UNIVERSITY OF NOTTINGHAM

Institute of Engineering Surveying and Space Geodesy

Crustal Deformation Monitoring by the Kalman Filter Method

by Cahit Tağı Çelik, *BSc, MSc*

Thesis submitted to the University of Nottingham

for the degree of Doctor of Philosophy, October 1998

Table of Contents

Table of Figures

Table of Tables

Acknowledgements

The author would like to thank his principle supervisor, Professor V Askenazi, for his invaluable guidance, advice, support and encouragement, and his associate supervisor, Dr. R M Bingley, for his great support guidance and proof reading throughout the course of this study.

The author would like to thank to Dr. W Chen, for his great support, discussion and encouraging ideas.

Thanks also to Dr. N Penna, for his advice and all colleagues for their understanding and personality, especialy D Baker for his proof reading.

The author would like to express his appreciation to his sponsor, the State Of Republic of Turkey and Nigde University, who have supported him in pursing higher education degrees for many years.

Finally, the author would like to acknowledge his family who have been indebted, especially his Mother, Hatice Celik, throughout his education and for their patience for his long term absence from home. And thanks also to his wife Guler Celik and his children, Merve F Celik and Sena H Celik, for their understanding, support and encouragement.

Abstract

The Earth's crust is deforming continuously due to plate tectonics. Deformation at plate boundaries causes volcanoes and most destructive earthquakes. Monitoring such deformation is essential to gaining an insight into the mechanisms of plate tectonics.

Deformation analysis is one of the most important aspects of geodetic research. Space geodesy, with which long baselines can be measured to millimetre accuracy, plays an important role in determining crustal deformation parameters, since deformation in general, means a change in geometric configuration. The main deformation monitoring problem is to determine the spatial relationship of a set of object points relative to a number of reference points. Ideally reference and object point observations are made at regular intervals. After mathematical adjustment of each epoch's observations, which includes 'data snooping', a displacement vector is obtained by simply differencing the estimated coordinates at consecutive epochs. The use of this method also however, increases the noise level.

In this thesis, the author proposes a deformation analysis technique which mainly uses a Kalman Filter. However, Kalman filter estimation may not be optimal if local movement occurs between observation epochs. To overcome this kind of deficiency, two sub-optimal filters have been proposed: Fading Memory Filter and Adaptive Kalman Filter for a System with Unknown Measurement Bias. These two filtering techniques have been used in this research and tested on real/simulated data based on the EASTMED project. In addition to this, data from the EUREF Permanent GPS Network, and from the UK Tide Gauge Monitoring Project are also processed and the result presented.

Chapter 1

Introduction

Monitoring the Earth's deformation is important in order to understand geodynamics. The movement of the Earth's crust comprises both global and local elements. Global in this context means tectonic motion and local means local motion (e.g. earthquakes). Tectonic motion is described by the plate tectonic theory. This divides the lithosphere into a number of rigid plates, which move relative to one other. Plate tectonic motion is generally governed by convection currents. This motion causes earthquakes, faults, plate boundaries and volcanoes. Hence, precisely monitoring Earth deformation is a primary task in geodesy. Global motion models (e.g. NNR-NUVEL-1) describe plate velocities based on the data from earthquakes, transform fault azimuths and spreading rates (Argus and Gordon, 1991). However, there is little knowledge of the mechanism that creates earthquakes, which may be associated with strain accumulation. One method of determining strain is to directly monitor the relative movements of the Earth's crust using geodetic methods.

Classical and space geodesy play important roles in determining crustal deformation parameters, due to the fact that deformation, in general, means a change in geometric configuration. Classical geodesy, unlike space geodesy, does not provide precise measurements over long distances. However, since the 1960's space geodesy (VLBI, SLR and GPS) has been widely used for monitoring crustal movements, enabling precise vector measurements to be made between ground stations anywhere on the Earth (Davies, 1997). One of the aims of modern space geodesy is to monitor crustal movements.

A number of research centres have developed various deformation analysis techniques. In general, deformation monitoring by geodetic methods can be divided into two parts: firstly, estimation of coordinates of stations which

constitute the network and elimination of noisy data (data snooping), and secondly, defining the reference frame (or datum). Definition of the reference frame can be further split into two categories: the conventional definition of a reference frame, and reference frame definition using the IGS stations and the precise International Terrestrial Reference Frame (ITRF).

Classical deformation analysis techniques in general use reference frames that are defined in conventional ways, either by an absolute or a relative network. The Hannover approach (Heck et al, 1983), is a conventional analysis technique. In this approach, a reference frame for a relative network is provided by a congruency test. The Delft approach, which uses the B-method of testing (Baarda, 1968) is used to define a relative network. In the Munich approach, (Chrazanowsky et al, 1981) and the Generalised approach (Chen, 1983), the reference frames are solved in a similar way to the previous methods. These methods differ in the use of test statistics, but have a common element in the calculation of the displacement vector, where the simple coordinate differences are taken. Significance tests are then applied to determine whether the movement occurred has actualy occured. The determination of displacement vectors is straightforward and simple, but this process also increases the noise level associated with the displacement vector. Simple differencing is also used in the Nottingham Approach (Dodson, 1977), and by many others such as Segall et al (1993) and Drewes et al (1995). An alternative technique used by some research groups uses linear regression to derive the station velocities. This is simple, but is sensitive to large movements and smoothes them out. For example, EUREF uses linear regression method to derive the velocities of the stations in the EUREF Permanent GPS Network.

A precise method is needed to derive station velocities from epochal geodetic measurements. This is one of the main aims of this study. The chosen precise method is Kalman Filtering. This method has already been used in many studies such as Donnellan et al (1993), and Feigl et al (1993). Although Kalman Filtering is a precise method, suitable for crustal deformation

monitoring it is in fact sensitive to the large movement induced by earthquakes which are associated with crustal movement. Hence the filter is contaminated for a number of epochs after the earthquake has occurred. The treatment of this is the main aim of this study and adressed using two adapted sub-optimal filters. These are the Fading Memory Filter and the Adaptive Kalman Filter for a System with an Unknown Measurement Bias.

The author was also involved in a project called the East Mediterranean GPS Geodynamic Project (EASTMED). One of the main aims of this project was to monitor the crustal deformation occurring in the East Mediterranean region. This project produced data from two GPS campaigns (October and November 1995). Between these two campaigns the Nuweiba earthquake (Mw=7.1) occurred. In the thesis, these data were used in association with the NNR-NUVEL-1 plate motion model as input to a simulation experiment. These data are used to test the proposed deformation analysis technique. Two disparate data sets were also used for further test purposes, taken from the EUREF Permanent GPS Network and the UK Tide Gauge Monitoring Project.

In this thesis, the main objectivies can be summarised as follows,

- To develop an approach for monitoring crustal deformations by using the Kalman filter method.

- To study and select suitable statistical tests and step functions that are convenient for the detection and treatment of an earthquake or bias occurring between episodic measurements.

- To test and assess the approach using suitable data.

- To process GPS measurements from the EASTMED project, and investigate if any stations were affected by the Nuweiba earthquake.

Basic information about Earth deformations is given in Chapter 2 including, plate tectonic theory, plate motion models and the possible direction of movement of different plate boundaries. A tectonic plate motion model, NNR-NUVEL-1 is used in the simulation process, (which is described in Chapter 5). Additionally, the tectonic setting of the East Mediterranean Region and information on vertical land movements are given. (as background to Chapters 5 and 6). Chapter 3 covers the high precision GPS techniques which were used by the author to observe and process the GPS data from the EASTMED Project. In Chapter 4, the method proposed to analyse the crustal deformation using Kalman filtering is detailed. Hence the title of this thesis: Crustal Deformation Monitoring by the Kalman Filter Method. Chapter 5 describes the data sets used and in Chapter 6, results and analyses are discussed.

Chapther 2

Deformations of the Earth

The main objective of this Chapter is to give a background on Earth deformations, which can be divided into two groups, global and regional deformations. Global deformations, as can be understood from its name, involve very large areas or plates. The movements of large plates can be described by the theory of plate tectonics which divides the lithosphere into a number of plates using data from paleomagnetic studies, seismological studies and many others. Therefore, the theory of plate tectonics provides very clear motion models at the plate boundaries. Regional deformations, however, involve smaller areas where the motions of small plates are controlled largely by the forces of large plates, but are not clearly delineated.

The theory of plate tectonics resulted from a combination of adequate parts from the hypotheses of both continental drift and sea-floor spreading. Therefore, in order to understand the Earth's deformation, these two hypotheses are essential.

The theory of plate tectonics has been used for a couple of decades to form plate motion models for global reference frames. For instance, the velocity fields of ITRF90 and of earlier realisations of the International Terrestrial Reference Frame (ITRF) were obtained by using an absolute geophysical plate motion model, i.e. 'AM0-2' (Boucher and Altamimi, 1996). Moreover, most results of individual studies are compared to plate motion models. However, these models represent the results over a number of different data and different time periods. For this reason most geodesists prefer current motions obtained mainly by using space geodetic techniques, i.e. VLBI, SLR, and GPS. For example from ITRF91 to ITRF94 the respective velocity fields have been adjusted by a combination of velocities resulting from VLBI, SLR and GPS (since 1993).

Consequently, this Chapter reviews the theory of plate tectonics and gives details on the tectonic setting of the East Mediterranean, as a background to the results presented in § 6.1. The Chapter is concluded with some background on vertical land movements, also in relation to the results presented in § 6.3.

2.1 Continental Drift and Sea-Floor Spreading

Ever since man chartered the coastlines of continents around the Atlantic Ocean in the 16th Century, the similarity of the coastlines of the Americas and of Europe and Africa have been noticed. Abraham Ortelius in 1596 appears to have been the first to note the similarity and suggests an ancient separation (Kearay and Vine, 1996). In 1620, Francis Bacon in 'conformable instances', commented on the similar form of the West coast of Africa and South America. He also suggested that they were once together and had drifted apart. In 1756, Theodor Christoph Liliental was another person to note the similarity or 'fit' of the Atlantic coastlines of South America and Africa and to suggest that they might once have been side by side. Then many more such as Snider in 1858, Taylor in 1910 wrote about the 'fit' of opposing continents and speculated on its meaning (Ollier, 1981).

In 1915, Alfred Wegener stated that "Continents were once combined together to form one single block, *pangea*, in the Late Carboniferous, since then they have been moving apart from each other" and published his first book, "*The Origin of Continents and Oceans*". In Figure 2.1 he reconstructed the positions of continents. In the book he gave evidence that was based on the distribution of plants and animals, distribution of fossils, ancient deserts, glaciated rocks and other geological reasons. However, he could not explain how this had occurred. Therefore, he could not convince many scientists who were against the idea of continental drift.

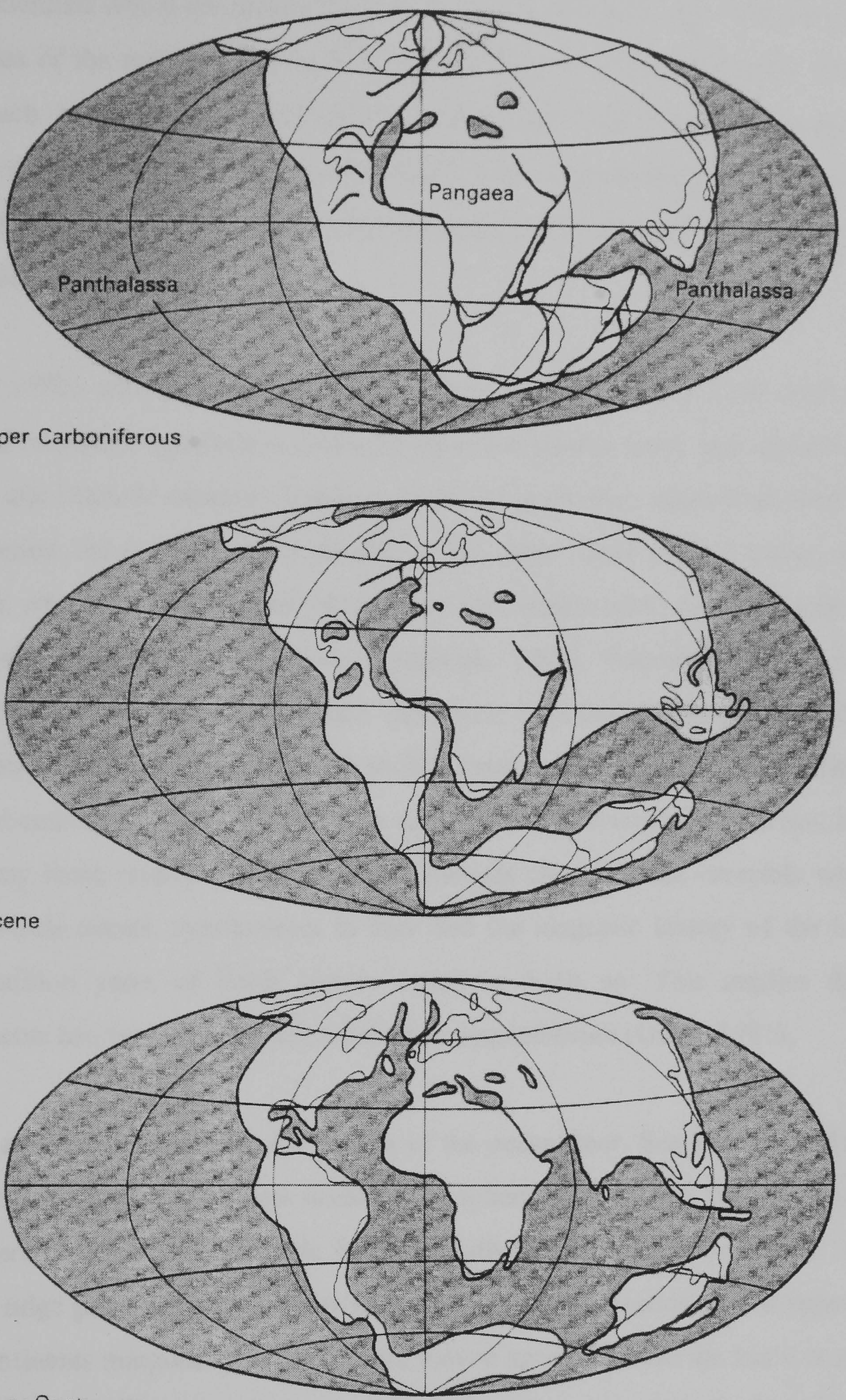

Figure 2.1 Wegener's Reconstruction of the Positions of the Continents from Carboniferous to Quaternary Times (Kearey and Vine, 1996)

The scientists who were against the idea of continental drift were familiar with the idea of the mobile Earth with a crust floating on a molten interior. Their approach is based on the idea that if a catastrophic event powerful enough to split a continental mass had occurred, then the newly generated margins would be stretched and severely deformed and they could not possibly fit so well (Wyllie, 1971).

In the 1950s, other evidence came from paleomagnetism, which is the study of natural remnant magnetism in rocks. Rocks that contain a small amount of iron oxide and sulphide minerals acquire a weak but permanent magnetism with an orientation and polarity that is parallel to the Earth's field at the location and time at which the rock cooled through its Curie temperature, which is defined as natural remnant magnetisation (Lambeck, 1988). Paleomagnetic studies showed that there is a systematic difference between the position of the magnetic pole. This results from the studies based on the same age rocks. Many special-case explanations were tried to account for this reversed magnetism, but as many more results were collected it became clear that the reversals were world-wide events, synchronous in time and the magnetic history of the last few million years of Earth history could be built up. This implies that continents had been drifting since their first magnetisation (Ollier, 1981).

More evidence results from the studies of the ocean floor. Sea-floor spreading is a phenomena in which new oceanic lithosphere is created by the upwelling and partial melting of materials from the asthenosphere at ocean ridges. As ocean ridge gradually grows wider with the progressive creation of lithosphere, the continents marginal to the ocean are moved apart. Because the Earth is not increasing in surface area by any significant amount, the increase in size of those oceans growing by the sea floor spreading would be balanced by the destruction of lithosphere at the same rate in another, shrinking, ocean by subduction at deep sea trenches situated around its margins.

The driving mechanism of these movements was believed to be convection currents in the sublithospheric mantle. These were thought to form cells in which mantle ascended beneath ocean ridges, bringing hot materials to the surface and giving rise to new lithosphere. The flow then moved horizontally away from the ridge, driving the lithosphere laterally in the same direction by viscous drag on its base and finally descended back into the deep mantle at the ocean trenches, assigning the subduction of the lithosphere (Kearey and Vine, 1996).

Some of the evidence for sea floor spreading is based on the magnetic field anomalies resulting from the magnetometer surveys. The anomalies were symmetrical about, and parallel to the ridge axes. Moreover, dating the mid-Atlantic ridge showed that the outer layer of the ocean floor is younger than the one underneath. All this evidence indicates that the ocean floor is spreading (Lambeck, 1988).

2.2 Plate Tectonics

The theory of plate tectonics in which the Earth's surface is divided into a number of plates (or aseismic units) moving relative to each other and carrying both the continental and oceanic crust, resulted from the combination of the adequate parts of the hypotheses of continental drift and sea-floor spreading. Continental drift and sea-floor spreading indicated that movements of the continents and of the sea-floor can be accepted as large-scale movements of plates. The movements of plates may be governed by convection currents. Convection is defined as the vertical transfer of the heat by a circulation of movement of a gas, liquid or plastic solid. Veining Meinesz stated that convection currents exist within the Earth's mantle. He experienced large negative anomalies from his gravity measurements in the East Indies associated with the oceanic trench in Indonesia. He provided the relationship between negative anomalies and convection currents in the Earth's mantle that is how

the Earth's crust gets pulled down into the mantle by sinking convection currents (Seyfert and Sirkin, 1979).

In fact, a large amount of information on modern plate tectonics comes from seismology and geomagnetism. The latter has already been mentioned above in the concept of sea-floor spreading. Seismology involves using waves produced by earthquakes. When an earthquake occurs it reveals two types of elastic waves, namely body waves and surface waves. The former travel through the earth and are of two types; P waves (compressional) and S waves (shear waves). P waves are always faster than S waves, and S waves can not be transmitted through a liquid. Surface waves that propagate along the earth's surface consist of two types, Rayleigh and Lowe waves. The former has a motion within the vertical plane containing the direction of propagation, while the second one has horizontal motion normal to the direction of the propagation. Elastic waves can be detected by seismometers which respond to ground movements. Figure 2.2 shows epicentres, which are the points above the hypocentres where elastic waves are produced by an earthquake. These occurred between 1961-1969.

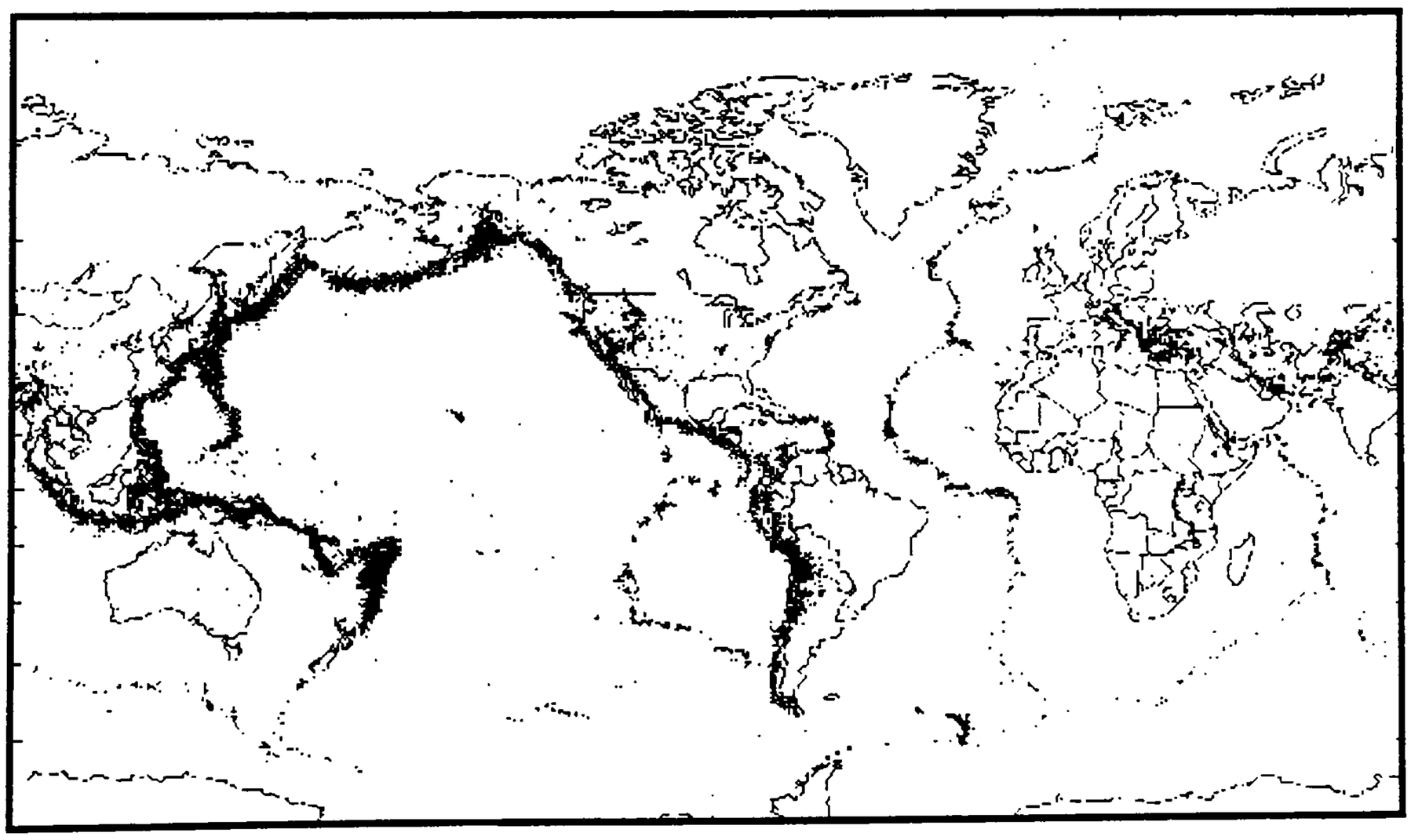

Figure 2.2 Distribution of World Earthquakes 1961-1969 (Condie,1989)

As can be seen from Figure 2.2, earthquakes occur along the rather narrow belts on the plate boundaries between the lithospheric plates. There are three types of seismic boundaries, distinguished by their epicentre distributions and geological characteristics. These are constructive (ocean ridges), destructive (trenches), and conservative (transform faults) boundaries (Rayson, 1990).

Constructive Boundaries: This type of boundary is where two plates separate from each other. Magma and depleted mantle upwell between separating plates giving rise to new oceanic lithosphere. Figure 2.3 represents the direction of motion being, in general, perpendicular to the strike of the boundary.

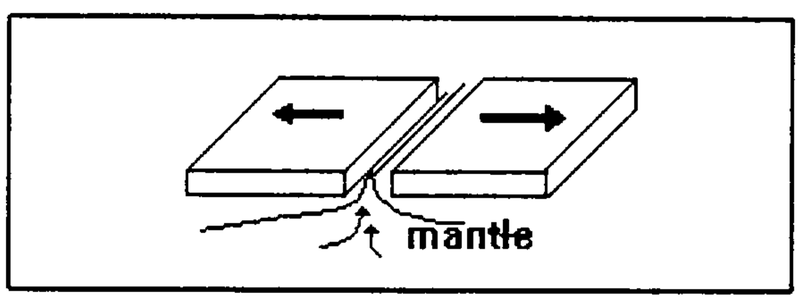

Figure 2.3 Constructive Boundary

Destructive Boundaries: These boundaries are where two plates have convergent movement. This type of boundary occurs under oceans and one plate usually bends under the other plate and sinks to the mantle, which causes the greatest depths. Since the Earth is not expanding significantly the rate of lithospheric destruction at trenches is virtually the same as the rate of creation at ocean ridges. Figure 2.4 shows an example of this type of boundary and possible deformations in the region.

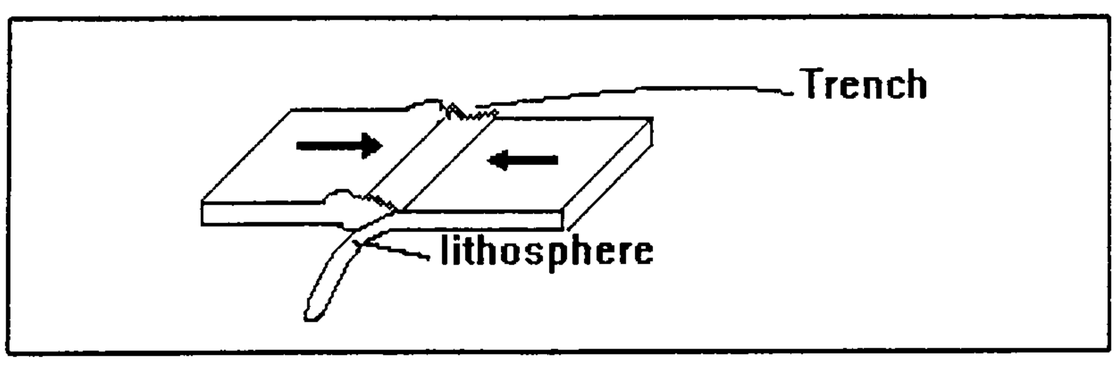

Figure 2.4 Destructive Boundary

Conservative Boundaries: Conservative boundaries are where two plates slide past each other without deformation, due to the plates having the same density. The relative motion is usually parallel to the fault. In these boundaries, there

are two possible movements namely sinistral and dextral. Sinistral movement is known as left-lateral movement. Dextral movement is known as right-lateral movement. Figure 2.5 shows the boundaries and their possible movements.

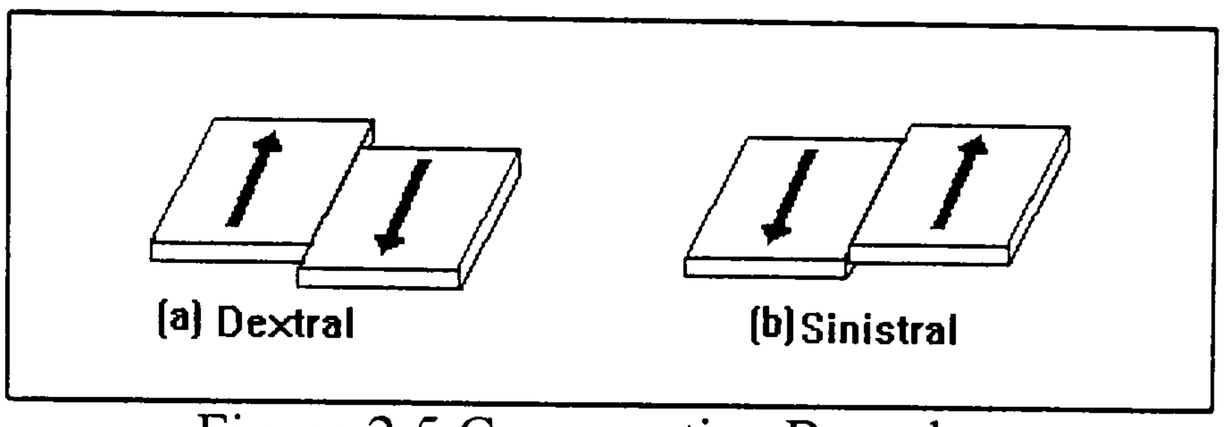

Figure 2.5 Conservative Boundary

According to the plate tectonic theory, plates are considered to be internally rigid, and to act as extremely efficient stress guides. A stress applied to one margin of a plate is transmitted to its opposite margin with no deformation of the plate interior. Deformation then takes place only at plate margins. Therefore the motion of the large plates are well characterised. However, since these boundaries are dynamic, not only migrating about the Earth's surface but changing from one type of boundary to another, new plate boundaries can be created in response to changes in the lithosphere (Condie, 1989).

2.3 Plate Motion Models

The Earth's crust is moving continuously due to plate tectonics (Cox, 1986). In plate tectonics, the Earth lithosphere is divided into a number of plates moving relative to each other.

A plate tectonic model first introduced by Morgan, (1968) extended Wilson's transform fault concept based on Euler's theorem describing the relative motion of two plates. Wilson's transform fault is based on the two plates (a and b) on a sphere moving relative to each other. This movement happens around a Euler pole (Ep) that has a datum common with the stable one of the two plates as seen in Figure 2.6.

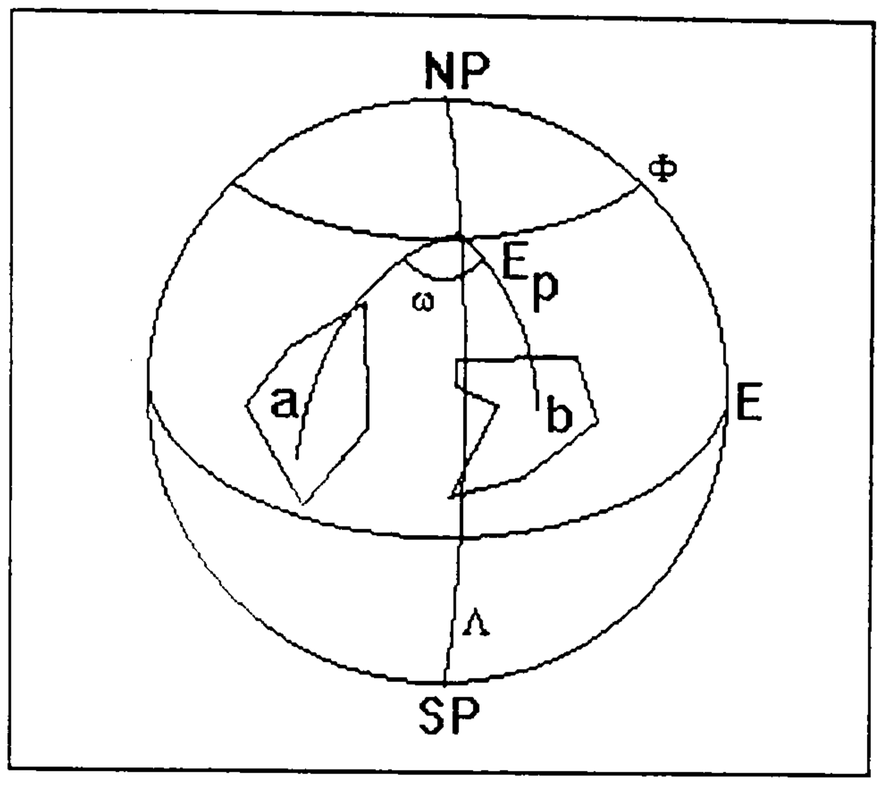

Figure 2.6 Description of Euler Vector

This relative movement is expressed by three parameters, two of them are location of the Euler pole (latitude Φ, longitude Λ) and the third one is rate of motion (ω). These three parameters are called the Euler vector.

Morgan divided the lithosphere into 13 plates bounded by the Mid-Atlantic Ridge and the Mid-Indian Ocean Ridge (divergent), oceanic trenches (convergent), great faults (transform) and active fold belts (collisional boundaries). Figure 2.7 shows Morgan's division of the lithosphere into 13 plates. The movements on the Mid-Atlantic Ridge, as mentioned earlier in the concept of sea-floor spreading, are of the divergent type. Therefore, plates move apart from each other. The Peru-Chile Trench, an example of a convergent boundary, is the zone of descending oceanic crust and upper mantle. The San Andreas Fault is an example of a transform boundary that slides past each other or strike-slip, while the Himalayan mountain belts demonstrate active folds (Seyfert and Sirkin, 1979; Condie, 1989). This was followed by a number of global plate motion models, such as CH72 (Chase, 1972), RM1 (Minster, et al., 1974), P071 (Chase. 1978), RM2 (Minster and Jordan, 1978), NUVEL-1 (DeMets, et al., 1990) and NUVEL-1A (DeMets, et al., 1994).

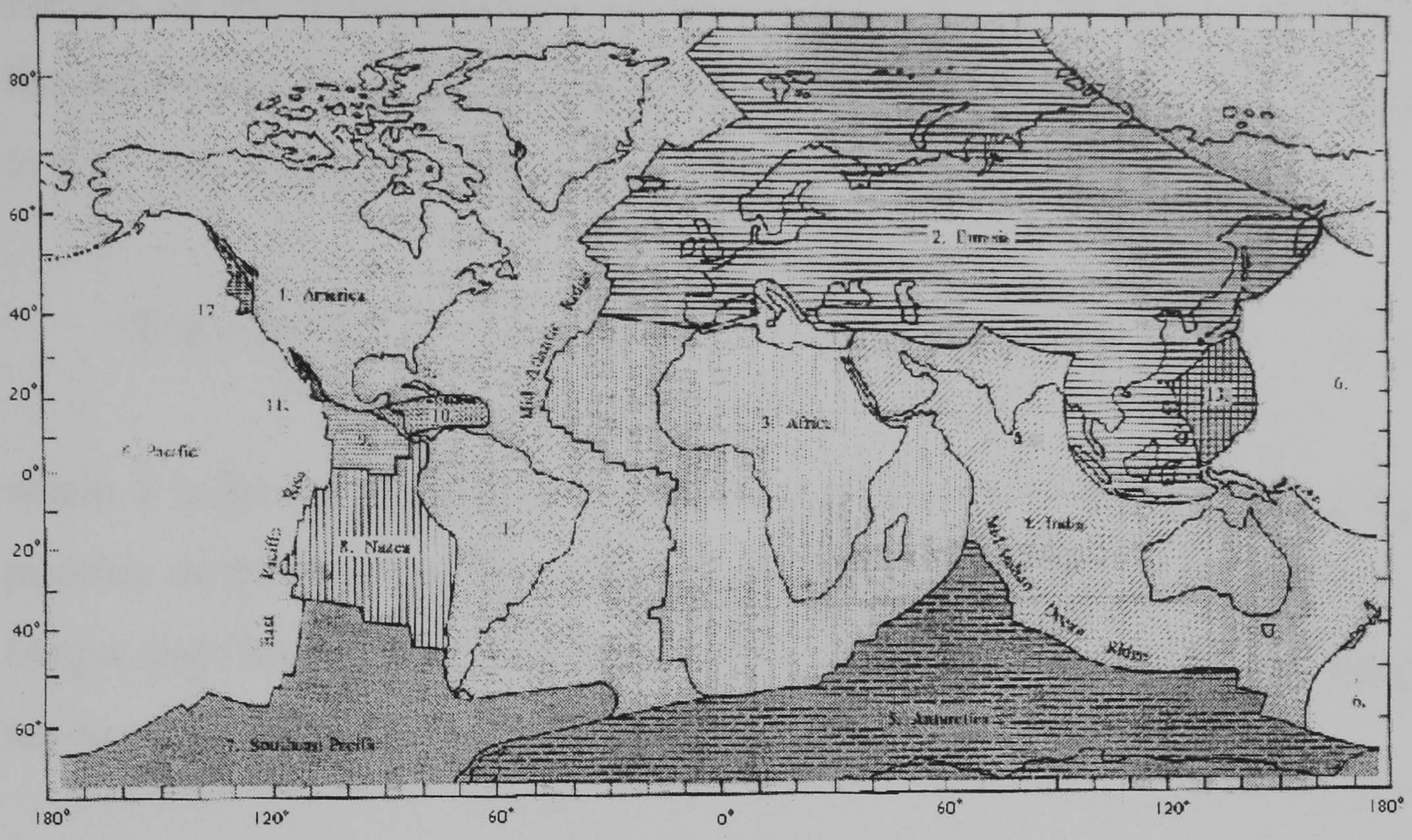

Figure 2.7 Division of the Earth's Crust into 13 Plates. The Unlabeled Plates are: 9-Cocos Plate; 10-Caribbean Plate; 11-Baja Plate; 12-Juan de Fuca Plate; and 13-Marianas Plate. (Seyfert and Sirkin, 1979)

There are two types of plate motion models; absolute plate motion models and relative plate motion models. An absolute plate motion model, defined as motion relative to mesosphere, can be obtained by various methods such as using hotspots data, using no-net-rotation frame and using space geodetic methods such as VLBI, SLR, and GPS.

Hotspots are believed to be stable in the deep mantle. When the plates moves from one position to the other, hotspots stays stable in the deep mantle. That makes a trace on the lithosphere as hotspots. Hotspot tracks form along small circles around the Euler pole describing the motion of a plate relative to the mesosphere. HS2-NUVEL-1 (Gripp and Gordon, et al., 1990) is an absolute plate motion model obtained from hotspots data and the incorporation of NUVEL-1.

Another method for obtaining the absolute plate motion is the one using no-net-rotation frame. This method is based on the calculation of total torque

exerted on the mesosphere by the lithosphere due to different velocities of lithosphere and mesosphere. This method assumes that the total torque is equal to zero. This is given by a cross product as,

$$\mathbf{T}=\mathbf{r} \times D\mathbf{v}=0 \qquad (2.1)$$

where **T** is the total torque, **r** is a radius position vector, **v** is a velocity of the position on the plate and D is a drag coefficient (Cox, 1986). NNR-NUVEL-1 (Argus and Gordon, et al., 1991) is an example of a plate motion model using no-net-rotation frame.

Relative motion defined as motion relative to an arbitrary fixed tectonic plate can be obtained by various data, including geological seismic and geodetic.

Geodetic techniques can directly measure the relative plate motions. The results from conventional geodetic methods may be inefficient for crustal movement over the long baselines. However, space-based techniques, ie VLBI, SLR, and GPS, provide sufficiently high accuracy over long base lines from which plate motions can be detected in a few years (Stein, 1993).

Plate motion models which use geological and seismic data, are based on the estimation of Euler poles of each pair of plates and their angular velocities corresponding to each Euler pole. An example is the NUVEL-1 model, (Table 2.1). NUVEL-1 divides the Earth's lithosphere into 13 assumed-rigid plates. These plates described by their Euler poles and their corresponding angular velocities. An estimation of an Euler vector is based on the inversion of plate motion data.

Table 2.1 NUVEL-1 Euler Vectors (DeMets, et al., 1990)

Plate Name	Lat(N)	Long(E)	ω(deg/m.a)	ωχ (Rad/m.a)	ωγ (Rad/m.a)	ωz(Rad/m.a)
African	59.160	-73.174	0.9695	0.002511	-0.008303	0.014529
Antartican	64.315	-83.984	0.9093	0.000721	-0.006841	0.014302
Arabian	59.658	-33.193	1.1616	0.008570	-0.005607	0.017496
Australian	60.080	1.742	1.1236	0.009777	0.000297	0.016997
Caribbean	54.195	-80.802	0.8534	0.001393	-0.008602	0.012080
Cocos	36.823	-108.629	2.0890	-0.009323	-0.027657	0.021853
Eurasian	61.066	-85.819	0.8985	0.000553	-0.007567	0.013724
Indian	60.494	-30.403	1.1539	0.008555	-0.005020	0.017528
Nazca	55.578	-90.096	1.4222	-0.000023	-0.014032	0.020476
N.American	48.709	-78.167	0.7829	0.001849	-0.008826	0.010267
S.American	54.999	-85.752	0.6657	0.000494	-0.006646	0.009517
Additional Euler vectors (Pacific plate fixed)						
J.de Fuca	35.0	26.0	0.53	0.00681	0.00332	0.00531
Philippi	0.0	-47.0	1.0	0.0119	0.0128	0.000

Each named plate moves counterclockwise relative to the Pacific Plate. The Juan de Fuca-Pacific 3.0 Ma Euler vector is taken from Wilson (1988) and the Philippine-Pacific Euler vector is taken from Seno et al, (1987).

Figure 2.8 shows the geometric division of the lithosphere into a number of plates. This model is represented by a set of angular velocity vectors defining the motion of each plate relative to one arbitrarily fixed plate. The angular velocity vectors are determined in a spherical coordinate system together with their rotation rate and Euler pole.

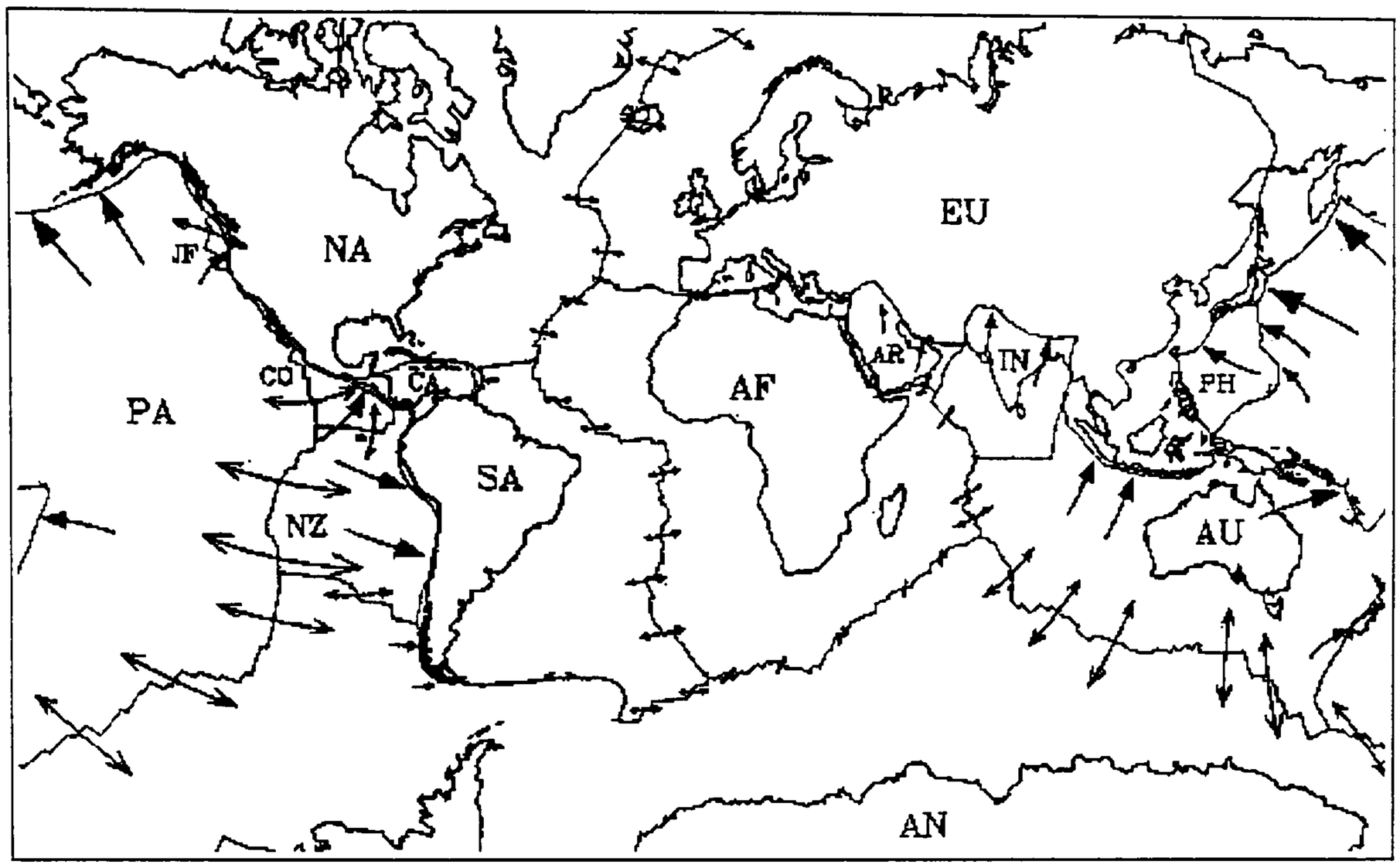

Figure 2.8 Plate Motions and Assumed Geometry for the NUVEL-1 Global Relative Plate Motion Model (DeMets, et al, 1990)

Table 2.1 shows the Euler vectors relative to the Pacific Plate. The relative velocity of one plate to another at any point along their boundary is the cross product of the appropriate angular velocity vector and the point position vector (Smith and Turcotte, 1993). It is given in terms of spherical coordinates i.e., Latitude and Longitude, by

$$\begin{aligned} \Delta\varphi &= \Delta t.\omega.\cos\Phi.\sin(\lambda-\Lambda) \\ \Delta\lambda &= \Delta t.\omega.(\sin\Phi-\cos(\lambda-\Lambda).\tan\varphi.\cos\Phi) \end{aligned} \tag{2.2}$$

where

ω is the rate of rotation

Φ is Latitude of the Pole of Rotation

Λ is the Longitude of the Pole of Rotation

φ is the Latitude of a location whose velocities are in question

λ is the Longitude of a location whose velocities are in question

or in three-dimensional cartesian coordinates (x, y, z), by

$$\Delta x = \omega(y).z - \omega(z).y$$
$$\Delta y = \omega(z).x - \omega(x).z \qquad (2.3)$$
$$\Delta z = \omega(x).y - \omega(y).x$$

where,

$\omega(x) = \omega.\cos\Phi.\cos\Lambda$

$\omega(y) = \omega.\cos\Phi.\sin\Lambda$

$\omega(z) = \omega.\sin\Phi$

x, y, z are the cartesian coordinates of a location whose velocities are in question

There are two disadvantages of the conventional global plate motion models. One of them is the assumption that the plates are thought to be rigid. The other is the fact that different data types that represent the motions of plates averaged over different time periods are combined.

In the NUVEL-1 model there are three types of data used. These are namely; transform fault azimuths, earthquake slip vectors and spreading rates (DeMets et al., 1990). These three types of data will be briefly described here for completion.

Transform Fault Azimuth: A transform fault azimuth is described by an horizontal angle between the North pole and the direction of a great circle that is tangent and parallel to the transform fault at a locality where the transform fault is. In Figure 2.9 transform fault azimuth is represented. An Euler pole azimuth corresponding to the transform fault azimuth is 90° plus the azimuth of the transform fault. A transform fault azimuth averages the direction of plate motion over an unknown time interval, which may be several millions of years long (DeMets et al, 1990).

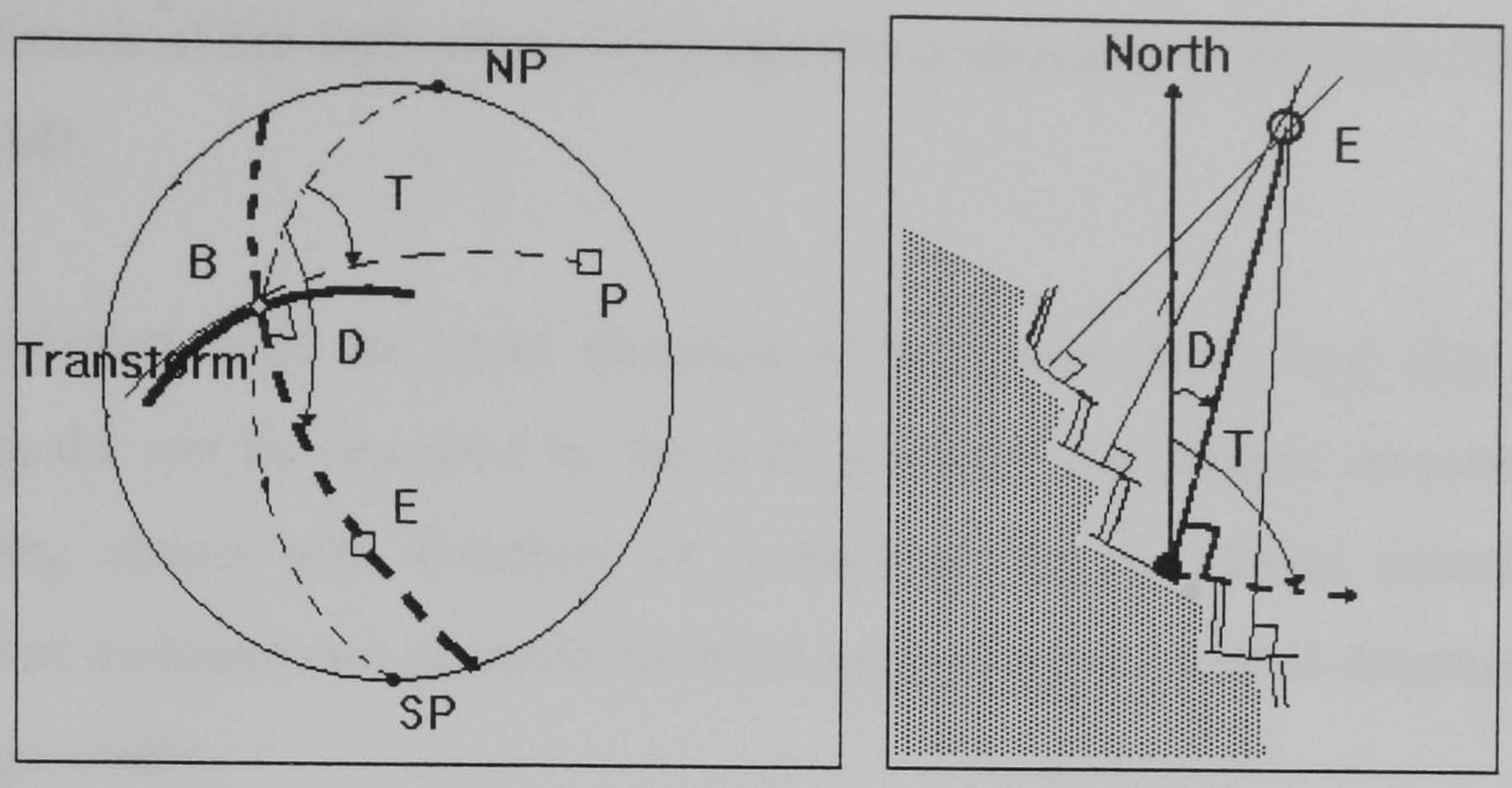

Figure 2.9 Transform Fault Azimuth. Euler pole E is on the Great Circle Perpendicular to the Trend of Transform. P is the Pole of Great Circle <BE> (Cox, 1986)

Earthquake Slip Vector: An earthquake slip vector provides the same information as a transform fault azimuth does but over a known time interval that is over years, tens of years or hundreds of years depending on repeat cycles. Earthquake slips vectors are found from the radiation pattern of seismic waves from earthquakes along transforms. They describe the relative motion of the plates on opposite sides of the transforms.

When an earthquake happens, it transmits seismic waves in certain directions. The directions of these seismic energy are directly related to the stresses released at the time of an earthquake and indirectly to the direction of plate motion.

Descriptions of point seismic sources from analysing the radiation pattern of an earthquake are of two types. One of them is in terms of an angular description of the nodal planes in the P radiation from a purely slip motion on a fault. The other is the description of source by the six independent components of the moment tensor inversion of body and surface waves, which are assumed to have a common dependence on time. As a result of this, a fault geometry is yielded. This is described in the focal mechanism by focal sphere parameters;

the azimuth of the fault plane, strike and dip component of the fault (Udias et al, 1988).

The orientation of the fault, direction of fault movement, and size of an earthquake can be described by the fault geometry and seismic moment. The differing shapes and directions of motion of the waveforms recorded at different distances and azimuths from the earthquake are used to determine the fault geometry.

Spreading Rates: In plate tectonics, a chronometer used to determine isocrons on the seafloor is provided by the Earth's magnetic field. The heart of the timing system is located in the Earth's liquid core where the geomagnetic field is generated by electrical currents. This chronometer is binary in the sense that it has two stable states: a normal state in which the magnetic field is directed toward the North, and a reversed state in which the field is directed toward the South. For at least two billion years the field has switched back and forth between these two states at irregular intervals that may be as short as 20 thousand years or as long as several tens of millions of years or more. The geomagnetic field aligns the ferromagnetic domains in rocks on the seafloor as they cool from a molten state at ridge. From sensitive magnetometer readings made at the sea surface, it is possible to "read the magnetic memory" of the rocks on the sea floor.

The seafloor is generally magnetised in stripes of alternating polarity. Like tree rings, the stripes are of varying widths, and ages can be determined by a comparison with a standard pattern of known age as determined by isotopic dating. As a result, a spreading velocity can be determined.

2.4 Tectonic Setting of the East Mediterranean

The Mediterranean province is one of the areas where adequate explanation of plate boundaries is expected due to the belief among geologists that a large ocean, *Tethys*, once existed between Eurasia and Africa during the Cretaceous and early Tertiary periods. Therefore, the present tectonic setting of the area is believed to be the remnant of this ocean.

The tectonic setting of the East Mediterranean region is largely governed by three major plates together with some small plates (McKenzie, 1970). These plates are the African, Eurasian and Arabian plates (Figure 2.10). Present day tectonic deformation of the area is closely related to the northerly motion of the African-Arabian plate relative to Eurasia and to the medial to late Eocene events(23-50 ma) in the Red Sea. During this period, Africa and Arabia combined as a single plate closing the back arc basin of the Tethys (Hempton, 1987). Then the process of combination continued forming subduction of Africa underneath Eurasia. As this continued, the extension in the Red Sea and Gulf of Aden formed by the separation of Arabia from Africa, caused a convergence of the Arabian plate against Eurasia. The stresses by the convergent motion were relieved by the extrusion of continental wedges along transform faults. Consequently, Anatolion strike slip faults formed (Barka and Hancock, 1984). Westward lateral motion of the Anatolian plate is due to the forces concerned with the Eurasia/ Arabia collision. The Anatolian Fault that extends from East to West defines the Northern boundary of the block. In the Marmara Sea, the boundary spread out series of parallel fault systems extending into the Northern Aegean Sea. The westerly motion of Anatolia relative to Eurasia, continental collision by the Adriatic plate against Northwest Greece and Albania, and by Arabia against Eurasia, and the subduction at the Hellenic arc control the present-day kinematics of deformation in the eastern Mediterranean (Oral, 1994).

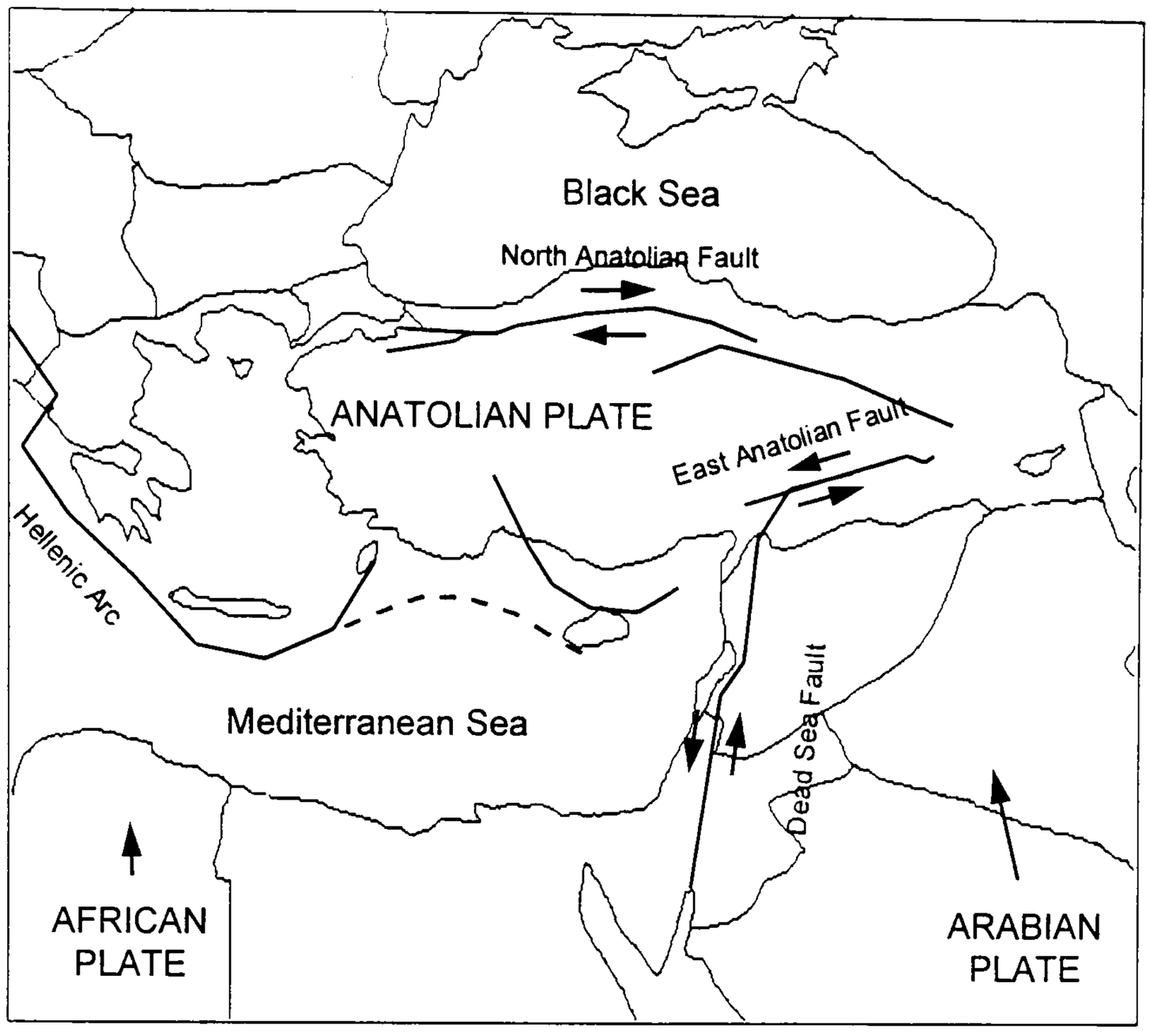

Figure 2.10 Simplified Tectonic Framework of East Mediterranean (Oral, 1994)

According to a study by Nooman et al, (1993) of the episodic crustal motions in the geologicaly active Mediterranean region using satellite laser ranging (SLR) techniques supports the hypothesis that the obliquely convergent motion between the Arabian and Eurasian plates is largely partitioned into right-lateral strike slip faulting in eastern Turkey and shortening farther North.

Another study done by Noomen et al., (1995) showed the deformation taking place in the area as: the Northward motion of Arabia, the lateral escape to the West of Anatolia, the NE-SW expansion in the Aegean Basin and the Northward motion of Africa being transduced into the central part of the Mediterranean.

The Arabian plate appears moving Northward and pushing Turkey (Figure 2.10). The motion of Eastern Turkey is characterised by distributed deformation while the motion of Central/ Western Turkey by coherent plate motion involving Westward displacement and counterclockwise rotation of the

Anatolian plate. This difference in Eastern and Western Turkey to collision of Arabia may result from the different boundary conditions, the Hellenic arc forming a free boundary to the West and the Asian continent and oceanic lithosphere of the Black and Caspian Seas forming a resistant boundary to the North and the East (Reilinger et al, 1997).

The East Mediterranean Region has undergone several destructive earthquakes most of which are now close to modern population centers (Ambraseys and Finkel, 1995). Most of these earthquakes resulted from the relative motions between the African, Arabian and Eurasian plates.

The motion of the Arabian plate is constrained from several plate boundaries in the region (Jestin et al, 1994). These boundaries are the Gulf of Aden, the Dead Sea Transform Fault, the Red Sea, the Suez Rift and East African Rift.

The seismic slip rate calculated for the Dead Sea Transform Fault is 1-2mm per year, which is an order of magnitude smaller than Arabia-African motion (Salamon, 1993). Spatial distribution of earthquakes along the Israel-Jordan section of the Dead Sea Transform Fault is also non-uniform (Figure 2.11). Activity is mostly localised at large basins along its strike, ie the Kinneret-Hula, the Dead Sea and the Gulf of Eilat/Aqaba, whereas the inter-basin segments are quiet. This non-uniform strain release may indicate non-uniform slip rates and strain accumulation along various sections of the Dead Sea Transform Fault.

The Gulf of Eilat/Aqaba is currently the most active segment of the Dead Sea Transform Fault (Shamir and Shapira, 1994) and produced the Mw=7.1 Nuweiba earthquake in November 1995 with a mean dislocation of 3m (Shamir, 1996). This level of activity implies that large strains are accumulating along the Arava Valley segment of the Dead Sea Transform Fault (Figure 2.11).

The Nuweiba earthquake in 1995 is important for this study since we have two campaigns of GPS data (October 1995, and just after the earthquake, November 1995) from the East Mediterranean GPS Geodynamics Project(EASTMED).

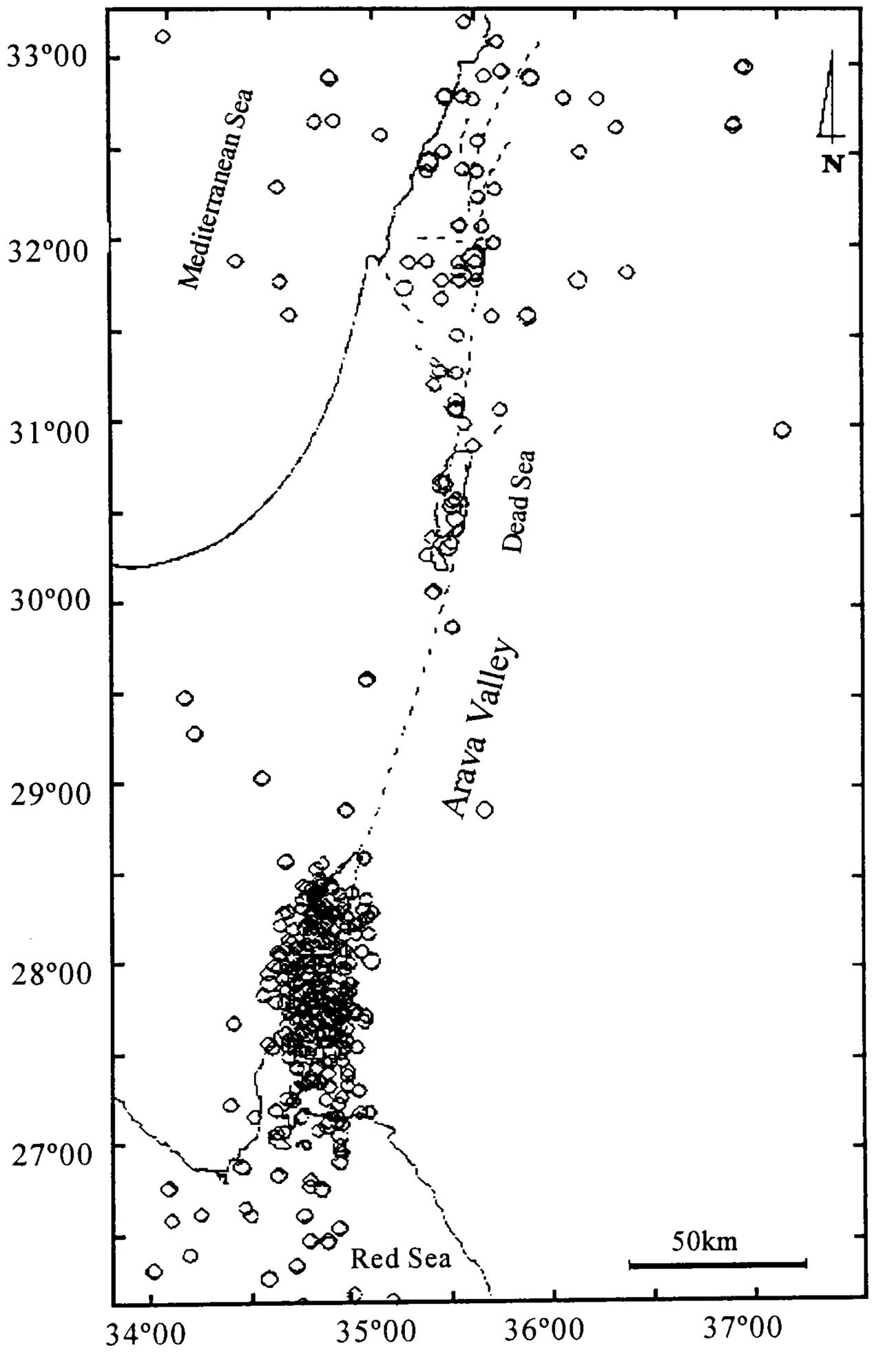

Figure 2.11 Seismicty Along the Dead Sea Transform Fault: 1900-1996

2.5 Vertical Land Movements

Up to now, this Chapter has dealt with the plate tectonic and plate motion models, which are basically two dimensional. There remains a third part, the vertical component, which is barely mentioned in plate tectonics. A good reference for this is Lambeck, (1988). Vertical movements of the Earth's crust, either uplift or subsidence, occur local and world-wide, at plate boundaries, and in plate interiors with an order of magnitude smaller than horizontal movements. Major uplifts associated with the tectonics of continent-continent, continent-ocean collision are examples of movements at plate boundaries. Within plate interiors, there might be a number of causes for vertical movements, i.e. lateral variations in the thermal regime, the response of the crust to variations in surface loading resulting from the erosion of elevated regions and the deposition of sediments away from these regions or from the vertical response of the crust to horizontal forces. These processes occur on variying time scales. Figure 2.12 represents responses due to different causes on different time scales.

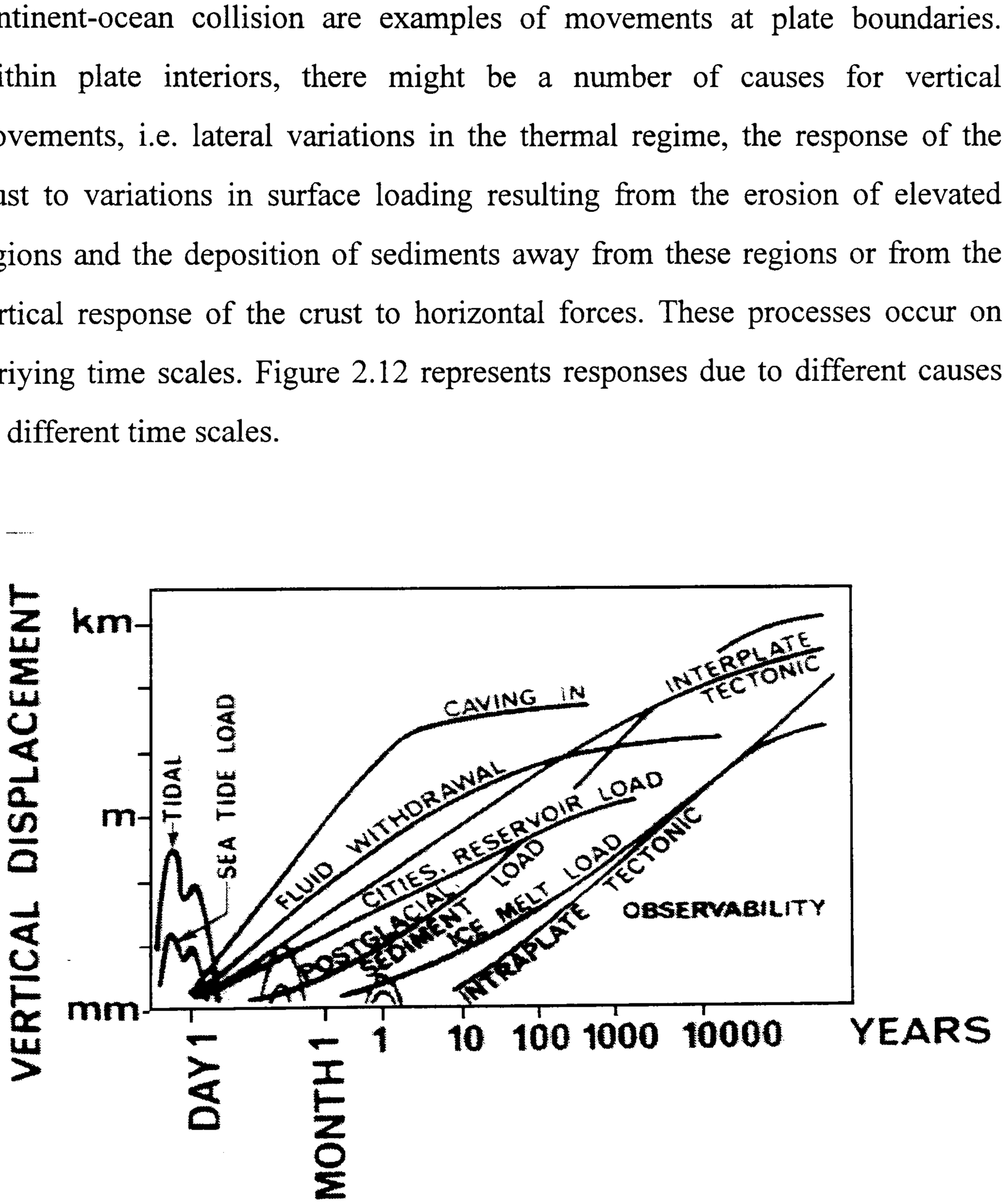

Figure 2.12 Characteristics Vertical Displacements due to the Most Conspicuous Phenomena (Vanicek and Krakiwsky,1986)

The time scales vary from an hour to millions of years. For long term movements, the most important phenomena is rebound. When the ice melted, the elastic relaxation took place instantaneously, while the non-elastic part of the deformation persisted. In other words, the lithosphere found itself and remained in a state of non-equilibrium. Since that time the crust has been rebounding, due to its buoyancy, to attain the isostatic equilibrium. This process is known as the *postglacial isostatic rebound* (Vanicek and Krakiwsky, 1986). The immediate consequence of melting of the Late Pleistocene ice caps was to raise sea-level on average by about 120-130m. Much of this rise occurred within about 6000 years from 14000 to 8000 years ago. Secondary and more subtle, consequences of the melting of ice sheets is that the crust rebounds in response to unloading by amounts that reach several hundreds of metres in some instances.

In Fennoscandia as well as in Canada the crust has been rising continuously since the deloading of the ice sheets at the end of the last Ice Age; a small contribution also comes due to from the deloading of sea water due to crustal uplift itself, which is an example of postglacial rebound as defined above. The maximum apparent uplift (relative to mean sea level) in the northern part of Gulf of Bothnia in Fennoscandia amounts to 9.2 mm/year, +/- 0.2mm/year (Ekman, 1992) based on Fennoscandian land uplift map of Ekman in 1989 compiled from the national land uplift maps and data of Denmark, Norway, Sweden, Findland Estonia and Latvia and the northwestern corner of the Russia.

Sea surface height is recorded continuously by tide gauges. From tide gauge records relative mean sea levels are obtained. The tide gauges are assumed on the stable land. However, the Earth's crust is subject to vertical land movements as described above. Therefore to obtain absolute changes in mean sea level, any vertical land movements of tide gauges must be considered and removed. For more information the reader is refered to §5.3.1

Chapter 3

High Precision GPS Techniques

The main objective of this Chapter is to give an introduction to the use of GPS in association with the International GPS Service for Geodynamics (IGS) and the International Terrestrial Reference System (ITRS), for high precision positioning.

The NAVSTAR GPS (Navigation Satellite Timing and Ranging Global Positioning System) is a satellite based positioning system developed by the US Department of Defence (DoD). The development of GPS began in 1973. At this time, the TRANSIT (Doppler) system was operational. However, there were deficiencies with coverage and continuity of this service. GPS set out to address these with the aims of providing a real-time positioning service of high accuracy and continuous global coverage. For these reasons, carrier frequency was modified from 400 Mhz to 1574.42 MHz and the altitude of satellite constellation was changed from 1075 km for Transit to 20200 km for GPS (Eren and Uzel, 1995). GPS provides a global, three-dimensional positioning, velocity and time information system. For more information the reader is referred to Seeber, (1993), Kaplan, (1996) and Hofmann-Wellenhof et al, (1997).

GPS provides a global three-dimensional positioning capability, through a terrestrial reference system, the World Geodetic System 1984 (WGS84). Initially the WGS84 reference frame was accurate to 1-2m, with the improvement of the frame, it is currently accurate to cm level (Malys, 1997). Alternatively another reference frame is the International Terrestrial Reference Frame (ITRF). The ITRF represents the realisation of the ITRS (International Terrestrial Reference System). The relationship between the ITRF and GPS became more important with the establishment of the International GPS Service for Geodynamics (IGS) in 1992. IGS analysis centres use an ITRF

coordinated subset of their global network of stations to determine precise GPS ephemerides. They are consistent with the ITRF. In turn, IGS precise ephemerides are used in high precision GPS positioning computations.

3.1 General Description of GPS

The main aim of this system is to determine the position of a GPS receiver by measuring ranges from satellites. These range measurements can be obtained provided that the signals transmitted continuously from the satellite are recorded by a synchronised receiver. Once the period in which a signal travelled from a satellite to receiver has been obtained, a range measurement can be computed as a product of the speed of light and the time period obtained. This is known as a pseudo-range. Using a number of pseudo-range measurements from different satellites the position of the receiver can be determined explicitly using the well known resection method. In this process, the clock errors must be taken into account, since the synchronisation of both satellite and receiver to the real GPS time are not perfectly achieved. Therefore, the number of unknowns are four for each receiver i.e. the X, Y, Z coordinate components of the receiver position and one clock offset between satellite and receiver. Thus at least four satellites must be available during the observation period to determine the four unknowns explicitly.

This system is conventionally divided into three main segments, namely, the space segment, the control segment and the user segment (Seeber, 1993).

3.1.1 Space Segment

The space segment of GPS was designed to consists of 24 satellites orbiting the earth in six orbital planes in planning stage. At present there are 27 operational GPS satellite. The satellites are neither polar nor equatorial, but slice the Earth's latitude at about 55°, executing a single revolution every 12 hours (Kennedy, 1996). There are six orbital planes. In each orbital plane, there are four satellites at an altitude of approximately 20,200 km. This provides at least

four satellites above an elevation of 15°, to be visible at any time and any place on the Earth. Each satellite is identified by two different numbering schemes. The SVN (Satellite Vehicle Number) or NAVSTAR number, based on the launch sequence and the PRN (Pseudo-Random Noise) or SVID (Space Vehicle Identity) numbers based on the orbit arrangement and the particular PRN segment assigned to the each satellite.

There are two carrier frequencies transmitted by the satellites namely, L1 and L2 as shown in Table 3.1. The frequencies are obtained from the fundamental L-band 10.23 MHz by multiplying by 154 and 120 respectively. They are transmitted at the same time so that a user can receive both signals to calibrate for ionospheric delay and apply the correction for this refraction (Schofield, 1993).

Table 3.1 Carrier Phase and Embedded Codes

L1 10.23*150=1575.42Mhz	C/A -Code Wavelength 300m	P - Code Wavelength 30m
L2 10.23*120=1227.60Mhz	-	P - Code Wavelength 30m

There are two codes employed in GPS, and modulated on these two L1 and L2 carrier waves, namely, the so-called P-code (precise), primarily for military use and the C/A-code (Coarse-Acquisition), mainly used by civilians. The P-code is modulated on both L1 and L2 and has a wavelength of 30m. Since this code is only available for military use, the code is encrypted and becomes the Y code so that civilian users can not use it. This is known as Anti-Spoofing (A-S) and has been operational since 31 January 1994. The C/A code is only modulated on the L1 carrier wave and has a wavelength of 300 m. This code and is not encrypted, but its accuracy is degraded. This degrading is known as Selective Availability (SA) whereby the satellite transmission is modified to introduce errors in pseudo-range measurement. These errors are introduced in

two types, namely EPSILON that is alteration of the broadcast ephemerides, and DITHER that is the manipulation of the satellite clock.

3.1.2 Control Segment

The control segment is responsible for supervising the satellite timing system, the orbits and the mechanical condition of the individual satellites. To achieve these tasks, there are five Monitor Stations distributed around the World (Hawaii, Kwajalein, Ascencion Islands, Diego Garcia, Colorado Springs) and one Master Control Station at Falcon Air Force Base in Colorado Springs (Shank and Lavrakas, 1994). All the satellites are being tracked by these Monitor Stations. Signals from the satellites are recorded and satellite orbits are predicted for several hours ahead. Then these satellite ephemerides and clock corrections are uploaded to the satellites via ground antennas as satellites pass overhead.

All computations involve two reference systems and their corresponding frames namely, the Conventional Inertial System (CIS) and the Conventional Terrestrial System (CTS) (Eren and Uzel, 1995). The CIS is a system of coordinates whose origin is at the centre of mass of the Earth, whose X-Y plane is taken to coincide with the Earth's equatorial plane, and +X-axis is permanently fixed in a particular direction relative to the celestial sphere, +Z-axis is taken normal to the X-Y plane in the direction of the North pole, and +Y- axis is chosen so as to form a right-handed coordinate system. However, in the definition of the CIS, the irregularies of the Earth rotation have to be taken into account. Therefore, the CIS can only be defined with an orientation of axes at a particular instant in time. Typically, the GPS uses the orientation of the equatorial plane at 1200 hr UTC on 1 January 2000, as its basis. The +X-axis of the system is defined to point from the centre of mass of the Earth to the direction of the vernal equinox, and the other two axes are defined as above (Kaplan, 1996).

Satellites orbit the Earth in an inertial system due to Newton's law of motion, their orbit estimation and predictions are made in an inertial system. However, receiver coordinates on the Earth surface, are required in an Earth centred Earth fixed coordinate system, i.e. CTS. For this, the GPS uses WGS84.

3.1.2.1 World Geodetic Reference System (WGS84)

The US DoD has developed a series of global terrestrial reference frames for the need of a range of world-wide applications. These are WGS60, WGS66, WGS72 and WGS84. The WGS84 provides the basic reference frame and geometric figure of the Earth, models the Earth gravimetrically and provides the means for relating positions on various local geodetic coordinate systems. The definition of WGS84 is that its origin is at the centre of mass of the Earth, its positive directions of Z and of X axes are directed to the pole and the Greenwich zero meridian determined by BIH at epoch 1984.0 respectively, and the positive direction of Y axis completes the right hand system (Figure 3.1).

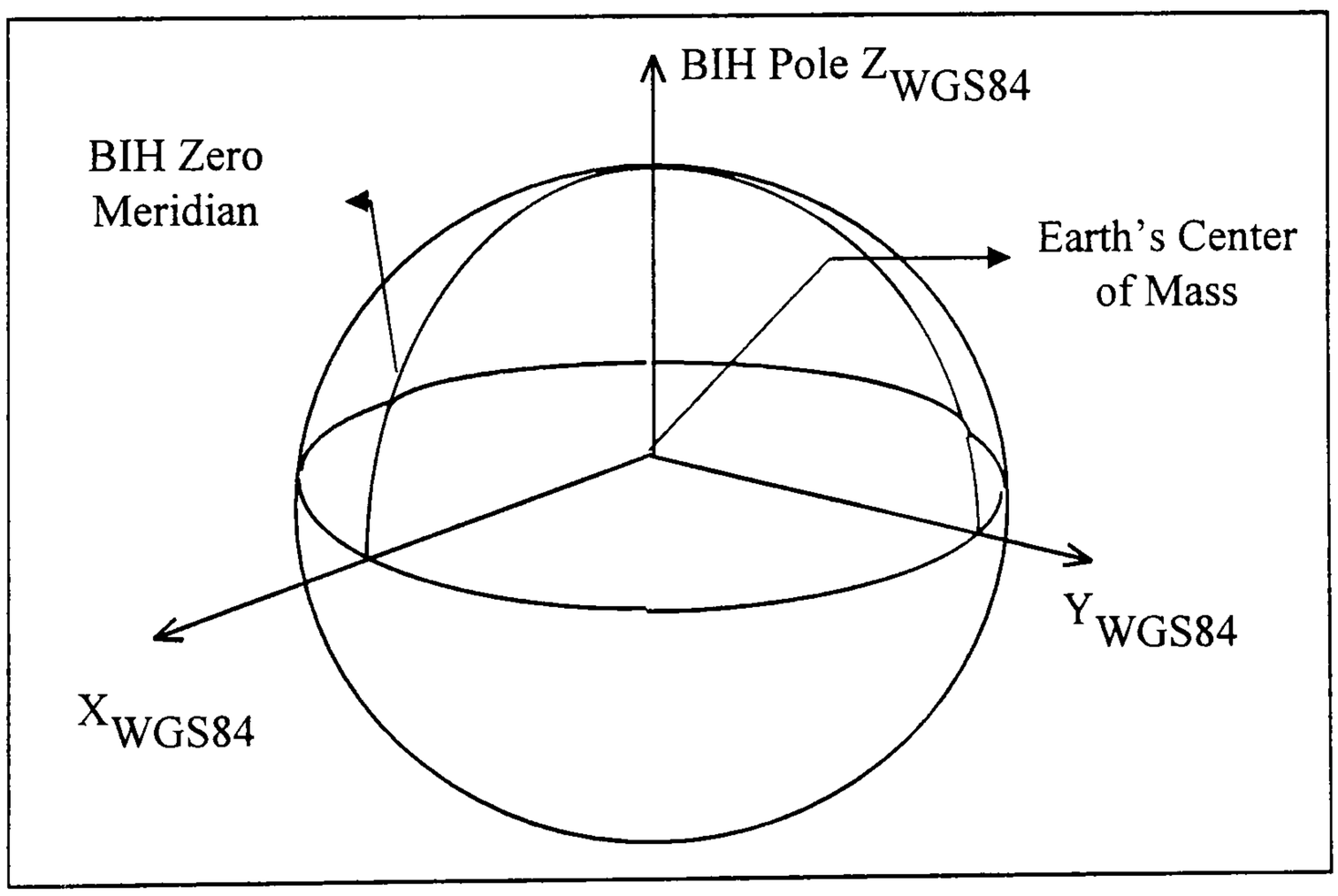

Figure 3.1 WGS84 Reference Frame

The ellipsoid adopted for the system is the WGS84 ellipsoid. The realisation of WGS84 included the available data from WGS72, which was global astronomical data, geodetic and gravimetric data, from techniques up to early 1984. The new and more extensive data sets included the coordinates of 1591

Doppler-derived stations for many more local geodetic coordinate systems around the world, improved sets of ground-based Doppler and Laser satellite tracking data and surface gravity and geoid height reduced from satellite radar altimetry (DMA, 1987). The parameters of WGS84 are tabulated in Table 3.2.

Table 3.2 Geodetic Parameters of the WGS84 (Hofmann-Wellenhof et al., 1997)

Parameter	WGS84
Semi-Major Axis (a)	6378137.0
Flattening (f)	1/298.25722356
Angular Velocity (ω)	7292115×10^{-11} rad s^{-1}
Earth's Gravitational Constant (GM)	3986005×10^{8} m^3s^{-2}
Normalised 2nd Degree Zonal Gravitational Coefficient (C_2)	-484.16685×10^{-6}

The broadcast ephemerides of satellites are given in the WGS84 reference frame.

3.1.2.2 GPS Reference Time

GPS involves three basic groups of time scales namely, Sidereal Time or Universal Time, Dynamical Time and Atomic Time. Sidereal Time is defined as an hour angle between the mean equinox and a particular meridian (Typically, Greenwich Zero Meridian). As this time scale is connected with the diurnal rotation of the Earth, it relates the Earth-based observations to a space-fixed reference frame. For more information the reader is referred to Seeber, (1993) and Hofmann-Wellenhof et al, (1997). Universal Time is the Greenwich hour angle of the mean sun, as follows,

$$UT=12h + \text{Greenwich hour angle of the mean sun.} \tag{3.1}$$

Due to the effect of the polar motion on UT, the UT1 time scale is created by removing the effect of polar motion,

$$UT1 = UT + \text{effect of polar motion} \tag{3.2}$$

UT1 is known as a fundamental time scale in geodetic astronomy and satellite geodesy due to the fact that it describes the actual orientation of the CTS with respect to space. Side real time and universal time are mathematically related through the mean time scale. Specifically (Moore, 1986)

$$\begin{aligned} GMST = {} & 6^h\,41^m\,50.^s5481 + 8640184.^s812866T_u \\ & + 0.^s093104T_u^2 - 6.^s2\times10^{-6}T_u^3 \\ & + (1.00273709350795 + 5.9006\times10^{-11}\,T_U - 5.9\times10^{-15}\,T_U^2)t_{UT1} \end{aligned} \tag{3.3}$$

where T_u is the time difference from the epoch J2000, ie 1 January 2000, 12^h UT1 and t_{UT1} is UT1 time elapsed since 0.0hrs UT1 of the particular day.

Dynamic Times can be derived from planetary motions in the solar system. This time scale is needed to describe satellite motion, which can be used as the independent variable in the equations of motion.

GPS involves pseudo-range determination based on the measurement of travel time of a signal from a satellite to a receiver. Therefore, it requires a uniform time system. Such a time system is known as an atomic time system. It is called International Atomic Time (TAI). TAI is a uniform time scale based on the atomic second which is defined as the fundamental unit of time in the International System of Units. The Bureau International des Poids et Measures (BIPM) is responsible for computing TAI. TAI is referred to as a 'paper' time scale since it is not kept by a physical clock.

GPS system time is referenced to UTC (Universal Coordinated Time). UTC is a sort of atomic time which is tied to the rotation of the Earth in the sense that the UTC second is the SI second and the epoch of UTC is occasionally adjusted

in leap seconds to maintain the agreement with UT1 to within the 0.9 seconds. UTC provides the compatibility for time synchronisation of users world-wide. The Master Control Station ensures that GPS time does not deviate from its expected offset from UTC by more than 1 millisecond. Unlike UTC, a true atomic time scale does not suffer any discontinuities such as leap seconds, hence its offset from UTC will only change periodically. The relationship between GPS time and UTC is given by

$$\text{GPS time UTC} = n\,s - Co \tag{3.4}$$

Where n is integer number, and Co is the correction term.

The precise time is maintained at the Master Control Station using two caesium beam frequency standards and three hydrogen maser frequency standards.

3.1.2.3 Satellite Orbits

Satellite orbits can be described by Kepler's three laws derived from the planets' motions around the sun (Schofield, 1993). These three laws are,

- Satellites move around the Earth in elliptical orbits, with the centre of mass of the Earth situated at one of the focal points
- The radius vector from the Earth's centre to the satellite sweeps out equal area at equal time intervals
- The square of the orbital period is proportional to the cube of the semi-major axis a, i.e. $T^2=a^3\times constant$.

In the description of the above laws, T stands for time period and 'a' represents the semi-major axis of the ellipse corresponding to the orbit of the particular planet or satellite. The geometric shape of the orbit is defined by the first law, velocity variation of the satellite along its path is described by the second law and the time that it takes to complete the whole orbit is determined by the third law.

Having defined the geometric shape of the orbits, it has to be specified in a space-fixed reference frame (ie inertial reference frame). This is achieved by

the definition of three angles. In Figure 3.2 an orbit and its description in an inertial frame are depicted. Two important satellite positions at which the three angles in an inertial frame define the orientation of the orbit are the ascending node and perigee. Ascending node is a point when the satellite crosses the equator and perigee is a point when the satellite position is closest to the Earth.

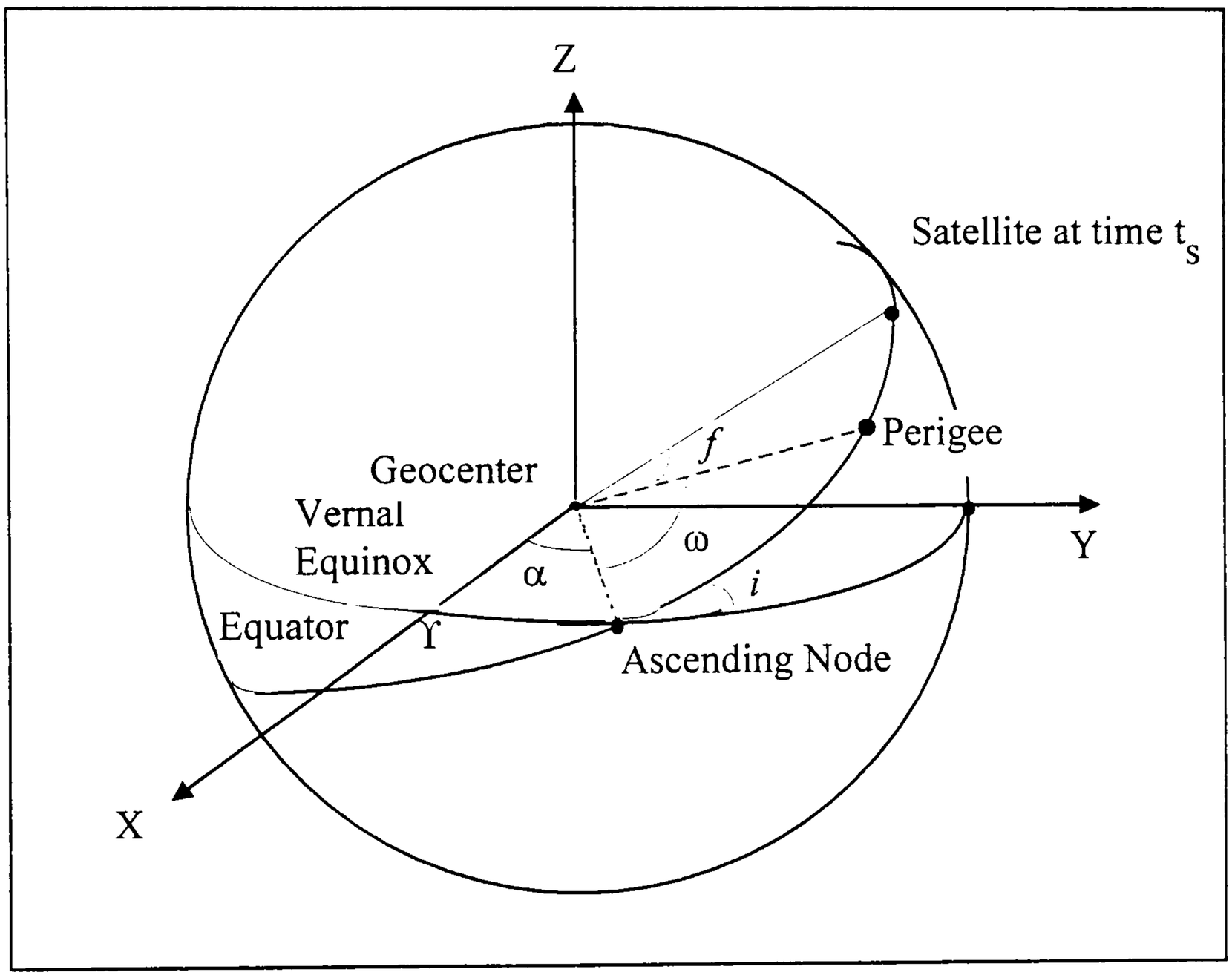

Figure 3.2 A Satellite Orbit in Space

In an inertial reference frame, the right ascension , (α), of the ascending node is measured on the equator from the vernal equinox to the ascending node, inclination of the orbit, (*i*), defines the inclination of the orbit and the argument of perigee, (ω), is the angle measured in the plane of the orbit from the ascending node to the perigee. Finally, the position of a satellite on the orbit can be described by a distance from the centre of the mass of the Earth to the satellite s and f is an angle called true anomaly measured along the orbit from the perigee to the satellite s. For a full treatment of orbits and their calculation the reader is referred to Seeber, (1993) and Kaplan, (1996).

3.1.2.4 Broadcast Ephemerides

The broadcast ephemerides are part of the satellite message. They are generated from an orbit integration process. This process is based on the observations at the Monitor Stations. The Master Control Station is responsible for the computation of the ephemerides and upload to the satellites. The broadcast ephemerides, may be considered in three parts. as shown in Table 3.3.

Table 3.3 Broadcast Ephemerides

Satellite PRN number	
Current GPS week	
Ephemerides reference epoch	t_e
Square root of semi major axis in $\sqrt{meter}$	$\sqrt{a}$
Eccentricity	e
Mean anomaly at reference epoch	M_0
Argument of perigee	ω_0
Inclination	i_0
Longitude of the ascending node at weekly epoch	l_0
Mean motion difference	Δn
Rate of inclination angle	i
Rate of the ascending node's right ascension	$\dot{\Omega}$
Correction coefficients (argument of perigee)	Cuc, Cuc
Correction coefficients (geocentric distance)	Crc, Crs
Correction coefficients (inclination)	Cic, Cis
Satellite clock reference epoch	t_c
Satellite clock offset	a_0
Satellite clock drift	a_1
Satellite clock frequency drift	a_2

The first part contains records with general information. The second part contains records with orbital information. The parameters in this part are the

reference epoch, six parameters describing Kepler's ellipse at the reference epoch namely, three secular correction terms and six periodic correction terms. The third part contains records with information on the satellite clocks. The ephemerides are broadcast every hour and are valid for 4 hours (Ashkenazi and Moore, 1986). Then the user can determine the satellite position in the CTS using the procedures given in Seeber, (1995) and Kaplan, (1996).

3.1.3 User Segment

The user segment consists of the necessary equipment to convert the GPS signals into pseudo-range measurements. These equipment are receiver, antenna and power supply. In GPS, the user (receiver) is able to determine its position and velocity in three dimensions, if it receives signals simultaneously from at least four satellites. This is mainly based on the pseudo-range measurements, using the available positioning services, i.e. standard positioning (C/A-code) and precise positioning (P- or Y- Code), the user can determine his instantaneous position to within an accuracy of 100m and 20m respectively. For higher accuracy positioning, special receiver specifications are required in order to record carrier phase measurements. To find out more about receivers the reader is referred to Langley, (1991).

3.2 GPS Positioning

This section will describe the principles of determination of receiver positions in an Earth fixed Earth centered reference frame using GPS observables.

3.2.1 GPS Observables

There are many types of GPS user, each requiring a different accuracy. There are four basic observables introduced in GPS (Seeber, 1993):

- pseudo-range from code measurements,
- pseudo-range difference from integrated Doppler counts,
- carrier phase or carrier phase difference, and

In practice, howerver, only two of them are used namely, pseudo-range from code measurements and carrier phase.

3.2.1.1 Pseudorange Observable

To determine the receiver position on the Earth, in the air, at sea or in space ranges from the receiver to satellites have to be measured. A range between a receiver and a satellite can be obtained as the product of the period through which the signal travelled and the speed of light. The period is obtained by comparing the received timing codes with a replica code generated within the receiver. These two codes are out of alignment, and the difference between them (in seconds) is the travel time between satellite and receiver, although because these ranges are contaminated by a number of error sources, e.g. atmospheric delay biases and clock offsets, they are known as pseudo-ranges. The fundamental observation equation for a single pseudorange is given, as

$$R_i = \left|X^s - X_r\right| + cdt_u = c\tau_i$$

$$= \left\{(X^s - X_r)^2 + (Y^s - Y_r)^2 + (Z^s - Z_r)^2\right\}^{1/2} + cdt_u \qquad (3.5)$$

where R_i is the geometrical distance between satellite antenna s and receiver antenna r; X^S is the satellite position vector in the geocentric CTS system (WGS84) X^S ,Y^S ,Z^S; X_r is the Position vector of the receiver antenna r in CTS system (WGS84) X_r, Y_r , Z_r ; τ_i is the observed signal propagation time between satellite antenna s and receiver antenna r; dt_u is the clock synchronisation error between GPS system time and receiver clock; and c is the signal propagation velocity.

Pseudo-range measurements may be taken on either the C/A-code or P-code signals. Due to the length of the PRN codes a P-code pseudo-range will be an

absolute measurement, whereas a C/A-code pseudo-range will have a 300 km ambiguity. In general, the resolution of pseudo-range measurements is 1% of the period between successive code epochs. For the P-code with a 0.1 microsecond period, this implies a range measurement resolution of 30 cm. For the C/A code, the numbers are ten times less precise than the P code, i.e. a range measurement resolution of 3m (Wells et al, 1986).

3.2.1.2 Carrier Phase Observable

GPS surveying requires the use of the carrier phase (L1, L2) instead of the timing codes used for navigation. The frequency of satellite signal will change due to the Doppler effect, as there is a relative motion between the satellite and the receiver. However, the phase of the satellite signal will not be affected. Therefore the carrier phase of the signal transmitted and received is the same. In carrier phase observation theory, this is the most important aspect.

Let $\Phi^S(t)$ be the phase of the signal transmitted by the satellite s at time t, and $\Phi_r(\tau)$ be the phase at the receiver r at the reception time τ then the difference between the incoming, Doppler shifted, satellite carrier signal and the nominally constant reference frequency generated in the receiver is the carrier phase observable $\Phi_r^s(\tau)$. The basic equation of this carrier phase observable is given by

$$\Phi_r^s(\tau) = \Phi^S(t) - \Phi_r(\tau) + N_r^s \qquad (3.6)$$

where N_r^s is the number of integer wavelength between satellite s and receiver r.

The instantaneous fractional part of the carrier phase is measured at every epoch by a GPS receiver. However, the integer number of cycles between the

satellite and the receiver can not be obtained. This unknown cycle count N is the so-called integer ambiguity (Figure 3.3).

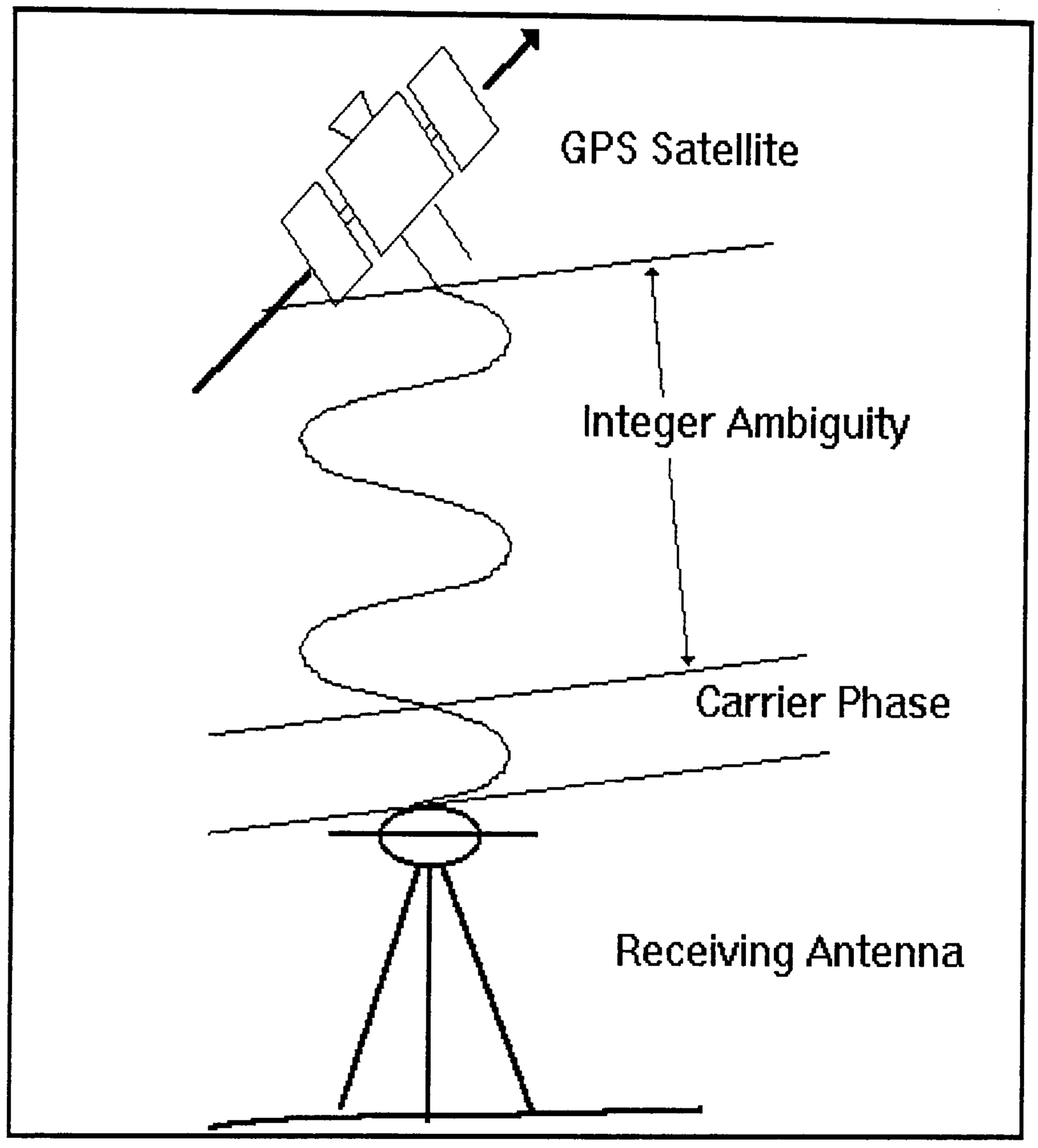

Figure 3.3 Carrier Phase and Integer Ambiguity

As a result, as long as tracking is continued without any loss of lock, the unknown number of integer wavelengths at lock-on remains the same during an observation session. The following formula is the full carrier phase observation equation between satellite s and receiver r,

$$\Phi_r^s(\tau) = \frac{f}{c}\,\rho_r^s(T^S, T_r) - f\,[d\tau_r(\tau), dt^S(t)] + d_{atm} + N_r^s \qquad (3.7)$$

where ρ_r^s is the geometric range between satellite s and receiver r,

f is the frequency of the carrier wave ,

c is the speed of light,

$d\tau_r$ is the receiver clock offset in receiver time frame,

dt^s is the satellite clock offset in satellite time frame,

T^s, T_r is the time in GPS time frame at satellite and receiver respectively,

d_{atm} is the atmospheric effects of the signal propagation.

In the case of relative positioning, there must be more than one geodetic receiver collecting data simultaneously. Then equation 3.7 can be used to derive the differential mode of observation equations. As a result, Single Difference, Double Difference and Triple Difference Carrier Phase observables can be obtained. Single Difference Carrier Phase Observables are obtained by subtracting the carrier phase observations made at two receivers to a common satellite (Figure 3.4a).

$$\Phi^s_{r1,r2} = \Phi^s_{r1} - \Phi^s_{r2} \tag{3.8}$$

In equation 3.8, s is the satellite from which carrier phase observations are made, Φ^s_{r1} and Φ^s_{r2} are the carrier phase observations made at receiver r1 and r2 respectively. By this procedure, the satellite clock offset term is eliminated assuming that the satellite clock offset is common to both receivers. This single differencing procedure can also help to reduce the effect of common atmospheric signal propagation effects and to reduce the effects of satellite orbital errors.

The double difference carrier phase observable is obtained by subtracting the single differenced carrier phase observable made to two different satellites, s_1 and s_2 (Figure 3.4b). The corresponding equation is given by

$$\Phi^{s1,s2}_{r1,r2} = \Phi^{s2}_{r1,r2} - \Phi^{s1}_{r1,r2} \tag{3.9}$$

From this, the receiver clock offsets at each station are eliminated, assuming that the receiver records its observations to satellite 1 and 2 simultaneously. In processing, if the coordinates of the satellites and one of the receivers are known, the second receiver position, atmospheric corrections and double difference integer ambiguity are the unknowns in this equation.

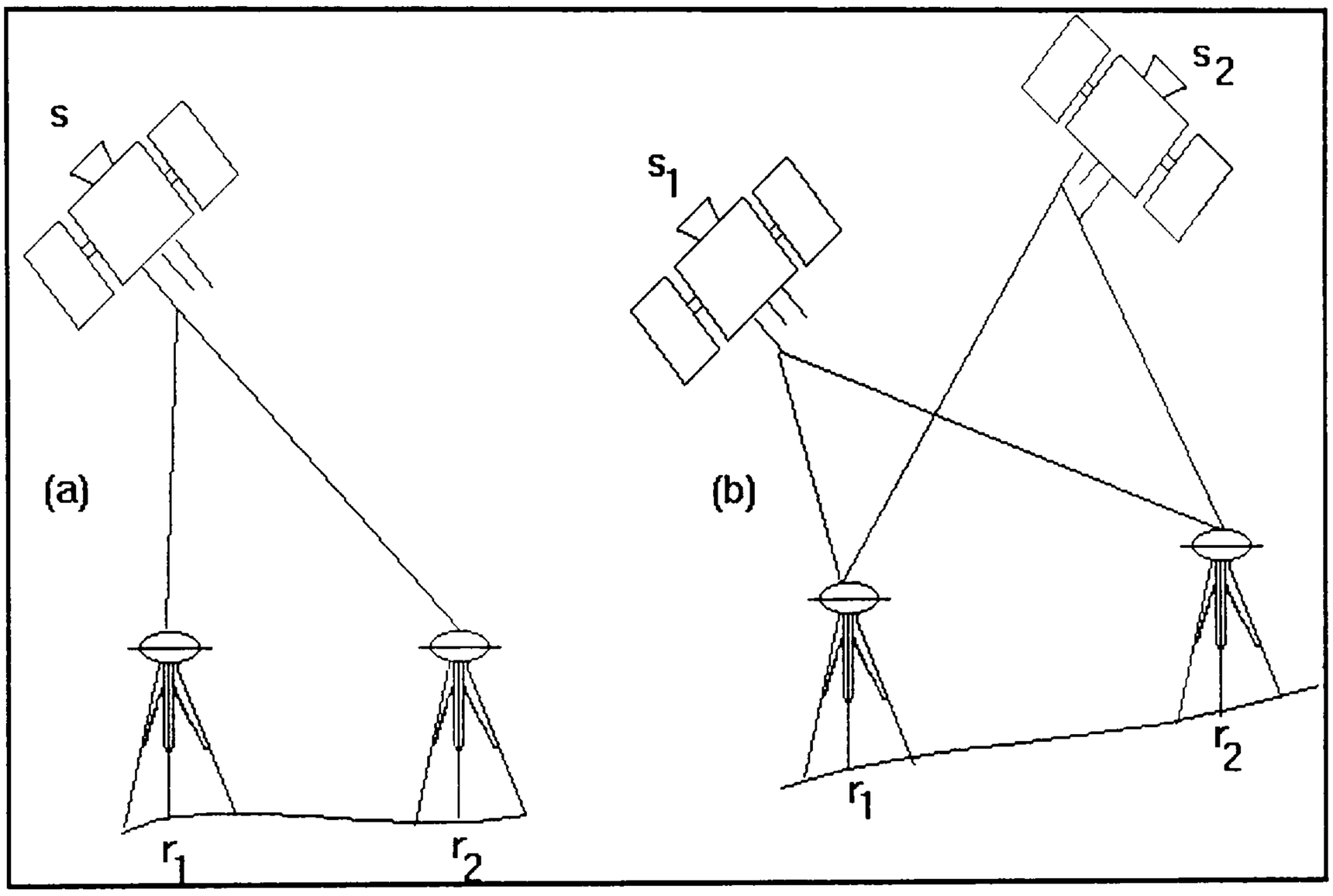

Figure 3.4 Single and Double Differencing

There are linear frequency combinations of L1 and L2 used during processing, due the properties of the combinations. For example, widelane (L3), is the difference between L1 and L2 which has a wavelength of 86.2cm. This combination makes it easier to resolve integer ambiguities. Another combination is ionospherically free (L0). This is the sum of L1*2.545 and L2*(-1.984). By this combination, it eliminates first order ionospheric effects (Penna, 1997).

3.2.2 GPS Errors

Errors can be thought of in three parts as conventionally in geodesy namely, systematic, random and blunder errors. Systematic errors can be either

modelled in a mathematical model or eliminated in some way. Random errors, however, can not be related to measurement, but are the discrepancies after removing all systematic errors and blunders.

The errors can be grouped into four sources as follows,

- Satellite related errors
  - Orbit, clock and relativity
- Signal propagation and atmospheric errors
  - Ionosphere, troposphere, cycle slips and multipath effects
- Receiver related errors
  - Antenna phase centre variations
- Station dependent errors
  - Earth body tides, ocean tide loading, and atmospheric pressure loading

3.2.2.1 Satellite Related Errors

Orbit Errors: For the broadcast ephemerides, satellite orbits are predicted for several hours ahead, from the observations collected up to the prediction time. Hence, there are discrepancies between the satellite orbit predicted and the actual orbit. This error directly propagates into user position. Differencing the observations eliminates most of the orbital errors. However, the remaining errors degrade the baseline accuracy. The rule of thumb relates the ratio of *dr/db* (*dr* orbit error, *db* baseline error) to the ratio of ρ/b (where ρ is the geometric range between satellite and receiver, *b* is the baseline length) (Vanicek and Krakiwsky, 1986).

$$\frac{\rho}{b} = \frac{dr}{db} \tag{3.10}$$

For the broadcast ephemerides, the orbital error is known to be in the order of 20m which is equivalent to a baseline error of 1ppm.

For the precise ephemerides, orbital error may be assessed by comparing coordinate root mean square (RMS) agreements of CODE precise ephemerides and combined IGS precise ephemerides. The agreement was 10 cm in 1994 and improved to 6cm in 1995 (Springer et al, 1996). To work out the corresponding effect on baseline error, equation 3.10 can be used, which is equivalent to 0.05ppm in 1994 and about 0.025 in 1995.

Clock Errors: The offset between the time provided by the satellite and GPS time is known as the satellite clock bias, being in the order of 1 millisecond (Wells et al, 1986). The amount of offset is determined by the Control Segment using the following equation, without considering the Selective Availability,

$$dt(t) = a_0 + a_1 (t - t_{oc}) + a_2 (t - t_{oc})^2 \qquad (3.11)$$

where a_0 represents the clock offset at reference time

a_1 is the clock drift term at reference time

a_2 represent the clock ageing term at reference time and t_{oc} is the satellite clock reference time.

Relativity: Satellite orbit and clock error as well as signal propagation and receiver clock are considered in the relativity error. This kind of error cancels out when differencing the observables and are usually neglected (Wellenhof et al., 1997).

3.2.2.2 Atmospheric and Signal Propagation Errors

Atmospheric Errors: The media in which the GPS signal travels between satellite and receiver effect almost all frequencies, resulting in refraction with a time delay of arriving signals. Since GPS satellites are in the altitude of 20,200 km above the Earth surface, signals first travel through a vacuum, in

which there is no problem in terms of time delay, then travel through the ionosphere that has a dispersive effect.

Ionospheric Errors: Since there are two carrier wavelengths the delay in the ionosphere can be modelled as the difference in group delay at each frequency as

$$dt = \Delta t_{L1} - \Delta t_{L2} \tag{3.12}$$

Therefore, an expression can be derived for a constant A, that can be used to compute the group delay,

$$A = dt \left(\frac{f_{L1}^2 f_{L2}^2}{f_{L2}^2 - f_{L1}^2} \right) \tag{3.13}$$

This ionospheric delay error can be mostly eliminated by using the L1/L2 ionospherically free observable (L0).

Tropospheric Errors: The troposheric delay can not be eliminated as in ionospheric delay, but has to be modelled. As mentioned earlier, tropospheric delay depends on temperature, humidity and pressure (Shardlow, 1994). The refractivity is given by

$$N = 77.6 \frac{P}{T} + 3.73 \times 10^5 \frac{e}{T^2} \tag{3.14}$$

where, P represent pressure

T stands for temperature in Kelvin

e is the partial water vapour pressure.

As can be seen from the above equation there are two parts a dry and a wet component. The dry component accounts for about 90 % of the total tropospheric delay and can be empirically modelled. However, since water vapour varies with height, accurate prediction of the wet component is more difficult. Nevertheless, there are a number of models for estimating the tropospheric effect. In practice, one of these models is made as choice. These models differ in obtaining the values either using surface meteorological observation or a surface meteorological model. One of the empirical models is the Magnet model. It uses a standard atmosphere in which the values vary with respect to position of the station and the Julian day. During processing a scale factor can be solved as an unknown parameter, as a correction to the above model.

Cycle Slips: If the receiver loses lock on the carrier phase for some reason such as a high moving speed of antenna, an obstruction between the satellite and the receiver, signal noise or low satellite elevation angle, a cycle slip occurs (Figure 3.5). This appears as a jump in the carrier phase data. This means that the receiver loses its initial integer ambiguity and re-acquires a new integer ambiguity. The difference between these two ambiguities is a cycle slip which is an arbitrary integer that must be added or subtracted from the initial ambiguity. All cycle slips have to be detected and cleaned at the pre-processing stage of computation to obtain a precise positioning solution.

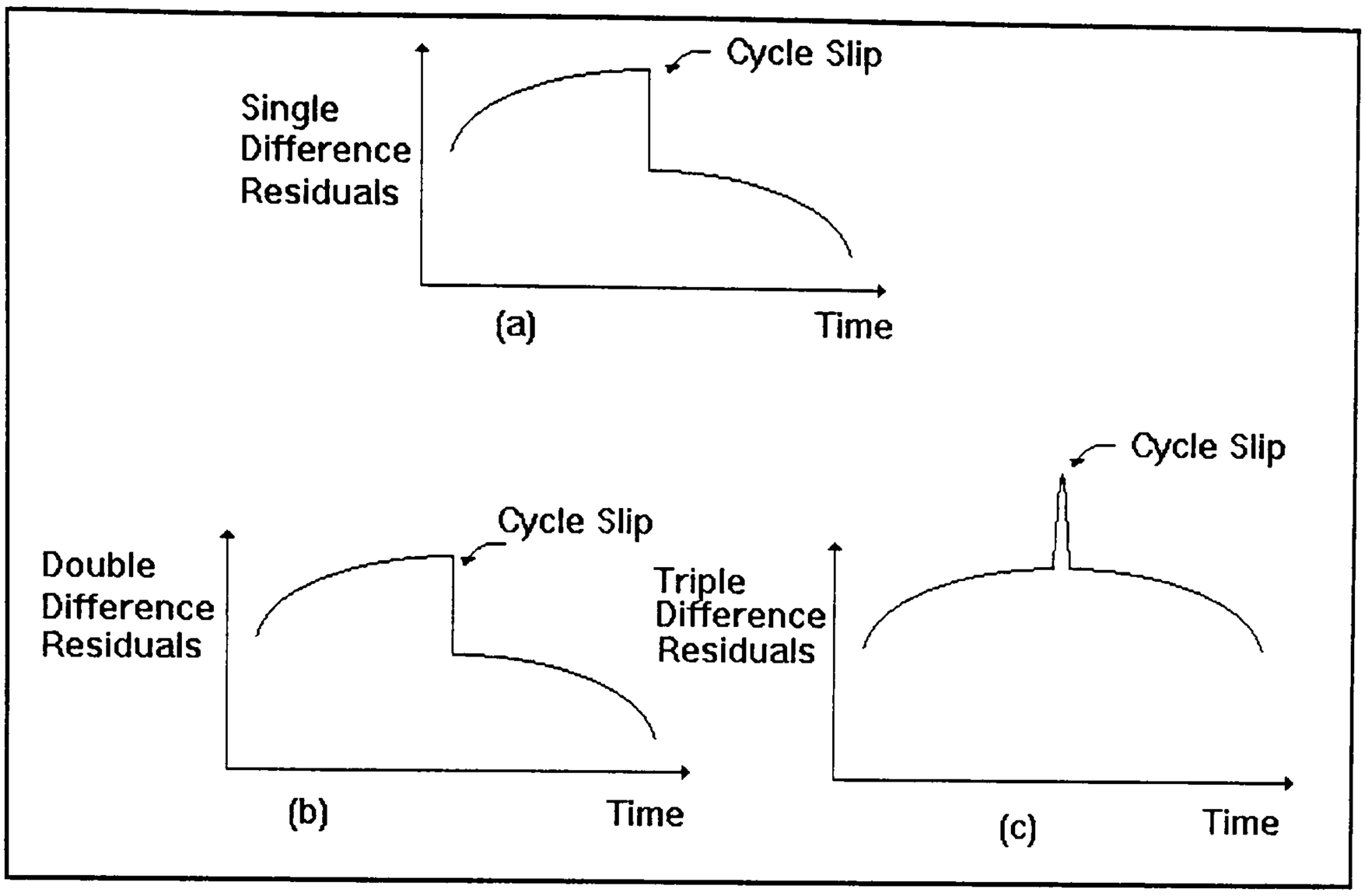

Figure 3.5 Graphic Representations of a Cycle Slip at Time t

Multipath: When a transmitted signal from a satellite reflects from surfaces, a receiver measures both signals coming in, resulting in relative phase offsets and phase differences being proportional to the differences of the path lengths. This depends on the environment of the antenna and can not be eliminated by combinations of observables. In practice, they are treated as random errors (Jack, 1994).

3.2.2.3 Receiver Related Errors

Antenna Phase Centre Variations: Receiver related errors are mainly related to the antenna design. Physical antenna phase centres are not coincident with the electrical phase centre of the antenna. As a result, offsets occur and vary with intensity and direction of the incident signals. Therefore this effect must be modelled in order to avoid direct error propagation to the station coordinates. The corrections are tabulated over a complete range of elevation angles for different types of antenna by so-called Chamber tests (Schupler and Clark, 1991), and more recently in-situ measurements based on the GPS data gathered over short baselines, ie approximately 10m. With this method, relative antenna phase centre caracteristics can be determined using in-situ generated variations

with respect to a mean offsets and a reference antenna obtained from chamber tests (Rothacher et al, 1995). Therefore, these two methods are complementary and each can be used to remove the effect of antenna phase centre variation error.

3.2.2.4 Station Dependent Errors

A point position on the Earth's surface changes continuously due to geophysical phenomenon during an observation period such as Earth body tides, ocean tide loading and atmospheric pressure loading.

Earth Body Tides: Gravity forces of the Sun and the Moon subject the Earth to tidal changes occurring in 12 and 24 hour intervals, so-called semi diurnal and diurnal tides. This means that station coordinates on the Earth surface are subject to changes due to Earth body tides. The magnitude of the changes depends on both the position of the station and the position of the Sun and Moon and can be in the range of over 40 cm in the period of 6 hours (Baker, 1984). Therefore, for accurate positioning, it ought to be modelled in the parameter estimation process. Apart from short period tidal effect on station position, in long term, the Earth's surface is also subject to displacement due to tidal forces. This effect may be cancelled out by differencing procedures for short baselines. However, it has to be modelled by a suitable 'model' for longer baselines.

Ocean Tide Loading: In addition to Earth body tides, the ocean tides can also give periodic variations of surface mass loading on Earth surface which cause further tidal deformation of the Earth (Baker, 1984). The magnitude of the effect depends on the alignment of the Earth, Sun and Moon and the position of the observer and can be in the range of more than 10 cm at some parts of the earth and 1 cm in continental regions about 500 km from the ocean. Therefore, depending on station position it may have to be modelled in high precision surveying (Baker et al, 1995).

Atmospheric Pressure Loading: The Earth and the atmosphere interact through pressure loading at the Earth's surface and gravitational attraction of the atmospheric mass. A time-varying atmospheric pressure mass can lead to Earth deformation. It has been reported that global seasonal fluctuations in barometric pressure contribute less than 1 cm to surface displacements. The largest displacement are associated with synoptic scale storms i.e. 10 mm in the vertical directions. Therefore, in high precision surveying, the observation time may be extended by up to 2 weeks, in order to model atmospheric loading (Blewitt et al, 1994).

3.3 Fiducial GPS

The accuracy of a baseline in a GPS network depends on the accuracy of the satellite coordinates. In order to obtain accurate results from GPS applications, accurate satellite coordinates are needed. Satellite coordinates provided via the broadcast ephemerides result in baseline accuracies in the order of 1 ppm. Prior to the establishment of the IGS the fiducial GPS technique was developed to overcome the limitation in accurray of the broadcast ephemerides.

This technique is based on a network adjustment in which at least three fiducial stations are held fixed (Ashkenazi and Ffoulkes-Jones, 1990). The fiducial station coordinates have to be known to a high accuracy in a global reference frame, that can only be achieved via SLR, VLBI and more recently global GPS. In a normal solution of the network, corrections are brought to coordinates of stations on the Earth surface. However, in fiducial GPS, corrections to the satellite coordinates are also made. This means that fiducial GPS involves the determination of high precision satellite orbits. In a fiducial GPS network, simultaneous recording of carrier phase measurements are made at fiducial and new stations whose coordinates are to be estimated. By holding the fiducial stations (at least three) fixed, in the process of a least squares adjustment, the satellite orbits are improved through the solving of satellite orbital parameters.

The orbit integration requires force modelling acting on satellites such as Earth, Moon and Sun gravitational forces, surface forces and other perturbing forces . The result of integration is a satellite state-vector. Then a fiducial network adjustment is performed to obtain improved satellite coordinates (Moore, 1993).

In summary, a fiducial GPS network solution involves the three major procedures. These are,

- Observe the data simultaneously at both fiducial stations and the station whose coordinates are in question
- Determination of orbits based on the fiducial stations in the network
- Using the well-determined orbits, to estimate the unknown station coodinates.

It is noted that the choice of a global reference frame and its treatment is a very important factor to the accuracy which can be achieved by the fiducial GPS technique. Moreover, for the two main applications of the fiducial GPS technique, ie the establishment of new geodetic reference network and the monitoring of deformation. In the first case, the new geodetic reference network will be required in a particular reference frame and in the second case, the consistency between successive observation epochs has to be ensured (Bingley, 1993).

3.4 The International Terrestrial Reference System (ITRS)

The International Terrestrial Reference System (ITRS) is an Earth centred and Earth fixed reference system. Its origin is at the centre of the mass of the Earth obtained by precise space geodetic techniques, such as VLBI, LLR, SLR, GPS(since 1991) and DORIS(since 1994). Its orthogonal axis are defined to be consistent with those of the Bureau International de l' Heure (BIH) at epoch 1984.0. The unit of length is a metre (SI). Its time evolution of orientation is

ensured by using a no-net-rotation condition with respect to horizontal tectonic motions over the whole Earth. If ellipsoidal coordinates are required, the IERS uses the International Union of Geodesy and Geophysics (IUGG) recommended GRS80 ellipsoid. Its realisations are produced by the Terrestrial Frame Section of the International Earth Rotation Service (IERS) Central Bureau in France. The realisation of the ITRS is the International Terrestrial Reference Frame (ITRF) (Boucher and Altamimi, 1991). ITRF is a global network of basic stations whose coordinates are well-determined by the most precise space geodetic techniques including the coordinate changes by crustal movements. The ITRF is realised through a list of coordinates of stations along with their velocity fields. The quality of coordinates estimated at some sites in the ITRF are generally believed to be accurate to 2 cm.

The up to date global solutions are ITRF88.0, ITRF89, ITRF90, ITRF91, ITRF92, ITRF93, ITRF94 and ITRF96. From ITRF88 to ITRF92, the reference frame realisation was based on the estimation of a set of station coordinates at epoch 1988.0, and to map the coordinates to the required epoch, a plate motion model was used. To map the station coordinates from the epoch 1988.0 to at any epoch can be accomplished by

$$\text{Coordinate}_{(\text{at any epoch})} = \text{Coordinate}(\text{ITRF-yy}(1988.0) + \text{Velocity}_{(\text{ITRF-yy})}\,[t_{(\text{at any epoch})} - 1988.0] \qquad (3.15)$$

The ITRF93 and ITRF94 reference frame realisations differ significantly from the previous ones in that they are defined by two sets of station coordinates at epoch 1988.0 and 1993.0 with their corresponding velocity field consistent between the two. The ITRF93 velocity field was constrained to be consistent with the IERS series of Earth rotation parameters, and consequently has a small rate of rotation in comparison NNR-NUVEL-1A model, which is an update from NNR-NUVEL-1 (Boucher and Altamimi, 1996). For this reason, a second velocity field ITRF93N is also provided whose time evolution is consistent

with the NNR-NUVEL-1A model. The velocity field of the ITRF94 is consistent with the NNR-NUVEL-1A.

The ITRF solutions were estimated by the IERS. In addition to ITRF station coordinates and velocities it also provides Earth rotation parameters in collaboration with the IGS. In turn, the IGS supports the objective of realisation of global accesibility to the improvement of the ITRF, and the IGS analysis centers use the ITRF coordinated subsets in their orbit computations.

The ITRF coordinates are vital for monitoring applications that require precisions of a few millimetres.

3.5 International GPS Service for Geodynamics (IGS)

The IGS is an international collaborative organisation set up by the International Association of Geodesy (IAG) in 1993 to support geodetic and geophysical research activities by supplying standard GPS products. The IGS products are 'precise' ephemerides (orbits), Earth orientation parameters, coordinate network solutions and station tracking data from a world-wide network of fiducial stations. These products are very accurate, and contribute to the improvement and densification of the ITRF. Since January 1st, 1994, the IGS has made available to its user community the IGS orbits based on contributions from seven IGS Analysis Centres (Zumberge and Liu, 1995).

The IGS consists of various groups whose functions are different. These are a global network of permanent GPS tracking stations (observatories), Data Centres (operational centres, regional centres, network centres, data flow/management coordinator) , Analysis Centres (processing centres, associate analysis centres and evaluation centres) and a Central Bureau (Muller, 1991). Operational data centres regularly download, monitor, reformat (RINEX) and archive the data from the tracking stations, and send it to Regional or Global Data Centres. Then, all data are being sent to Global Data

Centres to Global Data Centres, who archive and provide on-line access to tracking data and data products, accessible via the internet.

To meet the IGS objectives of a wide range of scientific and engineering applications and studies, accurate GPS data sets are being collected, archived and distributed by the IGS. GPS satellite ephemerides, Earth rotation parameters, IGS tracking station coordinates and velocities, and GPS satellite and IGS tracking station clock information are produced by using the GPS data sets. The IGS is very important for scientific activities. The IGS gradually improves and extends the ITRF, monitors the Earth deformations and variations in the liquid Earth, and in Earth rotation and determines orbits of scientific satellite and monitors the ionosphere. More importantly, for the investigations of geodynamics by GPS on a regional scale, one can use the data from one or more nearby IGS stations as fiducial stations with coordinates fixed to their ITRF values, and use the IGS precise ephemerides for high precision GPS positioning.

3.6 The GAS Suite

The GPS **A**nalysis **S**oftware (GAS) is a software suite developed for more than 10 years at the University of Nottingham (Stewart et al,1995). In this thesis, GAS has been used to process the GPS measurements obtained during the East Mediterranean GPS Geodynamics Project (EASTMED). GAS consists of a number of separate individual programs providing entities for processing. The individual programs are CON2SP3, FILTER, PANIC(cleaning mode), SLIPCOR, MKGAF, GPSORBIT, PANIC (Network mode), CARNET, and REPDIF. From these individual programs, results can be obtained either by an ordinary network solution, fiducial network solution or free network solution depending on the requirements. Therefore, GAS can be grouped into three main phases.

- Pre-Processing
- Processing

- Post-Processing

3.6.1 Pre-Processing

In this phase, the main aim is to clean the data from cycle slips and prepare them for the processing stage. This is illustrated in Figure 3.6. This phase takes the data from the RINEX format to network processing stage using CON2SP3, FILTER, PANIC (cleaning mode) and SLIPCOR programs.

For the aim of data preparation to FILTER and PANIC, CON2SP3 is used to convert RINEX format ephemerides files to the NGS SP3 format that is the format used in GAS. Then FILTER is ready to be used to convert the observation data files to the GAS NOTT2 format. FILTER also performs the following tasks,

- Removes unwanted data
- Specify a time-span for the required NOTT2 observation files
- Detects large cycle slips and removes them, and
- Computes single point pseudorange solution.

Obtained NOTT2 format data are then cleaned using PANIC in cleaning mode. Cleaning is based on a baseline solution. Therefore, an origin station which is assumed to be clean from cycle slips, has to be chosen.

Since the double difference carrier phase observable is used, base satellites have also to be defined. Relative to the specified base satellite, differencing is performed. The other stations which are assumed as having cycle slips, are assigned a slip file, which the user has an opportunity to manually edit. Cycle slips detected occur as a jump in the residuals. Therefore, minimum sigma zero is looked for on the L1/L2 ionospherically free observable residuals in the slip file. Once at an acceptable magnitude, all cycle slips detected in the individual baseline are corrected using the SLIPCOR program. All stations are cleaned using the same procedure so that the data is ready for processing.

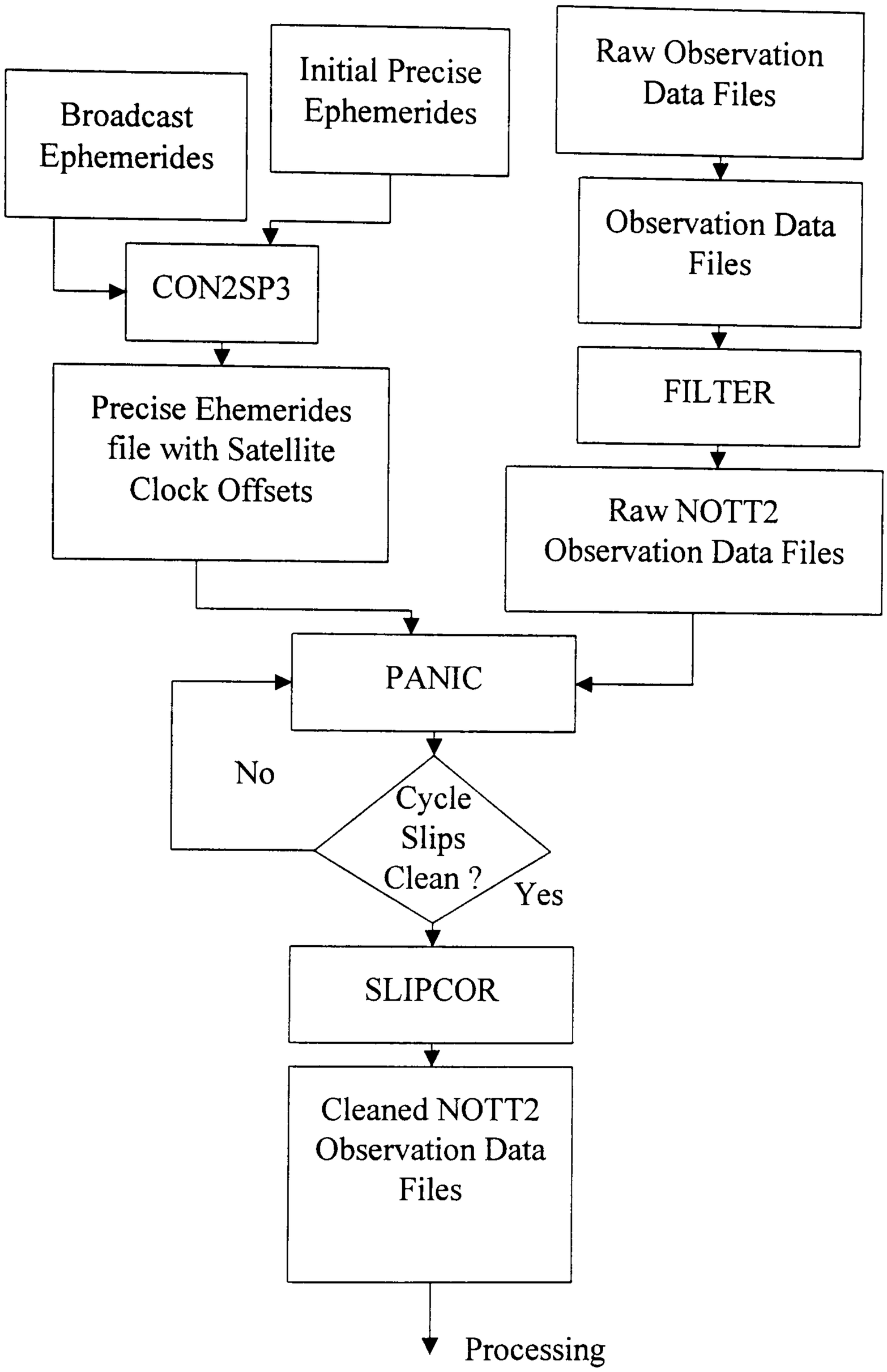

Figure 3.6 Flow Diagram for GAS Pre-Processing

3.6.2 Processing

The PANIC program is the main processor in the GAS suite, which is run in network adjustment or single baseline processing modes. In PANIC a number of options are available. They include pseudo-range or carrier phase solutions, simultaneous frequency combination solutions, varying tropospheric models.

There are three network solutions available, normal network, fiducial network and free network. The procedures are illustrated in Figure 3.7.

In normal network adjustment mode, the satellite coordinates are computed from either broadcast ephemerides or precise ephemerides and known coordinates of stations in the network are held fixed. If Earth body tide (EBT) corrections are needed, the GAF file is required to be used. In the free network adjustment mode, the satellite coordinates are computed from broadcast or precise ephemerides but no stations are fixed. In the fiducial network adjustment mode, more information is required. To obtain the additional information such as integrated orbit and their partial derivatives, the GPSORBIT program is used. This requires a Global Gravity file, a tidal model file and the GAF file, which may already be available, if the EBT corrections were applied during the ordinary network adjustment. Otherwise, the module MKGAF has to be run to produce the GAF file, that is valid for a 40-day period. Then PANIC is run with a minimum of three stations fixed in the network adjustment.

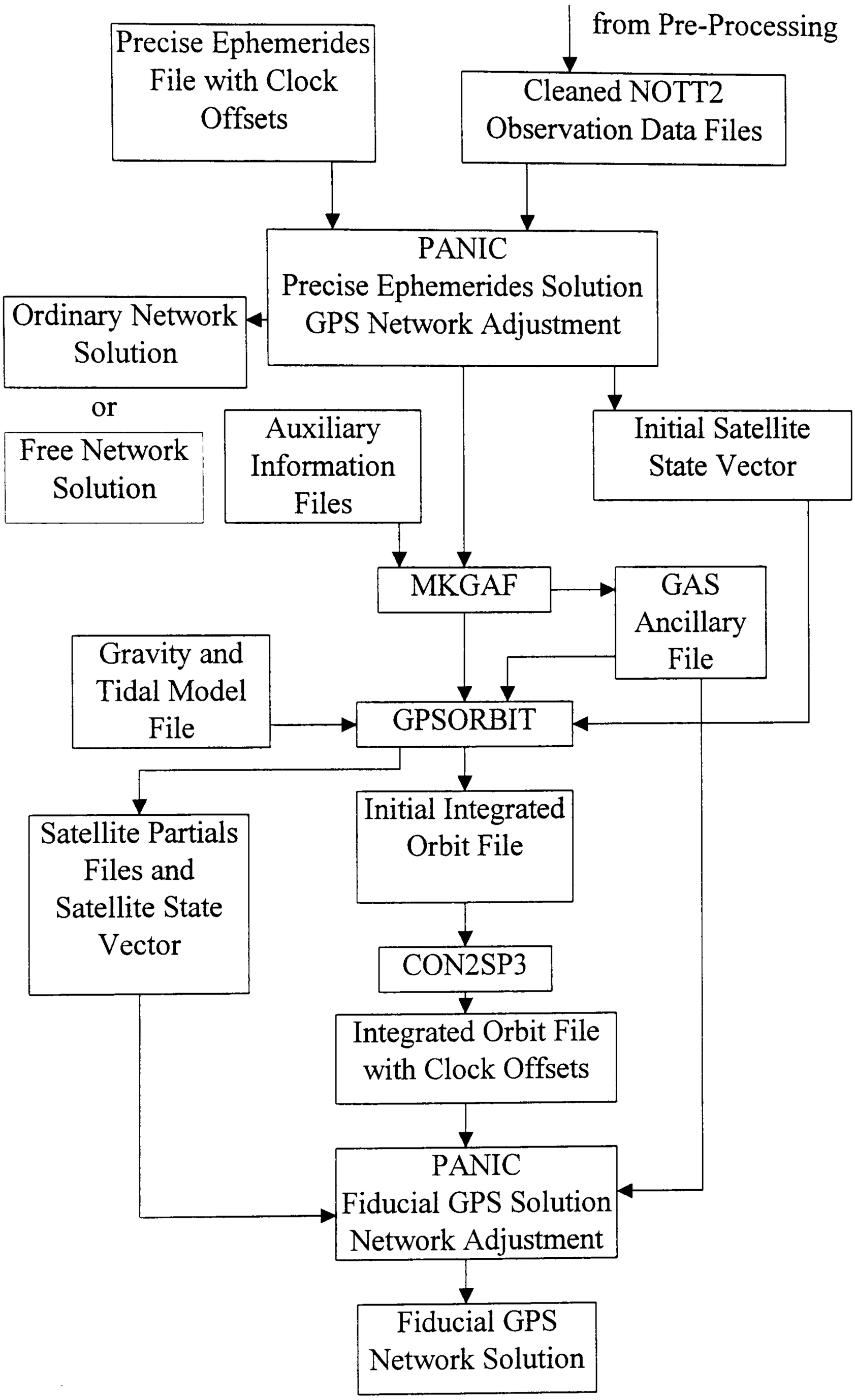

Figure 3.7 Flow Diagram for GAS Processing

3.6.3 Post-Processing

Post-processing is necessary to obtain a campaign solution, ie a unique result including all of the sessional network solutions available. To achieve this, the CARNET program, which is a Cartesian Network adjustment program is used. Then the quality of the network can be obtained using REPDIF. This is a program based on the criteria given in §3.6.4., for calculating repeatabilities of both coordinates and baselines.

3.6.4 Quality Assessment Criteria

It is necessary to determine a set of criteria for the error analysis, because error analysis is an important quality assessment indication for the result estimated from a computation technique or model. For example, the precision and accuracy of GPS measurements have been widely adopted for the quality assessment. Accuracy is how close the estimates are to the true value whereas precision is a measure of how close the individual estimates are from the mean estimate, i.e. a measure of repeatability, which can be defined as,

$$\text{Repeatability} = \sqrt{\sum_{i=1}^{n} \frac{(r_i - r)^2}{n}} \qquad (3.16)$$

where r is a mean estimate,

r_i is a single-session estimates and

n is the number of session.

This can be computed by using the program REPDIF as mentioned in § 3.6.3.

Chapter 4

Proposed Deformation Analysis Technique

Deformation analysis is one of the most important aspects in geodetic research. Various techniques have been developed by different research centres, as mentioned in the introduction of this thesis. Those techniques differ from each other in a way in which the datum problem is resolved, and in using different test statistics.

The University of Nottingham has been involved in this research for a number of years and a method to analyse the earth deformation was developed. This approach basically consists of two steps. Firstly, the station coordinates in the network are adjusted epoch by epoch using least squares method. Simple coordinate differences from two successive epochs are then computed to form the displacement vector or velocities. The deformations of the network are analysed based on the displacement of stations. However, this differencing procedure also increases the noise level of the displacement vectors.

From the plate tectonic theory, for most earth deformations, the stations do not move randomly from epoch to epoch. Therefore, if measurements for all available epochs are used, it is possible to improve the accuracy of the estimated velocity or displacement vector. Based on this idea, a technique proposed by Napier (1990), which uses Kalman Filtering to analyse the deformation of a geodetic network has been developed. However, because crustal deformation involves dynamic systems with epochal measurements, if any bias occurs between two epochal measurements, with Kalman Filtering the estimation is no longer unbiased for those parameters after the bias had occurred. Such a bias may be the effect of local movements (Earthquakes) in the measurements. Therefore, as one of the main aims of this research two sub-optimal filters (ie Fading Memory Filter and Adaptive Estimation for an

Unknown Measurement Bias) have been adopted to overcome this sort of problems from which Kalman filtering suffers.

In this Chapter, first, the description of the optimal estimation and Kalman Filtering will be given, as it is a main mathematical approach to deformation problems. Secondly, smoothing techniques will be discussed. Following this, the statistical tests which have been used in this study to detect the bias are described. Then the concepts of the two sub- optimal filters mentioned above are outlined and the proposed deformation analysis technique is detailed Finally, a description of the program VEBUK (Velocity Estimation By Using Kalman Filter) developed by the author and strain analysis background will be detailed in this Chapter.

4.1 General Description of Optimal Estimation and the Kalman Filter

Kalman filtering is an optimal estimation method to analyse a dynamic system, developed by Kalman, (1960). In this method, parameters to be estimated vary with time or have temporal variations. Kalman Filter is the 'modern' form of Least Squares Estimation technique. The Least Squares Estimation was first used by K. F. Gauss in 1795. The developments from Least Squares up to Kalman Filter is well documented by Sorenson, (1970). The principles of Least Square estimation technique can be found in many mathematical books, and it is well described by Cross, (1994).

The Least Squares technique provides an 'optimal' estimation in a time-invariant regime using over-determined measurements. Therefore, parameters such as velocity and acceleration can not be estimated from the positional data. To estimate this kind of parameters, it requires separate calculations from each time-invariant least squares estimation.

Least Squares is based on two models corresponding to the measurements, ie mathematical and stochastic model. The mathematical model involves a function that relates the measurements to the parameters in question. The stochastic model describes the stochastic nature of the measurements. In other words, it describes the statistics of the measurements, ie variance-covariance matrix. The mathematical model is described by

$$z = Ax + v \tag{4.1}$$

where, z is the measurement vector,

x is the parameter vector,

v is the vector of measurement noise,

A is the coefficient matrix.

The stochastic model is given by

$$W = R^{-1} \tag{4.2}$$

Where, R is the variance-covariance matrix, W is the weight matrix.

Because the Least Squares technique is an optimisation problem, its criteria is to minimise the quadratic form of residuals and it is expressed by

$$v^T W v \rightarrow minimum \tag{4.3}$$

It is noted that for most applications the Least Squares observation equations are not linear. Therefore, the equations must be linearised before the minimisation takes place.

Equations (4.1), (4.2), and (4.3) have a solution, that is only the estimation of time-invariant parameters. However, dynamic problems such as the

determination of crustal movements, involve time-variant measurements. For this reason, the parameters to be estimated include velocity, and acceleration, depending on the dynamic model.

Optimal estimation is described by Gelb, (1974) as '*an optimal estimator is a computational algorithm that processes measurements to deduce a minimum error, estimate of the state of a system by utilising: knowledge of system and measurement dynamics, assumed statistics of the system noises and measurement errors, and initial condition information.*' Obviously, this kind of data processor has a number of advantages. These are that it minimises the estimation error in a well defined statistical sense and that it uses all measurement data and includes prior knowledge about the system. However, the main disadvantages are that it is sensitive to its erroneous prior models and statistics, and that it requires more computations. The computation takes place in a consecutive manner and consists of three main parts, namely, prediction, filtering and smoothing. This is shown in Figure 4.1. When the estimates are desired at time t, when the last observations were made, the problem is called **filtering**. When the estimates desired fall within the span of data, the problem is called **smoothing**. When the estimates are desired after the last available data, the problem is called **prediction**.

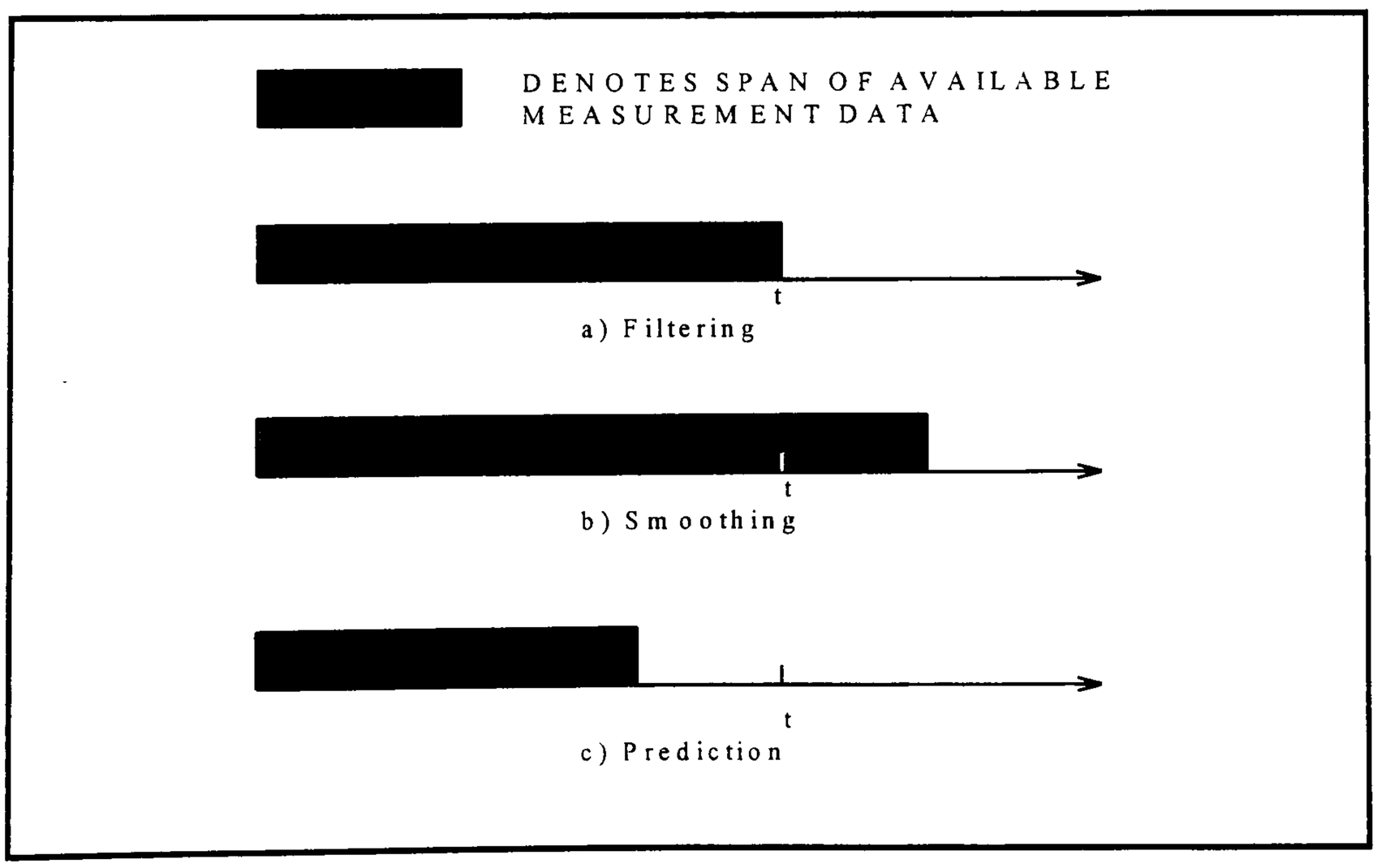

Figure 4.1 Three Types of Estimation Problems at Time t. (Gelb, 1974)

Kalman Filtering is probably one of the most common optimal filtering techniques. This technique can perform all of the above estimation problems, as is depicted in Figure 4.2.

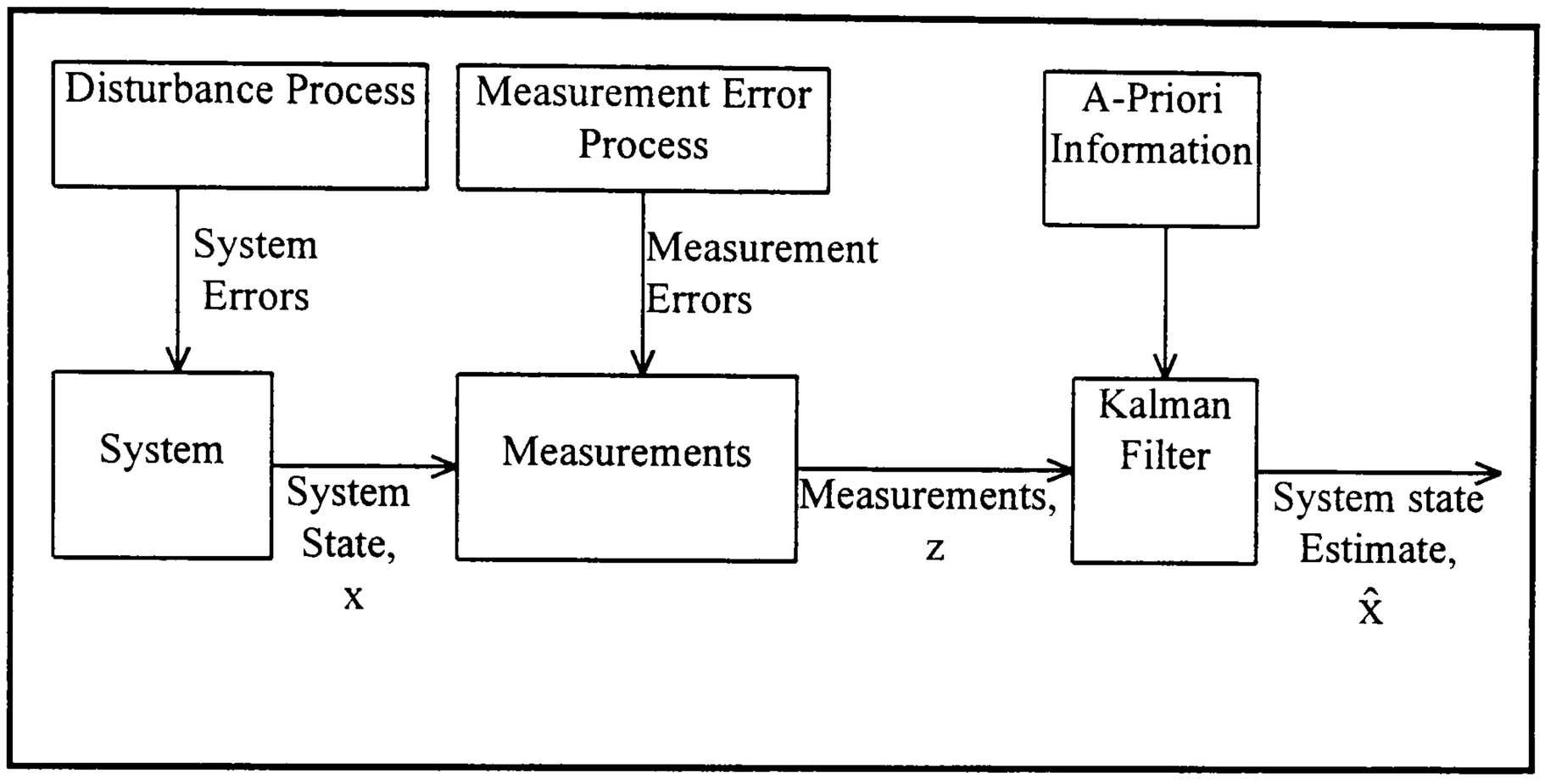

Figure 4.2 Block Diagram for Description of System, Measurement and Estimator (Gelb, 1974)

This provides a convenient example, which illustrates the capabilities and limitations of optimal estimators. For example, if we know the linear system model, any measurements of its behaviour and statistical models and initial condition information, then the Kalman filter describes how to process the measurement data.

There are a number of areas where optimal estimation theory is applied. These are *communication systems* which involve processing a received signal that has both message and errors in coding and transmission; *navigation* which is that of determining position and velocity of a vehicle in some suitable coordinate system by utilising the data from navigational fixes such as range, range rate, and angular measurements; *post-experimental data analysis* , in which following the completion of an experiment, it is desired to reduce the data which were taken during the experiment to asses the experiment, such as tracking and telemetry data during a space vehicle launch, orbit injection and

subsequent orbital flights (Meditch, 1969); and *deformation monitoring*, which involves time series of measurement from which, positions, velocities and accelerations are estimated (Napier, 1990). The latter will be described in more detail in §4.5

The Kalman filter estimation process can be mainly divided into two parts namely, Continuous and Discrete Kalman Filter. In this study, details of the Continuous Kalman filter are not given. The reader who is interested in the continuous Kalman filter is referred to Meditch, (1969) and Gelb, (1974). Discrete Kalman filtering is a processing procedure in which a sequence of data collected in discrete steps, without considering whether the event occurrences are continuous or discrete. For example, in crustal deformation monitoring, although the deformation of the lithosphere is continuous, the data collected to detect the movement in the crust, represent the events in discrete time when the data was collected. Discrete Kalman filter equations are given in § 4.1.1.4.

4.1.1 Kalman Filtering

Kalman filtering is an optimal estimation method to analyse a dynamic system, developed in the early 1960's. This technique involves two basic models, the primary (observation or measurement), and secondary (dynamic) models. These two models are given below in detail.

4.1.1.1 Primary (Measurement) Model

Primary model defines the relationship between the measurements and the state vector of the system (unknown parameters). For instance, in the case of deformation monitoring, the state vector contains not only positions but also velocities and accelerations.

The measurement model can be described as follows,

$$z_{(k)} = A_{(k)}x_{(k)} + v_{(k)} \tag{4.4}$$

where, $z_{(k)}$ is the vector of measurements observed at time t_k,

$A_{(k)}$ is the measurement model matrix defining the linear relationship between the measurements and the state measurement residual vector,

$x_{(k)}$ is the discrete system state vector (parameter vector),

$v_{(k)}$ is the measurement residual vector, which has a zero mean and normal distribution with covariance.

it is based on the assumption that the measurements are linearly related to the unknown quantities.

It is noted that equations (4.4) and (4.1) are the same, except that the state vector contains more parameters which are time dependent. This means that the system state vector can not be estimated by Least Squares unless the excess parameters are omitted. However, it can be estimated by the Kalman filter, if the system model is defined. This is because the system model describes how the state varies with time.

4.1.1.2 Secondary (Dynamic) Model

This model is also known as the system model. It describes the physical model as close as possible. It can be achieved by relationships close to physical reality or empirical rules, in the form of differential equations. This first-order linear difference equation can be represented as,

$$x_{(k+1)} = \Phi_{(k+1,k)}x_{(k)} + \Gamma_{(k+1,k)}w_{(k)} \tag{4.5}$$

where, $x_{(k+1)}$ is the state vector at time k+1,

$\Phi_{(k+1,k)}$ is the state transition matrix that describes the relationship between the state vector at time k and the state vector at time k+1,

$x_{(k)}$ is the state vector at time k,

$\Gamma_{(k+1,k)}$ is the disturbance transition matrix,

$w_{(k)}$ is the disturbance vector,

The matrix $\Phi_{(k+1,k)}$ is called the *transition matrix* for the system of equation (4.5). Figure 4.3 depicts the time evolution of a state vector.

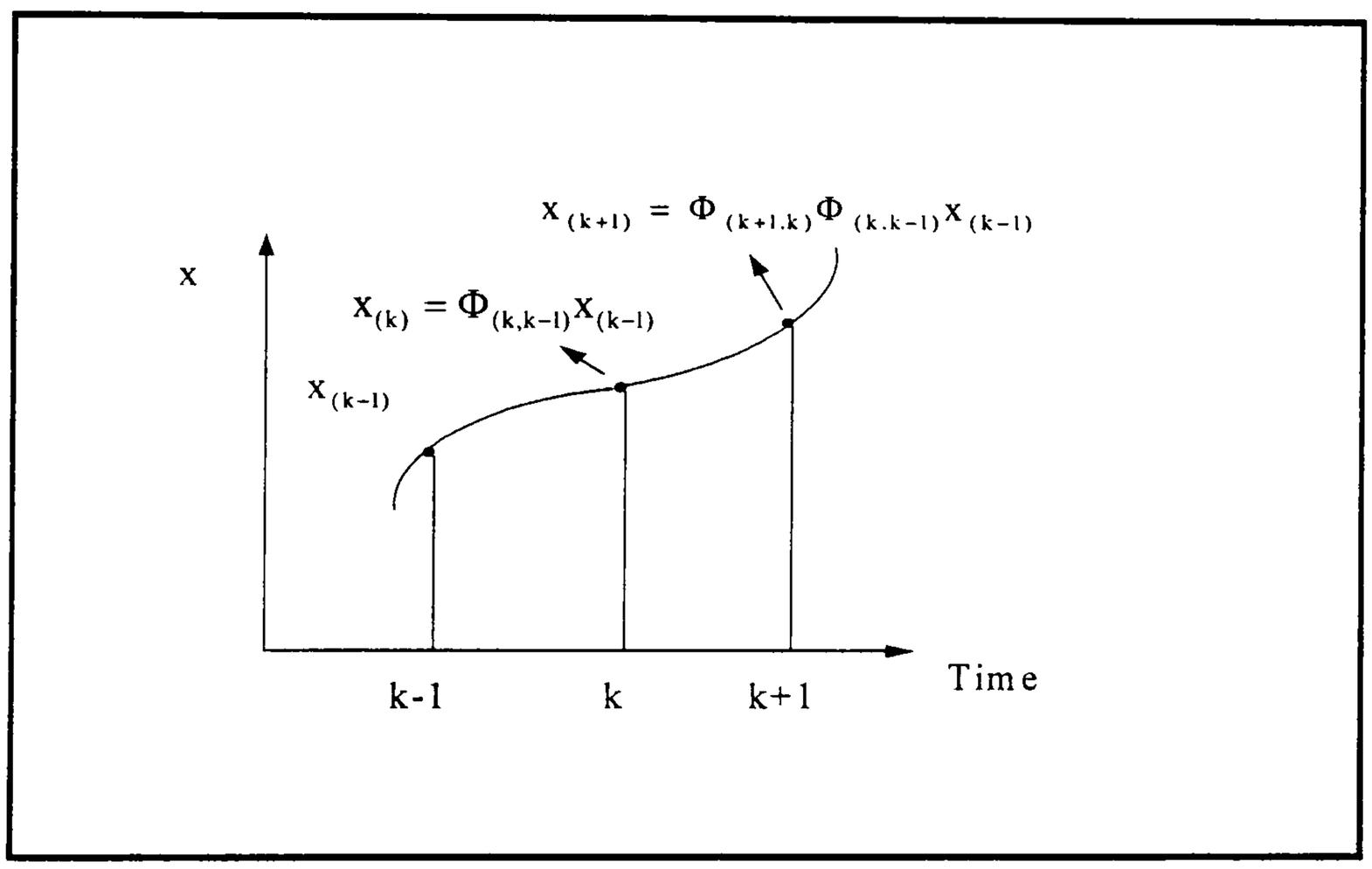

Figure 4.3 Conceptual Illustration of the Time Evolution of a State Vector in (n+1) Dimensional Space (Gelb, 1974)

This matrix allows the calculation of a state vector at some time k+1, given complete knowledge of the state vector at time k. The matrix describes the influence of $x_{(k)}$ on $x_{(k+1)}$. The properties of the transition matrix can be found in (Gelb, 1974).

The system description which is given in equations (4.4) and (4.5) is designated a *discrete linear system.* The block diagram is given in Figure 4.4. In the diagram, 'delay' refers to the act of storing or retaining the value of x

from the present computational cycle for use in the succeeding one. That is after $x_{(k)}$ is computed it must be stored until time k+1 for use in determining $x_{(k+1)}$.

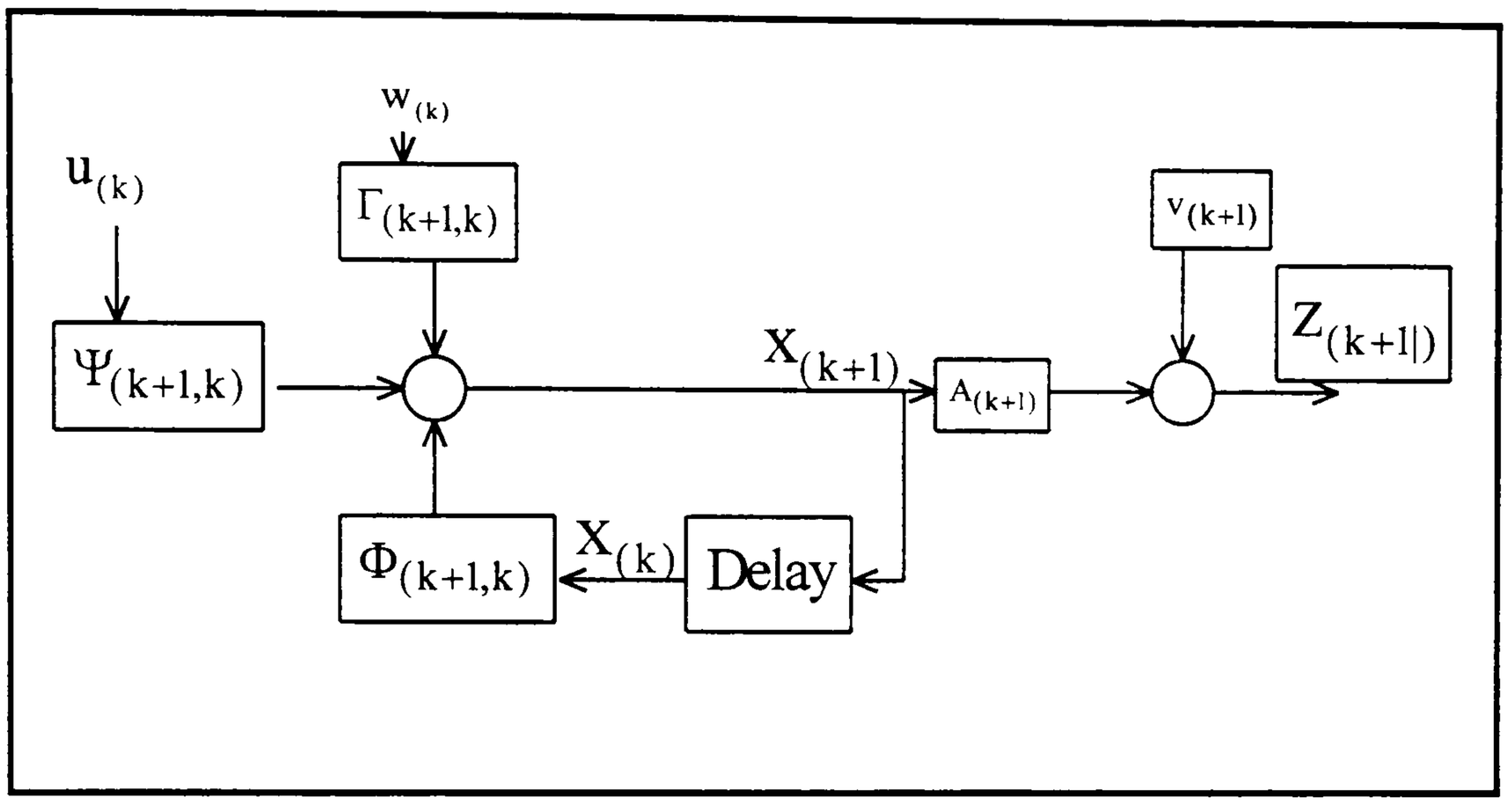

Figure 4.4 Block Diagram for Discrete Linear System Description (Meditch, 1969)

4.1.1.3 Covariance Matrix

A covariance matrix describes the relationship between the random variables. For a full explanation of the covariance matrix, the reader is referred to Meditch, (1969), Gelb, (1974) and Cross, (1994). The covariance matrix is described as the expectation of the square of difference of a random variable from its expected value, typically the mean of the set of random variables. It is given by

$$P = E\left[(x - \mu)(x - \mu)^T\right] \tag{4.6}$$

Where, P is the covariance matrix,

x is the random variables,

μ is the mean of the set of random variables.

E is the expectation

The random state and forcing function vectors are frequently described in terms of the covariance matrix. A statistical measure of the uncertainty in these two vectors is provided by their covariance matrices P and Q respectively. Equation (4.6) is re-written considering the vector of unknowns $\widetilde{X}_{(k)}$, covariance $P_{(k)}$ and time t_k as,

$$P_{(k)} = E[\widetilde{x}_{(k)}\widetilde{x}_{(k)}^T] \tag{4.7}$$

the Gauss propagation of error law is applied to equation (4.5) ignoring the control part to obtain the covariance matrix at a later time, as

$$P_{(k+1)} = E[(\Phi_{(k+1,k)}x_{(k)} - \Gamma_{(k+1,k)}w_{(k)})(\Phi_{(k+1,k)}x_{(k)} - \Gamma_{(k+1,k)}w_{(k)})^T] \tag{4.8}$$

Where, $w_{(k)}$ term has a zero mean and is uncorelated and $P_{(k+1)}$ is the covariance matrix at time t_{k+1}.

Opening the equation (4.8) and after mathematical processes,

$$P_{(k+1)} = \Phi_{(k+1,k)}P_{(k)}\Phi_{(k+1,k)}^T + \Gamma_{(k+1,k)}Q_{(k)}\Gamma_{(k+1,k)}^T \tag{4.9}$$

where, $Q_{(k)}$ is the covariance of $w_{(k)}$.

It is noted that the term $\Gamma_{(k+1,k)}Q_{(k)}\Gamma_{(k+1,k)}^T$ has a direct effect on the covariance matrix at any point in time. Therefore, special care for this term is necessary. This term $Q_{(k)}$ is , in this study, called as system noise.

4.1.1.4 Recursive Kalman Filter

In this section, the procedures of recursive Kalman filtering (including prediction and filter equations) are given without derivations of these formulae.

The equations can be obtained by Standard Least Squares procedures from Cross, (1987).

Before describing recursive Kalman filter equations, It is important to note that the following notation has been used in this section.

Optimal estimation, as stated in §4.1, consists of prediction, filtering (updating) and smoothing. Assuming $x_{(k|j)}$ is the state vector, the meaning of (k|j) being time indicator, changes depending on,

- Filtering : $k = j$
- Smoothing : $k < j$
- Prediction : $k > j$

Corresponding covariances are treated in the same manner as above.

Details on smoothing are given in §4.2. For prediction and filtering the equations are,

Prediction:

$$x_{(k+1|k)} = \Phi_{(k+1,k)} x_{(k|k)} \tag{4.10}$$

$$P_{(k+1|k)} = \Phi_{(k+1,k)} P_{(k|k)} \Phi^{T}_{(k+1,k)} + \Gamma_{(k+1,k)} Q_{(k|k)} \Gamma^{T}_{(k+1,k)} \tag{4.11}$$

Filtering:

$$x_{(k+1|k+1)} = x_{(k+1|k)} K_{(k+1)} \left[z_{(k+1)} - A_{(k+1)} x_{(k+1|k)} \right] \tag{4.12}$$

$$P_{(k+1|k+1)} = \left[I - K_{(k+1)} A_{(k+1)} \right] P_{(k+1|k)} \tag{4.13}$$

$$K_{(k+1)} = P_{(k+1|k)} A^{T}_{(k+1)} \left[A_{(k+1)} P_{(k+1|k)} A^{T}_{(k+1)} + R_{(k+1)} \right]^{-1} \tag{4.14}$$

where $K_{(k+1)}$ is the gain matrix calculate at time k+1,

$x_{(k+1|k)}$ is the predicted state vector of the system,

$P_{(k+1|k)}$ is the predicted covariance matrix,

$A_{(k+1)}$ is the coefficient matrix in equation (4.4).

In equation (4.10), $x_{(k|k)}$, $P_{(k|k)}$ are an initial state vector and an initial covariance matrix respectively. For the first time the calculation from equation (4.10) to (4.14) are performed using initial values. The final estimates of the state vector $x_{(k+1|k+1)}$ and the covariance matrix $P_{(k+|k+1)}$ will be the initial state vector and the initial covariance matrix for a second computation at a later time, and so on.

The equations (4.10) and (4.11) are called prediction equations, and equations (4.12), (4.13), and (4.14) are called the filtering equations.

4.2 Smoothing Techniques

Smoothing is a method to estimate the state vector at epoch k, using all measurements from epoch 0 to epoch N, where 0<k<N. Obviously it requires the measurements from a future time and therefore is not a real-time processing schame (Salzman, 1988). The notation for smoothing was given as the state vector donated by $x_{(k|j)}$, where, j>k, and 0<j≤N. There are a number of optimal smoothing algorithms. These are driven to obtain suitable algorithms from the system model in equations (4.4), and (4.5). There are three smoothing algorithms considered in this study, which were used by the author and included in the program VEBUK (detailed in §4.6), to get the best estimates. These are,

- A linear Smoothing based on forward and backward filtering procedures, this will be called backward and forward smoothing in this study,
- Fixed-Interval Smoothing, and
- Fixed-Point Smoothing

Theses three smoothing techniques are now described.

4.2.1 Backward and Forward Smoothing

This linear smoothing algorithm is known as two stage smoothing and is based on the forward and backward filtering procedures. Therefore, forward filtering procedures can be achieved using equations (4.10) to (4.14). Backward filtering is the same procedure and the same equations as forward filtering but the only difference is the time difference haing a negative sign, which begins from the last epoch to the first epoch. This two stage filter is shown in Figure 4.5.

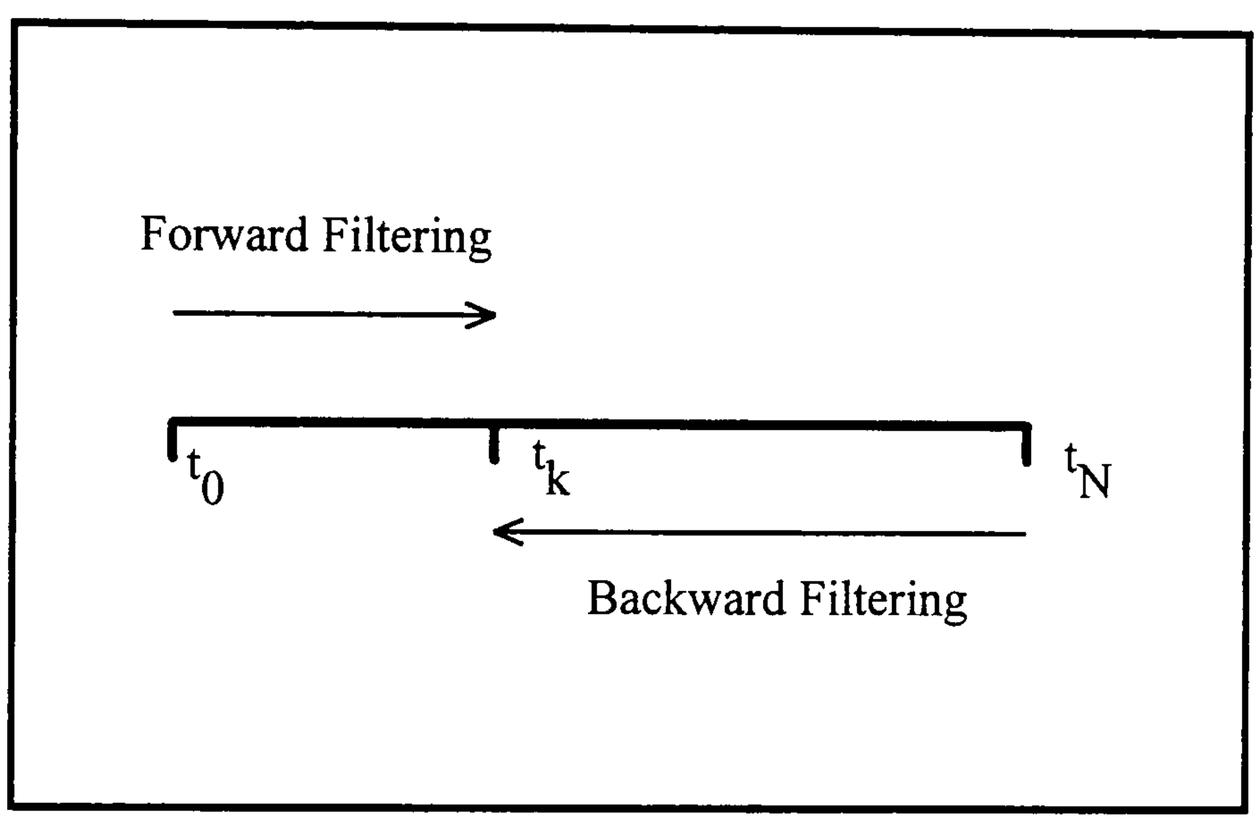

Figure 4.5 Forward and Backward Filtering

The smoothened state vector for any epoch t_k, is given by the weighted average of the filtering state vectors from forward and backward filtering as,

$$x_{(k|N)} = P_{(k|N)}[(P_{(k|k)}(f))^{-1} x_{(k|k)}(f) + (P_{(k|k-1)}(b))^{-1} x_{(k|k-1)}(b)] \quad (4.15)$$

where, $x_{(k|N)}$ represents the smoothed state vector, and

$P_{(k|k)}(f)$ is the estimated covariance matrix with f standing for the forward filtering at time t_k

$P_{(k|k-1)}(b)$ is the predicted covariance matrix with b representing the backward filter at time t_k , and similarly,

$x_{(k|k)}(f)$ is the estimated state vector by the forward filter at time t_k ,

$x_{(k|k-1)}(b)$ is the predicted state vector by the backward filter at time t_k .

$P_{(k|N)}$ is the smoothed covariance matrix corresponding to the smoothed state vector $x_{(k|N)}$, and it is given by

$$P_{(k|N)} = [(P_{(k|k)}(f))^{-1} + (P_{(k|k-1)}(b))^{-1}]^{-1} \tag{4.16}$$

It is obvious from equation (4.16) that $P_{(k|N)}$ is smaller then $P_{(k|k)}(f)$, which means that $x_{(k|N)}$ is always more precise or equally as precise to its filtered estimate. This is depicted in Figure 4.6.

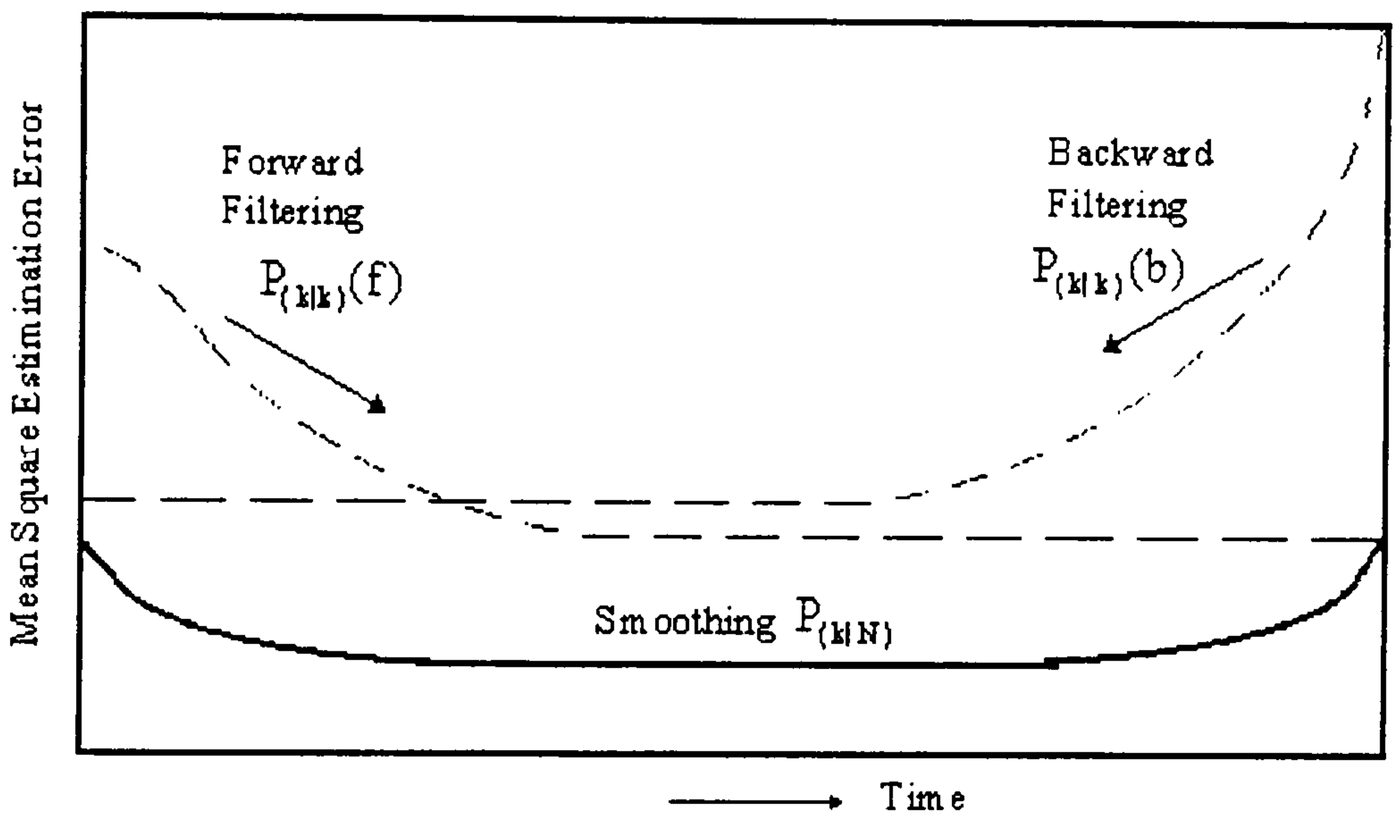

Figure 4.6 Advantage of Performing Optimal Smoothing (Gelb, 1974)

4.2.2 Optimal Fixed-Interval Smoothing

This smoothing technique is one stage smoothing and based on the estimation of a state vector at a required time t_k, using all the available measured data over the fixed interval [0, N]. This estimation is termed the optimal fixed-interval smoothed estimate of $x_{(k|k)}$. Of all the estimates for k=0. 1,...N, only $x_{(N|N)}$ is recognised as this point is the starting point in fixed interval smoothing and the appropriate algorithm is backward recursive in time. Therefore, fixed-interval smoothing is post-experimental processing. The derivation of the fixed-interval smoothing is well described in Meditch, (1969). Here only final forms

of the fixed-interval smoothing will be given. The optimal fixed-interval smoothed estimate $x_{(k|N)}$ is governed by

$$x_{(k|N)} = x_{(k|k)} + B_{(k)}\left[x_{(k+1|N} - x_{(k+1|k)}\right] \tag{4.17}$$

where $x_{(k|k)}$ is the state vector estimated at time t_k by forward filtering,

$x_{(k+1|k)}$ is the predicted state vector at time t_k,

where for k=N-1, N-2, ..., 0, $x_{(N|N)}$ is the boundary condition for k=N-1.

$B_{(k)}$ is the smoothing gain matrix, which is given by

$$B_{(k)} = P_{(k|k)}\Phi^{T}_{(k+1,k)}P^{-1}_{(k+1|k)} \tag{4.18}$$

where $P^{-1}_{(k+1|k)}$ is the inverse of the predicted covariance matrix at time t_k.

The optimal fixed-interval smoothing error, stochastic process is a zero mean whose covariance matrix is given by the system of equations

$$P_{(k|N)} = P_{(k|k)} + B_{(k)}\left[P_{(k+1|N)} - P_{(k+1|k)}\right]B^{T}_{(k)} \tag{4.19}$$

where, for k=N-1, N-2, ..., 0, $P_{(N|N)}$ is the boundary condition for k=N-1.

Equation (4.17) specifies the algorithm for optimal fixed-interval smoothing. At each time k, it requires the optimal filtered and predicted estimates as input.

It is noted that computations must be carried out in reverse time. This is because initial conditions for equation (4.17) are required. It is obvious that

only for k=N-1 within the interval [0,N] will we have all the information which we need. Specifically, for k=N-1, equation (4.17) becomes,

$$x_{(N-1|N)} = x_{(N-1|N-1)} + B_{(N-1)}\left[x_{(N|N} - x_{(N|k)}\right] \tag{4.20}$$

Having so determined $x_{(N-1|N)}$, we then proceed successively to determine $x_{(N-2|N)}$, $x_{(N-3|N)}$, ..., $x_{(0|N)}$, in that order. Therefore indexing on k in equation (4.17) is k=N-1, N-2, ..., 0, and the boundary condition is the optimal filtered estimate $x_{(N|N)}$. The sequence of computations is depicted in Figure 4.7. It is obvious that this is not a procedure for on-line processing.

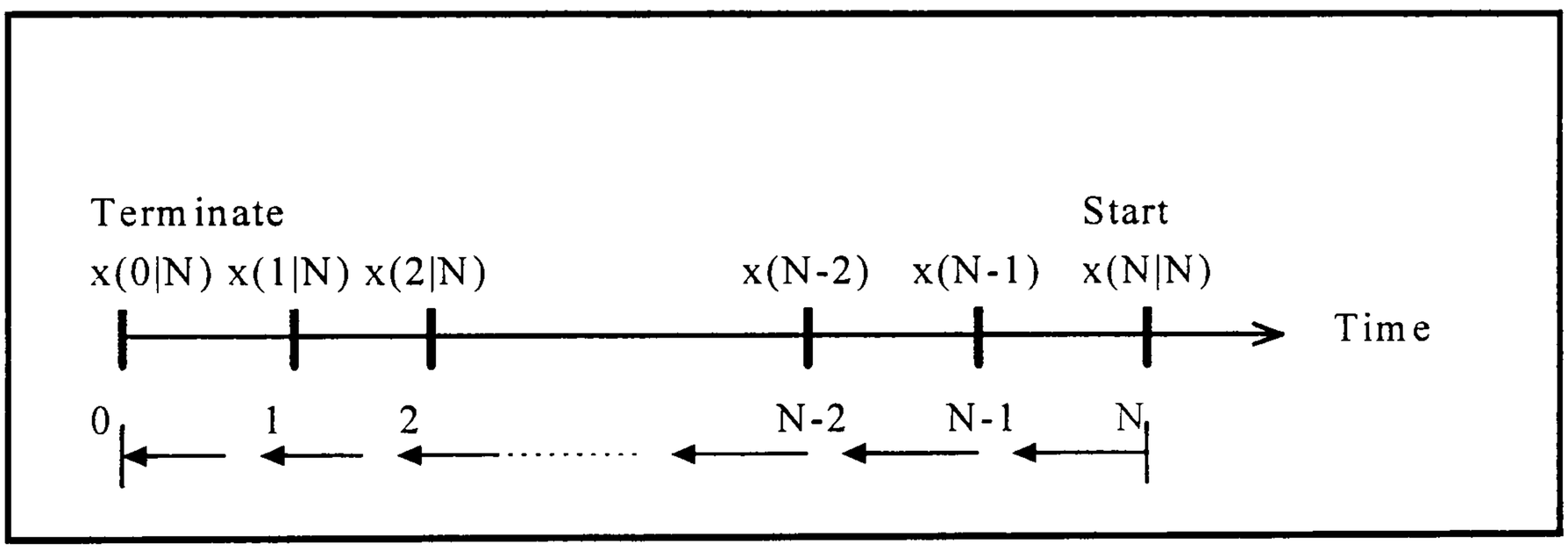

Figure 4.7 Computational Sequence for Optimal Fixed-Interval Smoothing (Meditch, 1969)

4.2.3 Optimal Fixed-Point Smoothing

A smoothing solution is sometimes sought for a specific time of interest, therefore, it is efficient to reformulate the smoothing equation to perform the task. Fixed-Point means a fixed epoch with respect to which smoothing is performed. Here the final formulation is given, the reader is referred to Gelb, (1974) and Meditch, (1969) for further information.

The optimal fixed-point estimate $x_{(k|j)}$, is given by the system of equations

$$x_{(k|j)} = x_{(k|j-1)} + G_{(j)}[x_{(j|j)} - x_{(j|j-1)}] \tag{4.21}$$

for a fixed k and j=k+1, k+2, where the initial condition is $x_{(k|k)}$ and $G_{(j)}$ is the fixed-point smoothing gain matrix, and it is given by

$$G_{(j)} = \prod_{i=k}^{j-1} B_{(i)} \tag{4.22}$$

where $\prod$ stands for a product,

and

$$B_{(i)} = P_{(i|i)} \Phi^{T}_{(i+1,i)} P^{-1}_{(i|i)} \tag{4.23}$$

for j=k+1, k+2.

The optimal fixed-point smoothing error process, ($x_{(k|j)}$, j=k+1, k+2, ..) is a zero mean whose covariance matrix is described by the system of equations as

$$P_{(k|j)} = P_{(k|j-1)} + G_{(j)}[P_{(j|j)} - P_{(j|j-1)}]G^{T}_{(j)} \tag{4.24}$$

for j=k+1, k+2, ..., subject to initial condition $P_{(k|k)}$.

It is noted that the error in the inverse of the covariance matrix in equation (4.23) is cumulative, since the gain matrix is a continuing product. Therefore, if any error is made at time i>k, the value of $G_{(j)}$ would be in error for all j>k as this is clear from the equation, (4.22). There are alternative algorithms, which avoid the inverse of the covariance matrix, but these algorithms will not be given here, and the reader is referred to Meditch, (1969) for more information.

It is clear from the fixed-point smother equations that it can be used for on-line processing in conjunction with optimal filtering and prediction. Optimal fixed-

point smoothing, at any time point, requires an additional correction term to the estimate $x_{(k|j-1)}$ which was the smoothened state vector obtained at the preceeding time. The basic idea is depicted in Figure 4.8.

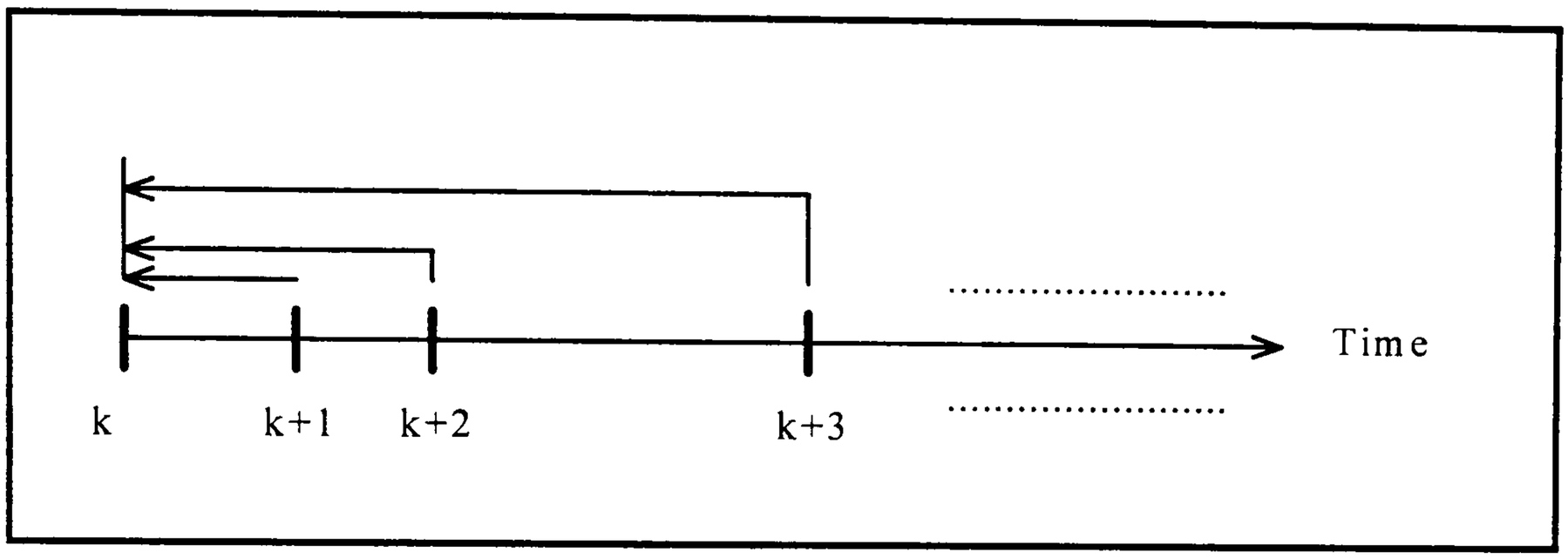

Figure 4.8 Notion of 'reflection' of Measurement Data in Optimal Fixed-Point Smoothing (Meditch, 1969)

4.3 Statistical Tests

There are two statistical tests adapted in this study, for the detection of sudden movements; Local Overall Model Test (LOM) and Local Slippage Test (LST). These two tests are recommended for detecting the performance of a Kalman filter, by Teunissen and Salzmann (1988). These tests will be described next.

4.3.1 Local Overall Model Test (LOM)

This test is a hypothesis testing procedure as applied to the linear discrete time Kalman Filter. The term 'Local' means that the tests (LOM & LST) when performed at time t_{k+1} only depend on the predicted state at time t_{k+1} , and the observations at time t_{k+1}. The main aim of this test is to detect mis-specifications in the mathematical model occurring at time t_{k+1}. As mis-specifications in the model effect the predicted state vector, the LOM test can detect them. Therefore, the test is applied to the innovation sequence (predicted residuals). The test statistic can be obtained by

$$T_{(k+1)} = \frac{\tilde{z}^{T}_{(k+1|k)}(\tilde{P}_{(k+1|k)})^{-1}\tilde{z}_{(k+1|k)}}{m_{k+1}} \tag{4.25}$$

where, $\tilde{z}_{(k+1|k)}$ and $\tilde{P}_{(k+1|k)}$ are the predicted residuals and covariance matrix respectively and

m_{k+1} is the number of observations at time t_{k+1}

The decision that mis-specification in the model has occurred, is made if the following expression holds true.

$$T_{k+1} \geq \chi^{2}_{\alpha(mk)} \tag{4.26}$$

where, $\chi^{2}_{\alpha(mk)}$ is the upper α probability point of the Chi-squared distribution with m_{k+1} degrees of freedom.

Once the test fails, further investigation is done by the Local Slippage Test (LST).

4.3.2 Local Slippage Test (LST)

This is a one-dimensional slippage test. This test is necessary to identify the errorneous observations when the LOM test fails. This test is described in Teunissen and Salzmann (1988). Here the test statistic is described as

$$s_{k+1} = \frac{c^{T}(\tilde{P}_{(k+1|k)})^{-1}\tilde{z}_{(k+1|k)}}{\sqrt{(c^{T}(\tilde{P}_{(k+1|k)})^{-1}c)}} \tag{4.27}$$

where, the c- vector depends on the type of mis-specification one can test.

With equation (4.27), it is possible to detect a departure from the mean of the predicted state vector, or from the mean of the measurement noise, or from

both. For example, for a sensor failure detection or outlying observations the c-vector can be adapted as follows,

$$c_i = (0,\cdots,0,1,0,\cdots,0)^T \tag{4.28}$$

where, $i=1,...m_{k+1}$.

It is noted that, in equation (4.27), the inverse of the predicted covariance matrix governs the detectability of the mis-specification in the model. Therefore, special attention must be paid to the inverse of the predicted covariance matrix. In the case of data snooping, one should aim at a diagonal dominant matrix $\widetilde{P}_{(k+1|k)}$.

In equation (4.27), maximum values of the s_{k+1} test statistic for the observation represent the outlying observation.

4.4 Sub-Optimal Filters

Until now in this chapter, optimal filtering and smoothing have been detailed. However, when the Kalman filter equations are applied to practical problems, several difficulties become obvious. The optimal filter must model all the error sources in the system at hand. However, it is not always possible to model all the error sources that physically exist. Therefore, the assumption that exact descriptions of system dynamics, error statistics and the measurement process are known is made in the filter equations. For these reasons, one can make his own assumptions or ignore certain effects deliberately. The result is sub-optimal filtering. There are two sub-optimal filters that have been adapted in the VEBUK program, written by the author, to overcome the problem of sudden movements when monitoring the crustal deformation. These are the Recursive Fading Memory Filter and the Adaptive Kalman Filter for a System With Unknown Measurement Bias.

4.4.1 Recursive Fading Memory Filter

This method is described by Sorenson and Sacks, (1971). The method can be used for overcoming the destructive influence of model errors in Kalman Filter application that cause the creation of divergence. Divergence is said to occur when the actual errors in the estimates of state becomes inconsistent with the error covariance predicted. This causes breakdown in the processing method. The Recursive Fading Memory Filter is a method that overcomes the divergence problem. The method is based on discounting the effect of past data. This is accomplished through the choice of the Least-Squares weighting matrices. The weighting matrices are the same if all the data are treated equally. In order to discount the data obtained at earlier time than more recent data, this can be achieved by assigning smaller values to the associated weighting matrices. It can be shown that the Kalman Filter equations can be obtained as a solution to the unbiased, linear, mean square filtering problem. From the solution, it can be understood that the role of least squares weighting matrices are the same as the a-priori covariance matrices of noise processes of the filtering problem. Therefore, the procedures for discounting the data in the filtering context are performed by the appropriate selection of the noise covariances. This is the basic criteria from which fading memory filter equations are obtained.

The state behaviour is described by the linear difference equation and measurements occurring at discrete instants:

$$x^{N}_{(k|k-1)} = \Phi_{(k,k-1)} x^{N}_{(k-1|k-1)} + \Gamma_{(k,k-1)} w_{(k-1)} \tag{4.29}$$

and

$$z_{(k)} = A_{(k)} x^{N}_{(k|k)} + v^{N}_{(k)} \tag{4.30}$$

where, N represents the current time, and the sequences $w_{(k-1)}$ and $v_{(k)}$ are zero mean white noise with covariance matrices $Q_{(k)}$ and $R_{(k)}$ respectively.

Then the initial state and the noise covariances are assumed as,

$$E[(x^N_{(0|0)} - \bar{x})(x^N_{(0|0)} - \bar{x})^T] = P_{(0|0)} \exp \sum_{i=0}^{N-1} c_i \tag{4.31}$$

$$E[w_{(k)} w^T_{(k)}] = Q_{(k-1)} \exp \sum_{i=k}^{N-1} c_i \tag{4.32}$$

$$E[v_{(k)} v^T_{(k)}] = R_{(k)} \exp \sum_{i=k}^{N-1} c_i \tag{4.33}$$

Then the recursive fading memory equations are as follows,

$$x_{(n|n)} = \Phi_{(n,n-1)} x_{(n-1|n-1)} + K^c_n [z_n - A_n x_{(n|n-1)}] \tag{4.34}$$

$$P^c_{(n|n-1)} = \Phi_{(n,n-1)} P^c_{(n-1|n-1)} \Phi^T_{(n,n-1)} (e^{c_{n-1}}) + Q_{(n-1)} \tag{4.35}$$

$$K^c_n = P^c_{(n|n-1)} A^T_n [A_{(n)} P^c_{(n|n-1)} A^T_{(n)} + R_{(n)}]^{-1} \tag{4.36}$$

$$P^c_{(n|n)} = P^c_{(n|n-1)} - K^c_{(n)} A_{(n)} P^c_{(n|n-1)} \tag{4.37}$$

where, $x_{(n|n)}$, $P^c_{(n|n-1)}$, $P^c_{(n|n)}$, and $K^c_{(n)}$ are the sub-optimal state vector, predicted covariance matrix, estimated covariance matrix respectively and gain matrix at time n and they satisfy the above system.

It is noted that the data can be discounted by multiplying the covariance matrix $P^{c}_{(n-1|n-1)}$ by exp (c_{n-1}), providing that $c_{n-1} \geq 1$ before updating the estimate to the n*th* sampling time.

4.4.2 Adaptive Kalman Filter for a System With Unknown Measurement Bias

This approach was developed by Richard et al, (1986) for passive underwater tracking of manoeuvring targets. In this approach, the state estimator is designed specifically for a system containing unknown or randomly switching biased measurements. The stochastic system is modelled assuming that the bias sequence dynamics can be modelled by a Semi-Markov process. The Semi-Markov process is defined as ' *a probabilistic system that made its transitions according to the transition probability matrix of a markov process, but whose time between transitions could be an arbitrary random variable that depend on the transition.*' (Howard, 1964).

By incorporating the Semi-Markovian concept into a Bayesian estimation technique an estimator consisting of a bank of parallel, adaptively weighted, Kalman filter equations can be obtained. The reader is referred to Richard et al, (1986) for derivation of the equations, here only the final product of the Adaptive Kalman filter equations for a system with unknown measurement bias are given. The system can be described as

$$x_{(k|k+1)} = \Phi_{(k,k+1)} x_{(k|k)} + \Gamma_{(k,k+1)} w_{(k)} \tag{4.38}$$

and

$$z_{(k+1)} = A_{(k+1)} x_{(k+1)} + v_{(k+1)} + v_{(b)} \tag{4.39}$$

where, all the terms have being explained in equation (4.4) and (4.5) except $\nu_{(b)}$.

The new term, $\nu_{(b)}$ is the unknown bias vector which is governed by a Semi-Markov process which assumes that the bias can take any of N possible discrete vectors $\{ \nu^{(i)}, ..., \nu^{(N)} \}$ for a random duration of time before a transition occurs. This range of $\nu^{(i)}$ is modelled to span the entire possible range of $\nu_{(b)}$.

The adaptive estimator for the system described by the equations (4.38) and (4.39) is given by

$$x_{(k+1|k+1)} = \sum_{i=1}^{N} x^{(i)}_{(k+1|k+1)} S^{(i)}_{(k+1)} \tag{4.40}$$

where, $S^{(i)}_{(k+1)}$ is the weight determined for every possibility N, (i=1,...N), and its computation is given in equation (4.45)

$$x^{(i)}_{(k+1|k+1)} = \Phi_{(k+1,k)} x^{(i)}_{(k|k)} + \Gamma_{(k+1,k)} w_{(k)} + K_{(k+1)} [z_{(k+1)} - \nu^{(i)} - A_{(k+1)} x^{(i)}_{(k+1|k)} - A_{(k+1)} \Gamma_{(k+1,k)} w_{(k)}] \tag{4.41}$$

Equations (4.40) and (4.41) are the i*th* conditioned estimators. Their auxiliary equations are

$$P_{(k+1|k)} = \Phi_{(k+1,k)} P_{(k|k)} \Phi^{T}_{(k+1,k)} + \Gamma_{(k+1,k)} Q_{(k)} \Gamma^{T}_{(k+,k)} \tag{4.42}$$

$$K_{(k+1)} = P_{(k+1|k)} A_{(k+1)} [A_{(k+1)} P_{(k+1|k)} A^{T}_{(k+1)} + R_{(k+1)} + R_{(b)}]^{-1} \tag{4.43}$$

$$P_{(k+1|k+1)} = [I - K_{(k+1)} A_{(k+1)}] P_{(k+1|k)} \tag{4.44}$$

and the adaptive weighting functions are given by

$$S_{(k+1)}^{(i)} = c_{(k+1)} e^{q_i} \sum_{\alpha=1}^{N} \theta_{\alpha i} S_{(k)}^{\alpha} \tag{4.45}$$

where, $\theta_{\alpha i}$ is the Markov transition probabilities and it can be determined by the appropriate selection of θ_{ii}=0.95 and $\theta_{\alpha i}$=(1-0.95)/(N-1), which is the standard distribution. The $c_{(k+1)}$ is the scale factor determined for every iteration so that it provides the sum of the weights equal to 1. It is defined as

$$\sum_{i=1}^{N} S_{(k+1)}^{(i)} = 1 \tag{4.46}$$

In equation (4.45) q_i is calculated as follows

$$q_i = -\frac{1}{2}\left[\left(z_{(k+1)} - \bar{z}^{(i)}\right) Q_z^{(-1)} \left(z_{(k+1)} - \bar{z}^{(i)}\right)^T\right] \tag{4.47}$$

and

$$\left(z_{(k+1)} - \bar{z}^{(i)}\right) = \left(z_{(k+1)} - \nu^{(i)} - A_{(k+1)} x_{(k+1|k)}^{(i)} - A_{(k+1)} \Gamma_{(k+1,k)} w_{(k)}\right) \tag{4.48}$$

In equation (4.47) Q_z is given by

$$Q_z = A_{(k+1)} P_{(k+1|k)} A_{(k+1)}^T + R_{(k+1)} + R_{(b)} \tag{4.49}$$

where $R_{(b)}$ is the covariance of bias vector v_b.

For some applications, the estimation of the bias vector is necessary such as the magnitude of local movement, an estimate of v_b is formulated as follows

$$v_{b(k+1)} = \sum_{i=1}^{N} \nu^{(i)} S_{(k+1)}^{(i)} \tag{4.50}$$

The block diagram of the state estimator is depicted in Figure 4.9.

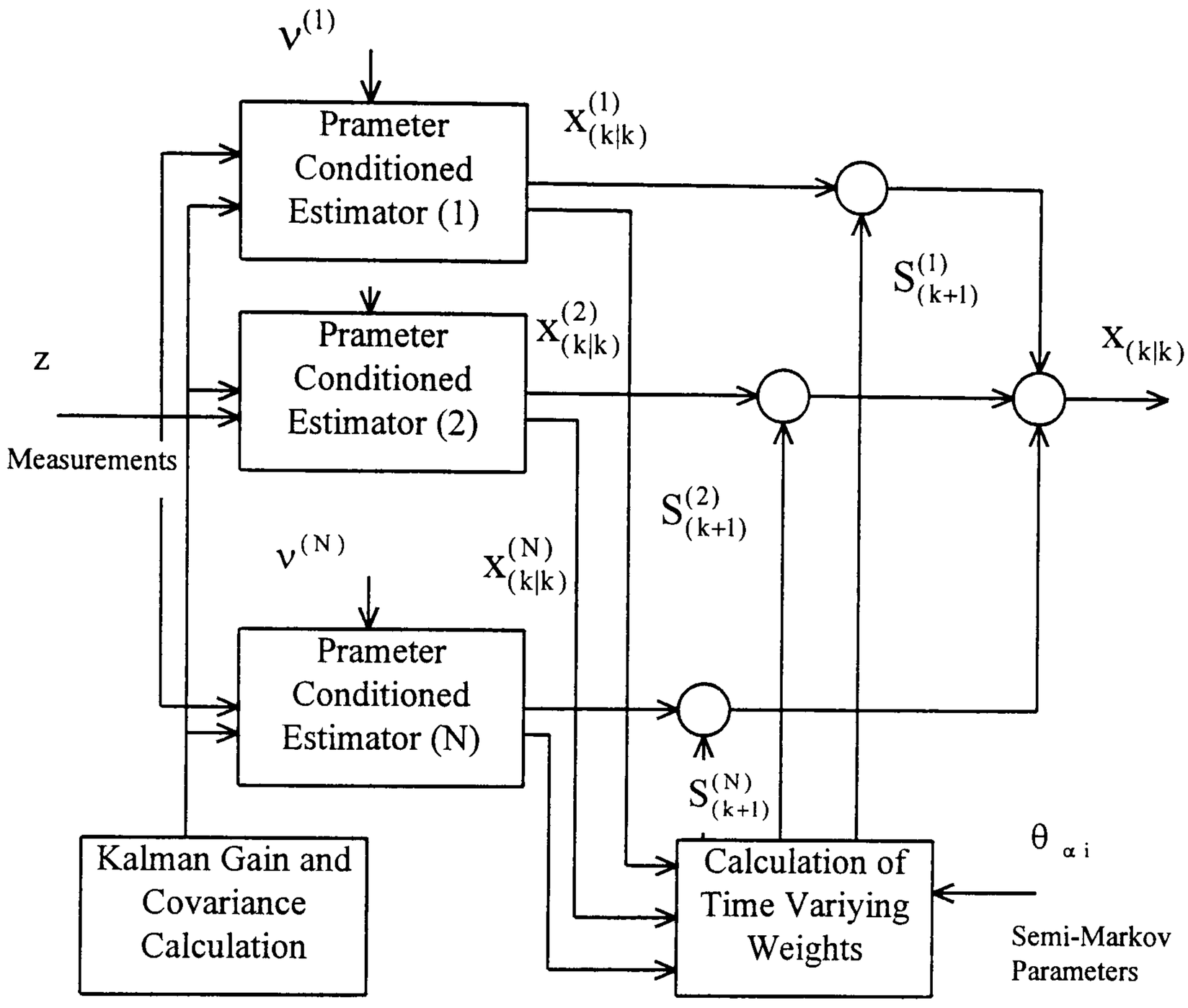

Figure 4.9 Adaptive Estimator for Random Switching Measurements Bias (Richard et al, 1986)

The advantages of the adaptive filter are that it isolates the local motion from the tectonic motion, and that it is possible to estimate the magnitude of the local motion. However it is sub-optimal and it requires more computation.

4.5 Kalman Filtering in Deformation Monitoring

The deformation monitoring problem is mainly that of detecting the movement of a set of object points compared with a number of reference points. The reference points can be obtained, in a conventional manner, by two network models, an absolute network and a relative network. The absolute network involves points (stations) which are not subject to movement, for example in dam deformation, the reference points can be located away from the area that is subjected to forces due to water loading. Relative networks involve reference

points and object points which are both subject to movement. In this case, the minimum configuration defect is sought. Once a set of points which have the minimum configuration defect are found, these points form the reference network relative to which displacements (movements) can be determined. However, for the aim of monitoring the crustal movements, which involves large areas, this is a bit tedious considering the multiple epochs of observations. Fortunately, the International GPS Service for Geodynamics (IGS) stations can be used as reference stations, by fixing station coordinates to a precise terrestrial reference frame and its velocity field (ITRFxx), and using the IGS precise ephemerides, a well-defined reference frame can be obtained.

Observations, which connect the fixed (reference) and object (subject to movement) points in a defined network (one of above reference network), are made at separate epochs, usually at regular intervals of time.

In classical (conventional) deformation analysis, the network is adjusted for individual epochs. At this stage, data snooping is performed to detect any possible blunders or gross errors in the observations . One of the procedures of data snooping can be found in Baarda, (1968). From the results of two such adjustments at consecutive epochs, the displacement vector for each object point is computed and, if appropriate, significance testing is applied .

Napier, (1990), suggested an approach for deformation monitoring . '*Pelzer (1986) proposes an advanced deformation analysis using Kalman filtering.*' This approach was also adapted to monitor dam deformations in two dimensions by Celik, (1995). Based on this, the procedure is to model the trajectory of each of the object points with a special kinematic model:

$$y(t_k) = y(t_{k-1}) + \dot{y}(t_{k-1})\Delta t + \cdots \tag{4.51}$$

where, $y(t_k)$ is the trajectory of a station,

$\dot{y}(t_{k-1})$ is the rate of movement (velocity) of $y(t_{k-1})$, at time t_{k-1},

Δt is the time difference $(t_k - t_{k-1})$.

Then the state vector is formed as,

$$x(t_k) = \begin{bmatrix} y(t_k) \\ \dot{y}(t_k) \end{bmatrix} \tag{4.52}$$

where, $x(t_k)$ is the state vector at time t_k,

and the secondary model can be written as,

$$x(t_{k+1}) = \Phi_{(k+1,k)} x(t_k) + \Gamma_{(k+1,k)} w(t_k) \tag{4.53}$$

where, $w(t_k)$ is a vector of system noise.

Having defined the above dynamic model, the fixed points are easily catered for by setting,

$$\dot{y}(t_k) = 0 \tag{4.54}$$

Such a Kalman filter can be used to analyse for changes in the steady state conditions, for example changes in velocity, in addition to changes in position. The deformation analysis can be carried out using the following procedures,

1. Prediction of the state vector at an actual epoch,
2. Comparison with actual observations, ie innovations (predicted residuals),
3. Updating of the state vector from the observations,
4. Testing the change in state vector resulting from the update for any significant change in state.

The application of the standard Kalman filter equations can perform steps 1 and 3. The prediction equation is given in equations (4.10), and (4.11), and updating (filtering) is given in equations (4.12) to (4.14). Step 2 can be performed from equation (4.13) by,

$$\tilde{z}_{(k+1|k)} = (z_{(k+1)} - A_{(k+1)}x_{(k+1|k)}) \tag{4.55}$$

where, $\tilde{z}_{(k+1|k)}$ is the innovation residuals vector at time k+1,

and its corresponding covariance matrix from equation (4.12) is,

$$\tilde{P}_{(k+1|k)} = (A_{(k+1)}P_{(k|k)}A^{T}_{(k+1)} + R_{(k+1)}) \tag{4.56}$$

where, $R_{(k+1)}$ is the measurement covariance matrix at time t_{k+1}.

In step 4, the change to the state vector due to the update is obtained from equation (4.14) by

$$\Delta x_{(k+1|k)} = K_{(k+1)}\tilde{z}_{(k+1|k)} \tag{4.57}$$

The advantages of this approach over the conventional (classical) approaches are,

- The deformation model includes position, and velocity,
- A Least Squares solution at any epoch uses historical information as well as the actual observation at that epoch,
- The calculation of the actual state of the point field includes position, and velocity,
- Prediction is easy to make,
- It can handle the variation of the motion.

However, sudden change in positions due to local movements such as an earthquake, may affect a number of epochs after it. This problem arises in the case of monitoring crustal dynamics. As, this study mainly involves the crustal deformation monitoring, this problem, can be detected by the statistical tests given in §4.3 and eliminated using the two alternatively proposed sub-optimal filters. These are Fading Memory Filter which has been described in §4.4.1, and the adaptive Kalman Filter for a System With Unknown Bias given in §4.4.2. In Figure 4.10 procedures proposed by the author are depicted.

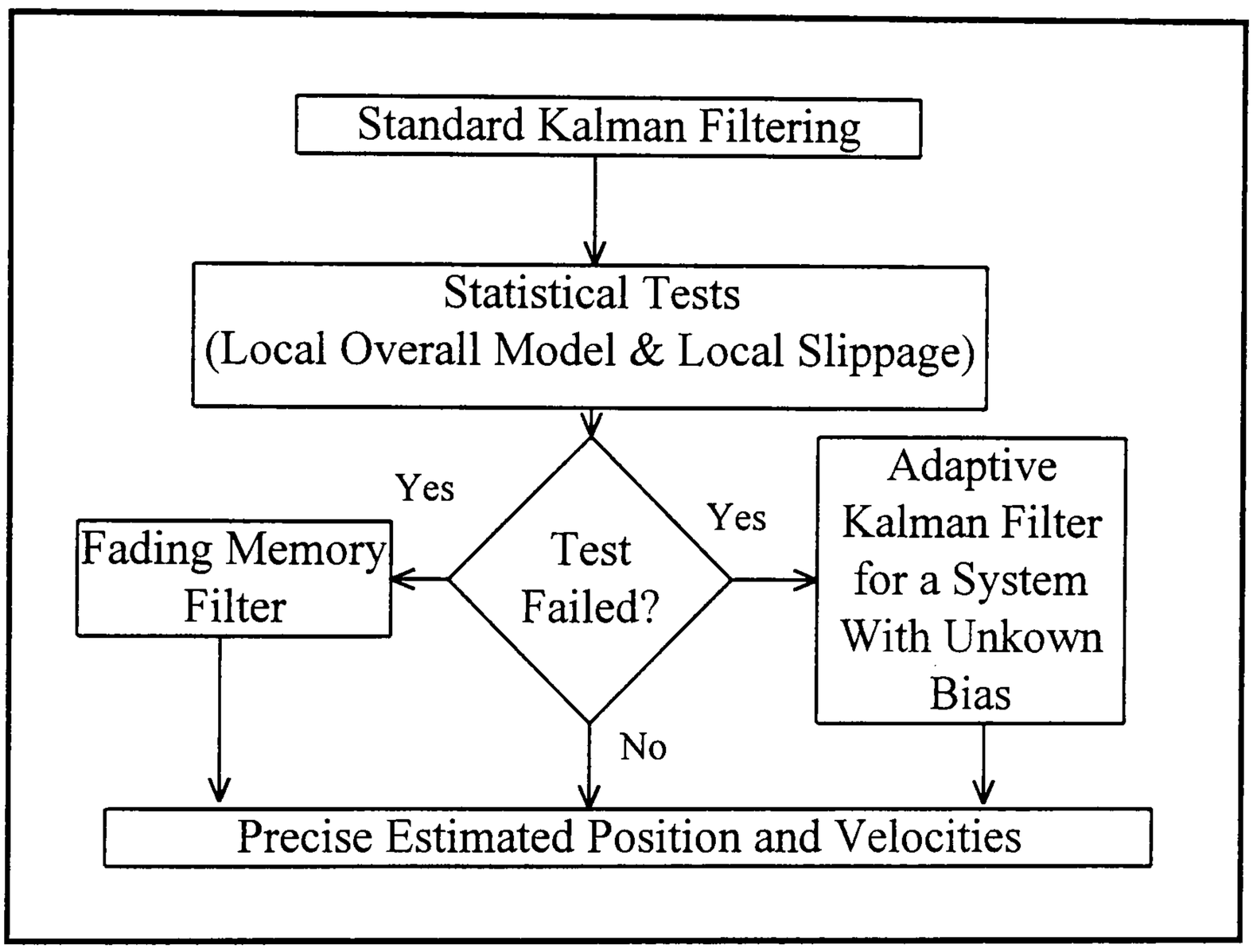

Figure 4.10 Proposed Processing Procedure

In this proposed procedure, standard Kalman filtering means that equations (4.10) to (4.14) are used. In this study, the standard Kalman filter model is a constant velocity with system noise. The measurements are the estimated coordinates z_k at time t_k (k=1, 2,.....,N) obtained by the Least Squares method. The initial state vector is formed by combining the z_k and velocity, which is zero for the first epoch. In a similar way, the initial covariance is formed by combining the covariance matrix that corresponds to the measurement vector and the variance for the velocity chosen by the user. The choice of the initial covariance for the initial zero velocity will effect a few epochs, then the effect

will vanish as the Kalman filter is not sensitive to initial covariances for all the epochs.

By applying the standard Kalman filter and the testing procedures given in §4.3, to the innovation vector, any sudden movement or bias will be revealed, then one can chose one of the two sub-optimal filters proposed to eliminate the problem.

4.6 The VEBUK Program

The VEBUK (**V**elocity **E**stimation **B**y **U**sing **K**alman Filter) program has been developed by the author, and is designed to estimate the velocities of stations in a deformation monitoring network. The program basically accepts the sets of coordinates and corresponding covariances, estimated by the Least Squares technique at every epoch, as inputs. This is achieved by using GAS as described in §3.6 in the case of GPS measurements. The outputs of each sessions from GAS can be combined to obtain campaign solutions using the program CARNET (**CAR**tesian **NET**work Adjustment Program). The CARNET is designed for network adjustments by the Least Squares technique and analysis, and can be used with many types of observations including GPS Cartesian baseline vectors (Lowe, 1994). This program also has an option to obtain the covariances as outputs. One of the methods described in §4.5, can be used to define the reference frame for the aim of deformation monitoring. It is important here to note that before the VEBUK program run, data snooping has to be performed in order to eliminate the blunders or outlier for each coordinate set at every epoch t_k. The outputs of CARNET are the inputs of VEBUK. The outputs of VEBUK are the filtered and smoothed coordinates and velocities for each time t_k. In addition to these, VEBUK also calculates the single differenced velocities for the aim of comparison. For each station, VEBUK creates an output file corresponding to that station.

The format of VEBUK has been designed to be compatable with other programs in GAS. It uses a control file in which options are specified as well as input and output filenames. The control file consists of six blocks, FILES (input), OPTION, NOISE, MODELS, SMOOTHINGS and OUTPUTS.

A flow chart for the VEBUK program is depicted in Figure 4.11. First, the initial state vector is formed by combining the coordinates and velocity (that is assigned to zero for the first epoch), then the initial covariance matrix corresponding to the initial state vector is formed. Next, using the initial state vector and covariances, a prediction is made. Then following the introduction of new measurements into the system, Local Overall Model (LOM) and Local slippage tests (LST) are performed. Depending on the result of the statistical tests and the preferred sub-optimal filter, filtering (updating) is performed using the measurements. Then for the next time, the filtered state vector and the covariances are accepted as initial values, and so on. Having finished all of the filtering jobs for all of the data span, then the smoothing is performed and finally simple differenced velocities are calculated and recorded to the output files.

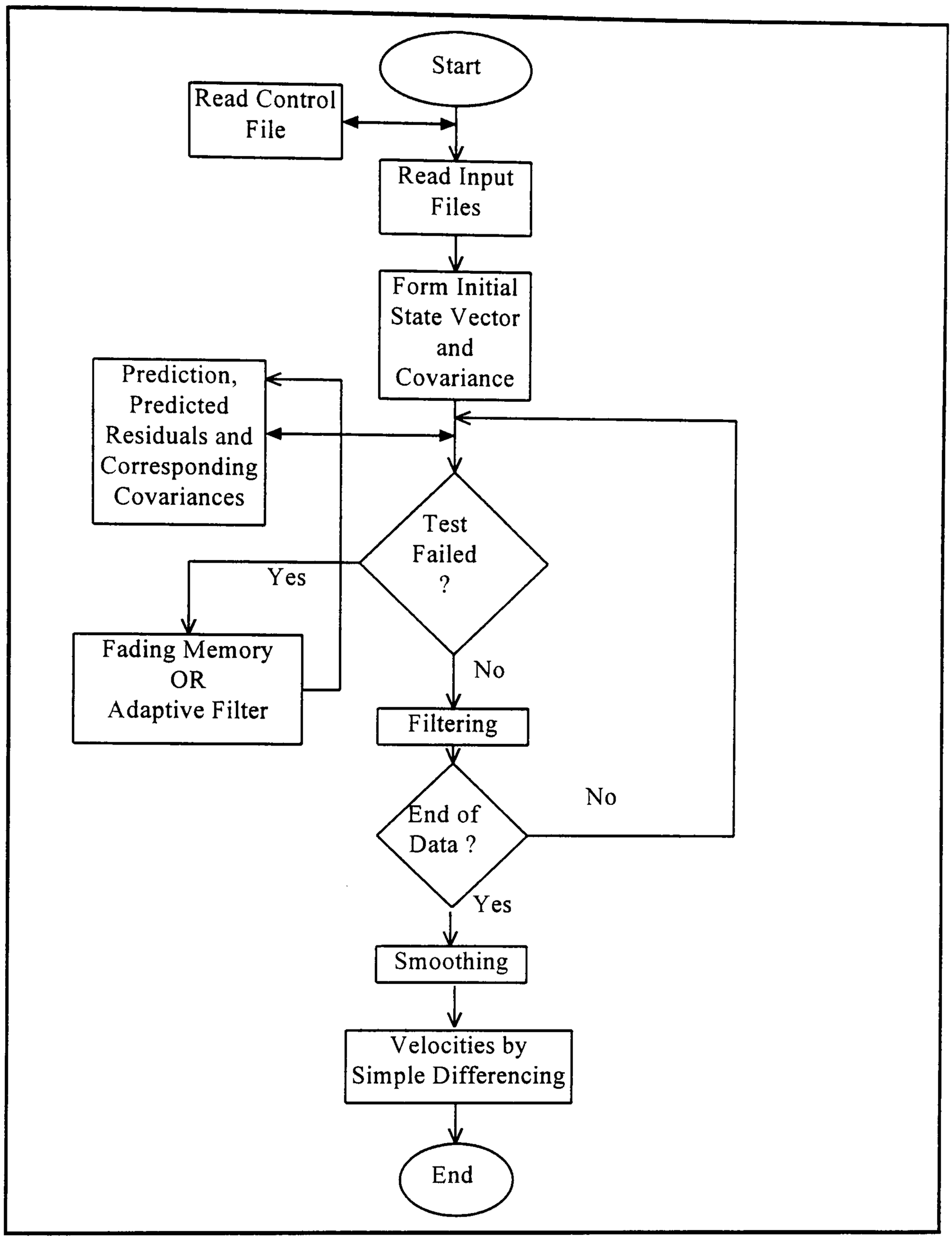

Figure 4.11 Program Flow Chart for the VEBUK

4.7 Strain Analysis

Having obtained velocities by VEBUK program, then using these, one can obtain strain rates, and rotation occurring in the area. The author has developed a program with which strain rates and rotation are obtained using the outputs from VEBUK. Here, a background for strain analysis is given by using relative velocities.

The Earth's crust is deforming continuously due to plate tectonics, and external forces such as gravitational forces, Earth rotation and heat transfer. Deformation is defined as the movement of points of a body relative to each other and a translation and rotation of the body as a whole. The movement of an arbitrary point is a vector quantity known as displacement.

Strain is defined as change in length per unit of initial length. The translation and rotation of a body as a whole is known as rigid body motion and this does not produce strain (Dally and Riley, 1991).

In Figure 4.12, considering a deformable body S, and a and b as two points in the body. After a certain time, the body S moves to S' and the points a and b move to a' and b' respectively (Malvern 1969). The displacements of aa' and bb' consist of three parts of movement, namely the translation, rotation and deformation between points a and b. The deformation along the line ab can be described by the strain, which is given as

$$s = (a'b'-ab)/ab \tag{4.58}$$

The distribution and accumulation of strain is responsible for the occurrence of earthquakes, as an earthquake releases the accumulated strain in the Earth's crust. Therefore, in crustal deformation monitoring, strain analysis is very important. In this section, the strain analysis method is used to obtain the deformation movement from the total displacement.

Deformation can be represented, in principle, by the trajectory of every point X,

$$x = x(X, t) \text{ or } x = x(X, Y, Z, t) \tag{4.59}$$

The rate-of-deformation tensor (also called the stretching tensor, velocity tensor) and the spin tensor are important tensors in linear viscosity and most

plasticity theories. Their rectangular Cartesian components will be defined in terms of velocity components,

$$v_i = \frac{dx_i}{dt} \tag{4.60}$$

and this is expressed in terms of spatial coordinates and the time

$$v_i = v(X, Y, Z, t) \tag{4.61}$$

These velocity components describe the tangential motions.

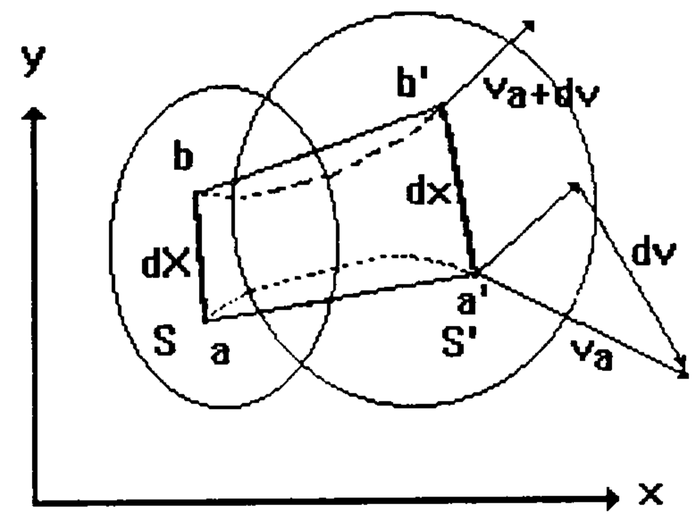

Figure 4.12 Relative Displacement

Given two points a and b in a geodetic network (Figure 4.12), the relative velocity Jacobean Equation can be formed as

$$dv_x = \frac{\partial v_x}{\partial X} dX + \frac{\partial v_x}{\partial Y} dY + \frac{\partial v_x}{\partial Z} dZ \tag{4.62}$$

$$dv_y = \frac{\partial v_y}{\partial X} dX + \frac{\partial v_y}{\partial Y} dY + \frac{\partial v_y}{\partial Z} dZ \tag{4.63}$$

$$dv_z = \frac{\partial v_z}{\partial X} dX + \frac{\partial v_z}{\partial Y} dY + \frac{\partial v_z}{\partial Z} dZ \tag{4.64}$$

where dv_x, dv_y, dv_z are the relative velocity,

dX, dY, dZ are the displacement components of a point relative to the other.

Since in this study only two dimensional strain analysis is considered, It is now continued in two dimension, i.e. x, and y or Latitude or Longitude. The notation from dv_x, dv_y to Δv_x, Δv_y, and from dX, dY to ΔX, ΔY respectively will be considered. Equation (4.62) and (4.63) are re-written considering the above notation as

$$\begin{bmatrix} \Delta v_x \\ \Delta v_y \end{bmatrix} = \begin{bmatrix} e_{xx} & e_{xy} \\ e_{yx} & e_{yy} \end{bmatrix} \begin{bmatrix} \Delta x \\ \Delta y \end{bmatrix} = E \begin{bmatrix} \Delta x \\ \Delta y \end{bmatrix} \tag{4.65}$$

where, Δx, Δy are coordinate differences between two points

$\Delta v_{X,y}$ are velocity difference between two points

E is the displacement matrix, and its components are described in equations (4.62) and (4.63) as

$$e_{xx} = \frac{\partial v_x}{\partial X}, \qquad e_{xy} = \frac{\partial v_x}{\partial Y}$$

$$e_{yx} = \frac{\partial v_y}{\partial Y}, \qquad e_{yy} = \frac{\partial v_y}{\partial Y} \tag{4.66}$$

Because the relative velocity is used in equation. 4.65, the movement of translation has been removed. The displacement matrix E, therefore, only contains the information of rotation and deformation. As seen in equation. (4.65), for each baseline two equations can be formed. In order to solve for the four elements of the displacement matrix, at least two baselines , or three points are needed.

The displacement matrix E can further be divided in to two parts

$$E = S+W \tag{4.67}$$

S is the symmetric part, representing strain matrix (rate-of-deformation tensor or stretching tensor),

$$\mathbf{S} = \frac{1}{2}\left[\mathbf{E} + \mathbf{E}^{\mathrm{T}}\right] \tag{4.68}$$

W is the asymmetric part of E, representing the rotation rate matrix (spin tensor)

$$\mathbf{W} = \frac{1}{2}\left[\mathbf{E} - \mathbf{E}^{\mathrm{T}}\right] \tag{4.69}$$

From the strain matrix S, the principal strain rates can be obtained by solving for the eigenvalues of the matrix

$$\begin{bmatrix} s_{11}-\lambda & s_{12} \\ s_{21} & s_{22}-\lambda \end{bmatrix} = 0 \tag{4.70}$$

From equation. (4.70), the maximum and minimum strain rates along the principal axes are

$$\lambda_{max} = S_{max} = \frac{1}{2}\left[(s_{11}+s_{22}) + \sqrt{(s_{11}-s_{22})^2 + 4s_{12}^2}\right] \tag{4.71}$$

$$\lambda_{min} = S_{min} = \frac{1}{2}\left[(s_{11}+s_{22}) - \sqrt{(s_{11}-s_{22})^2 + 4s_{12}^2}\right]$$

The direction of the principal axis for the maximum strain rate can also be calculated by

$$\Theta = \tan^{-1}\left(\frac{s_{12}}{S_{max} - s_{22}}\right) \tag{4.72}$$

In the deformation analysis, the velocities of all stations, together with their covariance matrix can be obtained from the Kalman filter/smoother. First, the network is divided into sub-triangles. The sub-triangles are chosen with respect to Delaunay triangles (Davis, 1986). Then for each triangle the strain rate and rotation rate are estimated based the theory discussed above.

Given the velocities and coordinates of three points, the relative velocity and coordinates can be obtained by

$$\Delta v = Mv = \begin{bmatrix} \Delta v_{x,1,2} \\ \Delta v_{y,1,2} \\ \Delta v_{x,1,3} \\ \Delta v_{y,1,3} \end{bmatrix} = \begin{bmatrix} -1 & 0 & 1 & 0 & 0 & 0 \\ 0 & -1 & 0 & 1 & 0 & 0 \\ -1 & 0 & 0 & 0 & 1 & 0 \\ 0 & -1 & 0 & 0 & 0 & 1 \end{bmatrix} \begin{bmatrix} v_{x1} \\ v_{y1} \\ v_{x2} \\ v_{y2} \\ v_{x3} \\ v_{y3} \end{bmatrix} \tag{4.73}$$

and

$$\Delta x = Mx = \begin{bmatrix} -1 & 0 & 1 & 0 & 0 & 0 \\ 0 & -1 & 0 & 1 & 0 & 0 \\ -1 & 0 & 0 & 0 & 1 & 0 \\ 0 & -1 & 0 & 0 & 0 & 1 \end{bmatrix} \begin{bmatrix} x_1 \\ y_1 \\ x_2 \\ y_2 \\ x_3 \\ y_3 \end{bmatrix} \tag{4.74}$$

where 1, 2, 3 donates sub-triangle corner numbers

The covariance matrix for the relative velocity Δv is

$$C_{\Delta v} = MC_V M^T \tag{4.75}$$

From equation. (4.65), the elements of the displacement matrix can be determined using the following equation

$$\Delta v = \begin{bmatrix} \Delta x & \Delta y & 0 & 0 \\ 0 & 0 & \Delta x & \Delta y \end{bmatrix} \begin{bmatrix} e_{xx} \\ e_{xy} \\ e_{yx} \\ e_{xx} \end{bmatrix} \quad \text{or } \Delta v = A \begin{bmatrix} e_{xx} \\ e_{xy} \\ e_{yx} \\ e_{xx} \end{bmatrix} \tag{4.76}$$

The variance-covariance of E can be obtained by,

$$C_E = \left(A^T C_{\Delta v}^{-1} A\right)^{-1} \tag{4.77}$$

Finally the other parameters, such as maximum, minimum strain rates and the rotation rate can be obtained using equations. (4.62) to (4.66). Their corresponding variance can also be calculated based on the error propagation law. The author wrote a program STRAIN that performs above calculations using the outputs from VEBUK.

Chapter 5

Deformation Data Sets

The deformation data sets which have been used in this thesis are of three types; *Real/Simulated* data based on two GPS campaigns, ie October, 1995 and November, 1995, from the East Mediterranean GPS Geodynamic Project (EASTMED), *real data* from the EUREF Permanent GPS Network; and *real data* from nine GPS campaigns in the UK. In this chapter the formation of the above mentioned data sets and the UK Tide Gauge Monitoring Project (UKGAUGE) will be described, with particular emphasis on the EASTMED data processed by the author.

5.1 East Mediterranean GPS Geodynamics Project (EASTMED)

The East Mediterranean GPS Geodynamics project involves representatives from a number of countries namely Egypt, Israel, Jordan, Turkey and the UK. On 19 May 1995, an inaugural meeting was held at the University of Nottingham. At the meeting, it was proposed that, the project should aim at defining a **Zero Order Network,** based on the ITRF, which could be used as

a) *A base framework for monitoring crustal dynamics in a region of high interest in tectono-physics and geodynamics,*

b) *A network for monitoring high precision vertical displacements of major tide gauges, and hence mean sea level, for a region stretching from the Black Sea to the Red Sea, and including the Eastern Mediterranean, and*

c) *A common high precision horizontal and (especially) vertical datum for large engineering projects in the region, e.g. hydro-dynamic projects where high precision heighting control is essential.*

It was noted that the Zero Order Network could also be used as a framework for national GPS networks of the individual countries in the region, to help them define

d) *A common mapping datum, compatible with the ETRF89, the European mapping datum,*

e) *A common coordinate reference framework for sea, land and air navigation, compatible with WGS84,*

f) *A framework for future DGPS and Wide-Area-DGPS regional networks, and*

g) *A geo-referencing system for continuous environmental monitoring in the region, in terms of water and land resources, and general ecological purposes.*

After some discussion of these proposals a consensus view emerged. The project should concentrate on the monitoring of vertical land movement and changes in mean sea level at major tide gauges in the region, which includes the Black Sea, the Mediterranean and the Red Sea. Other stations should also be included in order to study the interaction of the African, Arabian, Anatolian and Eurasian plates, and the crustal dynamics in the Dead Sea fault region. Based on these broad objectives, a Zero Order Network was designed, which comprises 22 stations in the East Mediterranean region (Figure 5.1). Of the 22 stations, 10 were in Egypt (including the SLR stations and 6 tide gauges), 3 in Israel (including the SLR station and 2 tide gauges), 3 in Jordan (including 1 tide gauge), 5 in Turkey (including 2 SLR stations and 3 tide gauges), and one in Cyprus.

It was agreed that the project would be carried out in two phases, starting as soon as possible. For Phase I, it was agreed that a First-Epoch GPS Campaign would be carried out from Monday 23 October to Friday 27 October 1995. The reconnaissance, station monumentation and GPS observations would be the responsibility of the organisations from the East Mediterranean countries, with some assistance from the UK Military Survey, if requested. The University of

Nottingham would act as coordinators of Phase I, and would collect and distribute all of the GPS data to all of the participants, along with the following information.

a) IGS Precise ephemerides.

b) GPS data from the IGS stations.

c) Fiducial station coordinates in the ITRF for the IGS stations.

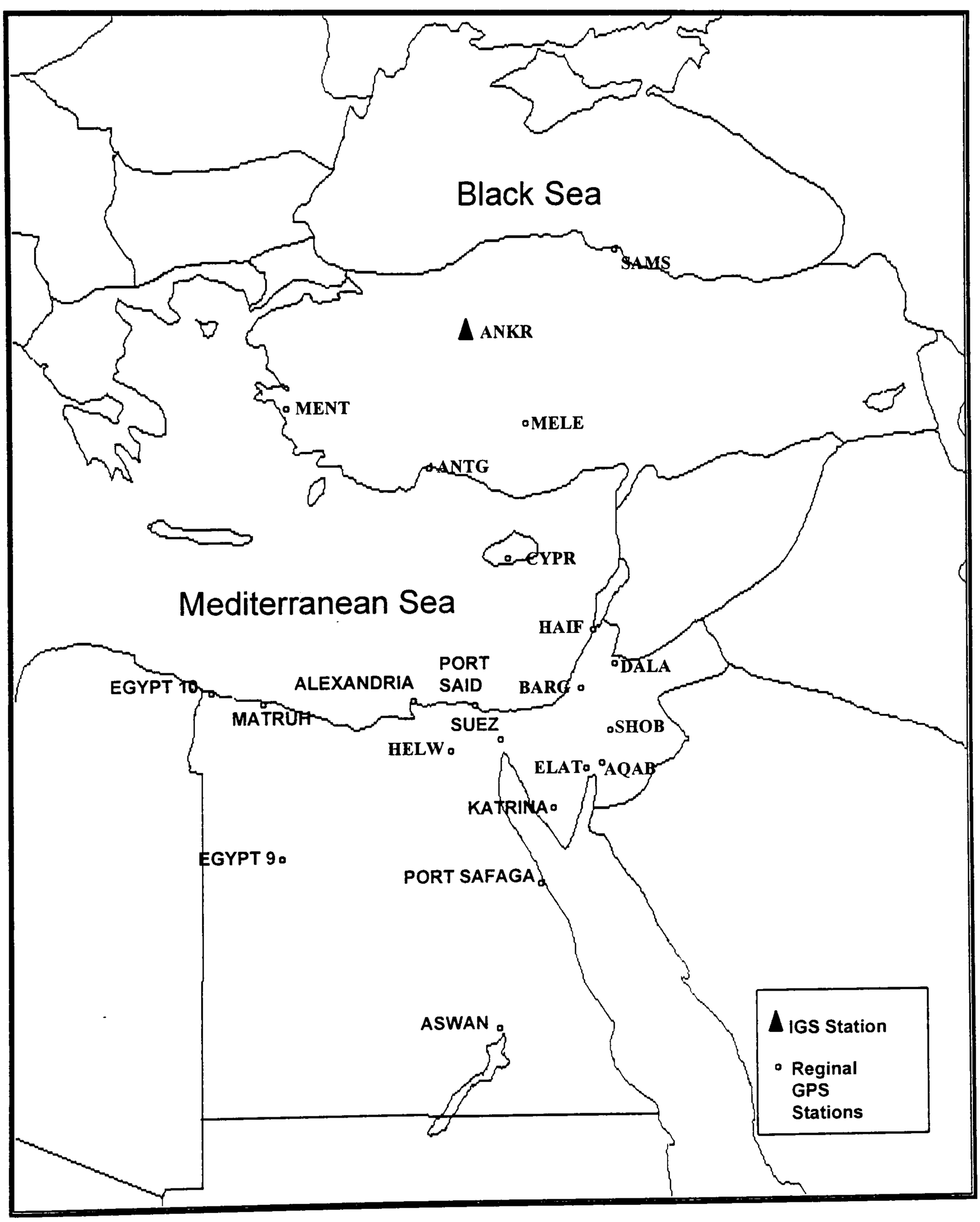

Figure 5.1 Proposed Network Including IGS Stations

Following the meeting in Nottingham in May 1995, a network of seventeen survey stations was established within the region. A preliminary GPS campaign was carried out at these survey stations from 23 to 27 October 1995, with five days of 24 hour observation at each survey station. Shortly after the campaign ended, the 22 November 1995 Earthquake (M_w = 7.1) took place in the Gulf of Eilat/Aqaba, with reports of ground fractures, damage and collapse of buildings in Eilat in Israel, Aqaba in Jordan and the Sinai Peninsula in Egypt (Kimata et al, 1997). A repeat GPS campaign was quickly organised, and five of the fifteen survey stations were re-observed from 29 November to 2 December 1995, with five days of 24 hour observations at each survey station.

5.1.1 Field Campaigns Summary

Although a total of 22 stations (Figure 5.1) were proposed, the October 1995 Campaign measurements were carried out at a total of seventeen stations being five in Turkey, one in Cyprus, seven in Israel, three in Jordan and one in Egypt. A summary of the stations is given in Table 5.1 and their locations in Figure 5.2.

In the November 1995 Campaign, measurements were carried out at a total of seven stations being four in Israel, two in Jordan and one in Egypt. A summary of the stations is given in Table 5.2 and their location in Figure 5.3.

Table 5.1 Satiation and Observation Information in October 95 Campaign

Station Information

Station Name	Station Type	Station Code	Approx Coordinates	
			Latitude	Longitude
Samsun	Tide Gauge	SAMS	41 20 N	36 20 E
Ankara IGS	Other	ANKR	39 41 N	32 44 E
Mentes	Tide Gauge	IZMI		
Melengicik SLR	Other	MELE	37 12 N	33 11 E
Antalya	Tide Gauge	ANTG	36 49 N	30 36 E
Cyprus	Other	CYPR	34 42 N	32 51 E
Haifa	Tide Gauge	HAIF	32 50 N	34 57 E
Haifa Technion)	Other	TECH	32 47 N	35 01 E
Tel Aviv	Other	TARD	32 04 N	34 47 E
Bar Giy SLR	Other	BARG	31 43 N	35 05 E
Beer Sheva	Other	BEER	31 16 N	34 48 E
Mizpe Roman	Other	MIZP	30 36 N	34 46 E
Eliat	Tide Gauge	ELAT	29 31 N	34 55 E
Dala	Other	DALA	32 08 N	35 37 E
Shobak	Other	SHOB	30 33 N	35 32 E
Aqaba Area	Tide Gauge	AQAB	29 31 N	35 00 E
Helwan SLR	Other	HELW	29 52 N	31 21 E

Observation Information

Date	Day of the week	Julian day & Session	START Time (UT)	STOP Time (UT)
23.10.1995	Monday	296-1	0000	1200
		296-2	1230	2359
24.10.1995	Tuesday	297-1	0000	1200
		297-2	1230	2359
25.10.1995	Wednesday	298-1	0000	1200
		298-2	1230	2359
26.10.1995	Thursday	299-1	0000	1200
		299-2	1230	2359
27.10.1995	Friday	300-1	0000	1200
		300-2	1230	2359

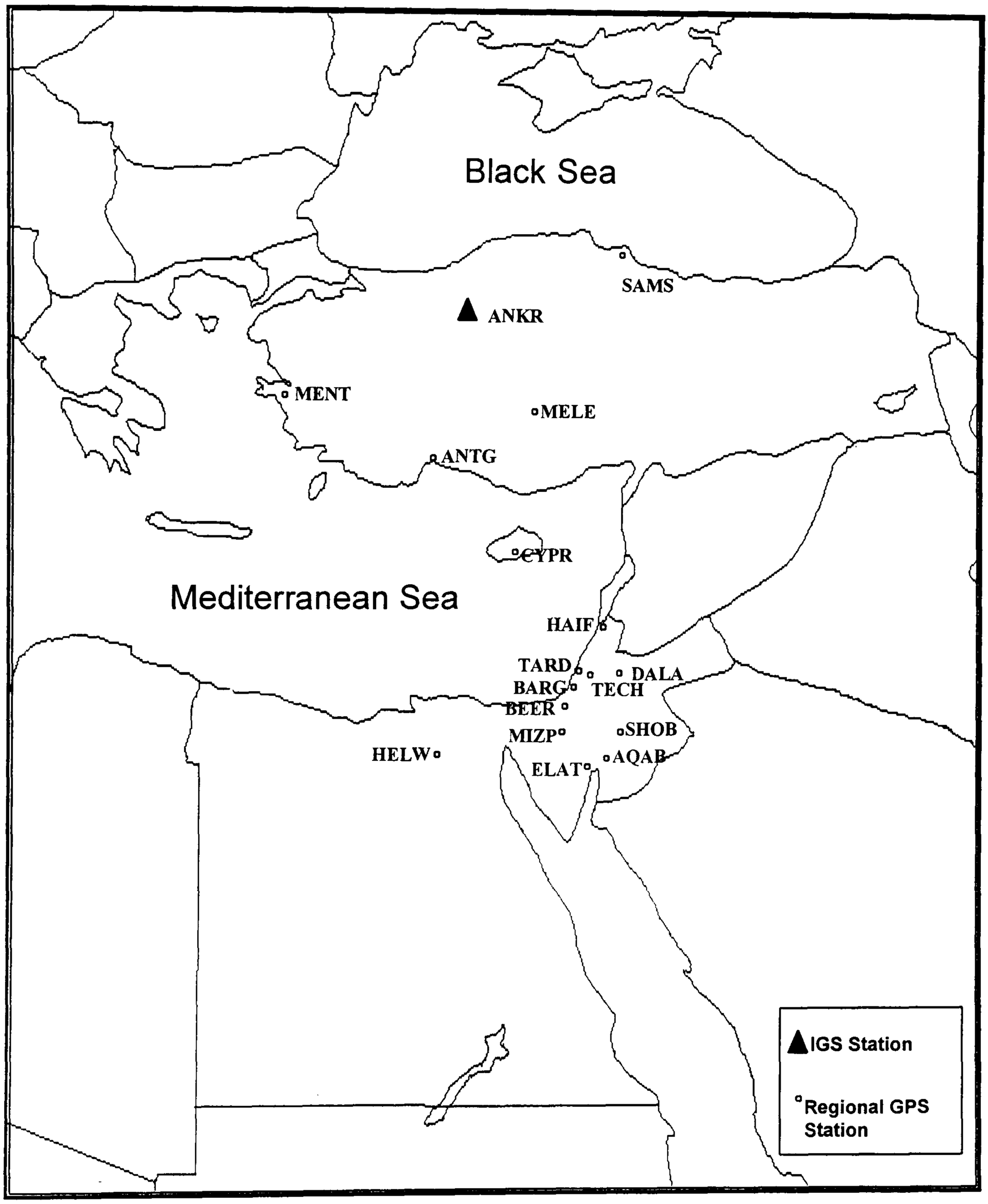

Figure 5.2 Regional Network in October 95 Campaign

Table 5.2 Station and Observation Information in November 95 Campaign

Station Information

Station Name	Station Type	Station Code	Approx Coordinates Latitude	Longitude
KATZ	Other	KATZ	33 00 N	35 41 E
Tel Aviv	Other	TARD	32 04 N	34 47 E
Bar Giyorra SLR	Other	BARG	31 43 N	35 05 E
Eilat	Tide Gauge	ELAT	29 31 N	34 55 E
Dala	Other	DALA	32 08 N	35 37 E
Aqaba	Tide Gauge	AQAB	29 31 N	35 00 E
Helwan SLR	Other	HELW	29 52 N	31 21 E

Observation Information

Date	Day of the week	Julian day & Session	START Time (UT)	STOP Time (UT)
29.11.1995	Wednesday	333-1	0000	1200
		333-2	1230	2359
30.11.1995	Thursday	334-1	0000	1200
		334-2	1230	2359
01.12.1995	Friday	335-1	0000	1200
		335-2	1230	2359
02.12.1995	Saturday	336-1	0000	1200
		336-2	1230	2359

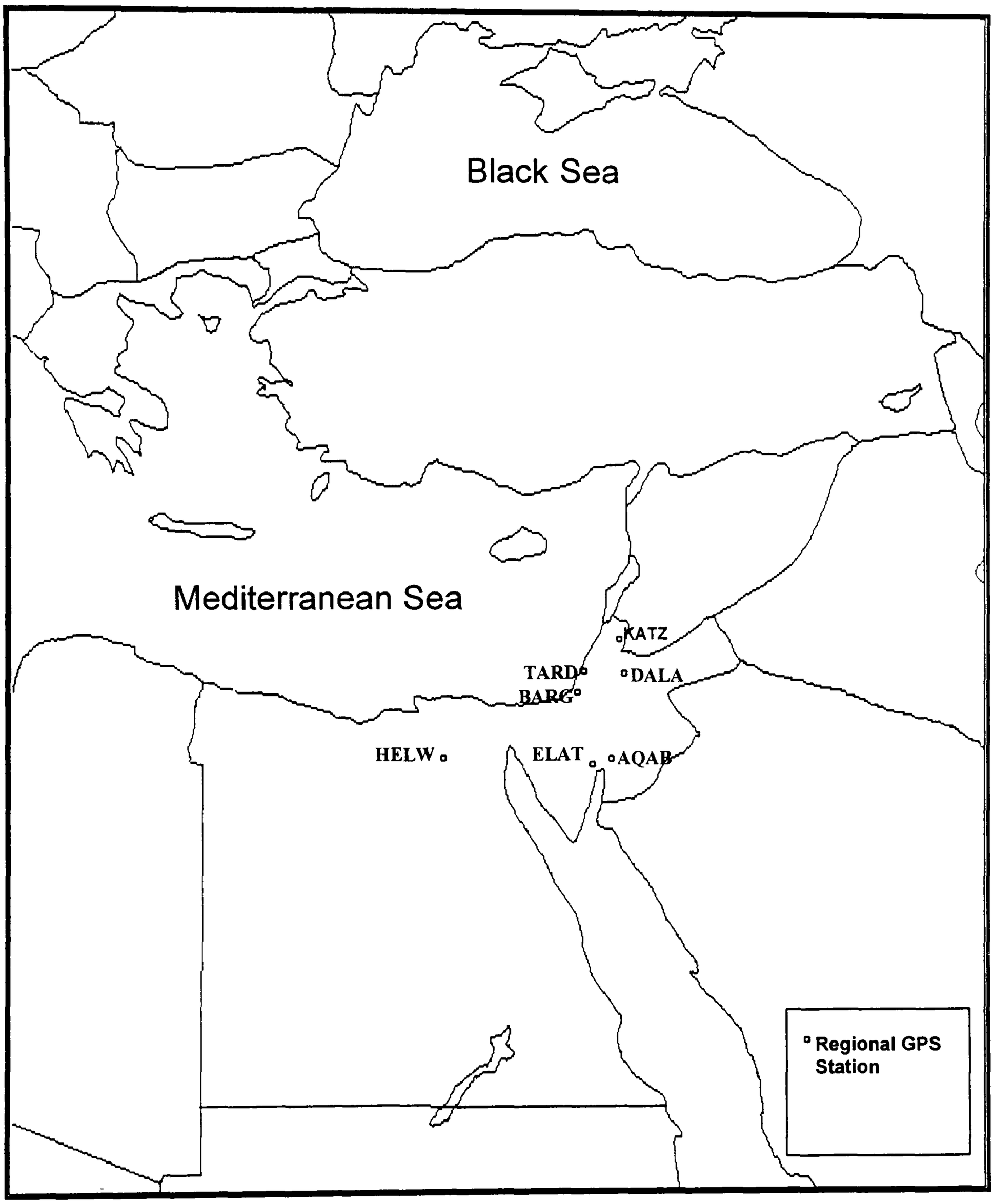

Figure 5.3 Regional Network in November 95 Campaign

5.1.2 GPS Processing Strategy

The EASTMED data have been processed by using the software GAS described in §3.6. In processing, the IGS precise ephemeris and ionosphericly free observable were used, and corrections were applied for tropospheric delay (using the Magnet standard model and solving for tropospheric scale foctors as a stepwise function per station) and a model for antenna phase centre variations. The estimation of the coordinates of the stations were computed with respect to the ITRF93 (epoch 1995.82). Details of the whole strategy are given in the following.

The available data were collected in floppy discs form the observing agencies along with their booking sheets. The conversion of the observation data files from the manufacturers' raw format to RINEX format is carried out using the Bernese Programs TRRINEXO for Trimble receivers and ASRINEXO for Ashtech receivers. Any 24 hour observation data files in RINEX Format were edited using WS (Wordstar) to produce two separate 12 hour observed data files in RINEX format. Then all of the 12 hour observation data files were edited using WS in order to input the L1/L2 phase centre, antenna heights used in GAS.

From the RINEX format observation data file headers, the coordinates were collected for the station from all sessions. Then the collected coordinates were averaged to improve the approximate station positions. The conversion of observation data files from RINEX format to the GAS NOTT2 format was then carried out using the IESSG Program FILTER, with the pseudo-range option used to check the approximate station positions. FILTER was also used to correct large cycle slips and delete any unwanted data, such as satellites which fall and then rise again in the same processing session.

When using GAS in the cleaning stage, cycle slips are detected using double and triple differences for a specified baseline. The station TARD was accepted as the origin station with good approximate coordinates. The source coordinates computed in the ITRF93 (epoch 1995.82) with repect to the IGS station in Wettzell, and with TARD being assumed to be clean from cycle slips.

The baselines relative to TARD were then cleaned using the IESSG Program PANIC in single baseline mode. In this mode, six base satellites were defined providing whole 12 hours cover without a break. If any slips detected on a particular baseline, the slips are cleaned using the IESSG Program SLIPCOR.

This procedures was repeated for all stations and all the sessions. Once all of the baselines in the regional network were cleaned, a network solution was computed for each session using the IESSG Program PANIC, in network adjustment mode. The baseline used in the cycle slip cleaning and network solution are shown in Figure 5.4. After computations of these session solutions, a campaign solution was then computed using the IESSG Program CARNET. Once a campaign solution had been obtained, repeatabilities of the coordinates and baselines were computed using the IESSG Program REPDIF in order to obtain precision estimates (see §3.6.4).

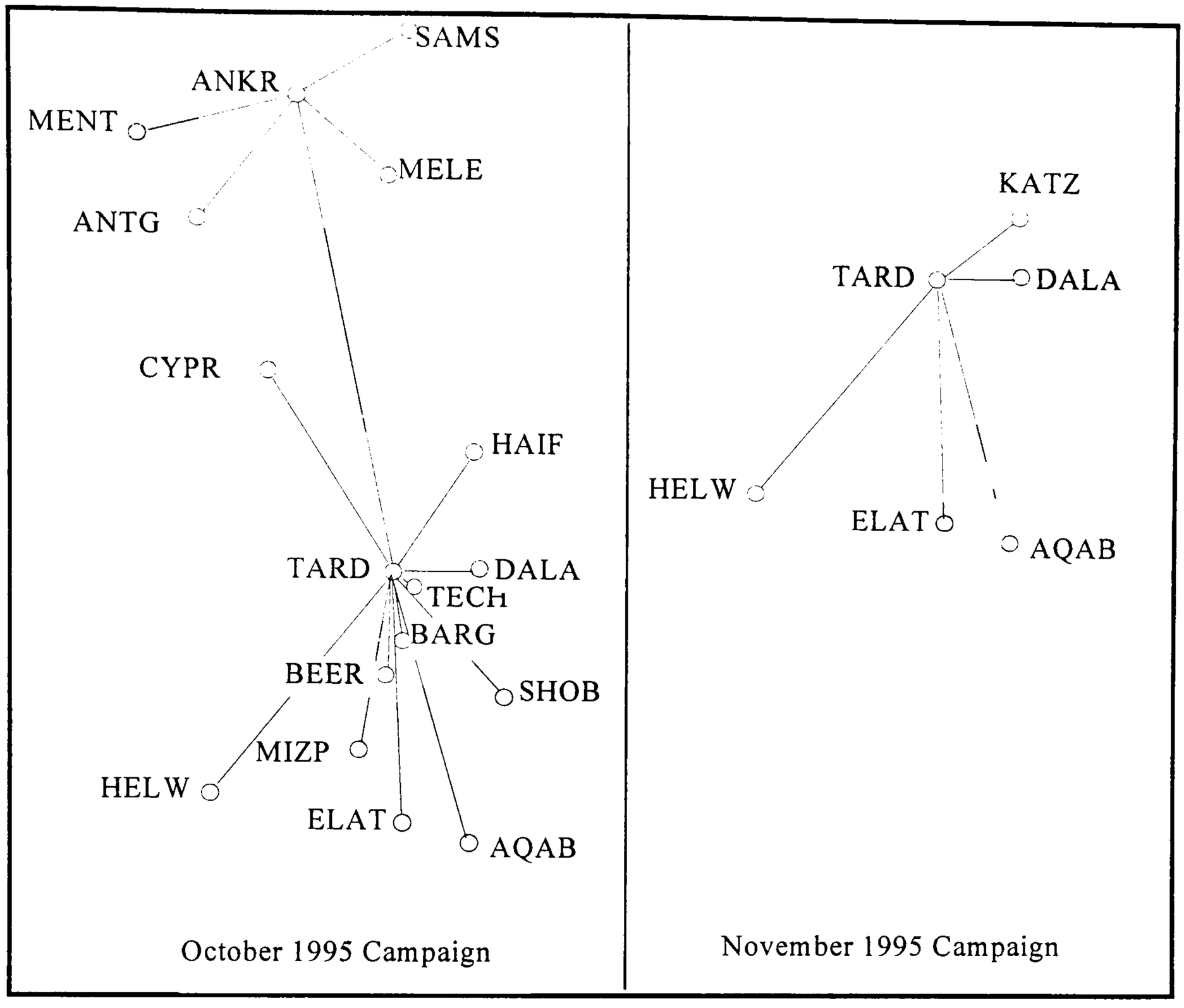

Figure 5.4 Baselines Used in the Cycle Slip Cleaning and Network Solution

5.1.3 Results

The repeatabilities of station coordinates are given in Figure 5.5 for the October 1995 Campaign and and Figure 5.6 for the November 1995 Campaign. In these figures only the five stations common to both campaigns are illustrated.

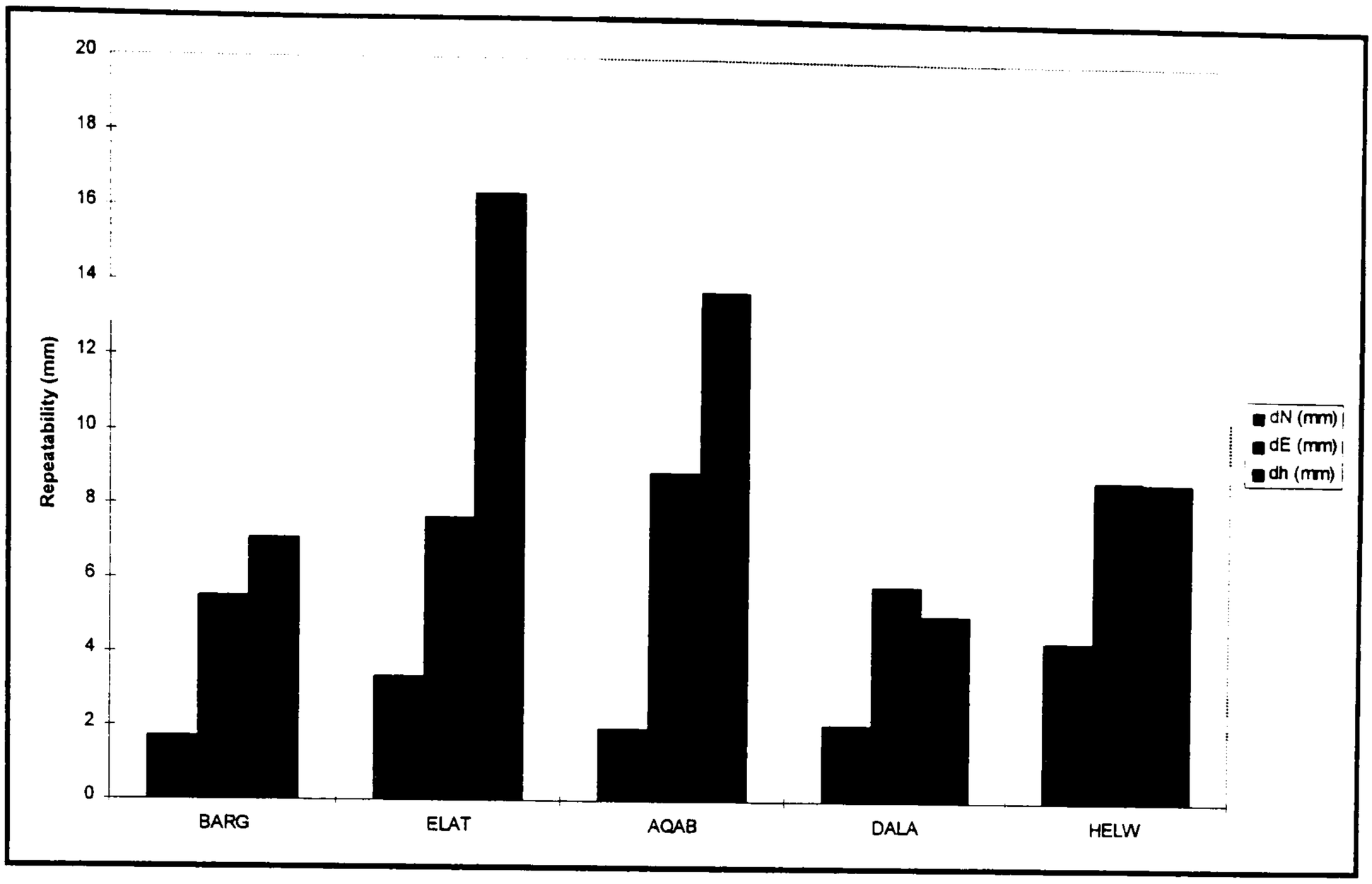

Figure 5.5 Coordinate Repeatabilities in October 95 Campaign

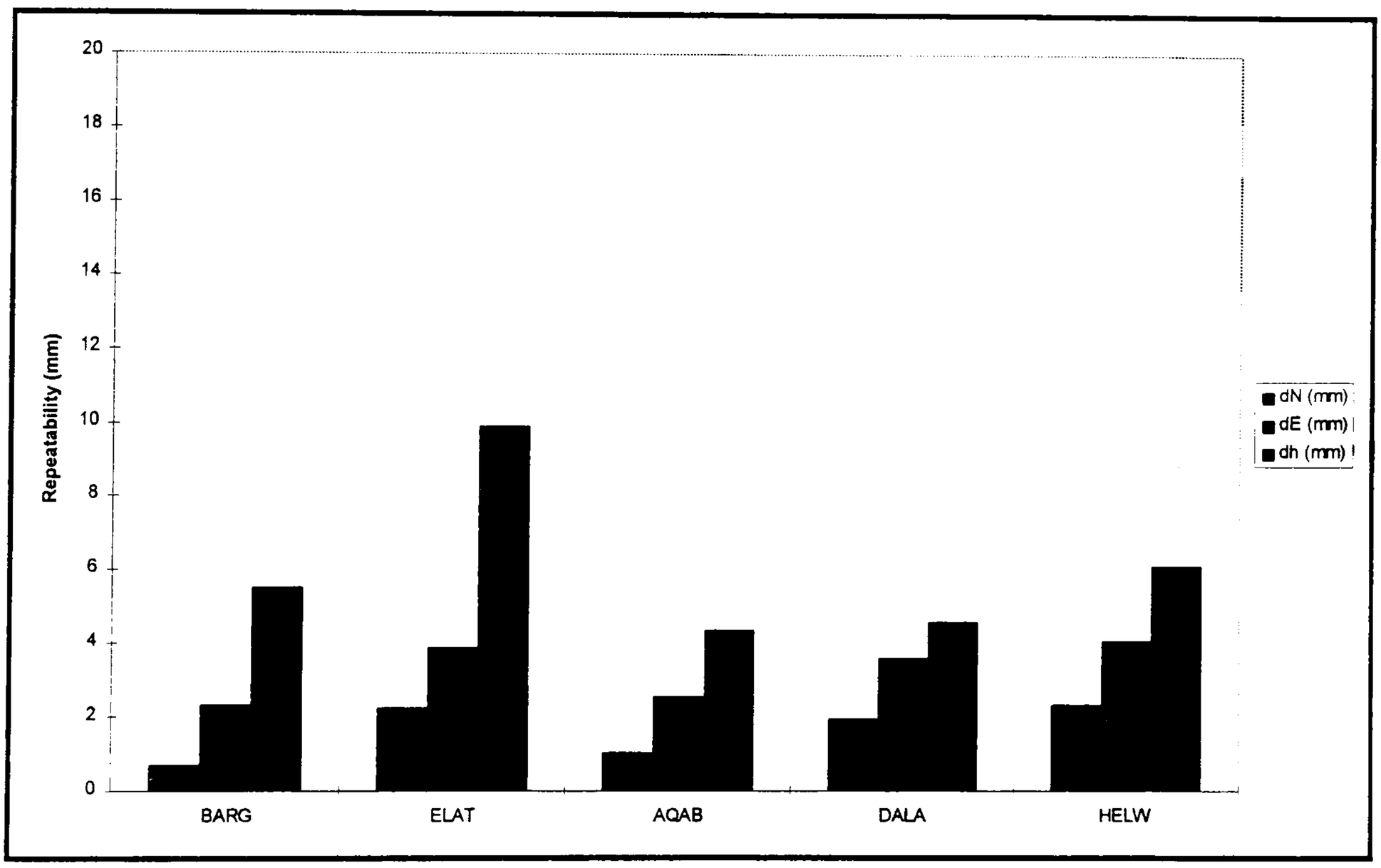

Figure 5.6 Coordinate Repeatabilities in November 95 Campaign

These results demonstrate that the coordinate precisions were slightly better in the November 95 compaign. The plan coordinate precisions being 2 to 9 mm and 1 to 4 mm in the two campaigns. The height precisions being 7 to 16 and 4 to 10 mm in the two campaigns. Here it should be noted that these values are based on the deviations of a single sessional solution from the weighted mean

campaign solution, and do not involve any transformations between sessional and campaign solutions.

The corresponding standard errors for these stations are given in Figure 5.7 for the October 95 Campaign and Figure 5.8 for the November 95 Campaign.

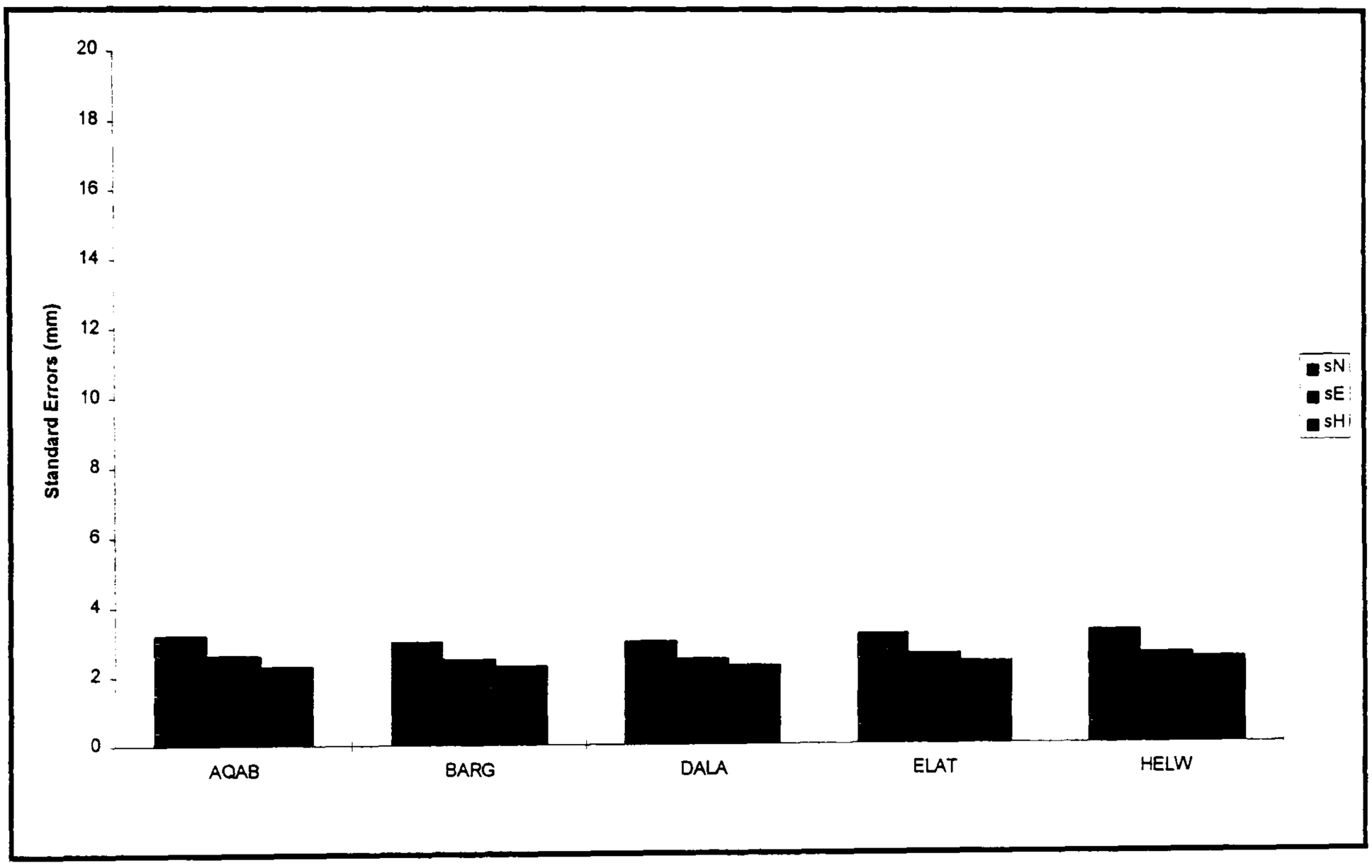

Figure 5.7 Standard Errors in October 95 Campaign

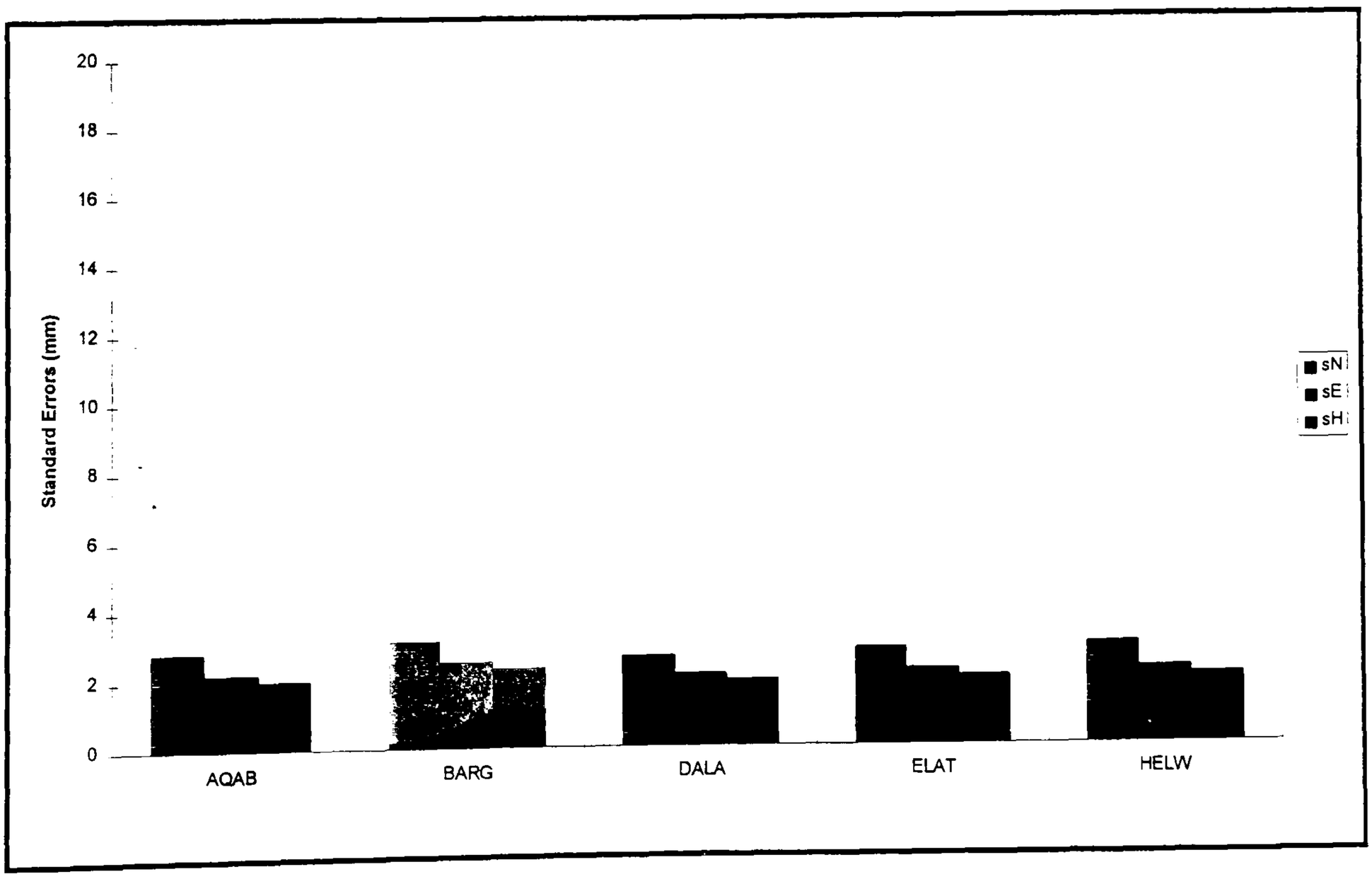

Figure 5.8 Standard Errors in November 95 Campaign

A comparison of the baseline components determined for the two campaigns (October and November 1995) is presented in Table 5.3. These baseline differences are also divided by the baseline length to give the equivalent ppm value from which a station movement may be apparent.

Table 5.3 Baseline Vector Differences (mm & ppm) (Oct 95 minus Nov 95)

From	To	dx (mm)	ppm	dy (mm)	ppm	dz (mm)	ppm	db (mm)	ppm
TARD	BARG	-2.20	-0.04	12.0	0.24	-7.30	-0.15	13.79	0.28
TARD	ELAT	7.50	0.02	17.0	0.06	-23.7	-0.08	28.91	0.10
TARD	AQAB	-11.3	-0.4	19.3	0.068	-2.80	-0.01	4.93	0.01
TARD	DALA	-3.9	-0.04	2.3	0.02	0.1	0.0	4.22	0.05
TARD	HELW	4.9	0.01	-1.8	-0.0	-0.50	-0.0	4.57	0.01
BARG	ELAT	9.7	0.03	5.0	0.02	-16.4	-0.06	19.67	0.08
BARG	AQAB	-9.1	-0.03	7.3	0.03	4.50	0.01	-5.93	-0.02
BARG	DALA	-1.7	-0.02	-9.7	-0.14	7.4	0.10	1.73	0.02
BARG	HELW	7.1	0.01	-13.8	-0.03	6.8	0.01	10.04	0.02
ELAT	**AQAB**	**-18.8**	**-2.5**	**2.3**	**0.3**	**20.9**	**2.79**	**14.87**	**1.99**
ELAT	DALA	-11.4	-0.3	-14.7	-0.049	23.8	0.08	27.62	0.09
ELAT	HELW	-2.6	-0.0	-18.8	-0.05	23.2	0.06	17.19	0.04
AQAB	DALA	7.4	0.02	-17.0	-0.05	2.90	0.01	0.73	0.00
AQAB	HELW	16.2	0.04	-21.1	-0.05	2.3	0.0	26.48	0.07
DALA	HELW	8.8	0.01	-4.1	-0.0	-0.6	0.0	8.68	0.01

It was anticipated that the three survey stations which were not close to the Earthquake epicentre, ie Helwan (HELW) in Egypt, Bar Giyorra (BARG) in Israel, and Dala (DALA) in Jordan, would not have been affected by the Earthquake and would not have moved over the short period of 5 weeks between the two preliminary GPS campaigns. However, we did expect that the two survey stations at Eilat (ELAT) in Israel and Aqaba (AQAB) in Jordan, which are located on either side of the Dead Sea Transform Fault (DSTF) to the North of the Gulf of Eilat/Aqaba, could have been affected by the Earthquake some 120 km to the South.

For the two campaigns the author performed two sequential tests of a global congruency, and detection for significant movement. The procedure of the tests is given by Caspary, (1987).

From the tests, it was found that the two networks were incongruent ($T=7.66 > F_{(11,18)} = 2.375$ with 95% confidence). Then an identification process was run to determine which station (s) contributed most to the failure of the test. Contributions for each stations are tabulated in Table 5.4.

Table 5.4. Contributions of Stations to the Failure of the Congruency Test

Station Code	Contributions
BARG	0.217
ELAT	**6.254**
AQAB	0.338
DALA	0.608
HELW	1.037

From Table 5.4, it is clear that station ELAT had the most effect. From the displacement vector and its corresponding covariances, the significance of displacements are given in Table 5.5.

Table 5.5 Displacement and Corresponding 95% Standard Errors

Station Code	dN (mm)	σN (mm)	dE (mm)	σE (mm)	dH (mm)	σH (mm)
BARG	-8.9	±2.6	12.9	±5.1	0.4	±10.0
ELAT	**-28.5**	**±2.7**	**11.0**	**±4.7**	2.1	±9.9
AQAB	-3.2	±2.7	**25.6**	**±4.8**	0.8	±10.1
DALA	1.0	±2.4	4.8	±4.9	-0.6	±9.4
HELW	-2.0	±2.6	-4.7	±5.0	-0.5	±9.8

From Table 5.5, it is clear that station ELAT moved significanly in a North-Easterly direction and station AQAB moved significantly in an Easting direction. In Table 5.3 it can also be seen that the ELAT/AQAB baseline shows the largest proportional difference which can be attributed to ground movement occurring within the 37 days between the two campaigns. In Figure 5.9, the ELAT/AQAB baseline is illustrated in both October and November 1995 campaigns.

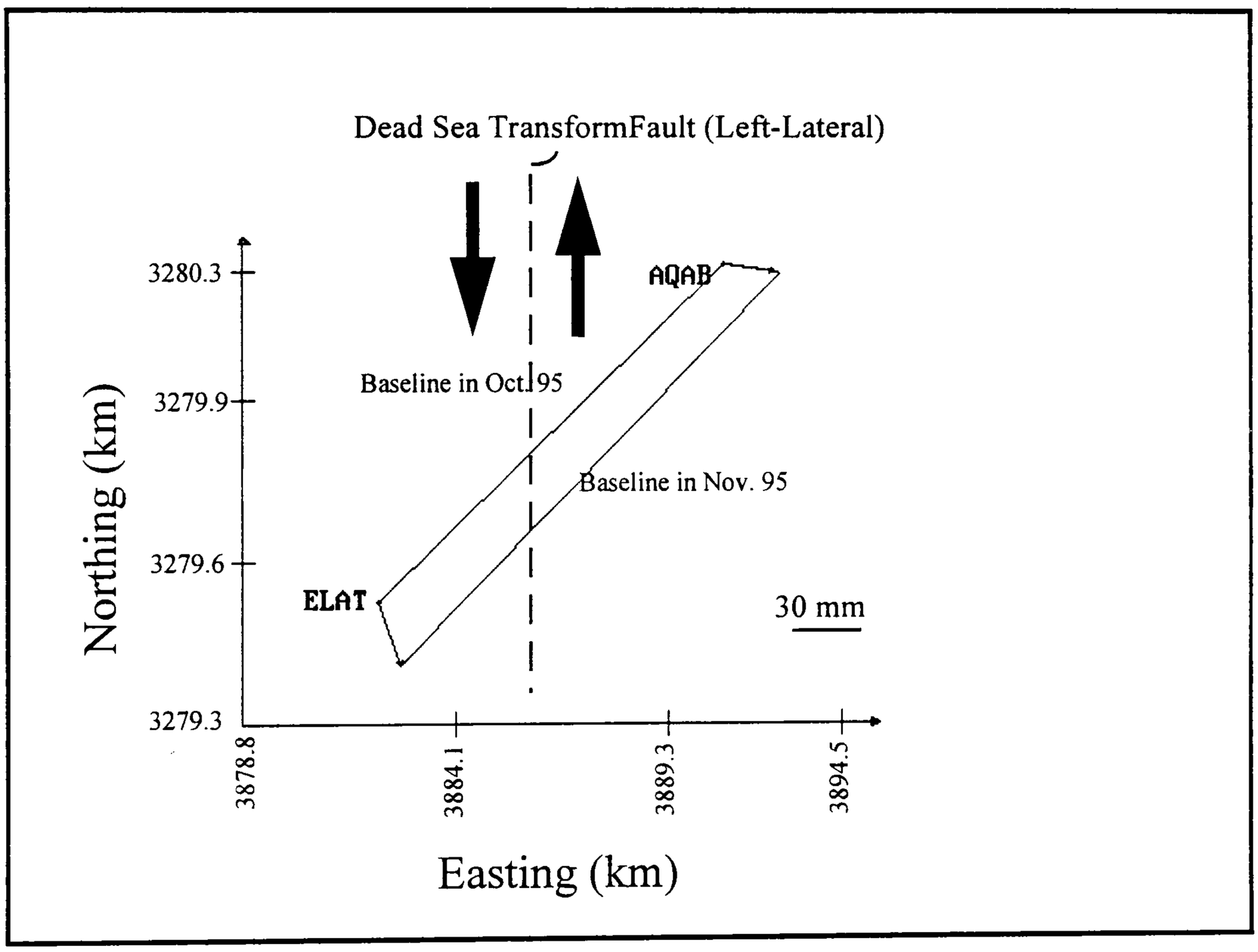

Figure 5.9 Baseline Extension Between Eilat/Aqab

According to the DSTF, it is clear that the station Elat moved in an anticipated direction. The baseline experienced 15mm (or 2 ppm) extension and 0″.68 seconds anticlockwise rotation.

5.1.4 Data Simulation

From the EASTMED Project therefore, there are two campaign solutions available, spanning the Nuweiba earthquake of 22 November 1995. These

campaign solutions have been used as the basis for simulation by the author. From the October 95 Campaign solution, using the NNR NUVEL-1 tectonic plate motion model and adding random noise to it according to its covariances, 10 epochs of simulated backward coordinates have been obtained. Similarly from the November 95 Campaign, by using the same method as before, ten epochs of simulated forward coordinates have been determined. This simulation is illustrated in Figure 5.10 which shows the Latitude-component for ELAT.

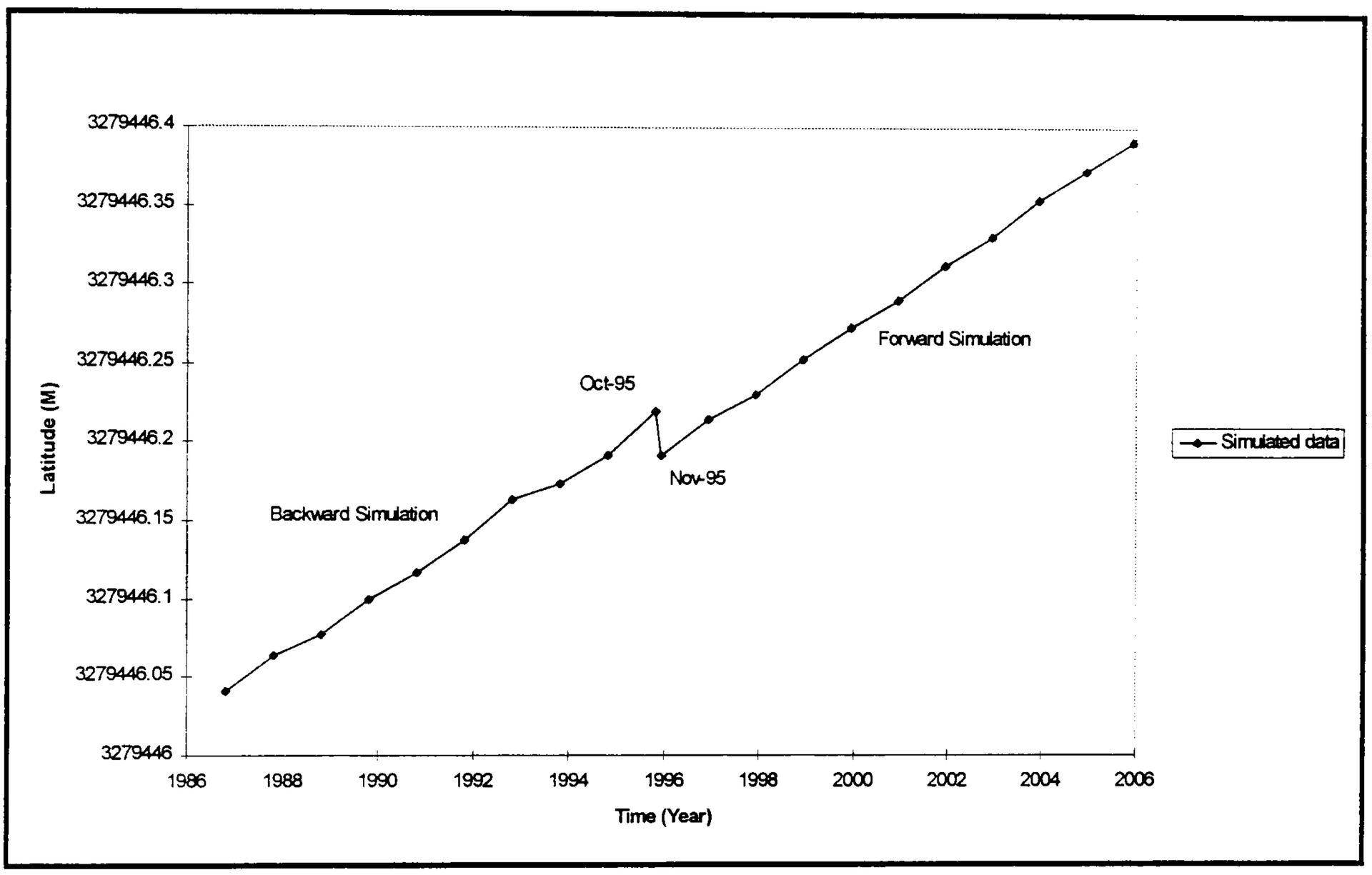

Figure 5.10 Simulation on Station Elat Latitude Component

5.2 EUREF Permanent GPS Network

In August 1987, The International Union of Geodesy and Geophysics (IUGG) held its 19th General Assembly , in Vancouver, Canada. At this assembly, the International Association of Geodesy (IAG) decided to form a new subcommission called EUropean REference Frame (EUREF) within Commission X (Continental Networks), according to the resolutions No.3 and No.4 of the Paris Symposium of Redjustment of the European Triangulation Network (RETrig) Subcommission from May 1987.

Resolution No. 3 of the IAG Subcommission for RETrig : The IAG Subcommission for RETrig stated that there was a need for a continuing evaluation and maintenance of three dimensional reference frames and noted the rapid development of geodetic techniques. Based on this, the Subcommision recommended a new permanent Subcommission of Commission X to replace the RETrig Subcommission for the maintenance and promotions of a three dimensional geometric reference frame for Europe to be established by the IUGG General Assembly in Vancouver.

Resolution No. 4 of the IAG Subcommission for RETrig : The IAG Subcommission for RETrig noted existing specifications for terrestrial measurements refer to conventional techniques and suggested new technology such as GPS is now available for establishing control networks and that an IAG agreed specification is required for general use within Europe. The Subcommission recommended that the new Subcommission recommended in Resolution No.3 of the 1987 Paris Symposium undertakes the design of such specifications.

The EUREF Subcommission started working during the final RETrig symposium in Lisbon in May 1988. In July 1996, at the 21st General Assembly of the IUGG in Boulder, Colorado, USA. it was decided to form a new subcommission called 'Subcommission for Europe' within the frame of Commission X, to take over the functions of the previous 'EUREF Subcommission'.

The EUREF reference frame has mainly been realised using the GPS measurement technique. A first measurement campaign covering Western Europe was carried out in 1989 and since then other GPS campaigns have been carried out, improving the results of previous campaigns and enlarging the territory covered to Eastern Europe.

Taking into account the growing number of permanent GPS stations in Europe, the EUREF subcommission decided to take advantage of this situation for the maintenance of the European Reference Frame (Resolution No.2 of the EUREF Symposium in Helsinki). The permanent GPS stations forming backbone of the EUREF network, which could be densified using local campaigns of finite duration.

The organisation of the EUREF Permanent GPS Network includes the following components: permanent GPS stations, Operational Centres, Local Data Centres, a Regional Data Centre, Local Analysis Centres, a Regional Analysis Centre and a Network Coordinator.

5.2.1 Continuous Data Sets

The EUREF Local Analysis Centres deliver weekly sub-network solutions in SINEX format to the Regional Data Centre. Then a combined weekly solution (European Combined Solution) is computed available using all the data from the Local Analysis Centres and made available in SINEX format within twenty days.

The SINEX stands for **S**olution (Software/technique) **IN**dependent **EX**change Format. It consists of a number of blocks which are mutually related through station codes/names, epochs and/or index counters. Some blocks consist of descriptive lines and/or fixed format fields with numerous headers and descriptive annotations.

The combination of the SINEX files from the Local Analysis Centers is done using the Bernese software which includes a program, ADDNEQ, for the combination of SINEX files together with the estimation of all types of unknowns (coordinates, troposphere, orbit parameters, ERP, etc.).

Only coordinates are estimated during the combination. The geodetic datum of the coordinates is defined by forcing the total free coordinate solution to have no translation and no rotation (for a selected number of 'fiducial' stations) with respect to the ITRF96. The fiducial stations currently used are Brussels (BRUS), Graz (GRAZ), Kootwijk (KOSG), Matera (MATE), Onsala (ONSA), Wettzell (WTZR) and Zimmerwald (ZIMM). The EUREF Permanent GPS Network is shown in Figure 5.11.

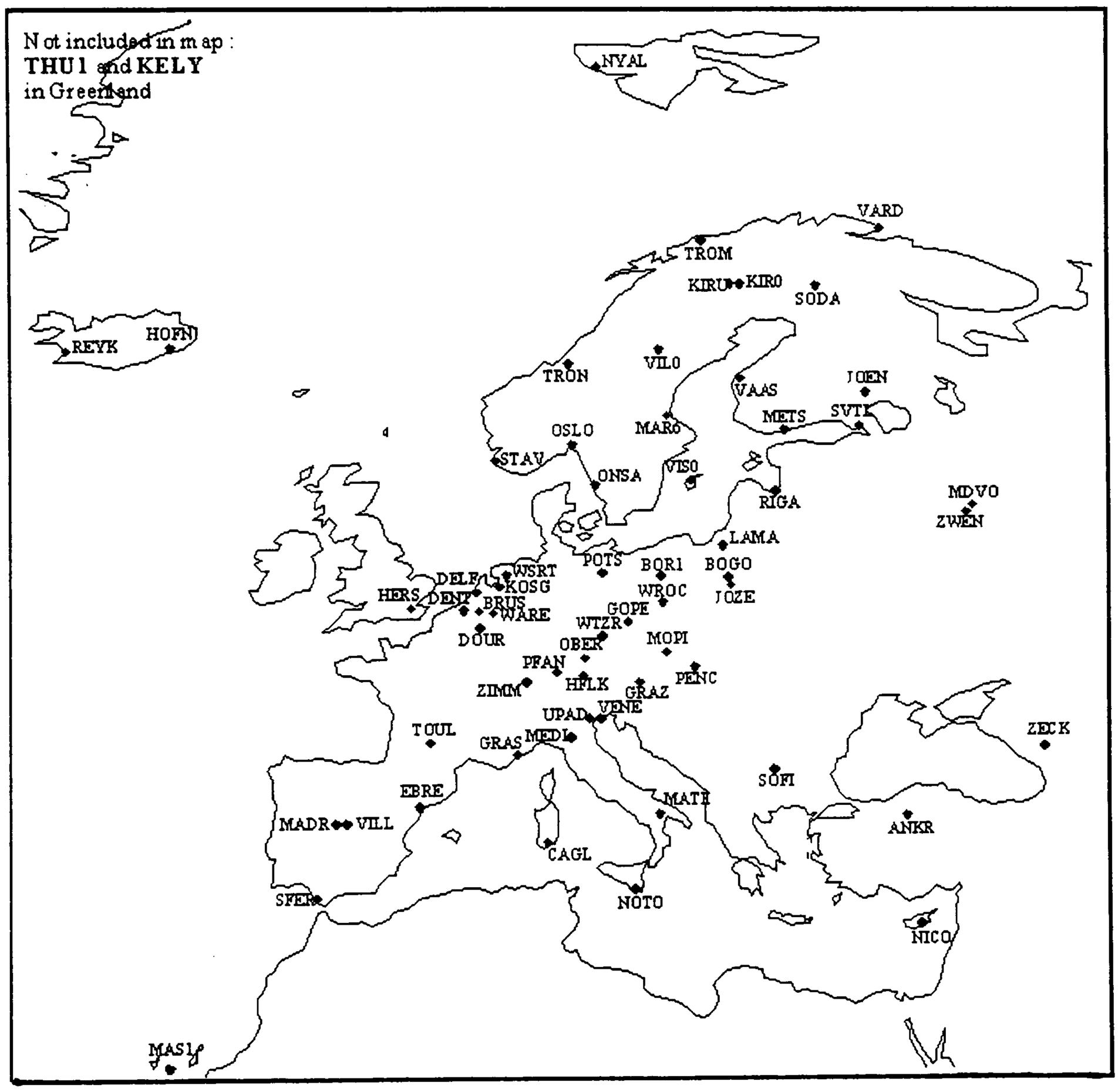

Figure 5.11 EUREF Network of Permanent GPS Stations

For input to the program VEBUK, the author wrote a program to extract the final estimated coordinates and their corresponding variance-covariances from the combined weekly solutions in SINEX format.

For the porpose of this thesis, 111 combined weekly solutions for GPS weeks 834 to 944 have been extracted. In these solutions the EUREF Permanent GPS Network included up to 65 stations located in a number of different countries. For a number of stations, however, the data availability is not continuous. These stations and corresponding unavailability are specified below. Full data availability is given in Appendix A.

There are three stations from *Austria*, Graz (GRAZ), Hafelekar (HLFK) and Pfander (PFAN). Data from GRAZ are fully available. Data from HLFK are unavailable for GPS weeks; 861, 885 to 888, 923, 937, 938, 939 and 940. Data from PFAN are unavailable for GPS weeks; 834 to 900.

There are four stations from *Belgium*, Brussels (BRUS), Dentergem (DENT), Dourbes (DOUR) and Waremme (WARE). Data from BRUS are fully available. Data from DENT and DOUR are unavailable for GPS weeks; 834 and 835. Data from WARE are unavailable for GPS weeks; 834, 835 and 897.

There is one station from *Bulgaria*, Sofia (SOFI) from which data are unavailable for GPS weeks; 834 to 910.

There is one station from *Cyprus*, Nicosia (NICO) from which data are unavailable for GPS weeks; 834 to 910.

There is one station from *Czech Republic*, Pency (GOPE) from which data are fully available.

There is one station from *England*, Hersmonceux (HERS) from which data are unavailable for GPS weeks; 834, 835, 854, 855, 868, 869, 911, 912, 913, 927, 928 and 931 to 944.

There are four stations from *Finland*, Joensuu (JOEN), Metsahovi (METS), Sodankskaya (SODA) and Vaasa (VAAS). Data from JOEN are unavailable for

GPS weeks; 834 to 877 and 880. Data from METS are unavailable for GPS week; 841. Data from SODA are unavailable for GPS weeks; 834 to 892 and 935. Data from VAAS are unavailable for GPS weeks; 834 to 877, 880 and 884 to 887.

There are two stations from *France*, Grasse (GRAS) and Toulouse (TOUL). Data from GRAS are unavailable for GPS weeks; 853 to 872. Data from TOUL are unavailable for GPS weeks; 834 to 913 and 930.

There are four stations from *Germany*, Oberpfaffenhofen (OBER), Potsdam (POTS), Wettzell (WETT) and Wettzell (WTZR). Data from WTZR and POTS are fully available. Data from OBER are unavailable for GPS weeks; 834 to 886. Data from WETT are unavailable for GPS weeks; 871 to 944.

There are two stations from *Greenland*, Kellyville (KELY) and Thule (THU1). Data from KELY are unavailable for GPS weeks; 834, 835, 836 and 847. Data from THU1 are unavailable for GPS weeks; 836, 894 to 900, 921, 922, 930 and 931.

There is one station from *Hungary*, Penc (PENC) from which data are unavailable for GPS weeks; 834 to 842 and 887.

There are two stations from *Iceland*, Hoefn (HOFN) and Reykjavik (REYK). From REYK data are fully available. From HOFN data are unavailable for GPS weeks; 834 to 924.

There are six stations from *Italy*, Cagliari (CAGL), Matera (MATE), Medicina (MEDI), Noto (NOTO), Padova (UPAD) and Venezia (VENE). From NOTO data are fully available. From CAGL data are unavailable for GPS weeks; 834, 835, 836. Data from MATE are unavailable for GPS weeks; 849 to 860. From MEDI data are unavailable for GPS weeks; 834, 835, 836 and 884. From UPAD data are unavailable for GPS weeks; 865, 866, 922, 923, 937, and 938.

Data from VENE are unavailable for GPS weeks; 834 to 862, 864, 865 and 866.

There is one station from *Latvia*, Riga (RIGA) from which data are unavailable for GPS weeks; 834 to 877, 880 and 927 to 942.

There are three stations from *Netherlands*, Delft (DELF), Kootwijk (KOSG) and Westerbork (WSRT). From KOSG data are fully available. Data from DELF are unavailable for GPS weeks; 834 to 840. From WSRT data are unavailable for GPS weeks; 834 to 918.

There are six stations from *Norway*, Ny-Alasund (NYAL), Oslo (OSLO), Stavanger (STAV), Tromsø (TROM), Trondheim (TRON) and Vardo (VARD). From NYAL data are unavailable for GPS weeks; 921 to 944. Data from OSLO, STAV, TRON and VARD are unavailable for GPS weeks; 834 to 877, 880 and 927 to 942. From TROM data are unavailable for GPS weeks; 836, 872, 873, 880, and 891 to 944.

There are five stations from *Poland*, Borowa Gora (BOGO), Borowiec (BOR1), Jozefoslaw (JOZE), Lamkowko (LAMA) and Wroclaw (WROC). Data from BOR1 and JOZE are fully available. From BOGO data are unavailable for GPS weeks; 834 to 859. Data from LAMA are unavailable for GPS weeks; 842 to 848. From WROC data are unavailable for GPS weeks; 834 to 880.

There are four stations from *Russia*, Mendeleevo (MDVO), Svetloe (SVTL), Zelenchukskaya (ZECK) and Zwenigorod (ZWEN). From MDVO data are fully available. From STVL data are unavailable for GPS weeks; 834 to 913 and 930. Data from ZECK are unavailable for GPS weeks; 871 to 944. From ZWEN data are unavailable for GPS weeks; 864 to 967, 902 and 905.

There is one station from *Slovak Republic*, Modra-Piesok (MOPI) from which data are unavailable for GPS weeks; 834 to 877 and 940.

There are five stations from *Spain*, Ebre (EBRE), Madrid (MADR), Maspalomas (MASP), San Fernando (SFER) and Villafranca (VILL). From VILL data are fully available. Data from EBRE are unavailable for GPS weeks; 834 to 874. From MADR data are unavailable for GPS weeks; 872, 873, 888 to 908, 931 to 938, 942 and 943. Data from MASP are unavailable for GPS weeks; 845 to 847. From SFER data are unavailable for GPS weeks; 834 to 856, 891, 934, 935, and 938 to 944.

There are six stations from *Sweden*, Kiruna (KIR0), Kiruna (KIRU), Maartsbo (MAR6), Onsala (ONSA), Vilhelmina (VIL0) and Visby (VIS0). From ONSA data are fully available. From KIRU data are unavailable for GPS weeks; 889 to 893. Data from KIR0 are unavailable for GPS weeks; 834 to 877, 880 and 883 to 887. From MAR6, VIL0 and VIS0 data are unavailable for GPS weeks; 834 to 877 and 880.

There is one station from *Switzerland*, Zimmerwald (ZIMM) from which data are fully available.

There is one station from *Turkey*, Ankara (ANKR) from which data are unavailable for GPS weeks; 856 to 863, 879 and 914.

5.2.2 Stations Not on the Stable Part of Eurasian Plate

Before carrying out any analysis on the data from the EUREF Permanent GPS Network it is worth considering stations which are not located on the stable part of the Eurasian plate, due to the fact that this study is about crustal deformation.

Deformation of the Earth's crust in the Mediterranean Region is governed by the movement of the three major plates, Eurasian, African and Arabian (Figure 5.12). The boundary of the African and the Eurasian plates is delineated by the Azores-Gibraltar Ridge. According to focal plane solutions, the motion between Africa and Eurasia is to be strike-slip at the Azores, changing to overthrust South of Spain and in North Africa (McKenzie, 1970; Udias, 1982). In the plate motion model NUVEL-1 (DeMets et al, 1990), the Eurasian and African plates converge at a rate of 7 mm/year. Between the Eurasian and African plates, the Mediterranean region is characterised by the fragmentation of minor plates from North Africa, followed by collisions of these plates with Southern Europe. Such collision is responsible for wide spread compressive and extensive deformation that play a major role in the formation of the Alpine Orogenic Belt in Western and Central Europe (Le Pichon and Angelier, 1979).

There are at present a number of microplates between Africa and Europe, each in motion with respect to all adjacent plates. The present motion of these plates are complex as shown in Figure 5.12 (Dewey et al, 1973).

The western part of the Eurasia-Africa plate boundary extends from the Azores to Tunisia and is known as the'Iberian-Magrebian' region. This region includes the Gulf of Cadez, the Alboran Sea and the North-Western part of Africa. The seismicity in this region shows earthquakes (M<5) are spread over a wide area, but condencing around the Alboran Sea and surrounding zone. This region is experiencing convergent motion between Iberia and Africa as shown in seismotectonic studies (Davila et al, 1998). In Spain, stations from the EUREF Permanent GPS Network are EBRE located on the Iberic (Eurasiatic), MADR located on Eurasian, MASP located on the African and VILL located on the Eurasian plate.

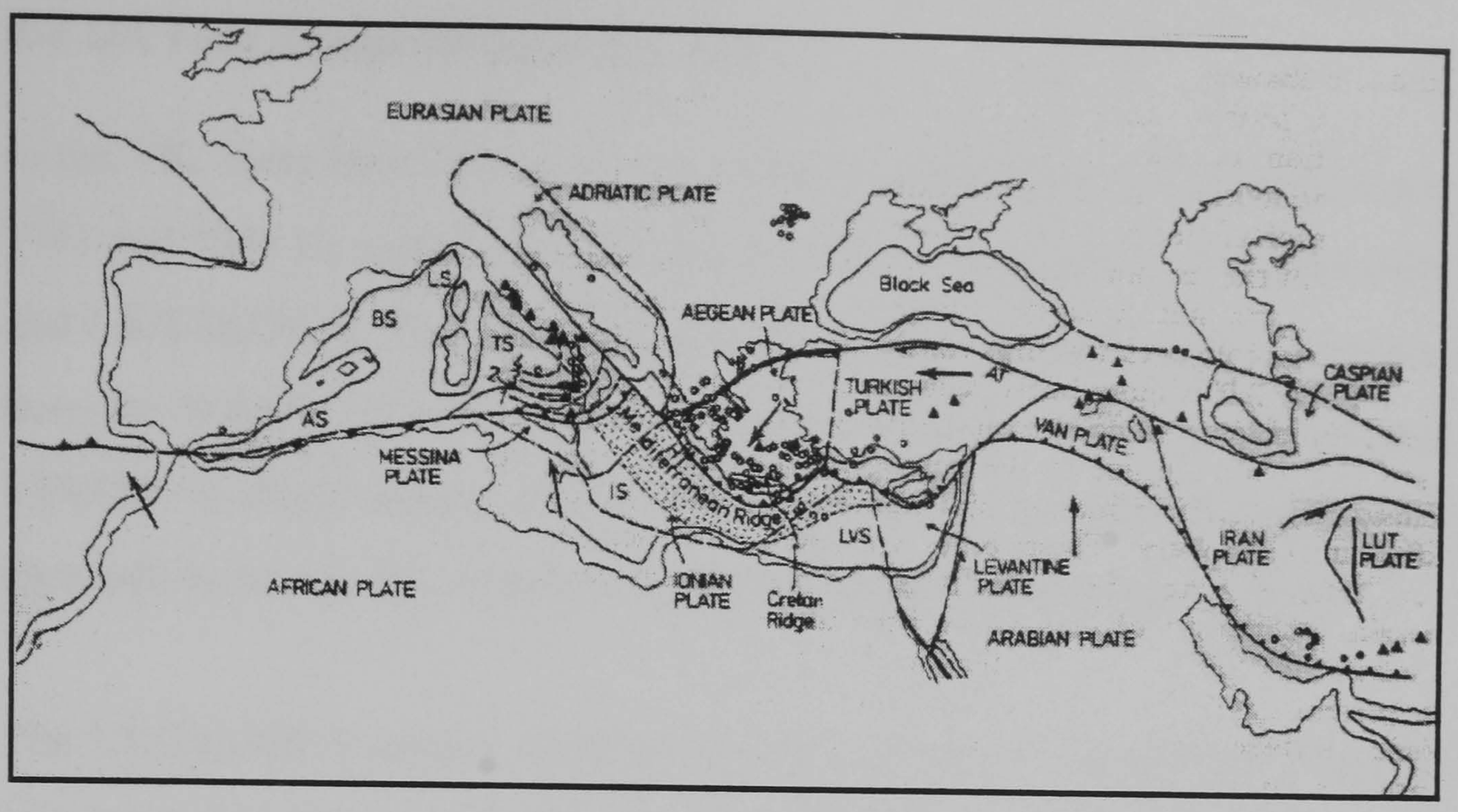

Figure 5.12 Neotectonoics of Alpine System (Dewey et al, 1973). Key to Symbols: triangles=Quatenary and Holocene volcanoes; circles=epicenters of earthquakes deeper than 100km; arrows=slip direction of plate with respect to the Eurasian plate; dashed lines=contours on Benioff zone in hundreds of kilometres. Key to abbreviations: As=Alboran Sea; AT= Anatolian Transform; BS= Balearic Sea; HT=Hellenic Trench; IS=Ionian Sea; LS=Ligurian Sea; LVS=Levantine Sea; TS=Tyrrhenian Sea

Another geodynamically active area is Adria, the African promontory which covers the Adriatic Sea and the Eastern part of the Italian peninsula (Channel et al, 1979). A recent study by Tomasi and Rioja (1998) stated that stations such as MATE and NOTO in Southern Italy are moving by 5mm/year in both a North and East direction with respect to the Eurasian plate. They indicated that these stations are not on the stable part of the Eurosian plate, whereas MEDI shows a small North-Eastern displacement at half the rate of MATE, indicating Adriatic micro plate. In Italy, therefore, the stations in the EUREF Permanent GPS Network are all located on the Adriatic-African plate.

Another geodynamically active area is Turkey. The tectonic setting of this area is well described in §2.4. In Turkey, the ANKR station is located on the Anatolian plate.

5.3 UK Tide Gauge Monitoring Project

In the UK, there have been nine episodic GPS campaigns carried out between 1991 and 1996 as part of three projects namely, UKGAUGE I, EUROGAUGE and UKGAUGE II. The combined data set from these three projects and data from the IRENET 95 GPS camapign, have been used, as input to the program VEBUK, to obtain station velocities for each site. This is mainly for testing the approach to monitoring crustal movement proposed by the author in § 4.5.

The UKGAUGE I project, initiated by the Ministry of Agriculture Fisheries and Food (MAFF) and the Proudman Oceanographic Laboratory (POL), was for monitoring vertical land movements at selected sites of the UK National Tide Gauge Network using GPS between 1991 and 1993. This and the European Commission funded EUROGAUE project which involved sixteen station, including five station in the UK, between 1993 and 1994, were feasibility studies which aimed at establishing the accuracy of GPS height determination. Following on from the success of these projects, MAFF and POL initiated another project (UKGAUGE II) between 1995 and 1996. Details of the combined data set and the GPS processing strategies are detailed in Penna (1997) and summarised in Ashkenazi et al (1998).

5.3.1 Background on Vertical Land Movement and Mean Sea Level

Vertical land movements as described in general in Chapter 2, occur world-wide, at plate boundaries and in plate interiors. Hence any region on the Earth is subject to vertical land movement over different time scales. Tide gauge benchmarks (TGBM) fixed to the Earth are subject to long term vertical land movement. Since TGBMs are used to measure physical sea surface height, it is necessary to distinguish between mean sea level (MSL) changes and vertical land movements.

Mean sea level is a mean of sea level height readings. It is obtained from tide gauge measurements over a certain period at coastal sites. There is numerous

evidence of relative changes in the level of land and sea. In the sea, many of the rocks on continents, including the mountain regions, were laid down as well and consequently uplifted. There are also places where rocks or sediments deposited on land, such as sand dunes are now covered by the sea.

Sea Level changes have been evidenced by studies in many part of the world. In summary, some changes are of limited extent, and presumably reflect local tectonic movement, resulting in local uplift or subsidence. Other changes act over large areas possibly the whole Earth. World-wide simultaneous change in sea level is known as eustatic change. This change spans over half a million years and is associated with the decline of ice caps. In other words, these are glacio-eustatic sea level changes and they may go back well into the Cenozoic glaciation. For further information about sea level changes, the reader is referred to (Ollier, 1981).

A number of studies have been carried out to investigate the secular global sea level change from tide gauge measurements. In one study by Woodworth et al (1990), some results of annual MSLs from some of the longest tide gauge records available in Europe showed that MSLs at Cascais (Portugal) for a period from 1880 to 1985, Brest (France) for a period from 1810 to 1985, Newlyn (UK) for a period from 1915 to 1985, had risen by approximately 15 to 20 cm over 100 years. In Figure 5.13 , a plot of MSLs at different sites is represented. Here it can be seen that in Northern Europe, the MSL trend, is completely different. For example, at Aberdeen (UK) for a period from 1860 to 1985 MSL had been almost constant, however, at Stockholm (Sweden) for a period from 1895 to 1985, the MSL had declined by approximately 40 cm. These results are a combination of a rise in global sea level and local ground movement at the tide gauge site, because of the post-glacial uplift happening in Northern Europe.

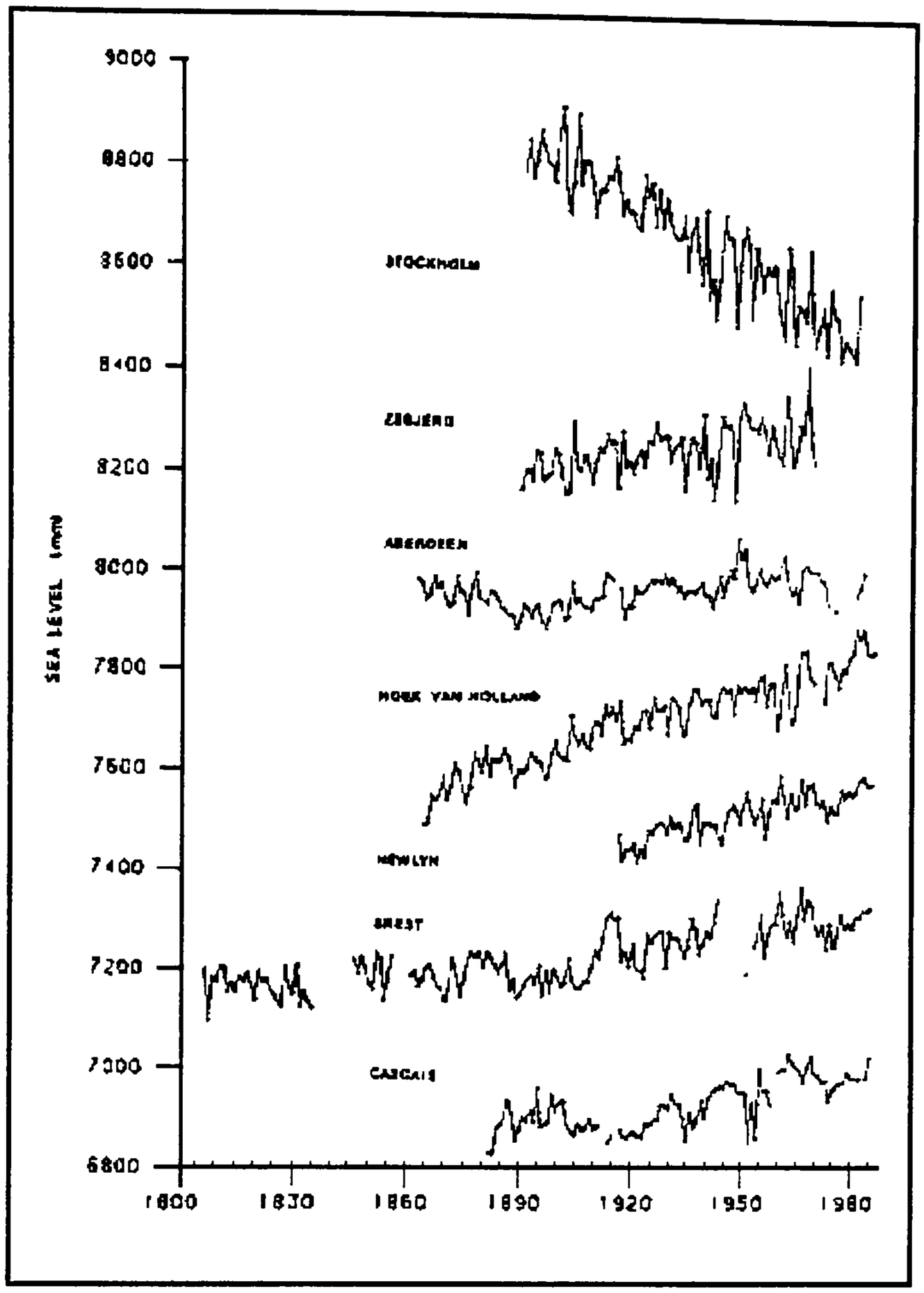

Figure 5.13 European Tide Gauge Records (Woodworth et al, 1990)

As a result, to determine absolute changes in sea level any vertical movements of the TGBM must be isolated from the changes in mean sea level determined from tide gauge records. This may be achieved by the determination of vertical land movements of TGBMs from methods such as space geodesy.

By using GPS and apropriate processing software, it is possible to determine the heights of TGBMs precise enough to determine certain magnitudes of vertical land movement over certain periods of time. From the tide gauge records, typical expected land movements at the tide gauge sites range from 1 to 2 mm per year, up to about 6 to 7 mm per year (Chang, 1995; Penna, 1997).

The GPS measurement strategy employed at UK tide gauge sites to determine the height of a TGBM in the ITRF and to monitor vertical land movement is depicted in Figure 5.14.

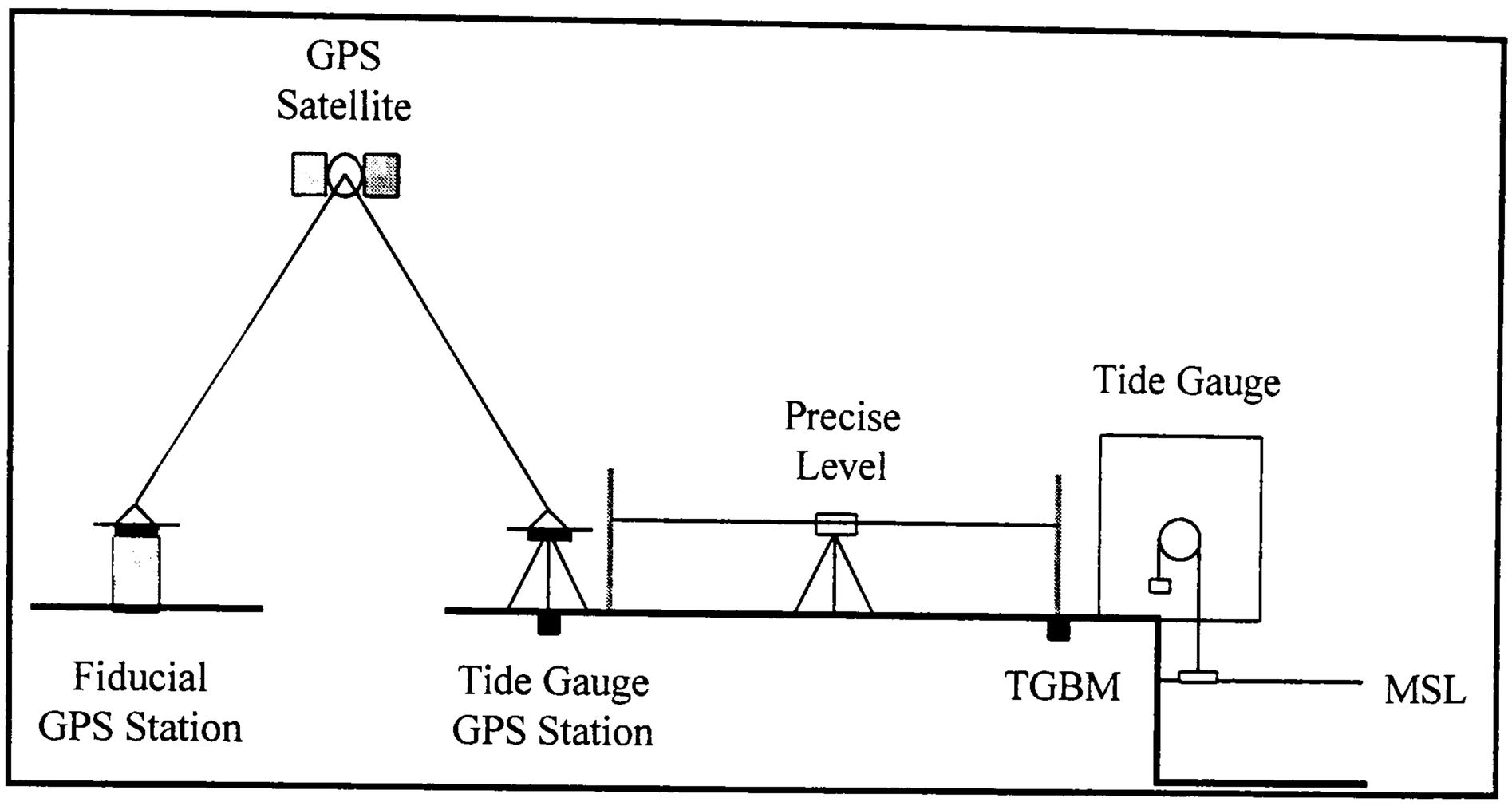

Figure 5.14 Schematic Diagram of the UK Tide Gauge Measurement Strategy (Ashkenazi et al, 1998)

The procedure is that a tide gauge GPS station (TGGS) has been established as close to the tide gauge bench mark (TGBM) as possible, but in a location suitable for GPS measurements and installed in bedrock or a substantial concrete structure such as a pier or sea wall piled down to bedrock. Then the coordinates of the TGGSs are determined in ITRF by making simultaneous GPS observations at both TGGSs and fiducial GPS stations. Following on from this the height of TGBM can be determined by making a local precise levelling connection between the TGGS and the TGBM (Baker, 1993). This is repeated for each episodic GPS campaign which is essential for the determination of vertical land movement.

5.3.2 The Episodic GPS Campaigns

The UKGAUGE I project involved nine tide gauge sites, mainly on the South and East coasts of the UK, observed during three campaigns in September 1991 (UK 91), August 1992 (UK 92) and August 1993 (UK 93). The TGGSs were

occupied for between 8 and 10 hours per day, for 5 consecutive days in all three campaigns (Ashkenazi et al 1993).

The EUROGAUGE project followed this and involved sixteen tide gauge sites, mainly situated along the Atlantic Coast of Europe, including five in the UK, five in France, three in Spain and three in Portugal, observed during two campaigns in November 1993 (EU 93) and March 1994 (EU 94). The TGGSs were occupied for 24 hours per day, for 5 consecutive days in both campaigns (Ashkenazi et al 1996a).

Then, in 1995, the IESSG were responsible for the computation of a new GPS-based zero order control network for Ireland, termed IRENET. For this project, a 6 days duration campaign was carried out in April 1995 (IR 95), involving 24 hour observation sessions at fifteen GPS stations throughout Ireland and Great Britain, including Newlyn and Nottingham (Ashkenazi et al 1996b).

Finally, the UKGAUGE II project was carried out, which involved sixteen tide gauge sites, evenly distributed around the coast of the UK, observed during three campaigns in September 1995 (UK 95A), November 1995 (UK 95B) and September 1996 (UK 96). During each campaign, the TGGSs were occupied for 10 hours per day, for 5 consecutive days.

The 'combined data set' used in this study comprises the data from the nine episodic GPS campaigns which have included observations to one, or more, of the sixteen tide gauge sites in the UK, as detailed above. The availability of the data in the combined data set is summarised in Table 5.6

Table 5.6 Data Availability and GPS Station IDs for the Combined Data Set

Station	**Campaign and Epoch**								
	UK 91	**UK 92**	**UK 93**	**EU 93**	**EU 94**	**IR 95**	**UK 95A**	**UK 95B**	**UK 96**
	91.70	**92.60**	**93.61**	**93.88**	**94.21**	**95.32**	**95.68**	**95.91**	**96.70**
Tide Gauge GPS Stations									
Newlyn	NEW1	NEW1	NEW1	NEW2	NEW2	NEW1	NEW1	NEW1	
Portsmouth	POR1	POR1	POR2	POR3	POR3		POR1	POR1	POR1
Newhaven	NWH1	NWH1	NWH1					NWH1	
Dover	DOV1	DOV1	DOV1	DOV2	DOV2			DOV1	
Sheerness	SHE1	SHE1	SHE1				SHE1		SHEE
Avonmouth							AVO1		AVO1
Lowestoft	LOW1	LOW1	LOW1					LOW1	
Holyhead							HOL1		HOL1
Immingham								IMM1	
Heysham							HEY1		HEY1
Portpatrick	PPA1	PPA1	PPA1				PPA1	PPA1	PPA1
North Shields							NSH1	NSH1	NSH2
Millport							MIL1		MIL1
Aberdeen	ABE1		ABE1				ABE1	ABE1	ABE1
Stornoway				STO1	STO1		STO1		
Lerwick	LER1	LER2	LER2	LER3	LER3			LER2	
Other Stations									
Hermitage	HRM1		HRM1				HRM1	HRM1	HRM1
Nottingham	NOT1		NOT1	NOT1	NOT1	NOT1	NOT1	NOT1	NOT1
IGS Stations									
Tromso	TROM	TROM	TROM	TROM			TROM	TROM	
Metsahovi			METS	METS	METS		METS	METS	METS
Onsala	ONSA	ONSA	ONSA	ONSA	ONSA	ONSA	ONSA	ONSA	ONSA
Kootwijk		KOSG	KOSG	KOSG	KOSG	KOSG	KOSG	KOSG	KOSG
Herstmonceux	HER1	HER1	HER1	HERS	HERS	HERS	HER1	HER1	HER1
Wettzell	WETT	WETT	WETT	WETT	WETT	WETT	WETT	WETT	WTZR
Zimmerwald				ZIMM	ZIMM	ZIMM	ZIMM	ZIMM	ZIMM
Matera		MATE	MATE	MATE	MATE	MATE	MATE	MATE	MATE
Madrid	MADR	MADR	MADR	MADR	MADR	MADR	MADR	MADR	MADR

KEY For Tables 5.6

NEW1 = Newlyn UKGAUGE GPS Station.

NEW2 = Newlyn EUROGAUGE GPS Station.

POR1 = Portsmouth UKGAUGE GPS Station.

POR2 = Portsmouth UKGAUGE Auxiliary GPS Station.

POR3 = Portsmouth EUROGAUGE GPS Station.

NWH1 = Newhaven UKGAUGE GPS Station.

DOV1 = Dover UKGAUGE GPS Station.

DOV2 = Dover EUROGAUGE GPS Station.

SHE1 = Sheerness UKGAUGE GPS Station.

SHEE = Sheerness COGR Station.

AVO1 = Avonmouth UKGAUGE GPS Station.

LOW1 = Lowestoft UKGAUGE GPS Station.

HOL1 = Holyhead UKGAUGE GPS Station.

IMM1 = Immingham UKGAUGE GPS Station.

HEY1 = Heysham UKGAUGE GPS Station.

PPA1 = Portpatrick UKGAUGE GPS Station.

NSH1 = North Shields UKGAUGE GPS Station 1.

NSH2 = North Shields UKGAUGE GPS Station 2.

MIL1 = Millport UKGAUGE GPS Station.

ABE1 = Aberdeen UKGAUGE GPS Station.

STO1 = Stornoway EUROGAUGE GPS Station.

LER1 = Lerwick UKGAUGE Auxiliary GPS Station.

LER2 = Lerwick UKGAUGE GPS Station.

LER3 = Lerwick EUROGAUGE GPS Station.

HRM1 = Hermitage UKGAUGE GPS Station.

NOT1 = Nottingham UKGAUGE GPS Station.

TROM = Tromso IGS Station.

METS = Metsahovi IGS Station.

ONSA = Onsala IGS Station.

KOSG = Kootwijk IGS Station.

HER1 = Herstmonceux Solar Pillar.

HERS = Herstmonceux IGS Station.

WETT = Wettzell Original IGS Station.

WTZR = Wettzell New IGS Station.

ZIMM = Zimmerwald IGS Station.

MATE = Matera IGS Station.

MADR = Madrid IGS Station.

Chapter 6

Deformation Analysis: Testing and Results

In this Chapter, by using the data sets described in Chapter 5, the VEBUK and STRAIN programs will be tested and the results presented.

6.1 Results and Analysis of the EASTMED Project

As detailed in §5.1 a real/simulated data set was formed for the EASTMED Project based on ten epochs of backward station coordinates from the October 95 Campaign, and ten epochs of forward station coordinates from the November 95 Campaign. Between the EASTMED October 95 and November 95 Campaigns, there happened an earthquake (Mw=7.1).

So the data set consists of 22 sets of estimated station coordinates for a 20 year period, beginning in the year 1985 and ending in the year 2005. The question is how to estimate the station velocity, and how to separate the local motion (due to the earthquake) from the global motion (due to plate tectonics).

First, let us consider what happens when a standard Kalman Filter is used to estimate velocities where the measurements (coordinates and their corresponding covariances) are contaminated by an earthquake. In the velocity estimation process, an initial velocity of zero was set and the initial covariances were big (eg 4 cm^2y^{-2}) due to the fact that the velocity is in the order of squared millimeters and the Kalman filter is not sensitive to the initial covariances. The system noise can be determined by experience, hence it has been determined as 0.1 mm^2y^{-4}. Figures 6.1, 6.2 and 6.3 show the velocity components of the station ELAT in the directions Northing, Easting, and Vertical. The station ELAT has been chosen based on the results presented in Table 5.3, where the ELAT/AQAB baseline underwent a significant extension due to the earthquake.

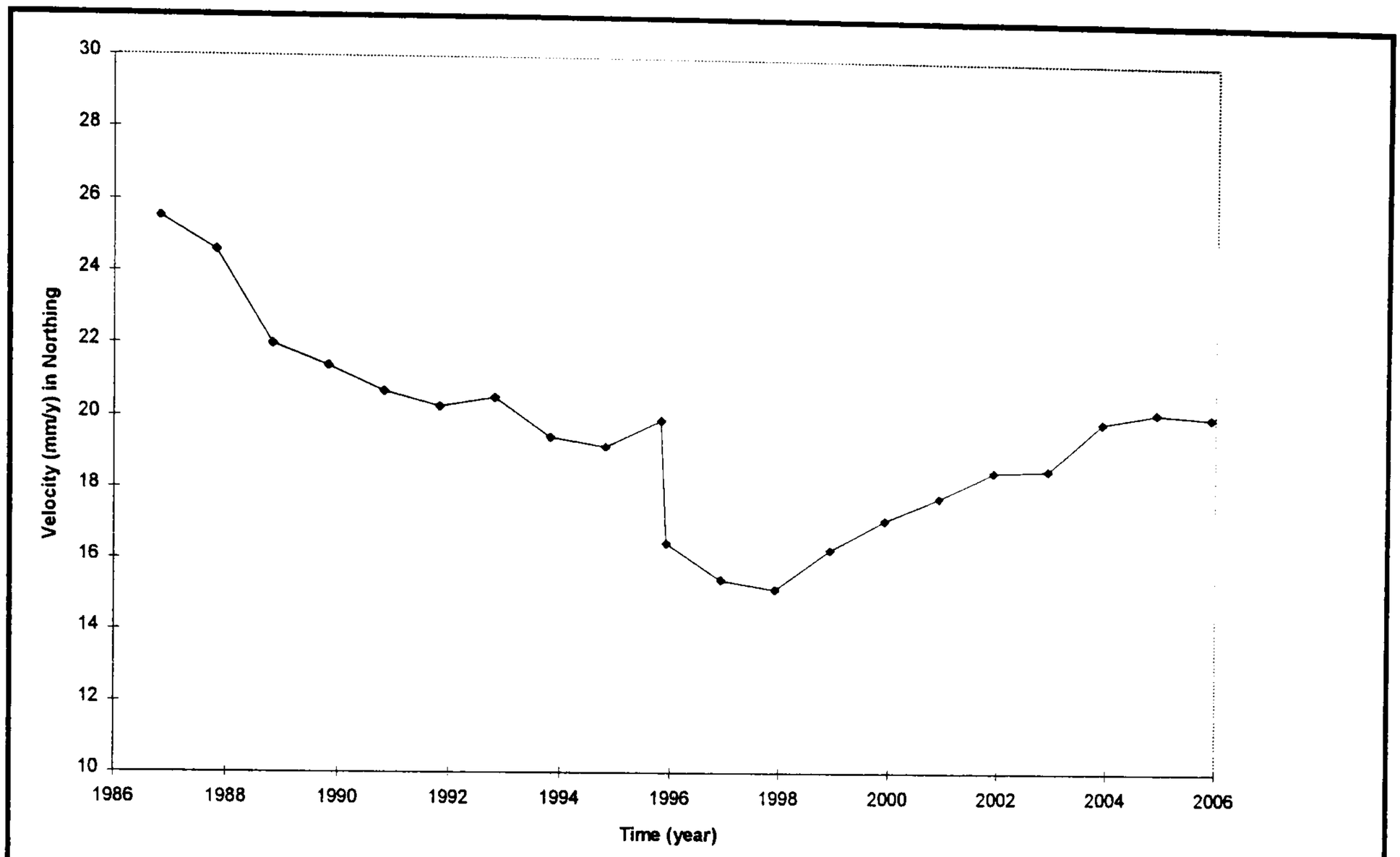

Figure 6.1 ELAT Northing Velocity Estimated by Standard Kalman Filter

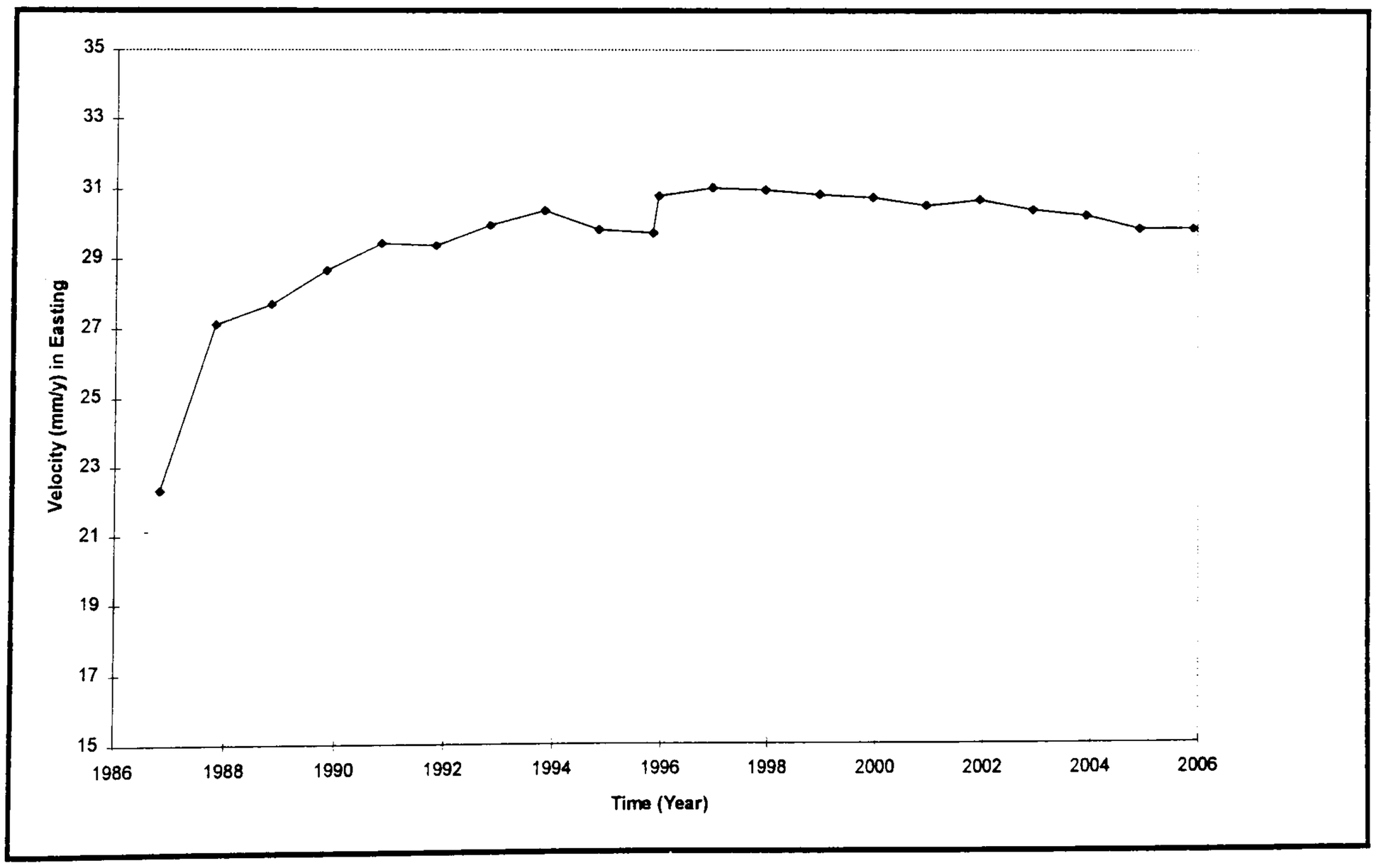

Figure 6.2 ELAT EastingVelocity Estimated by Standard Kalman Filter

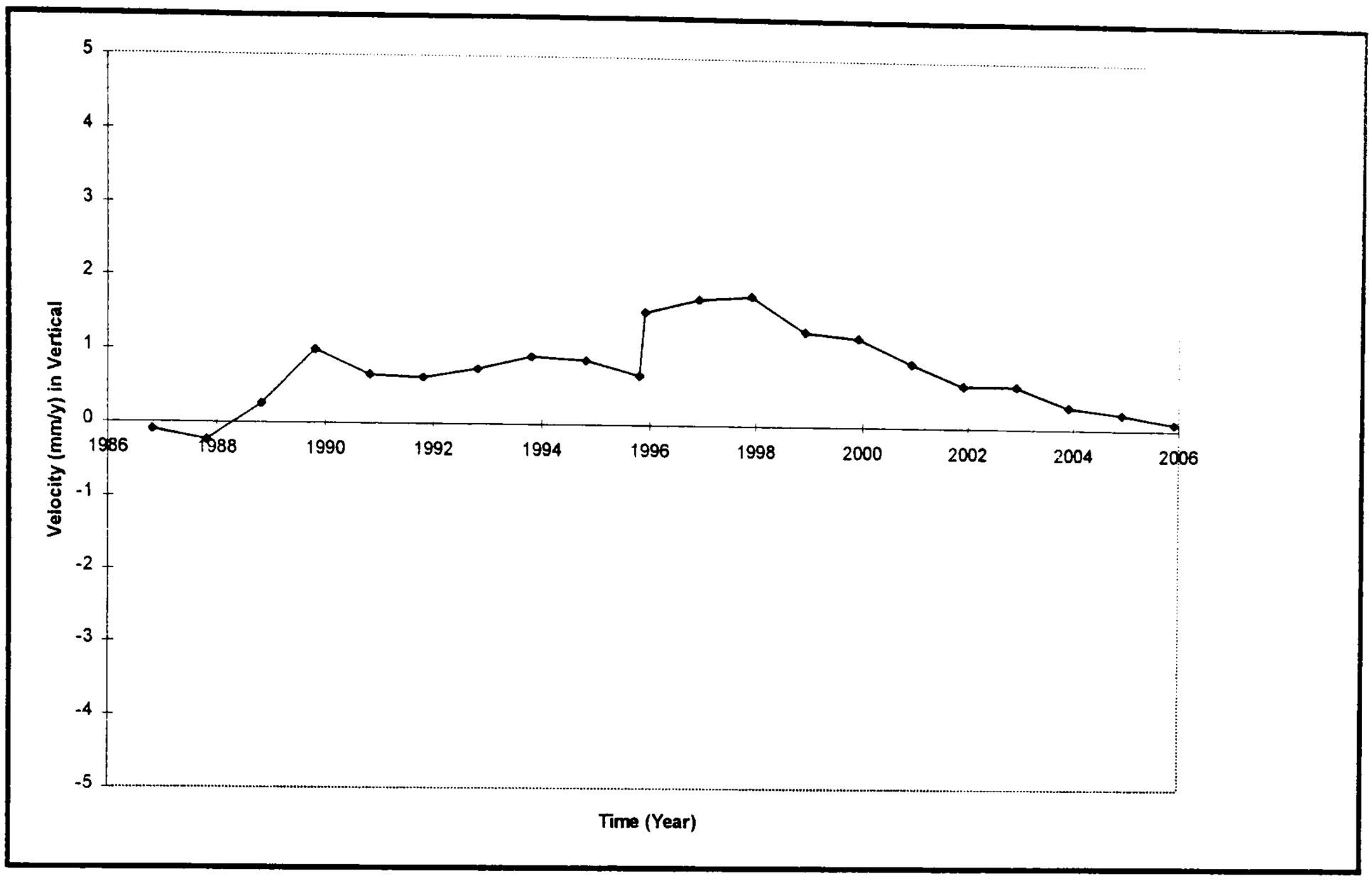

Figure 6.3 ELAT Vertical Velocity Estimated by Standard Kalman Filter

As can be seen from the above figures the earthquake, between 1995.82 and 1995.92, affected the velocity estimated for a number of epochs after it. Using the deformation analysis techniques proposed in § 4.5, the local movement can be detected by carrying out the statistical tests detailed in § 4.3. In Table 6.1, the results of the Local Overall Model (LOM) tests are tabulated. In the table, it can be seen that the LOM statistics are the largest at epoch 12. Although it is below the Chi-square Percentile corresponding to it, at this epoch one can see from the Local Slippage test results, which stations are making the largest contribution to the LOM statistics. This situation can happen if there are a few stations effected by the local motion. Therefore, one can set a scale factor to automatically detect it as part of the test. In this case, the test scale factor was 0.6 which can be specified in the VEBUK control file. In Table 6.2, the Local Slippage test results for epoch 12 only are tabulated. It can be seen that, the maximum values in Table 6.2 correspond to the station Eilat (ELAT), and that these values are significantly different from the other stations.

Table 6.1 LOM Test Statistics Versus Chi-square Percentiles

Epoch Number	LOM Test Statistic	Chi-square Percentile
2	0.25	62.77
3	17.91	62.77
4	16.29	62.77
5	29.58	62.77
6	25.56	62.77
7	25.34	62.77
8	17.40	62.77
9	33.52	62.77
10	18.53	62.77
11	6.15	62.77
12	**47.90**	**66.19**
13	7.58	66.19
14	5.57	66.19
15	6.34	66.19
16	3.30	66.19
17	6.29	66.19
18	10.96	66.19
19	5.06	66.19
20	6.05	66.19
21	1.05	66.19
22	7.47	66.19

Table 6.2 Local Slippage Test Results for epoch 12

Station Name	(LST) in Northing	(LST) in Easting	(LST) in Vertical
BARG	-8.17	6.06	5.42
ELAT	**-41.47**	**21.13**	**29.02**
DALA	3.36	-6.37	-0.94
AQAB	4.71	11.43	-2.74
HELW	11.45	-10.88	-4.39
KATZ	2.83	-3.76	0.37
CYPR	1.44	-1.31	-1.29
HAIF	1.99	-1.48	-0.71
TECH	2.11	-1.51	-0.84
BEER	2.46	-1.45	-0.90
MIZP	2.37	-1.27	-0.79
SHOB	2.71	-1.58	-1.06
ANKR	0.81	-1.19	0.07
SAMS	0.51	-1.29	0.16
MELE	1.19	-1.12	-0.34
MENT	1.33	-0.80	0.20
ANTG	1.51	-0.99	-0.28

After the detection, according to the procedures outlined in § 4.5, one can either select a Fading Memory or Adaptive Filter approach to overcome this problem. In Figures 6.4, 6.5 and 6.6, the effect of local motion (at epoch 12) on the consecutive epochs has been reduced by using the Fading Memory approach.

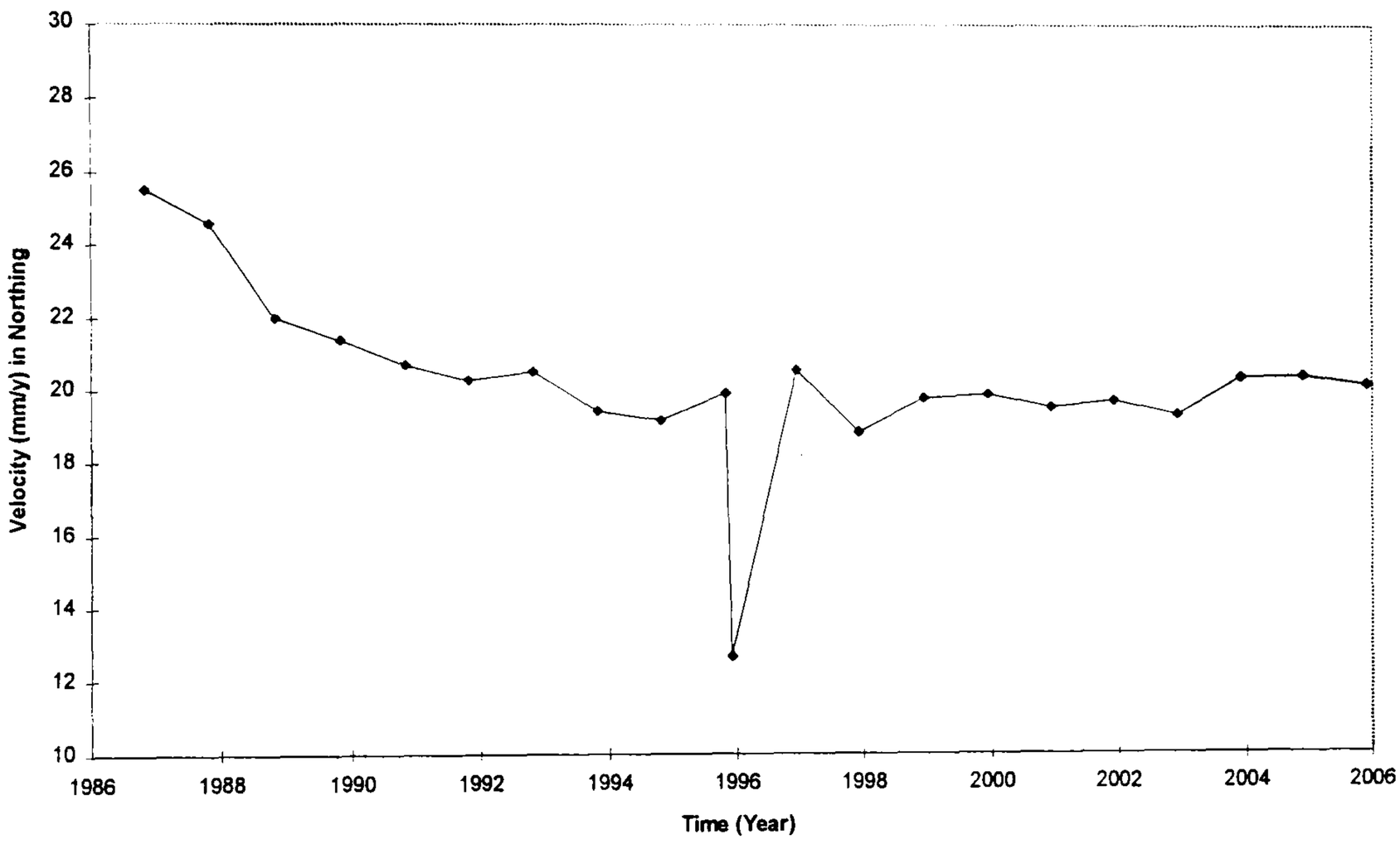

Figure 6.4 ELAT Northing Velocity Estimated by Fading Memory Approach

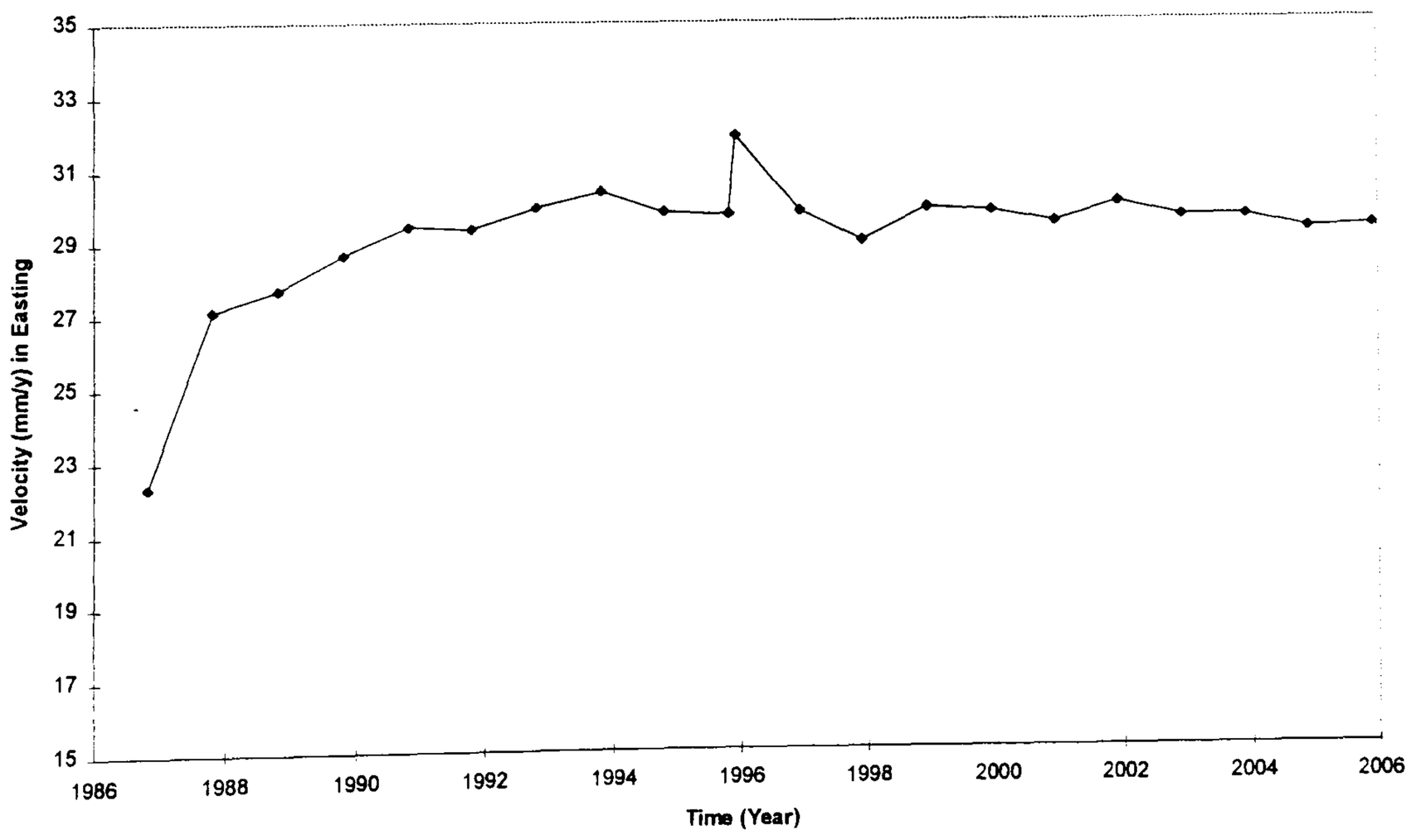

Figure 6.5 ELAT Easting Velocity Eastimated by Fading Memory Approach

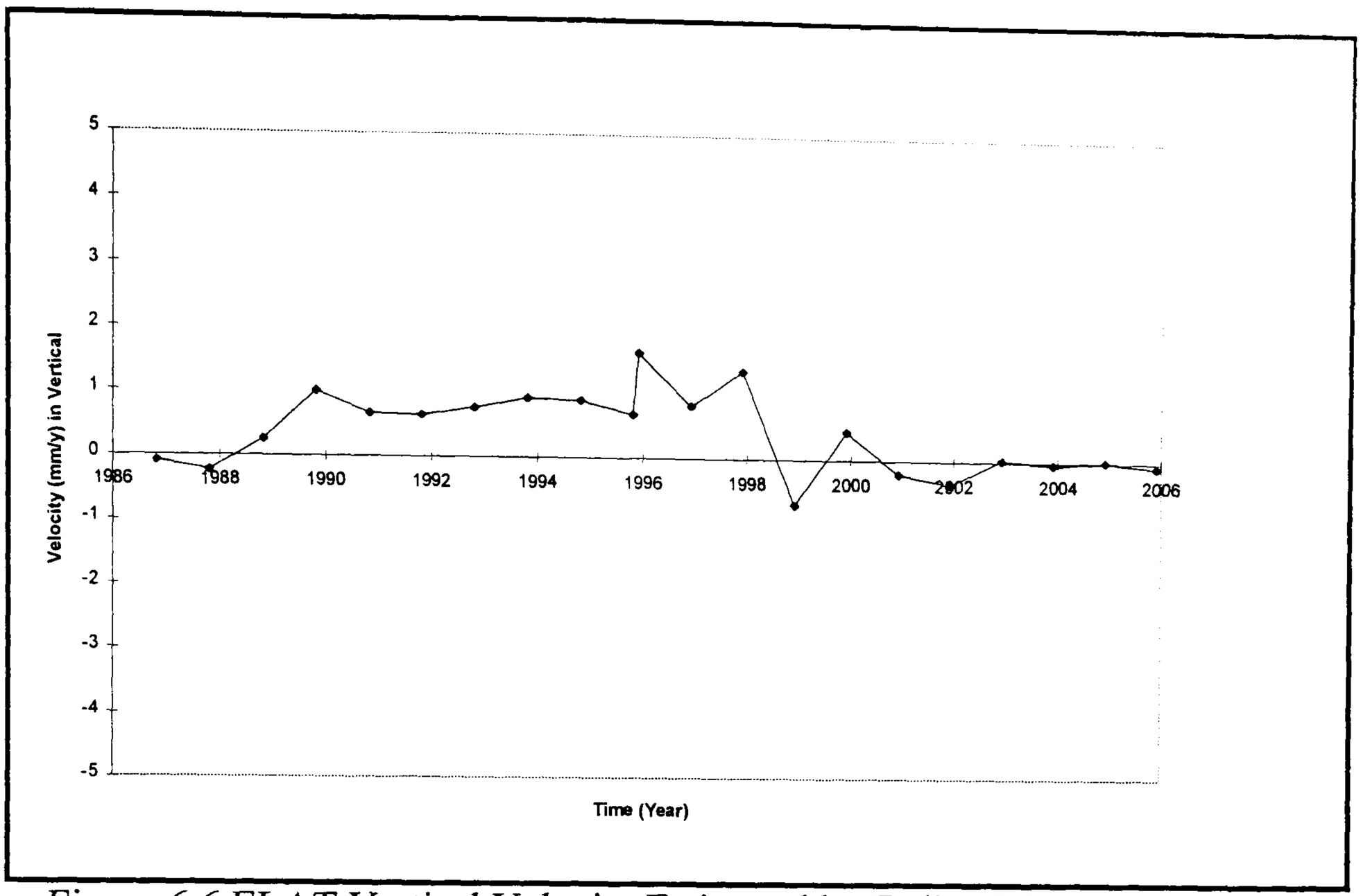

Figure 6.6 ELAT Vertical Velocity Estimated by Fading Memory Approach

Using the Fading Memory approach, the decay factor (Equation 4.42) has to be determined by experience. In this case, the decay factor was set to 5. From Figures 6.4 and 6.5, the Northing and Easting velocities are relatively much better than those estimated by the standard Kalman filter, shown in Figures 6.1 and 6.2. However, in the Fading Memory approach, the vertical velocity component is slightly worsened. This is due to the fact that the height component covariances are higher than those of the plan coordinates.

Figures 6.7, 6.8 and 6.9 show the velocities when the local motion at epoch 12 has been estimated and eliminated by the Adaptive Filter approach. In the Adaptive Filter approach the local motion has been estimated for ELAT as -28 mm in Northing, 12 mm in Easting and 3 mm in Vertical. These local motions are subtracted from the coordinates and filtered by using the Standard Kalman filter. As the Adaptive Filter approach involves complex computation and requires more computer power, it is only used when a local motion (or bias) has occurred.

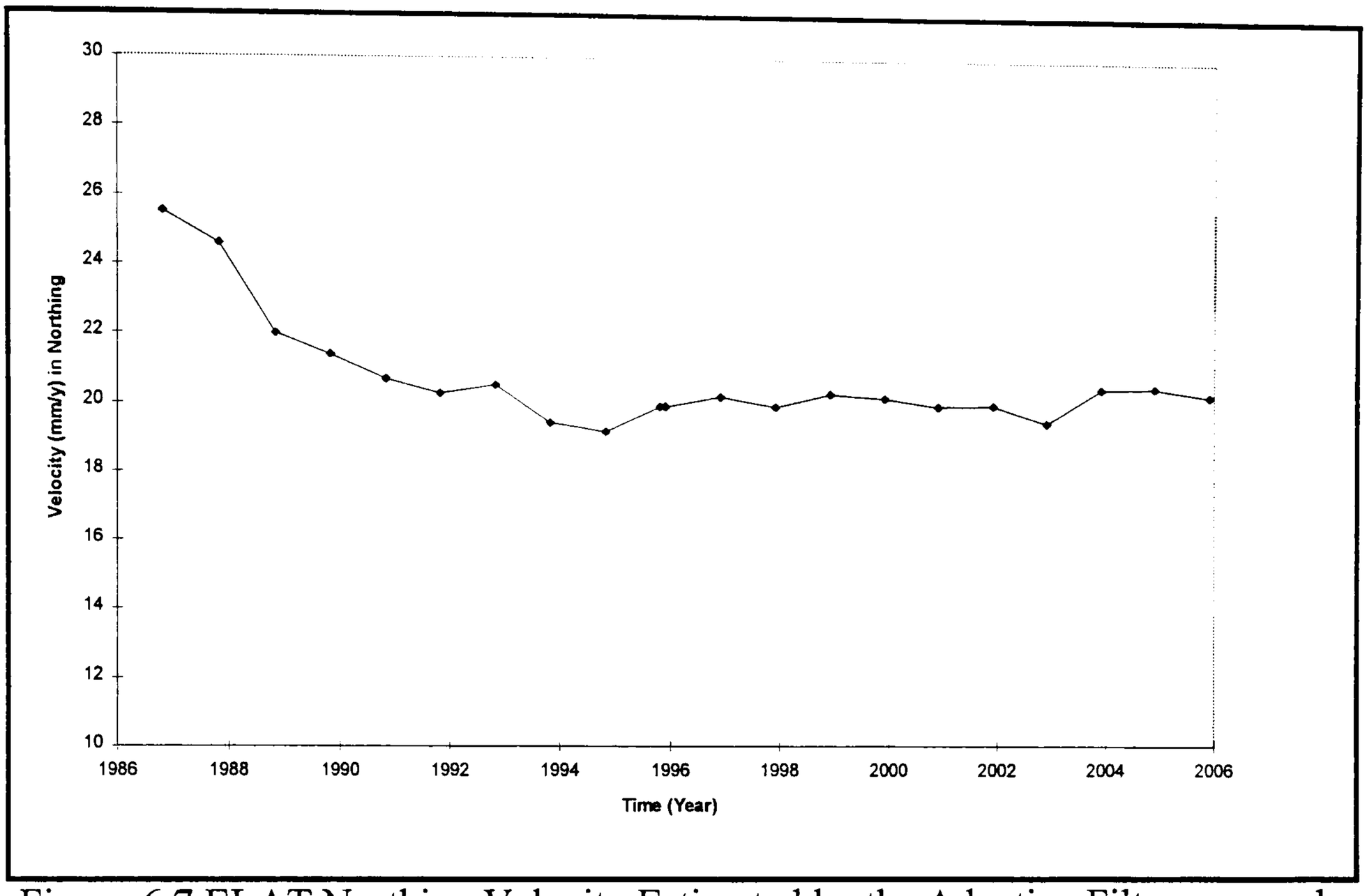

Figure 6.7 ELAT Northing Velocity Estimated by the Adaptive Filter approach

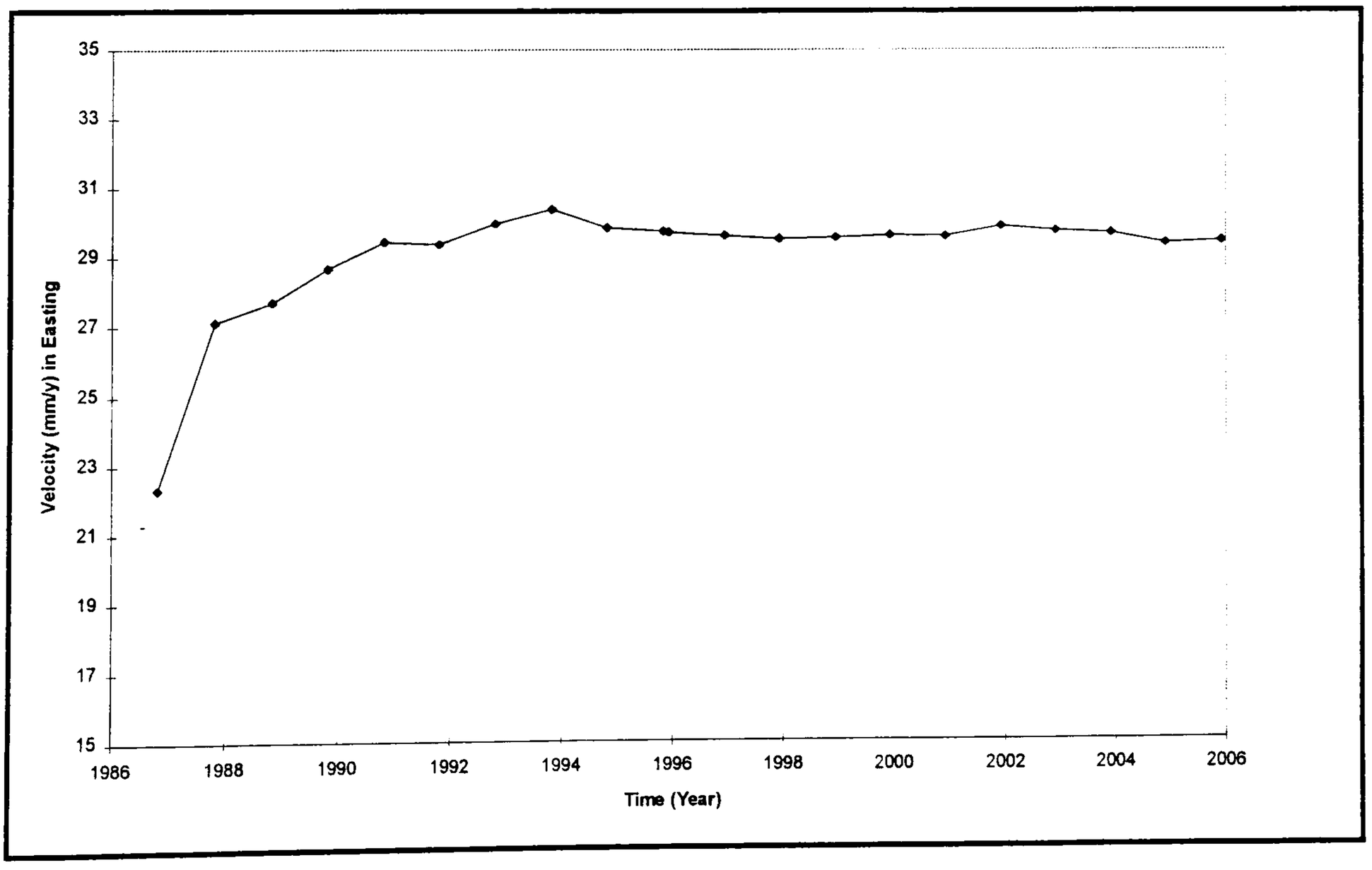

Figure 6.8 ELAT EastingVelocity Estimated by the Adaptive Filter Approach

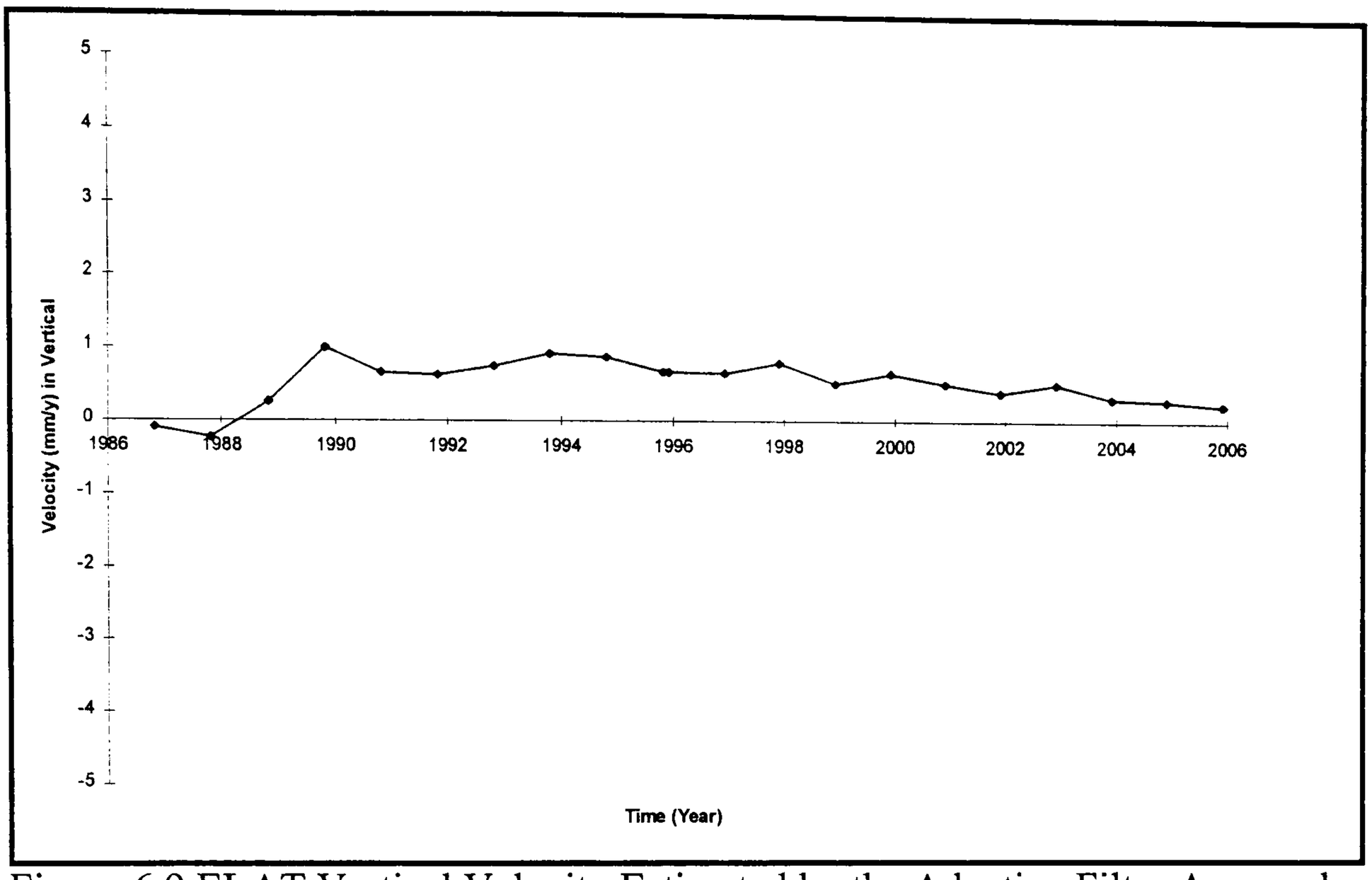

Figure 6.9 ELAT Vertical Velocity Estimated by the Adaptive Filter Approach

Having shown that the VEBUK program can detect a local motion (or bias), estimate the magnitude, eliminate it from the coordinates and then estimate the velocity, the question at this stage is how accurate the estimated velocity is. The following comparisons are made for three stations ELAT, ANKR and KATZ.

The criteria used to choose the above stations were

- ELAT - contaminated by the effect of the earthquake,
- ANKR - not available after the October 95 Campaign,
- KATZ - not available until the November 95 Campaign

In the following figures the computed velocities are compared with those calculated by simple differencing and those calculated using the NNR-NUVEL-1 model. In this section, only one horizontal component is presented as the velocities of the second horizontal component follow the same pattern, and the plate tectonic motion model only represents horizontal movement.

Figures 6.10, 6.11 and 6.12 represent the Northing velocities for ELAT, ANKR and KATZ respectively. In each case, the dotted line represents the velocity calculated by simple differencing, the dashed line represents the NNR-NUVEL-1 velocity, and the solid line represents the velocity estimated by using the deformation analysis technique proposed in § 4.5. In the latter case, the Adaptive Filter approach was used to overcome the local motion that occurred between the two campaigns of the EASTMED Project.

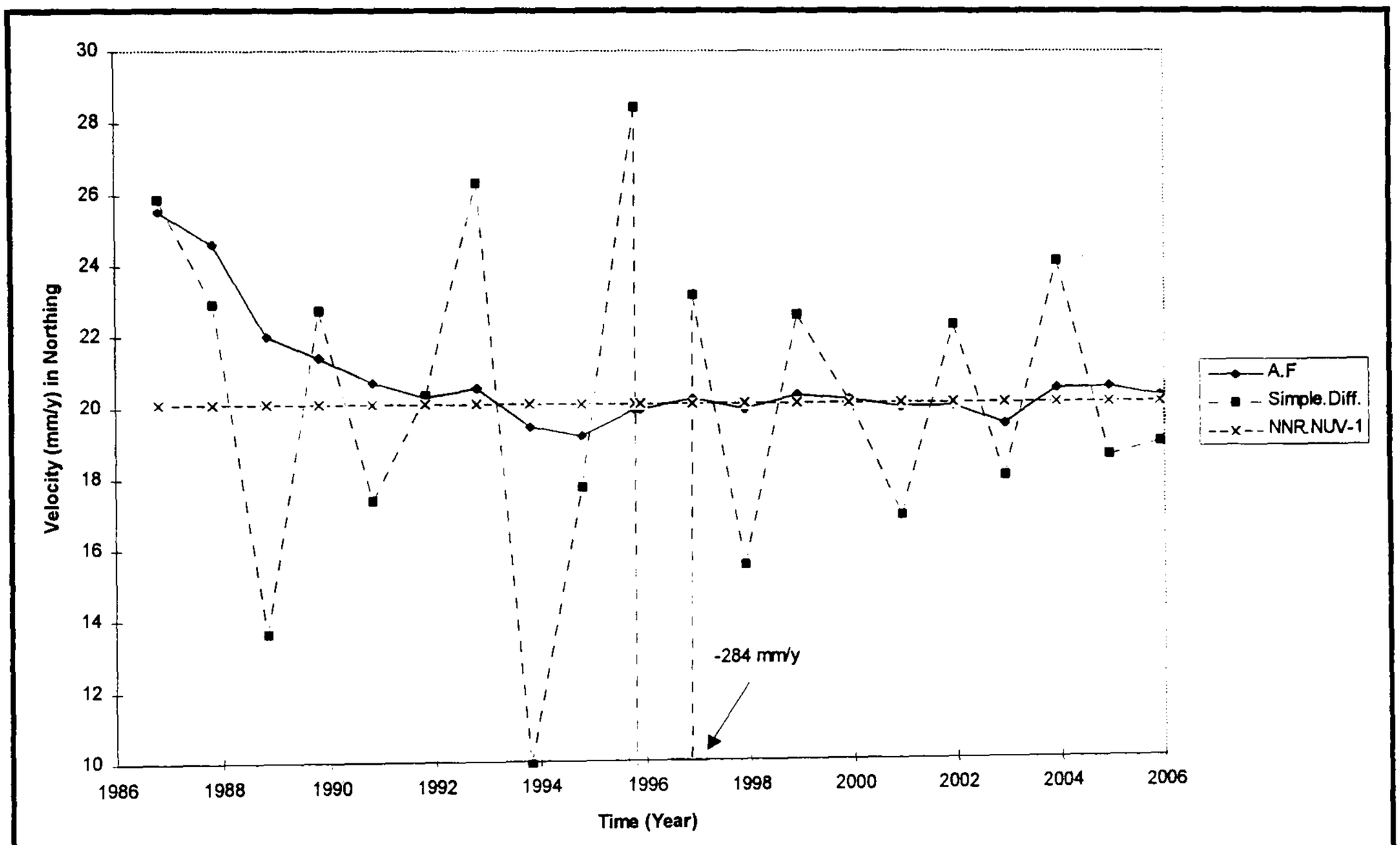

Figure 6.10 Velocity Comparison for ELAT

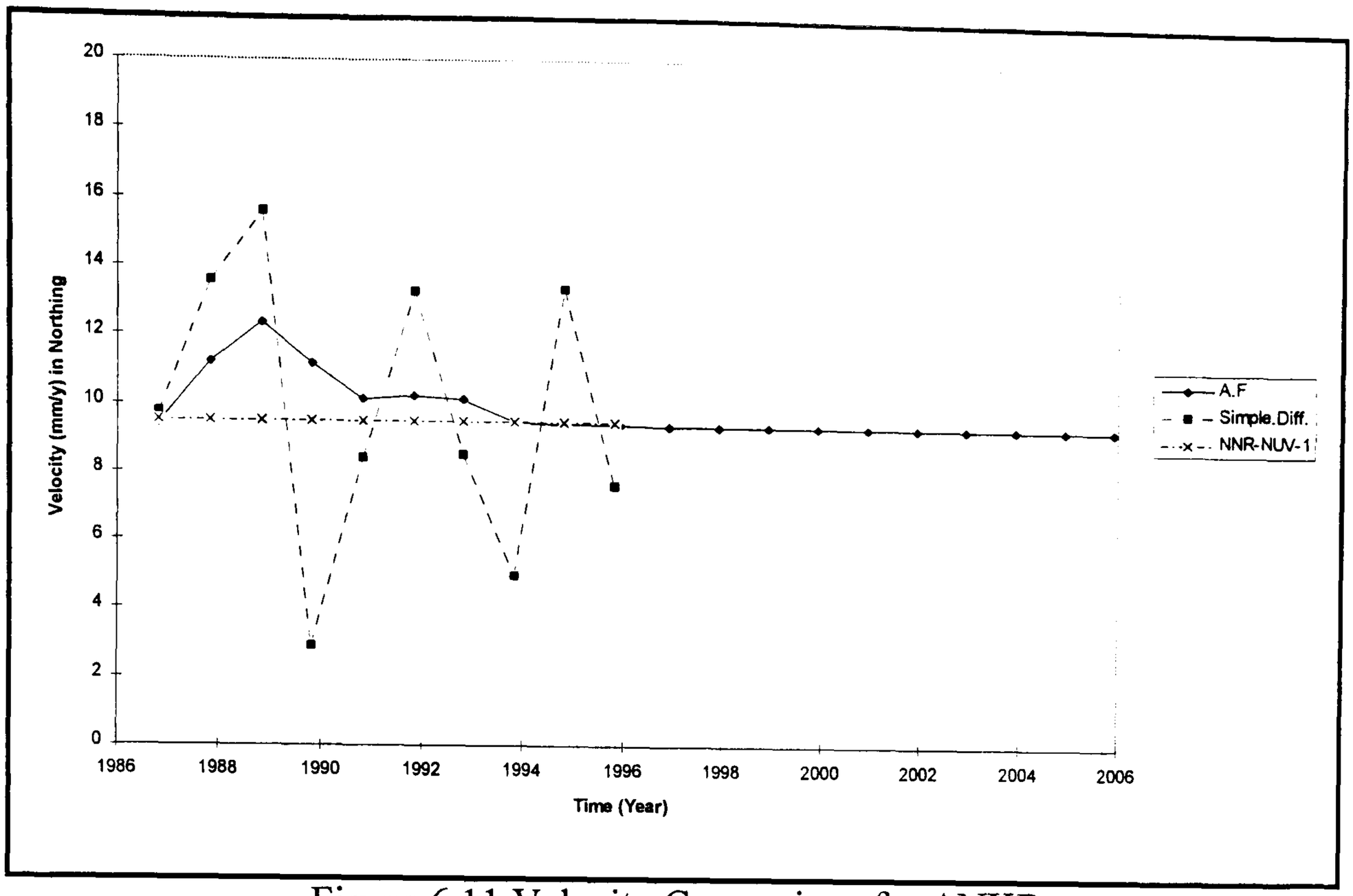

Figure 6.11 Velocity Comparison for ANKR

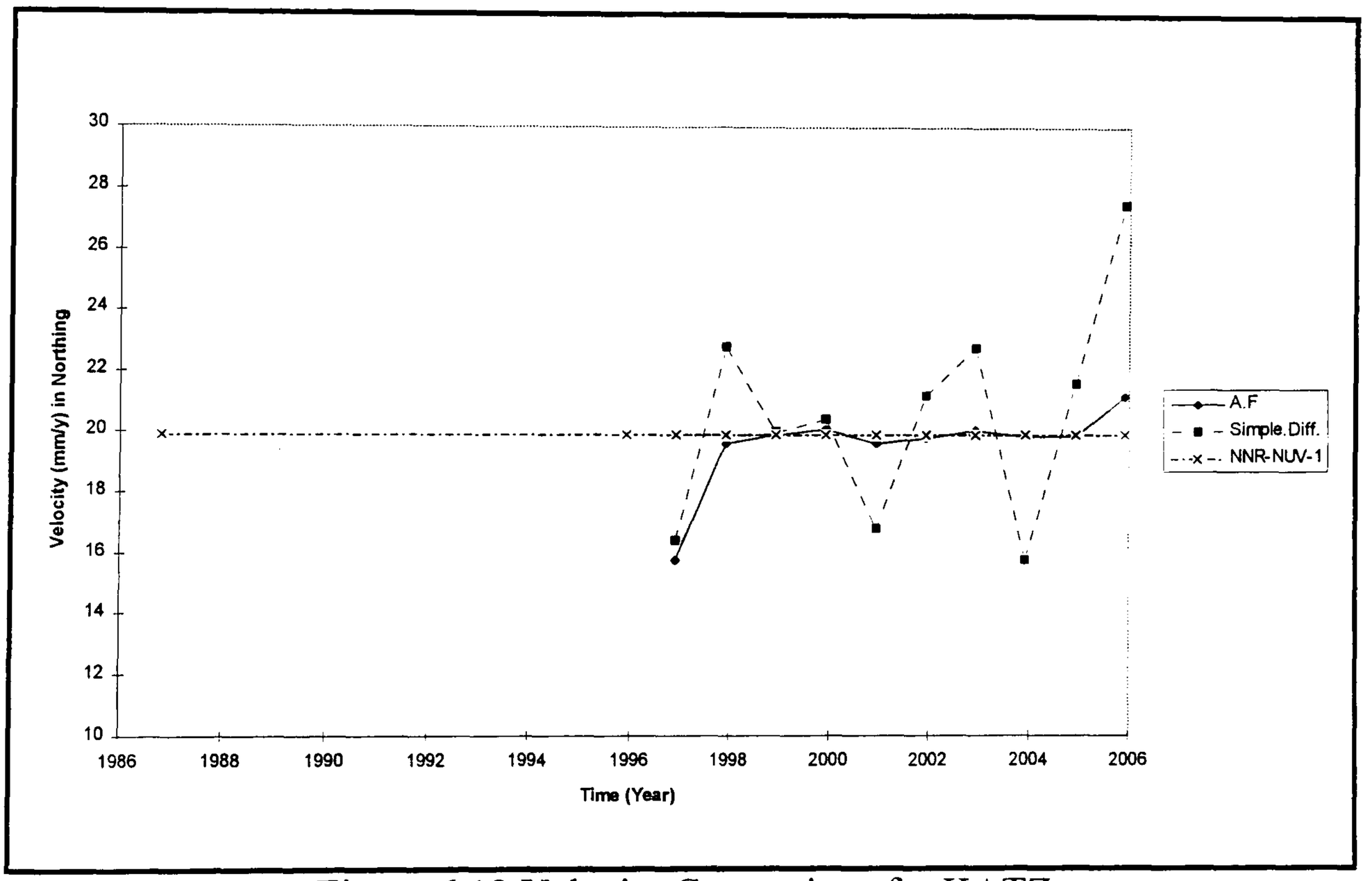

Figure 6.12 Velocity Comparison for KATZ

It is important to note that the simulated station coordinates were actually generated by using the NNR-NUVEL-1 plate motion model with added noise so that the results from the Adaptive Filter approach are as expected.

Now let us consider the three types of smoothing algorithm included in the VEBUK program. The results presented here are those for the station ELAT. Figures 6.13, 6.14 and 6.15 show comparisons of filtered, and smoothened by the three smoothing approaches (forward and backward, fixed-interval and fixed-point), and the velocity from the NNR-NUVEL-1 model.

In Figure 6.15, the fixed-point is the first epoch 1985.82. As discussed in §4.2.3, if any errors occur after this fixed point, the errors are cumulative, since the gain matrix is a continuing product. Such errors may be caused by the local movement estimation not being very accurate. The error in Figure 6.15 is approximately 3mm. The estimated local movement is -28 mm. Figure 6.16 shows the effect of selecting the fixed point after the local movement (say epoch 1996.92). In this case there is no such bias in the measurement.

Of the three smoothing approaches the best result is given by the fixed-interval smoothing method. Within the network, some other stations were also affected by the earthquake and their results are similar to ELAT as shown in Appendix B.

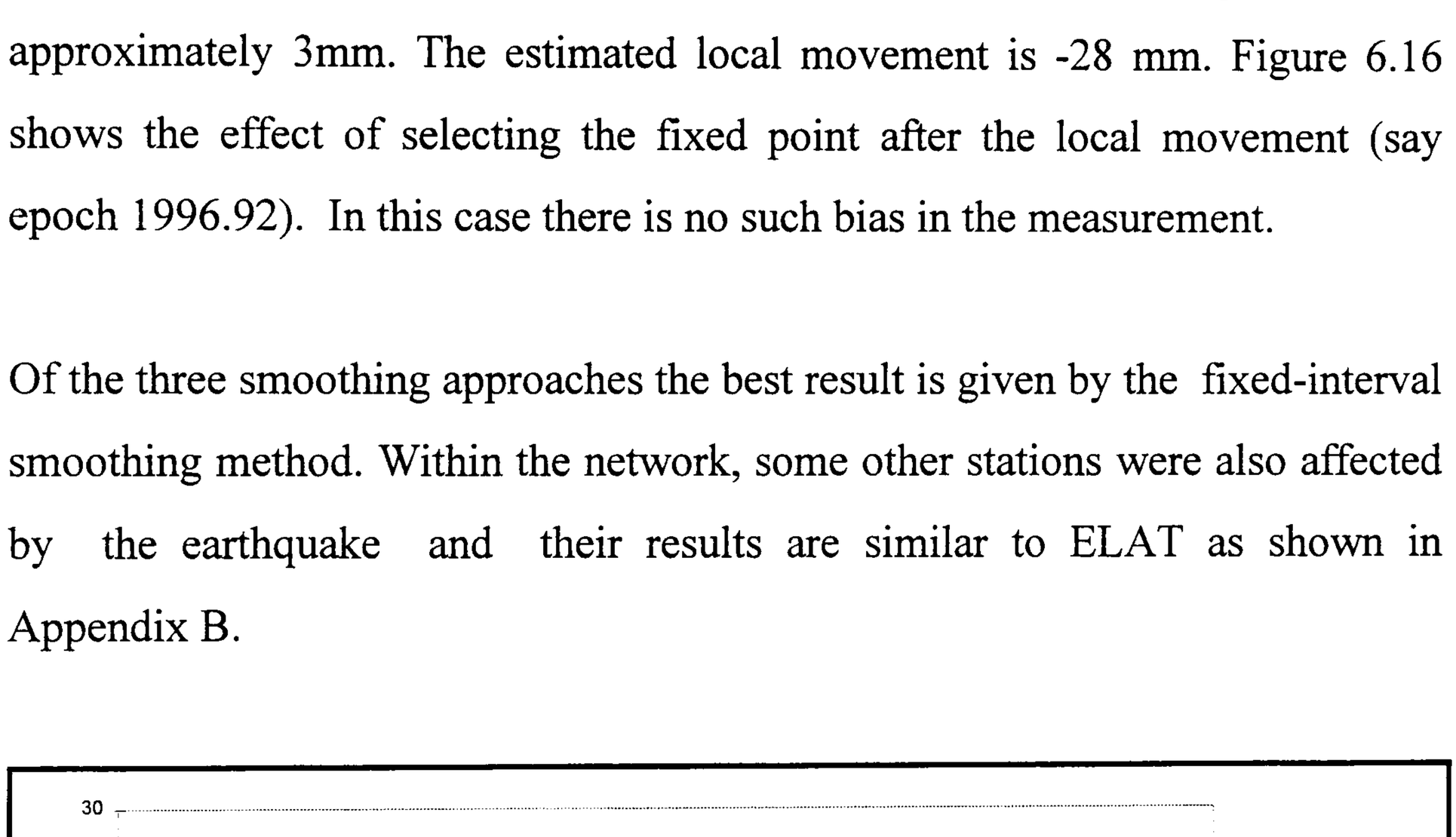

Figure 6.13 Forward and Backward Smoothened NorthingVelocity for ELAT

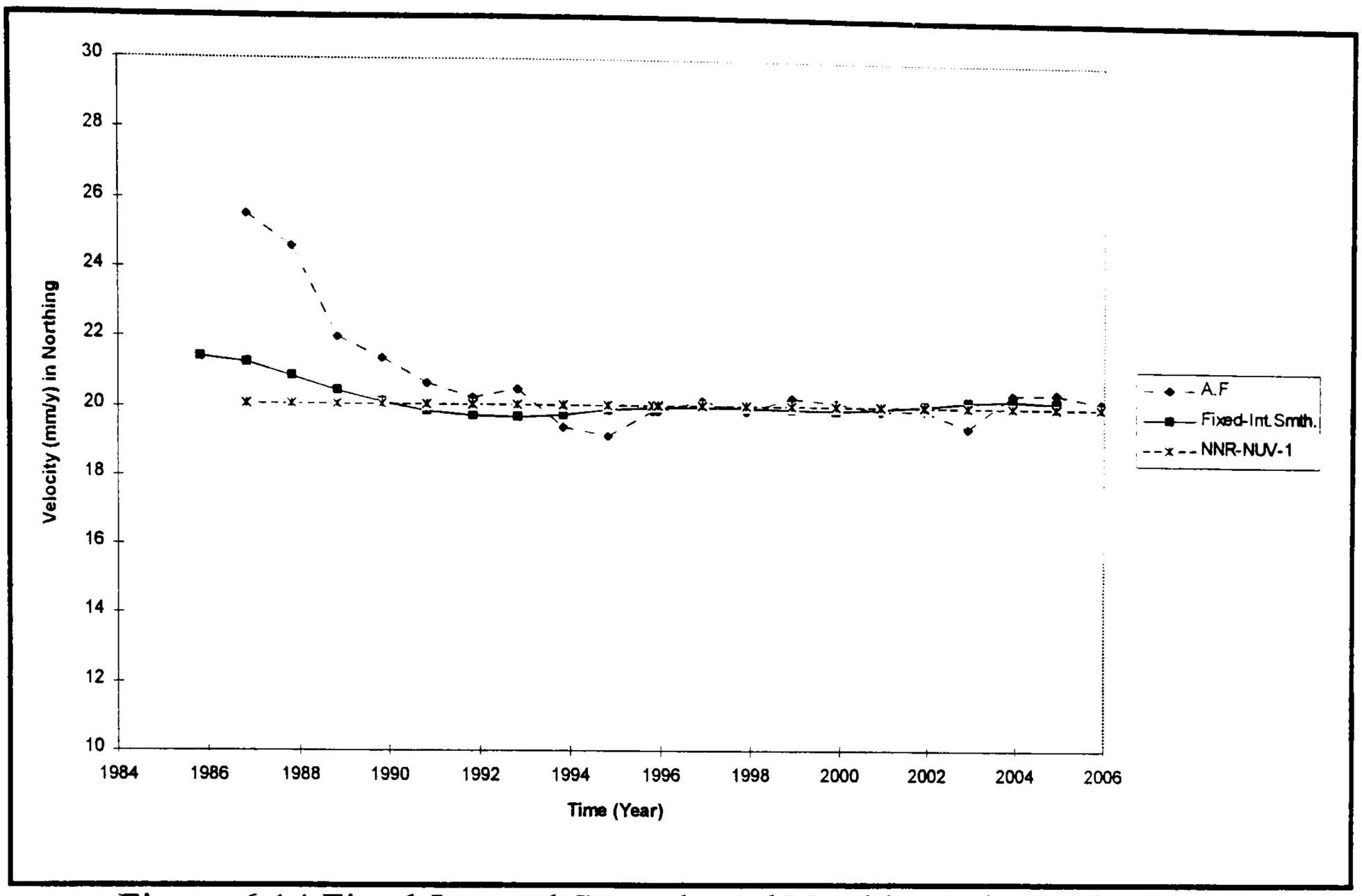

Figure 6.14 Fixed-Interval Smoothened NorthingVelocity for ELAT

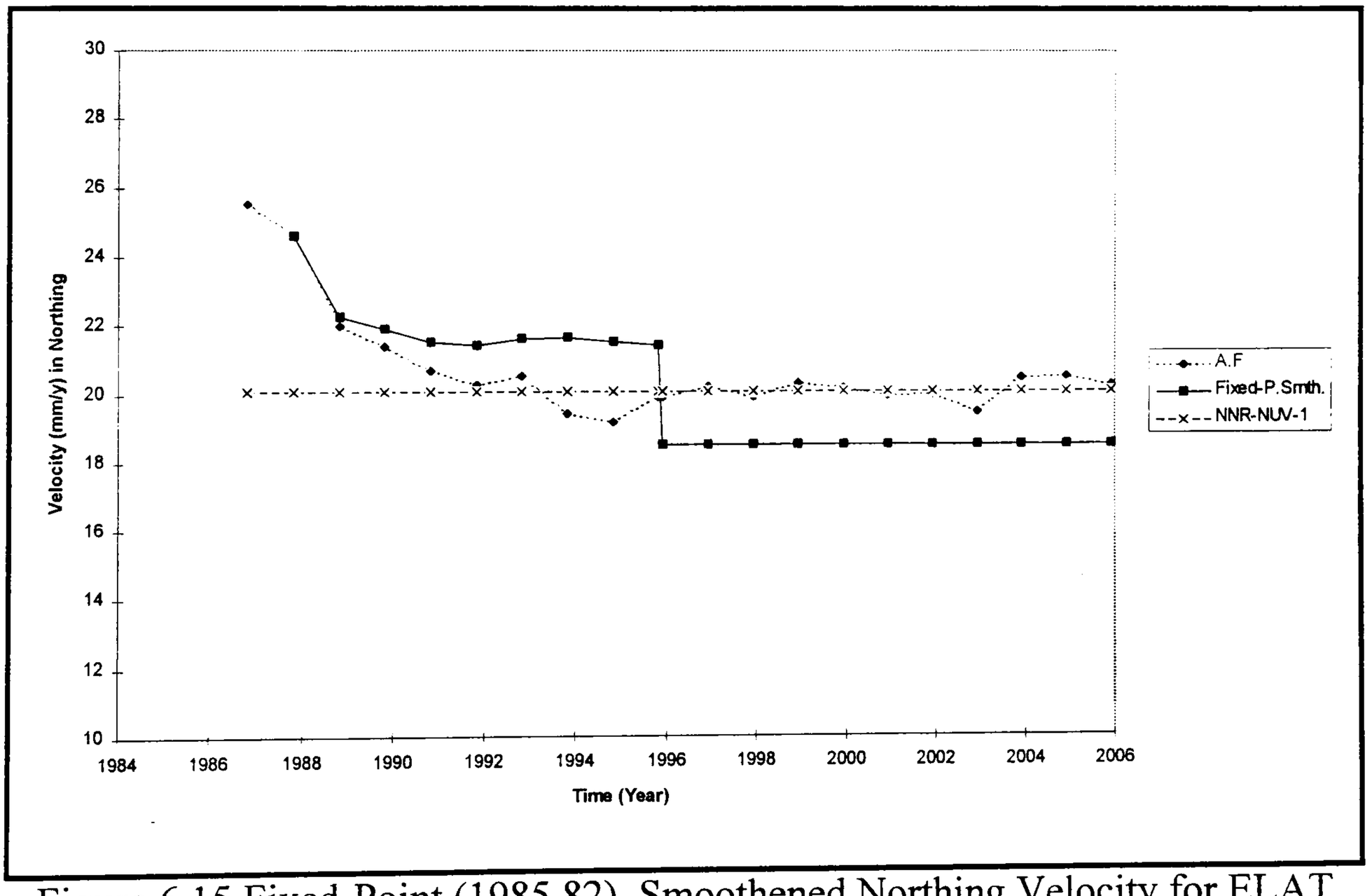

Figure 6.15 Fixed-Point (1985.82), Smoothened Northing Velocity for ELAT

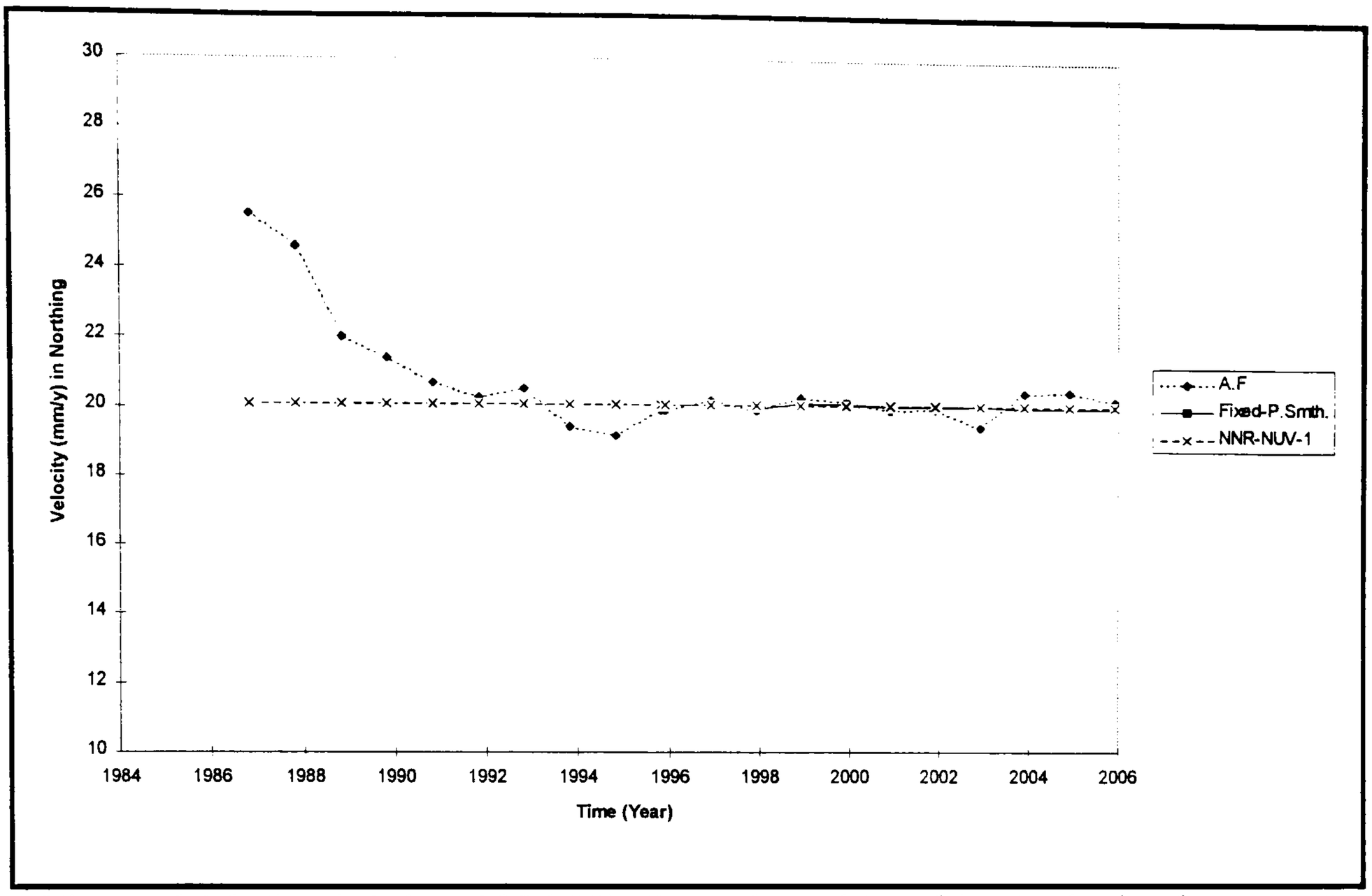

Figure 6.16 Fixed-Point (1996.92), Smoothened Northing Velocity for ELAT

A velocity field for all of the stations in the EASTMED Project is presented in Figure 6.17. This velocity field has been computed based on the Adaptive Filter approach, using Fixed-interval smoothing. In Figure 6.17, the station velocities reflect the results according to the plate motion model for that particular station. The station coordinates and the plate to which the station is associated are given in Appendix C.

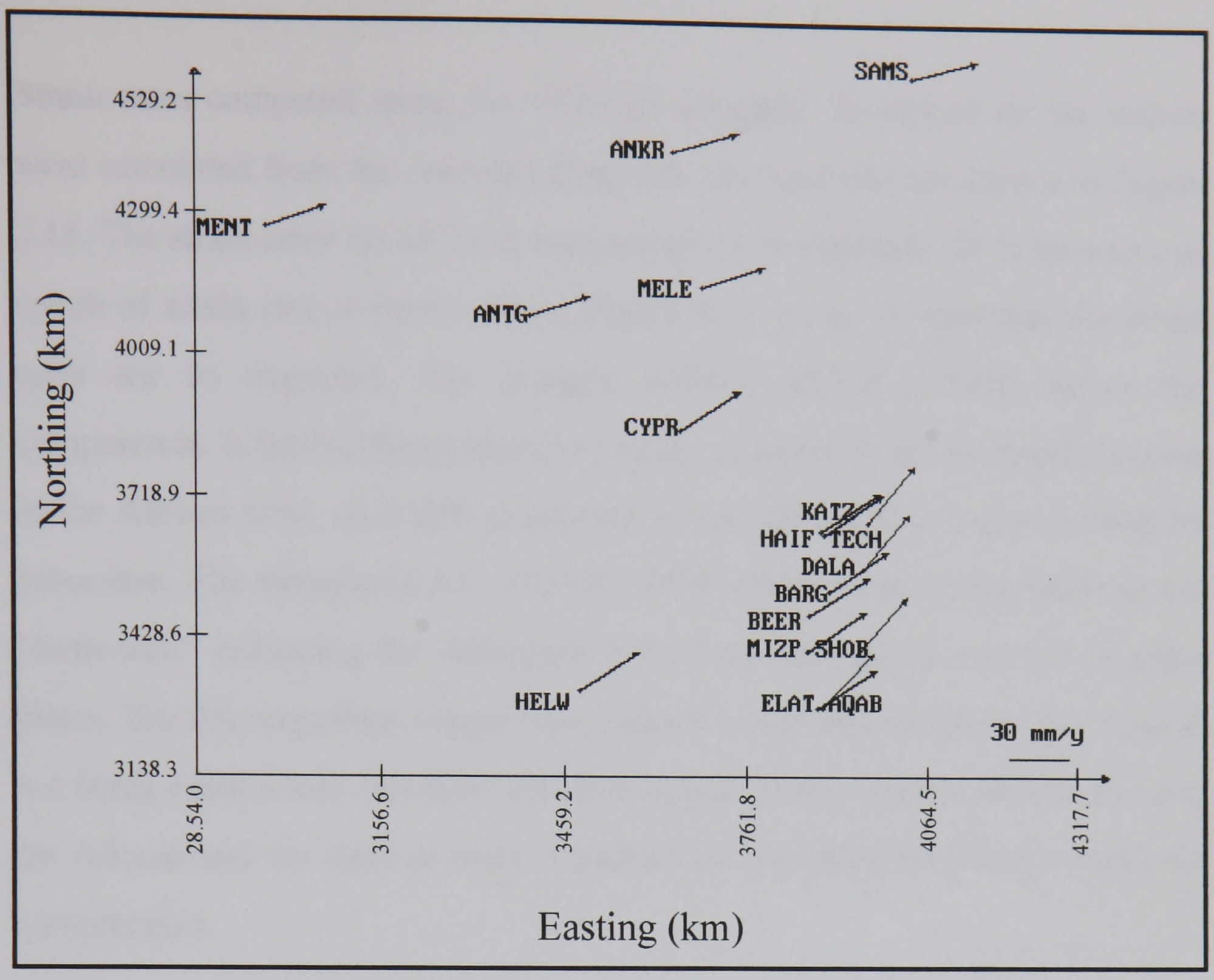

Figure 6.17 Estimated Velocity Field of the Stations in the EASTMED Project

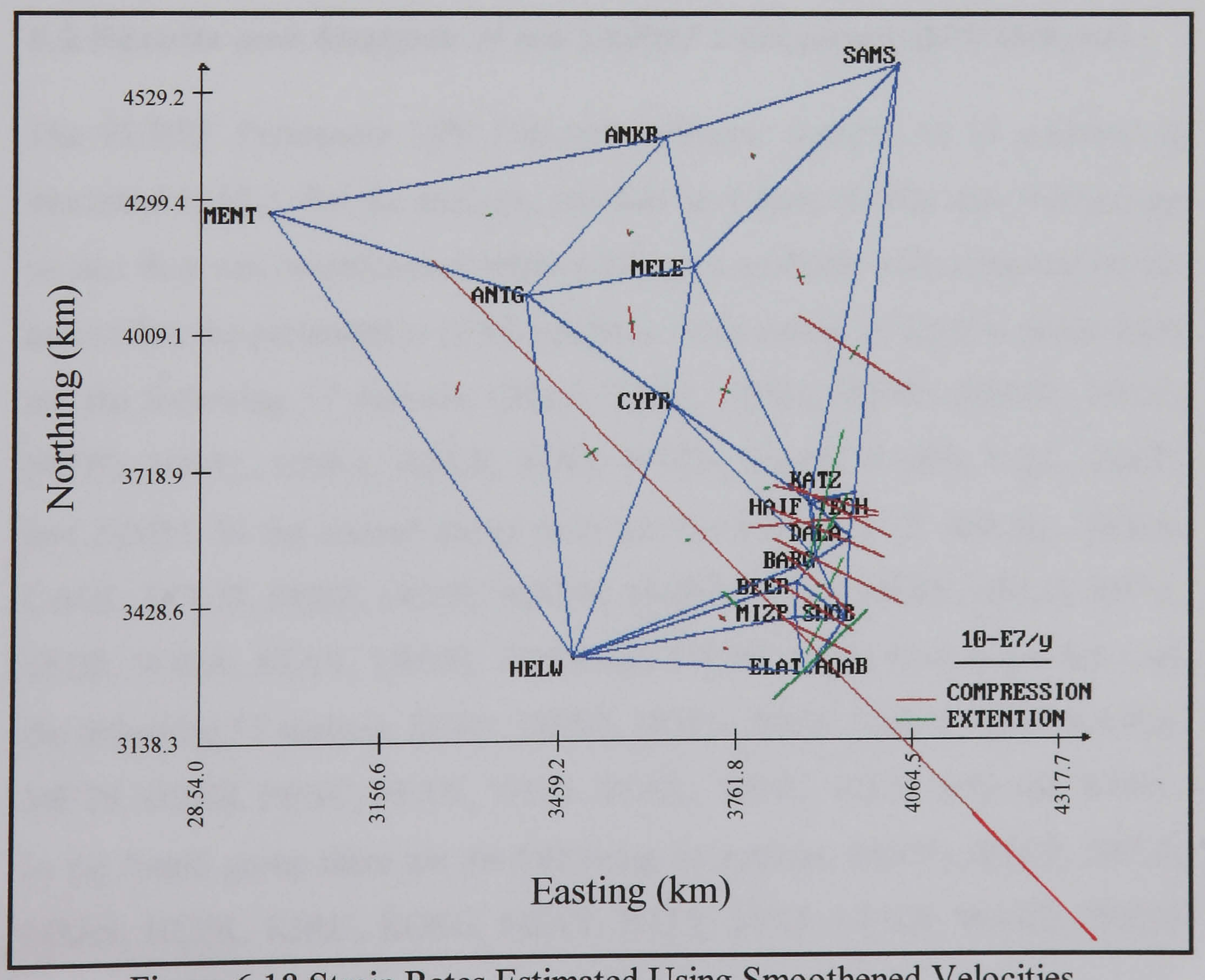

Figure 6.18 Strain Rates Estimated Using Smoothened Velocities

Strain rates computed using the STRAIN program, developed by the author, were calculated from the corresponding velocity field and are shown in Figure 6.18. The strain rates for all 22 epochs are given in Appendix D. Here only one epoch of strain rate is shown. From Figure 6.18 it can be seen that the strain rates are as expected. The triangle ANTG, MELE, CYPR shows the compression in the Northing direction which is caused by the Northerly motion of the African plate, as CYPR is located on the African plate in the simulation procedure. The triangle ELAT, AQAB, SHOB shows large compression to the North-west indicating the deformation between the African and the Arabian plates. But the magnitude bigger than expected, this may be due to the triangle not being equal sided. Similarly all the triangles which contain stations on both the African and the Arabian plate, separated by the Dead Sea Fault, underwent compression.

6.2 Results and Analysis of the EUREF Permanent GPS Network

The EUREF Permanent GPS Network currently consists of 65 stations, as described in §5.2. For the analysis, the data have been divided into four groups so that they can be processed without having a problem with computer power and so that the presentation of the results is made easier. In the first group there are the following 17 stations, GRAZ, JOZE, HERS, MASP, MDVO, NICO, NOTO, NYAL, ONSA, REYK, SOFI, WTZR, VAAS, VARD, VILL, ZECK and ZIMM. In the second group there are the following 17 stations, ANKR, CAGL, DOUR, EBRE, GOPE, MADR, MAR6, MATE, MEDI, OSLO, RIGA, SFER, SODA, STAV, TROM, TRON and ZWEN. In the third group there are the following 17 stations, BOR1, DENT, HOFN, JOEN, KELY, KIR0, LAMA, METS, OBER, PENC, PFAN, THU1, TOUL, VENE, VIL0, VIS0 and WSRT. In the fourth group there are the following 14 stations, BOGO, BRUS, DELF, GRAS, HLFK, KIRU, KOSG, MOPI, POTS, SVTL UPAD, WARE, WETT

and WROC. The data have been processed at one month intervals, on the assumption that crustal movement is a slow process.

The first results presented are for Zimmerwald (ZIMM), in the first group, by using the standard Kalman filter. During the processing, the initial value of the covariance for the velocity was chosen as 4 cm^2y^{-2}, and the system noise as $1mm^2y^{-4}$. Figure 6.19 represents the Northing coordinates component of the actual (dotted line) and estimated (solid line) coordinates. Figure 6.20 represents the Northing velocities computed by simple differencing (dotted line) and by the standard Kalman filter approach (solid line). Here It should be noted that the station ZIMM has a bias between the GPS weeks 0858 and 0862. This bias is present in the other coordinate components of the station ZIMM, and for the other stations in the network. This bias was caused from the two reference frame, ITRF93 and ITRF94, used during the combined estimation process .

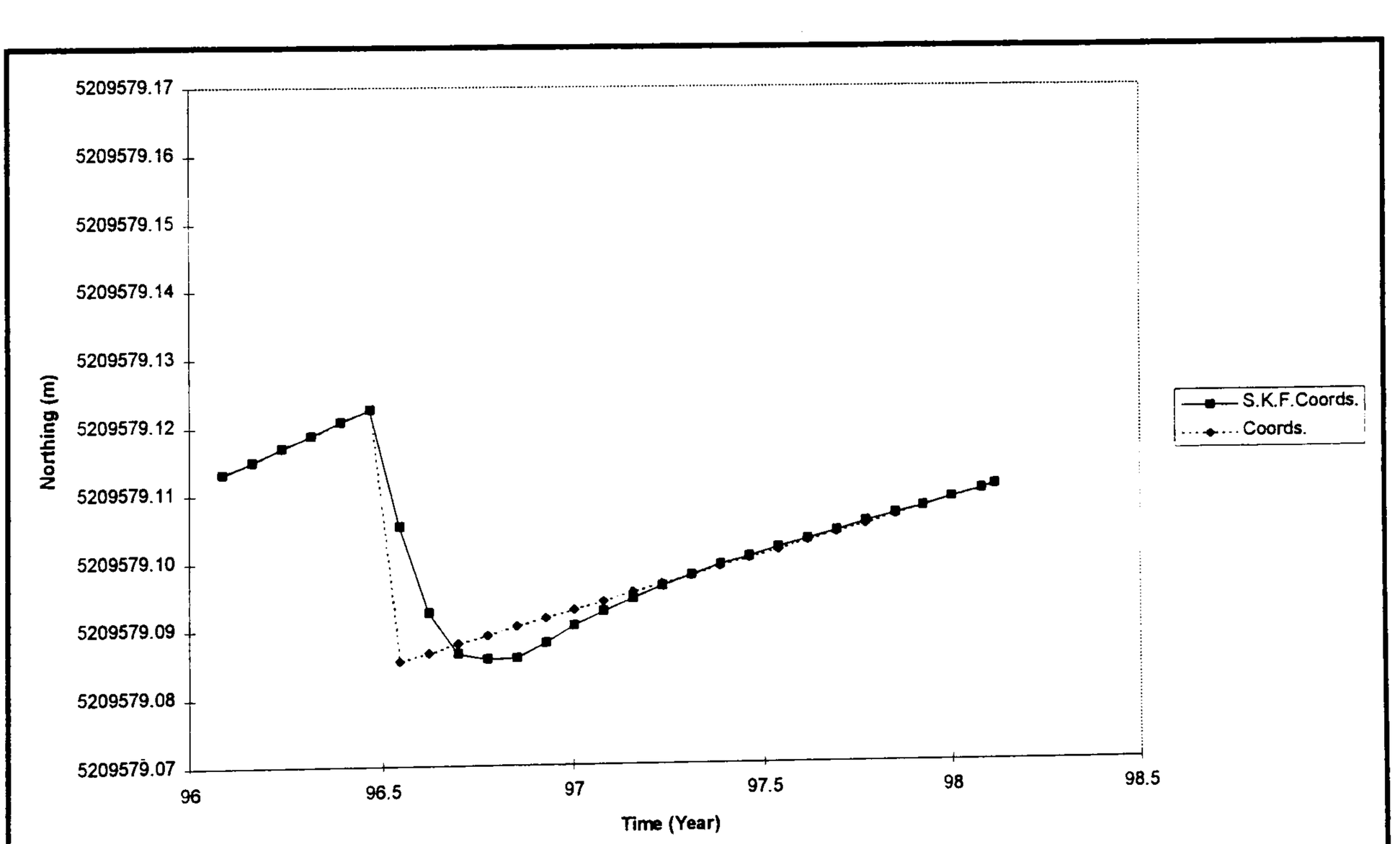

Figure 6.19 ZIMM Northing Coordinates Estimated by Standard Kalman Filter

In Figure 6.20, the effect of the bias can be seen in velocity terms. The level of this effect depends on the sytem noise. If the system noise is set to be small, the effect is larger, whereas if the system noise is set to be large the effect is

smaller. However, under large system errors, the estimation will not differ from the one obtained by simple differencing. Therefore, this effect can not be removed by the Kalman filter itself.

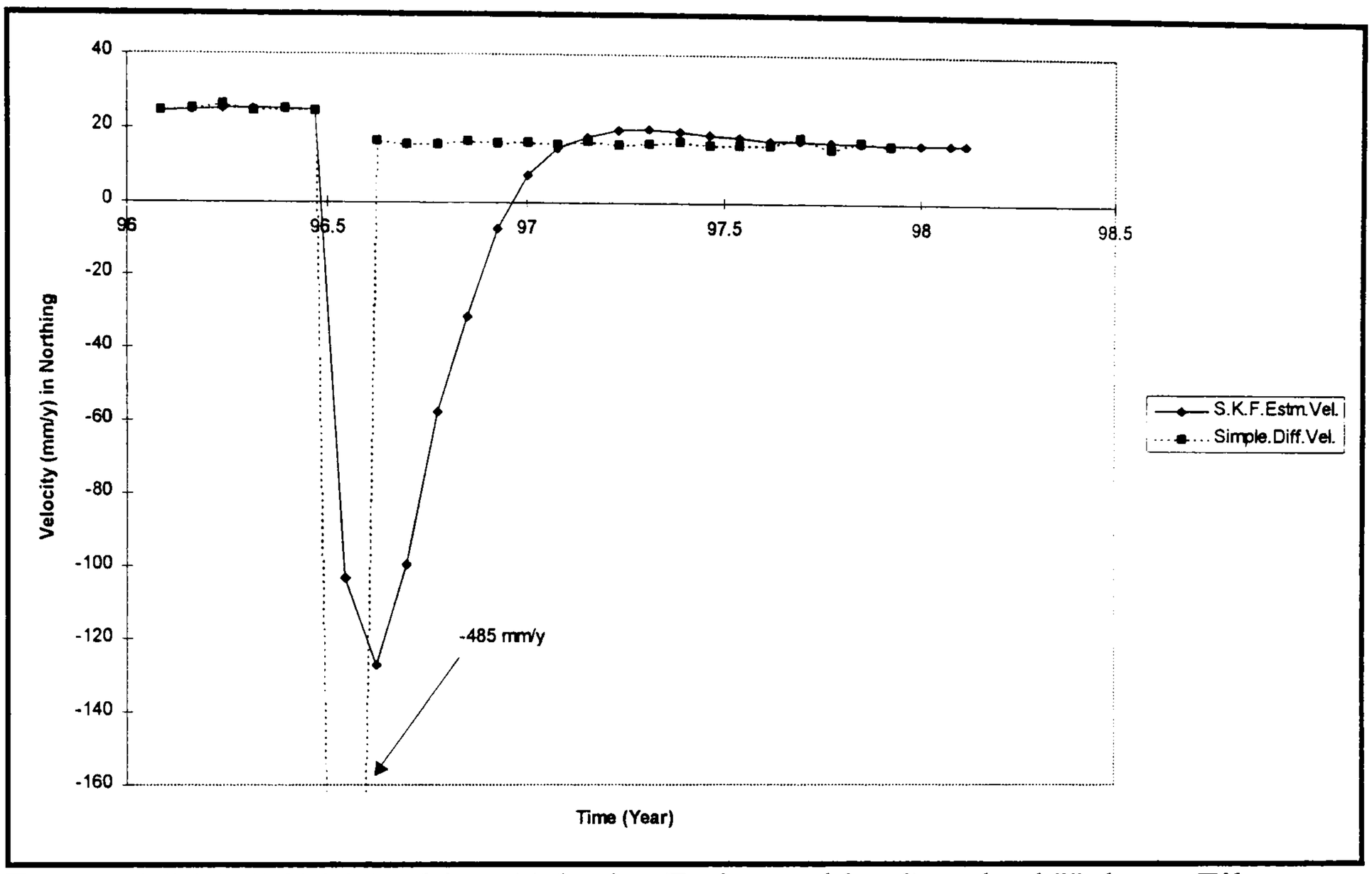

Figure 6.20 ZIMM Northing Velocity Estimated by Standard Kalman Filter

By using the proposed deformation analysis technique, detailed in Section §4.5, and with the Adaptive Filtering approach, the estimated bias for the Northing component of the station ZIMM is -39 mm. If this bias is removed from the coordinates, the new estimated coordinates and velocity for the station ZIMM are given in Figures 6.21 and 6.22 respectively.

From Figures 6.21 and 6.22, it can be seen that this bias not only occured in the coordinates, but the rate of movement is also changed. Therefore even with this complexity the estimation is succesful.

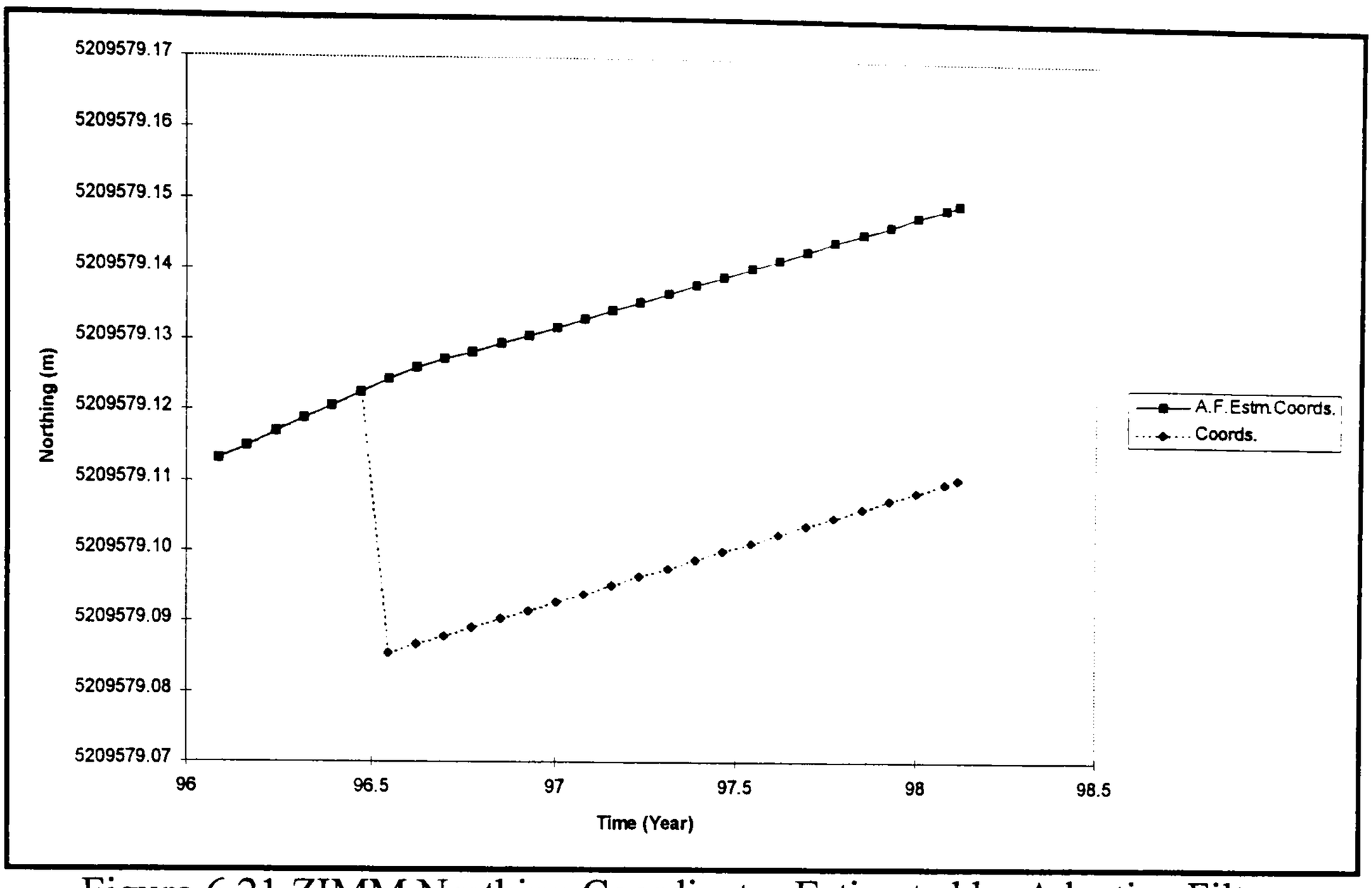

Figure 6.21 ZIMM Northing Coordinates Estimated by Adaptive Filter

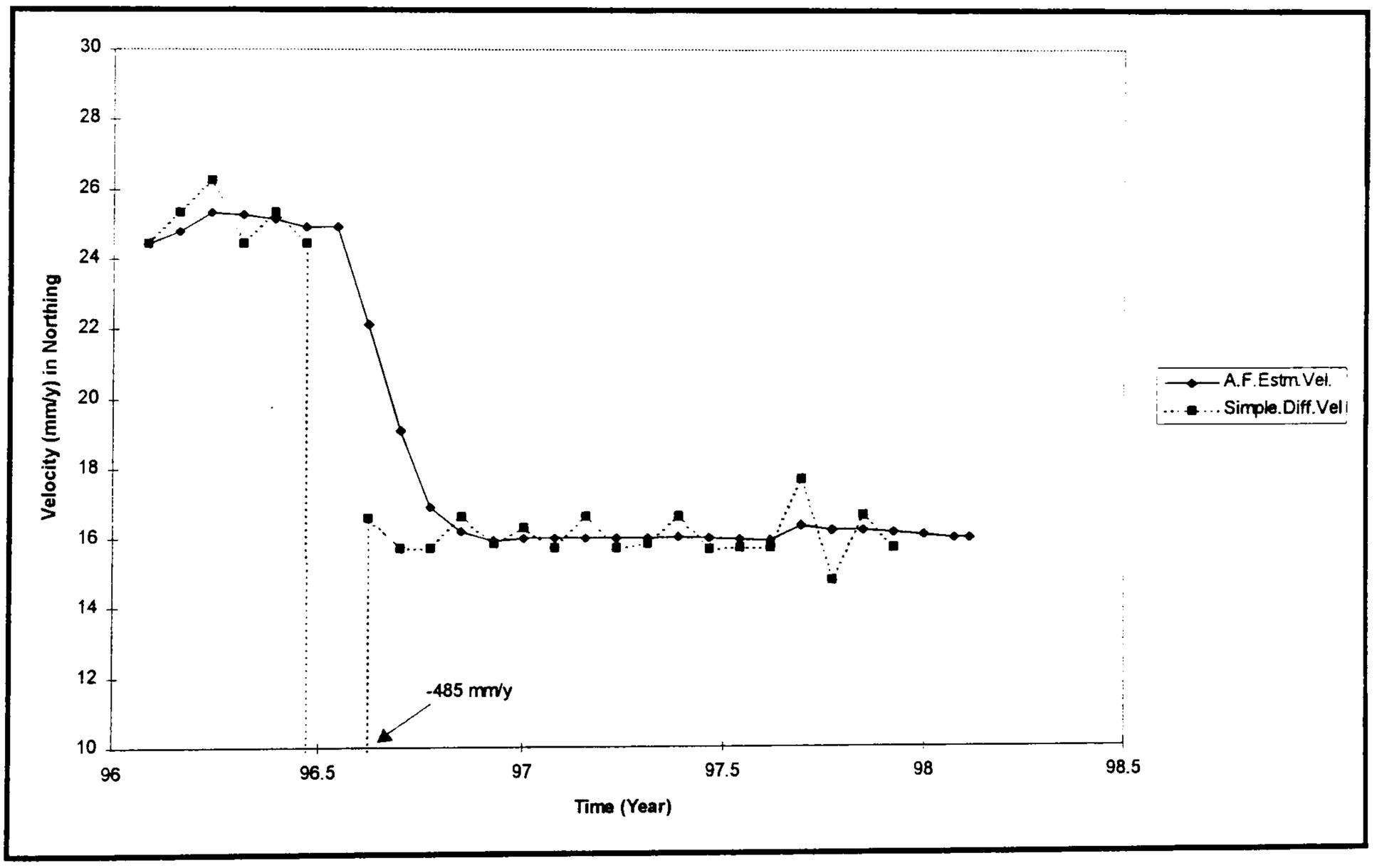

Figure 6.22 ZIMM Northing Velocity Estimated by Adaptive Filter

A comparison of the velocities computed by using the Adaptive Filter with the ITRF93 and ITRF94 velocities, is presented in Figures 6.23 and 6.24 for the station ZIMM.

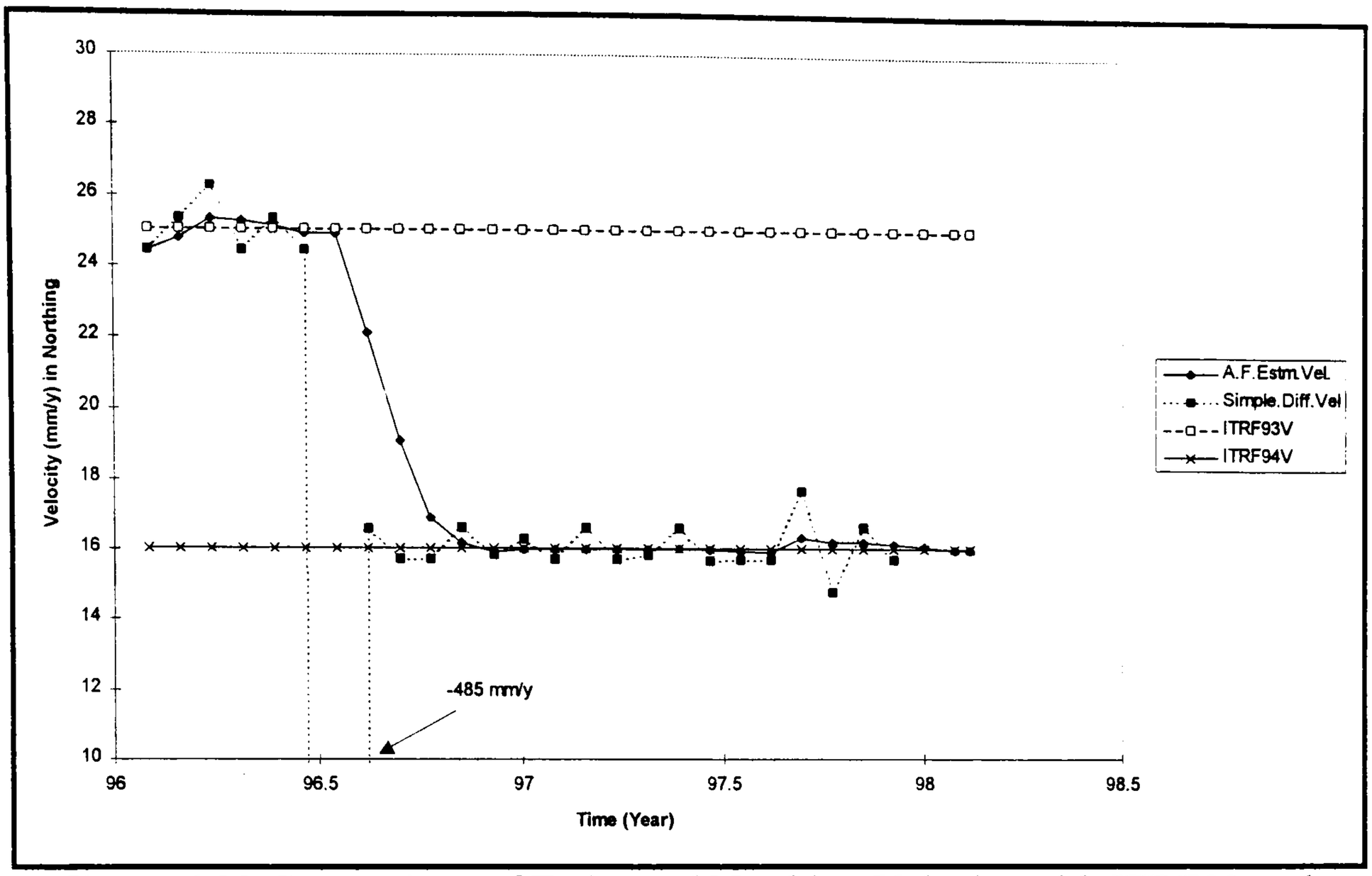

Figure 6.23 Comparison of Estimated Northing Velocity with ITRF93 and ITRF94 Velocities for Station ZIMM

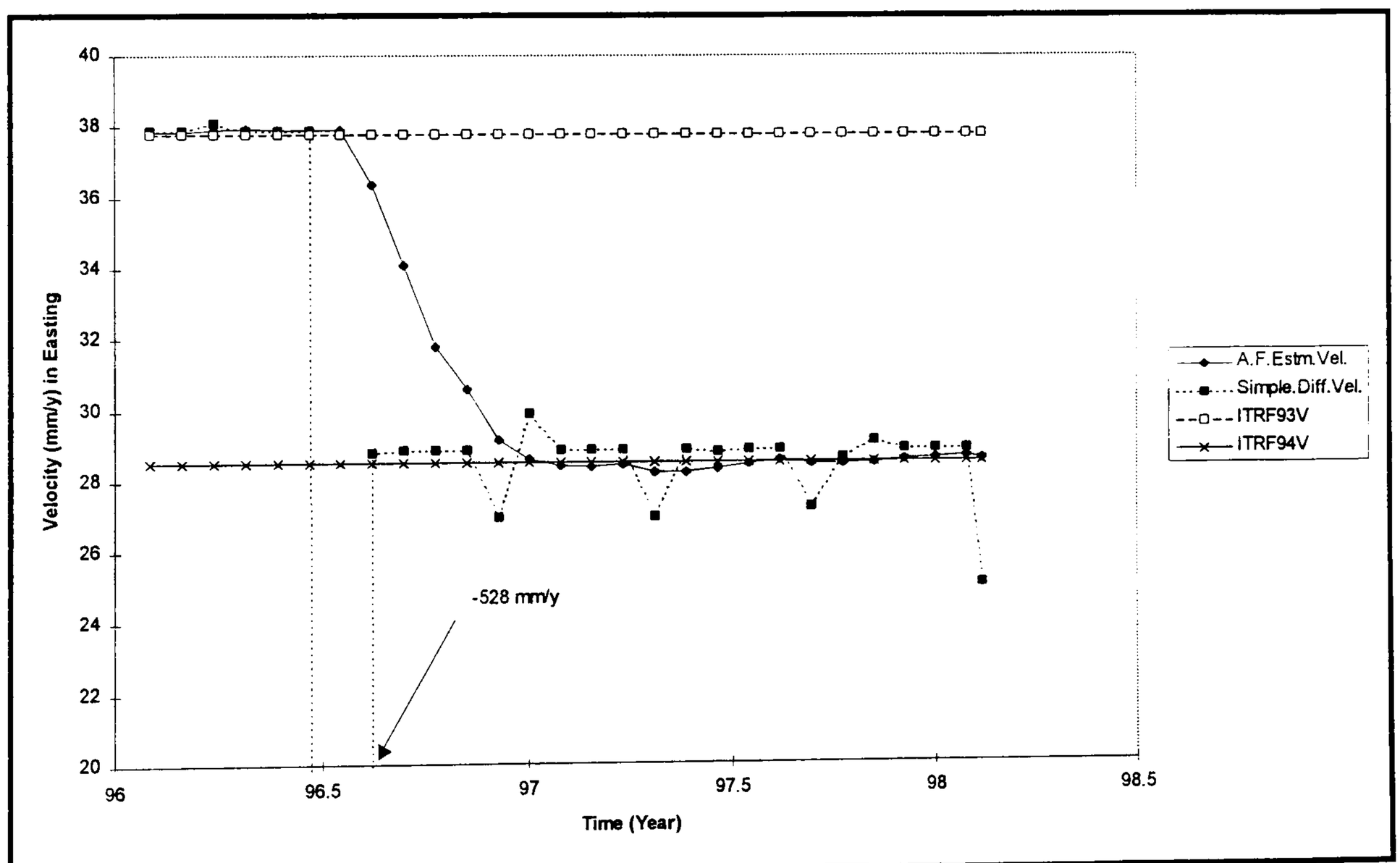

Figure 6.24 Comparison of Estimated Easting Velocity with ITRF93 and ITRF94 Velocities for Station ZIMM

From Figures 6.23 and 6.24, the effect of changing from the ITRF93 reference frame to the ITRF94 reference frame for the combined EUREF permanent GPS network solution can be clearly seen.

The horizontal velocity field estimated using the Adaptive Filter approach for the stations in the first and second groups are plotted in Figures 6.25 and 6.27 respectively, with the ITRF94 velocities for some stations being plotted in Figures 6.26 and 6.28. The full results including the estimated station velocities and their standard errors for all four groups are given in Appendix E.

It can be seen from Figures 6.25 and 6.27, that stations VILL, GRAZ, ZIMM, WTZR, HERS, ONSA, JOZE, MDVO, DOUR, GOPE, EBRE, MADR, MATE and CAGL to appear to be on the stable part of the Eurasian plate and have velocities that are consistent with the ITRF94 velocity field shown in Figures 6.26 and 6.28.

As discussed in §5.2.2, some stations in the EUREF Permanent GPS Network are not on the stable part of the Eurasian plate. From Figures 6.27, it can be seen that ANKR is moving in a North -West direction with a magnitude of 6 mm/y. This may be explained as ANKR is located on the Anatolian plate, which is rotated anti-clockwise by the motion of the Arabian plate.

Similarly, in Figure 6.25, the station NICO is moving in a North direction, due to the motion of Cyprus which is controlled by the African and Arabian plates. In Southern Italy, the station NOTO is moving in a North - East direction due to the fact that it is located on the Adriatic - African Plate.

In the North of the EUREF Permanent GPS Network, REYK is moving mainly North due to motion of Iceland, which is controlled by the North American and Eurasian plates. Furthermore, four stations in Fennoscandia namely NYAL, VARD, TRON and SODA exhibit large unexpected motions of about 80 mm/y.

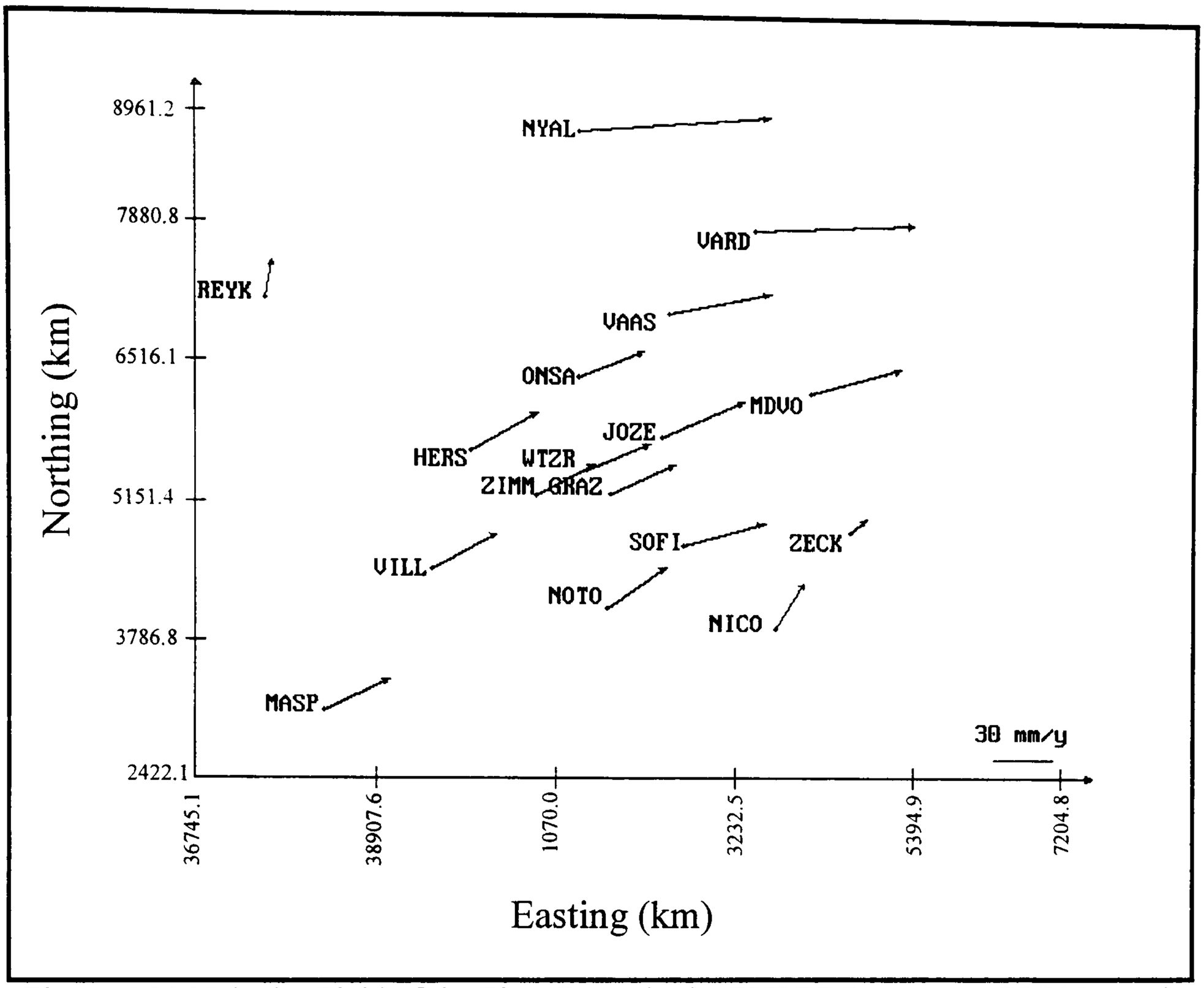

Figure 6.25 Velocity Field of the First Group in the EUREF Permanent GPS Network

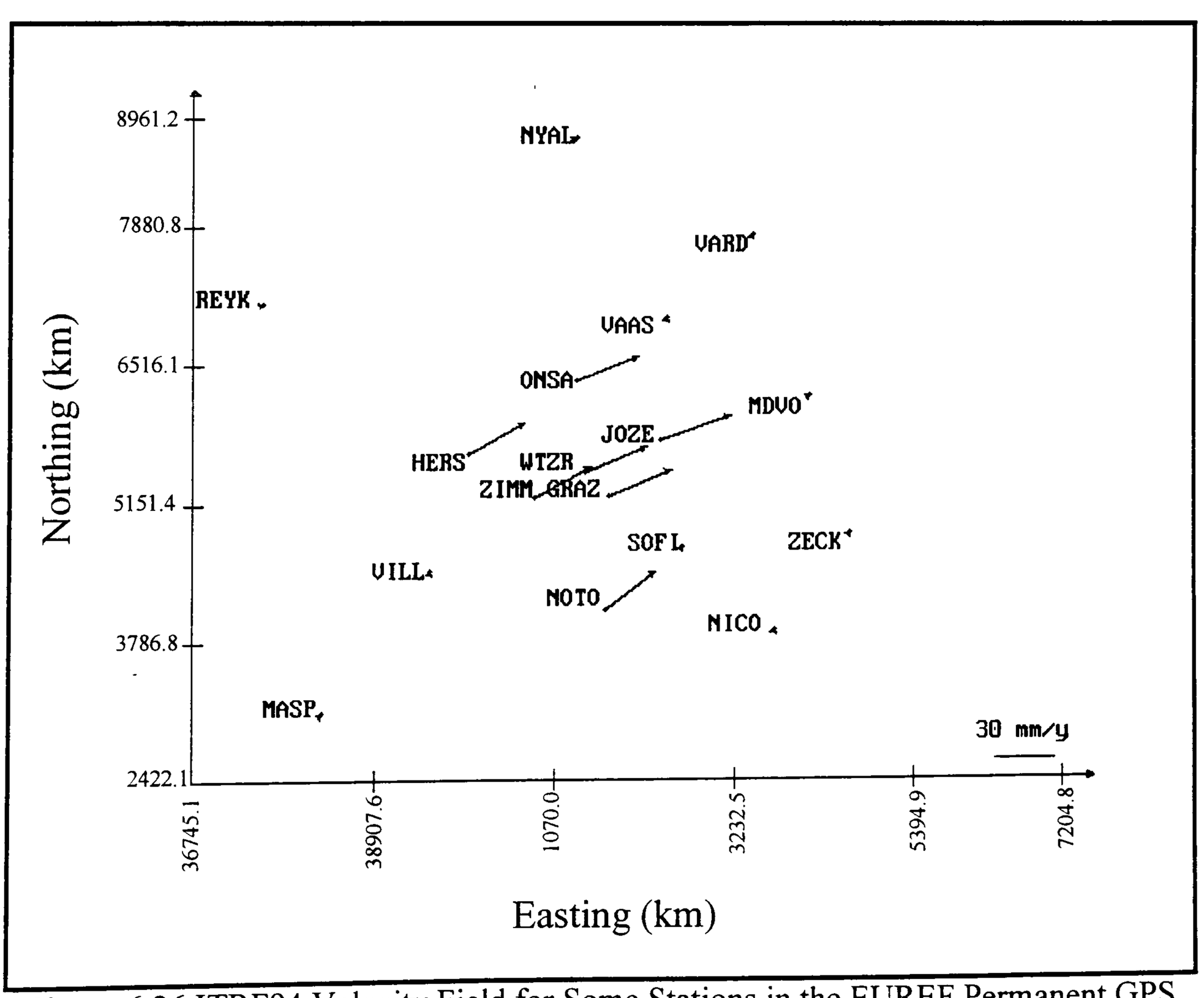

Figure 6.26 ITRF94 Velocity Field for Some Stations in the EUREF Permanent GPS Network

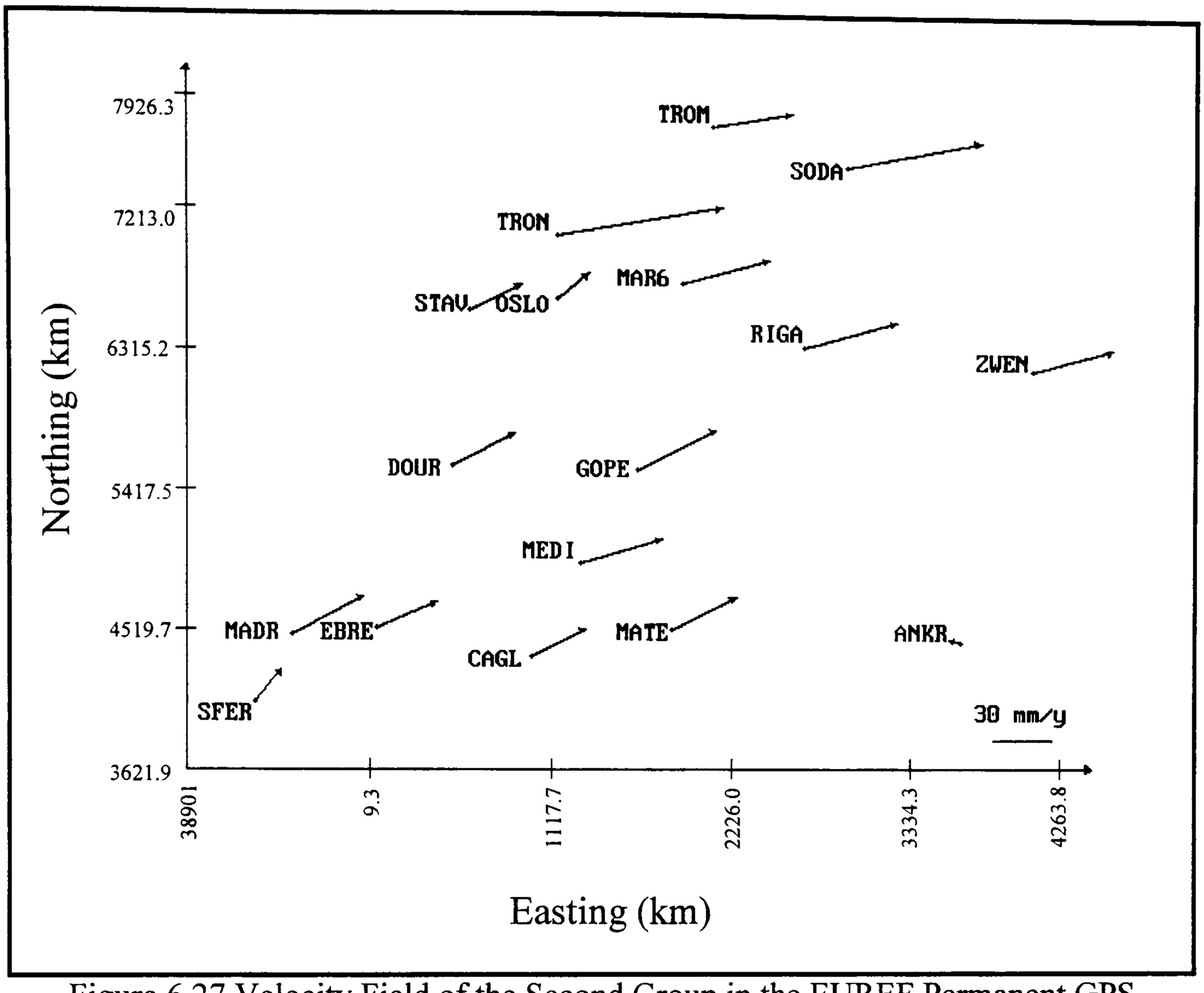

Figure 6.27 Velocity Field of the Second Group in the EUREF Permanent GPS Network

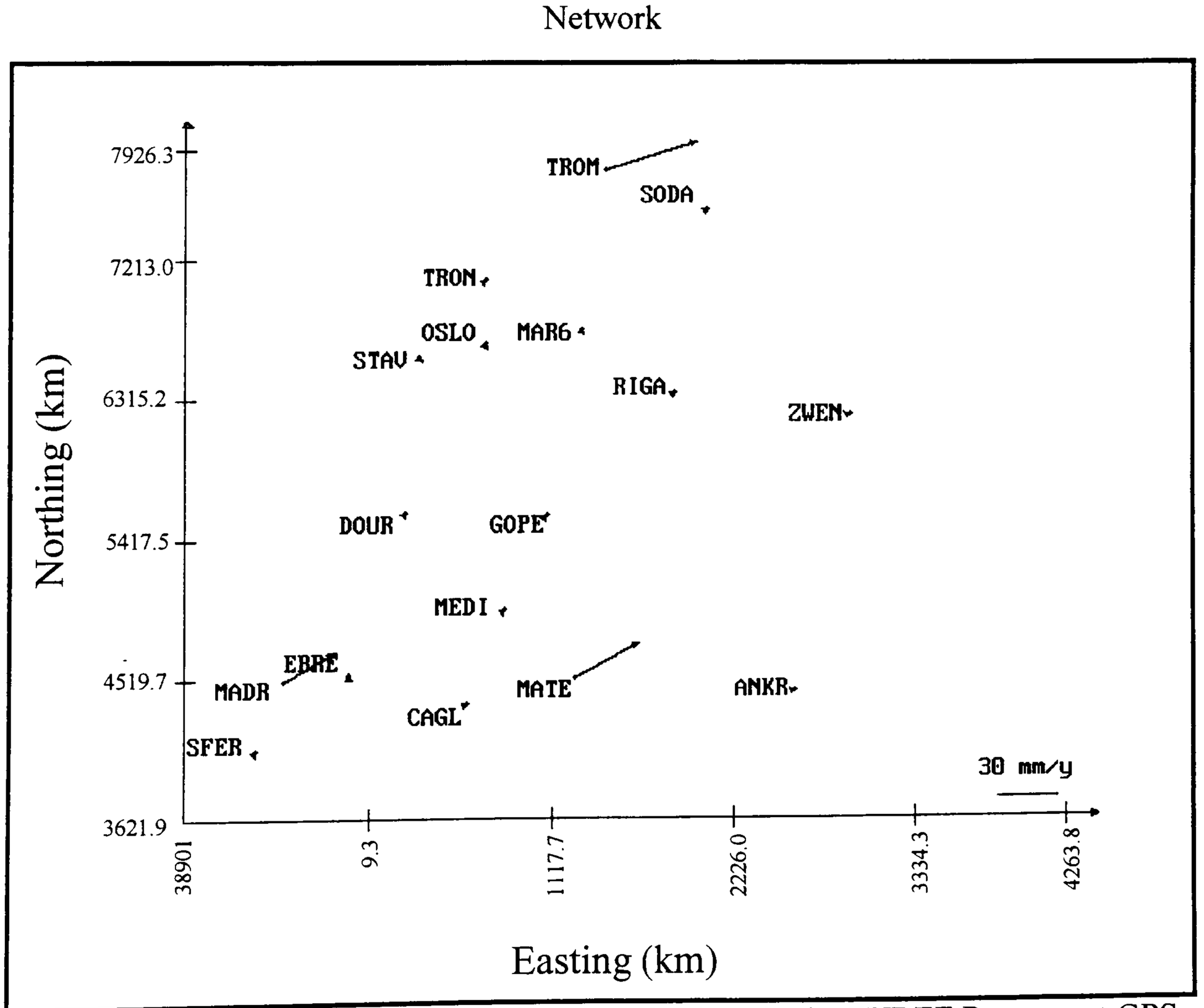

Figure 6.28 ITRF94 Velocity Field for Some Stations in the EUREF Permanent GPS Network

The vertical velocity fields of the first and second groups are given in Figures 6.29 and 6.31. The analysis suggests that stations in the North of the EUREF Permanent GPS Network, namely, NYAL, REYK, VAAS JOZE, SODA, TRON, MAR6, STAV and OSLO all appear to be rising at the rates from 8 to 30 mm/y respectively which may be connected to post-glacial rebound (as described in §2.5), but are greater than would be expected.

In the South of the EUREF Permanent GPS Network, the stations NICO, SOFI, NOTO and VILL also appear to be rising, whereas the stations MADR, WTZR and MASP are in downward motion. Figures 6.30 and 6.32 show the ITRF94 vertical velocity field for some stations in the EUREF Permanent GPS Network, which suggest that there is no significant vertical motion taking place.

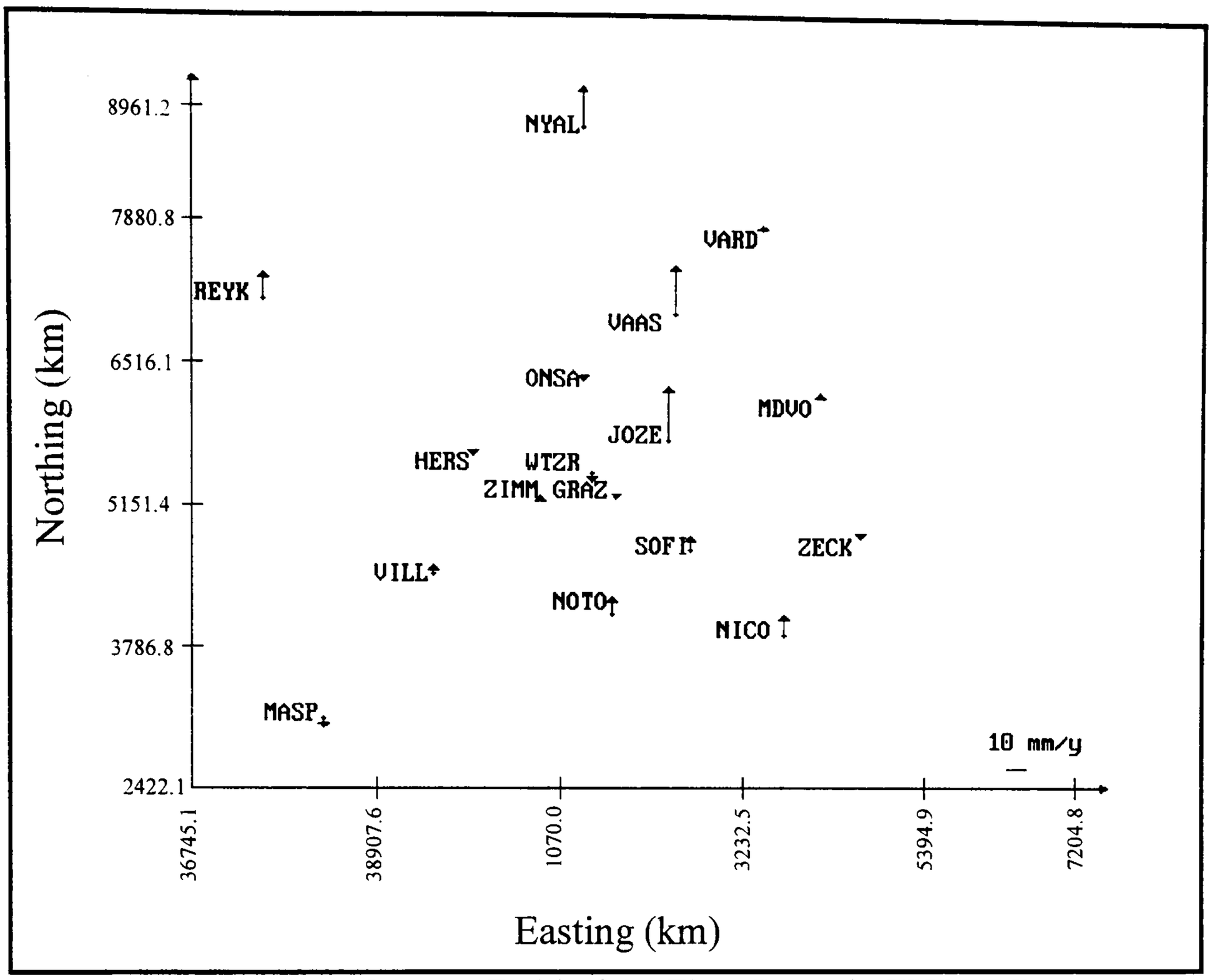

Figure 6.29 Vertical Velocity Field of the First Group in EUREF Permanent GPS Network

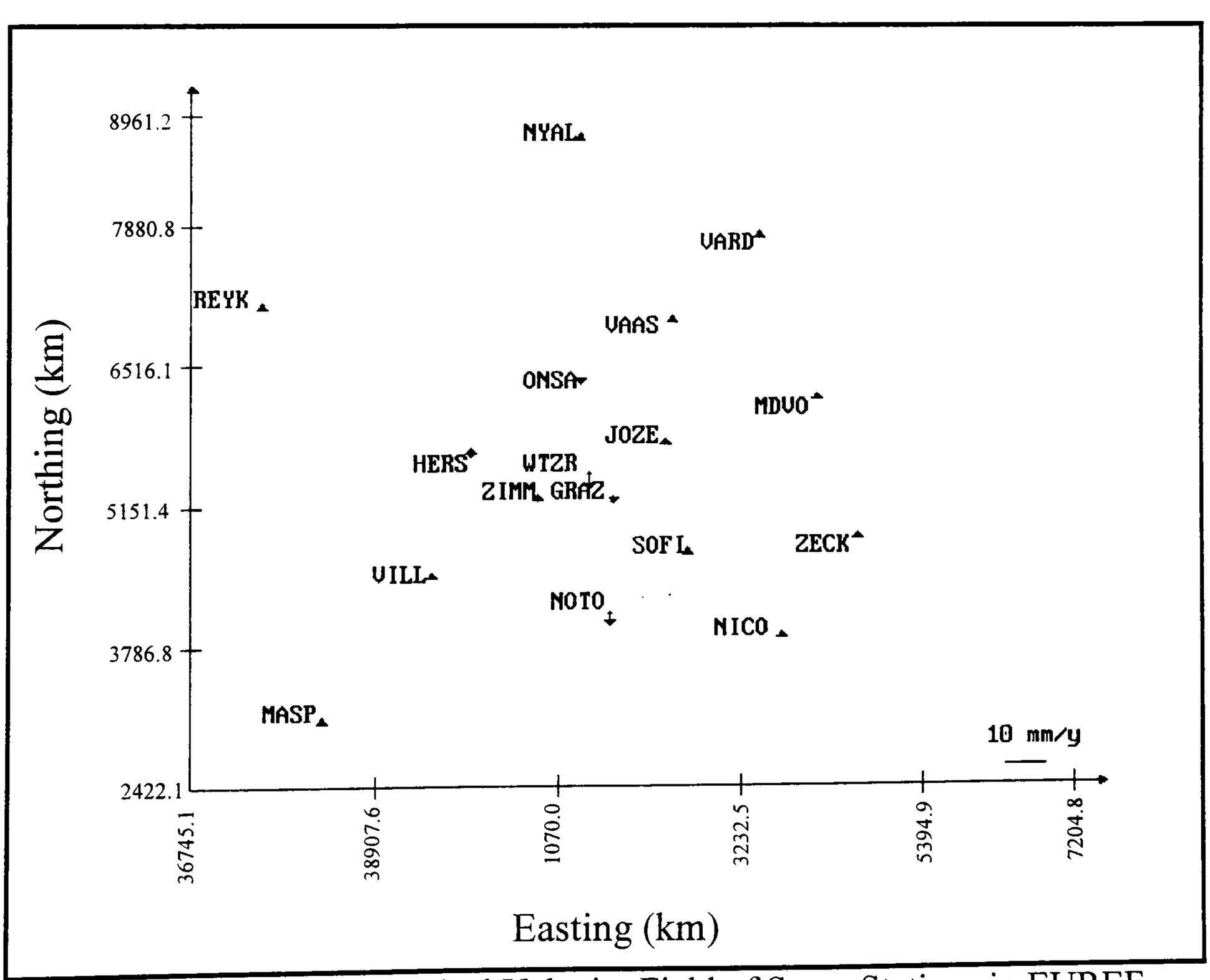

Figure 6.30 ITRF94 Vertical Velocity Field of Some Stations in EUREF Permanent GPS Network

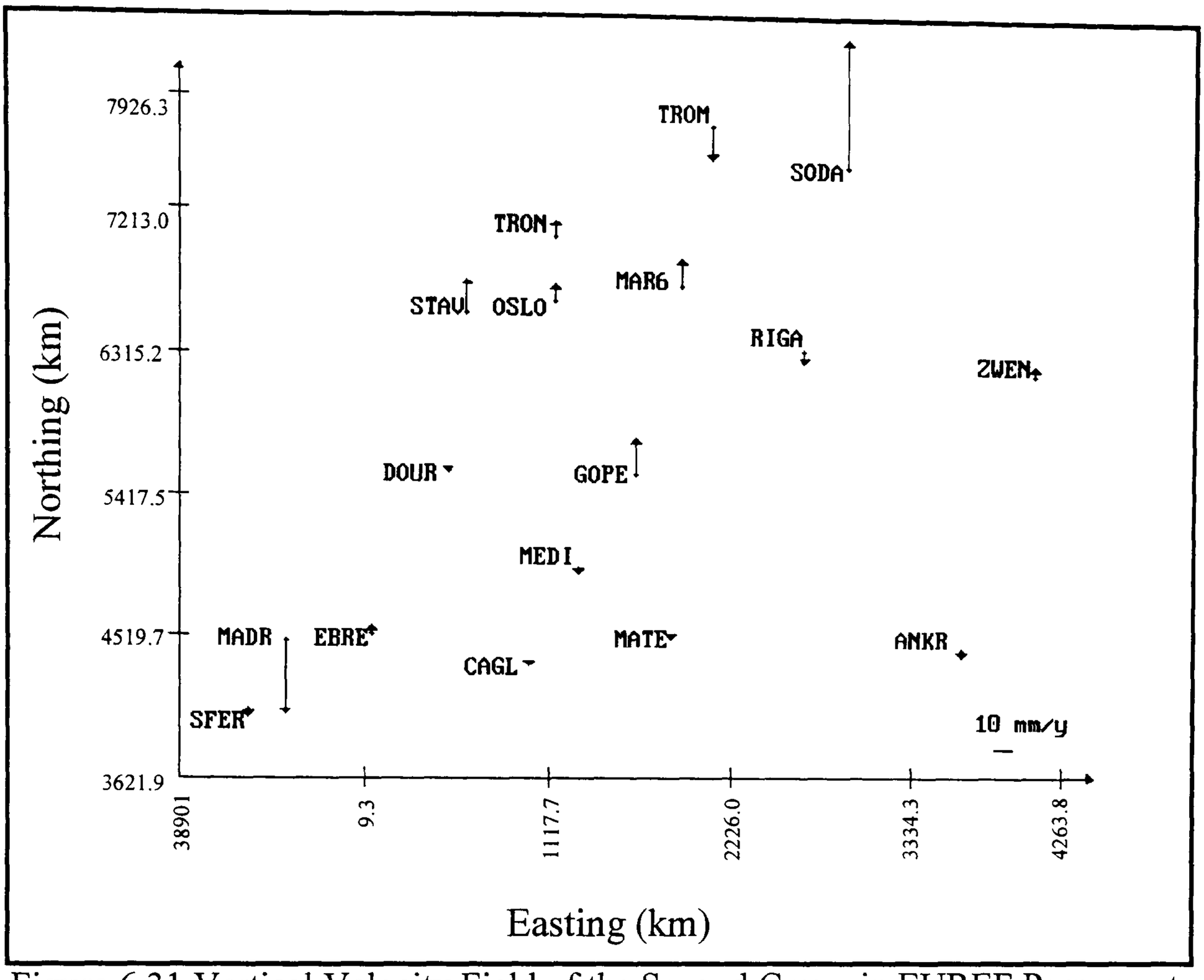

Figure 6.31 Vertical Velocity Field of the Second Group in EUREF Permanent GPS Network

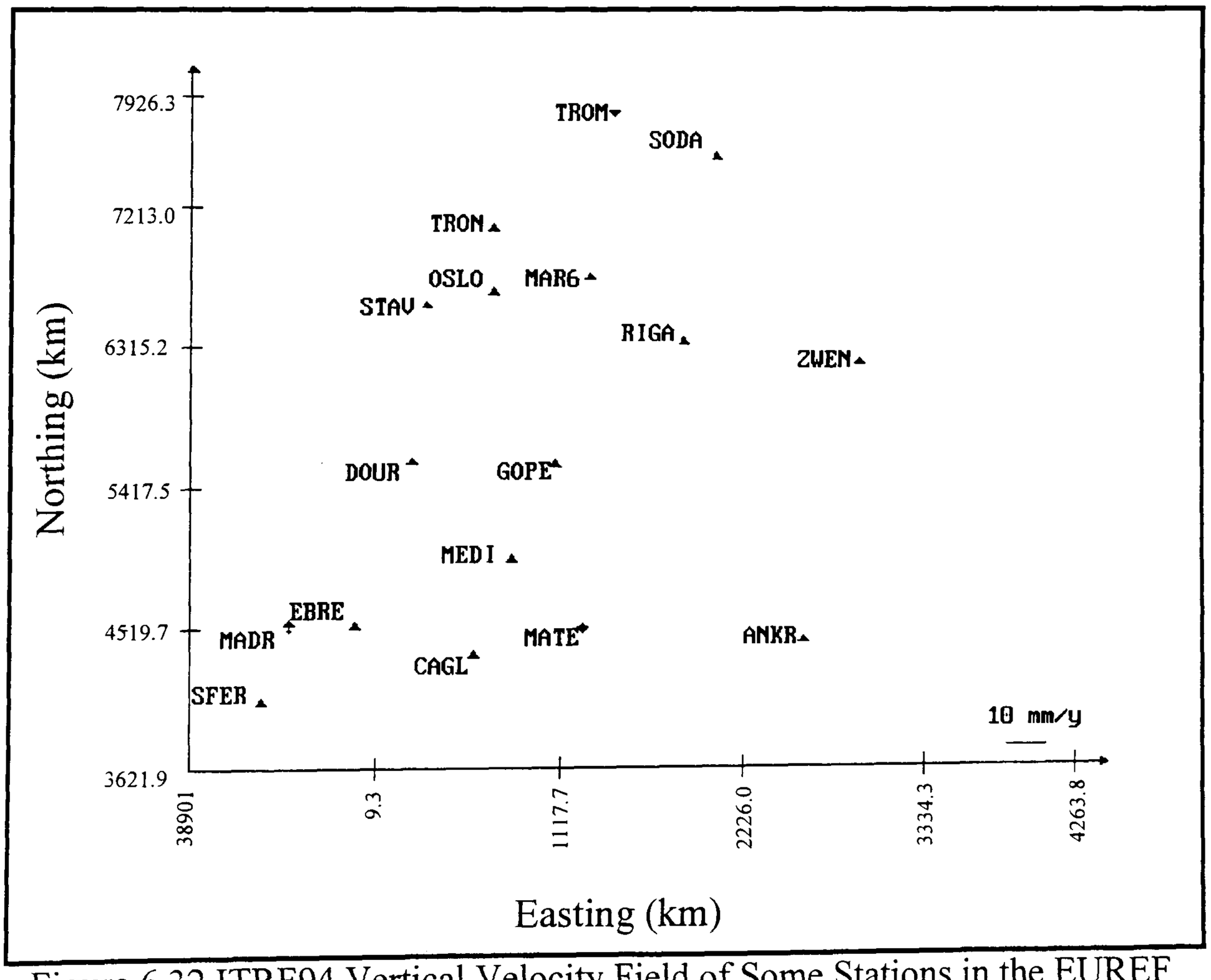

Figure 6.32 ITRF94 Vertical Velocity Field of Some Stations in the EUREF Permanent GPS Network

In Figures 6.33 and 6.34, strain rates for the first and second groups of stations are plotted. The results for all the epochs and all groups are given in Appendix F. From Appendix F, it can be seen that there is no significant rotation taking place. In Figures 6.33 and 6.34, however, the triangles NOTO, NICO, SOFI; NICO, SOFI, ZECK; MAPS, NOTO, NICO; SFER, MADR, CAGL; EBRE, CAGL, MEDI; CAGL, MEDI, MATE; and MATE RIGA, ANKR, all experience compression towards the North - West. This suggests that the Southern part of the Eurasian plate experiences compression, which may be connected to the Northerly motion of the African Plate.

From Figure 6.34, it can be seen that the triangles STAV, OSLO, TRON; TRON, MAR6, TROM; and TRON, OSLO, MAR6, also underwent compression along the direction of North - West.

In Central Europe, it can be seen from Figures 6.33 and 6.34 that there is no significant deformation encountered.

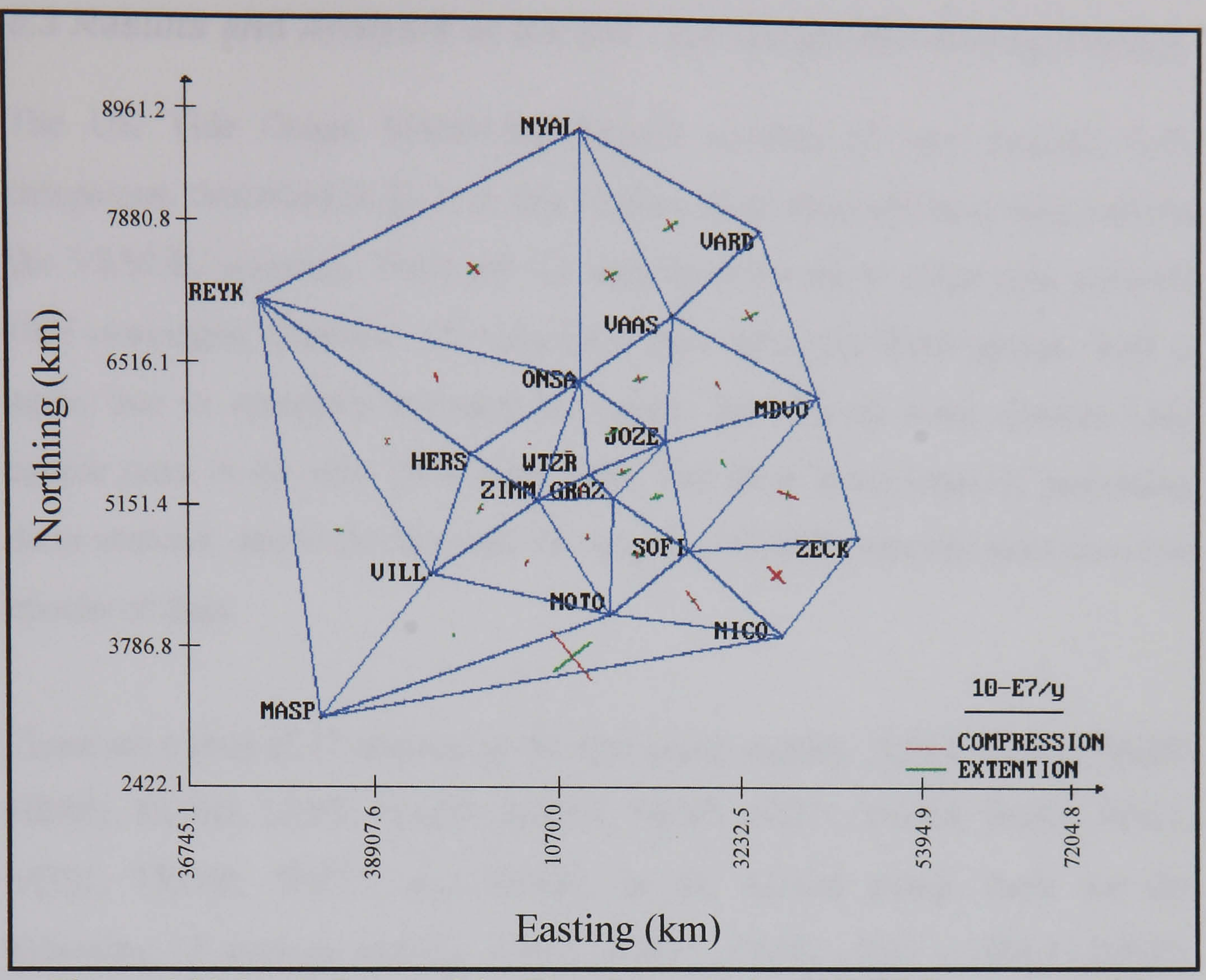

Figure 6.33 Strain Rates of the First Group in the EUREF Permanent GPS Network

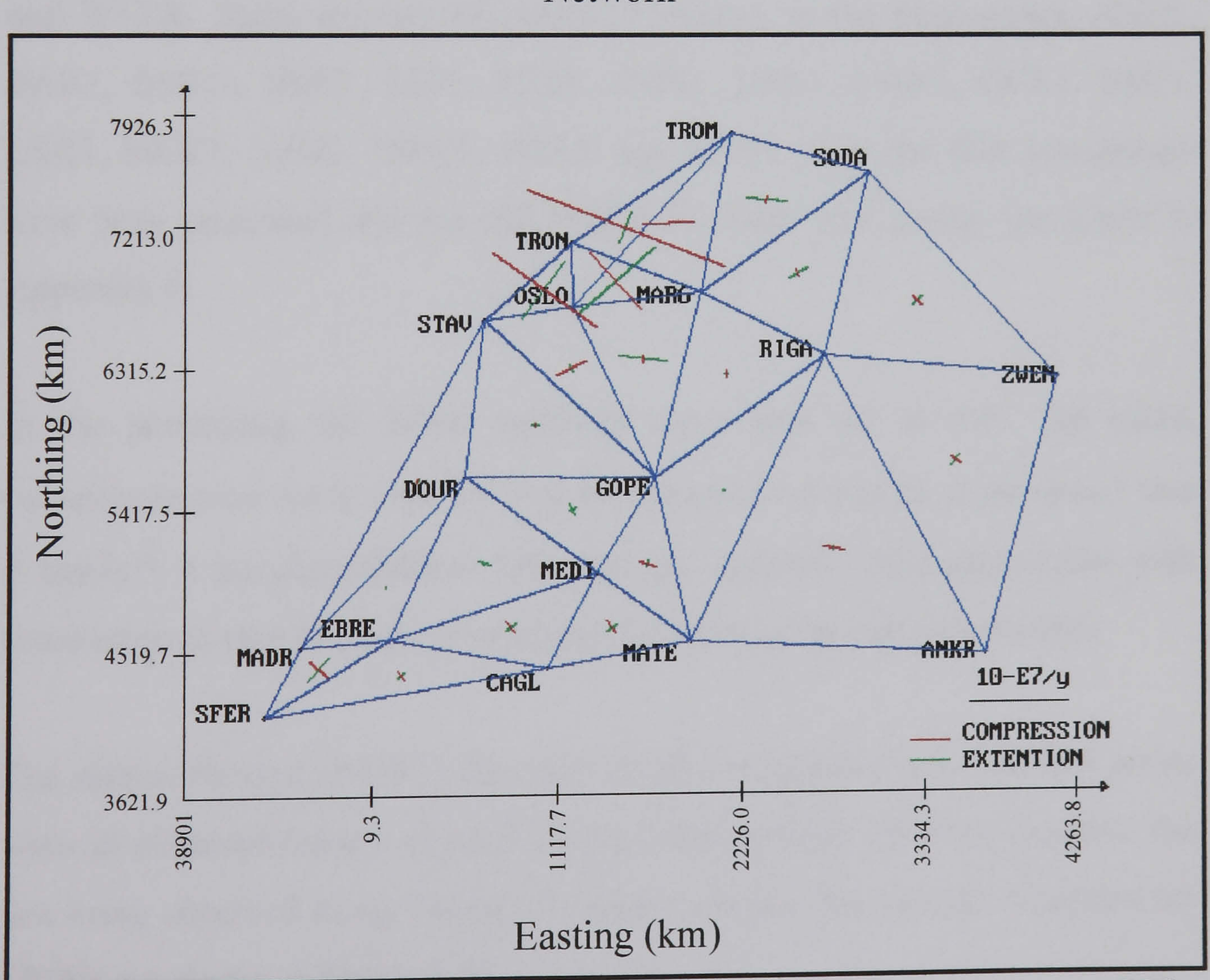

Figure 6.34 Strain Rates of the Second Group in the EUREF Permanent GPS Network

6.3 Results and Analysis of the UK Tide Gauge Monitoring Project

The UK Tide Guage Monitoring Project consists of nine episodic GPS campaigns, described in §5.3. In this section, these data sets have been input to the VEBUK program. There are 51 stations involved in these nine episodic GPS campagns, therefore, the data have been split into three groups. This is again due to computer memory limitation, but also as some stations only appear once in the nine GPS campaigns, and there is no sense in processing these stations, due to the fact that the program VEBUK requires more then two epochs of data.

There are a total of 17 stations in the first group namely, ABE1, HER1, HERS, HRM1, KOSG, LER2, MADR, METS, NEW1, NOT1, ONSA, POR1, PPA1, STO1, TROM, WETT, and ZIMM. In the second group, there are the following 17 stations namely, AVO1, DOV1, DOV2, HEY1, HOL1, IMM1, LER3, LOW1, MATE, MIL1, NEW2, NSH1, NWH1, POR3, SHE1, SHEE, and WTZR. There are the following 17 stations in the third group, ANC1, BAR1, BMO1, BRE1, BRI1, BUD1, CHS1, DAL1, DAN1, GCL1, KST1, LER1, MOE1, NSH2, NWC1, POR2, and RAT1. Only the first two groups have been processed and the full results for these two groups are given in Appendix G.

In the processing, the initial velocities have been set to zero, the initial covariances were set to 4 cm^2y^{-2} and the system noise was set to between 1 and 5 mm^2y^{-4} A standard Kalman filter and the Adaptive filter approaches with fixed-interval smoothing have been used to estimate the station velocities.

The station Newlyn (NEW1) has eight epochs of observations. The first seven were all observed using a standard antenna type, namely Trimble Geodetic, the last being observed using Trimble Compact antenna.The vertical velocities for NEW1 are shown in Figure 6.35 .

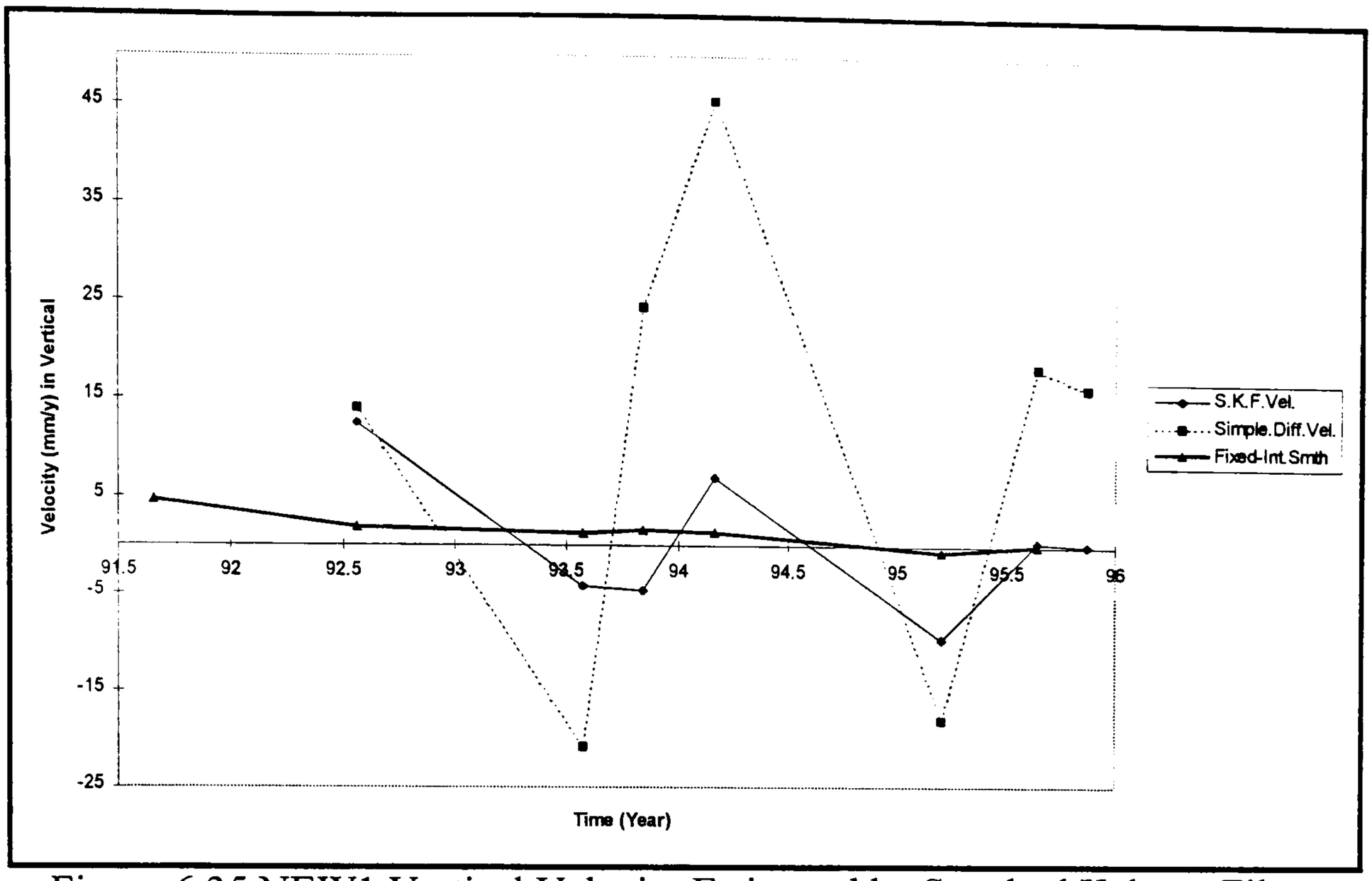

Figure 6.35 NEW1 Vertical Velocity Estimated by Standard Kalman Filter with Fixed-Interval Smoothing

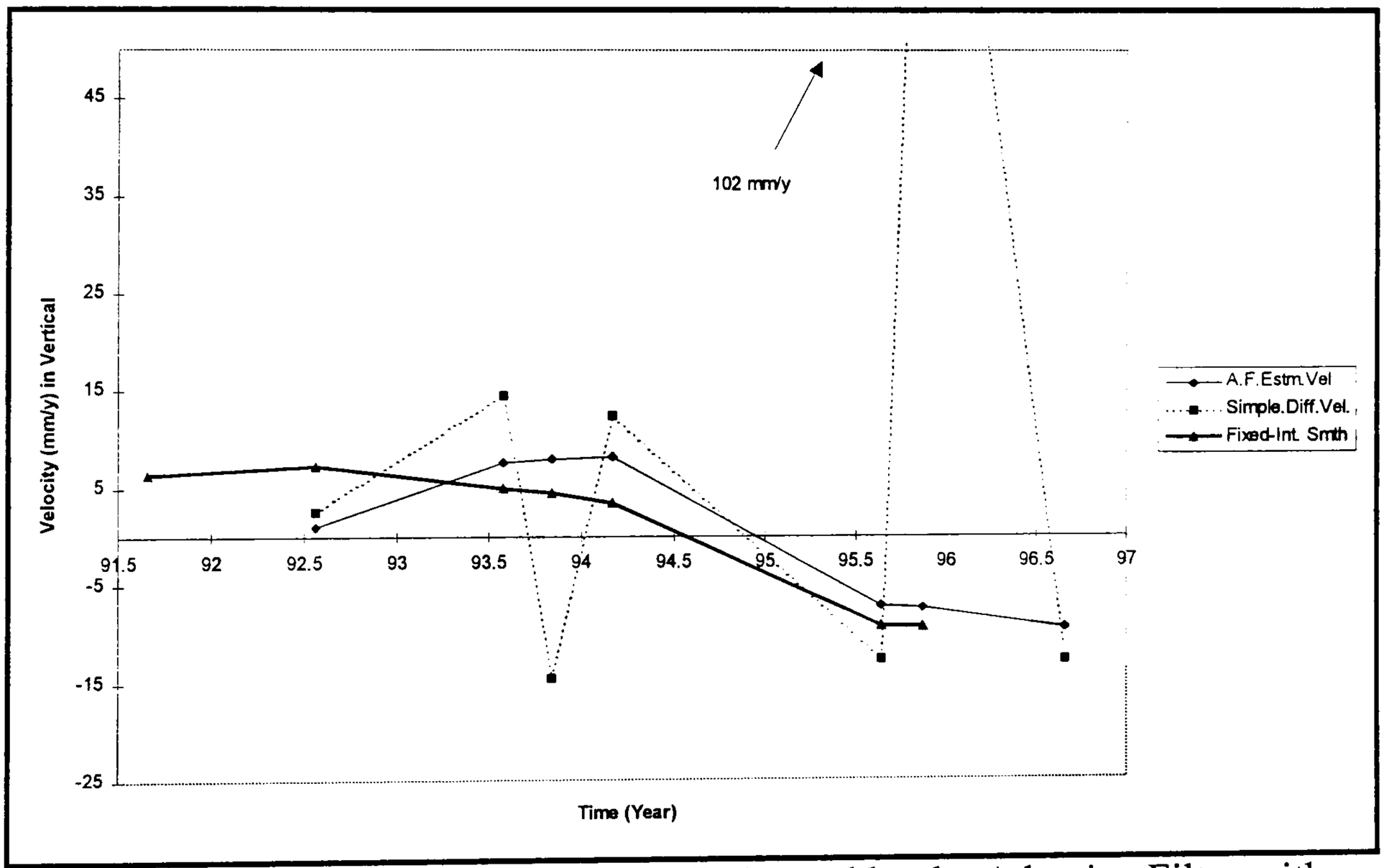

Figure 6.36 POR1 Vertical Velocity Estimated by the Adaptive Filter with Fixed-Interval Smoothing

The station Portsmouth (POR1) also has eight epochs, however two very different antenna types were used. A Trimble geodetic antenna for the first six epochs and an Ashtech compact antenna for the last two epochs. In this case, it is anticipated that the station will experience a bias in the height component due to the changes in antenna type. It can be seen from Figure 6.36 that at

epoch 5, there is a systematic bias due to antenna changes. The magnitude of this bias was estimated to be 12 mm by using the Adaptive filter.

In Figure 6.37 vertical velocity field of the first group of stations is illustrated. Here It can be seen that in general, the stations in the UK appear to be stable.

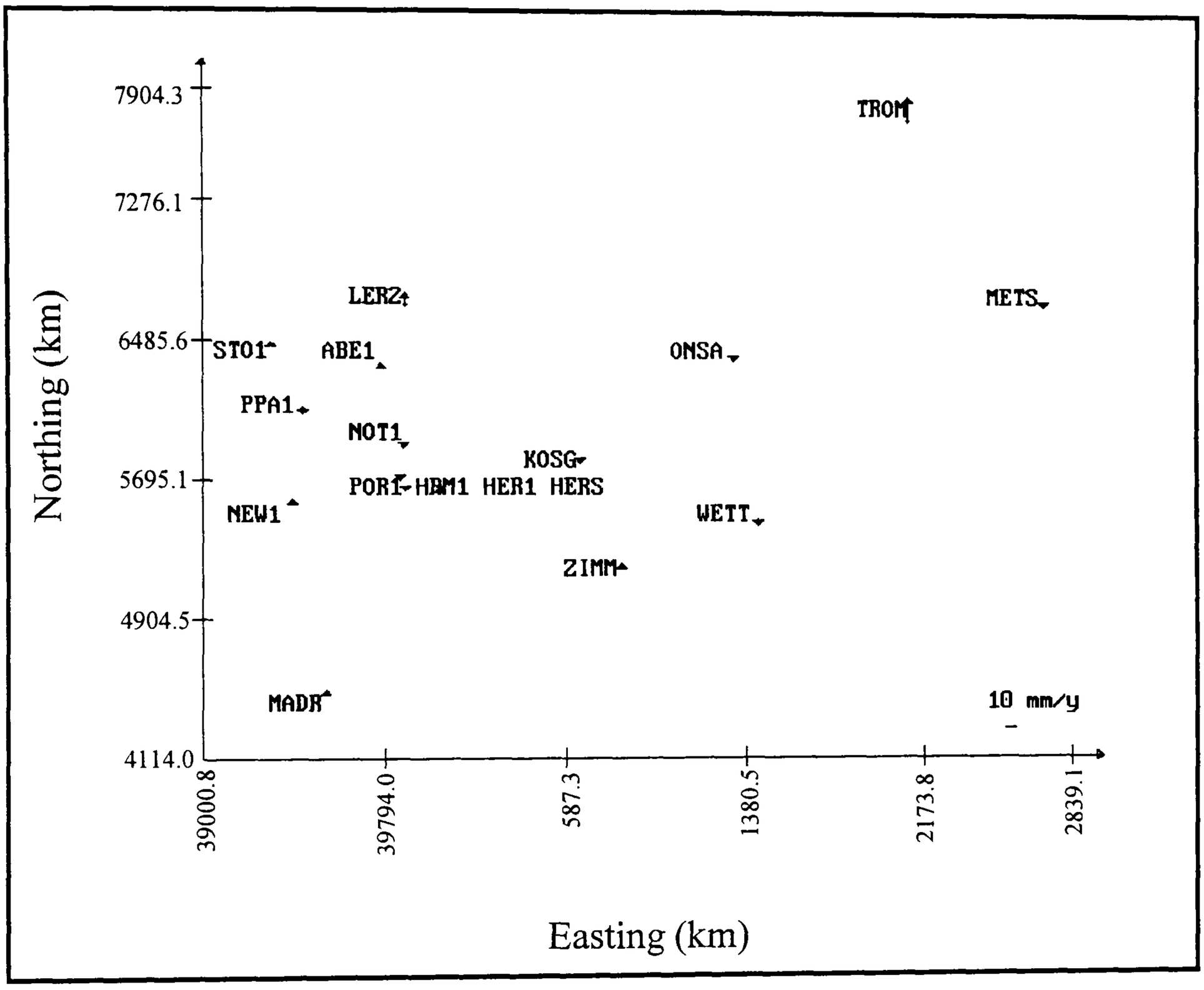

Figure 6.37 Vertical Velocity Field for the First Group in UK Tide Gauge Monitoring Data

From all of the results in Appendix G, it is possible to compute a single vertical velocity and standard error. For each station based on all epochs observed, Table 6.3 shows the values computed for those stations with five or more observation epochs.

Table 6. 3 Single Velocities and Standard Errors for Stations Five or More Epochs Observed

Station Name	Number of. Epoch	System Noise (mm)	Avarage Vel (mm/year)	Standard Error (mm/year)
NEW1	8	5	1.29	±2.78
POR1	8	4	-0.20	±2.28
PPA1	6	3	-0.41	±2.36
ABE1	5	2.5	-0.06	±2.34
HRM1	5	3	-1.00	±2.86
NOT1	8	3	-0.09	±1.90

From Table 6.3, it can be seen that the vertical velocities are not statistically significant at this stage. In general, it is expected that 10 to 20 years of such episodic GPS measurements are required to determine a reliable velocity with vertical and movement of the order of 1 mm/year. These first estimates should, therefore, improve as more episodic or continuous GPS observations are made at these stations. The data from which can be included in the future runs of VEBUK to obtain updated velocity estimates.

Chapter 7

Conclusions and Suggestions for Future Work

In this Chapter, the main objectives are to draw overall conclusions from the studies undertaken and, based on the research in this thesis, to make some suggestions for future work.

7.1 Conclusions

Conclusions are made from five main areas of reference: the new deformation analysis technique proposed by the author; the processed GPS measurements for the two EASTMED campaigns (October 1995 and November 1995); EASTMED real/simulated data test results; EUREF Permanent GPS Network test results; and the analysis of the UK Tide Gauge Monitoring Project data.

7.1.1 Proposed Deformation Analysis Technique

In this thesis, the author has proposed a new deformation analysis technique based on standard Kalman Filtering , Fading Memory Filtering and Adaptive Kalman Filtering for a System With Unknown Bias. This technique consists of five main steps:

1. Adjustment of measurements at each epoch by the least squares method, including data snooping.
2. Reference frame definition.
3. Kalman Filter estimation of station kinematics.
4. Result evaluations using the two statistical tests of; Local Overall Model Test (LOM) and Local Slippage Test (LST) to check whether any bias or local movement has occurred.
5. If any local movement or bias has occurred in one or more epochs as detected by (4), then use either Fading Memory Filtering to mitigate the effect of historical data on the next estimation, or use Adaptive

Kalman Filtering to estimate and remove the effect of this bias (or local movement) from the estimation.

This technique is based on modelling the trajectory of stations at which a series of measurements have been made. Hence, the method can be used in both crustal deformation monitoring and other local deformation monitoring applications such as dam deformation and subsidence monitoring.

From the two sub-optimal filters, it was found that the Adaptive filter has advantages over the Fading Memory filter. The advantages are as follows,

- The Adaptive filter can be used for all the coordinate components to detect and remove the effect of earthquake or bias.

- The Adaptive filter can be used to estimate the magnitude of station displacement due to an earthquake or bias.

The technique is powerful, enabling precise velocities and coordinates of stations to be estimated. Using these velocities, precise strain rates can be calculated which allow an understanding of Earth geodynamics. These data, in association with earthquake history, may be used to assess seismic hazard in earthquake zones.

The VEBUK program has been developed by the author to perform the proposed deformation analysis steps 3, 4 and 5 with three smoothing-techniques: *Backward and Forward Smoothing*, *Fixed-Interval Smoothing, and Fixed-Point Smoothing.*

The VEBUK output can be directly input to a plotting package such as Microsoft Excel to give a spatial appreciation of the measurements and velocities.

The STRAIN program was also developed by the author to perform the calculation of strain rates and rotation using outputs from VEBUK.

7.1.2 East Mediterranean GPS Geodynamics Project

One of the main aims of this project was to monitor crustal deformations. Therefore, the author used the GPS measurements from the EASTMED project to investigate crustal movements.

Two campaigns from the EASTMED project, October 1995 and November 1995 were processed by the author using GAS. Note that between the two campaigns, the Nuweiba earthquake occurred (M=7.1).

Plan coordinate precisions obtained for the October 95 campaign were 2 to 9 mm, and for the November 95 campaign 1 to 4 mm. Height precisions were 7 to 16 mm, and 4 to10 mm in the two campaigns respectively.

It was anticipated that the two survey stations at Eilat (ELAT) in Israel and Aqaba (AQAB) in Jordan, which are located on either side of the Dead Sea Transform Fault (DSTF) to the North of the Gulf of Eilat/Aqaba, could have been affected by the the Nuweiba earthquake that occurred some 120 km to the South. However other network stations farther away from the earthquake epicentres were not expected to move within the 5 week period.

A congruency test was applied to the two campaigns. It was found that the test failed against 95% $F_{(11,18)}$. From a search of which station(s) made a contribution to the failure of the test, station ELAT was found to have made the maximum contribution. Then from the significant movement search, it was found that the Northing and Easting components of station ELAT and the Easting component of AQAB were subject to significant movement.

From these station movements it would appear that between the two epochs the ELAT/AQAB baseline underwent 15 mm extension (or 2 ppm), and 0″.68 seconds anticlockwise rotation.

7.1.3 Real/Simulated Data Based on the EASTMED Project

To test the proposed deformation analysis technique, simulated data based on the two real campaigns from the EASTMED project was created, 10 epochs backwards from October 95 and 10 epochs forward from November 95, using the plate tectonic motion model NNR-NUVEL-1.

The VEBUK program was run in Standard Kalman Filtering mode. At epoch 12, it was found that the Kalman filtering estimates were not optimal, due to the earthquake that occurred between the two EASTMED campaigns. Using the proposed deformation analysis technique, applying the Fading Memory and Adaptive Filter approaches separately, the bias was obtained and removed. The estimated bias for the Northing component of station ELAT was about 3 cm. The RMS of the estimated Northing velocity of station ELAT with respect to NNR-NUVEL-1 is ±0.65mm.

From the result of running both the Fading Memmory and Adaptive filter separately, it was found that the Adaptive filter is the best for the real/simulated data.

Using these precise velocities, strain rates were also estimated and plotted. The deformation pattern was found to be in agreement with the NNR-NUVEL-1 motion model as would be expected as simulation was based on the NNR-NUVEL-1 model.

7.1.4 EUREF Permanent GPS Network

Combined data sets in SINEX format for GPS weeks 834 to 944 of the EUREF Permanent GPS Network, were downloaded from the EUREF Internet site. The

network then (1996) consisted of 65 stations. Data from the SINEX files were extracted so that the coordinates and their covariances could be input to the VEBUK program.

The processed results revealed an inconsistency in the coordinates supplied. This was due to the fact that the reference frame was changed from ITRF93 to ITRF94 during the data interval used. This was readily identified by the VEBUK program, and station velocities were estimated without this anomaly. The estimated bias for Northing component of station ZIMM was about 4 cm.

The level of agreement between the estimated velocities and the ITRF published velocities illustrated the power of the proposed deformation analysis technique. The RMS of the estimated Northing velocity of station ZIMM was ±0.23mm with respect to the ITRF94 velocity filed.

From the strain rates calculated, it can be seen that no significant strain accumulation took place in Central Europe. The average velocity of stations in Central Europe was found to be 33 mm along a North-East direction. However, some evidence of significant crustal deformation were found in Cyprus and Southern Italy.

7.1.5 UK Tide Gauge Monitoring Project

Data from the UK Tide Gauge Monitoring Projects was processed using the VEBUK program in standard Kalman filter and Adaptive filter modes.

The vertical velocities obtained are not statistically significant at this stage. However VEBUK can be used to obtain updated velocity estimates from the episodic or continuous GPS observations planned for the future.

7.1.6 Recommendations on use of VEBUK

The VEBUK program uses the output from CARNET directly, therefore the covariance matrix has to be in upper triangle form.

The author suggests that initial covariances should be set large (4 to 5 cm^2y^{-2}) and system noise small (1 to 2 mm^2y^{-4}). With these constraints, VEBUK should be run in the standard Kalman Filter mode. Depending on the results, ie velocities, predicted residuals, and the tests carried out, system noise can be determined by experience.

If the data contains no bias, VEBUK should be run with one of the smoothing (Forward and Backward, Fixed-Intervals and Fixed-Point Smoothing) option.

If any bias is encountered during one of the two statistical tests, VEBUK should be run with one of the two eliminating filtering techniques, ie Fading Memory Filter and Adaptive Kalman Filter mode.

If Fading Memory Filter mode is chosen, the determination of a decay factor is necessary. The author suggests that it should be set to more than 1. Depending on the resultant velocities, the decay factor can be increased until a satisfactory result is obtained.

If Adaptive Filtering is chosen, the parameter for covariances of the N possible range has to be set up. The author suggests that this parameter should be set up small (say 0.1 mm^2y^{-2}). Depending on the resultant velocities, it can be increased until a satisfactory result is obtained.

In the treatment of earthquake or bias, the author suggest that both methods run separately to find out which one is the best.

The VEBUK produces outputs can be used directly as input to the STRAIN program, for calculation of strain rates and rotations.

7.2 Suggestions for Future Work

From the research carried out in this thesis and the results obtained, the following suggestions for future work can be given.

The proposed deformation analysis technique proved itself to be powerful, enabling precise velocities to be estimated. Precise velocities from a large network may be used to form a velocity field. Using these velocities, one might investigate a good conversion method and testing procedure for whether a station belongs to one particular tectonic plate or another.

The reference frame determination problem was hardly touched in this study, where the reference frame was defined using IGS stations and their coordinates fixed with respect to ITRFyy frame. However, the potential discrepancies introduced by successive realisations of the ITRS were highlighted in §6.2. Hence reference frame definition for deformation monitoring purposes is still worthy of further investigation.

There is little knowledge of the mechanism that creates earthquakes, which may be associated with strain accumulation. Using precise velocities and estimated strain rates, one might research a relationship between strain and earthquake mechanism for seismic hazard assessment in earthquake zones.

More data from crustal deformation, dam deformation or subsidence areas should be used to carry out more tests on the proposed deformation analysis technique.

References

Ambraseys, N. N., and Finkel, C., ,1995 : **The Seismicity of Turkey and Adjacent Areas**, a historical Review, 1500-1800, Eren Press, Istanbul.

Argus, D. F., and Gordon, R. G., 1991 : **No-Net-Rotation Model of Current Plate Motion Model NUVEL-1**, Geophys. Res. Lett, 18, 2039-2042.

Argus, D. F., Gordon, R. G., 1991: **No-Net-Rotation Model of Current Plate Velocities Incorporating Plate Motion Model Nuvel 1.** Geophys. Res. Lett, 18, 2039-2042.

Ashkenazi, V. and Moore, T., 1986 : **The Navigation of Navigation Satellites**, Journal of Navigation, Vol 3.

Ashkenazi, V. Bingley, R. M., Whitmore, G. M., and Baker, T. F., 1993 : **Monitoring Mean Sea Level to Millimetres Using GPS**, Geophysical Research Letters, V.20, No.18, September, p1951-1954.

Ashkenazi, V., and Ffoulkes-Jones, G. H., 1990 : **Millimetres over Hundreds of Kilometres by GPS**, GPS World, Nov/Dec.

Ashkenazi, V., Bingley, R. M., Chang, C. C., Dodson, A. H., Baker, T. F., Ruis, A., Cross, P. A., Torres, J. A., Boucher, C., Fagard, H., Caturla, J. L., Quiros, R., and Calvert, C., 1996a : **The Results of the EUROGAUGE: The West European Tide Gauge Monitoring Project**, XXI General Assembly of the European Geophysical Society, The Hague, May.

Ashkenazi, V., Bingley, R. M., Codd, J. F., and Cory, M. J., 1996b : **Results and Analysis of the EUREF EIR/GB 95 Campaign**, Report on symposium of the IAG Subcommission for European Reference Frame (EUREF), Ankara, p.59-72.

Ashkenazi, V., Bingley, R. M., Dodson, A. H., Penna, N. T., and Baker, T. F., 1998 : **Monitoring Tide Gauge Heights in the UK with GPS**, paper presented in the proceedings of the FIG 98 Congress Brighton, UK.

Baarda, W., 1968 : **A Testing Procedure for Use in Geodetic Networks**, Publications on geodesy, Volume 2, Number 5, Netherlands Geodetic Commission, Netherlands.

Baker, T. F, 1993 : **Absolute Sea Level Measurements, Climate Change and Vertical Crustal Movements**, Elsevier Science Bubls BV, 8, p.149-159.

Baker, T. F., Curtis, D. J., and Dodson, A. H., 1995 : **Ocean Tide Loading and GPS**, GPS World March, 54-59

Baker, T. F., 1984 : **Tidal Deformation of the Earth**, Sci. Prog., 69,197-233, Oxford.

Barka, A. A. and Hancock, P.L., 1984 : **Neotectonic Deformation Patterns in the Convex-Northwards Arc of the North Anotolian Fault in the Geological Evolution of Eastern Mediterranean.** edited by Dixon, J. G., and Robertson, A. H. F., 763-773, Geological Soc. of London.

Bingley, R. M., 1993 : **High Accuracy Monitoring of Movements by Fiducial GPS**, IESSG, University of Nottingham, Nottingham.

Blewitt, G. Vandam, T. M., and Heflin, M. B., 1994 : **Atmospheric Loading Effects and GPS Time Averaged Vertical Positions**, Proceedings of first International Sysmposium on Deformations in Turkey, Istanbul, Turkey.

Boucher, C., and Altamimi, Z., 1991 : **ITRF89 and Other Realisations of the IERS Terrestrial Reference System for 1989**, IERS Technical Note 6, Observatorire de Paris.

Boucher, C., and Altamimi, Z., 1996 : **International Terrestrial Reference Frame**, GPS World, 71-74, September.

Caspary, W. F., 1987 : **Concepts of Network and Deformation Analysis.** Monografh 11, School of Surveying The University of New South Wales, Kesington, N.S.W., Australia.

Celik, C. T., 1995 : **Deformation Monitoring for Crustal Dynamics**, M.Sc. Dissertation, University of Nottingham, Nottingham, UK.

Chang, C. C., 1995 : **Monitoring of Tide Gauge Heights in Western Europe by GPS**, Ph.D Thesis, University of Nottingham, Nottingham, UK.

Channel, J. E. T., D`Argenio, B., and Horvath, F., 1979 : **Adria, the African Promontory, in Mesozoic Mediterranean Palaeogeography**, Earth Science Reviews, 15, p.213-292.

Chase, C. G., 1972 : **The n-plate Problem of Plate Tectonics.** Geophys. J. R. Astrm. Soc., 29, 117-122.

Chase, C. G., 1978 : **Plate Kinematics.** The Americas, East Africa, and the rest of the World, Earth Planet Sci. Lett., 37, 355-368.

Chen Young-qi, 1983 : **Analysis of Deformation Surveys ----A Generalised Method**, TR. 94, UNB, Canada.

Chrazanowsky, A. et al, 1981 : **A comparison of Different Approaches into the Analysis of Deformation Measurements**, Proceedings FIG XVI Congress, No. 602.3, Monrteux.

Condie, K. C., 1989 : **Plate Tectonics and Crustal Evolution.** Third edition, New Mexico Institute of Mining and Technology, Socorro, New Mexico

Cox, A. 1986: **Plate Tectonics How It Works**. Stanford University, London.

Cross, P. A., 1987 : **Derivation of Kalman Filter Equations**, Department of Surveying University of Newcastle Upon Tyne, the paper presented at the Royal Institution of Chartered Surveyors/ Hydrographic Society seminar on Kalman Filtering held at the University of Nottingham, 4 February .

Cross, P. A., 1994 : **Advanced Least Square Applied to Position-Fixing**. Working Paper no: 6, School of Surveying, University of East London, London.

Dally, J. W., and Riley, W. F., 1991 : **Experimental Stress Analysis**, Third editrion, Singapore.

Davies, P. B. H., 1997 : **Assembling the IGS Polyhedron A identified Weekly GPS Terrestrial Reference Frame**, Ph.D Thesis, University of New Castle-Upon-Tyne.

Davila, J. M., Pasquin, J. G., and Dominguez, M. B., 1998 : **A New Permanent San Fernado Observatory GPS Network for Monitoring Crustal Deformations in the South Spain-North Africa Plate Boundary**, Book of Extended Abstracts, The 9th General Assembly of the Working Group of European Geoscientists for the Establishment of Networks for Earth-Science Research, WEGENER 98 , Edited by Hans-Peter Plag, Krokkleiva, Norway.

Davis, J. C., 1986 : **Statistics and Data Analysis in Geology**, 646pp, New York.

Defence Mapping Agency, 1987 : **Department of Defence World Geodetic System 1984 - its Definitions and Relationships with Local Geodetic Systems**, DMA Technical Report 8350.2 NOAA Reprint, USA.

DeMets, C., Gordon, R. G., Argus, D. F., Stein, S., 1990 : **Current Plate Motions.** Geophys. J. int. 101, 425-478.

DeMets, C., Gordon, R. G., Argus, D. F., Stein, S., 1994 : **Effect of Recent Revisions to the Geomagnatic Reversal Time Scale on Estimates of Current Plate Motion.** Geophys. Res. Lett., 21, 2191-2194.

Dewey, J. F., Pitman III, W. C., Ryan, W. B. F., and Bonn, J., 1973 :**Plate Tectonics and the Evolution of the Alpine System**, Geological society of America Bulletin, V.84, p.3137-3180, October.

Dodson, A. H., 1977: **The Measurements of Spatial Displacements by Geodetic Methods**, Ph.D Thesis, University of Nottingham, Nottingham.

Donnellan, A., Hager, B. H., King, R. W., and Herring, T. A., 1993 : **Geodetic Measurement of Deformation in the Ventura Basin Region, Southern California**, Journal of Geophysical Research Vol. 98, No. B12, 21727-21739.

Drewes, H., Kaniuth, K., Stuber, K., Tremel, H., Kahle, H. G., Straub, CH., Hernandez, N., Hoyer, M., and Wildermann, E., 1995 : **The Casa'93 GPS Campaign for Crustal Deformation Research along the South Caribbean Plate Boundary**, J. Geodynamics, Vol. 20, No. 2 129-144.

Ekman, M., 1992 : **Postglacial Rebound and Sea Level Phenomena, with Special Reference to Fennoscandia and Baltic Sea**, Lecturer notes, NKG Autumn School in Helsinki, September, Sweden.

Eren, K. and Uzel, T., 1995 **GPS Olcmeleri**, Yildiz Teknik Universitesi, Insaat Fakultesi Jeodezi ve Fotgrametri Muhendisligi Bolumu, Yayin No:301.

Feigl, K. L., Agnew, D. C., Bock, Y., Dong, D., Donnellan, A., Hager, B. H., Herring, T. A., Jackson, D. D., Jordan, T. H., King, R. W., Larsen, S., Larson, K. M., Murray, M. H., Shen, Z., and Webb, F. H., 1993 : **Space Geodetic Measurement of Crustal Deformation in Central and Southern California, 1984-1992**, Journal of Geophysical Research Vol. 98, No. B12, 21677-21712.

Gelb, A., 1974 : **Applied Optimal Estimation**, written by the Technical Staff, The Analytical Sceince Corporation, Massachusetts Institute of Technology, Cambridge, Massachusetts, and London, England.

Gripp, A. E., and Gordon, R. G., 1990:**Current Plate Velocities Relative to The Hotspots Incorporating The Nuvel 1.** Geophys. Res. Lett, 17, 1109-1112.

Heck, B., Kok, J. J., Welh, W. M., Baumer, R., Chrazanowsky, A., Chen, Y. Q., and Secord, J., 1983: **Report of the FIG-Working Group on the Analysis of Deformation Measurements by Geodetic Methods**, Budapest.

Hempton, M. R., 1987 : **Constrains on the Arabian Plate Moions and Extentional History of the Red Sea.** Tectonics, 6, 686-705.

Hofmann-Wellenhof, B., Lichtenegger, H., and Collins, J., 1997 :**GPS Theory and Practice**, Fourth revised edition, New York.

Howard, R. A., 1964 : **System Analysis of Semi-Morkov Process**, IEEE Transactions on Military Electronics, Mil-8 114-124.

Jack, O. T. L., 1994 : **Multipath Effects on GPS Observations**, Msc Dissertation, University of Nottingham, Nottingham.

Jestin, F., Huchon, P., and Gaulier, J. M., 1994 :**The Somalia Plate and the East African Rift System; Present Day-Kinematics**, Geophysical Journal International, 116, 635-654.

Kalman, R. E., 1960 : **A New Approach to Linear Filtering and Prediction Problems**. Trans. ASME, J. Basic Engineering, Series 82D, pp, 35 - 45, Edited by H.W. Sorenson, **Kalman Filtering**, Theory and Applications, 1985.

Kaplan, E. D., (eds) 1996 : **Understanding GPS Principles and Applications**, Boston, London.

Kearey, P., & Vine, F. J., 1996: **Global Tectonics**, second edition, Cambridge.

Kennedy, M., 1996 : **The Global Positioning System and CIS**, an Introduction, University of Kentucky, Chelsea, Michigan.

Kimata, F., Tealep, A., Murakami, H., Furukawa, N., Mahmoud, S., Kalil, H., Sakr, K. O., and Hamdy, A. M., 1997 : **The Aqaba Earthquake of November 22, 1995, and Co-Seismic Deformation in Sinai Peninsula, Deduced from Repeated GPS Measurements.** Bulletin of the National Research Institude for Astronomy and Geophysics, Helwan, Cairo.

Lambeck, K., 1988:**Geophysical Geodesy the slow deformations of the Earth.**, clarendon press, Oxford.

Langley, R., 1991 : **The GPS Receiver**, an Introduction, GPS World 2(1), pp50-53.

Le Pichon, X., and Angelier, J., 1979 : **The Helenic arc and Trench System: A Key to Neotectonic Evolution of the Eastern Mediterranean Area**, Tectonophysics, Vol. 60, pp1-42.

Lowe, D., 1994 : **CARNET Version 3.13 User Guide**, IESSG, University of Nottingham, Nottingham.

Malvern, L. E., 1969 : **Introduction to the Mechanics of a Continuous Medium**, Engineering of the physical Sceince Michigan state Universty, New Jersey, USA.

Malys, S., James, A. S., Randall, W. S., Larry, E. K., and Steven, C. K. 1997 : **Refinements to The World Geodetic System 1984.** Institute of Navigation, ION GPS-97, Kansas City, MO, September 16-19.

McKenzie, D. P., 1970 : **Plate Tectonics of the Mediterranean Region.** Nature, 226, 239-243.

Meditch, J. S., 1969 : **Stochastic Optimal Linear Estimation and Control**, Boing Scientific Reseach Laboratories, Seattle, Washington, publised in New York, St. Louis, San Francisco, London, Sydney, Toronto, Mexico, Panamas.

Minster, J. B., Jordon, T. H., Molnar, P. and Haines, E., 1974 : **Numerical Modelling of Instantaneous Plate Tectonics.** Geopys. J. R., Astrm. Soc., 36, 541-576.

Minster, J. B. and Jordan, T. H., 1978 : **Present Day Plate Motions.** Geophys. J. Res., 83, 5331-5354.

Moore, T, 1986 : **Satellite Laser Ranging and the Determination of Earth Rotation Parametres.** PHD Thesis, University of Nottingham.

Moore, T., 1993 : **GPS Orbit Determination and Fiducial Network**, IESSG Internal Publication, University of Nottingham, Nottingham.

Morgan, W. J., 1968 : **Rises, Trenches, Great Foults and Crustal Blocks.** Journal of Geophys, 73, 1959-1982.

Muller, I. I., 1991 : **Planning an International Service Using the Global Positioning System (GPS) for Geodynamic Applications**, IAG Symposia no 109, Permanent Satellite Tracking Networks for Geodesy and Geodynamics, Edited by G L Mader, Springer Verlag, pp1-22.

Napier, M., 1990 : **Kalman Filtering**. Internal Paper, in the Institute of Engineering Surveying and Space Geodesy, University of Nottingham, Nottingham.

Nooman, R., Ambrosius, B. A. C., and Walker, K. F., 1993 : **Crustal Motions in the Mediterranean Region Determined from Laser Ranging to Lageos**, Contributions of Space Geodesy to Geodynamics: Crustal Dynamics 23, 331-346.

Noomen, R., Springer, T. A., Ambrosious, A. C., Herzberger, K., Kuijper, D. C., Mets, G. J., Overgaauw, B. and Wakker, K. F., 1995 : **Crustal Deformations in the Mediterranean Area Computed from SLR and GPS Observations.** J. Geodynamics., 21, 1, 73-96.

Ollier, C. D., 1981 : **Tectonics and Landforms.** Geomorphology texts, Horlow, Essex, UK.

Oral, M. B., 1994 : **Global Positioning System (GPS) Measurements in Turkey (1988-1992), Kinematics of the Africa-Arabia-Eurosia Plate Collision Zone.** Ph.D thesis at the University of Massachutsetts Institude of Tecnology.

Penna, N. T., 1997 : **Monitoring Land Movements at UK Tide Gauge Sites Using GPS**, PhD Thesis, University of Nottingham, Nottingham.

Rayson, M. W., 1990 : **Computer Aided Design Geodetic Networks for Monitoring Crustal Tectonics.** Ph.D thesis at the University of Newcastle.

Reilinger, R. E., McClusky, S. C., Oral. M. B., King, R. W., Toksoz, M. N., Barka, A. A., Kinik, I., Lenk, O., and Sanli, I., 1997 : **Global Positioning System Measurements of Present -Day Crustal Movements in the Arabia-Africa-Eurosia Plate Collision Zone**, JGR-Solid Earth, Vol 102, 9983.

Richard, L. M., Mohammad, K. S., and Gisli, S., 1986 : **Adaptive Estimation for a System With Unkown Measurement Bias**, IEEE Transactions on Aerospace and Electronic Ssytems, Vol AES-22, no:6.

Rothacher, M., Schaer, S., Mervart, L., and Beutler, G., 1995 : **Determination of Antenna Phase Centre Variations Using GPS Data**, IGS Workshop, Potsdam, May.

Salamon, A., 1993 : **Seismotectonic Analysis of Earthquakes in Israel and Adjecent Areas**, PhD Theses Hebrew University, Jerusalem, 135pp (in Hebrew, English abstract).

Salzmann, M. A., 1988 : **Some Aspects of Kalman Filtering**, Dep. of Surveying Engineering, University of New Brunswick, Canada.

Schofield, W., 1993 : **Engineering Surveying**, Theory and Examination Problems for Students, fourth edition, Great Britain.

Schupler, B., and Clark, T. A., 1991 : **How Different Antennas Effect the GPS Observables**, GPS World, 32-36.

Seeber, G., 1993 :**Satellite Geodesy**, Foundations, Methods and Applications, New York.

Segall, P., Williams, C. R., and Arnadottir, T., 1993 : **Coseicmic Deformation and Dislocation Models of the 1989 Loma Prieta Earthquake Derived from Global Positioning System Measurements**, Journal of Geophysical Research Vol. 98, No. B3, 4567-4578.

Seno, T., Moriyama, T., Stein, S., Woods, D. F., DeMets, C., Argus, D. and Gordon, R., 1987 : **Redetermination of the Philippine Sea Plate Motion.** EOS. Trans. Am. Geophys. Union, 68.

Seyfert, C. K., and Sirkin, L. A., 1979 : **Earth History and Plate Tectonics**, An introduction to Historical Geology, second edition, New York, Hagerstown,, Philadelphia, San Francisco, London.

Shamir, G., 1996 : **The November 22, 1995, Nuweiba Earthquake, Gulf of Elat (Aqaba): Mechanical Analysis**, The Geophysical Institude of Israel, 550/87/96(114).

Shamir, G., and Shapira, A., 1994 : **Earthquake Sequences in the Gulf of Elat**, In 27th General Assembly of the International Association of Seismology and Physics of the Earth's Interior.

Shank, C. and Lavrakas, J. W., 1994 : **Inside GPS, The Master Control Station**, GPS World, September.

Shardlow, P. J., 1994 : **Propagation Effects on Precise GPS Heighting**, PhD Thesis, University of Nottingham.

Smith, D. E. and Torcotte, D. L., 1993 : **Contributions of Space Geodesy to Geodynamics.** Geodynamics series, 23, 5-20, Washington, D. C.

Sorenson, H. W., 1970 : **Least Square Estimation: from Gauss to Kalman**. IEEE spectrum, vol. 7, pp 63-68, Edited by H.W. Sorenson, **Kalman Filtering**, Theory and Applications, 1985.

Sorenson, H. W., and Sacks, J. E., 1971 : **Recursive fading Memory Filtering**, Information Sciences, 3, 101-109.

Springer, T. A., Rothacher, M. and Beutler, G., 1996 : **Using the Extended CODE Orbit Model- First Experiences**, IGS 1996 Analysis Workshop Proceedings 13-31, March, IGS Central Bureau , Jet Propulsion Laboratory, California Institude of Tecnology, Pasadena, California, USA.

Stein, S., 1993:**Space Geodesy and Plate Motions, Contributions of Space Geodesy to Geodynamics,** Crustal Dynamics, Geodynamics 23 by the American Geophsical Union.

Stewart, M. P., FFoulkes-Jones G. H., Ochieng, W. Y., and Shardlow, P. J., 1995 : **GAS: GPS Analysis Software User Manuel, Version 2.3**, IESSG , University of Nottingham.

Teunessian, P. J. G., and Salzmann, M. A., 1988 : **Performance analysis of Kalman Filters**, Delft University of Technology Reports of the Faculty of Geodesy Mathematical and Physical Geodesy, No: 88.2, Delft, Netherlands.

Tomasi, P., and Rioja, M., 1998 : **South-Western Europe Movements with VLBI**, Book of Extended Abstracts, 9th General Assembly of the Working Group of European Geoscientists for the Establishment of Networks for Earth-science Research, WEGENER 98 , Edited by Hans-Peter Plag, Krokkleiva, Norway.

Udias, A., 1982 :**Seismicity and Seismotectonic Stress Field in the Alpine Mediterranean Region**, Alpine-Mediterranean Geodynamics, edited by

Berkhermer, H., and Hsu, K., Geodynamics series Vol. 7, AGU, Washington, USA.

Udias, A., and Buforn, E., 1988: **Single and Joint Fault-Plane Solution from First-Motion Data** , Seismological Algorithms edited by Durk J. Doornbos. Institute of Geophysics, University of Oslo, Norway.

Vanicek, P., and Krakiwsky, E., 1986: **Geodesy the Concept**, second editoion, North-Holland, Amsterdam, New York, Tokyo.

Wells, D. N., Beck, N., Delikaraoglu, D., Kleusberg, A., Krakiwsky, E. J., Lacchapelle, G., Langley, R. B., Nakiboglu, M., Schwarz, K. P., Tranquillia, J. M., and Vanicek, P., 1986 : **Guide to GPS Positioning**, Canadian GPS Association, Canada.

Wilson, D. S., 1988 : **Tectonic History of the Juan de Fuca Ridge over the Last 40 Million Years.** J. Geophys. Res., 93, 11863-11876.

Woodworth, P. L., Spencer, W. E., and Alcock, G., 1990 : **On the Availability of European Mean Sea Level Data**, International Hydrographic Review, Vol 67, No 1, pp 131-146.

Wyllie, P. J., 1971 : **The Dynamic Earth**, Textbook in geosciences. Newyork, London, Sydney, Toronto.

Zumberge, J. F., and Liu, R., 1995 : **Densification of IERS Terrestrial Reference Frame through Regional GPS Networks**, IGS Workshop Proceedings, Pasadana, California.

Appendix A

(Data Availability Table for EUREF Permanent GPS Network)

STN CODE	1	2	3	4	5	6	7	8	9	10	11	12	13	14	15
ANKR	x	x	x	x	x	x	x	x	x	x	x	x	x	x	x
BOR1	x	x	x	x	x	x	x	x	x	x	x	x	x	x	x
CAGL				x	x	x	x	x	x	x	x	x	x	x	x
EBRE															
GRAS	x	x	x	x	x	x	x	x	x	x	x	x	x	x	x
KOSG	x	x	x	x	x	x	x	x	x	x	x	x	x	x	x
MASP	x	x	x	x	x	x	x	x	x	x	x	x	x	x	x
MATE	x	x	x	x	x	x	x	x	x	x	x				x
MEDI				x	x	x	x	x	x	x	x	x	x	x	x
NOTO	x	x	x	x	x	x	x	x	x	x	x	x	x	x	x
SFER															
UPAD	x	x	x	x	x	x	x	x	x	x	x	x	x	x	x
VENE															
VILL	x	x	x	x	x	x	x	x	x	x	x	x	x	x	x
WTZR	x	x	x	x	x	x	x	x	x	x	x	x	x	x	x
ZIMM	x	x	x	x	x	x	x	x	x	x	x	x	x	x	x
BOGO															
BRUS	x	x	x	x	x	x	x	x	x	x	x	x	x	x	x
GOPE	x	x	x	x	x	x	x	x	x	x	x	x	x	x	x
GRAZ	x	x	x	x	x	x	x	x	x	x	x	x	x	x	x
HERS			x	x	x	x	x	x	x	x	x	x	x	x	x
JOZE	x	x	x	x	x	x	x	x	x	x	x	x	x	x	x
KELY				x	x	x	x	x	x	x	x	x	x		x
KIRU	x	x	x	x	x	x	x	x	x	x	x	x	x	x	x
LAMA	x	x	x	x	x	x	x	x							
MDVO	x	x	x	x	x	x	x	x	x	x	x	x	x	x	x
METS	x	x	x	x	x	x	x		x	x	x	x	x	x	x
ONSA	x	x	x	x	x	x	x	x	x	x	x	x	x	x	x
PENC										x	x	x	x	x	x
POTS	x	x	x	x	x	x	x	x	x	x	x	x	x	x	x
REYK	x	x	x	x	x	x	x	x	x	x	x	x	x	x	x
ZWEN	x	x	x	x	x	x	x	x	x	x	x	x	x	x	x
HFLK	x	x	x	x	x	x	x	x	x	x	x	x	x	x	x
JOEN															
KIR0															
MAR6															
MOPI															
NYAL	x	x	x	x	x	x	x	x	x	x	x	x	x	x	x
OBER															
OSLO															
RIGA															
STAV															
TRON															
VAAS															
VARD															
VIL0															
VIS0															
WROC															
DELF								x	x	x	x	x	x	x	x
DENT			x	x	x	x	x	x	x	x	x	x	x	x	x
DOUR			x	x	x	x	x	x	x	x	x	x	x	x	x
HOFN															
MADR	x	x	x	x	x	x	x	x	x	x	x	x	x	x	x
NICO															
PFAN															
SODA															
SOFI															
SVTL															
THU1	x	x		x	x	x	x	x	x	x	x	x	x	x	x
TOUL															
TROM	x	x		x	x	x	x	x	x	x	x	x	x	x	x
WARE			x	x	x	x	x	x	x	x	x	x	x	x	
WSRT															
ZECK															
WETT	x	x	x	x	x	x	x	x	x	x	x	x	x	x	x

STN CODE	16	17	18	19	20	21	22	23	24	25	26	27	28	29	30
ANKR	x	x	x	x	x	x	x								
BOR1	x	x	x	x	x	x	x	x	x	x	x	x	x	x	x
CAGL	x	x	x	x	x	x	x	x	x	x	x	x	x	x	x
EBRE															
GRAS	x	x	x	x											
KOSG	x	x	x	x	x	x	x	x	x	x	x	x	x	x	x
MASP	x	x	x	x	x	x	x	x	x	x	x	x	x	x	x
MATE													x	x	x
MEDI	x	x	x	x	x	x	x	x	x	x	x	x	x	x	x
NOTO	x	x	x	x	x	x	x	x	x	x	x	x	x	x	x
SFER									x	x	x	x	x	x	x
UPAD	x	x	x	x	x	x	x	x	x	x	x	x	x	x	x
VENE															x
VILL	x	x	x	x	x	x	x	x	x	x	x	x	x	x	x
WTZR	x	x	x	x	x	x	x	x	x	x	x	x	x	x	x
ZIMM	x	x	x	x	x	x	x	x	x	x	x	x	x	x	x
BOGO												x	x	x	x
BRUS	x	x	x	x	x	x	x	x	x	x	x	x	x	x	x
GOPE	x	x	x	x	x	x	x	x	x	x	x	x	x	x	x
GRAZ	x	x	x	x	x	x	x	x	x	x	x	x	x	x	x
HERS	x	x	x	x	x			x	x	x	x	x	x	x	x
JOZE	x	x	x	x	x	x	x	x	x	x	x	x	x	x	x
KELY	x	x	x	x	x	x	x	x	x	x	x	x	x	x	x
KIRU	x	x	x	x	x	x	x	x	x	x	x	x	x	x	x
LAMA	x	x	x	x	x	x	x	x	x	x	x	x	x	x	x
MDVO	x	x	x	x	x	x	x	x	x	x	x	x	x	x	x
METS	x	x	x	x	x	x	x	x	x	x	x	x	x	x	x
ONSA	x	x	x	x	x	x	x	x	x	x	x	x	x	x	x
PENC	x	x	x	x	x	x	x	x	x	x	x	x	x	x	x
POTS	x	x	x	x	x	x	x	x	x	x	x	x	x	x	x
REYK	x	x	x	x	x	x	x	x	x	x	x	x	x	x	x
ZWEN	x	x	x	x	x	x	x	x	x	x	x	x	x	x	x
HFLK	x	x	x	x	x	x	x	x	x	x	x	x		x	x
JOEN															
KIR0															
MAR6															
MOPI															
NYAL	x	x	x	x	x	x	x	x	x	x	x	x	x	x	x
OBER															
OSLO															
RIGA															
STAV															
TRON															
VAAS															
VARD															
VIL0															
VIS0															
WROC															
DELF	x	x	x	x	x	x	x	x	x	x	x	x	x	x	x
DENT	x	x	x	x	x	x	x	x	x	x	x	x	x	x	x
DOUR	x	x	x	x	x	x	x	x	x	x	x	x	x	x	x
HOFN															
MADR	x	x	x	x	x	x	x	x	x	x	x	x	x	x	x
NICO															
PFAN															
SODA															
SOFI															
SVTL															
THU1	x	x	x	x	x	x	x	x	x	x	x	x	x	x	x
TOUL															
TROM	x	x	x	x	x	x	x	x	x	x	x	x	x	x	x
WARE	x	x	x	x	x	x	x	x	x	x	x	x	x	x	
WSRT															
ZECK															
WETT	x	x	x	x	x	x	x	x	x	x	x	x	x	x	x

STN CODE	31	32	33	34	35	36	37	38	39	40	41	42	43	44	45
ANKR	x	x	x	x	x	x	x	x	x	x	x	x	x	x	x
BOR1	x	x	x	x	x	x	x	x	x	x	x	x	x	x	x
CAGL	x	x	x	x	x	x	x	x	x	x	x	x	x	x	x
EBRE												x	x	x	x
GRAS										x	x	x	x	x	x
KOSG	x	x	x	x	x	x	x	x	x	x	x	x	x	x	x
MASP	x	x	x	x	x	x	x	x	x	x	x	x	x	x	x
MATE	x	x	x	x	x	x	x	x	x	x	x	x	x	x	x
MEDI	x	x	x	x	x	x	x	x	x	x	x	x	x	x	x
NOTO	x	x	x	x	x	x	x	x	x	x	x	x	x	x	x
SFER	x	x	x	x	x	x	x	x	x	x	x	x	x	x	x
UPAD	x			x	x	x	x	x	x	x	x	x	x	x	x
VENE				x	x	x	x	x	x	x	x	x	x	x	x
VILL	x	x	x	x	x	x	x	x	x	x	x	x	x	x	x
WTZR	x	x	x	x	x	x	x	x	x	x	x	x	x	x	x
ZIMM	x	x	x	x	x	x	x	x	x	x	x	x	x	x	x
BOGO	x	x	x	x	x	x	x	x	x	x	x	x	x	x	x
BRUS	x	x	x	x	x	x	x	x	x	x	x	x	x	x	x
GOPE	x	x	x	x	x	x	x	x	x	x	x	x	x	x	x
GRAZ	x	x	x	x	x	x	x	x	x	x	x	x	x	x	x
HERS	x	x		x			x	x	x	x	x	x	x	x	x
JOZE	x	x	x	x	x	x	x	x	x	x	x	x	x	x	x
KELY	x	x	x	x	x	x	x	x	x	x	x	x	x	x	x
KIRU	x	x	x	x	x	x	x	x	x	x	x	x	x	x	x
LAMA	x	x	x	x	x	x	x	x	x	x	x	x	x	x	x
MDVO	x	x	x	x	x	x	x	x	x	x	x	x	x	x	x
METS	x	x	x	x	x	x	x	x	x	x	x	x	x	x	x
ONSA	x	x	x	x	x	x	x	x	x	x	x	x	x	x	x
PENC	x	x	x	x	x	x	x	x	x	x	x	x	x	x	x
POTS	x	x	x	x	x	x	x	x	x	x	x	x	x	x	x
REYK	x	x	x	x	x	x	x	x	x	x	x	x	x	x	x
ZWEN			x		x	x	x	x	x	x	x	x	x	x	x
HFLK	x	x	x	x	x	x	x	x	x	x	x	x	x	x	x
JOEN															x
KIR0															x
MAR6															x
MOPI															
NYAL	x	x	x	x	x	x	x	x	x	x	x	x	x	x	x
OBER															
OSLO															x
RIGA															x
STAV															x
TRON															x
VAAS															x
VARD															x
VIL0															x
VIS0															x
WROC															
DELF	x	x	x	x	x	x	x	x	x	x	x	x	x	x	x
DENT	x	x	x	x	x	x	x	x	x	x	x	x	x	x	x
DOUR	x	x	x	x	x	x	x	x	x	x	x	x	x	x	x
HOFN															
MADR	x	x	x	x	x	x	x	x			x	x	x	x	x
NICO															
PFAN															
SODA															
SOFI															
SVTL															
THU1	x	x	x	x	x	x	x	x	x	x	x	x	x	x	x
TOUL															
TROM	x	x	x	x	x	x	x	x			x	x	x	x	x
WARE	x	x	x	x	x	x	x	x	x	x	x	x	x	x	x
WSRT															
ZECK															
WETT	x	x	x	x	x	x	x								

STN CODE	46	47	48	49	50	51	52	53	54	55	56	57	58	59	60
ANKR		x	x	x	x	x	x	x	x	x	x	x	x	x	x
BOR1	x	x	x	x	x	x	x	x	x	x	x	x	x	x	x
CAGL	x	x	x	x	x	x	x	x	x	x	x	x	x	x	x
EBRE	x	x	x	x	x	x	x	x	x	x	x	x	x	x	x
GRAS	x	x	x	x	x	x	x	x	x	x	x	x	x	x	x
KOSG	x	x	x	x	x	x	x	x	x	x	x	x	x	x	x
MASP	x	x	x	x	x	x	x	x	x	x	x	x	x	x	x
MATE	x	x	x	x	x	x	x	x	x	x	x	x	x	x	x
MEDI	x	x	x	x	x		x	x	x	x	x	x	x	x	x
NOTO	x	x	x	x	x	x	x	x	x	x	x	x	x	x	x
SFER	x	x	x	x	x	x	x	x	x	x	x	x	x	x	x
UPAD	x	x	x	x	x	x	x	x	x	x	x	x		x	x
VENE	x	x	x	x	x	x	x	x	x	x	x	x	x	x	x
VILL	x	x	x	x	x	x	x	x	x	x	x	x	x	x	x
WTZR	x	x	x	x	x	x	x	x	x	x	x	x	x	x	x
ZIMM	x	x	x	x	x	x	x	x	x	x	x	x	x	x	x
BOGO	x	x	x	x	x	x	x	x	x	x	x	x	x	x	x
BRUS	x	x	x	x	x	x	x	x	x	x	x	x	x	x	x
GOPE	x	x	x	x	x	x	x	x	x	x	x	x	x	x	x
GRAZ	x	x	x	x	x	x	x	x	x	x	x	x	x	x	x
HERS	x	x	x	x	x	x	x	x	x	x	x	x	x	x	x
JOZE	x	x	x	x	x	x	x	x	x	x	x	x	x	x	x
KELY	x	x	x	x	x	x	x	x	x	x	x	x	x	x	x
KIRU	x	x	x	x	x	x	x	x	x	x					
LAMA	x	x	x	x	x	x	x	x	x	x	x	x	x	x	x
MDVO	x	x	x	x	x	x	x	x	x	x	x	x	x	x	x
METS	x	x	x	x	x	x	x	x	x	x	x	x	x	x	x
ONSA	x	x	x	x	x	x	x	x	x	x	x	x	x	x	x
PENC	x	x	x	x	x	x	x	x		x	x	x	x	x	x
POTS	x	x	x	x	x	x	x	x	x	x	x	x	x	x	x
REYK	x	x	x	x	x	x	x	x	x	x	x	x	x	x	x
ZWEN	x	x	x	x	x	x	x	x	x	x	x	x	x	x	x
HFLK	x	x	x	x	x	x					x	x	x	x	x
JOEN	x		x	x	x	x	x	x	x	x	x	x	x	x	x
KIR0	x		x	x						x	x	x	x	x	x
MAR6	x		x	x	x	x	x	x	x	x	x	x	x	x	x
MOPI		x	x	x	x	x	x	x	x	x	x	x	x	x	x
NYAL	x	x	x	x	x	x	x	x	x	x	x	x	x	x	x
OBER									x	x	x	x	x	x	x
OSLO	x		x	x	x	x	x	x	x	x	x	x	x	x	x
RIGA	x		x	x	x	x	x	x	x	x	x	x	x	x	x
STAV	x		x	x	x	x	x	x	x	x	x	x	x	x	x
TRON	x		x	x	x	x	x	x	x	x	x	x	x	x	x
VAAS	x		x	x	x					x	x	x	x	x	x
VARD	x		x	x	x	x	x	x	x	x	x	x	x	x	x
VIL0	x		x	x	x	x	x	x	x	x	x	x	x	x	x
VIS0	x		x	x	x	x	x	x	x	x	x	x	x	x	x
WROC			x	x	x	x	x	x	x	x	x	x	x	x	x
DELF	x	x	x	x	x	x	x	x	x	x	x	x	x	x	x
DENT	x	x	x	x	x	x	x	x	x	x	x	x	x	x	x
DOUR	x	x	x	x	x	x	x	x	x	x	x	x	x	x	x
HOFN															
MADR	x	x	x	x	x	x	x	x	x						
NICO															
PFAN															
SODA															x
SOFI															
SVTL	x		x	x	x	x	x	x	x	x	x	x	x	x	x
THU1	x	x	x	x	x	x	x	x	x	x	x	x	x	x	x
TOUL															
TROM	x		x	x	x	x	x	x	x	x	x	x			
WARE	x	x	x	x	x	x	x	x	x	x	x	x	x	x	x
WSRT															
ZECK															
WETT															

STN CODE	61	62	63	64	65	66	67	68	69	70	71	72	73	74	75
ANKR	x	x	x	x	x	x	x	x	x	x	x	x	x	x	x
BOR1	x	x	x	x	x	x	x	x	x	x	x	x	x	x	x
CAGL	x	x	x	x	x	x	x	x	x	x	x	x	x	x	x
EBRE	x	x	x	x	x	x	x	x	x	x	x	x	x	x	x
GRAS	x	x	x	x	x	x	x	x	x	x	x	x	x	x	x
KOSG	x	x	x	x	x	x	x	x	x	x	x	x	x	x	x
MASP	x	x	x	x	x	x	x	x	x	x	x	x	x	x	x
MATE	x	x	x	x	x	x	x	x	x	x	x	x	x	x	x
MEDI	x	x	x	x	x	x	x	x	x	x	x	x	x	x	x
NOTO	x	x	x	x	x	x	x	x	x	x	x	x	x	x	x
SFER	x	x	x	x	x	x	x	x	x	x	x	x	x	x	x
UPAD	x	x	x	x	x	x	x	x	x	x	x	x	x	x	x
VENE	x	x	x	x	x	x	x	x	x	x	x	x	x	x	x
VILL	x	x	x	x	x	x	x	x	x	x	x	x	x	x	x
WTZR	x	x	x	x	x	x	x	x	x	x	x	x	x	x	x
ZIMM	x	x	x	x	x	x	x	x	x	x	x	x	x	x	x
BOGO	x	x	x	x	x	x	x	x	x	x	x	x	x	x	x
BRUS	x	x	x	x	x	x	x	x	x	x	x	x	x	x	x
GOPE	x	x	x	x	x	x	x	x	x	x	x	x	x	x	x
GRAZ	x	x	x	x	x	x	x	x	x	x	x	x	x	x	x
HERS	x	x	x	x	x	x	x	x	x	x	x	x	x	x	x
JOZE	x	x	x	x	x	x	x	x	x	x	x	x	x	x	x
KELY	x	x	x	x	x	x	x	x	x	x	x	x	x	x	x
KIRU	x		x	x	x	x	x	x	x	x	x	x	x	x	x
LAMA	x	x	x	x	x	x	x	x	x	x	x	x	x	x	x
MDVO	x	x	x	x	x	x	x	x	x	x	x	x	x	x	x
METS	x	x	x	x	x	x	x	x	x	x	x	x	x	x	x
ONSA	x	x	x	x	x	x	x	x	x	x	x	x	x	x	x
PENC	x	x	x	x	x	x	x	x	x	x	x	x	x	x	x
POTS	x	x	x	x	x	x	x	x	x	x	x	x	x	x	x
REYK	x	x	x	x	x	x	x	x	x	x	x	x	x	x	x
ZWEN	x	x	x	x	x	x	x	x		x		x	x	x	x
HFLK	x	x	x	x	x	x	x	x	x	x	x	x	x	x	x
JOEN	x	x	x	x	x	x	x	x	x	x	x	x	x	x	x
KIR0	x	x	x	x	x	x	x	x	x	x	x	x	x	x	x
MAR6	x	x	x	x	x	x	x	x	x	x	x	x	x	x	x
MOPI	x	x	x	x	x	x	x	x	x	x	x	x	x	x	x
NYAL	x	x	x	x	x	x	x	x	x	x	x	x	x	x	x
OBER	x	x	x	x	x	x	x	x	x	x	x	x	x	x	x
OSLO	x	x	x	x	x	x	x	x	x	x	x	x	x	x	x
RIGA	x	x	x	x	x	x	x	x	x	x	x	x	x	x	x
STAV	x	x	x	x	x	x	x	x	x	x	x	x	x	x	x
TRON	x	x	x	x	x	x	x	x	x	x	x	x	x	x	x
VAAS	x	x	x	x	x	x	x	x	x	x	x	x	x	x	x
VARD	x	x	x	x	x	x	x	x	x	x	x	x	x	x	x
VIL0	x	x	x	x	x	x	x	x	x	x	x	x	x	x	x
VIS0	x	x	x	x	x	x	x	x	x	x	x	x	x	x	x
WROC	x	x	x	x	x	x	x	x	x	x	x	x	x	x	x
DELF	x	x	x	x	x	x	x	x	x	x	x	x	x	x	x
DENT	x	x	x	x	x	x	x	x	x	x	x	x	x	x	x
DOUR	x	x	x	x	x	x	x	x	x	x	x	x	x	x	x
HOFN															
MADR															
NICO															
PFAN								x	x	x	x	x	x	x	x
SODA	x	x	x	x	x	x	x	x	x	x	x	x	x	x	
SOFI															
SVTL	x	x	x	x	x	x	x	x	x	x	x	x	x	x	x
THU1								x	x	x	x	x	x	x	x
TOUL															
TROM															
WARE	x	x	x		x	x	x	x	x	x	x	x	x	x	x
WSRT															
ZECK															
WETT															

STN CODE	76	77	78	79	80	81	82	83	84	85	86	87	88	89	90
ANKR	x	x	x	x	x		x	x	x	x	x	x	x	x	x
BOR1	x	x	x	x	x	x	x	x	x	x	x	x	x	x	x
CAGL	x	x	x	x	x	x	x	x	x	x	x	x	x	x	x
EBRE	x	x	x	x	x	x	x	x	x	x	x	x	x	x	x
GRAS	x	x	x	x	x	x	x	x	x	x	x	x	x	x	x
KOSG	x	x	x	x	x	x	x	x	x	x	x	x	x	x	x
MASP	x	x	x	x	x	x	x	x	x	x	x	x	x	x	x
MATE	x	x	x	x	x	x	x	x	x	x	x	x	x	x	x
MEDI	x	x	x	x	x	x	x	x	x	x	x	x	x	x	x
NOTO	x	x	x	x	x	x	x	x	x	x	x	x	x	x	x
SFER	x	x	x	x	x	x	x	x	x	x	x	x	x	x	x
UPAD	x	x	x	x	x	x	x	x	x	x	x	x	x		
VENE	x	x	x	x	x	x	x	x	x	x	x	x	x	x	x
VILL	x	x	x	x	x	x	x	x	x	x	x	x	x	x	x
WTZR	x	x	x	x	x	x	x	x	x	x	x	x	x	x	x
ZIMM	x	x	x	x	x	x	x	x	x	x	x	x	x	x	x
BOGO	x	x	x	x	x	x	x	x	x	x	x	x	x	x	x
BRUS	x	x	x	x	x	x	x	x	x	x	x	x	x	x	x
GOPE	x	x	x	x	x	x	x	x	x	x	x	x	x	x	x
GRAZ	x	x	x	x	x	x	x	x	x	x	x	x	x	x	x
HERS	x	x				x	x	x	x	x	x	x	x	x	x
JOZE	x	x	x	x	x	x	x	x	x	x	x	x	x	x	x
KELY	x	x	x	x	x	x	x	x	x	x	x	x	x	x	x
KIRU	x	x	x	x	x	x	x	x	x	x	x	x	x	x	x
LAMA	x	x	x	x	x	x	x	x	x	x	x	x	x	x	x
MDVO	x	x	x	x	x	x	x	x	x	x	x	x	x	x	x
METS	x	x	x	x	x	x	x	x	x	x	x	x	x	x	x
ONSA	x	x	x	x	x	x	x	x	x	x	x	x	x	x	x
PENC	x	x	x	x	x	x	x	x	x	x	x	x	x	x	x
POTS	x	x	x	x	x	x	x	x	x	x	x	x	x	x	x
REYK	x	x	x	x	x	x	x	x	x	x	x	x	x	x	x
ZWEN	x	x	x	x	x	x	x	x	x	x	x	x	x	x	x
HFLK	x	x	x	x	x	x	x	x	x	x	x	x	x	x	
JOEN	x	x	x	x	x	x	x	x	x	x	x	x	x	x	x
KIR0	x	x	x	x	x	x	x	x	x	x	x	x	x	x	x
MAR6	x	x	x	x	x	x	x	x	x	x	x	x	x	x	x
MOPI	x	x	x	x	x	x	x	x	x	x	x	x	x	x	x
NYAL	x	x	x	x		x	x	x	x	x	x	x			
OBER	x	x	x	x	x	x	x	x	x	x	x	x	x	x	x
OSLO	x	x	x	x	x	x	x	x	x	x	x	x	x	x	x
RIGA	x	x	x	x	x	x	x	x	x	x	x	x	x	x	x
STAV	x	x	x	x	x	x	x	x	x	x	x	x	x	x	x
TRON	x	x	x	x	x	x	x	x	x	x	x	x	x	x	x
VAAS	x	x	x	x	x	x	x	x	x	x	x	x	x	x	x
VARD	x	x	x	x	x	x	x	x	x	x	x	x	x	x	x
VIL0	x	x	x	x	x	x	x		x	x	x	x	x	x	x
VIS0	x	x	x	x	x	x	x	x	x	x	x	x	x	x	x
WROC	x	x	x	x	x	x	x	x	x	x	x	x	x	x	x
DELF	x	x	x	x	x	x	x	x	x	x	x	x	x	x	x
DENT	x	x	x	x	x	x	x	x	x	x	x	x	x	x	x
DOUR	x	x	x	x	x	x	x	x	x	x	x	x	x	x	x
HOFN															
MADR	x	x	x	x	x	x	x	x	x	x	x	x	x	x	x
NICO			x	x	x	x	x	x	x	x	x	x	x	x	x
PFAN	x	x	x	x	x	x	x	x	x	x	x	x	x	x	x
SODA	x	x	x	x	x	x	x	x	x	x	x	x	x	x	x
SOFI			x	x	x	x	x	x	x	x	x	x	x	x	x
SVTL	x	x	x	x	x	x	x	x	x	x	x	x	x	x	x
THU1	x	x	x	x	x	x	x	x	x	x	x	x			x
TOUL						x	x	x	x	x	x	x	x	x	x
TROM															
WARE	x	x	x	x	x	x	x	x	x	x	x	x	x	x	x
WSRT											x	x	x	x	x
ZECK															
WETT															

STN CODE	91	92	93	94	95	96	97	98	99	100	101	102	103	104
ANKR	x	x	x	x	x	x	x	x	x	x	x	x	x	x
BOR1	x	x	x	x	x	x	x	x	x	x	x	x	x	x
CAGL	x	x	x	x	x	x	x	x	x	x	x	x	x	x
EBRE	x	x	x	x	x	x	x	x	x	x	x	x	x	x
GRAS	x	x	x	x	x	x	x	x	x	x	x	x	x	x
KOSG	x	x	x	x	x	x	x	x	x	x	x	x	x	x
MASP	x	x	x	x	x	x	x	x	x	x	x	x	x	x
MATE	x	x	x	x	x	x	x	x	x	x	x	x	x	x
MEDI	x	x	x	x	x	x	x	x	x	x	x	x	x	x
NOTO	x	x	x	x	x	x	x	x	x	x	x	x	x	x
SFER	x	x	x	x	x	x	x	x	x	x			x	x
UPAD	x	x	x	x	x	x	x	x	x	x	x	x	x	
VENE		x	x	x	x	x	x	x	x	x	x	x	x	x
VILL	x	x	x	x	x	x	x	x	x	x	x	x	x	x
WTZR	x	x	x	x	x	x	x	x	x	x	x	x	x	x
ZIMM	x	x	x	x	x	x	x	x	x	x	x	x	x	x
BOGO	x	x	x	x	x	x	x	x	x	x	x	x	x	x
BRUS	x	x	x	x	x	x	x	x	x	x	x	x	x	x
GOPE	x	x	x	x	x	x	x	x	x	x	x	x	x	x
GRAZ	x	x	x	x	x	x	x	x	x	x	x	x	x	x
HERS	x	x	x			x	x							
JOZE	x	x	x	x	x	x	x	x	x	x	x	x	x	x
KELY	x	x	x	x	x	x	x	x	x	x	x	x	x	x
KIRU	x	x	x	x	x	x	x	x	x	x	x	x	x	x
LAMA	x	x	x	x	x	x	x	x	x	x	x	x	x	x
MDVO	x	x	x	x	x	x	x	x	x	x	x	x	x	x
METS	x	x	x	x	x	x	x	x	x	x	x	x	x	x
ONSA	x	x	x	x	x	x	x	x	x	x	x	x	x	x
PENC	x	x	x	x	x	x	x	x	x	x	x	x	x	x
POTS	x	x	x	x	x	x	x	x	x	x	x	x	x	x
REYK	x	x	x	x	x	x	x	x	x	x	x	x	x	x
ZWEN	x	x	x	x	x	x	x	x	x	x	x	x	x	x
HFLK	x	x	x	x	x	x	x	x	x	x	x	x	x	
JOEN	x	x	x	x	x	x	x	x	x	x	x	x	x	x
KIR0	x	x	x	x	x	x	x	x	x	x	x	x	x	x
MAR6	x	x	x	x	x	x	x	x	x	x	x	x	x	x
MOPI	x	x	x	x	x	x	x	x	x	x	x	x	x	x
NYAL														
OBER	x	x	x	x	x	x	x	x	x	x	x	x	x	x
OSLO	x	x	x											
RIGA	x	x	x	x	x	x	x	x	x	x	x	x	x	x
STAV	x	x	x											
TRON	x	x	x											
VAAS	x	x	x	x	x	x	x	x	x	x	x	x	x	x
VARD	x	x	x											
VIL0	x	x	x	x	x	x	x	x	x	x	x	x	x	x
VIS0	x	x	x	x	x	x	x	x	x	x	x	x	x	x
WROC	x	x	x	x	x	x	x	x	x	x	x	x	x	x
DELF	x	x	x	x	x	x	x	x	x	x	x	x	x	x
DENT	x	x	x	x	x	x	x	x	x	x	x	x	x	x
DOUR	x	x	x	x	x	x	x	x	x	x	x	x	x	x
HOFN		x	x	x	x	x	x	x	x	x	x	x	x	x
MADR	x	x	x	x	x	x	x							
NICO	x	x	x	x	x	x	x	x	x	x	x	x	x	x
PFAN	x	x	x	x	x	x	x	x	x	x	x	x	x	x
SODA	x	x	x	x	x	x	x	x	x	x	x		x	x
SOFI	x	x	x	x	x	x	x	x	x	x	x	x	x	x
SVTL	x	x	x	x	x	x	x	x	x	x	x	x	x	x
THU1	x	x	x	x	x	x			x	x	x	x	x	x
TOUL	x	x	x	x	x	x		x	x	x	x	x	x	
TROM														
WARE	x	x	x	x	x	x	x	x	x	x	x	x	x	x
WSRT	x	x	x	x	x	x	x	x	x	x	x	x	x	x
ZECK		x	x	x	x	x	x	x	x	x		x	x	x
WETT														

STN CODE	105	106	107	108	109	110	111
ANKR	x	x	x	x	x	x	x
BOR1	x	x	x	x	x	x	x
CAGL	x	x	x	x	x	x	x
EBRE	x	x	x	x	x	x	x
GRAS	x	x	x	x	x	x	x
KOSG	x	x	x	x	x	x	x
MASP	x	x	x	x	x	x	x
MATE	x	x	x	x	x	x	x
MEDI	x	x	x	x	x	x	x
NOTO	x	x	x	x	x	x	x
SFER							
UPAD		x	x	x	x	x	x
VENE	x	x	x	x	x	x	x
VILL	x	x	x	x	x	x	x
WTZR	x	x	x	x	x	x	x
ZIMM	x	x	x	x	x	x	x
BOGO	x	x	x	x	x	x	x
BRUS	x	x	x	x	x	x	x
GOPE	x	x	x	x	x	x	x
GRAZ	x	x	x	x	x	x	x
HERS							
JOZE	x	x	x	x	x	x	x
KELY	x	x	x	x	x	x	x
KIRU	x	x	x	x	x	x	x
LAMA	x	x	x	x	x	x	x
MDVO	x	x	x	x	x	x	x
METS	x	x	x	x	x	x	x
ONSA	x	x	x	x	x	x	x
PENC	x	x	x	x	x	x	x
POTS	x	x	x	x	x	x	x
REYK	x	x	x	x	x	x	x
ZWEN	x	x	x	x	x	x	x
HFLK				x	x	x	x
JOEN	x	x	x	x	x	x	x
KIR0	x	x	x	x	x	x	x
MAR6	x	x	x	x	x	x	x
MOPI	x	x		x	x	x	x
NYAL							
OBER	x	x	x	x	x	x	x
OSLO						x	x
RIGA	x	x	x	x	x	x	x
STAV						x	x
TRON						x	x
VAAS	x	x	x	x	x	x	x
VARD						x	x
VIL0	x	x	x	x	x	x	x
VIS0	x	x	x	x	x	x	x
WROC	x	x	x	x	x	x	x
DELF	x	x	x	x	x	x	x
DENT	x	x	x	x	x	x	x
DOUR	x	x	x	x	x	x	x
HOFN	x	x	x	x	x	x	x
MADR		x	x	x			x
NICO	x	x	x	x	x	x	x
PFAN	x	x	x	x	x	x	x
SODA	x	x	x	x	x	x	x
SOFI	x	x	x	x	x	x	x
SVTL	x	x	x	x	x	x	x
THU1	x	x	x	x	x	x	x
TOUL	x	x	x	x	x	x	x
TROM							
WARE	x	x	x	x	x	x	x
WSRT	x	x	x	x	x	x	x
ZECK	x	x	x	x	x	x	x
WETT							

Key for the Table

1-eur08347.snx
2-eur08357.snx
3-eur08367.snx
4-eur08377.snx
5-eur08387.snx
6-eur08397.snx
7-eur08407.snx
8-eur08417.snx
9-eur08427.snx
10-eur08437.snx
11-eur08447.snx
12-eur08457.snx
13-eur08467.snx
14-eur08477.snx
15-eur08487.snx
16-eur08497.snx
17-eur08507.snx
18-eur08517.snx
19-eur08527.snx
20-eur08537.snx
21-eur08547.snx
22-eur08557.snx
23-eur08567.snx
24-eur08577.snx
25-eur08587.snx
26-eur08597.snx
27-eur08607.snx
28-eur08617.snx
29-eur08627.snx
30-eur08637.snx
31-eur08647.snx
32-eur08657.snx
33-eur08667.snx
34-eur08677.snx
35-eur08687.snx
36-eur08697.snx
37-eur08707.snx
38-eur08717.snx
39-eur08727.snx
40-eur08737.snx
41-eur08747.snx
42-eur08757.snx
43-eur08767.snx
44-eur08777.snx
45-eur08787.snx
46-eur08797.snx
47-eur08807.snx
48-eur08817.snx
49-eur08827.snx
50-eur08837.snx
51-eur08847.snx
52-eur08857.snx
53-eur08867.snx
54-eur08877.snx
55-eur08887.snx
56-eur08897.snx
57-eur08907.snx
58-eur08917.snx
59-eur08927.snx
60-eur08937.snx
61-eur08947.snx
62-eur08957.snx
63-eur08967.snx
64-eur08977.snx
65-eur08987.snx
66-eur08997.snx
67-eur09007.snx
68-eur09017.snx
69-eur09027.snx
70-eur09037.snx
71-eur09047.snx
72-eur09057.snx
73-eur09067.snx
74-eur09077.snx
75-eur09087.snx
76-eur09097.snx
77-eur09107.snx
78-eur09117.snx
79-eur09127.snx
80-eur09137.snx
81-eur09147.snx
82-eur09157.snx
83-eur09167.snx
84-eur09177.snx
85-eur09187.snx
86-eur09197.snx
87-eur09207.snx
88-eur09217.snx
89-eur09227.snx
90-eur09237.snx
91-eur09247.snx
92-eur09257.snx
93-eur09267.snx
94-eur09277.snx
95-eur09287.snx
96-eur09297.snx
97-eur09307.snx
98-eur09317.snx
99-eur09327.snx
100-eur09337.snx
101-eur09347.snx
102-eur09357.snx
103-eur09367.snx
104-eur09377.snx
105-eur09387.snx
106-eur09397.snx
107-eur09407.snx
108-eur09417.snx
109-eur09427.snx
110-eur09437.snx
111-eur09447.snx

Appendix B

(Estimated Velocities for the Real/Simulated Data Based on EASTMED Project)

fixed-interval smoothing results (vN=Velocity in Northing, vE=Velocity in Easting)
2004.920000000000 (vH=Velocity in Height, svN,svE and svH are standard errors)

Ep.N	S.Name	vN	vE	vH	svN	svE	svH
21	BARG	20.116	29.743	0.378	0.142	0.210	0.257
21	ELAT	20.256	29.445	0.225	0.136	0.197	0.250
21	DALA	28.408	23.298	0.187	0.130	0.196	0.241
21	AQAB	28.889	25.444	-0.124	0.137	0.196	0.249
21	HELW	19.507	29.358	0.473	0.138	0.202	0.249
21	KATZ	21.029	30.614	-0.329	0.140	0.205	0.285
21	CYPR	20.548	29.899	-0.540	0.127	0.136	0.146
21	HAIF	20.261	29.990	-0.412	0.128	0.136	0.147
21	TECH	20.192	29.082	-0.002	0.127	0.136	0.147
21	BEER	19.673	30.278	-0.573	0.127	0.136	0.148
21	MIZP	19.865	29.498	0.069	0.128	0.137	0.149
21	SHOB	28.822	24.597	0.480	0.127	0.136	0.148
21	ANKR	9.416	32.050	0.216	0.128	0.137	0.144
21	SAMS	8.864	32.857	0.405	0.128	0.138	0.143
21	MELE	10.469	30.844	0.822	0.128	0.138	0.145
21	MENT	10.867	29.181	0.566	0.128	0.139	0.146
21	ANTG	9.975	29.566	-0.267	0.128	0.138	0.146
fixed-interval smoothing results							
2003.920000000000				20			
20	BARG	20.139	29.740	0.378	0.121	0.189	0.239
20	ELAT	20.314	29.438	0.221	0.116	0.176	0.232
20	DALA	28.549	23.293	0.152	0.109	0.175	0.222
20	AQAB	28.677	25.470	-0.090	0.116	0.175	0.230
20	HELW	19.671	29.350	0.445	0.117	0.181	0.231
20	KATZ	20.752	30.647	-0.279	0.120	0.185	0.270
20	CYPR	20.548	29.899	-0.540	0.105	0.115	0.126
20	HAIF	20.261	29.990	-0.412	0.105	0.115	0.127
20	TECH	20.192	29.082	-0.002	0.105	0.115	0.126
20	BEER	19.673	30.278	-0.573	0.105	0.115	0.128
20	MIZP	19.865	29.498	0.069	0.106	0.115	0.129
20	SHOB	28.822	24.597	0.480	0.105	0.115	0.128
20	ANKR	9.416	32.050	0.216	0.106	0.115	0.124
20	SAMS	8.864	32.857	0.405	0.106	0.117	0.122
20	MELE	10.469	30.844	0.822	0.106	0.117	0.125
20	MENT	10.867	29.181	0.566	0.106	0.117	0.126
20	ANTG	9.975	29.566	-0.267	0.106	0.117	0.126
fixed-interval smoothing results							
2002.920000000000				19			
19	BARG	20.216	29.726	0.374	0.107	0.171	0.221
19	ELAT	20.256	29.461	0.240	0.103	0.159	0.215
19	DALA	28.668	23.316	0.114	0.098	0.158	0.205
19	AQAB	28.498	25.463	-0.062	0.104	0.158	0.213
19	HELW	19.918	29.340	0.405	0.104	0.163	0.214
19	KATZ	20.467	30.681	-0.228	0.108	0.169	0.259
19	CYPR	20.548	29.899	-0.540	0.093	0.103	0.114
19	HAIF	20.261	29.990	-0.412	0.093	0.102	0.116
19	TECH	20.192	29.082	-0.002	0.093	0.103	0.115
19	BEER	19.673	30.278	-0.573	0.093	0.103	0.116
19	MIZP	19.865	29.498	0.069	0.093	0.103	0.118
19	SHOB	28.822	24.597	0.480	0.093	0.102	0.116
19	ANKR	9.416	32.050	0.216	0.093	0.103	0.112
19	SAMS	8.864	32.857	0.405	0.093	0.105	0.111
19	MELE	10.469	30.844	0.822	0.093	0.105	0.113
19	MENT	10.867	29.181	0.566	0.093	0.105	0.114
19	ANTG	9.975	29.566	-0.267	0.093	0.105	0.114
fixed-interval smoothing results							
2001.920000000000				18			
18	BARG	20.340	29.704	0.368	0.100	0.156	0.206
18	ELAT	20.104	29.508	0.275	0.097	0.145	0.199
18	DALA	28.644	23.390	0.093	0.093	0.144	0.190
18	AQAB	28.357	25.418	-0.043	0.097	0.144	0.198
18	HELW	20.253	29.324	0.354	0.098	0.149	0.198
18	KATZ	20.239	30.708	-0.190	0.102	0.158	0.250
18	CYPR	20.548	29.899	-0.540	0.088	0.098	0.110
18	HAIF	20.261	29.990	-0.412	0.088	0.098	0.112
18	TECH	20.192	29.082	-0.002	0.088	0.098	0.111
18	BEER	19.673	30.278	-0.573	0.088	0.098	0.113

18	MIZP	19.865	29.498	0.069	0.088	0.099	0.114
18	SHOB	28.822	24.597	0.480	0.088	0.098	0.113
18	ANKR	9.416	32.050	0.216	0.088	0.099	0.108
18	SAMS	8.864	32.857	0.405	0.088	0.101	0.107
18	MELE	10.469	30.844	0.822	0.088	0.101	0.110
18	MENT	10.867	29.181	0.566	0.088	0.101	0.110
18	ANTG	9.975	29.566	-0.267	0.088	0.101	0.110

fixed-interval smoothing results

2000.920000000000 17

17	BARG	20.358	29.708	0.389	0.096	0.145	0.191
17	ELAT	20.002	29.547	0.306	0.093	0.135	0.185
17	DALA	28.635	23.491	0.061	0.090	0.134	0.176
17	AQAB	28.257	25.356	-0.037	0.093	0.134	0.184
17	HELW	20.517	29.317	0.315	0.094	0.139	0.184
17	KATZ	20.044	30.727	-0.157	0.099	0.153	0.247
17	CYPR	20.548	29.899	-0.539	0.087	0.099	0.111
17	HAIF	20.261	29.990	-0.412	0.087	0.099	0.113
17	TECH	20.192	29.083	-0.002	0.087	0.099	0.112
17	BEER	19.673	30.278	-0.573	0.087	0.099	0.114
17	MIZP	19.865	29.498	0.069	0.087	0.100	0.115
17	SHOB	28.822	24.597	0.480	0.087	0.099	0.114
17	ANKR	9.416	32.050	0.216	0.087	0.100	0.109
17	SAMS	8.865	32.857	0.405	0.088	0.101	0.108
17	MELE	10.469	30.844	0.822	0.088	0.102	0.111
17	MENT	10.867	29.181	0.566	0.088	0.102	0.112
17	ANTG	9.975	29.566	-0.267	0.087	0.102	0.112

fixed-interval smoothing results

1999.920000000000 16

16	BARG	20.213	29.738	0.450	0.094	0.136	0.178
16	ELAT	19.957	29.567	0.335	0.091	0.128	0.173
16	DALA	28.798	23.589	-0.012	0.088	0.127	0.165
16	AQAB	28.198	25.317	-0.049	0.092	0.128	0.172
16	HELW	20.677	29.308	0.298	0.092	0.132	0.172
16	KATZ	19.908	30.726	-0.134	0.099	0.154	0.248
16	CYPR	20.548	29.899	-0.539	0.087	0.102	0.114
16	HAIF	20.261	29.990	-0.412	0.087	0.102	0.116
16	TECH	20.193	29.083	-0.002	0.087	0.102	0.115
16	BEER	19.673	30.278	-0.573	0.087	0.102	0.117
16	MIZP	19.865	29.498	0.069	0.088	0.103	0.118
16	SHOB	28.823	24.597	0.480	0.087	0.102	0.117
16	ANKR	9.416	32.050	0.216	0.088	0.103	0.113
16	SAMS	8.865	32.857	0.405	0.088	0.105	0.111
16	MELE	10.469	30.844	0.822	0.088	0.105	0.114
16	MENT	10.867	29.181	0.566	0.088	0.106	0.115
16	ANTG	9.975	29.566	-0.267	0.088	0.105	0.115

fixed-interval smoothing results

1998.920000000000 15

15	BARG	19.972	29.769	0.539	0.093	0.130	0.167
15	ELAT	19.981	29.570	0.360	0.091	0.124	0.163
15	DALA	28.982	23.712	-0.096	0.088	0.124	0.156
15	AQAB	28.082	25.329	-0.063	0.091	0.124	0.162
15	HELW	20.867	29.277	0.280	0.091	0.127	0.162
15	KATZ	19.867	30.692	-0.126	0.102	0.162	0.254
15	CYPR	20.548	29.899	-0.539	0.088	0.106	0.118
15	HAIF	20.262	29.990	-0.412	0.088	0.105	0.119
15	TECH	20.193	29.083	-0.002	0.088	0.106	0.118
15	BEER	19.673	30.278	-0.573	0.088	0.105	0.119
15	MIZP	19.865	29.498	0.069	0.089	0.106	0.121
15	SHOB	28.823	24.597	0.480	0.088	0.106	0.120
15	ANKR	9.416	32.050	0.216	0.089	0.107	0.116
15	SAMS	8.865	32.857	0.405	0.090	0.109	0.115
15	MELE	10.469	30.844	0.822	0.089	0.109	0.117
15	MENT	10.867	29.181	0.566	0.090	0.109	0.118
15	ANTG	9.975	29.566	-0.267	0.089	0.109	0.118

fixed-interval smoothing results

1997.920000000000 14

14	BARG	19.772	29.773	0.630	0.092	0.126	0.158
14	ELAT	20.009	29.565	0.388	0.091	0.122	0.154
14	DALA	29.049	23.869	-0.159	0.088	0.121	0.148
14	AQAB	28.008	25.363	-0.098	0.091	0.122	0.153
14	HELW	21.044	29.237	0.268	0.091	0.125	0.154
14	KATZ	19.862	30.656	-0.125	0.112	0.176	0.264

14 CYPR	20.549	29.899	-0.540	0.089	0.109	0.120
14 HAIF	20.262	29.990	-0.412	0.089	0.108	0.121
14 TECH	20.193	29.083	-0.002	0.089	0.109	0.120
14 BEER	19.674	30.278	-0.573	0.089	0.109	0.121
14 MIZP	19.866	29.498	0.069	0.090	0.109	0.122
14 SHOB	28.823	24.597	0.480	0.089	0.109	0.122
14 ANKR	9.416	32.050	0.216	0.091	0.110	0.118
14 SAMS	8.865	32.857	0.405	0.091	0.112	0.117
14 MELE	10.469	30.844	0.822	0.091	0.112	0.120
14 MENT	10.867	29.181	0.566	0.091	0.113	0.120
14 ANTG	9.976	29.566	-0.267	0.090	0.112	0.120

fixed-interval smoothing results

1996.920000000000 13

13 BARG	19.716	29.736	0.702	0.092	0.124	0.150
13 ELAT	20.016	29.561	0.423	0.091	0.121	0.146
13 DALA	28.996	24.047	-0.200	0.088	0.120	0.141
13 AQAB	28.089	25.383	-0.171	0.091	0.120	0.146
13 HELW	21.102	29.208	0.279	0.092	0.123	0.146
13 KATZ	19.816	30.645	-0.118	0.131	0.195	0.278
13 CYPR	20.548	29.899	-0.540	0.091	0.111	0.120
13 HAIF	20.261	29.990	-0.412	0.090	0.110	0.120
13 TECH	20.193	29.083	-0.002	0.090	0.111	0.120
13 BEER	19.673	30.278	-0.573	0.090	0.110	0.121
13 MIZP	19.865	29.498	0.069	0.090	0.110	0.121
13 SHOB	28.822	24.598	0.480	0.090	0.111	0.121
13 ANKR	9.417	32.050	0.216	0.092	0.112	0.118
13 SAMS	8.865	32.857	0.405	0.093	0.113	0.118
13 MELE	10.469	30.844	0.822	0.092	0.113	0.120
13 MENT	10.867	29.181	0.565	0.093	0.114	0.120
13 ANTG	9.976	29.566	-0.267	0.092	0.114	0.120

fixed-interval smoothing results

1995.920000000000 12

12 BARG	19.764	29.670	0.762	0.092	0.121	0.143
12 ELAT	20.018	29.565	0.459	0.092	0.119	0.140
12 DALA	28.907	24.215	-0.236	0.089	0.118	0.136
12 AQAB	28.206	25.394	-0.252	0.092	0.118	0.139
12 HELW	21.075	29.202	0.306	0.093	0.120	0.139
12 KATZ	19.773	30.647	-0.110	0.159	0.217	0.294
12 CYPR	20.548	29.899	-0.540	0.091	0.111	0.118
12 HAIF	20.261	29.990	-0.412	0.091	0.110	0.119
12 TECH	20.192	29.083	-0.002	0.091	0.111	0.119
12 BEER	19.673	30.279	-0.573	0.090	0.110	0.119
12 MIZP	19.864	29.498	0.069	0.091	0.110	0.119
12 SHOB	28.822	24.598	0.480	0.091	0.111	0.119
12 ANKR	9.417	32.050	0.216	0.093	0.112	0.117
12 SAMS	8.866	32.857	0.405	0.094	0.113	0.117
12 MELE	10.469	30.845	0.822	0.092	0.113	0.118
12 MENT	10.868	29.182	0.565	0.093	0.114	0.118
12 ANTG	9.976	29.566	-0.268	0.092	0.113	0.119

fixed-interval smoothing results

1995.820000000000 11

11 CYPR	20.548	29.899	-0.540	0.091	0.111	0.118
11 HAIF	20.261	29.990	-0.412	0.091	0.110	0.119
11 TECH	20.192	29.083	-0.002	0.091	0.111	0.119
11 BARG	19.765	29.670	0.763	0.092	0.121	0.143
11 BEER	19.673	30.279	-0.573	0.090	0.110	0.119
11 MIZP	19.864	29.498	0.069	0.091	0.110	0.119
11 ELAT	20.017	29.565	0.459	0.092	0.119	0.140
11 DALA	28.906	24.217	-0.237	0.089	0.118	0.136
11 AQAB	28.207	25.395	-0.252	0.092	0.118	0.139
11 SHOB	28.822	24.598	0.480	0.091	0.111	0.119
11 HELW	21.075	29.202	0.306	0.093	0.120	0.139
11 ANKR	9.417	32.050	0.216	0.093	0.112	0.117
11 SAMS	8.866	32.857	0.405	0.094	0.113	0.117
11 MELE	10.469	30.845	0.822	0.092	0.113	0.118
11 MENT	10.868	29.182	0.565	0.093	0.114	0.118
11 ANTG	9.976	29.566	-0.268	0.092	0.113	0.119

fixed-interval smoothing results

1994.820000000000 10

10 CYPR	20.566	29.900	-0.546	0.092	0.110	0.115
10 HAIF	20.254	29.993	-0.412	0.091	0.110	0.116
10 TECH	20.238	29.072	-0.010	0.091	0.110	0.116

10	BARG	19.810	29.600	0.825	0.092	0.118	0.137
10	BEER	19.673	30.282	-0.575	0.091	0.110	0.116
10	MIZP	19.856	29.498	0.070	0.091	0.109	0.116
10	ELAT	19.949	29.587	0.504	0.092	0.117	0.134
10	DALA	28.870	24.353	-0.280	0.089	0.116	0.131
10	AQAB	28.223	25.413	-0.312	0.092	0.116	0.134
10	SHOB	28.831	24.597	0.477	0.091	0.110	0.116
10	HELW	21.064	29.213	0.331	0.093	0.118	0.134
10	ANKR	9.413	32.051	0.217	0.093	0.111	0.114
10	SAMS	8.858	32.857	0.408	0.094	0.112	0.114
10	MELE	10.480	30.844	0.821	0.093	0.112	0.116
10	MENT	10.842	29.183	0.570	0.094	0.112	0.116
10	ANTG	10.013	29.556	-0.274	0.093	0.112	0.116

fixed-interval smoothing results

1993.820000000000 9

9	CYPR	20.663	29.888	-0.570	0.091	0.108	0.112
9	HAIF	20.290	29.997	-0.424	0.091	0.107	0.112
9	TECH	20.278	29.053	-0.017	0.091	0.108	0.112
9	BARG	19.845	29.537	0.888	0.091	0.116	0.133
9	BEER	19.695	30.292	-0.585	0.091	0.107	0.113
9	MIZP	19.904	29.497	0.060	0.091	0.108	0.113
9	ELAT	19.805	29.635	0.557	0.092	0.114	0.130
9	DALA	28.870	24.467	-0.327	0.089	0.113	0.126
9	AQAB	28.208	25.419	-0.361	0.092	0.113	0.129
9	SHOB	28.858	24.592	0.472	0.091	0.108	0.113
9	HELW	21.023	29.235	0.362	0.092	0.115	0.130
9	ANKR	9.412	32.056	0.216	0.093	0.108	0.111
9	SAMS	8.803	32.868	0.424	0.094	0.109	0.111
9	MELE	10.460	30.841	0.831	0.093	0.109	0.112
9	MENT	10.771	29.183	0.586	0.094	0.109	0.112
9	ANTG	10.107	29.521	-0.290	0.093	0.109	0.112

fixed-interval smoothing results

1992.820000000000 8

8	CYPR	20.742	29.877	-0.596	0.091	0.105	0.109
8	HAIF	20.236	30.033	-0.425	0.090	0.105	0.109
8	TECH	20.253	29.037	-0.015	0.090	0.105	0.109
8	BARG	19.963	29.470	0.936	0.091	0.113	0.130
8	BEER	19.745	30.309	-0.604	0.090	0.105	0.110
8	MIZP	20.116	29.486	0.021	0.090	0.105	0.110
8	ELAT	19.723	29.692	0.598	0.092	0.111	0.128
8	DALA	28.848	24.555	-0.366	0.090	0.110	0.124
8	AQAB	28.205	25.396	-0.408	0.092	0.110	0.127
8	SHOB	28.930	24.568	0.460	0.091	0.105	0.110
8	HELW	20.856	29.287	0.412	0.092	0.112	0.127
8	ANKR	9.462	32.061	0.203	0.092	0.105	0.108
8	SAMS	8.801	32.871	0.432	0.093	0.106	0.108
8	MELE	10.340	30.846	0.871	0.092	0.106	0.109
8	MENT	10.662	29.182	0.611	0.094	0.106	0.109
8	ANTG	10.235	29.466	-0.317	0.092	0.106	0.109

fixed-interval smoothing results

1991.820000000000 7

7	CYPR	20.674	29.893	-0.605	0.090	0.103	0.108
7	HAIF	20.027	30.110	-0.402	0.090	0.102	0.108
7	TECH	20.193	29.027	-0.009	0.090	0.103	0.108
7	BARG	20.044	29.421	0.988	0.091	0.110	0.130
7	BEER	19.832	30.327	-0.634	0.089	0.103	0.109
7	MIZP	20.444	29.462	-0.037	0.090	0.103	0.109
7	ELAT	19.766	29.729	0.617	0.092	0.108	0.128
7	DALA	28.833	24.604	-0.400	0.090	0.107	0.123
7	AQAB	28.153	25.355	-0.439	0.091	0.108	0.127
7	SHOB	29.006	24.528	0.451	0.090	0.103	0.109
7	HELW	20.667	29.366	0.461	0.092	0.109	0.128
7	ANKR	9.574	32.058	0.181	0.091	0.103	0.107
7	SAMS	8.919	32.850	0.419	0.092	0.104	0.106
7	MELE	10.132	30.875	0.933	0.091	0.104	0.107
7	MENT	10.576	29.175	0.637	0.092	0.104	0.108
7	ANTG	10.427	29.392	-0.357	0.091	0.104	0.108

fixed-interval smoothing results

1990.820000000000 6

6	CYPR	20.495	29.928	-0.601	0.089	0.102	0.109
6	HAIF	19.812	30.191	-0.380	0.088	0.101	0.110
6	TECH	20.080	29.025	0.009	0.088	0.102	0.110

6 BARG	19.862	29.427	1.083	0.090	0.109	0.132
6 BEER	19.921	30.355	-0.666	0.088	0.101	0.111
6 MIZP	20.704	29.451	-0.082	0.088	0.102	0.112
6 ELAT	19.902	29.739	0.619	0.090	0.107	0.132
6 DALA	28.961	24.610	-0.459	0.089	0.106	0.126
6 AQAB	28.133	25.285	-0.466	0.090	0.107	0.131
6 SHOB	29.022	24.486	0.455	0.089	0.102	0.111
6 HELW	20.576	29.445	0.492	0.091	0.109	0.131
6 ANKR	9.695	32.060	0.158	0.090	0.102	0.108
6 SAMS	9.152	32.806	0.386	0.090	0.103	0.107
6 MELE	9.893	30.917	1.003	0.090	0.103	0.109
6 MENT	10.512	29.156	0.662	0.091	0.104	0.110
6 ANTG	10.681	29.306	-0.406	0.090	0.104	0.110

fixed-interval smoothing results

1989.820000000000

5 CYPR	20.195	29.982	-0.576	0.086	0.104	0.115
5 HAIF	19.560	30.270	-0.352	0.086	0.103	0.116
5 TECH	20.046	29.005	0.015	0.086	0.104	0.116
5 BARG	19.427	29.476	1.216	0.088	0.110	0.139
5 BEER	19.986	30.406	-0.698	0.086	0.103	0.117
5 MIZP	20.867	29.458	-0.110	0.086	0.104	0.118
5 ELAT	20.137	29.721	0.604	0.088	0.109	0.139
5 DALA	29.285	24.591	-0.554	0.087	0.108	0.133
5 AQAB	28.200	25.188	-0.500	0.088	0.108	0.138
5 SHOB	28.972	24.455	0.476	0.086	0.104	0.118
5 HELW	20.563	29.511	0.509	0.089	0.111	0.138
5 ANKR	9.887	32.051	0.119	0.088	0.105	0.113
5 SAMS	9.509	32.747	0.329	0.088	0.107	0.113
5 MELE	9.592	30.971	1.086	0.087	0.106	0.115
5 MENT	10.369	29.140	0.700	0.088	0.107	0.116
5 ANTG	10.928	29.228	-0.457	0.087	0.107	0.116

fixed-interval smoothing results

1988.820000000000 4

4 CYPR	19.830	30.049	-0.539	0.085	0.111	0.126
4 HAIF	19.258	30.332	-0.311	0.084	0.110	0.127
4 TECH	20.163	28.961	-0.003	0.084	0.111	0.127
4 BARG	18.848	29.549	1.367	0.086	0.116	0.149
4 BEER	20.068	30.462	-0.733	0.084	0.110	0.128
4 MIZP	21.010	29.467	-0.134	0.084	0.110	0.130
4 ELAT	20.474	29.674	0.571	0.087	0.116	0.151
4 DALA	29.654	24.571	-0.655	0.085	0.114	0.143
4 AQAB	28.302	25.092	-0.536	0.087	0.115	0.149
4 SHOB	28.973	24.417	0.489	0.084	0.111	0.129
4 HELW	20.474	29.583	0.533	0.087	0.119	0.150
4 ANKR	10.219	32.018	0.052	0.087	0.113	0.123
4 SAMS	9.928	32.686	0.255	0.088	0.115	0.123
4 MELE	9.120	31.058	1.199	0.086	0.115	0.126
4 MENT	10.145	29.130	0.750	0.087	0.116	0.126
4 ANTG	11.160	29.162	-0.509	0.086	0.115	0.127

fixed-interval smoothing results

1987.820000000000 3

3 CYPR	19.496	30.119	-0.504	0.088	0.125	0.142
3 HAIF	18.926	30.370	-0.260	0.087	0.123	0.144
3 TECH	20.354	28.913	-0.036	0.087	0.125	0.143
3 BARG	18.222	29.629	1.518	0.089	0.129	0.164
3 BEER	20.200	30.500	-0.773	0.087	0.123	0.145
3 MIZP	21.149	29.468	-0.156	0.087	0.123	0.146
3 ELAT	20.892	29.606	0.520	0.091	0.129	0.166
3 DALA	29.985	24.554	-0.744	0.088	0.127	0.158
3 AQAB	28.439	25.013	-0.574	0.090	0.128	0.165
3 SHOB	29.047	24.374	0.488	0.088	0.125	0.146
3 HELW	20.242	29.668	0.574	0.091	0.132	0.165
3 ANKR	10.580	31.981	-0.020	0.091	0.127	0.139
3 SAMS	10.358	32.631	0.175	0.093	0.129	0.139
3 MELE	8.554	31.162	1.325	0.090	0.129	0.142
3 MENT	9.917	29.121	0.797	0.092	0.131	0.143
3 ANTG	11.339	29.109	-0.552	0.090	0.129	0.143

fixed-interval smoothing results

1986.820000000000 2

2 CYPR	19.303	30.168	-0.487	0.103	0.146	0.163
2 HAIF	18.632	30.398	-0.214	0.102	0.144	0.164
2 TECH	20.493	28.880	-0.059	0.102	0.146	0.164

2 BARG	17.705	29.692	1.639	0.103	0.148	0.183
2 BEER	20.360	30.518	-0.815	0.101	0.144	0.166
2 MIZP	21.297	29.455	-0.179	0.102	0.144	0.167
2 ELAT	21.268	29.541	0.471	0.106	0.149	0.186
2 DALA	30.237	24.543	-0.809	0.102	0.147	0.178
2 AQAB	28.523	24.972	-0.601	0.105	0.148	0.184
2 SHOB	29.083	24.347	0.490	0.103	0.145	0.167
2 HELW	20.036	29.737	0.607	0.107	0.152	0.185
2 ANKR	10.838	31.950	-0.072	0.107	0.148	0.159
2 SAMS	10.684	32.591	0.113	0.109	0.150	0.159
2 MELE	8.083	31.249	1.426	0.106	0.149	0.163
2 MENT	9.750	29.112	0.829	0.109	0.152	0.163
2 ANTG	11.455	29.073	-0.581	0.106	0.150	0.164

fixed-interval smoothing results

1985.820000000000 1

1 CYPR	19.271	30.180	-0.488	0.134	0.172	0.188
1 HAIF	18.517	30.409	-0.196	0.132	0.171	0.189
1 TECH	20.517	28.870	-0.062	0.133	0.172	0.189
1 BARG	17.501	29.715	1.688	0.134	0.174	0.205
1 BEER	20.434	30.523	-0.834	0.132	0.170	0.190
1 MIZP	21.375	29.447	-0.191	0.132	0.170	0.191
1 ELAT	21.420	29.513	0.451	0.136	0.175	0.208
1 DALA	30.328	24.539	-0.832	0.133	0.173	0.201
1 AQAB	28.531	24.964	-0.607	0.136	0.174	0.207
1 SHOB	29.088	24.336	0.492	0.133	0.172	0.191
1 HELW	19.967	29.762	0.618	0.137	0.178	0.207
1 ANKR	10.929	31.936	-0.090	0.137	0.174	0.185
1 SAMS	10.804	32.577	0.090	0.139	0.176	0.185
1 MELE	7.888	31.287	1.467	0.136	0.176	0.188
1 MENT	9.687	29.107	0.841	0.139	0.178	0.188
1 ANTG	11.508	29.059	-0.594	0.137	0.176	0.189

Appendix C

(Station Coordinates and their Corresponding Plate Name in the Simulation Process)

Forward Simulation

Station Name	X (m)	Y (m)	Z (m)	Plate Name
!TARD	4443540.7000	3086145.6500	3366846.1500	afrc
BARG	4443959.2384	3121953.1477	3334710.3625	afrc
ELAT	4555028.9629	3180067.3098	3123164.3408	afrc
DALA	4394744.5076	3147950.7403	3373291.9330	arab
AQAB	4550488.9936	3185967.8268	3123743.5182	arab
HELW	4728074.2310	2879731.5443	3157180.5420	afrc
KATZ	4349389.4799	3124004.7743	3453705.2978	arab

Backward Simulation

CYPR	4410424.2383	2848192.1609	3609955.2998	afrc
!TARD	4443540.7000	3086145.6500	3366846.1500	afrc
HAIF	4397078.2433	3073881.2879	3437798.4947	afrc
TECH	4395949.4978	3080709.1995	3433497.4365	afrc
BARG	4443959.2412	3121953.1359	3334710.3702	afrc
BEER	4481586.8819	3114267.9402	3290665.0272	afrc
MIZP	4514790.9960	3133457.5705	3228006.1149	afrc
ELAT	4555028.9553	3180067.2882	3123164.3628	afrc
DALA	4394744.5121	3147950.7356	3373291.9325	arab
AQAB	4550489.0045	3185967.8017	3123743.5190	arab
SHOB	4474714.5606	3195547.4395	3224298.7363	arab
HELW	4728074.2266	2879731.5455	3157180.5431	afrc
ANKR	4121948.6084	2652188.0166	4069023.6731	eura
SAMS	3865672.2672	2843377.6753	4187436.9490	eura
MELE	4247620.3832	2778639.0870	3851607.6405	eura
MENT	4468969.4993	2249289.9103	3942762.3010	eura
ANTG	4399214.8005	2602657.5934	3802195.0846	eura

Appendix D

(Calculated Strain Rates Using Estimated Velocities for the Real/Simulated Data Based on EASTMED Project)

Epno	Trig	max deformation (10-7) E1	(10-7) sE1	min deformation (10-7) E2	(10-7) sE2	max direction (deg) teta	(deg) steta	rotation (sec) R	(sec) sR
1	1	0.1	0.0	-0.1	0.0	61.83	2.0	0.00	0.0
1	2	0.1	0.0	0.0	0.0	-5.60	2.9	0.00	0.0
1	3	0.1	0.0	0.0	0.0	-41.31	3.0	0.00	0.0
1	4	0.1	0.0	-0.4	0.0	-88.84	0.6	0.00	0.0
1	5	0.1	0.0	-0.2	0.0	58.55	0.8	0.00	0.0
1	6	0.1	0.0	-0.4	0.0	-70.72	0.9	0.00	0.0
1	7	0.1	0.0	0.0	0.0	39.58	8.2	0.00	0.0
1	8	1.0	0.1	-2.8	0.3	23.20	2.5	0.03	0.0
1	9	0.7	0.0	-1.7	0.0	34.41	0.5	0.02	0.0
1	10	-0.4	0.0	-0.9	0.0	55.87	2.0	0.00	0.0
1	11	0.2	0.0	-1.0	0.0	34.38	1.0	0.01	0.0
1	12	0.3	0.0	-0.8	0.0	24.06	0.8	0.01	0.0
1	13	0.8	0.1	-10.8	0.3	42.18	0.8	0.06	0.0
1	14	0.0	0.0	0.0	0.0	37.13	14.5	0.00	0.0
1	15	0.0	0.0	-0.2	0.0	56.54	3.9	0.00	0.0
1	16	0.1	0.0	-0.8	0.1	86.83	2.2	0.01	0.0
1	17	0.0	0.0	0.0	0.0	-38.36	3.8	0.00	0.0
1	18	0.0	0.0	-0.1	0.0	-86.58	1.8	0.00	0.0
1	19	0.1	0.0	-0.2	0.0	59.53	1.0	0.00	0.0
1	20	0.9	0.0	-1.3	0.0	28.39	0.5	0.02	0.0

Epno	Trig	max deformation (10-7) E1	(10-7) sE1	min deformation (10-7) E2	(10-7) sE2	max direction (deg) teta	(deg) steta	rotation (sec) R	(sec) sR
2	1	0.1	0.0	-0.1	0.0	62.11	1.7	0.00	0.0
2	2	0.1	0.0	0.0	0.0	-4.61	2.6	0.00	0.0
2	3	0.1	0.0	0.0	0.0	-42.71	2.8	0.00	0.0
2	4	0.1	0.0	-0.4	0.0	-89.28	0.5	0.00	0.0
2	5	0.1	0.0	-0.2	0.0	59.15	0.6	0.00	0.0
2	6	0.1	0.0	-0.4	0.0	-70.85	0.7	0.00	0.0
2	7	0.1	0.0	0.0	0.0	41.70	6.7	0.00	0.0
2	8	0.9	0.1	-2.7	0.2	22.45	2.1	0.03	0.0
2	9	0.7	0.0	-1.7	0.0	34.28	0.4	0.02	0.0
2	10	-0.4	0.0	-0.9	0.0	53.81	1.6	0.00	0.0
2	11	0.2	0.0	-1.0	0.0	34.45	0.8	0.01	0.0
2	12	0.3	0.0	-0.8	0.0	24.05	0.6	0.01	0.0
2	13	0.8	0.1	-10.9	0.2	42.38	0.7	0.06	0.0
2	14	0.0	0.0	0.0	0.0	30.91	13.4	0.00	0.0
2	15	0.0	0.0	-0.2	0.0	56.89	3.3	0.00	0.0
2	16	0.1	0.0	-0.7	0.0	87.93	2.0	0.01	0.0
2	17	0.0	0.0	0.0	0.0	-38.85	3.4	0.00	0.0
2	18	0.0	0.0	-0.1	0.0	-85.88	1.5	0.00	0.0
2	19	0.1	0.0	-0.2	0.0	59.46	0.8	0.00	0.0
2	20	0.8	0.0	-1.3	0.0	28.43	0.4	0.02	0.0

Epno	Trig	max deformation (10-7) E1	(10-7) sE1	min deformation (10-7) E2	(10-7) sE2	max direction (deg) teta	(deg) steta	rotation (sec) R	(sec) sR
3	1	0.0	0.0	-0.1	0.0	63.19	1.6	0.00	0.0
3	2	0.1	0.0	0.0	0.0	-0.88	3.0	0.00	0.0
3	3	0.1	0.0	0.0	0.0	-48.78	3.3	0.00	0.0
3	4	0.1	0.0	-0.4	0.0	89.53	0.5	0.00	0.0
3	5	0.1	0.0	-0.2	0.0	60.73	0.6	0.00	0.0
3	6	0.1	0.0	-0.4	0.0	-71.02	0.7	0.00	0.0
3	7	0.1	0.0	0.0	0.0	48.19	5.8	0.00	0.0
3	8	0.7	0.1	-2.5	0.2	19.51	2.1	0.02	0.0
3	9	0.7	0.0	-1.6	0.0	33.92	0.4	0.02	0.0
3	10	-0.3	0.0	-0.9	0.0	49.41	1.3	0.00	0.0
3	11	0.2	0.0	-1.0	0.0	34.61	0.7	0.01	0.0
3	12	0.3	0.0	-0.8	0.0	23.86	0.5	0.01	0.0
3	13	0.9	0.1	-11.2	0.2	42.82	0.6	0.07	0.0
3	14	0.0	0.0	0.0	0.0	7.25	14.5	0.00	0.0
3	15	0.0	0.0	-0.2	0.0	58.12	3.0	0.00	0.0
3	16	0.1	0.0	-0.5	0.0	-88.28	2.1	0.00	0.0

3	17	0.0	0.0	0.0	0.0	-39.52	3.7	0.00	0.0
3	18	0.0	0.0	-0.1	0.0	-84.35	1.2	0.00	0.0
3	19	0.1	0.0	-0.2	0.0	59.00	0.7	0.00	0.0
3	20	0.7	0.0	-1.2	0.0	28.65	0.4	0.02	0.0

Epno	Trig	max deformation (10-7) E1	(10-7) sE1	min deformation (10-7) E2	(10-7) sE2	max direction (deg) teta	(deg) steta	rotation (sec) R	(sec) sR
4	1	0.0	0.0	-0.1	0.0	64.86	1.5	0.00	0.0
4	2	0.0	0.0	0.0	0.0	11.24	4.6	0.00	0.0
4	3	0.1	0.0	0.0	0.0	-66.60	4.2	0.00	0.0
4	4	0.1	0.0	-0.4	0.0	87.85	0.4	0.00	0.0
4	5	0.1	0.0	-0.2	0.0	62.89	0.5	0.00	0.0
4	6	0.1	0.0	-0.4	0.0	-71.01	0.6	0.00	0.0
4	7	0.1	0.0	0.0	0.0	59.25	5.5	0.00	0.0
4	8	0.3	0.1	-2.1	0.2	14.35	2.3	0.02	0.0
4	9	0.6	0.0	-1.5	0.0	33.41	0.4	0.02	0.0
4	10	-0.2	0.0	-0.9	0.0	45.43	1.1	0.00	0.0
4	11	0.2	0.0	-1.0	0.0	34.72	0.6	0.01	0.0
4	12	0.4	0.0	-0.8	0.0	23.56	0.5	0.01	0.0
4	13	1.0	0.1	-11.4	0.2	43.30	0.5	0.07	0.0
4	14	0.0	0.0	0.0	0.0	-7.93	8.3	0.00	0.0
4	15	0.0	0.0	-0.2	0.0	59.32	3.0	0.00	0.0
4	16	0.1	0.0	-0.3	0.0	-80.94	2.5	0.00	0.0
4	17	0.0	0.0	0.0	0.0	-38.77	4.5	0.00	0.0
4	18	0.0	0.0	-0.1	0.0	-82.47	1.0	0.00	0.0
4	19	0.1	0.0	-0.2	0.0	58.12	0.6	0.00	0.0
4	20	0.7	0.0	-1.2	0.0	28.96	0.4	0.02	0.0

Epno	Trig	max deformation (10-7) E1	(10-7) sE1	min deformation (10-7) E2	(10-7) sE2	max direction (deg) teta	(deg) steta	rotation (sec) R	(sec) sR
5	1	0.0	0.0	0.0	0.0	66.39	1.6	0.00	0.0
5	2	0.0	0.0	0.0	0.0	38.28	6.4	0.00	0.0
5	3	0.1	0.0	0.0	0.0	89.78	3.9	0.00	0.0
5	4	0.1	0.0	-0.4	0.0	86.15	0.4	0.00	0.0
5	5	0.1	0.0	-0.2	0.0	64.95	0.5	0.00	0.0
5	6	0.1	0.0	-0.4	0.0	-70.85	0.6	0.00	0.0
5	7	0.1	0.0	0.0	0.0	70.98	5.8	0.00	0.0
5	8	0.1	0.0	-1.9	0.2	8.33	2.7	0.01	0.0
5	9	0.5	0.0	-1.5	0.0	32.93	0.4	0.02	0.0
5	10	-0.1	0.0	-0.9	0.0	42.83	1.0	0.00	0.0
5	11	0.2	0.0	-1.0	0.0	34.76	0.6	0.01	0.0
5	12	0.4	0.0	-0.8	0.0	23.55	0.5	0.01	0.0
5	13	1.1	0.1	-11.6	0.2	43.78	0.5	0.07	0.0
5	14	0.1	0.0	0.0	0.0	-12.41	5.8	0.00	0.0
5	15	0.0	0.0	-0.2	0.0	59.61	3.1	0.00	0.0
5	16	0.2	0.0	-0.2	0.0	-69.79	3.0	0.00	0.0
5	17	0.0	0.0	0.0	0.0	-32.58	6.6	0.00	0.0
5	18	0.0	0.0	-0.1	0.0	-80.69	0.9	0.00	0.0
5	19	0.1	0.0	-0.2	0.0	56.96	0.5	0.00	0.0
5	20	0.6	0.0	-1.2	0.0	29.12	0.4	0.02	0.0

Epno	Trig	max deformation (10-7) E1	(10-7) sE1	min deformation (10-7) E2	(10-7) sE2	max direction (deg) teta	(deg) steta	rotation (sec) R	(sec) sR
6	1	0.0	0.0	0.0	0.0	67.07	1.8	0.00	0.0
6	2	0.0	0.0	0.0	0.0	54.93	5.5	0.00	0.0
6	3	0.0	0.0	0.0	0.0	78.68	3.1	0.00	0.0
6	4	0.1	0.0	-0.4	0.0	84.76	0.4	0.00	0.0
6	5	0.1	0.0	-0.2	0.0	66.46	0.5	0.00	0.0
6	6	0.1	0.0	-0.4	0.0	-70.72	0.6	0.00	0.0
6	7	0.1	0.0	0.0	0.0	78.72	6.1	0.00	0.0
6	8	0.1	0.0	-1.7	0.2	4.21	3.0	0.01	0.0
6	9	0.4	0.0	-1.4	0.0	32.57	0.4	0.02	0.0
6	10	-0.1	0.0	-0.9	0.0	41.38	0.9	0.01	0.0
6	11	0.2	0.0	-1.0	0.0	34.74	0.6	0.01	0.0
6	12	0.4	0.0	-0.8	0.0	23.85	0.4	0.01	0.0
6	13	1.1	0.1	-11.7	0.2	44.23	0.5	0.08	0.0

6	14	0.1	0.0	0.0	0.0	-14.71	5.1	0.00	0.0
6	15	0.0	0.0	-0.2	0.0	59.13	3.4	0.00	0.0
6	16	0.2	0.0	-0.1	0.0	-57.59	3.5	0.00	0.0
6	17	0.0	0.0	0.0	0.0	-19.86	9.2	0.00	0.0
6	18	0.0	0.0	-0.1	0.0	-79.49	0.9	0.00	0.0
6	19	0.1	0.0	-0.2	0.0	55.94	0.5	0.00	0.0
6	20	0.5	0.0	-1.1	0.0	28.97	0.4	0.02	0.0

Epno	Trig	max deformation (10-7) E1	(10-7) sE1	min deformation (10-7) E2	(10-7) sE2	max direction (deg) teta	(deg) steta	rotation (sec) R	(sec) sR
7	1	0.0	0.0	0.0	0.0	67.21	2.1	0.00	0.0
7	2	0.0	0.0	0.0	0.0	62.46	4.4	0.00	0.0
7	3	0.0	0.0	0.0	0.0	72.45	2.6	0.00	0.0
7	4	0.1	0.0	-0.4	0.0	83.52	0.4	0.00	0.0
7	5	0.1	0.0	-0.2	0.0	67.53	0.6	0.00	0.0
7	6	0.1	0.0	-0.4	0.0	-70.72	0.6	0.00	0.0
7	7	0.1	0.0	0.0	0.0	78.02	7.1	0.00	0.0
7	8	0.0	0.0	-1.6	0.2	2.06	3.3	0.00	0.0
7	9	0.4	0.0	-1.4	0.0	32.30	0.4	0.02	0.0
7	10	0.0	0.0	-0.9	0.0	40.85	0.9	0.01	0.0
7	11	0.3	0.0	-1.0	0.0	34.54	0.6	0.01	0.0
7	12	0.4	0.0	-0.8	0.0	24.52	0.4	0.01	0.0
7	13	1.2	0.1	-11.7	0.2	44.68	0.5	0.08	0.0
7	14	0.1	0.0	0.0	0.0	-19.76	5.8	0.00	0.0
7	15	0.0	0.0	-0.1	0.0	57.45	4.0	0.00	0.0
7	16	0.3	0.0	-0.1	0.0	-50.09	3.6	0.00	0.0
7	17	0.0	0.0	0.0	0.0	-16.97	10.4	0.00	0.0
7	18	0.0	0.0	-0.1	0.0	-78.78	0.8	0.00	0.0
7	19	0.1	0.0	-0.2	0.0	55.41	0.5	0.00	0.0
7	20	0.5	0.0	-1.1	0.0	28.66	0.4	0.02	0.0

Epno	Trig	max deformation (10-7) E1	(10-7) sE1	min deformation (10-7) E2	(10-7) sE2	max direction (deg) teta	(deg) steta	rotation (sec) R	(sec) sR
8	1	0.0	0.0	0.0	0.0	67.83	2.5	0.00	0.0
8	2	0.0	0.0	0.0	0.0	65.60	3.6	0.00	0.0
8	3	0.0	0.0	0.0	0.0	69.12	2.3	0.00	0.0
8	4	0.0	0.0	-0.4	0.0	82.52	0.4	0.00	0.0
8	5	0.1	0.0	-0.2	0.0	68.21	0.6	0.00	0.0
8	6	0.1	0.0	-0.4	0.0	-70.93	0.6	0.00	0.0
8	7	0.1	0.0	0.0	0.0	60.89	9.1	0.00	0.0
8	8	0.0	0.0	-1.4	0.2	-1.64	3.6	0.00	0.0
8	9	0.4	0.0	-1.4	0.0	32.11	0.4	0.02	0.0
8	10	0.0	0.0	-0.9	0.0	41.26	0.9	0.01	0.0
8	11	0.3	0.0	-1.0	0.0	34.12	0.6	0.01	0.0
8	12	0.4	0.0	-0.8	0.0	25.43	0.5	0.01	0.0
8	13	1.2	0.1	-11.8	0.2	45.05	0.5	0.08	0.0
8	14	0.0	0.0	0.0	0.0	-32.06	7.3	0.00	0.0
8	15	0.0	0.0	-0.1	0.0	53.29	5.3	0.00	0.0
8	16	0.3	0.0	-0.1	0.0	-49.03	3.7	0.00	0.0
8	17	0.0	0.0	0.0	0.0	-31.20	9.1	0.00	0.0
8	18	0.0	0.0	-0.2	0.0	-78.28	0.8	0.00	0.0
8	19	0.1	0.0	-0.2	0.0	55.36	0.5	0.00	0.0
8	20	0.5	0.0	-1.1	0.0	28.30	0.4	0.02	0.0

Epno	Trig	max deformation (10-7) E1	(10-7) sE1	min deformation (10-7) E2	(10-7) sE2	max direction (deg) teta	(deg) steta	rotation (sec) R	(sec) sR
9	1	0.0	0.0	0.0	0.0	68.35	2.9	0.00	0.0
9	2	0.0	0.0	0.0	0.0	66.50	3.3	0.00	0.0
9	3	0.0	0.0	0.0	0.0	67.58	2.1	0.00	0.0
9	4	0.0	0.0	-0.4	0.0	81.90	0.5	0.00	0.0
9	5	0.1	0.0	-0.2	0.0	68.44	0.6	0.00	0.0
9	6	0.1	0.0	-0.3	0.0	-71.16	0.6	0.00	0.0
9	7	0.1	0.0	0.0	0.0	46.88	9.5	0.00	0.0
9	8	0.0	0.0	-1.4	0.2	-2.36	3.8	0.00	0.0
9	9	0.4	0.0	-1.4	0.0	31.84	0.4	0.02	0.0
9	10	0.0	0.0	-0.9	0.0	41.88	0.9	0.01	0.0

9	11	0.3	0.0	-1.0	0.0	33.82	0.6	0.01	0.0
9	12	0.4	0.0	-0.8	0.0	26.18	0.5	0.01	0.0
9	13	1.2	0.1	-11.6	0.2	45.17	0.5	0.08	0.0
9	14	0.0	0.0	0.0	0.0	-48.75	7.7	0.00	0.0
9	15	0.0	0.0	-0.1	0.0	48.58	6.6	0.00	0.0
9	16	0.2	0.0	-0.1	0.0	-49.84	4.0	0.00	0.0
9	17	0.0	0.0	0.0	0.0	-43.27	7.6	0.00	0.0
9	18	0.0	0.0	-0.2	0.0	-77.83	0.8	0.00	0.0
9	19	0.1	0.0	-0.2	0.0	55.64	0.5	0.00	0.0
9	20	0.5	0.0	-1.2	0.0	27.86	0.4	0.02	0.0

Epno	Trig	max deformation (10-7) E1	(10-7) sE1	min deformation (10-7) E2	(10-7) sE2	max direction (deg) teta	(deg) steta	rotation (sec) R	(sec) sR
10	1	0.0	0.0	0.0	0.0	68.19	3.3	0.00	0.0
10	2	0.0	0.0	0.0	0.0	66.24	3.3	0.00	0.0
10	3	0.1	0.0	0.0	0.0	66.66	2.1	0.00	0.0
10	4	0.0	0.0	-0.4	0.0	81.60	0.5	0.00	0.0
10	5	0.1	0.0	-0.2	0.0	68.34	0.6	0.00	0.0
10	6	0.1	0.0	-0.3	0.0	-71.27	0.7	0.00	0.0
10	7	0.1	0.0	0.0	0.0	43.78	10.4	0.00	0.0
10	8	0.0	0.0	-1.3	0.2	-2.60	3.8	0.00	0.0
10	9	0.4	0.0	-1.4	0.0	31.46	0.4	0.02	0.0
10	10	0.0	0.0	-0.9	0.0	42.25	0.9	0.01	0.0
10	11	0.3	0.0	-1.0	0.0	33.76	0.6	0.01	0.0
10	12	0.4	0.0	-0.8	0.0	26.57	0.5	0.01	0.0
10	13	1.2	0.1	-11.5	0.2	45.11	0.5	0.08	0.0
10	14	0.0	0.0	0.0	0.0	-60.22	7.8	0.00	0.0
10	15	0.0	0.0	-0.1	0.0	47.81	7.0	0.00	0.0
10	16	0.2	0.0	0.0	0.0	-49.60	4.3	0.00	0.0
10	17	0.0	0.0	0.0	0.0	-50.08	7.3	0.00	0.0
10	18	0.0	0.0	-0.2	0.0	-77.49	0.8	0.00	0.0
10	19	0.1	0.0	-0.2	0.0	55.81	0.5	0.00	0.0
10	20	0.5	0.0	-1.2	0.0	27.50	0.4	0.02	0.0

Epno	Trig	max deformation (10-7) E1	(10-7) sE1	min deformation (10-7) E2	(10-7) sE2	max direction (deg) teta	(deg) steta	rotation (sec) R	(sec) sR
11	1	0.0	0.0	0.0	0.0	68.00	3.4	0.00	0.0
11	2	0.0	0.0	0.0	0.0	66.14	3.3	0.00	0.0
11	3	0.1	0.0	0.0	0.0	66.33	2.1	0.00	0.0
11	4	0.0	0.0	-0.4	0.0	81.53	0.5	0.00	0.0
11	5	0.1	0.0	-0.2	0.0	68.28	0.6	0.00	0.0
11	6	0.1	0.0	-0.3	0.0	-71.34	0.7	0.00	0.0
11	7	0.1	0.0	0.0	0.0	38.33	10.8	0.00	0.0
11	8	0.0	0.0	-1.3	0.2	-4.26	3.8	0.00	0.0
11	9	0.4	0.0	-1.5	0.0	31.06	0.4	0.02	0.0
11	10	0.0	0.0	-0.9	0.0	42.69	0.9	0.01	0.0
11	11	0.3	0.0	-1.0	0.0	33.76	0.6	0.01	0.0
11	12	0.4	0.0	-0.8	0.0	26.67	0.5	0.01	0.0
11	13	1.2	0.1	-11.4	0.2	45.00	0.5	0.08	0.0
11	14	0.0	0.0	0.0	0.0	-64.04	7.9	0.00	0.0
11	15	0.0	0.0	-0.1	0.0	48.34	7.0	0.00	0.0
11	16	0.2	0.0	0.0	0.0	-50.54	4.7	0.00	0.0
11	17	0.0	0.0	0.0	0.0	-52.72	6.5	0.00	0.0
11	18	0.0	0.0	-0.2	0.0	-77.35	0.8	0.00	0.0
11	19	0.1	0.0	-0.2	0.0	55.82	0.5	0.00	0.0
11	20	0.5	0.0	-1.2	0.0	27.13	0.4	0.02	0.0

Epno	Trig	max deformation (10-7) E1	(10-7) sE1	min deformation (10-7) E2	(10-7) sE2	max direction (deg) teta	(deg) steta	rotation (sec) R	(sec) sR
12	1	0.0	0.0	0.0	0.0	68.00	3.4	0.00	0.0
12	2	0.0	0.0	0.0	0.0	66.14	3.3	0.00	0.0
12	3	0.1	0.0	0.0	0.0	66.33	2.1	0.00	0.0
12	4	0.0	0.0	-0.4	0.0	81.53	0.5	0.00	0.0
12	5	0.1	0.0	-0.2	0.0	68.28	0.6	0.00	0.0
12	6	0.1	0.0	-0.3	0.0	-71.34	0.7	0.00	0.0
12	7	0.1	0.0	0.0	0.0	38.28	10.8	0.00	0.0

12	8	0.0	0.0	-1.3	0.2	-4.26	3.8	0.00	0.0
12	9	0.4	0.0	-1.5	0.0	31.06	0.4	0.02	0.0
12	10	0.0	0.0	-0.9	0.0	42.69	0.9	0.01	0.0
12	11	0.3	0.0	-1.0	0.0	33.76	0.6	0.01	0.0
12	12	0.4	0.0	-0.8	0.0	26.67	0.5	0.01	0.0
12	13	1.2	0.1	-11.4	0.2	45.00	0.5	0.08	0.0
12	14	0.0	0.0	0.0	0.0	-64.03	7.9	0.00	0.0
12	15	0.0	0.0	-0.1	0.0	48.34	7.0	0.00	0.0
12	16	0.2	0.0	0.0	0.0	-50.54	4.7	0.00	0.0
12	17	0.0	0.0	0.0	0.0	-52.76	6.5	0.00	0.0
12	18	0.0	0.0	-0.2	0.0	-77.35	0.8	0.00	0.0
12	19	0.1	0.0	-0.2	0.0	55.82	0.5	0.00	0.0
12	20	0.5	0.0	-1.2	0.0	27.13	0.4	0.02	0.0
12	21	1.3	0.2	-1.1	0.1	14.41	2.3	0.00	0.0
12	22	0.2	0.0	-1.1	0.0	30.22	0.8	0.01	0.0
12	23	0.1	0.0	-1.3	0.0	32.84	0.6	0.01	0.0

Epno	Trig	max deformation (10-7) E1	(10-7) sE1	min deformation (10-7) E2	(10-7) sE2	max direction (deg) teta	(deg) steta	rotation (sec) R	(sec) sR
13	1	0.0	0.0	0.0	0.0	68.02	3.4	0.00	0.0
13	2	0.0	0.0	0.0	0.0	66.14	3.3	0.00	0.0
13	3	0.1	0.0	0.0	0.0	66.34	2.1	0.00	0.0
13	4	0.0	0.0	-0.4	0.0	81.53	0.5	0.00	0.0
13	5	0.1	0.0	-0.2	0.0	68.28	0.6	0.00	0.0
13	6	0.1	0.0	-0.3	0.0	-71.34	0.7	0.00	0.0
13	7	0.1	0.0	0.0	0.0	33.38	11.0	0.00	0.0
13	8	0.0	0.0	-1.3	0.2	-4.26	3.8	0.00	0.0
13	9	0.4	0.0	-1.5	0.0	30.64	0.4	0.02	0.0
13	10	0.0	0.0	-0.9	0.0	43.13	0.9	0.01	0.0
13	11	0.3	0.0	-1.0	0.0	33.76	0.6	0.01	0.0
13	12	0.4	0.0	-0.8	0.0	26.67	0.5	0.01	0.0
13	13	1.2	0.1	-11.3	0.2	44.79	0.5	0.08	0.0
13	14	0.0	0.0	0.0	0.0	-63.73	7.9	0.00	0.0
13	15	0.0	0.0	-0.1	0.0	48.36	7.1	0.00	0.0
13	16	0.2	0.0	0.0	0.0	-51.67	5.0	0.00	0.0
13	17	0.0	0.0	0.0	0.0	-53.90	5.8	0.00	0.0
13	18	0.0	0.0	-0.2	0.0	-77.35	0.8	0.00	0.0
13	19	0.1	0.0	-0.2	0.0	55.86	0.5	0.00	0.0
13	20	0.5	0.0	-1.2	0.0	26.70	0.4	0.02	0.0
13	21	1.3	0.2	-1.1	0.1	14.43	2.3	0.00	0.0
13	22	0.2	0.0	-1.1	0.0	30.47	0.7	0.01	0.0
13	23	0.1	0.0	-1.3	0.0	32.90	0.6	0.01	0.0

Epno	Trig	max deformation (10-7) E1	(10-7) sE1	min deformation (10-7) E2	(10-7) sE2	max direction (deg) teta	(deg) steta	rotation (sec) R	(sec) sR
14	1	0.0	0.0	0.0	0.0	68.02	3.4	0.00	0.0
14	2	0.0	0.0	0.0	0.0	66.12	3.3	0.00	0.0
14	3	0.1	0.0	0.0	0.0	66.33	2.1	0.00	0.0
14	4	0.0	0.0	-0.4	0.0	81.53	0.5	0.00	0.0
14	5	0.1	0.0	-0.2	0.0	68.28	0.6	0.00	0.0
14	6	0.1	0.0	-0.3	0.0	-71.33	0.6	0.00	0.0
14	7	0.1	0.0	0.0	0.0	32.72	12.8	0.00	0.0
14	8	0.0	0.0	-1.3	0.2	-4.44	3.8	0.00	0.0
14	9	0.4	0.0	-1.5	0.0	30.12	0.4	0.02	0.0
14	10	0.0	0.0	-0.9	0.0	43.07	0.9	0.01	0.0
14	11	0.3	0.0	-1.0	0.0	33.76	0.6	0.01	0.0
14	12	0.4	0.0	-0.8	0.0	26.65	0.5	0.01	0.0
14	13	1.1	0.1	-11.2	0.2	44.59	0.5	0.07	0.0
14	14	0.0	0.0	0.0	0.0	-63.22	8.1	0.00	0.0
14	15	0.0	0.0	-0.1	0.0	48.05	6.9	0.00	0.0
14	16	0.2	0.0	0.0	0.0	-49.51	5.4	0.00	0.0
14	17	0.0	0.0	0.0	0.0	-54.95	6.2	0.00	0.0
14	18	0.0	0.0	-0.2	0.0	-77.27	0.7	0.00	0.0
14	19	0.1	0.0	-0.2	0.0	55.75	0.5	0.00	0.0
14	20	0.5	0.0	-1.3	0.0	26.31	0.4	0.02	0.0
14	21	1.4	0.2	-1.1	0.1	14.45	2.3	0.00	0.0
14	22	0.2	0.0	-1.1	0.0	30.68	0.6	0.01	0.0
14	23	0.1	0.0	-1.3	0.0	32.99	0.5	0.01	0.0

Epno	Trig	max deformation (10-7) E1	(10-7) sE1	min deformation (10-7) E2	(10-7) sE2	max direction (deg) teta	(deg) steta	rotation (sec) R	(sec) sR
15	1	0.0	0.0	0.0	0.0	68.01	3.3	0.00	0.0
15	2	0.0	0.0	0.0	0.0	66.12	3.2	0.00	0.0
15	3	0.1	0.0	0.0	0.0	66.32	2.1	0.00	0.0
15	4	0.0	0.0	-0.4	0.0	81.52	0.4	0.00	0.0
15	5	0.1	0.0	-0.2	0.0	68.28	0.6	0.00	0.0
15	6	0.1	0.0	-0.3	0.0	-71.34	0.6	0.00	0.0
15	7	0.0	0.0	0.0	0.0	42.59	19.7	0.00	0.0
15	8	0.0	0.0	-1.3	0.2	-4.76	3.8	0.00	0.0
15	9	0.4	0.0	-1.5	0.0	29.48	0.4	0.02	0.0
15	10	0.0	0.0	-0.9	0.0	42.37	0.9	0.01	0.0
15	11	0.3	0.0	-1.0	0.0	33.76	0.6	0.01	0.0
15	12	0.4	0.0	-0.8	0.0	26.60	0.5	0.01	0.0
15	13	1.1	0.1	-11.4	0.2	44.65	0.5	0.08	0.0
15	14	0.0	0.0	0.0	0.0	-62.43	9.2	0.00	0.0
15	15	0.0	0.0	-0.1	0.0	47.61	6.4	0.00	0.0
15	16	0.2	0.0	0.0	0.0	-43.04	5.4	0.00	0.0
15	17	0.0	0.0	0.0	0.0	-58.14	9.9	0.00	0.0
15	18	0.0	0.0	-0.2	0.0	-77.15	0.7	0.00	0.0
15	19	0.1	0.0	-0.2	0.0	55.46	0.5	0.00	0.0
15	20	0.4	0.0	-1.3	0.0	25.90	0.4	0.02	0.0
15	21	1.4	0.2	-1.1	0.1	14.52	2.3	0.00	0.0
15	22	0.2	0.0	-1.2	0.0	30.69	0.6	0.01	0.0
15	23	0.1	0.0	-1.3	0.0	33.07	0.5	0.01	0.0

Epno	Trig	max deformation (10-7) E1	(10-7) sE1	min deformation (10-7) E2	(10-7) sE2	max direction (deg) teta	(deg) steta	rotation (sec) R	(sec) sR
16	1	0.0	0.0	0.0	0.0	68.01	3.2	0.00	0.0
16	2	0.0	0.0	0.0	0.0	66.12	3.1	0.00	0.0
16	3	0.1	0.0	0.0	0.0	66.32	2.0	0.00	0.0
16	4	0.0	0.0	-0.4	0.0	81.52	0.4	0.00	0.0
16	5	0.1	0.0	-0.2	0.0	68.29	0.6	0.00	0.0
16	6	0.1	0.0	-0.3	0.0	-71.33	0.6	0.00	0.0
16	7	0.0	0.0	0.0	0.0	74.14	21.6	0.00	0.0
16	8	0.0	0.0	-1.3	0.2	-5.07	3.8	0.00	0.0
16	9	0.3	0.0	-1.5	0.0	28.83	0.5	0.02	0.0
16	10	0.1	0.0	-0.9	0.0	41.48	0.9	0.01	0.0
16	11	0.3	0.0	-1.0	0.0	33.76	0.5	0.01	0.0
16	12	0.4	0.0	-0.8	0.0	26.57	0.4	0.01	0.0
16	13	1.2	0.1	-11.5	0.2	44.85	0.5	0.08	0.0
16	14	0.0	0.0	0.0	0.0	-62.20	11.1	0.00	0.0
16	15	0.0	0.0	-0.1	0.0	47.28	5.9	0.00	0.0
16	16	0.3	0.0	0.0	0.0	-37.07	5.0	0.00	0.0
16	17	0.0	0.0	0.0	0.0	-74.96	25.5	0.00	0.0
16	18	0.0	0.0	-0.2	0.0	-77.05	0.7	0.00	0.0
16	19	0.1	0.0	-0.2	0.0	55.16	0.5	0.00	0.0
16	20	0.4	0.0	-1.3	0.0	25.43	0.5	0.02	0.0
16	21	1.4	0.2	-1.1	0.1	14.60	2.2	0.00	0.0
16	22	0.3	0.0	-1.2	0.0	30.39	0.5	0.01	0.0
16	23	0.1	0.0	-1.3	0.0	33.20	0.5	0.01	0.0

Epno	Trig	max deformation (10-7) E1	(10-7) sE1	min deformation (10-7) E2	(10-7) sE2	max direction (deg) teta	(deg) steta	rotation (sec) R	(sec) sR
17	1	0.0	0.0	0.0	0.0	68.01	3.1	0.00	0.0
17	2	0.0	0.0	0.0	0.0	66.12	3.0	0.00	0.0
17	3	0.1	0.0	0.0	0.0	66.32	2.0	0.00	0.0
17	4	0.0	0.0	-0.4	0.0	81.52	0.4	0.00	0.0
17	5	0.1	0.0	-0.2	0.0	68.29	0.6	0.00	0.0
17	6	0.1	0.0	-0.3	0.0	-71.33	0.6	0.00	0.0
17	7	0.0	0.0	0.0	0.0	86.54	16.6	0.00	0.0
17	8	0.0	0.0	-1.3	0.2	-5.30	3.9	0.00	0.0
17	9	0.3	0.0	-1.5	0.0	28.36	0.5	0.02	0.0
17	10	0.1	0.0	-0.9	0.0	40.92	0.8	0.01	0.0
17	11	0.3	0.0	-1.0	0.0	33.76	0.5	0.01	0.0

17	12	0.4	0.0	-0.8	0.0	26.66	0.4	0.01	0.0
17	13	1.2	0.1	-11.5	0.2	45.05	0.5	0.08	0.0
17	14	0.0	0.0	0.0	0.0	-68.53	13.2	0.00	0.0
17	15	0.0	0.0	-0.1	0.0	47.17	5.6	0.00	0.0
17	16	0.3	0.0	0.0	0.0	-34.55	4.8	0.00	0.0
17	17	0.0	0.0	0.0	0.0	60.36	27.7	0.00	0.0
17	18	0.0	0.0	-0.2	0.0	-77.01	0.7	0.00	0.0
17	19	0.1	0.0	-0.2	0.0	54.92	0.5	0.00	0.0
17	20	0.4	0.0	-1.3	0.0	25.03	0.5	0.02	0.0
17	21	1.4	0.2	-1.1	0.1	14.61	2.2	0.00	0.0
17	22	0.3	0.0	-1.2	0.0	29.99	0.5	0.01	0.0
17	23	0.1	0.0	-1.3	0.0	33.39	0.5	0.01	0.0

Epno	Trig	max deformation (10-7) E1	(10-7) sE1	min deformation (10-7) E2	(10-7) sE2	max direction (deg) teta	(deg) steta	rotation (sec) R	(sec) sR
18	1	0.0	0.0	0.0	0.0	68.01	3.1	0.00	0.0
18	2	0.0	0.0	0.0	0.0	66.13	3.0	0.00	0.0
18	3	0.1	0.0	0.0	0.0	66.32	2.0	0.00	0.0
18	4	0.0	0.0	-0.4	0.0	81.52	0.4	0.00	0.0
18	5	0.1	0.0	-0.2	0.0	68.29	0.6	0.00	0.0
18	6	0.1	0.0	-0.3	0.0	-71.33	0.6	0.00	0.0
18	7	0.0	0.0	0.0	0.0	84.95	17.5	0.00	0.0
18	8	0.0	0.0	-1.3	0.2	-5.26	3.9	0.00	0.0
18	9	0.3	0.0	-1.5	0.0	28.18	0.5	0.02	0.0
18	10	0.1	0.0	-0.9	0.0	40.96	0.9	0.01	0.0
18	11	0.3	0.0	-1.0	0.0	33.76	0.5	0.01	0.0
18	12	0.4	0.0	-0.8	0.0	26.87	0.4	0.01	0.0
18	13	1.2	0.1	-11.4	0.2	45.35	0.6	0.08	0.0
18	14	0.0	0.0	0.0	0.0	-83.32	15.3	0.00	0.0
18	15	0.0	0.0	-0.1	0.0	47.07	5.3	0.00	0.0
18	16	0.3	0.0	0.0	0.0	-35.23	5.2	0.00	0.0
18	17	0.0	0.0	0.0	0.0	40.86	18.7	0.00	0.0
18	18	0.0	0.0	-0.1	0.0	-76.95	0.8	0.00	0.0
18	19	0.1	0.0	-0.2	0.0	54.53	0.5	0.00	0.0
18	20	0.4	0.0	-1.3	0.0	24.82	0.5	0.02	0.0
18	21	1.4	0.2	-1.1	0.1	14.63	2.2	0.00	0.0
18	22	0.3	0.0	-1.2	0.0	29.89	0.5	0.01	0.0
18	23	0.1	0.0	-1.3	0.0	33.61	0.5	0.01	0.0

Epno	Trig	max deformation (10-7) E1	(10-7) sE1	min deformation (10-7) E2	(10-7) sE2	max direction (deg) teta	(deg) steta	rotation (sec) R	(sec) sR
19	1	0.0	0.0	0.0	0.0	68.01	3.2	0.00	0.0
19	2	0.0	0.0	0.0	0.0	66.13	3.1	0.00	0.0
19	3	0.1	0.0	0.0	0.0	66.32	2.0	0.00	0.0
19	4	0.0	0.0	-0.4	0.0	81.52	0.5	0.00	0.0
19	5	0.1	0.0	-0.2	0.0	68.29	0.6	0.00	0.0
19	6	0.1	0.0	-0.3	0.0	-71.33	0.6	0.00	0.0
19	7	0.0	0.0	0.0	0.0	74.15	22.7	0.00	0.0
19	8	0.0	0.0	-1.3	0.2	-5.09	4.1	0.00	0.0
19	9	0.3	0.0	-1.5	0.0	28.19	0.6	0.02	0.0
19	10	0.1	0.0	-0.9	0.0	41.42	0.9	0.01	0.0
19	11	0.3	0.0	-1.0	0.0	33.76	0.6	0.01	0.0
19	12	0.4	0.0	-0.8	0.0	27.16	0.5	0.01	0.0
19	13	1.2	0.1	-11.3	0.2	45.62	0.6	0.08	0.0
19	14	0.0	0.0	0.0	0.0	82.88	12.6	0.00	0.0
19	15	0.0	0.0	-0.1	0.0	46.92	5.1	0.00	0.0
19	16	0.2	0.0	0.0	0.0	-38.16	6.3	0.00	0.0
19	17	0.0	0.0	0.0	0.0	29.36	13.9	0.00	0.0
19	18	0.0	0.0	-0.1	0.0	-76.85	0.8	0.00	0.0
19	19	0.1	0.0	-0.2	0.0	54.04	0.5	0.00	0.0
19	20	0.4	0.0	-1.3	0.0	24.63	0.6	0.02	0.0
19	21	1.4	0.2	-1.1	0.1	14.62	2.3	0.00	0.0
19	22	0.3	0.0	-1.2	0.0	29.78	0.5	0.01	0.0
19	23	0.1	0.0	-1.3	0.0	33.85	0.5	0.01	0.0

Epno	Trig	max deformation (10-7) E1	(10-7) sE1	min deformation (10-7) E2	(10-7) sE2	max direction (deg) teta	(deg) steta	rotation (sec) R	(sec) sR

20	1	0.0	0.0	0.0	0.0	68.01	3.6	0.00	0.0
20	2	0.0	0.0	0.0	0.0	66.13	3.5	0.00	0.0
20	3	0.1	0.0	0.0	0.0	66.32	2.3	0.00	0.0
20	4	0.0	0.0	-0.4	0.0	81.52	0.5	0.00	0.0
20	5	0.1	0.0	-0.2	0.0	68.29	0.7	0.00	0.0
20	6	0.1	0.0	-0.3	0.0	-71.33	0.7	0.00	0.0
20	7	0.0	0.0	0.0	0.0	64.05	26.9	0.00	0.0
20	8	0.0	0.0	-1.3	0.2	-4.99	4.6	0.00	0.0
20	9	0.3	0.0	-1.5	0.0	28.18	0.6	0.02	0.0
20	10	0.0	0.0	-0.9	0.0	41.71	1.1	0.01	0.0
20	11	0.3	0.0	-1.0	0.0	33.76	0.6	0.01	0.0
20	12	0.4	0.0	-0.8	0.0	27.28	0.5	0.01	0.0
20	13	1.3	0.1	-11.4	0.2	45.90	0.7	0.08	0.0
20	14	0.0	0.0	0.0	0.0	77.38	12.0	0.00	0.0
20	15	0.0	0.0	-0.1	0.0	46.83	5.4	0.00	0.0
20	16	0.2	0.1	0.0	0.0	-40.59	7.7	0.00	0.0
20	17	0.0	0.0	0.0	0.0	25.42	11.7	0.00	0.0
20	18	0.0	0.0	-0.1	0.0	-76.78	1.0	0.00	0.0
20	19	0.1	0.0	-0.2	0.0	53.68	0.5	0.00	0.0
20	20	0.4	0.0	-1.3	0.0	24.34	0.6	0.02	0.0
20	21	1.5	0.2	-1.1	0.1	14.62	2.5	0.00	0.0
20	22	0.4	0.0	-1.2	0.0	29.31	0.6	0.01	0.0
20	23	0.2	0.0	-1.3	0.0	34.15	0.5	0.01	0.0

Epno	Trig	max deformation (10-7) E1	(10-7) sE1	min deformation (10-7) E2	(10-7) sE2	max direction (deg) teta	(deg) steta	rotation (sec) R	(sec) sR
21	1	0.0	0.0	0.0	0.0	68.01	4.3	0.00	0.0
21	2	0.0	0.0	0.0	0.0	66.13	4.1	0.00	0.0
21	3	0.1	0.0	0.0	0.0	66.32	2.7	0.00	0.0
21	4	0.0	0.0	-0.4	0.0	81.52	0.6	0.00	0.0
21	5	0.1	0.0	-0.2	0.0	68.29	0.8	0.00	0.0
21	6	0.1	0.0	-0.3	0.0	-71.33	0.8	0.00	0.0
21	7	0.0	0.0	0.0	0.0	60.90	32.0	0.00	0.0
21	8	0.0	0.0	-1.3	0.3	-4.95	5.6	0.00	0.0
21	9	0.3	0.0	-1.5	0.0	28.15	0.7	0.02	0.0
21	10	0.0	0.0	-0.9	0.0	41.79	1.2	0.01	0.0
21	11	0.3	0.0	-1.0	0.0	33.76	0.8	0.01	0.0
21	12	0.4	0.0	-0.8	0.0	27.18	0.6	0.01	0.0
21	13	1.3	0.1	-11.7	0.3	46.21	0.8	0.08	0.0
21	14	0.0	0.0	0.0	0.0	73.95	14.8	0.00	0.0
21	15	0.0	0.0	-0.1	0.0	46.76	6.3	0.00	0.0
21	16	0.2	0.1	0.0	0.0	-41.64	9.2	0.00	0.0
21	17	0.0	0.0	0.0	0.0	24.60	11.1	0.00	0.0
21	18	0.0	0.0	-0.1	0.0	-76.73	1.1	0.00	0.0
21	19	0.1	0.0	-0.2	0.0	53.44	0.6	0.00	0.0
21	20	0.4	0.0	-1.3	0.0	24.10	0.7	0.02	0.0
21	21	1.5	0.2	-1.1	0.1	14.61	2.9	0.00	0.0
21	22	0.4	0.0	-1.2	0.0	28.81	0.6	0.01	0.0
21	23	0.2	0.0	-1.4	0.0	34.42	0.6	0.01	0.0

KEY FOR TRIANGLE NUMBER

1	MENT	ANKR	ANTG
2	ANKR	SAMS	MELE
3	ANTG	ANKR	MELE
4	ANTG	MELE	CYPR
5	MELE	SAMS	HAIF
6	CYPR	MELE	HAIF
7	BARG	HAIF	CYPR
8	BARG	HAIF	TECH
9	BARG	DALA	SHOB
10	BARG	SHOB	BEER
11	BEER	MIZP	SHOB
12	MIZP	ELAT	SHOB
13	ELAT	SHOB	AQAB
14	MIZP	ELAT	HELW
15	MIZP	BEER	HELW
16	HELW	BEER	BARG
17	HELW	BARG	CYPR
18	MENT	ANTG	HELW
19	ANTG	CYPR	HELW
20	BARG	TECH	DALA
21	HAIF	TECH	KATZ
22	TECH	KATZ	DALA
23	HAIF	SAMS	KATZ

Appendix E

(Estimated Velocities for the EUREF Permanent GPS Network)

GROUP ONE

fixed-interval smoothing results (vN=Velocity in Northing, vE=Velocity in Easting)
(vH=Velocity in Height, svN,svE and svH are standard errors)

Ep.N	S.Name	vN	vE	vH	svN	svE	svH
98.07680000000001			28				
28	REYK	19.396	3.261	13.046	0.312	0.448	0.266
28	MDVO	12.633	45.775	1.520	0.317	0.365	0.442
28	ZECK	6.489	8.219	-1.344	5.178	4.828	14.633
28	NICO	24.041	15.133	10.618	2.571	2.640	10.195
28	NOTO	21.667	30.095	8.914	0.308	0.315	0.658
28	MASP	16.443	32.504	-4.357	0.350	0.352	1.204
28	SOFI	11.183	41.011	6.513	1.924	2.186	6.660
28	JOZE	18.146	41.413	27.041	0.287	0.306	0.342
28	GRAZ	14.746	32.497	-0.390	0.107	0.129	0.054
28	WTZR	13.100	31.487	-4.028	0.107	0.131	0.053
28	ZIMM	16.013	28.570	1.517	0.108	0.130	0.053
28	VILL	17.888	32.198	4.275	0.319	0.337	0.758
28	ONSA	12.949	32.957	-1.005	0.105	0.139	0.049
28	VAAS	10.850	51.345	24.743	0.770	1.179	1.359
28	HERS	19.287	33.125	-0.996	0.197	0.229	0.199
28	VARD	3.769	81.489	2.186	0.679	1.284	0.900
28	NYAL	8.341	97.777	20.289	0.233	0.265	0.096
fixed-interval smoothing results							
98.00010000000000			27				
27	REYK	19.399	3.261	13.046	0.302	0.442	0.264
27	MDVO	12.639	45.778	1.520	0.308	0.357	0.441
27	ZECK	6.491	8.220	-1.344	5.177	4.828	14.633
27	NICO	24.043	15.133	10.618	2.570	2.639	10.195
27	NOTO	21.667	30.097	8.914	0.298	0.306	0.657
27	MASP	16.439	32.505	-4.357	0.341	0.344	1.204
27	SOFI	11.184	41.010	6.513	1.922	2.185	6.660
27	JOZE	18.145	41.414	27.041	0.277	0.296	0.340
27	GRAZ	14.742	32.499	-0.389	0.087	0.110	0.046
27	WTZR	13.125	31.482	-4.032	0.087	0.111	0.045
27	ZIMM	16.025	28.577	1.511	0.088	0.110	0.046
27	VILL	17.888	32.199	4.275	0.310	0.328	0.757
27	ONSA	12.961	32.952	-1.010	0.086	0.120	0.041
27	VAAS	10.849	51.345	24.744	0.767	1.177	1.359
27	HERS	19.287	33.125	-0.996	0.184	0.217	0.197
27	VARD	3.752	81.489	2.189	0.675	1.282	0.900
27	NYAL	8.341	97.777	20.289	0.221	0.254	0.091
fixed-interval smoothing results							
97.92340000000000			26				
26	REYK	19.409	3.264	13.046	0.293	0.435	0.262
26	MDVO	12.652	45.785	1.519	0.299	0.349	0.440
26	NICO	24.045	15.134	10.618	2.570	2.638	10.195
26	NOTO	21.665	30.100	8.914	0.289	0.297	0.656
26	MASP	16.430	32.508	-4.357	0.333	0.336	1.204
26	SOFI	11.187	41.006	6.513	1.922	2.184	6.660
26	JOZE	18.142	41.419	27.042	0.267	0.286	0.339
26	GRAZ	14.741	32.504	-0.390	0.074	0.094	0.040
26	WTZR	13.159	31.467	-4.036	0.074	0.096	0.039
26	ZIMM	16.057	28.584	1.498	0.075	0.094	0.040
26	VILL	17.888	32.201	4.275	0.301	0.319	0.757
26	ONSA	12.979	32.946	-1.019	0.074	0.104	0.035
26	VAAS	10.846	51.346	24.745	0.764	1.174	1.359
26	ZECK	6.494	8.221	-1.344	5.177	4.828	14.633
26	HERS	19.287	33.125	-0.996	0.177	0.209	0.197
26	VARD	3.726	81.489	2.194	0.672	1.280	0.899
26	NYAL	8.340	97.777	20.289	0.209	0.244	0.087
fixed-interval smoothing results							
97.84670000000000			25				
25	REYK	19.430	3.270	13.044	0.284	0.429	0.261
25	MDVO	12.673	45.794	1.518	0.290	0.341	0.439
25	ZECK	6.495	8.222	-1.344	5.178	4.828	14.633
25	NICO	24.048	15.135	10.618	2.570	2.638	10.195
25	NOTO	21.663	30.107	8.914	0.279	0.287	0.656
25	MASP	16.415	32.514	-4.357	0.325	0.328	1.203
25	SOFI	11.190	41.000	6.512	1.922	2.184	6.660
25	JOZE	18.137	41.429	27.044	0.257	0.277	0.338
25	GRAZ	14.726	32.500	-0.387	0.067	0.083	0.036

25 WTZR	13.192	31.447	-4.042	0.067	0.084	0.035
25 ZIMM	16.105	28.583	1.480	0.068	0.083	0.035
25 HERS	19.288	33.124	-0.996	0.173	0.203	0.198
25 VILL	17.889	32.205	4.275	0.292	0.310	0.756
25 ONSA	12.985	32.940	-1.027	0.067	0.092	0.031
25 VAAS	10.839	51.348	24.747	0.761	1.173	1.358
25 VARD	3.695	81.490	2.199	0.669	1.279	0.899
25 NYAL	8.339	97.777	20.289	0.198	0.234	0.082
fixed-interval smoothing results						
97.77000000000000			24			
24 REYK	19.464	3.281	13.040	0.275	0.423	0.259
24 VARD	3.662	81.491	2.205	0.667	1.278	0.899
24 MDVO	12.704	45.806	1.515	0.282	0.333	0.438
24 ZECK	6.495	8.222	-1.344	5.178	4.828	14.633
24 NICO	24.050	15.137	10.617	2.570	2.638	10.195
24 NOTO	21.663	30.118	8.914	0.270	0.278	0.655
24 MASP	16.396	32.521	-4.357	0.317	0.320	1.203
24 SOFI	11.192	40.996	6.512	1.922	2.184	6.660
24 JOZE	18.129	41.445	27.047	0.247	0.267	0.337
24 GRAZ	14.716	32.481	-0.383	0.065	0.077	0.033
24 WTZR	13.212	31.431	-4.049	0.065	0.078	0.032
24 ZIMM	16.149	28.570	1.467	0.065	0.077	0.033
24 HERS	19.288	33.123	-0.996	0.169	0.198	0.199
24 VILL	17.892	32.210	4.275	0.283	0.302	0.756
24 ONSA	12.996	32.933	-1.039	0.064	0.085	0.029
24 VAAS	10.830	51.350	24.749	0.759	1.171	1.358
24 NYAL	8.338	97.777	20.289	0.187	0.224	0.078
fixed-interval smoothing results						
97.69329999999999			23			
23 REYK	19.511	3.299	13.036	0.266	0.417	0.257
23 VARD	3.627	81.493	2.211	0.666	1.277	0.899
23 MDVO	12.750	45.820	1.512	0.274	0.326	0.437
23 NICO	24.051	15.138	10.617	2.571	2.639	10.195
23 NOTO	21.664	30.131	8.914	0.261	0.269	0.655
23 MASP	16.373	32.531	-4.357	0.309	0.312	1.203
23 SOFI	11.193	40.994	6.512	1.923	2.185	6.660
23 JOZE	18.118	41.467	27.051	0.237	0.258	0.335
23 GRAZ	14.735	32.447	-0.387	0.064	0.074	0.031
23 WTZR	13.214	31.419	-4.054	0.064	0.075	0.031
23 ZIMM	16.198	28.548	1.456	0.064	0.075	0.031
23 HERS	19.289	33.122	-0.996	0.166	0.194	0.200
23 VILL	17.897	32.218	4.275	0.274	0.293	0.755
23 ONSA	13.030	32.932	-1.064	0.063	0.081	0.028
23 VAAS	10.821	51.353	24.751	0.757	1.170	1.358
23 NYAL	8.336	97.776	20.289	0.177	0.215	0.074
fixed-interval smoothing results						
97.61660000000001			22			
22 REYK	19.572	3.322	13.030	0.258	0.411	0.256
22 NYAL	8.335	97.775	20.290	0.167	0.207	0.070
22 VARD	3.589	81.495	2.217	0.665	1.277	0.899
22 MDVO	12.816	45.834	1.507	0.266	0.319	0.437
22 NICO	24.052	15.139	10.617	2.571	2.640	10.195
22 NOTO	21.668	30.148	8.914	0.252	0.261	0.654
22 MASP	16.346	32.545	-4.358	0.301	0.304	1.202
22 SOFI	11.194	40.992	6.512	1.924	2.186	6.660
22 JOZE	18.105	41.496	27.055	0.228	0.249	0.334
22 GRAZ	14.760	32.410	-0.393	0.063	0.073	0.030
22 WTZR	13.218	31.403	-4.066	0.062	0.074	0.030
22 ZIMM	16.196	28.529	1.459	0.063	0.073	0.030
22 HERS	19.289	33.121	-0.996	0.163	0.190	0.201
22 VILL	17.904	32.227	4.275	0.265	0.285	0.755
22 ONSA	13.045	32.935	-1.089	0.061	0.078	0.028
22 VAAS	10.811	51.356	24.753	0.756	1.170	1.358
fixed-interval smoothing results						
97.53990000000000			21			
21 REYK	19.647	3.352	13.022	0.250	0.406	0.255
21 NYAL	8.334	97.774	20.290	0.159	0.199	0.067
21 VARD	3.548	81.499	2.223	0.665	1.277	0.899
21 MDVO	12.907	45.847	1.501	0.259	0.312	0.436
21 NICO	24.052	15.139	10.617	2.573	2.641	10.195
21 NOTO	21.674	30.167	8.914	0.243	0.253	0.653
21 MASP	16.313	32.561	-4.358	0.294	0.297	1.202

```
 21 SOFI       11.194       40.992        6.512        1.925        2.187        6.660
 21 JOZE       18.088       41.534       27.061        0.219        0.240        0.333
 21 GRAZ       14.757       32.379       -0.396        0.060        0.071        0.029
 21 WTZR       13.225       31.383       -4.081        0.060        0.072        0.029
 21 ZIMM       16.117       28.513        1.481        0.061        0.071        0.029
 21 HERS       19.291       33.120       -0.997        0.161        0.187        0.202
 21 VILL       17.914       32.238        4.275        0.257        0.278        0.754
 21 ONSA       13.024       32.936       -1.099        0.059        0.076        0.027
 21 VAAS       10.802       51.360       24.755        0.756        1.169        1.358
fixed-interval smoothing results
   97.463200000000000                20
 20 REYK       19.735        3.390       13.013        0.242        0.401        0.253
 20 NYAL        8.332       97.773       20.291        0.151        0.192        0.063
 20 VARD        3.508       81.502        2.228        0.665        1.278        0.899
 20 MDVO       13.024       45.860        1.492        0.252        0.306        0.435
 20 NOTO       21.685       30.190        8.914        0.235        0.245        0.653
 20 MASP       16.277       32.581       -4.358        0.287        0.290        1.202
 20 JOZE       18.065       41.580       27.067        0.210        0.231        0.332
 20 GRAZ       14.779       32.369       -0.407        0.059        0.069        0.029
 20 WTZR       13.211       31.371       -4.089        0.059        0.070        0.028
 20 ZIMM       16.036       28.480        1.513        0.059        0.070        0.029
 20 HERS       19.295       33.120       -0.997        0.159        0.186        0.203
 20 VILL       17.927       32.251        4.276        0.250        0.270        0.754
 20 ONSA       12.978       32.929       -1.098        0.058        0.074        0.026
 20 VAAS       10.793       51.363       24.756        0.756        1.170        1.358
fixed-interval smoothing results
   97.386399999999990                19
 19 REYK       19.836        3.435       13.003        0.235        0.396        0.252
 19 NYAL        8.329       97.772       20.292        0.144        0.186        0.061
 19 VARD        3.473       81.506        2.233        0.667        1.279        0.899
 19 MDVO       13.175       45.871        1.481        0.246        0.300        0.434
 19 NOTO       21.701       30.214        8.915        0.228        0.237        0.652
 19 MASP       16.235       32.605       -4.358        0.280        0.284        1.202
 19 JOZE       18.036       41.635       27.075        0.202        0.223        0.331
 19 GRAZ       14.814       32.380       -0.423        0.058        0.068        0.028
 19 WTZR       13.183       31.369       -4.091        0.058        0.069        0.028
 19 ZIMM       15.986       28.427        1.543        0.058        0.068        0.028
 19 HERS       19.301       33.122       -0.997        0.159        0.185        0.204
 19 VILL       17.941       32.267        4.276        0.242        0.263        0.753
 19 ONSA       12.972       32.915       -1.106        0.057        0.073        0.026
 19 VAAS       10.785       51.366       24.757        0.757        1.170        1.358
fixed-interval smoothing results
   97.309700000000010                18
 18 REYK       19.947        3.488       12.993        0.229        0.392        0.251
 18 NYAL        8.325       97.770       20.294        0.138        0.181        0.058
 18 VARD        3.443       81.509        2.237        0.668        1.280        0.899
 18 MDVO       13.364       45.879        1.467        0.241        0.294        0.434
 18 NOTO       21.722       30.242        8.915        0.221        0.230        0.652
 18 MASP       16.191       32.635       -4.359        0.275        0.278        1.201
 18 JOZE       17.999       41.700       27.084        0.195        0.215        0.330
 18 GRAZ       14.777       32.394       -0.421        0.057        0.067        0.028
 18 WTZR       13.178       31.368       -4.101        0.057        0.068        0.027
 18 ZIMM       15.977       28.368        1.562        0.057        0.067        0.028
 18 HERS       19.309       33.124       -0.998        0.160        0.186        0.205
 18 VILL       17.958       32.286        4.276        0.236        0.257        0.753
 18 ONSA       12.976       32.877       -1.105        0.056        0.071        0.025
 18 VAAS       10.778       51.368       24.758        0.759        1.171        1.358
fixed-interval smoothing results
   97.233000000000000                17
 17 REYK       20.064        3.546       12.982        0.223        0.388        0.251
 17 NYAL        8.317       97.769       20.299        0.133        0.178        0.057
 17 VARD        3.422       81.511        2.240        0.671        1.281        0.899
 17 MDVO       13.596       45.882        1.450        0.236        0.290        0.433
 17 NOTO       21.750       30.271        8.915        0.214        0.224        0.652
 17 MASP       16.143       32.673       -4.359        0.269        0.273        1.201
 17 JOZE       17.956       41.773       27.094        0.188        0.208        0.329
 17 GRAZ       14.675       32.393       -0.400        0.056        0.066        0.027
 17 WTZR       13.196       31.373       -4.118        0.056        0.067        0.027
 17 ZIMM       15.982       28.332        1.573        0.057        0.066        0.027
 17 HERS       19.320       33.129       -0.999        0.161        0.188        0.207
 17 VILL       17.977       32.309        4.276        0.229        0.251        0.753
 17 ONSA       12.992       32.841       -1.100        0.055        0.070        0.025
```

```
 17 VAAS       10.773       51.369       24.758       0.761       1.172       1.358
fixed-interval smoothing results
   97.15630000000000                    16
 16 REYK       20.186        3.609       12.971       0.218       0.384       0.250
 16 NYAL        8.306       97.767       20.306       0.130       0.175       0.055
 16 VARD        3.408       81.512        2.242       0.674       1.283       0.900
 16 MDVO       13.869       45.881        1.430       0.232       0.285       0.433
 16 NOTO       21.782       30.304        8.915       0.209       0.218       0.651
 16 MASP       16.093       32.719       -4.359       0.264       0.268       1.201
 16 JOZE       17.907       41.855       27.105       0.181       0.202       0.329
 16 GRAZ       14.640       32.364       -0.385       0.055       0.065       0.027
 16 WTZR       13.203       31.406       -4.125       0.055       0.066       0.026
 16 ZIMM       15.983       28.325        1.586       0.056       0.065       0.027
 16 HERS       19.334       33.136       -1.000       0.164       0.191       0.208
 16 VILL       17.997       32.335        4.276       0.224       0.246       0.752
 16 ONSA       13.057       32.837       -1.111       0.054       0.069       0.025
 16 VAAS       10.770       51.369       24.759       0.763       1.174       1.359
fixed-interval smoothing results
   97.07960000000000                    15
 15 REYK       20.311        3.676       12.961       0.214       0.382       0.249
 15 NYAL        8.293       97.765       20.315       0.128       0.173       0.054
 15 VARD        3.399       81.512        2.243       0.677       1.284       0.900
 15 MDVO       14.176       45.876        1.407       0.228       0.282       0.433
 15 NOTO       21.820       30.339        8.915       0.204       0.213       0.651
 15 MASP       16.040       32.774       -4.360       0.260       0.264       1.201
 15 JOZE       17.852       41.945       27.117       0.176       0.196       0.328
 15 GRAZ       14.685       32.317       -0.380       0.055       0.065       0.027
 15 WTZR       13.206       31.475       -4.123       0.055       0.065       0.026
 15 ZIMM       15.988       28.334        1.598       0.055       0.065       0.027
 15 HERS       19.350       33.146       -1.001       0.168       0.195       0.209
 15 VILL       18.019       32.364        4.276       0.219       0.241       0.752
 15 ONSA       13.086       32.875       -1.106       0.054       0.069       0.024
 15 VAAS       10.769       51.369       24.759       0.766       1.176       1.359
fixed-interval smoothing results
   97.00290000000000                    14
 14 REYK       20.438        3.745       12.950       0.211       0.379       0.249
 14 NYAL        8.276       97.763       20.327       0.127       0.173       0.054
 14 VARD        3.392       81.512        2.244       0.681       1.286       0.900
 14 MDVO       14.514       45.867        1.383       0.225       0.279       0.433
 14 NOTO       21.861       30.375        8.915       0.200       0.209       0.651
 14 MASP       15.984       32.836       -4.360       0.257       0.261       1.201
 14 JOZE       17.791       42.043       27.129       0.171       0.191       0.328
 14 GRAZ       14.700       32.295       -0.357       0.055       0.064       0.027
 14 WTZR       13.213       31.549       -4.099       0.055       0.065       0.026
 14 ZIMM       15.981       28.370        1.618       0.055       0.064       0.026
 14 HERS       19.370       33.159       -1.003       0.173       0.200       0.211
 14 VILL       18.042       32.396        4.276       0.215       0.238       0.752
 14 ONSA       13.032       32.971       -1.074       0.054       0.068       0.024
 14 VAAS       10.768       51.369       24.759       0.769       1.178       1.359
fixed-interval smoothing results
   96.92890000000000                    13
 13 REYK       20.557        3.810       12.941       0.208       0.378       0.249
 13 NYAL        8.254       97.762       20.341       0.128       0.174       0.054
 13 VARD        3.387       81.512        2.245       0.684       1.288       0.901
 13 MDVO       14.852       45.857        1.358       0.223       0.277       0.432
 13 NOTO       21.902       30.410        8.914       0.197       0.206       0.651
 13 MASP       15.929       32.900       -4.361       0.255       0.258       1.201
 13 JOZE       17.730       42.140       27.142       0.167       0.188       0.327
 13 GRAZ       14.726       32.354       -0.325       0.054       0.064       0.026
 13 WTZR       13.179       31.610       -4.022       0.054       0.064       0.026
 13 ZIMM       15.936       28.469        1.662       0.054       0.064       0.026
 13 HERS       19.391       33.174       -1.005       0.179       0.205       0.212
 13 VILL       18.064       32.427        4.276       0.212       0.235       0.752
 13 ONSA       12.916       33.146       -1.035       0.053       0.068       0.024
 13 VAAS       10.768       51.369       24.759       0.772       1.180       1.359
fixed-interval smoothing results
   96.85220000000000                    12
 12 REYK       20.683        3.880       12.931       0.207       0.377       0.249
 12 NYAL        8.227       97.761       20.359       0.130       0.176       0.055
 12 VARD        3.385       81.512        2.245       0.689       1.291       0.901
 12 MDVO       15.231       45.844        1.330       0.222       0.276       0.432
 12 NOTO       21.947       30.449        8.914       0.195       0.204       0.651
```

12 MASP	15.867	32.975	-4.362	0.253	0.257	1.201
12 JOZE	17.663	42.247	27.155	0.164	0.185	0.327
12 GRAZ	14.812	32.590	-0.283	0.054	0.063	0.026
12 WTZR	13.142	31.721	-3.879	0.054	0.064	0.026
12 ZIMM	15.906	28.763	1.729	0.054	0.064	0.026
12 HERS	19.414	33.192	-1.006	0.186	0.212	0.214
12 VILL	18.087	32.463	4.276	0.210	0.233	0.752
12 ONSA	12.719	33.466	-0.978	0.053	0.068	0.024
12 VAAS	10.768	51.369	24.759	0.776	1.182	1.360
fixed-interval smoothing results						
96.77549999999999			11			
11 REYK	20.804	3.949	12.922	0.206	0.376	0.249
11 NYAL	8.197	97.761	20.378	0.134	0.180	0.057
11 MDVO	15.614	45.831	1.302	0.222	0.275	0.432
11 NOTO	21.991	30.488	8.914	0.194	0.203	0.651
11 MASP	15.804	33.054	-4.362	0.252	0.256	1.201
11 JOZE	17.594	42.356	27.170	0.162	0.183	0.327
11 GRAZ	14.988	33.096	-0.230	0.055	0.064	0.026
11 WTZR	13.323	31.935	-3.725	0.054	0.064	0.026
11 ZIMM	16.077	29.359	1.771	0.055	0.064	0.026
11 HERS	19.438	33.213	-1.008	0.193	0.219	0.216
11 VILL	18.110	32.501	4.276	0.209	0.232	0.752
11 ONSA	12.696	33.985	-0.975	0.054	0.068	0.024
fixed-interval smoothing results						
96.69880000000001			10			
10 REYK	20.922	4.016	12.912	0.207	0.377	0.249
10 NYAL	8.167	97.763	20.397	0.139	0.184	0.059
10 MDVO	15.987	45.819	1.275	0.222	0.276	0.433
10 NOTO	22.034	30.527	8.913	0.194	0.203	0.651
10 MASP	15.741	33.135	-4.363	0.252	0.256	1.201
10 JOZE	17.527	42.464	27.184	0.161	0.182	0.327
10 GRAZ	15.510	33.971	-0.221	0.054	0.063	0.026
10 WTZR	14.006	32.328	-3.618	0.054	0.064	0.026
10 ZIMM	16.748	30.309	1.730	0.054	0.063	0.026
10 HERS	19.461	33.235	-1.009	0.202	0.227	0.218
10 VILL	18.132	32.538	4.276	0.209	0.232	0.752
10 ONSA	13.303	34.817	-1.174	0.053	0.067	0.024
fixed-interval smoothing results						
96.62210000000000			9			
9 REYK	21.036	4.082	12.903	0.208	0.378	0.249
9 NYAL	8.140	97.766	20.415	0.146	0.190	0.061
9 MDVO	16.340	45.808	1.249	0.224	0.277	0.433
9 NOTO	22.073	30.563	8.913	0.195	0.205	0.651
9 MASP	15.679	33.214	-4.363	0.254	0.258	1.201
9 JOZE	17.461	42.569	27.198	0.162	0.183	0.327
9 GRAZ	16.748	35.281	-0.341	0.053	0.063	0.026
9 WTZR	15.486	32.979	-3.624	0.053	0.063	0.026
9 ZIMM	18.195	31.629	1.555	0.054	0.063	0.026
9 VILL	18.153	32.574	4.276	0.211	0.233	0.752
9 ONSA	14.998	36.020	-1.694	0.053	0.067	0.024
9 HERS	19.482	33.259	-1.010	0.210	0.235	0.220
fixed-interval smoothing results						
96.54530000000000			8			
8 REYK	21.148	4.145	12.894	0.211	0.379	0.250
8 NYAL	8.115	97.771	20.431	0.153	0.196	0.064
8 MDVO	16.668	45.797	1.225	0.226	0.280	0.433
8 NOTO	22.110	30.596	8.913	0.198	0.207	0.651
8 MASP	15.621	33.289	-4.363	0.256	0.260	1.201
8 JOZE	17.396	42.667	27.211	0.164	0.186	0.327
8 GRAZ	18.720	36.957	-0.603	0.054	0.063	0.026
8 WTZR	17.906	33.889	-3.805	0.054	0.064	0.026
8 ZIMM	20.416	33.251	1.232	0.054	0.063	0.026
8 HERS	19.501	33.283	-1.012	0.220	0.244	0.221
8 VILL	18.172	32.608	4.276	0.213	0.235	0.752
8 ONSA	17.922	37.549	-2.568	0.053	0.067	0.024
fixed-interval smoothing results						
96.46860000000000			7			
7 REYK	21.254	4.205	12.886	0.216	0.382	0.250
7 NYAL	8.096	97.776	20.444	0.162	0.204	0.068
7 MDVO	16.963	45.788	1.203	0.230	0.283	0.434
7 NOTO	22.143	30.623	8.912	0.202	0.211	0.651
7 MASP	15.567	33.357	-4.364	0.259	0.263	1.201

```
  7 JOZE       17.335       42.756       27.224    0.168    0.190    0.328
  7 GRAZ       20.733       38.707       -0.877    0.055    0.064    0.026
  7 WTZR       20.519       34.901       -4.050    0.055    0.064    0.026
  7 ZIMM       22.696       34.914        0.888    0.055    0.064    0.026
  7 HERS       19.517       33.305       -1.013    0.229    0.253    0.223
  7 VILL       18.188       32.638        4.276    0.217    0.239    0.752
  7 ONSA       20.802       39.155       -3.432    0.054    0.067    0.024
fixed-interval smoothing results
   96.39190000000001                  6
  6 REYK       21.350        4.258       12.878    0.221    0.385    0.251
  6 NYAL        8.078       97.782       20.455    0.171    0.212    0.071
  6 MDVO       17.221       45.780        1.183    0.235    0.288    0.434
  6 NOTO       22.173       30.647        8.912    0.207    0.217    0.652
  6 MASP       15.520       33.420       -4.364    0.264    0.268    1.201
  6 JOZE       17.280       42.834       27.235    0.173    0.195    0.328
  6 GRAZ       22.079       40.205       -1.029    0.054    0.063    0.026
  6 WTZR       22.366       35.770       -4.186    0.053    0.063    0.025
  6 ZIMM       24.285       36.309        0.668    0.054    0.063    0.025
  6 VILL       18.202       32.666        4.276    0.222    0.244    0.752
  6 ONSA       22.417       40.508       -3.923    0.052    0.066    0.024
  6 HERS       19.530       33.323       -1.014    0.240    0.263    0.225
fixed-interval smoothing results
   96.31520000000000                  5
  5 REYK       21.430        4.304       12.871    0.228    0.389    0.252
  5 NYAL        8.062       97.787       20.466    0.181    0.221    0.075
  5 MDVO       17.440       45.773        1.167    0.241    0.293    0.435
  5 NOTO       22.198       30.669        8.912    0.214    0.223    0.652
  5 MASP       15.479       33.475       -4.365    0.269    0.273    1.201
  5 JOZE       17.234       42.899       27.245    0.180    0.202    0.329
  5 GRAZ       22.752       41.319       -1.070    0.053    0.061    0.025
  5 WTZR       23.258       36.381       -4.192    0.053    0.061    0.024
  5 ZIMM       25.141       37.312        0.574    0.053    0.061    0.025
  5 HERS       19.538       33.337       -1.015    0.250    0.273    0.227
  5 VILL       18.213       32.689        4.276    0.229    0.250    0.753
  5 ONSA       22.967       41.486       -4.086    0.052    0.063    0.023
fixed-interval smoothing results
   96.23850000000000                  4
  4 REYK       21.493        4.341       12.866    0.235    0.394    0.254
  4 NYAL        8.045       97.791       20.476    0.192    0.231    0.080
  4 MDVO       17.615       45.768        1.154    0.248    0.299    0.436
  4 NOTO       22.218       30.688        8.912    0.222    0.231    0.653
  4 JOZE       17.198       42.950       27.252    0.188    0.210    0.330
  4 GRAZ       22.992       42.060       -1.047    0.052    0.058    0.024
  4 WTZR       23.504       36.785       -4.133    0.052    0.058    0.023
  4 ZIMM       25.489       37.958        0.563    0.052    0.058    0.023
  4 HERS       19.541       33.346       -1.015    0.260    0.282    0.229
  4 VILL       18.221       32.709        4.276    0.236    0.257    0.753
  4 ONSA       22.871       42.117       -4.027    0.051    0.060    0.022
  4 MASP       15.447       33.523       -4.365    0.276    0.280    1.202
fixed-interval smoothing results
   96.16180000000000                  3
  3 REYK       21.538        4.368       12.863    0.244    0.399    0.255
  3 NYAL        8.029       97.793       20.485    0.204    0.241    0.084
  3 MDVO       17.743       45.764        1.144    0.256    0.307    0.436
  3 NOTO       22.232       30.703        8.912    0.231    0.240    0.653
  3 MASP       15.423       33.560       -4.365    0.283    0.287    1.202
  3 JOZE       17.173       42.988       27.257    0.199    0.219    0.331
  3 GRAZ       22.939       42.513       -0.978    0.049    0.056    0.023
  3 WTZR       23.586       37.059       -4.106    0.049    0.057    0.023
  3 ZIMM       25.480       38.327        0.606    0.049    0.056    0.023
  3 HERS       19.542       33.350       -1.015    0.271    0.292    0.231
  3 VILL       18.225       32.725        4.276    0.245    0.265    0.754
  3 ONSA       22.574       42.507       -3.889    0.049    0.060    0.022
fixed-interval smoothing results
   96.08510000000000                  2
  2 REYK       21.566        4.384       12.860    0.254    0.406    0.257
  2 NYAL        8.017       97.794       20.492    0.216    0.251    0.089
  2 MDVO       17.822       45.761        1.138    0.266    0.315    0.437
  2 NOTO       22.240       30.713        8.911    0.242    0.250    0.654
  2 MASP       15.409       33.582       -4.365    0.292    0.296    1.202
  2 JOZE       17.157       43.010       27.261    0.210    0.230    0.332
  2 GRAZ       22.851       42.776       -0.928    0.051    0.064    0.027
```

2 WTZR	23.722	37.241	-4.134	0.051	0.065	0.026
2 ZIMM	25.315	38.507	0.657	0.052	0.064	0.027
2 HERS	19.541	33.351	-1.015	0.281	0.302	0.233
2 VILL	18.227	32.735	4.276	0.255	0.274	0.754
2 ONSA	22.529	42.748	-3.838	0.051	0.070	0.024
fixed-interval smoothing results						
96.00839999999999			1			
1 REYK	21.575	4.390	12.860	0.264	0.412	0.258
1 NYAL	8.013	97.794	20.495	0.229	0.262	0.094
1 MDVO	17.849	45.760	1.136	0.276	0.323	0.438
1 NOTO	22.242	30.716	8.911	0.253	0.260	0.654
1 MASP	15.404	33.590	-4.365	0.301	0.305	1.203
1 JOZE	17.152	43.018	27.262	0.223	0.242	0.334
1 GRAZ	22.841	42.867	-0.919	0.077	0.089	0.037
1 WTZR	23.803	37.313	-4.157	0.076	0.090	0.036
1 ZIMM	25.236	38.561	0.676	0.077	0.090	0.037
1 VILL	18.228	32.738	4.276	0.265	0.284	0.755
1 ONSA	22.587	42.833	-3.841	0.075	0.095	0.034
			GROUP TWO			
fixed-interval smoothing results						
98.07680000000001			28			
28 ANKR	2.510	-6.672	-2.255	0.319	0.329	0.652
28 ZWEN	10.649	39.367	6.454	0.335	0.383	0.515
28 SODA	12.041	75.480	77.503	1.283	2.278	1.871
28 DOUR	16.537	31.488	0.339	0.368	0.408	0.654
28 EBRE	14.522	30.760	7.635	0.604	0.664	2.224
28 CAGL	14.972	27.013	0.333	0.398	0.419	1.275
28 MATE	17.404	32.652	-1.606	0.109	0.125	0.056
28 MEDI	13.280	41.502	-1.748	0.364	0.395	0.895
28 GOPE	20.493	39.598	18.764	0.289	0.302	0.369
28 RIGA	13.333	46.039	-3.854	0.843	1.044	2.013
28 MAR6	12.083	44.968	16.133	0.700	0.981	1.318
28 MADR	19.820	35.927	-37.699	0.238	0.245	0.176
28 SFER	16.683	12.538	-3.426	0.394	0.423	1.708
28 TRON	17.493	84.646	-6.770	0.628	0.910	1.024
28 STAV	13.507	25.859	15.085	0.544	0.695	1.056
28 OSLO	17.233	9.885	-9.671	0.727	0.986	1.361
28 TROM	6.910	40.271	-16.748	0.183	0.210	0.090
fixed-interval smoothing results						
98.00010000000000			27			
27 ANKR	2.511	-6.671	-2.255	0.310	0.320	0.651
27 ZWEN	10.656	39.367	6.453	0.327	0.375	0.514
27 SODA	12.050	75.478	77.501	1.281	2.276	1.871
27 DOUR	16.538	31.489	0.339	0.360	0.401	0.653
27 EBRE	14.520	30.760	7.635	0.599	0.660	2.224
27 CAGL	14.971	27.014	0.333	0.391	0.412	1.274
27 MATE	17.402	32.653	-1.604	0.089	0.105	0.049
27 MEDI	13.278	41.504	-1.748	0.356	0.388	0.894
27 GOPE	20.495	39.601	18.764	0.279	0.292	0.367
27 RIGA	13.332	46.039	-3.854	0.840	1.041	2.013
27 MAR6	12.082	44.967	16.133	0.696	0.978	1.317
27 MADR	19.818	35.928	-37.699	0.226	0.234	0.174
27 SFER	16.683	12.538	-3.426	0.386	0.417	1.708
27 TRON	17.481	84.646	-6.768	0.624	0.907	1.023
27 STAV	13.510	25.856	15.086	0.539	0.691	1.056
27 OSLO	17.224	9.890	-9.669	0.723	0.983	1.361
27 TROM	6.910	40.271	-16.748	0.170	0.198	0.085
fixed-interval smoothing results						
97.92340000000000			26			
26 ANKR	2.510	-6.668	-2.255	0.301	0.311	0.651
26 ZWEN	10.668	39.368	6.452	0.318	0.368	0.513
26 SODA	12.063	75.475	77.499	1.279	2.275	1.871
26 DOUR	16.541	31.492	0.339	0.352	0.395	0.653
26 EBRE	14.517	30.761	7.635	0.595	0.656	2.224
26 CAGL	14.970	27.013	0.333	0.383	0.405	1.274
26 MATE	17.406	32.653	-1.601	0.075	0.090	0.042
26 MEDI	13.273	41.509	-1.748	0.348	0.381	0.894
26 GOPE	20.503	39.611	18.764	0.269	0.282	0.366
26 RIGA	13.331	46.039	-3.854	0.837	1.038	2.013
26 MAR6	12.081	44.966	16.133	0.692	0.976	1.317
26 MADR	19.815	35.928	-37.699	0.214	0.222	0.171
26 SFER	16.683	12.538	-3.426	0.380	0.410	1.707

```
 26 TRON        17.464        84.646        -6.764        0.620        0.904        1.023
 26 STAV        13.514        25.851        15.086        0.536        0.688        1.056
 26 OSLO        17.211         9.897        -9.667        0.720        0.980        1.360
 26 TROM         6.910        40.271       -16.748        0.161        0.187        0.081
fixed-interval smoothing results
   97.84670000000000                    25
 25 ANKR         2.507        -6.663        -2.256        0.291        0.302        0.650
 25 ZWEN        10.680        39.369         6.452        0.310        0.360        0.512
 25 SODA        12.080        75.472        77.496        1.278        2.275        1.871
 25 DOUR        16.547        31.497         0.339        0.345        0.388        0.652
 25 MADR        19.812        35.928       -37.700        0.203        0.211        0.169
 25 SFER        16.683        12.538        -3.426        0.374        0.405        1.707
 25 EBRE        14.514        30.761         7.635        0.591        0.653        2.224
 25 CAGL        14.968        27.010         0.333        0.377        0.399        1.274
 25 MATE        17.398        32.652        -1.594        0.068        0.079        0.038
 25 MEDI        13.264        41.523        -1.748        0.341        0.374        0.893
 25 GOPE        20.517        39.627        18.765        0.259        0.273        0.365
 25 RIGA        13.329        46.039        -3.854        0.835        1.036        2.013
 25 MAR6        12.078        44.966        16.134        0.689        0.973        1.317
 25 TRON        17.445        84.646        -6.760        0.617        0.902        1.022
 25 STAV        13.519        25.846        15.087        0.533        0.686        1.055
 25 OSLO        17.197         9.905        -9.664        0.718        0.978        1.360
 25 TROM         6.910        40.271       -16.748        0.154        0.177        0.076
fixed-interval smoothing results
   97.77000000000000                    24
 24 ANKR         2.503        -6.658        -2.256        0.283        0.293        0.649
 24 ZWEN        10.690        39.370         6.451        0.302        0.353        0.511
 24 SODA        12.101        75.469        77.493        1.277        2.274        1.871
 24 TRON        17.426        84.646        -6.756        0.614        0.900        1.022
 24 STAV        13.524        25.841        15.088        0.531        0.685        1.055
 24 DOUR        16.555        31.506         0.338        0.338        0.382        0.651
 24 MADR        19.811        35.926       -37.700        0.193        0.201        0.167
 24 SFER        16.684        12.538        -3.426        0.369        0.400        1.707
 24 EBRE        14.511        30.761         7.635        0.588        0.650        2.223
 24 CAGL        14.969        27.006         0.332        0.370        0.393        1.273
 24 MATE        17.386        32.652        -1.585        0.065        0.074        0.035
 24 MEDI        13.248        41.545        -1.748        0.334        0.367        0.893
 24 GOPE        20.540        39.654        18.766        0.249        0.263        0.364
 24 RIGA        13.325        46.039        -3.853        0.833        1.035        2.013
 24 MAR6        12.074        44.967        16.134        0.687        0.972        1.317
 24 OSLO        17.182         9.913        -9.661        0.715        0.977        1.360
 24 TROM         6.911        40.271       -16.748        0.148        0.168        0.072
fixed-interval smoothing results
   97.69329999999999                    23
 23 ANKR         2.499        -6.652        -2.256        0.274        0.285        0.649
 23 ZWEN        10.700        39.371         6.450        0.294        0.346        0.510
 23 SODA        12.120        75.466        77.489        1.277        2.274        1.871
 23 TRON        17.407        84.645        -6.752        0.613        0.899        1.022
 23 STAV        13.529        25.836        15.088        0.530        0.684        1.055
 23 DOUR        16.566        31.517         0.338        0.332        0.376        0.651
 23 MADR        19.815        35.920       -37.701        0.183        0.191        0.164
 23 SFER        16.684        12.537        -3.426        0.365        0.397        1.707
 23 EBRE        14.509        30.761         7.635        0.586        0.648        2.223
 23 CAGL        14.970        26.999         0.332        0.365        0.387        1.273
 23 MATE        17.374        32.652        -1.574        0.065        0.072        0.033
 23 MEDI        13.226        41.577        -1.748        0.327        0.361        0.892
 23 GOPE        20.572        39.691        18.767        0.240        0.254        0.363
 23 RIGA        13.320        46.039        -3.852        0.831        1.034        2.013
 23 MAR6        12.070        44.968        16.134        0.685        0.971        1.316
 23 OSLO        17.168         9.920        -9.659        0.714        0.976        1.360
 23 TROM         6.911        40.270       -16.748        0.144        0.160        0.068
fixed-interval smoothing results
   97.61660000000001                    22
 22 ANKR         2.495        -6.647        -2.257        0.265        0.276        0.648
 22 ZWEN        10.709        39.370         6.449        0.287        0.340        0.510
 22 SODA        12.135        75.465        77.486        1.277        2.274        1.871
 22 TRON        17.390        84.646        -6.749        0.612        0.899        1.022
 22 STAV        13.534        25.832        15.089        0.530        0.684        1.055
 22 DOUR        16.579        31.533         0.337        0.326        0.371        0.650
 22 MADR        19.828        35.905       -37.702        0.174        0.182        0.162
 22 SFER        16.685        12.535        -3.426        0.362        0.394        1.707
 22 EBRE        14.508        30.760         7.634        0.584        0.647        2.223
```

```
 22 CAGL        14.974        26.991         0.331        0.359        0.382        1.273
 22 MATE        17.350        32.647        -1.562        0.063        0.071        0.032
 22 MEDI        13.197        41.618        -1.748        0.321        0.356        0.892
 22 GOPE        20.613        39.739        18.768        0.230        0.245        0.362
 22 RIGA        13.314        46.040        -3.852        0.830        1.033        2.013
 22 MAR6        12.065        44.970        16.135        0.684        0.970        1.316
 22 OSLO        17.155         9.927        -9.656        0.713        0.975        1.360
 22 TROM         6.911        40.270       -16.748        0.140        0.153        0.064
fixed-interval smoothing results
   97.53990000000000                    21
 21 ZWEN        10.720        39.368         6.448        0.281        0.334        0.509
 21 SODA        12.146        75.465        77.484        1.278        2.274        1.871
 21 TRON        17.373        84.646        -6.745        0.612        0.899        1.022
 21 STAV        13.539        25.828        15.089        0.530        0.685        1.055
 21 DOUR        16.594        31.552         0.336        0.321        0.367        0.650
 21 MADR        19.852        35.878       -37.703        0.166        0.174        0.160
 21 SFER        16.685        12.532        -3.426        0.360        0.391        1.707
 21 EBRE        14.508        30.757         7.634        0.583        0.646        2.223
 21 CAGL        14.979        26.981         0.331        0.355        0.378        1.273
 21 MATE        17.340        32.641        -1.552        0.061        0.069        0.031
 21 MEDI        13.160        41.668        -1.749        0.316        0.351        0.892
 21 GOPE        20.664        39.800        18.770        0.221        0.236        0.361
 21 RIGA        13.308        46.040        -3.851        0.830        1.033        2.013
 21 MAR6        12.060        44.973        16.135        0.684        0.970        1.316
 21 OSLO        17.143         9.933        -9.654        0.713        0.975        1.360
 21 ANKR         2.494        -6.643        -2.258        0.257        0.269        0.647
 21 TROM         6.910        40.270       -16.748        0.136        0.146        0.061
fixed-interval smoothing results
   97.46320000000000                    20
 20 ANKR         2.496        -6.639        -2.259        0.250        0.261        0.647
 20 ZWEN        10.730        39.365         6.447        0.274        0.328        0.509
 20 SODA        12.152        75.466        77.482        1.279        2.275        1.871
 20 TRON        17.358        84.646        -6.742        0.613        0.899        1.022
 20 STAV        13.544        25.825        15.089        0.531        0.686        1.055
 20 DOUR        16.611        31.574         0.335        0.317        0.364        0.649
 20 MADR        19.894        35.832       -37.704        0.159        0.166        0.159
 20 SFER        16.685        12.527        -3.426        0.358        0.390        1.707
 20 EBRE        14.509        30.753         7.634        0.583        0.646        2.223
 20 CAGL        14.985        26.968         0.330        0.351        0.374        1.273
 20 MATE        17.347        32.629        -1.539        0.059        0.067        0.030
 20 MEDI        13.114        41.725        -1.749        0.311        0.346        0.892
 20 GOPE        20.724        39.873        18.773        0.213        0.227        0.360
 20 RIGA        13.303        46.041        -3.850        0.830        1.033        2.013
 20 MAR6        12.056        44.975        16.136        0.684        0.970        1.316
 20 OSLO        17.133         9.939        -9.653        0.714        0.976        1.360
 20 TROM         6.910        40.270       -16.748        0.132        0.139        0.058
fixed-interval smoothing results
   97.38639999999999                    19
 19 ANKR         2.502        -6.637        -2.260        0.242        0.254        0.646
 19 ZWEN        10.741        39.361         6.446        0.269        0.323        0.508
 19 SODA        12.154        75.467        77.481        1.280        2.276        1.871
 19 TRON        17.344        84.648        -6.740        0.614        0.900        1.022
 19 STAV        13.549        25.822        15.089        0.533        0.687        1.055
 19 DOUR        16.631        31.601         0.334        0.314        0.361        0.649
 19 SFER        16.686        12.522        -3.426        0.358        0.390        1.707
 19 EBRE        14.511        30.748         7.634        0.584        0.646        2.223
 19 CAGL        14.993        26.954         0.329        0.347        0.370        1.273
 19 MATE        17.331        32.608        -1.517        0.058        0.066        0.029
 19 MEDI        13.061        41.789        -1.749        0.308        0.343        0.891
 19 GOPE        20.794        39.960        18.775        0.205        0.219        0.359
 19 RIGA        13.298        46.042        -3.850        0.831        1.033        2.013
 19 MAR6        12.052        44.977        16.136        0.685        0.970        1.317
 19 OSLO        17.125         9.945        -9.652        0.715        0.976        1.360
 19 TROM         6.909        40.270       -16.748        0.128        0.133        0.055
 19 MADR        19.960        35.759       -37.707        0.153        0.159        0.157
fixed-interval smoothing results
   97.30970000000001                    18
 18 ANKR         2.511        -6.634        -2.261        0.236        0.247        0.646
 18 SODA        12.154        75.468        77.481        1.282        2.277        1.871
 18 TRON        17.333        84.649        -6.738        0.616        0.902        1.022
 18 STAV        13.554        25.821        15.089        0.536        0.689        1.056
 18 DOUR        16.652        31.630         0.332        0.311        0.358        0.649
```

18 SFER	16.686	12.517	-3.426	0.359	0.390	1.707
18 EBRE	14.514	30.744	7.634	0.585	0.647	2.223
18 CAGL	15.002	26.939	0.328	0.345	0.368	1.272
18 MATE	17.325	32.593	-1.503	0.058	0.065	0.029
18 MEDI	13.001	41.858	-1.749	0.305	0.340	0.891
18 GOPE	20.873	40.060	18.779	0.197	0.212	0.358
18 RIGA	13.294	46.043	-3.850	0.832	1.034	2.013
18 MAR6	12.049	44.978	16.136	0.687	0.972	1.317
18 OSLO	17.119	9.951	-9.651	0.716	0.977	1.360
18 ZWEN	10.755	39.354	6.445	0.264	0.319	0.508
18 TROM	6.908	40.270	-16.748	0.124	0.127	0.052
18 MADR	20.044	35.666	-37.709	0.147	0.152	0.156
fixed-interval smoothing results						
97.23300000000000			17			
17 ANKR	2.525	-6.628	-2.263	0.230	0.241	0.645
17 ZWEN	10.771	39.345	6.443	0.260	0.315	0.507
17 SODA	12.153	75.469	77.480	1.284	2.278	1.872
17 TRON	17.324	84.651	-6.737	0.619	0.904	1.023
17 STAV	13.557	25.821	15.088	0.539	0.692	1.056
17 DOUR	16.676	31.663	0.331	0.309	0.357	0.649
17 SFER	16.687	12.512	-3.426	0.360	0.392	1.707
17 EBRE	14.519	30.738	7.634	0.587	0.649	2.224
17 CAGL	15.014	26.923	0.327	0.343	0.366	1.272
17 MATE	17.332	32.590	-1.501	0.057	0.064	0.028
17 MEDI	12.936	41.930	-1.749	0.303	0.338	0.891
17 GOPE	20.963	40.173	18.782	0.190	0.205	0.357
17 RIGA	13.292	46.043	-3.849	0.834	1.036	2.013
17 MAR6	12.046	44.979	16.136	0.689	0.973	1.317
17 OSLO	17.115	9.958	-9.650	0.718	0.979	1.360
17 TROM	6.906	40.269	-16.748	0.120	0.122	0.050
17 MADR	20.134	35.565	-37.711	0.141	0.147	0.155
fixed-interval smoothing results						
97.15630000000000			16			
16 ANKR	2.544	-6.620	-2.265	0.224	0.236	0.645
16 ZWEN	10.791	39.333	6.442	0.256	0.312	0.507
16 SODA	12.152	75.469	77.480	1.286	2.279	1.872
16 TRON	17.317	84.652	-6.736	0.622	0.906	1.023
16 STAV	13.560	25.822	15.088	0.543	0.695	1.056
16 DOUR	16.701	31.699	0.329	0.308	0.356	0.649
16 SFER	16.687	12.508	-3.426	0.362	0.394	1.707
16 EBRE	14.524	30.733	7.634	0.590	0.652	2.224
16 CAGL	15.028	26.907	0.326	0.342	0.365	1.272
16 MATE	17.349	32.601	-1.512	0.056	0.063	0.028
16 MEDI	12.867	42.003	-1.750	0.302	0.337	0.891
16 GOPE	21.063	40.299	18.787	0.184	0.199	0.357
16 RIGA	13.291	46.042	-3.849	0.836	1.038	2.013
16 MAR6	12.045	44.978	16.136	0.692	0.975	1.317
16 OSLO	17.113	9.965	-9.650	0.721	0.981	1.361
16 TROM	6.904	40.269	-16.747	0.117	0.118	0.049
16 MADR	20.224	35.464	-37.714	0.136	0.142	0.154
fixed-interval smoothing results						
97.07960000000000			15			
15 ANKR	2.569	-6.607	-2.267	0.219	0.231	0.645
15 ZWEN	10.815	39.319	6.440	0.253	0.309	0.507
15 TROM	6.902	40.268	-16.747	0.114	0.116	0.048
15 TRON	17.312	84.652	-6.735	0.625	0.908	1.023
15 STAV	13.560	25.825	15.088	0.547	0.698	1.056
15 DOUR	16.728	31.738	0.328	0.308	0.356	0.649
15 SFER	16.687	12.506	-3.426	0.366	0.397	1.707
15 EBRE	14.529	30.728	7.633	0.593	0.655	2.224
15 CAGL	15.045	26.892	0.325	0.342	0.365	1.272
15 MATE	17.335	32.628	-1.536	0.056	0.063	0.028
15 MEDI	12.797	42.075	-1.751	0.302	0.336	0.891
15 GOPE	21.174	40.438	18.791	0.178	0.193	0.356
15 RIGA	13.291	46.042	-3.849	0.839	1.040	2.013
15 MAR6	12.045	44.976	16.136	0.695	0.977	1.317
15 OSLO	17.112	9.972	-9.650	0.724	0.983	1.361
15 MADR	20.311	35.364	-37.716	0.132	0.138	0.153
fixed-interval smoothing results						
97.00290000000000			14			
14 ANKR	2.599	-6.588	-2.269	0.215	0.228	0.644
14 ZWEN	10.842	39.304	6.438	0.251	0.307	0.507

14 TROM	6.899	40.268	-16.747	0.112	0.115	0.048
14 TRON	17.309	84.653	-6.734	0.629	0.911	1.024
14 STAV	13.560	25.827	15.088	0.551	0.702	1.057
14 DOUR	16.756	31.779	0.326	0.309	0.357	0.649
14 MADR	20.394	35.266	-37.718	0.129	0.135	0.153
14 SFER	16.686	12.505	-3.425	0.369	0.400	1.707
14 EBRE	14.534	30.724	7.633	0.597	0.659	2.224
14 CAGL	15.064	26.877	0.324	0.343	0.366	1.273
14 MATE	17.225	32.664	-1.564	0.056	0.062	0.028
14 MEDI	12.727	42.143	-1.752	0.303	0.337	0.891
14 GOPE	21.294	40.588	18.795	0.173	0.188	0.356
14 RIGA	13.292	46.041	-3.849	0.842	1.042	2.013
14 MAR6	12.046	44.975	16.136	0.699	0.980	1.318
14 OSLO	17.111	9.977	-9.650	0.728	0.986	1.361
fixed-interval smoothing results						
96.92890000000000		13				
13 ANKR	2.634	-6.561	-2.272	0.212	0.225	0.644
13 ZWEN	10.867	39.289	6.436	0.250	0.306	0.506
13 TROM	6.893	40.269	-16.746	0.111	0.115	0.048
13 TRON	17.307	84.654	-6.734	0.633	0.914	1.024
13 STAV	13.559	25.828	15.088	0.556	0.705	1.057
13 DOUR	16.784	31.820	0.324	0.311	0.359	0.649
13 MADR	20.468	35.180	-37.720	0.127	0.133	0.152
13 SFER	16.684	12.505	-3.425	0.374	0.404	1.707
13 EBRE	14.536	30.722	7.633	0.602	0.662	2.224
13 CAGL	15.082	26.864	0.323	0.345	0.367	1.273
13 MATE	17.100	32.721	-1.606	0.055	0.062	0.028
13 MEDI	12.666	42.202	-1.753	0.305	0.339	0.892
13 GOPE	21.414	40.738	18.800	0.170	0.185	0.355
13 RIGA	13.292	46.041	-3.849	0.845	1.044	2.014
13 MAR6	12.046	44.974	16.136	0.702	0.982	1.318
13 OSLO	17.111	9.980	-9.650	0.731	0.988	1.361
fixed-interval smoothing results						
96.85220000000000		12				
12 ANKR	2.677	-6.519	-2.275	0.210	0.223	0.644
12 ZWEN	10.892	39.274	6.434	0.249	0.305	0.506
12 TROM	6.883	40.272	-16.746	0.112	0.117	0.049
12 TRON	17.306	84.654	-6.734	0.638	0.917	1.025
12 STAV	13.558	25.829	15.088	0.561	0.709	1.058
12 DOUR	16.814	31.864	0.323	0.313	0.361	0.649
12 MADR	20.541	35.093	-37.722	0.126	0.133	0.152
12 SFER	16.682	12.506	-3.425	0.379	0.409	1.708
12 EBRE	14.537	30.721	7.633	0.606	0.667	2.224
12 CAGL	15.103	26.852	0.322	0.348	0.369	1.273
12 MATE	17.043	32.866	-1.698	0.055	0.062	0.028
12 MEDI	12.607	42.261	-1.754	0.308	0.341	0.892
12 GOPE	21.551	40.905	18.804	0.167	0.182	0.355
12 RIGA	13.292	46.041	-3.849	0.848	1.047	2.014
12 MAR6	12.046	44.973	16.136	0.706	0.985	1.318
12 OSLO	17.110	9.981	-9.650	0.735	0.991	1.362
fixed-interval smoothing results						
96.77549999999999		11				
11 ANKR	2.727	-6.459	-2.278	0.208	0.222	0.644
11 ZWEN	10.914	39.258	6.433	0.249	0.305	0.507
11 TROM	6.870	40.276	-16.745	0.114	0.121	0.051
11 DOUR	16.844	31.908	0.321	0.317	0.364	0.649
11 MADR	20.608	35.013	-37.724	0.126	0.134	0.153
11 SFER	16.678	12.508	-3.425	0.385	0.414	1.708
11 CAGL	15.123	26.842	0.321	0.351	0.372	1.273
11 MATE	17.192	33.181	-1.870	0.056	0.064	0.028
11 MEDI	12.555	42.316	-1.755	0.312	0.345	0.892
11 GOPE	21.695	41.075	18.809	0.165	0.180	0.355
fixed-interval smoothing results						
96.69880000000001		10				
10 ANKR	2.788	-6.379	-2.282	0.207	0.222	0.644
10 ZWEN	10.931	39.242	6.431	0.250	0.306	0.507
10 TROM	6.854	40.283	-16.744	0.117	0.126	0.053
10 DOUR	16.873	31.950	0.320	0.321	0.368	0.649
10 MADR	20.666	34.941	-37.725	0.128	0.136	0.153
10 SFER	16.675	12.509	-3.425	0.391	0.420	1.708
10 CAGL	15.142	26.833	0.320	0.355	0.376	1.273
10 MATE	17.940	33.740	-2.192	0.057	0.065	0.029

```
 10 MEDI       12.513       42.363      -1.757      0.317      0.349      0.892
 10 GOPE       21.840       41.245      18.813      0.164      0.179      0.355
fixed-interval smoothing results
   96.622100000000000                        9
  9 ZWEN       10.946       39.227       6.430      0.252      0.308      0.507
  9 TROM        6.836       40.293     -16.743      0.122      0.132      0.056
  9 DOUR       16.899       31.991       0.319      0.326      0.372      0.650
  9 MADR       20.715       34.878     -37.727      0.132      0.140      0.154
  9 SFER       16.672       12.510      -3.425      0.398      0.426      1.708
  9 CAGL       15.159       26.825       0.319      0.360      0.380      1.274
  9 MATE       19.592       34.555      -2.696      0.059      0.066      0.029
  9 MEDI       12.480       42.404      -1.758      0.323      0.354      0.893
  9 GOPE       21.984       41.411      18.817      0.164      0.180      0.355
  9 ANKR        2.861       -6.276      -2.286      0.208      0.223      0.644
fixed-interval smoothing results
   96.545300000000000                        8
  8 ZWEN       10.957       39.212       6.430      0.254      0.311      0.507
  8 TROM        6.816       40.304     -16.743      0.129      0.140      0.059
  8 DOUR       16.923       32.028       0.317      0.331      0.377      0.650
  8 MADR       20.755       34.823     -37.728      0.137      0.146      0.155
  8 SFER       16.671       12.511      -3.425      0.405      0.433      1.708
  8 CAGL       15.175       26.817       0.318      0.365      0.385      1.274
  8 MATE       22.001       35.543      -3.335      0.061      0.066      0.029
  8 MEDI       12.455       42.436      -1.758      0.329      0.360      0.893
  8 GOPE       22.121       41.570      18.820      0.166      0.182      0.355
  8 ANKR        2.943       -6.157      -2.291      0.209      0.225      0.644
fixed-interval smoothing results
   96.468600000000000                        7
  7 ZWEN       10.964       39.198       6.429      0.258      0.314      0.508
  7 TROM        6.795       40.317     -16.742      0.137      0.149      0.063
  7 DOUR       16.943       32.062       0.316      0.337      0.383      0.651
  7 MADR       20.788       34.774     -37.729      0.144      0.153      0.157
  7 SFER       16.670       12.511      -3.425      0.412      0.439      1.709
  7 CAGL       15.189       26.810       0.317      0.371      0.391      1.274
  7 MEDI       12.437       42.461      -1.759      0.336      0.366      0.894
  7 GOPE       22.249       41.717      18.823      0.170      0.186      0.356
  7 ANKR        3.022       -6.042      -2.295      0.212      0.228      0.644
  7 MATE       24.364       36.479      -3.949      0.059      0.065      0.028
fixed-interval smoothing results
   96.391900000000001                        6
  6 ANKR        3.093       -5.941      -2.299      0.216      0.232      0.644
  6 ZWEN       10.970       39.185       6.429      0.263      0.318      0.508
  6 TROM        6.774       40.330     -16.742      0.146      0.159      0.067
  6 DOUR       16.958       32.089       0.316      0.344      0.389      0.651
  6 MADR       20.815       34.735     -37.730      0.152      0.161      0.158
  6 CAGL       15.200       26.803       0.317      0.378      0.397      1.274
  6 MEDI       12.427       42.478      -1.759      0.343      0.373      0.894
  6 GOPE       22.363       41.846      18.826      0.175      0.191      0.356
  6 MATE       26.043       37.225      -4.418      0.058      0.063      0.027
fixed-interval smoothing results
   96.315200000000000                        5
  5 ANKR        3.156       -5.854      -2.302      0.222      0.238      0.645
  5 ZWEN       10.975       39.173       6.428      0.268      0.323      0.509
  5 TROM        6.754       40.340     -16.742      0.157      0.170      0.072
  5 DOUR       16.967       32.110       0.315      0.351      0.395      0.652
  5 MADR       20.835       34.704     -37.730      0.162      0.170      0.160
  5 CAGL       15.207       26.797       0.316      0.384      0.403      1.275
  5 MEDI       12.420       42.489      -1.760      0.351      0.380      0.895
  5 GOPE       22.459       41.953      18.828      0.182      0.198      0.357
  5 MATE       27.067       37.780      -4.743      0.058      0.063      0.027
fixed-interval smoothing results
   96.238500000000000                        4
  4 ANKR        3.207       -5.784      -2.305      0.229      0.245      0.645
  4 ZWEN       10.983       39.162       6.428      0.275      0.329      0.509
  4 TROM        6.739       40.347     -16.741      0.168      0.182      0.076
  4 DOUR       16.972       32.124       0.314      0.359      0.402      0.652
  4 MADR       20.851       34.682     -37.731      0.173      0.181      0.162
  4 CAGL       15.212       26.794       0.316      0.391      0.410      1.275
  4 MATE       27.463       38.141      -4.925      0.059      0.062      0.027
  4 MEDI       12.417       42.496      -1.760      0.359      0.387      0.895
  4 GOPE       22.536       42.036      18.830      0.191      0.206      0.358
fixed-interval smoothing results
```

96.16180000000000			3				
3 ANKR	3.243	-5.733	-2.307	0.237	0.254	0.646	
3 ZWEN	10.995	39.152	6.427	0.282	0.336	0.510	
3 TROM	6.727	40.352	-16.741	0.181	0.194	0.081	
3 DOUR	16.973	32.131	0.314	0.366	0.409	0.653	
3 MADR	20.862	34.668	-37.731	0.184	0.193	0.164	
3 CAGL	15.213	26.792	0.316	0.399	0.417	1.276	
3 MATE	27.429	38.341	-5.004	0.054	0.061	0.027	
3 MEDI	12.416	42.498	-1.760	0.367	0.395	0.896	
3 GOPE	22.591	42.095	18.831	0.201	0.216	0.359	
fixed-interval smoothing results							
96.08510000000000			2				
2 ANKR	3.265	-5.704	-2.308	0.247	0.263	0.646	
2 ZWEN	11.005	39.145	6.427	0.291	0.343	0.511	
2 TROM	6.721	40.354	-16.741	0.194	0.207	0.086	
2 DOUR	16.973	32.133	0.314	0.374	0.416	0.654	
2 MADR	20.868	34.660	-37.731	0.197	0.205	0.167	
2 CAGL	15.214	26.792	0.316	0.406	0.423	1.276	
2 MATE	27.273	38.449	-5.034	0.055	0.067	0.031	
2 MEDI	12.415	42.499	-1.760	0.375	0.402	0.896	
2 GOPE	22.626	42.131	18.832	0.212	0.226	0.360	
fixed-interval smoothing results							
96.00839999999999			1				
1 ANKR	3.272	-5.695	-2.309	0.258	0.273	0.647	
1 ZWEN	11.008	39.143	6.426	0.300	0.351	0.512	
1 TROM	6.719	40.355	-16.741	0.208	0.220	0.091	
1 MADR	20.870	34.657	-37.731	0.211	0.218	0.169	
1 MATE	27.192	38.490	-5.040	0.079	0.091	0.040	
1 GOPE	22.637	42.143	18.832	0.225	0.238	0.361	
GROUP THREE							
fixed-interval smoothing results							
98.07680000000001			28				
28 THU1	4.233	-96.033	-2.102	0.381	0.653	0.227	
28 KELY	16.393	-33.415	11.529	0.993	1.310	1.324	
28 HOFN	19.062	16.377	-3.325	4.330	7.956	5.611	
28 VIL0	13.468	48.950	13.611	0.678	1.105	1.037	
28 KIR0	11.669	71.178	6.724	0.772	1.430	1.038	
28 JOEN	9.188	60.379	15.066	0.876	1.262	1.694	
28 METS	11.135	37.912	0.152	0.104	0.141	0.047	
28 VIS0	14.257	45.720	4.068	0.705	0.916	1.555	
28 LAMA	17.322	42.792	20.005	0.294	0.316	0.359	
28 BOR1	14.958	41.879	8.711	0.297	0.313	0.363	
28 PENC	13.805	39.383	11.038	0.350	0.379	0.862	
28 VENE	12.025	35.467	11.833	0.694	0.872	1.928	
28 OBER	15.187	33.451	4.736	0.742	0.832	2.059	
28 PFAN	14.460	34.314	8.858	1.181	1.315	3.339	
28 TOUL	17.469	24.944	11.600	1.875	1.899	5.519	
28 DENT	16.825	30.334	-5.862	0.395	0.452	0.709	
28 WSRT	13.398	37.888	-9.481	2.879	3.373	6.086	
fixed-interval smoothing results							
98.00010000000000			27				
27 THU1	4.250	-96.033	-2.106	0.374	0.649	0.225	
27 KELY	16.396	-33.415	11.528	0.990	1.307	1.324	
27 HOFN	19.061	16.377	-3.325	4.329	7.956	5.611	
27 VIL0	13.468	48.950	13.612	0.674	1.102	1.037	
27 KIR0	11.668	71.179	6.724	0.769	1.428	1.038	
27 JOEN	9.188	60.380	15.066	0.873	1.260	1.694	
27 METS	11.089	37.901	0.173	0.084	0.123	0.040	
27 VIS0	14.257	45.719	4.069	0.701	0.913	1.555	
27 LAMA	17.319	42.794	20.005	0.284	0.307	0.357	
27 BOR1	14.956	41.881	8.711	0.287	0.304	0.362	
27 PENC	13.804	39.385	11.038	0.342	0.371	0.862	
27 VENE	12.024	35.468	11.833	0.690	0.869	1.928	
27 OBER	15.187	33.450	4.736	0.738	0.829	2.059	
27 PFAN	14.460	34.314	8.858	1.178	1.313	3.339	
27 TOUL	17.468	24.944	11.600	1.874	1.898	5.519	
27 DENT	16.826	30.334	-5.862	0.387	0.446	0.708	
27 WSRT	13.398	37.888	-9.481	2.879	3.372	6.086	
fixed-interval smoothing results							
97.92340000000000			26				
26 THU1	4.309	-96.031	-2.119	0.366	0.644	0.223	
26 KELY	16.405	-33.415	11.527	0.987	1.305	1.323	

```
 26 HOFN        19.059        16.378        -3.325         4.329         7.956         5.611
 26 VIL0        13.469        48.950        13.612         0.671         1.100         1.036
 26 KIR0        11.668        71.180         6.724         0.765         1.426         1.038
 26 JOEN         9.185        60.381        15.066         0.870         1.258         1.694
 26 METS        11.021        37.882         0.205         0.072         0.107         0.034
 26 VIS0        14.256        45.717         4.069         0.698         0.910         1.555
 26 LAMA        17.313        42.800        20.006         0.275         0.298         0.356
 26 BOR1        14.952        41.887         8.712         0.277         0.295         0.361
 26 PENC        13.801        39.390        11.038         0.334         0.364         0.861
 26 VENE        12.021        35.471        11.833         0.686         0.866         1.928
 26 OBER        15.188        33.449         4.736         0.735         0.826         2.059
 26 PFAN        14.459        34.315         8.858         1.177         1.311         3.339
 26 TOUL        17.467        24.946        11.600         1.873         1.897         5.519
 26 DENT        16.828        30.334        -5.862         0.380         0.439         0.707
 26 WSRT        13.397        37.888        -9.481         2.879         3.372         6.086
fixed-interval smoothing results
   97.84670000000000                    25
 25 KELY        16.417       -33.416        11.526         0.985         1.303         1.323
 25 HOFN        19.058        16.378        -3.324         4.330         7.956         5.611
 25 VIL0        13.469        48.950        13.612         0.668         1.098         1.036
 25 KIR0        11.667        71.182         6.724         0.763         1.425         1.037
 25 JOEN         9.176        60.383        15.067         0.868         1.256         1.693
 25 METS        10.982        37.857         0.226         0.066         0.095         0.030
 25 VIS0        14.254        45.715         4.070         0.695         0.908         1.554
 25 LAMA        17.301        42.811        20.008         0.265         0.288         0.355
 25 BOR1        14.945        41.898         8.713         0.268         0.285         0.359
 25 PENC        13.795        39.398        11.039         0.326         0.357         0.861
 25 VENE        12.016        35.476        11.833         0.683         0.864         1.928
 25 OBER        15.189        33.447         4.736         0.733         0.823         2.059
 25 PFAN        14.458        34.316         8.858         1.175         1.310         3.339
 25 DENT        16.831        30.335        -5.862         0.373         0.433         0.707
 25 WSRT        13.397        37.887        -9.481         2.879         3.372         6.086
 25 THU1         4.435       -96.028        -2.149         0.359         0.640         0.221
 25 TOUL        17.465        24.948        11.600         1.873         1.897         5.519
fixed-interval smoothing results
   97.77000000000000                    24
 24 THU1         4.634       -96.022        -2.195         0.352         0.635         0.219
 24 KELY        16.429       -33.417        11.524         0.983         1.302         1.323
 24 HOFN        19.058        16.378        -3.324         4.330         7.957         5.611
 24 VIL0        13.468        48.949        13.613         0.665         1.097         1.036
 24 KIR0        11.662        71.185         6.725         0.761         1.424         1.037
 24 JOEN         9.162        60.386        15.069         0.866         1.255         1.693
 24 METS        10.976        37.830         0.230         0.063         0.087         0.029
 24 VIS0        14.251        45.713         4.070         0.692         0.906         1.554
 24 LAMA        17.282        42.828        20.011         0.255         0.279         0.354
 24 BOR1        14.935        41.915         8.715         0.258         0.276         0.358
 24 PENC        13.787        39.411        11.039         0.319         0.350         0.860
 24 VENE        12.010        35.482        11.833         0.680         0.862         1.927
 24 OBER        15.190        33.446         4.736         0.731         0.822         2.059
 24 PFAN        14.458        34.317         8.858         1.175         1.309         3.339
 24 TOUL        17.462        24.949        11.600         1.874         1.897         5.519
 24 DENT        16.836        30.336        -5.862         0.367         0.428         0.706
 24 WSRT        13.397        37.886        -9.481         2.879         3.373         6.086
fixed-interval smoothing results
   97.69329999999999                    23
 23 KELY        16.441       -33.419        11.522         0.981         1.300         1.322
 23 VIL0        13.465        48.948        13.614         0.664         1.095         1.036
 23 KIR0        11.653        71.189         6.726         0.759         1.423         1.037
 23 JOEN         9.144        60.389        15.071         0.865         1.254         1.693
 23 METS        10.941        37.796         0.233         0.063         0.082         0.028
 23 VIS0        14.247        45.712         4.071         0.691         0.905         1.554
 23 LAMA        17.255        42.852        20.016         0.246         0.271         0.352
 23 BOR1        14.922        41.941         8.716         0.249         0.267         0.357
 23 PENC        13.778        39.428        11.039         0.313         0.344         0.860
 23 OBER        15.192        33.446         4.736         0.729         0.821         2.059
 23 PFAN        14.457        34.318         8.858         1.175         1.310         3.339
 23 TOUL        17.460        24.949        11.600         1.874         1.898         5.519
 23 DENT        16.842        30.337        -5.862         0.361         0.423         0.706
 23 WSRT        13.397        37.886        -9.481         2.880         3.373         6.086
 23 THU1         4.908       -96.015        -2.259         0.345         0.631         0.217
 23 VENE        12.004        35.489        11.833         0.678         0.860         1.927
fixed-interval smoothing results
```

```
  97.61660000000001                    22
 22 THU1        5.258      -96.006        -2.340    0.339    0.627    0.215
 22 KELY       16.456      -33.420        11.520    0.979    1.299    1.322
 22 VIL0       13.462       48.948        13.615    0.663    1.095    1.036
 22 KIR0       11.641       71.195         6.727    0.758    1.422    1.037
 22 JOEN        9.125       60.391        15.073    0.864    1.253    1.693
 22 METS       10.898       37.760         0.234    0.061    0.079    0.027
 22 VIS0       14.242       45.711         4.072    0.690    0.904    1.554
 22 LAMA       17.220       42.883        20.021    0.237    0.262    0.351
 22 BOR1       14.906       41.975         8.718    0.239    0.258    0.356
 22 PENC       13.767       39.449        11.040    0.307    0.339    0.859
 22 VENE       11.999       35.496        11.832    0.677    0.859    1.927
 22 OBER       15.195       33.447         4.736    0.729    0.820    2.059
 22 PFAN       14.457       34.319         8.858    1.175    1.310    3.339
 22 TOUL       17.459       24.949        11.600    1.876    1.899    5.519
 22 DENT       16.850       30.339        -5.863    0.356    0.418    0.705
fixed-interval smoothing results
  97.53990000000000                    21
 21 THU1        5.680      -95.995        -2.438    0.333    0.623    0.214
 21 KELY       16.473      -33.422        11.518    0.978    1.298    1.322
 21 VIL0       13.459       48.946        13.615    0.662    1.095    1.036
 21 KIR0       11.625       71.200         6.729    0.758    1.422    1.037
 21 JOEN        9.108       60.393        15.075    0.864    1.253    1.693
 21 METS       10.827       37.709         0.249    0.059    0.077    0.026
 21 VIS0       14.237       45.709         4.073    0.689    0.904    1.554
 21 LAMA       17.178       42.921        20.027    0.229    0.254    0.350
 21 BOR1       14.888       42.018         8.720    0.231    0.250    0.355
 21 PENC       13.756       39.475        11.040    0.302    0.334    0.859
 21 VENE       11.996       35.503        11.832    0.676    0.859    1.927
 21 OBER       15.197       33.447         4.736    0.729    0.820    2.059
 21 PFAN       14.456       34.319         8.858    1.177    1.311    3.339
 21 TOUL       17.458       24.949        11.600    1.877    1.900    5.519
 21 DENT       16.859       30.341        -5.863    0.351    0.414    0.705
fixed-interval smoothing results
  97.46320000000000                    20
 20 THU1        6.174      -95.982        -2.554    0.328    0.619    0.212
 20 KELY       16.492      -33.423        11.515    0.977    1.297    1.322
 20 VIL0       13.455       48.944        13.616    0.663    1.095    1.036
 20 KIR0       11.608       71.207         6.731    0.758    1.422    1.037
 20 JOEN        9.093       60.395        15.076    0.864    1.254    1.693
 20 METS       10.839       37.649         0.239    0.057    0.075    0.026
 20 VIS0       14.231       45.708         4.074    0.690    0.904    1.554
 20 LAMA       17.128       42.965        20.035    0.221    0.246    0.349
 20 BOR1       14.866       42.070         8.722    0.222    0.241    0.354
 20 PENC       13.744       39.505        11.040    0.297    0.331    0.859
 20 VENE       11.994       35.509        11.831    0.676    0.859    1.927
 20 OBER       15.199       33.448         4.736    0.730    0.821    2.059
 20 PFAN       14.456       34.319         8.858    1.178    1.313    3.339
 20 DENT       16.870       30.345        -5.863    0.347    0.411    0.705
fixed-interval smoothing results
  97.38639999999999                    19
 19 THU1        6.726      -95.968        -2.683    0.324    0.616    0.211
 19 KELY       16.514      -33.424        11.512    0.976    1.296    1.322
 19 VIL0       13.452       48.942        13.616    0.664    1.095    1.036
 19 KIR0       11.591       71.213         6.733    0.759    1.423    1.037
 19 JOEN        9.079       60.396        15.077    0.865    1.254    1.693
 19 METS       10.930       37.584         0.208    0.056    0.074    0.025
 19 VIS0       14.226       45.707         4.074    0.691    0.905    1.554
 19 LAMA       17.073       43.017        20.043    0.213    0.239    0.349
 19 BOR1       14.841       42.131         8.725    0.214    0.234    0.353
 19 PENC       13.732       39.540        11.041    0.294    0.328    0.859
 19 VENE       11.994       35.513        11.830    0.677    0.860    1.927
 19 OBER       15.200       33.448         4.736    0.732    0.823    2.059
 19 PFAN       14.456       34.318         8.858    1.180    1.315    3.339
 19 DENT       16.883       30.350        -5.864    0.343    0.408    0.704
fixed-interval smoothing results
  97.30970000000001                    18
 18 THU1        7.301      -95.954        -2.817    0.320    0.613    0.209
 18 KELY       16.539      -33.424        11.508    0.976    1.296    1.322
 18 VIL0       13.449       48.939        13.617    0.665    1.096    1.036
 18 KIR0       11.575       71.219         6.735    0.761    1.423    1.037
 18 JOEN        9.069       60.396        15.078    0.867    1.255    1.693
```

```
 18 METS      10.992      37.521       0.197      0.056      0.072      0.025
 18 VIS0      14.222      45.705       4.075      0.692      0.906      1.554
 18 LAMA      17.013      43.074      20.052      0.207      0.232      0.348
 18 BOR1      14.814      42.200       8.727      0.207      0.226      0.352
 18 PENC      13.720      39.579      11.041      0.292      0.325      0.859
 18 VENE      11.996      35.516      11.830      0.678      0.862      1.927
 18 OBER      15.202      33.449       4.736      0.734      0.825      2.059
 18 PFAN      14.456      34.318       8.858      1.183      1.317      3.340
 18 DENT      16.897      30.356      -5.865      0.341      0.406      0.704
fixed-interval smoothing results
   97.23300000000000                      17
 17 KELY      16.569     -33.422      11.504      0.975      1.295      1.322
 17 VIL0      13.447      48.935      13.617      0.668      1.098      1.036
 17 KIR0      11.561      71.224       6.736      0.763      1.424      1.037
 17 JOEN       9.063      60.395      15.078      0.869      1.256      1.694
 17 METS      11.019      37.488       0.195      0.055      0.071      0.024
 17 VIS0      14.219      45.703       4.076      0.694      0.908      1.554
 17 LAMA      16.948      43.135      20.063      0.200      0.226      0.347
 17 BOR1      14.785      42.280       8.730      0.200      0.220      0.351
 17 PENC      13.710      39.622      11.041      0.290      0.324      0.859
 17 VENE      12.001      35.517      11.829      0.680      0.864      1.927
 17 OBER      15.202      33.449       4.736      0.737      0.827      2.059
 17 DENT      16.912      30.365      -5.866      0.339      0.404      0.704
 17 THU1       7.881     -95.940      -2.953      0.316      0.611      0.208
fixed-interval smoothing results
   97.15630000000000                      16
 16 KELY      16.602     -33.418      11.500      0.976      1.296      1.322
 16 VIL0      13.447      48.932      13.617      0.670      1.099      1.037
 16 KIR0      11.552      71.227       6.737      0.765      1.426      1.038
 16 JOEN       9.060      60.394      15.079      0.871      1.258      1.694
 16 METS      10.947      37.491       0.225      0.054      0.070      0.024
 16 VIS0      14.216      45.702       4.076      0.697      0.910      1.555
 16 LAMA      16.879      43.201      20.074      0.195      0.220      0.346
 16 BOR1      14.755      42.369       8.732      0.194      0.214      0.351
 16 PENC      13.699      39.669      11.042      0.290      0.324      0.859
 16 VENE      12.007      35.516      11.828      0.683      0.866      1.927
 16 OBER      15.203      33.449       4.736      0.740      0.830      2.059
 16 DENT      16.929      30.376      -5.866      0.338      0.404      0.704
 16 THU1       8.461     -95.927      -3.089      0.312      0.608      0.207
fixed-interval smoothing results
   97.07960000000000                      15
 15 THU1       9.041     -95.913      -3.225      0.310      0.606      0.206
 15 KELY      16.642     -33.413      11.495      0.976      1.296      1.322
 15 VIL0      13.447      48.928      13.617      0.674      1.101      1.037
 15 KIR0      11.545      71.230       6.738      0.768      1.427      1.038
 15 JOEN       9.060      60.392      15.078      0.873      1.260      1.694
 15 METS      10.968      37.566       0.240      0.054      0.070      0.024
 15 VIS0      14.215      45.700       4.076      0.700      0.912      1.555
 15 LAMA      16.807      43.271      20.086      0.190      0.215      0.346
 15 BOR1      14.725      42.468       8.735      0.189      0.208      0.350
 15 PENC      13.689      39.720      11.042      0.291      0.325      0.859
 15 VENE      12.014      35.515      11.828      0.686      0.869      1.928
 15 OBER      15.203      33.449       4.736      0.744      0.834      2.060
 15 DENT      16.948      30.388      -5.867      0.337      0.403      0.704
fixed-interval smoothing results
   97.00290000000000                      14
 14 THU1       9.625     -95.900      -3.361      0.307      0.605      0.206
 14 KELY      16.686     -33.406      11.490      0.977      1.297      1.322
 14 VIL0      13.448      48.925      13.617      0.677      1.104      1.037
 14 JOEN       9.062      60.390      15.078      0.876      1.262      1.694
 14 METS      11.057      37.752       0.261      0.053      0.069      0.024
 14 VIS0      14.214      45.698       4.077      0.704      0.915      1.555
 14 LAMA      16.731      43.344      20.098      0.185      0.211      0.345
 14 BOR1      14.694      42.576       8.737      0.184      0.203      0.350
 14 PENC      13.679      39.773      11.042      0.292      0.326      0.859
 14 VENE      12.022      35.513      11.827      0.690      0.872      1.928
 14 OBER      15.203      33.449       4.736      0.744      0.834      2.060
 14 DENT      16.968      30.403      -5.869      0.338      0.404      0.704
 14 KIR0      11.541      71.231       6.738      0.772      1.429      1.038
fixed-interval smoothing results
   96.92890000000000                      13
 13 THU1      10.155     -95.888      -3.485      0.306      0.604      0.205
 13 KELY      16.727     -33.399      11.485      0.978      1.297      1.322
```

```
 13 VIL0        13.449        48.923        13.617    0.681    1.106    1.038
 13 KIR0        11.539        71.232         6.738    0.775    1.431    1.039
 13 JOEN         9.063        60.389        15.078    0.879    1.264    1.695
 13 METS        11.049        38.084         0.347    0.053    0.069    0.024
 13 VIS0        14.213        45.698         4.077    0.707    0.917    1.555
 13 LAMA        16.658        43.416        20.111    0.182    0.208    0.345
 13 BOR1        14.666        42.684         8.739    0.180    0.200    0.349
 13 PENC        13.669        39.823        11.042    0.295    0.328    0.859
 13 VENE        12.028        35.511        11.827    0.693    0.875    1.928
 13 DENT        16.988        30.417        -5.870    0.339    0.405    0.704
fixed-interval smoothing results
   96.852200000000000                  12
 12 THU1        10.720       -95.875        -3.617    0.304    0.604    0.205
 12 KELY        16.768       -33.391        11.480    0.980    1.298    1.322
 12 VIL0        13.449        48.922        13.617    0.685    1.109    1.038
 12 KIR0        11.538        71.232         6.738    0.779    1.433    1.039
 12 JOEN         9.064        60.389        15.078    0.883    1.266    1.695
 12 METS        11.036        38.746         0.464    0.053    0.069    0.023
 12 VIS0        14.213        45.697         4.077    0.711    0.920    1.556
 12 LAMA        16.576        43.500        20.125    0.179    0.205    0.345
 12 BOR1        14.637        42.805         8.742    0.177    0.197    0.349
 12 PENC        13.658        39.876        11.043    0.298    0.332    0.859
 12 VENE        12.032        35.511        11.826    0.697    0.878    1.928
 12 DENT        17.010        30.433        -5.871    0.341    0.407    0.704
fixed-interval smoothing results
   96.775499999999990                  11
 11 THU1        11.339       -95.861        -3.761    0.304    0.603    0.205
 11 KELY        16.802       -33.384        11.476    0.981    1.300    1.323
 11 METS        11.167        39.828         0.558    0.053    0.068    0.024
 11 LAMA        16.494        43.590        20.139    0.178    0.204    0.345
 11 BOR1        14.610        42.930         8.744    0.175    0.195    0.349
 11 PENC        13.648        39.926        11.043    0.303    0.336    0.860
 11 VENE        12.035        35.510        11.826    0.701    0.881    1.928
 11 DENT        17.032        30.449        -5.872    0.344    0.409    0.704
fixed-interval smoothing results
   96.698800000000010                  10
 10 THU1        12.029       -95.843        -3.921    0.304    0.604    0.205
 10 KELY        16.829       -33.379        11.473    0.983    1.301    1.323
 10 METS        11.620        41.373         0.588    0.053    0.068    0.023
 10 LAMA        16.412        43.684        20.153    0.177    0.204    0.345
 10 BOR1        14.583        43.056         8.746    0.174    0.194    0.349
 10 PENC        13.638        39.971        11.043    0.308    0.341    0.860
 10 VENE        12.035        35.510        11.826    0.705    0.885    1.929
 10 DENT        17.052        30.464        -5.874    0.347    0.412    0.704
fixed-interval smoothing results
   96.622100000000000                   9
  9 THU1        12.784       -95.823        -4.096    0.304    0.605    0.205
  9 KELY        16.852       -33.376        11.470    0.985    1.303    1.323
  9 METS        12.632        43.418         0.459    0.052    0.068    0.023
  9 LAMA        16.332        43.778        20.166    0.178    0.205    0.345
  9 BOR1        14.555        43.179         8.747    0.174    0.195    0.349
  9 PENC        13.629        40.009        11.044    0.315    0.347    0.860
  9 DENT        17.072        30.477        -5.875    0.351    0.416    0.704
fixed-interval smoothing results
   96.545300000000000                   8
  8 THU1        13.582       -95.801        -4.280    0.305    0.606    0.206
  8 KELY        16.871       -33.375        11.468    0.988    1.304    1.323
  8 METS        14.405        45.932         0.088    0.053    0.068    0.023
  8 LAMA        16.255        43.871        20.179    0.180    0.207    0.345
  8 BOR1        14.526        43.298         8.749    0.176    0.197    0.349
  8 PENC        13.620        40.038        11.045    0.322    0.353    0.861
  8 DENT        17.090        30.488        -5.876    0.356    0.421    0.705
fixed-interval smoothing results
   96.468600000000000                   7
  7 THU1        14.380       -95.778        -4.464    0.308    0.608    0.207
  7 KELY        16.887       -33.374        11.466    0.990    1.306    1.324
  7 METS        16.270        48.551        -0.308    0.053    0.068    0.024
  7 LAMA        16.184        43.957        20.190    0.184    0.211    0.346
  7 BOR1        14.498        43.409         8.751    0.180    0.200    0.350
  7 PENC        13.613        40.060        11.045    0.329    0.360    0.861
  7 DENT        17.107        30.497        -5.878    0.362    0.425    0.705
fixed-interval smoothing results
```

```
   96.39190000000001                          6
  6 THU1       15.130      -95.757      -4.637      0.311      0.610      0.207
  6 KELY       16.895      -33.375      11.464      0.993      1.308      1.324
  6 METS       17.408       50.793      -0.469      0.052      0.066      0.023
  6 LAMA       16.119       44.035      20.200      0.189      0.215      0.346
  6 BOR1       14.471       43.507       8.752      0.184      0.205      0.350
  6 PENC       13.608       40.074      11.045      0.337      0.367      0.862
  6 DENT       17.120       30.503      -5.879      0.368      0.431      0.706
fixed-interval smoothing results
   96.31520000000000                          5
  5 THU1       15.778      -95.739      -4.786      0.315      0.613      0.209
  5 KELY       16.896      -33.376      11.464      0.995      1.310      1.324
  5 METS       17.927       52.456      -0.431      0.052      0.064      0.023
  5 LAMA       16.064       44.103      20.209      0.196      0.222      0.347
  5 BOR1       14.447       43.590       8.754      0.191      0.212      0.351
  5 PENC       13.605       40.081      11.045      0.345      0.375      0.862
  5 DENT       17.128       30.507      -5.879      0.375      0.436      0.706
fixed-interval smoothing results
   96.23850000000000                          4
  4 THU1       16.295      -95.724      -4.905      0.320      0.616      0.210
  4 KELY       16.895      -33.377      11.464      0.998      1.313      1.325
  4 METS       18.034       53.550      -0.249      0.051      0.061      0.022
  4 BOR1       14.428       43.656       8.755      0.199      0.219      0.352
  4 PENC       13.604       40.083      11.045      0.353      0.382      0.863
  4 DENT       17.133       30.510      -5.880      0.382      0.442      0.707
  4 LAMA       16.020       44.157      20.216      0.204      0.229      0.348
fixed-interval smoothing results
   96.16180000000000                          3
  3 THU1       16.659      -95.714      -4.989      0.326      0.619      0.212
  3 KELY       16.893      -33.377      11.464      1.001      1.315      1.325
  3 METS       18.010       54.194      -0.039      0.048      0.061      0.021
  3 BOR1       14.413       43.704       8.755      0.208      0.228      0.353
  3 DENT       17.135       30.511      -5.880      0.389      0.449      0.708
  3 LAMA       15.988       44.197      20.221      0.213      0.238      0.349
fixed-interval smoothing results
   96.08510000000000                          2
  2 THU1       16.872      -95.708      -5.038      0.333      0.624      0.213
  2 KELY       16.892      -33.377      11.464      1.004      1.317      1.325
  2 METS       18.143       54.565       0.054      0.050      0.072      0.023
  2 LAMA       15.969       44.220      20.224      0.224      0.248      0.350
  2 BOR1       14.405       43.733       8.756      0.219      0.238      0.354
  2 DENT       17.135       30.511      -5.880      0.396      0.455      0.708
 fixed-interval smoothing results
   96.00839999999999                          1
  1 THU1       16.942      -95.705      -5.054      0.341      0.628      0.216
  1 METS       18.240       54.696       0.067      0.075      0.096      0.033
  1 LAMA       15.963       44.228      20.225      0.236      0.259      0.351
  1 BOR1       14.402       43.743       8.756      0.232      0.250      0.355
                                       GROUP FOUR
fixed-interval smoothing results
   98.07680000000001                         28
 28 KIRU       11.797       56.539      15.133      0.346      0.469      0.369
 28 SVTL       10.701       52.778      12.858      1.213      2.195      2.287
 28 BOGO       13.793       36.753      10.259      0.428      0.508      1.005
 28 KOSG       15.404       30.278      -0.631      0.111      0.134      0.090
 28 DELF       17.968       30.824       1.752      0.356      0.408      0.612
 28 WARE       16.278       31.673       3.201      0.403      0.452      0.753
 28 POTS       16.282       35.478       2.433      0.297      0.312      0.411
 28 WROC       14.997       34.229       3.407      0.658      0.757      1.815
 28 MOPI       14.392       32.850       0.402      0.558      0.623      1.640
 28 UPAD       20.531       39.706      20.404      0.223      0.226      0.237
 28 BRUS       16.969       30.526       1.929      0.112      0.133      0.092
 28 GRAS       -5.661       17.121       6.529      0.297      0.295      0.478
 28 HFLK       24.657       40.056      14.603      0.270      0.276      0.388
 28 WETT       27.157       59.420      -4.032      0.101      0.101      0.100
fixed-interval smoothing results
   98.00010000000000                         27
 27 KIRU       11.800       56.540      15.132      0.337      0.462      0.361
 27 SVTL       10.699       52.778      12.860      1.211      2.194      2.286
 27 BOGO       13.791       36.752      10.260      0.422      0.502      1.002
 27 KOSG       15.444       30.287      -0.692      0.091      0.115      0.071
 27 DELF       17.970       30.825       1.752      0.348      0.401      0.607
```

27 WARE	16.280	31.673	3.201	0.396	0.446	0.749
27 POTS	16.282	35.478	2.433	0.287	0.303	0.403
27 WROC	14.996	34.229	3.407	0.654	0.754	1.814
27 MOPI	14.393	32.851	0.401	0.553	0.619	1.638
27 BRUS	16.975	30.531	1.910	0.092	0.113	0.072
27 GRAS	-5.668	17.121	6.530	0.287	0.285	0.472
27 UPAD	20.531	39.709	20.405	0.209	0.212	0.224
27 HFLK	24.661	40.062	14.604	0.259	0.265	0.381
27 WETT	27.157	59.420	-4.032	0.081	0.081	0.080
fixed-interval smoothing results						
97.92340000000000			26			
26 KIRU	11.808	56.543	15.127	0.329	0.456	0.354
26 SVTL	10.694	52.779	12.863	1.209	2.193	2.285
26 BOGO	13.786	36.751	10.264	0.415	0.497	0.999
26 KOSG	15.508	30.296	-0.794	0.078	0.099	0.062
26 DELF	17.974	30.827	1.752	0.340	0.395	0.603
26 WARE	16.285	31.673	3.202	0.389	0.439	0.745
26 POTS	16.283	35.480	2.433	0.277	0.293	0.396
26 WROC	14.996	34.228	3.408	0.650	0.750	1.813
26 MOPI	14.394	32.852	0.400	0.548	0.615	1.637
26 UPAD	20.531	39.714	20.408	0.196	0.199	0.211
26 BRUS	16.957	30.541	1.914	0.078	0.097	0.063
26 GRAS	-5.685	17.119	6.532	0.277	0.275	0.466
26 HFLK	24.669	40.072	14.606	0.248	0.254	0.373
26 WETT	27.157	59.420	-4.032	0.070	0.070	0.069
fixed-interval smoothing results						
97.84670000000000			25			
25 KIRU	11.818	56.549	15.120	0.320	0.450	0.346
25 SVTL	10.687	52.780	12.869	1.207	2.192	2.284
25 BOGO	13.778	36.751	10.269	0.409	0.492	0.997
25 KOSG	15.546	30.303	-0.852	0.070	0.087	0.058
25 DELF	17.984	30.832	1.753	0.333	0.388	0.598
25 WARE	16.292	31.673	3.202	0.383	0.433	0.741
25 POTS	16.285	35.484	2.432	0.267	0.284	0.389
25 WROC	14.994	34.227	3.411	0.647	0.748	1.811
25 MOPI	14.394	32.855	0.399	0.544	0.611	1.636
25 UPAD	20.533	39.718	20.411	0.183	0.186	0.198
25 BRUS	16.923	30.553	1.934	0.070	0.086	0.058
25 GRAS	-5.715	17.115	6.538	0.268	0.265	0.460
25 HFLK	24.683	40.088	14.609	0.237	0.244	0.366
25 WETT	27.157	59.420	-4.032	0.066	0.066	0.065
fixed-interval smoothing results						
97.77000000000000			24			
24 KIRU	11.830	56.556	15.110	0.312	0.445	0.339
24 SVTL	10.676	52.781	12.876	1.206	2.191	2.284
24 BOGO	13.766	36.752	10.277	0.404	0.488	0.995
24 KOSG	15.546	30.311	-0.835	0.066	0.080	0.056
24 DELF	17.998	30.839	1.753	0.326	0.382	0.595
24 WARE	16.302	31.675	3.203	0.376	0.428	0.738
24 POTS	16.289	35.491	2.430	0.257	0.274	0.382
24 WROC	14.991	34.225	3.414	0.644	0.745	1.811
24 MOPI	14.394	32.860	0.396	0.541	0.608	1.634
24 UPAD	20.538	39.724	20.413	0.171	0.174	0.186
24 BRUS	16.913	30.564	1.919	0.066	0.079	0.057
24 GRAS	-5.759	17.110	6.546	0.258	0.256	0.454
24 HFLK	24.708	40.110	14.611	0.227	0.234	0.359
24 WETT	27.157	59.420	-4.032	0.065	0.065	0.065
fixed-interval smoothing results						
97.69329999999999			23			
23 KIRU	11.843	56.566	15.097	0.305	0.439	0.332
23 SVTL	10.663	52.783	12.885	1.205	2.191	2.283
23 BOGO	13.751	36.754	10.285	0.400	0.484	0.993
23 KOSG	15.538	30.321	-0.780	0.065	0.077	0.056
23 DELF	18.018	30.848	1.752	0.320	0.377	0.591
23 WARE	16.315	31.677	3.204	0.370	0.423	0.735
23 POTS	16.294	35.501	2.425	0.248	0.265	0.375
23 WROC	14.988	34.223	3.418	0.643	0.744	1.810
23 MOPI	14.393	32.866	0.393	0.539	0.606	1.634
23 UPAD	20.546	39.733	20.417	0.159	0.163	0.174
23 BRUS	16.938	30.569	1.849	0.066	0.076	0.057
23 GRAS	-5.818	17.103	6.558	0.248	0.246	0.449
23 HFLK	24.747	40.144	14.612	0.217	0.224	0.352

```
 23 WETT      27.157       59.420      -4.032      0.065      0.066      0.065
fixed-interval smoothing results
   97.61660000000001                      22
 22 KIRU      11.857       56.578      15.081      0.298      0.434      0.325
 22 SVTL      10.650       52.785      12.893      1.205      2.190      2.283
 22 BOGO      13.732       36.756      10.295      0.397      0.481      0.992
 22 KOSG      15.559       30.324      -0.758      0.064      0.075      0.054
 22 DELF      18.043       30.860       1.751      0.314      0.372      0.588
 22 WARE      16.329       31.680       3.205      0.365      0.418      0.732
 22 POTS      16.303       35.515       2.417      0.238      0.256      0.369
 22 WROC      14.984       34.220       3.423      0.642      0.743      1.810
 22 MOPI      14.392       32.874       0.389      0.537      0.605      1.633
 22 UPAD      20.559       39.744      20.421      0.149      0.153      0.163
 22 BRUS      16.931       30.547       1.848      0.064      0.075      0.055
 22 GRAS      -5.889       17.096       6.573      0.239      0.237      0.443
 22 HFLK      24.801       40.190      14.614      0.208      0.215      0.346
 22 WETT      27.157       59.420      -4.032      0.066      0.066      0.065
fixed-interval smoothing results
   97.53990000000000                      21
 21 KIRU      11.869       56.593      15.065      0.291      0.429      0.319
 21 SVTL      10.637       52.787      12.901      1.205      2.190      2.283
 21 BOGO      13.710       36.759      10.305      0.394      0.479      0.991
 21 KOSG      15.611       30.322      -0.818      0.062      0.073      0.052
 21 DELF      18.072       30.874       1.750      0.310      0.368      0.585
 21 WARE      16.345       31.684       3.206      0.361      0.414      0.730
 21 POTS      16.315       35.531       2.406      0.229      0.247      0.362
 21 WROC      14.980       34.217       3.427      0.642      0.743      1.810
 21 MOPI      14.391       32.881       0.383      0.536      0.604      1.633
 21 UPAD      20.579       39.759      20.427      0.141      0.143      0.153
 21 BRUS      16.891       30.494       1.940      0.062      0.073      0.053
 21 GRAS      -5.971       17.091       6.591      0.230      0.228      0.438
 21 HFLK      24.873       40.249      14.615      0.199      0.206      0.340
 21 WETT      27.157       59.420      -4.032      0.066      0.066      0.065
fixed-interval smoothing results
   97.46320000000000                      20
 20 KIRU      11.879       56.610      15.049      0.284      0.424      0.313
 20 SVTL      10.625       52.789      12.909      1.205      2.190      2.283
 20 BOGO      13.686       36.762      10.316      0.392      0.477      0.990
 20 KOSG      15.587       30.325      -0.808      0.061      0.072      0.051
 20 DELF      18.105       30.891       1.749      0.306      0.365      0.583
 20 WARE      16.363       31.689       3.207      0.357      0.411      0.728
 20 POTS      16.331       35.552       2.390      0.220      0.238      0.356
 20 WROC      14.976       34.213       3.432      0.642      0.743      1.810
 20 MOPI      14.391       32.889       0.376      0.536      0.604      1.633
 20 UPAD      20.606       39.777      20.433      0.133      0.136      0.143
 20 BRUS      16.916       30.433       1.934      0.061      0.071      0.052
 20 GRAS      -6.063       17.090       6.614      0.221      0.219      0.433
 20 HFLK      24.965       40.324      14.616      0.191      0.198      0.334
 20 WETT      27.157       59.420      -4.032      0.066      0.067      0.065
fixed-interval smoothing results
   97.38639999999999                      19
 19 KIRU      11.884       56.630      15.035      0.278      0.420      0.308
 19 SVTL      10.615       52.791      12.915      1.205      2.191      2.284
 19 BOGO      13.661       36.764      10.328      0.391      0.477      0.990
 19 KOSG      15.495       30.332      -0.735      0.060      0.070      0.050
 19 DELF      18.140       30.910       1.748      0.303      0.363      0.581
 19 WARE      16.382       31.694       3.208      0.353      0.408      0.726
 19 POTS      16.353       35.576       2.369      0.212      0.230      0.350
 19 WROC      14.973       34.210       3.436      0.644      0.745      1.811
 19 MOPI      14.390       32.896       0.368      0.538      0.605      1.633
 19 UPAD      20.642       39.799      20.441      0.126      0.129      0.135
 19 BRUS      17.002       30.377       1.831      0.060      0.070      0.051
 19 GRAS      -6.161       17.097       6.639      0.213      0.211      0.428
 19 HFLK      25.080       40.416      14.618      0.183      0.190      0.329
 19 WETT      27.157       59.420      -4.032      0.065      0.067      0.065
fixed-interval smoothing results
   97.30970000000001                      18
 18 KIRU      11.884       56.653      15.024      0.273      0.416      0.304
 18 SVTL      10.606       52.792      12.920      1.206      2.191      2.284
 18 BOGO      13.637       36.766      10.338      0.392      0.477      0.990
 18 KOSG      15.461       30.327      -0.774      0.059      0.069      0.050
 18 DELF      18.178       30.931       1.748      0.301      0.361      0.580
```

18 WARE	16.402	31.700	3.209	0.350	0.406	0.724
18 POTS	16.382	35.603	2.342	0.203	0.222	0.344
18 WROC	14.971	34.208	3.439	0.646	0.747	1.812
18 MOPI	14.391	32.902	0.359	0.539	0.607	1.634
18 UPAD	20.689	39.825	20.450	0.121	0.123	0.127
18 BRUS	17.025	30.328	1.854	0.059	0.069	0.050
18 GRAS	-6.261	17.116	6.669	0.205	0.203	0.424
18 HFLK	25.219	40.524	14.621	0.176	0.184	0.324
18 WETT	27.158	59.420	-4.032	0.065	0.067	0.064
fixed-interval smoothing results						
97.23300000000000			17			
17 KIRU	11.878	56.676	15.017	0.268	0.413	0.300
17 SVTL	10.600	52.792	12.923	1.208	2.192	2.285
17 BOGO	13.616	36.766	10.346	0.393	0.478	0.990
17 KOSG	15.494	30.310	-0.868	0.058	0.068	0.049
17 DELF	18.219	30.955	1.747	0.300	0.360	0.579
17 WARE	16.423	31.706	3.210	0.349	0.404	0.723
17 POTS	16.417	35.633	2.309	0.196	0.214	0.338
17 WROC	14.970	34.206	3.441	0.649	0.749	1.813
17 MOPI	14.390	32.908	0.351	0.542	0.609	1.635
17 UPAD	20.747	39.857	20.460	0.117	0.119	0.121
17 BRUS	17.004	30.293	1.915	0.058	0.067	0.050
17 GRAS	-6.360	17.152	6.702	0.198	0.196	0.420
17 HFLK	25.381	40.649	14.626	0.170	0.177	0.320
17 WETT	27.158	59.420	-4.032	0.065	0.068	0.063
fixed-interval smoothing results						
97.15630000000000			16			
16 KIRU	11.868	56.701	15.015	0.264	0.410	0.297
16 SVTL	10.596	52.793	12.926	1.210	2.193	2.286
16 BOGO	13.599	36.766	10.352	0.395	0.480	0.991
16 KOSG	15.549	30.300	-0.951	0.057	0.067	0.048
16 DELF	18.261	30.979	1.745	0.299	0.360	0.578
16 WARE	16.444	31.713	3.212	0.347	0.404	0.722
16 POTS	16.459	35.666	2.270	0.189	0.207	0.334
16 WROC	14.970	34.204	3.442	0.652	0.752	1.814
16 MOPI	14.388	32.912	0.344	0.546	0.612	1.636
16 UPAD	20.815	39.898	20.473	0.115	0.116	0.117
16 BRUS	17.023	30.282	1.853	0.057	0.067	0.049
16 GRAS	-6.453	17.210	6.738	0.191	0.189	0.416
16 HFLK	25.567	40.790	14.631	0.165	0.172	0.316
16 WETT	27.158	59.421	-4.032	0.067	0.071	0.064
fixed-interval smoothing results						
97.07960000000000			15			
15 SVTL	10.594	52.792	12.927	1.212	2.194	2.287
15 BOGO	13.586	36.764	10.355	0.398	0.482	0.993
15 KOSG	15.527	30.291	-0.922	0.057	0.067	0.048
15 DELF	18.307	31.005	1.744	0.300	0.361	0.578
15 WARE	16.465	31.720	3.214	0.347	0.403	0.722
15 POTS	16.509	35.703	2.225	0.182	0.200	0.329
15 WROC	14.970	34.203	3.443	0.656	0.756	1.816
15 MOPI	14.386	32.913	0.340	0.550	0.616	1.638
15 UPAD	20.894	39.948	20.487	0.113	0.114	0.114
15 BRUS	16.994	30.294	1.821	0.057	0.066	0.049
15 GRAS	-6.535	17.295	6.777	0.185	0.183	0.413
15 HFLK	25.775	40.946	14.637	0.160	0.167	0.313
15 KIRU	11.852	56.726	15.017	0.261	0.408	0.294
15 WETT	27.159	59.421	-4.032	0.071	0.076	0.067
fixed-interval smoothing results						
97.00290000000000			14			
14 KIRU	11.832	56.753	15.023	0.259	0.406	0.292
14 SVTL	10.593	52.792	12.928	1.214	2.195	2.288
14 BOGO	13.577	36.761	10.357	0.402	0.485	0.995
14 KOSG	15.439	30.310	-0.808	0.057	0.066	0.048
14 DELF	18.354	31.031	1.742	0.302	0.362	0.579
14 WARE	16.486	31.727	3.218	0.347	0.404	0.721
14 POTS	16.564	35.744	2.174	0.176	0.195	0.325
14 WROC	14.970	34.202	3.443	0.661	0.759	1.817
14 MOPI	14.385	32.914	0.338	0.555	0.620	1.639
14 UPAD	20.982	40.008	20.503	0.113	0.114	0.113
14 BRUS	16.926	30.333	1.854	0.057	0.066	0.048
14 GRAS	-6.598	17.410	6.819	0.179	0.178	0.410
14 HFLK	26.006	41.116	14.645	0.156	0.163	0.311

14 WETT	27.159	59.422	-4.032	0.079	0.084	0.074
fixed-interval smoothing results						
96.92890000000000			13			
13 KIRU	11.809	56.778	15.032	0.257	0.405	0.292
13 SVTL	10.593	52.791	12.928	1.216	2.196	2.289
13 BOGO	13.571	36.758	10.358	0.407	0.489	0.996
13 KOSG	15.401	30.407	-0.753	0.056	0.066	0.047
13 DELF	18.400	31.055	1.740	0.304	0.364	0.580
13 WARE	16.505	31.733	3.221	0.348	0.405	0.722
13 POTS	16.619	35.786	2.122	0.172	0.190	0.322
13 WROC	14.970	34.202	3.443	0.665	0.763	1.819
13 MOPI	14.384	32.914	0.338	0.559	0.624	1.641
13 UPAD	21.066	40.075	20.521	0.113	0.114	0.114
13 BRUS	16.908	30.398	1.893	0.056	0.065	0.048
13 GRAS	-6.628	17.553	6.861	0.175	0.174	0.408
13 HFLK	26.229	41.280	14.652	0.152	0.160	0.309
13 WETT	27.160	59.423	-4.032	0.088	0.091	0.085
fixed-interval smoothing results						
96.85220000000000			12			
12 KIRU	11.781	56.806	15.045	0.256	0.405	0.291
12 BOGO	13.567	36.754	10.360	0.412	0.494	0.999
12 KOSG	15.500	30.647	-0.737	0.056	0.066	0.047
12 DELF	18.450	31.080	1.738	0.307	0.367	0.581
12 WARE	16.524	31.740	3.226	0.350	0.407	0.722
12 POTS	16.682	35.834	2.061	0.168	0.186	0.319
12 UPAD	21.154	40.161	20.543	0.115	0.116	0.117
12 BRUS	16.982	30.533	1.919	0.056	0.065	0.047
12 GRAS	-6.608	17.756	6.907	0.171	0.170	0.406
12 HFLK	26.467	41.453	14.659	0.150	0.157	0.308
12 WETT	27.161	59.423	-4.032	0.094	0.095	0.092
fixed-interval smoothing results						
96.77549999999999			11			
11 KIRU	11.752	56.834	15.060	0.257	0.405	0.292
11 BOGO	13.566	36.750	10.361	0.418	0.499	1.001
11 KOSG	15.824	31.066	-0.674	0.056	0.065	0.048
11 DELF	18.499	31.105	1.737	0.311	0.371	0.583
11 WARE	16.543	31.747	3.231	0.353	0.409	0.723
11 POTS	16.749	35.886	1.994	0.165	0.183	0.317
11 UPAD	21.236	40.259	20.568	0.118	0.119	0.121
11 BRUS	17.101	30.778	2.130	0.056	0.065	0.048
11 GRAS	-6.523	18.019	6.954	0.168	0.167	0.405
11 HFLK	26.701	41.620	14.666	0.148	0.156	0.307
11 WETT	27.161	59.422	-4.032	0.094	0.094	0.093
fixed-interval smoothing results						
96.69880000000001			10			
10 KIRU	11.723	56.863	15.075	0.258	0.406	0.294
10 BOGO	13.566	36.747	10.361	0.425	0.504	1.004
10 KOSG	16.375	31.724	-0.453	0.056	0.065	0.047
10 DELF	18.546	31.129	1.736	0.316	0.375	0.586
10 WARE	16.560	31.754	3.236	0.356	0.412	0.725
10 POTS	16.819	35.940	1.922	0.163	0.181	0.316
10 UPAD	21.309	40.365	20.596	0.121	0.123	0.127
10 BRUS	17.443	31.175	2.399	0.056	0.065	0.048
10 HFLK	26.927	41.781	14.671	0.148	0.156	0.307
10 WETT	27.160	59.421	-4.032	0.091	0.091	0.091
10 GRAS	-6.348	18.355	7.000	0.166	0.166	0.404
fixed-interval smoothing results						
96.62210000000000			9			
9 KIRU	11.694	56.892	15.089	0.259	0.407	0.296
9 BOGO	13.567	36.746	10.362	0.431	0.510	1.007
9 KOSG	17.371	32.689	-0.486	0.055	0.065	0.047
9 DELF	18.589	31.150	1.735	0.322	0.380	0.589
9 WARE	16.575	31.761	3.241	0.360	0.416	0.727
9 POTS	16.888	35.997	1.847	0.162	0.181	0.316
9 WETT	27.159	59.418	-4.032	0.086	0.086	0.086
9 BRUS	18.423	31.752	2.070	0.055	0.064	0.047
9 HFLK	27.140	41.930	14.676	0.149	0.158	0.309
9 UPAD	21.370	40.474	20.626	0.126	0.128	0.135
9 GRAS	-6.102	18.742	7.044	0.165	0.165	0.404
fixed-interval smoothing results						
96.54530000000000			8			
8 KIRU	11.666	56.921	15.102	0.262	0.409	0.299

```
  8 BOGO       13.567      36.746      10.362      0.438      0.516      1.010
  8 KOSG       19.030      33.930      -1.254      0.056      0.065      0.047
  8 DELF       18.627      31.169       1.733      0.328      0.385      0.592
  8 WARE       16.589      31.769       3.244      0.365      0.420      0.729
  8 POTS       16.958      36.055       1.772      0.163      0.182      0.316
  8 UPAD       21.419      40.582      20.658      0.132      0.134      0.143
  8 WETT       27.157      59.413      -4.032      0.081      0.081      0.080
  8 BRUS       20.123      32.482       0.921      0.056      0.065      0.048
  8 HFLK       27.338      42.067      14.680      0.152      0.161      0.311
  8 GRAS       -5.834      19.134       7.085      0.165      0.167      0.405
fixed-interval smoothing results
   96.46860000000000                7
  7 KIRU       11.640      56.949      15.114      0.266      0.411      0.303
  7 KOSG       20.761      35.251      -2.112      0.057      0.066      0.048
  7 DELF       18.659      31.185       1.731      0.335      0.391      0.596
  7 WARE       16.601      31.776       3.247      0.370      0.425      0.732
  7 POTS       17.025      36.112       1.697      0.166      0.185      0.318
  7 UPAD       21.457      40.682      20.688      0.139      0.142      0.153
  7 WETT       27.156      59.407      -4.032      0.077      0.079      0.077
  7 BRUS       21.877      33.246      -0.225      0.057      0.065      0.049
  7 HFLK       27.515      42.189      14.684      0.156      0.165      0.314
  7 GRAS       -5.574      19.499       7.120      0.168      0.170      0.407
fixed-interval smoothing results
   96.39190000000001                6
  6 KIRU       11.616      56.975      15.125      0.271      0.415      0.308
  6 KOSG       22.009      36.391      -2.558      0.056      0.064      0.047
  6 DELF       18.683      31.198       1.729      0.342      0.398      0.600
  6 WARE       16.610      31.784       3.249      0.376      0.430      0.735
  6 POTS       17.085      36.166       1.630      0.171      0.189      0.321
  6 UPAD       21.487      40.771      20.716      0.148      0.150      0.163
  6 WETT       27.155      59.400      -4.032      0.078      0.080      0.076
  6 BRUS       22.938      33.897      -0.579      0.056      0.064      0.047
  6 HFLK       27.670      42.294      14.688      0.162      0.171      0.318
  6 GRAS       -5.338      19.823       7.150      0.172      0.175      0.409
fixed-interval smoothing results
   96.31520000000000                5
  5 KIRU       11.595      56.997      15.134      0.277      0.419      0.313
  5 KOSG       22.711      37.239      -2.653      0.055      0.062      0.047
  5 DELF       18.698      31.206       1.729      0.350      0.404      0.605
  5 WARE       16.616      31.789       3.250      0.383      0.436      0.738
  5 POTS       17.133      36.211       1.573      0.177      0.195      0.324
  5 UPAD       21.511      40.844      20.739      0.158      0.160      0.174
  5 WETT       27.153      59.394      -4.032      0.083      0.085      0.081
  5 BRUS       23.331      34.379      -0.364      0.055      0.062      0.047
  5 GRAS       -5.137      20.096       7.175      0.179      0.181      0.413
  5 HFLK       27.802      42.376      14.691      0.169      0.179      0.322
fixed-interval smoothing results
   96.23850000000000                4
  4 KIRU       11.577      57.015      15.142      0.284      0.423      0.319
  4 KOSG       22.925      37.831      -2.386      0.053      0.059      0.046
  4 DELF       18.707      31.211       1.729      0.358      0.411      0.609
  4 WARE       16.621      31.793       3.250      0.390      0.442      0.741
  4 POTS       17.172      36.247       1.527      0.185      0.203      0.329
  4 UPAD       21.529      40.902      20.757      0.169      0.171      0.186
  4 WETT       27.151      59.391      -4.032      0.093      0.096      0.091
  4 BRUS       23.393      34.739      -0.021      0.053      0.058      0.047
  4 GRAS       -4.977      20.314       7.194      0.187      0.190      0.417
  4 HFLK       27.907      42.437      14.693      0.178      0.188      0.328
fixed-interval smoothing results
   96.16180000000000                3
  3 KIRU       11.565      57.027      15.148      0.291      0.428      0.326
  3 KOSG       23.025      38.227      -2.292      0.050      0.058      0.044
  3 DELF       18.709      31.212       1.729      0.366      0.418      0.614
  3 WARE       16.622      31.795       3.250      0.397      0.448      0.745
  3 POTS       17.200      36.271       1.492      0.195      0.212      0.335
  3 UPAD       21.541      40.943      20.770      0.181      0.184      0.198
  3 WETT       27.148      59.390      -4.032      0.107      0.110      0.105
  3 BRUS       23.364      35.004       0.153      0.050      0.057      0.045
  3 GRAS       -4.860      20.473       7.207      0.196      0.199      0.422
  3 HFLK       27.986      42.479      14.696      0.189      0.198      0.334
fixed-interval smoothing results
   96.08510000000000                2
```

2 KIRU	11.558	57.034	15.153	0.299	0.434	0.334
2 KOSG	23.176	38.448	-2.497	0.054	0.067	0.043
2 WARE	16.623	31.796	3.250	0.404	0.455	0.749
2 POTS	17.218	36.285	1.470	0.207	0.223	0.342
2 UPAD	21.548	40.967	20.778	0.194	0.196	0.211
2 WETT	27.145	59.390	-4.032	0.124	0.127	0.123
2 BRUS	23.345	35.166	0.143	0.054	0.066	0.044
2 GRAS	-4.790	20.571	7.215	0.208	0.211	0.427
2 HFLK	28.035	42.503	14.698	0.201	0.210	0.342

fixed-interval smoothing results

96.00839999999999 1

1 KIRU	11.555	57.036	15.154	0.309	0.441	0.342
1 KOSG	23.240	38.513	-2.605	0.079	0.092	0.067
1 POTS	17.224	36.290	1.462	0.219	0.235	0.350
1 UPAD	21.551	40.975	20.781	0.207	0.210	0.224
1 WETT	27.143	59.390	-4.032	0.144	0.146	0.142
1 BRUS	23.339	35.220	0.119	0.079	0.092	0.068
1 GRAS	-4.766	20.604	7.218	0.221	0.223	0.434
1 HFLK	28.052	42.511	14.698	0.214	0.223	0.350

Appendix F

(Calculated Strain Rates Using Estimated Velocities for the EUREF Permanent GPS Network)

Strain Rates For Group One

Epno	Trig	max deformation (10-7) E1	(10-7) sE1	min deformation (10-7) E2	(10-7) sE2	max direction (deg) teta	(deg) steta	rotation (sec) R	(sec) sR
1	1	0.1	0.0	-0.2	0.0	50.59	0.1	0.00	0.0
1	11	0.1	0.0	0.0	0.0	58.32	0.9	0.00	0.0
1	12	0.0	0.0	0.0	0.0	34.64	0.9	0.00	0.0
1	13	0.0	0.0	0.0	0.0	-10.46	3.5	0.00	0.0
1	15	0.1	0.0	0.0	0.0	-63.87	0.9	0.00	0.0
1	19	0.0	0.0	-0.1	0.0	26.43	1.5	0.00	0.0
1	20	0.1	0.0	-0.1	0.0	-51.25	0.6	0.00	0.0
1	21	0.1	0.0	-0.1	0.0	-64.40	0.6	0.00	0.0
1	22	0.0	0.0	0.0	0.0	-89.48	1.4	0.00	0.0

Epno	Trig	max deformation (10-7) E1	(10-7) sE1	min deformation (10-7) E2	(10-7) sE2	max direction (deg) teta	(deg) steta	rotation (sec) R	(sec) sR
2	1	0.1	0.0	-0.2	0.0	50.55	0.1	0.00	0.0
2	11	0.1	0.0	0.0	0.0	58.39	0.8	0.00	0.0
2	12	0.1	0.0	0.0	0.0	34.31	0.9	0.00	0.0
2	13	0.0	0.0	0.0	0.0	-10.44	3.4	0.00	0.0
2	14	0.1	0.0	-0.1	0.0	-40.84	0.3	0.00	0.0
2	15	0.1	0.0	0.0	0.0	-63.90	0.9	0.00	0.0
2	16	0.1	0.0	-0.1	0.0	34.77	0.7	0.00	0.0
2	17	0.0	0.0	-0.2	0.0	-68.26	1.1	0.00	0.0
2	18	0.1	0.0	-0.1	0.0	77.02	0.8	0.00	0.0
2	19	0.0	0.0	-0.1	0.0	25.27	1.1	0.00	0.0
2	20	0.1	0.0	-0.1	0.0	-51.83	0.4	0.00	0.0
2	21	0.1	0.0	-0.1	0.0	-64.85	0.5	0.00	0.0
2	22	0.0	0.0	0.0	0.0	-89.85	1.2	0.00	0.0

Epno	Trig	max deformation (10-7) E1	(10-7) sE1	min deformation (10-7) E2	(10-7) sE2	max direction (deg) teta	(deg) steta	rotation (sec) R	(sec) sR
3	1	0.1	0.0	-0.2	0.0	50.55	0.1	0.00	0.0
3	11	0.1	0.0	0.0	0.0	58.32	0.8	0.00	0.0
3	12	0.1	0.0	0.0	0.0	33.53	0.8	0.00	0.0
3	13	0.0	0.0	0.0	0.0	-10.38	3.3	0.00	0.0
3	14	0.1	0.0	-0.1	0.0	-40.87	0.3	0.00	0.0
3	15	0.1	0.0	0.0	0.0	-63.95	0.9	0.00	0.0
3	16	0.1	0.0	-0.1	0.0	34.46	0.7	0.00	0.0
3	17	0.0	0.0	-0.2	0.0	-69.15	1.0	0.00	0.0
3	18	0.1	0.0	-0.1	0.0	76.65	0.7	0.00	0.0
3	19	0.0	0.0	0.0	0.0	21.96	1.0	0.00	0.0
3	20	0.1	0.0	-0.1	0.0	-53.15	0.4	0.00	0.0
3	21	0.1	0.0	-0.1	0.0	-66.04	0.4	0.00	0.0
3	22	0.0	0.0	0.0	0.0	89.91	1.1	0.00	0.0

Epno	Trig	max deformation (10-7) E1	(10-7) sE1	min deformation (10-7) E2	(10-7) sE2	max direction (deg) teta	(deg) steta	rotation (sec) R	(sec) sR
4	1	0.1	0.0	-0.2	0.0	50.66	0.1	0.00	0.0
4	11	0.1	0.0	0.0	0.0	58.41	0.8	0.00	0.0
4	12	0.0	0.0	0.0	0.0	32.97	0.8	0.00	0.0
4	13	0.0	0.0	0.0	0.0	-10.28	3.2	0.00	0.0
4	14	0.1	0.0	-0.1	0.0	-40.91	0.3	0.00	0.0
4	15	0.1	0.0	0.0	0.0	-64.05	0.8	0.00	0.0
4	16	0.1	0.0	-0.1	0.0	33.34	0.7	0.00	0.0
4	17	0.0	0.0	-0.2	0.0	-70.23	1.0	0.00	0.0
4	18	0.1	0.0	-0.1	0.0	75.49	0.7	0.00	0.0
4	19	0.0	0.0	0.0	0.0	18.95	1.1	0.00	0.0
4	20	0.1	0.0	-0.1	0.0	-53.96	0.4	0.00	0.0
4	21	0.1	0.0	-0.1	0.0	-67.22	0.5	0.00	0.0
4	22	0.0	0.0	0.0	0.0	-89.50	1.1	0.00	0.0

Epno	Trig	max deformation (10-7)	(10-7)	min deformation (10-7)	(10-7)	max direction (deg)	(deg)	rotation (sec)	(sec)

		E1	sE1	E2	sE2	teta	steta	R	sR
5	1	0.1	0.0	-0.2	0.0	50.65	0.1	0.00	0.0
5	11	0.1	0.0	0.0	0.0	59.66	0.9	0.00	0.0
5	12	0.0	0.0	0.0	0.0	33.17	0.9	0.00	0.0
5	13	0.0	0.0	0.0	0.0	-10.16	3.2	0.00	0.0
5	14	0.1	0.0	-0.1	0.0	-40.97	0.3	0.00	0.0
5	15	0.1	0.0	0.0	0.0	-64.17	0.8	0.00	0.0
5	16	0.1	0.0	-0.1	0.0	32.43	0.7	0.00	0.0
5	17	0.0	0.0	-0.2	0.0	-71.44	1.1	0.00	0.0
5	18	0.1	0.0	0.0	0.0	73.91	0.8	0.00	0.0
5	19	0.0	0.0	0.0	0.0	18.39	1.2	0.00	0.0
5	20	0.1	0.0	-0.1	0.0	-54.25	0.4	0.00	0.0
5	21	0.1	0.0	-0.1	0.0	-68.44	0.5	0.00	0.0
5	22	0.0	0.0	0.0	0.0	-89.38	1.1	0.00	0.0

Epno	Trig	max deformation (10-7) E1	(10-7) sE1	min deformation (10-7) E2	(10-7) sE2	max direction (deg) teta	(deg) steta	rotation (sec) R	(sec) sR
6	1	0.1	0.0	-0.2	0.0	50.30	0.1	0.00	0.0
6	11	0.1	0.0	0.0	0.0	62.83	0.9	0.00	0.0
6	12	0.0	0.0	0.0	0.0	35.01	1.0	0.00	0.0
6	13	0.0	0.0	0.0	0.0	-10.03	3.2	0.00	0.0
6	14	0.1	0.0	-0.1	0.0	-41.04	0.3	0.00	0.0
6	15	0.1	0.0	0.0	0.0	-64.32	0.8	0.00	0.0
6	16	0.1	0.0	-0.1	0.0	32.82	0.8	0.00	0.0
6	17	0.0	0.0	-0.1	0.0	-73.03	1.3	0.00	0.0
6	18	0.1	0.0	0.0	0.0	72.21	0.9	0.00	0.0
6	19	0.0	0.0	0.0	0.0	16.98	1.5	0.00	0.0
6	20	0.1	0.0	-0.1	0.0	-56.21	0.5	0.00	0.0
6	21	0.1	0.0	-0.1	0.0	-71.54	0.5	0.00	0.0
6	22	0.1	0.0	0.0	0.0	88.09	1.0	0.00	0.0

Epno	Trig	max deformation (10-7) E1	(10-7) sE1	min deformation (10-7) E2	(10-7) sE2	max direction (deg) teta	(deg) steta	rotation (sec) R	(sec) sR
7	1	0.1	0.0	-0.2	0.0	49.43	0.1	0.00	0.0
7	11	0.1	0.0	0.0	0.0	68.82	0.9	0.00	0.0
7	12	0.0	0.0	0.0	0.0	41.94	1.4	0.00	0.0
7	13	0.0	0.0	0.0	0.0	-9.90	3.2	0.00	0.0
7	14	0.1	0.0	-0.1	0.0	-41.12	0.3	0.00	0.0
7	15	0.1	0.0	0.0	0.0	-64.49	0.8	0.00	0.0
7	16	0.1	0.0	0.0	0.0	36.77	0.9	0.00	0.0
7	17	0.0	0.0	-0.1	0.0	-75.61	2.0	0.00	0.0
7	18	0.0	0.0	0.0	0.0	70.75	1.1	0.00	0.0
7	19	0.0	0.0	0.0	0.0	12.80	2.4	0.00	0.0
7	20	0.1	0.0	-0.1	0.0	-61.03	0.6	0.00	0.0
7	21	0.1	0.0	0.0	0.0	-78.18	0.6	0.00	0.0
7	22	0.1	0.0	0.0	0.0	82.06	0.8	0.00	0.0

Epno	Trig	max deformation (10-7) E1	(10-7) sE1	min deformation (10-7) E2	(10-7) sE2	max direction (deg) teta	(deg) steta	rotation (sec) R	(sec) sR
8	1	0.1	0.0	-0.2	0.0	47.99	0.1	0.00	0.0
8	11	0.0	0.0	0.0	0.0	76.32	0.8	0.00	0.0
8	12	0.0	0.0	0.0	0.0	62.43	2.0	0.00	0.0
8	13	0.0	0.0	0.0	0.0	-9.76	3.2	0.00	0.0
8	14	0.1	0.0	-0.1	0.0	-41.21	0.3	0.00	0.0
8	15	0.1	0.0	0.0	0.0	-64.68	0.7	0.00	0.0
8	16	0.0	0.0	-0.1	0.0	49.79	1.2	0.00	0.0
8	17	0.0	0.0	0.0	0.0	-89.29	7.6	0.00	0.0
8	18	0.0	0.0	0.0	0.0	70.89	1.7	0.00	0.0
8	19	0.0	0.0	0.0	0.0	-12.02	32.5	0.00	0.0
8	20	0.1	0.0	-0.1	0.0	-68.22	0.7	0.00	0.0
8	21	0.1	0.0	0.0	0.0	-89.42	0.8	0.00	0.0
8	22	0.1	0.0	0.0	0.0	75.64	0.6	0.00	0.0

Epno	Trig	max deformation (10-7)	(10-7)	min deformation (10-7)	(10-7)	max direction (deg)	(deg)	rotation (sec)	(sec)

		E1	sE1	E2	sE2	teta	steta	R	sR
9	1	0.1	0.0	-0.2	0.0	46.60	0.1	0.00	0.0
9	11	0.0	0.0	0.0	0.0	82.05	0.7	0.00	0.0
9	12	0.0	0.0	0.0	0.0	82.76	1.5	0.00	0.0
9	13	0.0	0.0	0.0	0.0	-9.61	3.3	0.00	0.0
9	14	0.1	0.0	-0.1	0.0	-41.31	0.3	0.00	0.0
9	15	0.1	0.0	0.0	0.0	-64.87	0.7	0.00	0.0
9	16	0.0	0.0	-0.1	0.0	67.12	1.2	0.00	0.0
9	17	0.0	0.0	0.0	0.0	26.67	3.1	0.00	0.0
9	18	0.0	0.0	0.0	0.0	72.42	3.7	0.00	0.0
9	19	0.0	0.0	0.0	0.0	-79.87	2.4	0.00	0.0
9	20	0.0	0.0	-0.1	0.0	-75.97	0.7	0.00	0.0
9	21	0.1	0.0	0.0	0.0	78.03	0.8	0.00	0.0
9	22	0.1	0.0	0.0	0.0	72.21	0.5	0.00	0.0

Epno	Trig	max deformation (10-7) E1	(10-7) sE1	min deformation (10-7) E2	(10-7) sE2	max direction (deg) teta	(deg) steta	rotation (sec) R	(sec) sR
10	1	0.1	0.0	-0.2	0.0	45.81	0.1	0.00	0.0
10	11	0.0	0.0	-0.1	0.0	85.37	0.6	0.00	0.0
10	12	0.0	0.0	0.0	0.0	-88.77	1.1	0.00	0.0
10	13	0.0	0.0	0.0	0.0	-9.44	3.4	0.00	0.0
10	14	0.1	0.0	-0.1	0.0	-41.40	0.3	0.00	0.0
10	15	0.1	0.0	0.0	0.0	-65.06	0.7	0.00	0.0
10	16	0.0	0.0	-0.1	0.0	76.45	1.0	0.00	0.0
10	17	0.1	0.0	0.0	0.0	24.39	1.6	0.00	0.0
10	18	0.0	0.0	0.0	0.0	41.76	26.1	0.00	0.0
10	19	0.0	0.0	0.0	0.0	-81.05	1.3	0.00	0.0
10	20	0.0	0.0	-0.1	0.0	-82.87	0.8	0.00	0.0
10	21	0.1	0.0	0.0	0.0	69.68	0.7	0.00	0.0
10	22	0.1	0.0	0.0	0.0	71.08	0.4	0.00	0.0

Epno	Trig	max deformation (10-7) E1	(10-7) sE1	min deformation (10-7) E2	(10-7) sE2	max direction (deg) teta	(deg) steta	rotation (sec) R	(sec) sR
11	1	0.1	0.0	-0.2	0.0	45.53	0.1	0.00	0.0
11	11	0.0	0.0	-0.1	0.0	87.16	0.6	0.00	0.0
11	12	0.0	0.0	-0.1	0.0	-84.70	1.0	0.00	0.0
11	13	0.0	0.0	0.0	0.0	-9.26	3.5	0.00	0.0
11	14	0.1	0.0	-0.1	0.0	-41.50	0.3	0.00	0.0
11	15	0.1	0.0	0.0	0.0	-65.25	0.7	0.00	0.0
11	16	0.0	0.0	-0.1	0.0	80.77	1.0	0.00	0.0
11	17	0.1	0.0	0.0	0.0	25.27	1.2	0.00	0.0
11	18	0.0	0.0	0.0	0.0	2.92	5.4	0.00	0.0
11	19	0.0	0.0	0.0	0.0	-80.55	1.0	0.00	0.0
11	20	0.0	0.0	-0.1	0.0	-88.23	0.8	0.00	0.0
11	21	0.1	0.0	0.0	0.0	65.52	0.6	0.00	0.0
11	22	0.1	0.0	0.0	0.0	70.90	0.4	0.00	0.0

Epno	Trig	max deformation (10-7) E1	(10-7) sE1	min deformation (10-7) E2	(10-7) sE2	max direction (deg) teta	(deg) steta	rotation (sec) R	(sec) sR
12	1	0.1	0.0	-0.2	0.0	45.53	0.1	0.00	0.0
12	2	0.1	0.0	-0.1	0.0	48.33	1.2	0.00	0.0
12	3	0.1	0.0	-0.1	0.0	55.28	0.9	0.00	0.0
12	4	0.2	0.0	-0.1	0.0	61.49	0.9	0.00	0.0
12	5	0.0	0.0	-0.1	0.0	63.90	3.0	0.00	0.0
12	11	0.0	0.0	-0.1	0.0	88.36	0.6	0.00	0.0
12	12	0.0	0.0	-0.1	0.0	-82.37	0.9	0.00	0.0
12	13	0.0	0.0	0.0	0.0	-9.11	3.6	0.00	0.0
12	14	0.1	0.0	-0.1	0.0	-41.60	0.3	0.00	0.0
12	15	0.1	0.0	0.0	0.0	-65.44	0.7	0.00	0.0
12	16	0.0	0.0	-0.1	0.0	82.86	1.0	0.00	0.0
12	17	0.1	0.0	0.0	0.0	26.63	1.0	0.00	0.0
12	18	0.0	0.0	0.0	0.0	5.01	3.2	0.00	0.0
12	19	0.0	0.0	0.0	0.0	-79.66	0.9	0.00	0.0
12	20	0.0	0.0	-0.1	0.0	88.74	0.8	0.00	0.0
12	21	0.1	0.0	0.0	0.0	63.52	0.6	0.00	0.0

12	22	0.1	0.0	0.0	0.0	71.08	0.4	0.00	0.0
12	23	0.1	0.0	-0.1	0.0	77.98	1.4	0.00	0.0

Epno	Trig	max deformation (10-7) E1	(10-7) sE1	min deformation (10-7) E2	(10-7) sE2	max direction (deg) teta	(deg) steta	rotation (sec) R	(sec) sR
13	1	0.1	0.0	-0.2	0.0	45.61	0.1	0.00	0.0
13	2	0.1	0.0	-0.1	0.0	48.64	1.1	0.00	0.0
13	3	0.1	0.0	-0.1	0.0	55.27	0.9	0.00	0.0
13	4	0.2	0.0	-0.1	0.0	61.43	0.9	0.00	0.0
13	5	0.0	0.0	-0.1	0.0	64.39	3.0	0.00	0.0
13	11	0.0	0.0	-0.1	0.0	89.20	0.6	0.00	0.0
13	12	0.0	0.0	-0.1	0.0	-81.19	1.0	0.00	0.0
13	13	0.0	0.0	0.0	0.0	-8.96	3.8	0.00	0.0
13	14	0.1	0.0	-0.1	0.0	-41.70	0.3	0.00	0.0
13	15	0.1	0.0	0.0	0.0	-65.63	0.7	0.00	0.0
13	16	0.0	0.0	-0.1	0.0	84.04	1.0	0.00	0.0
13	17	0.1	0.0	0.0	0.0	27.68	1.0	0.00	0.0
13	18	0.0	0.0	0.0	0.0	6.76	2.6	0.00	0.0
13	19	0.0	0.0	0.0	0.0	-78.87	0.9	0.00	0.0
13	20	0.0	0.0	-0.1	0.0	87.64	0.8	0.00	0.0
13	21	0.1	0.0	0.0	0.0	62.46	0.6	0.00	0.0
13	22	0.1	0.0	0.0	0.0	71.39	0.4	0.00	0.0
13	23	0.1	0.0	-0.1	0.0	78.26	1.4	0.00	0.0

Epno	Trig	max deformation (10-7) E1	(10-7) sE1	min deformation (10-7) E2	(10-7) sE2	max direction (deg) teta	(deg) steta	rotation (sec) R	(sec) sR
14	1	0.1	0.0	-0.2	0.0	45.65	0.1	0.00	0.0
14	2	0.1	0.0	-0.1	0.0	48.81	1.1	0.00	0.0
14	3	0.1	0.0	-0.1	0.0	55.26	0.9	0.00	0.0
14	4	0.2	0.0	-0.1	0.0	61.37	0.9	0.00	0.0
14	5	0.0	0.0	-0.1	0.0	64.83	3.0	0.00	0.0
14	11	0.0	0.0	-0.1	0.0	89.48	0.6	0.00	0.0
14	12	0.0	0.0	-0.1	0.0	-80.80	1.0	0.00	0.0
14	13	0.0	0.0	0.0	0.0	-8.85	4.0	0.00	0.0
14	14	0.1	0.0	-0.1	0.0	-41.80	0.3	0.00	0.0
14	15	0.1	0.0	0.0	0.0	-65.80	0.7	0.00	0.0
14	16	0.0	0.0	-0.1	0.0	84.68	1.0	0.00	0.0
14	17	0.1	0.0	0.0	0.0	28.19	0.9	0.00	0.0
14	18	0.0	0.0	0.0	0.0	7.25	2.4	0.00	0.0
14	19	0.0	0.0	0.0	0.0	-78.14	0.9	0.00	0.0
14	20	0.0	0.0	-0.1	0.0	87.70	0.8	0.00	0.0
14	21	0.1	0.0	0.0	0.0	62.21	0.6	0.00	0.0
14	22	0.1	0.0	0.0	0.0	71.50	0.5	0.00	0.0
14	23	0.1	0.0	-0.1	0.0	78.36	1.3	0.00	0.0

Epno	Trig	max deformation (10-7) E1	(10-7) sE1	min deformation (10-7) E2	(10-7) sE2	max direction (deg) teta	(deg) steta	rotation (sec) R	(sec) sR
15	1	0.1	0.0	-0.2	0.0	45.67	0.1	0.00	0.0
15	2	0.1	0.0	-0.1	0.0	48.90	1.1	0.00	0.0
15	3	0.1	0.0	-0.1	0.0	55.25	0.9	0.00	0.0
15	4	0.2	0.0	-0.1	0.0	61.30	0.9	0.00	0.0
15	5	0.0	0.0	-0.1	0.0	65.27	3.0	0.00	0.0
15	11	0.0	0.0	-0.1	0.0	89.42	0.6	0.00	0.0
15	12	0.0	0.0	-0.1	0.0	-80.73	1.0	0.00	0.0
15	13	0.0	0.0	0.0	0.0	-8.77	4.3	0.00	0.0
15	14	0.1	0.0	-0.1	0.0	-41.91	0.3	0.00	0.0
15	15	0.1	0.0	0.0	0.0	-65.97	0.7	0.00	0.0
15	16	0.0	0.0	-0.1	0.0	85.03	1.0	0.00	0.0
15	17	0.1	0.0	0.0	0.0	28.36	0.9	0.00	0.0
15	18	0.0	0.0	0.0	0.0	7.21	2.2	0.00	0.0
15	19	0.0	0.0	0.0	0.0	-77.53	0.9	0.00	0.0
15	20	0.0	0.0	-0.1	0.0	88.52	0.8	0.00	0.0
15	21	0.1	0.0	0.0	0.0	62.48	0.6	0.00	0.0
15	22	0.1	0.0	0.0	0.0	71.34	0.5	0.00	0.0
15	23	0.1	0.0	-0.1	0.0	78.34	1.3	0.00	0.0

Epno	Trig	max deformation (10-7) E1	(10-7) sE1	min deformation (10-7) E2	(10-7) sE2	max direction (deg) teta	(deg) steta	rotation (sec) R	(sec) sR
16	1	0.1	0.0	-0.2	0.0	45.65	0.1	0.00	0.0
16	2	0.1	0.0	-0.1	0.0	48.90	1.1	0.00	0.0
16	3	0.1	0.0	-0.1	0.0	55.24	0.9	0.00	0.0
16	4	0.2	0.0	-0.1	0.0	61.24	0.9	0.00	0.0
16	5	0.0	0.0	-0.1	0.0	65.66	3.1	0.00	0.0
16	11	0.0	0.0	-0.1	0.0	89.36	0.6	0.00	0.0
16	12	0.0	0.0	-0.1	0.0	-80.80	1.0	0.00	0.0
16	13	0.0	0.0	0.0	0.0	-8.72	4.5	0.00	0.0
16	14	0.1	0.0	-0.1	0.0	-42.01	0.3	0.00	0.0
16	15	0.1	0.0	0.0	0.0	-66.12	0.7	0.00	0.0
16	16	0.0	0.0	-0.1	0.0	85.17	1.0	0.00	0.0
16	17	0.1	0.0	0.0	0.0	28.40	0.9	0.00	0.0
16	18	0.0	0.0	0.0	0.0	7.05	2.2	0.00	0.0
16	19	0.0	0.0	0.0	0.0	-77.52	0.9	0.00	0.0
16	20	0.0	0.0	-0.1	0.0	89.57	0.8	0.00	0.0
16	21	0.1	0.0	0.0	0.0	62.77	0.7	0.00	0.0
16	22	0.1	0.0	0.0	0.0	71.14	0.5	0.00	0.0
16	23	0.1	0.0	-0.1	0.0	78.19	1.3	0.00	0.0

Epno	Trig	max deformation (10-7) E1	(10-7) sE1	min deformation (10-7) E2	(10-7) sE2	max direction (deg) teta	(deg) steta	rotation (sec) R	(sec) sR
17	1	0.1	0.0	-0.2	0.0	45.61	0.1	0.00	0.0
17	2	0.1	0.0	-0.1	0.0	48.86	1.1	0.00	0.0
17	3	0.1	0.0	-0.1	0.0	55.23	0.9	0.00	0.0
17	4	0.2	0.0	-0.1	0.0	61.18	0.9	0.00	0.0
17	5	0.0	0.0	-0.1	0.0	66.01	3.1	0.00	0.0
17	11	0.0	0.0	-0.1	0.0	89.11	0.6	0.00	0.0
17	12	0.0	0.0	-0.1	0.0	-80.93	1.1	0.00	0.0
17	13	0.0	0.0	0.0	0.0	-8.74	4.8	0.00	0.0
17	14	0.1	0.0	-0.1	0.0	-42.11	0.3	0.00	0.0
17	15	0.1	0.0	0.0	0.0	-66.27	0.7	0.00	0.0
17	16	0.0	0.0	-0.1	0.0	85.15	0.9	0.00	0.0
17	17	0.1	0.0	0.0	0.0	28.41	0.9	0.00	0.0
17	18	0.0	0.0	0.0	0.0	7.01	2.2	0.00	0.0
17	19	0.0	0.0	0.0	0.0	-77.71	0.9	0.00	0.0
17	20	0.0	0.0	-0.1	0.0	-89.99	0.8	0.00	0.0
17	21	0.1	0.0	0.0	0.0	63.09	0.7	0.00	0.0
17	22	0.1	0.0	0.0	0.0	70.92	0.5	0.00	0.0
17	23	0.1	0.0	-0.1	0.0	77.99	1.3	0.00	0.0

Epno	Trig	max deformation (10-7) E1	(10-7) sE1	min deformation (10-7) E2	(10-7) sE2	max direction (deg) teta	(deg) steta	rotation (sec) R	(sec) sR
18	1	0.1	0.0	-0.2	0.0	45.60	0.1	0.00	0.0
18	2	0.1	0.0	-0.1	0.0	48.82	1.1	0.00	0.0
18	3	0.1	0.0	-0.1	0.0	55.22	0.9	0.00	0.0
18	4	0.2	0.0	-0.1	0.0	61.12	0.9	0.00	0.0
18	5	0.0	0.0	-0.1	0.0	66.30	3.1	0.00	0.0
18	11	0.0	0.0	-0.1	0.0	88.70	0.6	0.00	0.0
18	12	0.0	0.0	-0.1	0.0	-81.18	1.1	0.00	0.0
18	13	0.0	0.0	0.0	0.0	-8.82	5.1	0.00	0.0
18	14	0.1	0.0	-0.1	0.0	-42.21	0.3	0.00	0.0
18	15	0.1	0.0	0.0	0.0	-66.40	0.8	0.00	0.0
18	16	0.0	0.0	-0.1	0.0	84.95	0.9	0.00	0.0
18	17	0.1	0.0	0.0	0.0	28.32	0.9	0.00	0.0
18	18	0.0	0.0	0.0	0.0	6.98	2.3	0.00	0.0
18	19	0.0	0.0	0.0	0.0	-77.59	0.9	0.00	0.0
18	20	0.0	0.0	-0.1	0.0	89.88	0.8	0.00	0.0
18	21	0.1	0.0	0.0	0.0	63.37	0.7	0.00	0.0
18	22	0.1	0.0	0.0	0.0	70.61	0.5	0.00	0.0
18	23	0.1	0.0	-0.1	0.0	77.84	1.3	0.00	0.0

Epno	Trig	max deformation (10-7) E1	(10-7) sE1	min deformation (10-7) E2	(10-7) sE2	max direction (deg) teta	(deg) steta	rotation (sec) R	(sec) sR

19	1	0.1	0.0	-0.2	0.0	45.59	0.1	0.00	0.0
19	2	0.1	0.0	-0.1	0.0	48.79	1.1	0.00	0.0
19	3	0.1	0.0	-0.1	0.0	55.20	0.9	0.00	0.0
19	4	0.2	0.0	-0.1	0.0	61.06	0.9	0.00	0.0
19	5	0.0	0.0	-0.1	0.0	66.53	3.1	0.00	0.0
19	11	0.0	0.0	-0.1	0.0	88.56	0.6	0.00	0.0
19	12	0.0	0.0	-0.1	0.0	-81.52	1.1	0.00	0.0
19	13	0.0	0.0	0.0	0.0	-8.94	5.4	0.00	0.0
19	14	0.1	0.0	-0.1	0.0	-42.30	0.3	0.00	0.0
19	15	0.1	0.0	0.0	0.0	-66.51	0.8	0.00	0.0
19	16	0.0	0.0	-0.1	0.0	84.75	0.9	0.00	0.0
19	17	0.1	0.0	0.0	0.0	28.21	0.9	0.00	0.0
19	18	0.0	0.0	0.0	0.0	6.85	2.4	0.00	0.0
19	19	0.0	0.0	0.0	0.0	-77.49	1.0	0.00	0.0
19	20	0.0	0.0	-0.1	0.0	89.89	0.8	0.00	0.0
19	21	0.1	0.0	0.0	0.0	63.32	0.7	0.00	0.0
19	22	0.1	0.0	0.0	0.0	70.39	0.5	0.00	0.0
19	23	0.1	0.0	-0.1	0.0	77.72	1.3	0.00	0.0

Epno	Trig	max deformation (10-7) E1	(10-7) sE1	min deformation (10-7) E2	(10-7) sE2	max direction (deg) teta	(deg) steta	rotation (sec) R	(sec) sR
20	1	0.1	0.0	-0.2	0.0	45.59	0.1	0.00	0.0
20	2	0.1	0.0	-0.1	0.0	48.77	1.1	0.00	0.0
20	3	0.1	0.0	-0.1	0.0	55.18	0.9	0.00	0.0
20	4	0.2	0.0	-0.1	0.0	61.00	0.9	0.00	0.0
20	5	0.0	0.0	-0.1	0.0	66.70	3.1	0.00	0.0
20	11	0.0	0.0	-0.1	0.0	88.77	0.7	0.00	0.0
20	12	0.0	0.0	-0.1	0.0	-81.77	1.2	0.00	0.0
20	13	0.0	0.0	0.0	0.0	-9.09	5.7	0.00	0.0
20	14	0.1	0.0	-0.1	0.0	-42.39	0.3	0.00	0.0
20	15	0.1	0.0	0.0	0.0	-66.62	0.8	0.00	0.0
20	16	0.0	0.0	-0.1	0.0	84.67	0.9	0.00	0.0
20	17	0.1	0.0	0.0	0.0	28.28	0.9	0.00	0.0
20	18	0.0	0.0	0.0	0.0	7.00	2.5	0.00	0.0
20	19	0.0	0.0	0.0	0.0	-77.24	1.0	0.00	0.0
20	20	0.0	0.0	-0.1	0.0	-89.81	0.9	0.00	0.0
20	21	0.1	0.0	0.0	0.0	63.04	0.7	0.00	0.0
20	22	0.1	0.0	0.0	0.0	70.30	0.6	0.00	0.0
20	23	0.1	0.0	-0.1	0.0	77.63	1.3	0.00	0.0

Epno	Trig	max deformation (10-7) E1	(10-7) sE1	min deformation (10-7) E2	(10-7) sE2	max direction (deg) teta	(deg) steta	rotation (sec) R	(sec) sR
21	1	0.1	0.0	-0.2	0.0	45.61	0.1	0.00	0.0
21	2	0.1	0.0	-0.1	0.0	48.79	1.1	0.00	0.0
21	3	0.1	0.0	-0.1	0.0	55.16	0.9	0.00	0.0
21	4	0.2	0.0	-0.1	0.0	60.94	0.9	0.00	0.0
21	5	0.0	0.0	-0.1	0.0	66.83	3.1	0.00	0.0
21	6	0.1	0.0	0.0	0.0	-21.82	13.1	0.00	0.0
21	9	0.0	0.0	-0.2	0.0	57.26	3.4	0.00	0.0
21	10	0.1	0.0	-0.1	0.0	-80.07	3.8	0.00	0.0
21	11	0.0	0.0	-0.1	0.0	89.00	0.7	0.00	0.0
21	12	0.0	0.0	-0.1	0.0	-81.90	1.3	0.00	0.0
21	13	0.0	0.0	0.0	0.0	-9.23	6.1	0.00	0.0
21	14	0.1	0.0	-0.1	0.0	-42.47	0.3	0.00	0.0
21	15	0.1	0.0	0.0	0.0	-66.70	0.8	0.00	0.0
21	16	0.0	0.0	-0.1	0.0	84.59	1.0	0.00	0.0
21	17	0.1	0.0	0.0	0.0	28.54	0.9	0.00	0.0
21	18	0.0	0.0	0.0	0.0	7.75	2.6	0.00	0.0
21	19	0.0	0.0	0.0	0.0	-76.47	1.0	0.00	0.0
21	20	0.0	0.0	-0.1	0.0	-89.50	0.9	0.00	0.0
21	21	0.1	0.0	0.0	0.0	62.88	0.8	0.00	0.0
21	22	0.1	0.0	0.0	0.0	70.19	0.6	0.00	0.0
21	23	0.1	0.0	-0.1	0.0	77.61	1.3	0.00	0.0
21	24	0.1	0.0	0.1	0.0	75.30	10.3	0.00	0.0
21	25	0.5	0.1	-0.6	0.1	50.82	4.8	-0.01	0.0

Epno Trig max deformation min deformation max direction rotation

		(10-7) E1	(10-7) sE1	(10-7) E2	(10-7) sE2	(deg) teta	(deg) steta	(sec) R	(sec) sR
22	1	0.1	0.0	-0.2	0.0	45.62	0.1	0.00	0.0
22	2	0.1	0.0	-0.1	0.0	48.80	1.1	0.00	0.0
22	3	0.1	0.0	-0.1	0.0	55.14	0.9	0.00	0.0
22	4	0.2	0.0	-0.1	0.0	60.89	0.9	0.00	0.0
22	5	0.0	0.0	-0.1	0.0	66.92	3.2	0.00	0.0
22	6	0.1	0.0	0.0	0.0	-22.31	12.9	0.00	0.0
22	9	0.0	0.0	-0.2	0.0	57.25	3.4	0.00	0.0
22	10	0.1	0.0	-0.1	0.0	-80.14	3.8	0.00	0.0
22	11	0.0	0.0	-0.1	0.0	89.12	0.7	0.00	0.0
22	12	0.0	0.0	-0.1	0.0	-81.95	1.3	0.00	0.0
22	13	0.0	0.0	0.0	0.0	-9.38	6.4	0.00	0.0
22	14	0.1	0.0	-0.1	0.0	-42.53	0.4	0.00	0.0
22	15	0.1	0.0	0.0	0.0	-66.78	0.8	0.00	0.0
22	16	0.0	0.0	-0.1	0.0	84.59	1.0	0.00	0.0
22	17	0.1	0.0	0.0	0.0	28.84	0.9	0.00	0.0
22	18	0.0	0.0	0.0	0.0	8.55	2.7	0.00	0.0
22	19	0.0	0.0	0.0	0.0	-75.65	1.0	0.00	0.0
22	20	0.0	0.0	-0.1	0.0	-89.26	0.9	0.00	0.0
22	21	0.1	0.0	0.0	0.0	62.91	0.8	0.00	0.0
22	22	0.1	0.0	0.0	0.0	70.09	0.6	0.00	0.0
22	23	0.1	0.0	-0.1	0.0	77.57	1.3	0.00	0.0
22	24	0.1	0.0	0.1	0.0	75.29	10.4	0.00	0.0
22	25	0.5	0.1	-0.6	0.1	50.84	4.9	-0.01	0.0

Epno	Trig	max deformation (10-7) E1	(10-7) sE1	min deformation (10-7) E2	(10-7) sE2	max direction (deg) teta	(deg) steta	rotation (sec) R	(sec) sR
23	1	0.1	0.0	-0.2	0.0	45.61	0.1	0.00	0.0
23	2	0.1	0.0	-0.1	0.0	48.78	1.1	0.00	0.0
23	3	0.1	0.0	-0.1	0.0	55.13	0.9	0.00	0.0
23	4	0.2	0.0	-0.1	0.0	60.85	0.9	0.00	0.0
23	5	0.0	0.0	-0.1	0.0	66.97	3.2	0.00	0.0
23	6	0.1	0.0	0.0	0.0	-22.67	12.8	0.00	0.0
23	9	0.0	0.0	-0.2	0.0	57.25	3.4	0.00	0.0
23	10	0.1	0.0	-0.1	0.0	-80.24	3.8	0.00	0.0
23	11	0.0	0.0	-0.1	0.0	89.08	0.7	0.00	0.0
23	12	0.0	0.0	-0.1	0.0	-82.11	1.4	0.00	0.0
23	13	0.0	0.0	0.0	0.0	-9.49	6.7	0.00	0.0
23	14	0.1	0.0	-0.1	0.0	-42.59	0.4	0.00	0.0
23	15	0.1	0.0	0.0	0.0	-66.84	0.9	0.00	0.0
23	16	0.0	0.0	-0.1	0.0	84.62	1.0	0.00	0.0
23	17	0.1	0.0	0.0	0.0	28.80	1.0	0.00	0.0
23	18	0.0	0.0	0.0	0.0	8.30	2.8	0.00	0.0
23	19	0.0	0.0	0.0	0.0	-75.58	1.1	0.00	0.0
23	20	0.0	0.0	-0.1	0.0	-89.05	0.9	0.00	0.0
23	21	0.1	0.0	0.0	0.0	62.90	0.8	0.00	0.0
23	22	0.1	0.0	0.0	0.0	70.05	0.6	0.00	0.0
23	23	0.1	0.0	-0.1	0.0	77.51	1.3	0.00	0.0
23	24	0.1	0.0	0.1	0.0	75.10	10.6	0.00	0.0
23	25	0.5	0.1	-0.6	0.1	50.84	4.9	-0.01	0.0

Epno	Trig	max deformation (10-7) E1	(10-7) sE1	min deformation (10-7) E2	(10-7) sE2	max direction (deg) teta	(deg) steta	rotation (sec) R	(sec) sR
24	1	0.1	0.0	-0.2	0.0	45.60	0.1	0.00	0.0
24	2	0.1	0.0	-0.1	0.0	48.76	1.1	0.00	0.0
24	3	0.1	0.0	-0.1	0.0	55.11	0.9	0.00	0.0
24	4	0.2	0.0	-0.1	0.0	60.81	0.9	0.00	0.0
24	5	0.0	0.0	-0.1	0.0	67.01	3.2	0.00	0.0
24	6	0.1	0.0	0.0	0.0	-22.92	12.7	0.00	0.0
24	7	0.1	0.0	-0.2	0.0	20.69	4.1	0.00	0.0
24	8	-0.1	0.0	-0.2	0.0	46.33	17.8	0.00	0.0
24	9	0.0	0.0	-0.2	0.0	57.25	3.4	0.00	0.0
24	10	0.1	0.0	-0.1	0.0	-80.33	3.8	0.00	0.0
24	11	0.0	0.0	-0.1	0.0	88.87	0.8	0.00	0.0
24	12	0.0	0.0	-0.1	0.0	-82.34	1.4	0.00	0.0
24	13	0.0	0.0	0.0	0.0	-9.61	7.1	0.00	0.0

24	14	0.1	0.0	-0.1	0.0	-42.63	0.4	0.00	0.0
24	15	0.1	0.0	0.0	0.0	-66.88	0.9	0.00	0.0
24	16	0.0	0.0	-0.1	0.0	84.64	1.0	0.00	0.0
24	17	0.1	0.0	0.0	0.0	28.53	1.0	0.00	0.0
24	18	0.0	0.0	0.0	0.0	7.40	2.9	0.00	0.0
24	19	0.0	0.0	0.0	0.0	-75.97	1.1	0.00	0.0
24	20	0.0	0.0	-0.1	0.0	-88.94	0.9	0.00	0.0
24	21	0.1	0.0	0.0	0.0	62.92	0.9	0.00	0.0
24	22	0.1	0.0	0.0	0.0	70.03	0.7	0.00	0.0
24	23	0.1	0.0	-0.1	0.0	77.43	1.3	0.00	0.0
24	24	0.1	0.0	0.1	0.0	74.94	10.7	0.00	0.0
24	25	0.5	0.1	-0.6	0.1	50.85	4.9	-0.01	0.0

Epno	Trig	max deformation (10-7) E1	sE1	min deformation (10-7) E2	sE2	max direction (deg) teta	steta	rotation (sec) R	sR
25	1	0.1	0.0	-0.2	0.0	45.59	0.1	0.00	0.0
25	2	0.1	0.0	-0.1	0.0	48.75	1.1	0.00	0.0
25	3	0.1	0.0	-0.1	0.0	55.10	0.9	0.00	0.0
25	4	0.2	0.0	-0.1	0.0	60.77	0.9	0.00	0.0
25	5	0.0	0.0	-0.1	0.0	67.02	3.2	0.00	0.0
25	6	0.1	0.0	0.0	0.0	-23.10	12.6	0.00	0.0
25	7	0.1	0.0	-0.2	0.0	20.69	4.1	0.00	0.0
25	8	-0.1	0.0	-0.2	0.0	46.32	17.8	0.00	0.0
25	9	0.0	0.0	-0.2	0.0	57.25	3.4	0.00	0.0
25	10	0.1	0.0	-0.1	0.0	-80.35	3.8	0.00	0.0
25	11	0.0	0.0	-0.1	0.0	88.64	0.8	0.00	0.0
25	12	0.0	0.0	-0.1	0.0	-82.51	1.5	0.00	0.0
25	13	0.0	0.0	0.0	0.0	-9.71	7.4	0.00	0.0
25	14	0.1	0.0	-0.1	0.0	-42.66	0.4	0.00	0.0
25	15	0.1	0.0	0.0	0.0	-66.91	0.9	0.00	0.0
25	16	0.0	0.0	-0.1	0.0	84.62	1.1	0.00	0.0
25	17	0.1	0.0	0.0	0.0	28.30	1.0	0.00	0.0
25	18	0.0	0.0	0.0	0.0	6.78	2.9	0.00	0.0
25	19	0.0	0.0	0.0	0.0	-76.08	1.1	0.00	0.0
25	20	0.0	0.0	-0.1	0.0	-89.07	1.0	0.00	0.0
25	21	0.1	0.0	0.0	0.0	62.97	0.9	0.00	0.0
25	22	0.1	0.0	0.0	0.0	69.95	0.7	0.00	0.0
25	23	0.1	0.0	-0.1	0.0	77.38	1.3	0.00	0.0
25	24	0.1	0.0	0.1	0.0	75.00	10.8	0.00	0.0
25	25	0.5	0.1	-0.6	0.1	50.84	4.9	-0.01	0.0

Epno	Trig	max deformation (10-7) E1	sE1	min deformation (10-7) E2	sE2	max direction (deg) teta	steta	rotation (sec) R	sR
26	1	0.1	0.0	-0.2	0.0	45.59	0.1	0.00	0.0
26	2	0.1	0.0	-0.1	0.0	48.73	1.1	0.00	0.0
26	3	0.1	0.0	-0.1	0.0	55.08	0.9	0.00	0.0
26	4	0.2	0.0	-0.1	0.0	60.74	0.9	0.00	0.0
26	5	0.0	0.0	-0.1	0.0	67.03	3.2	0.00	0.0
26	6	0.1	0.0	0.0	0.0	-23.23	12.6	0.00	0.0
26	7	0.1	0.0	-0.2	0.0	20.70	4.1	0.00	0.0
26	8	-0.1	0.0	-0.2	0.0	46.30	17.8	0.00	0.0
26	9	0.0	0.0	-0.2	0.0	57.26	3.4	0.00	0.0
26	10	0.1	0.0	-0.1	0.0	-80.34	3.8	0.00	0.0
26	11	0.0	0.0	-0.1	0.0	88.41	0.8	0.00	0.0
26	12	0.0	0.0	-0.1	0.0	-82.61	1.5	0.00	0.0
26	13	0.0	0.0	0.0	0.0	-9.77	7.7	0.00	0.0
26	14	0.1	0.0	-0.1	0.0	-42.68	0.4	0.00	0.0
26	15	0.1	0.0	0.0	0.0	-66.94	1.0	0.00	0.0
26	16	0.0	0.0	-0.1	0.0	84.60	1.1	0.00	0.0
26	17	0.1	0.0	0.0	0.0	28.10	1.0	0.00	0.0
26	18	0.0	0.0	0.0	0.0	6.29	3.0	0.00	0.0
26	19	0.0	0.0	0.0	0.0	-76.10	1.3	0.00	0.0
26	20	0.0	0.0	-0.1	0.0	-89.40	1.1	0.00	0.0
26	21	0.1	0.0	0.0	0.0	62.96	1.0	0.00	0.0
26	22	0.1	0.0	0.0	0.0	69.84	0.7	0.00	0.0
26	23	0.1	0.0	-0.1	0.0	77.35	1.3	0.00	0.0
26	24	0.1	0.0	0.1	0.0	75.13	10.9	0.00	0.0
26	25	0.5	0.1	-0.6	0.1	50.83	4.9	-0.01	0.0

Epno	Trig	max deformation (10-7) E1	(10-7) sE1	min deformation (10-7) E2	(10-7) sE2	max direction (deg) teta	(deg) steta	rotation (sec) R	(sec) sR
27	1	0.1	0.0	-0.2	0.0	45.58	0.1	0.00	0.0
27	2	0.1	0.0	-0.1	0.0	48.72	1.1	0.00	0.0
27	3	0.1	0.0	-0.1	0.0	55.07	0.9	0.00	0.0
27	4	0.2	0.0	-0.1	0.0	60.72	0.9	0.00	0.0
27	5	0.0	0.0	-0.1	0.0	67.04	3.2	0.00	0.0
27	6	0.1	0.0	0.0	0.0	-23.29	12.6	0.00	0.0
27	7	0.1	0.0	-0.2	0.0	20.70	4.1	0.00	0.0
27	8	-0.1	0.0	-0.2	0.0	46.29	17.8	0.00	0.0
27	9	0.0	0.0	-0.2	0.0	57.26	3.4	0.00	0.0
27	10	0.1	0.0	-0.1	0.0	-80.33	3.8	0.00	0.0
27	11	0.0	0.0	-0.1	0.0	88.32	0.9	0.00	0.0
27	12	0.0	0.0	-0.1	0.0	-82.64	1.6	0.00	0.0
27	13	0.0	0.0	0.0	0.0	-9.81	7.9	0.00	0.0
27	14	0.1	0.0	-0.1	0.0	-42.69	0.4	0.00	0.0
27	15	0.1	0.0	0.0	0.0	-66.95	1.0	0.00	0.0
27	16	0.0	0.0	-0.1	0.0	84.58	1.2	0.00	0.0
27	17	0.1	0.0	0.0	0.0	27.99	1.1	0.00	0.0
27	18	0.0	0.0	0.0	0.0	6.04	3.3	0.00	0.0
27	19	0.0	0.0	0.0	0.0	-76.08	1.5	0.00	0.0
27	20	0.0	0.0	-0.1	0.0	-89.69	1.3	0.00	0.0
27	21	0.1	0.0	0.0	0.0	62.89	1.1	0.00	0.0
27	22	0.1	0.0	0.0	0.0	69.75	0.8	0.00	0.0
27	23	0.1	0.0	-0.1	0.0	77.32	1.3	0.00	0.0
27	24	0.1	0.0	0.1	0.0	75.16	10.9	0.00	0.0
27	25	0.5	0.1	-0.6	0.1	50.83	4.9	-0.01	0.0

Epno	Trig	max deformation (10-7) E1	(10-7) sE1	min deformation (10-7) E2	(10-7) sE2	max direction (deg) teta	(deg) steta	rotation (sec) R	(sec) sR
28	1	0.1	0.0	-0.2	0.0	45.57	0.1	0.00	0.0
28	2	0.1	0.0	-0.1	0.0	48.71	1.1	0.00	0.0
28	3	0.1	0.0	-0.1	0.0	55.06	0.9	0.00	0.0
28	4	0.2	0.0	-0.1	0.0	60.70	0.9	0.00	0.0
28	5	0.0	0.0	-0.1	0.0	67.04	3.3	0.00	0.0
28	6	0.1	0.0	0.0	0.0	-23.31	12.6	0.00	0.0
28	7	0.1	0.0	-0.2	0.0	20.70	4.1	0.00	0.0
28	8	-0.1	0.0	-0.2	0.0	46.29	17.8	0.00	0.0
28	9	0.0	0.0	-0.2	0.0	57.26	3.4	0.00	0.0
28	10	0.1	0.0	-0.1	0.0	-80.33	3.8	0.00	0.0
28	11	0.0	0.0	-0.1	0.0	88.27	0.9	0.00	0.0
28	12	0.0	0.0	-0.1	0.0	-82.63	1.6	0.00	0.0
28	13	0.0	0.0	0.0	0.0	-9.83	8.2	0.00	0.0
28	14	0.1	0.0	-0.1	0.0	-42.69	0.4	0.00	0.0
28	15	0.1	0.0	0.0	0.0	-66.95	1.0	0.00	0.0
28	16	0.0	0.0	-0.1	0.0	84.57	1.3	0.00	0.0
28	17	0.1	0.0	0.0	0.0	27.96	1.2	0.00	0.0
28	18	0.0	0.0	0.0	0.0	6.01	3.6	0.00	0.0
28	19	0.0	0.0	0.0	0.0	-75.98	1.8	0.00	0.0
28	20	0.0	0.0	-0.1	0.0	-89.82	1.5	0.00	0.0
28	21	0.1	0.0	0.0	0.0	62.89	1.2	0.00	0.0
28	22	0.1	0.0	0.0	0.0	69.67	0.8	0.00	0.0
28	23	0.1	0.0	-0.1	0.0	77.30	1.4	0.00	0.0
28	24	0.1	0.0	0.1	0.0	75.20	10.9	0.00	0.0
28	25	0.5	0.1	-0.6	0.1	50.82	4.9	-0.01	0.0

Strain Rates For Group Two

Epno	Trig	max deformation (10-7) E1	(10-7) sE1	min deformation (10-7) E2	(10-7) sE2	max direction (deg) teta	(deg) steta	rotation (sec) R	(sec) sR
3	7	0.1	0.0	-0.2	0.0	38.92	0.8	0.00	0.0
3	8	0.2	0.0	-0.2	0.0	60.00	0.6	0.00	0.0
3	13	0.1	0.0	0.1	0.0	-2.85	4.4	0.00	0.0

Epno	Trig	max deformation (10-7) E1	(10-7) sE1	min deformation (10-7) E2	(10-7) sE2	max direction (deg) teta	(deg) steta	rotation (sec) R	(sec) sR
4	7	0.1	0.0	-0.2	0.0	38.74	0.8	0.00	0.0
4	8	0.2	0.0	-0.2	0.0	59.81	0.6	0.00	0.0
4	13	0.1	0.0	0.1	0.0	-3.49	4.3	0.00	0.0

Epno	Trig	max deformation (10-7) E1	(10-7) sE1	min deformation (10-7) E2	(10-7) sE2	max direction (deg) teta	(deg) steta	rotation (sec) R	(sec) sR
5	7	0.1	0.0	-0.2	0.0	38.03	0.8	0.00	0.0
5	8	0.2	0.0	-0.2	0.0	59.49	0.6	0.00	0.0
5	13	0.1	0.0	0.1	0.0	-4.36	4.3	0.00	0.0

Epno	Trig	max deformation (10-7) E1	(10-7) sE1	min deformation (10-7) E2	(10-7) sE2	max direction (deg) teta	(deg) steta	rotation (sec) R	(sec) sR
6	7	0.1	0.0	-0.2	0.0	36.50	0.8	0.00	0.0
6	8	0.2	0.0	-0.2	0.0	58.99	0.6	0.00	0.0
6	13	0.1	0.0	0.1	0.0	-5.44	4.2	0.00	0.0

Epno	Trig	max deformation (10-7) E1	(10-7) sE1	min deformation (10-7) E2	(10-7) sE2	max direction (deg) teta	(deg) steta	rotation (sec) R	(sec) sR
7	7	0.1	0.0	-0.2	0.0	34.01	0.8	0.00	0.0
7	8	0.2	0.0	-0.2	0.0	58.26	0.6	0.00	0.0
7	13	0.1	0.0	0.1	0.0	-6.71	4.1	0.00	0.0

Epno	Trig	max deformation (10-7) E1	(10-7) sE1	min deformation (10-7) E2	(10-7) sE2	max direction (deg) teta	(deg) steta	rotation (sec) R	(sec) sR
8	7	0.1	0.0	-0.2	0.0	30.37	0.9	0.00	0.0
8	8	0.2	0.0	-0.2	0.0	57.18	0.7	0.00	0.0
8	13	0.1	0.0	0.1	0.0	-8.11	4.1	0.00	0.0

Epno	Trig	max deformation (10-7) E1	(10-7) sE1	min deformation (10-7) E2	(10-7) sE2	max direction (deg) teta	(deg) steta	rotation (sec) R	(sec) sR
9	7	0.1	0.0	-0.2	0.0	26.40	0.9	0.00	0.0
9	8	0.1	0.0	-0.2	0.0	55.81	0.7	0.00	0.0
9	13	0.1	0.0	0.1	0.0	-9.60	4.0	0.00	0.0

Epno	Trig	max deformation (10-7) E1	(10-7) sE1	min deformation (10-7) E2	(10-7) sE2	max direction (deg) teta	(deg) steta	rotation (sec) R	(sec) sR
10	7	0.1	0.0	-0.2	0.0	23.49	0.9	0.00	0.0
10	8	0.1	0.0	-0.2	0.0	54.49	0.8	0.00	0.0
10	13	0.1	0.0	0.1	0.0	-11.13	4.0	0.00	0.0

Epno	Trig	max deformation (10-7) E1	(10-7) sE1	min deformation (10-7) E2	(10-7) sE2	max direction (deg) teta	(deg) steta	rotation (sec) R	(sec) sR
11	7	0.1	0.0	-0.2	0.0	22.00	0.8	0.00	0.0
11	8	0.1	0.0	-0.2	0.0	53.53	0.8	0.00	0.0
11	13	0.1	0.0	0.1	0.0	-12.68	4.0	0.00	0.0

Epno	Trig	max deformation (10-7) E1	(10-7) sE1	min deformation (10-7) E2	(10-7) sE2	max direction (deg) teta	(deg) steta	rotation (sec) R	(sec) sR
12	4	0.1	0.0	-0.1	0.0	37.13	0.9	0.00	0.0
12	5	0.0	0.0	-0.2	0.0	10.65	0.6	0.00	0.0
12	6	0.0	0.0	0.0	0.0	-17.15	5.6	0.00	0.0

12	7	0.1	0.0	-0.2	0.0	21.47	0.8	0.00	0.0
12	8	0.1	0.0	-0.2	0.0	52.98	0.8	0.00	0.0
12	9	0.1	0.0	-0.1	0.0	50.62	1.2	0.00	0.0
12	10	0.1	0.0	0.0	0.0	-69.38	2.4	0.00	0.0
12	11	0.0	0.0	0.0	0.0	15.45	8.3	0.00	0.0
12	12	0.3	0.0	-0.2	0.0	40.29	0.5	-0.01	0.0
12	13	0.1	0.0	0.1	0.0	-14.21	4.0	0.00	0.0
12	14	0.1	0.0	0.0	0.0	-83.09	2.0	0.00	0.0
12	15	0.1	0.0	-0.3	0.0	-27.25	1.4	0.00	0.0
12	16	0.5	0.0	-0.1	0.0	-83.07	0.8	0.00	0.0
12	17	0.0	0.0	-0.1	0.0	88.88	3.9	0.00	0.0
12	18	1.0	0.0	-0.8	0.0	48.55	0.4	-0.02	0.0
12	19	0.3	0.0	-2.1	0.0	21.81	0.4	-0.02	0.0
12	20	0.0	0.0	-0.5	0.0	-2.31	0.9	0.00	0.0
12	21	0.7	0.0	-1.3	0.0	36.51	0.5	-0.02	0.0
12	22	0.0	0.0	-0.1	0.0	-58.89	2.8	0.00	0.0
12	23	0.1	0.0	-0.1	0.0	48.94	5.5	0.00	0.0

Epno	Trig	max deformation (10-7) E1	(10-7) sE1	min deformation (10-7) E2	(10-7) sE2	max direction (deg) teta	(deg) steta	rotation (sec) R	(sec) sR
13	4	0.1	0.0	-0.1	0.0	37.13	0.9	0.00	0.0
13	5	0.0	0.0	-0.2	0.0	10.68	0.6	0.00	0.0
13	6	0.0	0.0	0.0	0.0	-16.81	6.2	0.00	0.0
13	7	0.1	0.0	-0.2	0.0	21.30	0.8	0.00	0.0
13	8	0.1	0.0	-0.2	0.0	52.71	0.8	0.00	0.0
13	9	0.1	0.0	-0.1	0.0	50.49	1.2	0.00	0.0
13	10	0.1	0.0	0.0	0.0	-69.51	2.4	0.00	0.0
13	11	0.0	0.0	0.0	0.0	15.14	8.4	0.00	0.0
13	12	0.3	0.0	-0.2	0.0	40.40	0.5	-0.01	0.0
13	13	0.1	0.0	0.1	0.0	-15.71	4.0	0.00	0.0
13	14	0.1	0.0	0.0	0.0	-82.92	2.0	0.00	0.0
13	15	0.1	0.0	-0.3	0.0	-27.12	1.4	0.00	0.0
13	16	0.5	0.0	-0.1	0.0	-83.12	0.8	0.00	0.0
13	17	0.0	0.0	-0.1	0.0	88.38	3.9	0.00	0.0
13	18	1.0	0.0	-0.8	0.0	48.55	0.4	-0.02	0.0
13	19	0.3	0.0	-2.1	0.0	21.81	0.4	-0.02	0.0
13	20	0.0	0.0	-0.5	0.0	-2.31	0.9	0.00	0.0
13	21	0.7	0.0	-1.3	0.0	36.51	0.5	-0.02	0.0
13	22	0.0	0.0	-0.1	0.0	-58.88	2.8	0.00	0.0
13	23	0.1	0.0	-0.1	0.0	48.79	5.5	0.00	0.0

Epno	Trig	max deformation (10-7) E1	(10-7) sE1	min deformation (10-7) E2	(10-7) sE2	max direction (deg) teta	(deg) steta	rotation (sec) R	(sec) sR
14	4	0.1	0.0	-0.1	0.0	37.14	0.9	0.00	0.0
14	5	0.0	0.0	-0.2	0.0	10.62	0.6	0.00	0.0
14	6	0.0	0.0	0.0	0.0	-17.14	7.0	0.00	0.0
14	7	0.1	0.0	-0.2	0.0	21.28	0.8	0.00	0.0
14	8	0.1	0.0	-0.2	0.0	52.58	0.8	0.00	0.0
14	9	0.1	0.0	-0.1	0.0	50.36	1.2	0.00	0.0
14	10	0.1	0.0	0.0	0.0	-69.65	2.3	0.00	0.0
14	11	0.0	0.0	0.0	0.0	14.82	8.6	0.00	0.0
14	12	0.3	0.0	-0.2	0.0	40.51	0.5	-0.01	0.0
14	13	0.1	0.0	0.1	0.0	-17.04	4.0	0.00	0.0
14	14	0.1	0.0	0.0	0.0	-82.77	2.1	0.00	0.0
14	15	0.1	0.0	-0.3	0.0	-27.00	1.4	0.00	0.0
14	16	0.5	0.0	-0.1	0.0	-83.16	0.8	0.00	0.0
14	17	0.0	0.0	-0.1	0.0	87.92	3.9	0.00	0.0
14	18	1.0	0.0	-0.8	0.0	48.55	0.4	-0.02	0.0
14	19	0.3	0.0	-2.1	0.0	21.81	0.4	-0.02	0.0
14	20	0.0	0.0	-0.5	0.0	-2.32	0.9	0.00	0.0
14	21	0.7	0.0	-1.3	0.0	36.51	0.5	-0.02	0.0
14	22	0.0	0.0	-0.1	0.0	-58.86	2.8	0.00	0.0
14	23	0.1	0.0	-0.1	0.0	48.66	5.4	0.00	0.0

Epno	Trig	max deformation (10-7) E1	(10-7) sE1	min deformation (10-7) E2	(10-7) sE2	max direction (deg) teta	(deg) steta	rotation (sec) R	(sec) sR

15	4	0.1	0.0	-0.1	0.0	37.14	0.9	0.00	0.0
15	5	0.0	0.0	-0.2	0.0	10.57	0.6	0.00	0.0
15	6	0.0	0.0	0.0	0.0	-17.83	8.1	0.00	0.0
15	7	0.1	0.0	-0.2	0.0	21.25	0.8	0.00	0.0
15	8	0.1	0.0	-0.2	0.0	52.47	0.8	0.00	0.0
15	9	0.1	0.0	-0.1	0.0	50.21	1.2	0.00	0.0
15	10	0.1	0.0	0.0	0.0	-69.79	2.3	0.00	0.0
15	11	0.0	0.0	0.0	0.0	14.45	8.7	0.00	0.0
15	12	0.3	0.0	-0.2	0.0	40.64	0.5	-0.01	0.0
15	13	0.1	0.0	0.1	0.0	-18.36	4.0	0.00	0.0
15	14	0.1	0.0	0.0	0.0	-82.61	2.1	0.00	0.0
15	15	0.1	0.0	-0.3	0.0	-26.88	1.4	0.00	0.0
15	16	0.5	0.0	-0.1	0.0	-83.21	0.8	0.00	0.0
15	17	0.0	0.0	-0.1	0.0	87.47	3.9	0.00	0.0
15	18	1.0	0.0	-0.8	0.0	48.55	0.4	-0.02	0.0
15	19	0.3	0.0	-2.1	0.0	21.81	0.4	-0.02	0.0
15	20	0.0	0.0	-0.5	0.0	-2.32	0.9	0.00	0.0
15	21	0.7	0.0	-1.3	0.0	36.51	0.5	-0.02	0.0
15	22	0.0	0.0	0.0	0.0	-58.85	2.8	0.00	0.0
15	23	0.1	0.0	-0.1	0.0	48.56	5.4	0.00	0.0

Epno	Trig	max deformation (10-7) E1	(10-7) sE1	min deformation (10-7) E2	(10-7) sE2	max direction (deg) teta	(deg) steta	rotation (sec) R	(sec) sR
16	1	0.4	0.0	-0.1	0.0	-85.36	1.1	0.00	0.0
16	2	0.2	0.0	-0.1	0.0	61.00	2.0	0.00	0.0
16	3	0.1	0.0	-0.1	0.0	43.03	1.6	0.00	0.0
16	4	0.1	0.0	-0.1	0.0	37.15	0.9	0.00	0.0
16	5	0.0	0.0	-0.2	0.0	10.56	0.6	0.00	0.0
16	6	0.0	0.0	0.0	0.0	-18.76	9.1	0.00	0.0
16	7	0.1	0.0	-0.2	0.0	21.10	0.9	0.00	0.0
16	8	0.1	0.0	-0.2	0.0	52.34	0.8	0.00	0.0
16	9	0.1	0.0	-0.1	0.0	50.06	1.2	0.00	0.0
16	10	0.1	0.0	0.0	0.0	-69.94	2.4	0.00	0.0
16	11	0.0	0.0	0.0	0.0	14.07	8.8	0.00	0.0
16	12	0.3	0.0	-0.2	0.0	40.76	0.5	-0.01	0.0
16	13	0.1	0.0	0.1	0.0	-19.58	4.1	0.00	0.0
16	14	0.1	0.0	0.0	0.0	-82.47	2.1	0.00	0.0
16	15	0.1	0.0	-0.3	0.0	-26.77	1.4	0.00	0.0
16	16	0.5	0.0	-0.1	0.0	-83.25	0.8	0.00	0.0
16	17	0.0	0.0	-0.1	0.0	87.04	3.9	0.00	0.0
16	18	1.0	0.0	-0.8	0.0	48.55	0.4	-0.02	0.0
16	19	0.3	0.0	-2.1	0.0	21.80	0.4	-0.02	0.0
16	20	0.0	0.0	-0.5	0.0	-2.32	0.9	0.00	0.0
16	21	0.7	0.0	-1.3	0.0	36.51	0.5	-0.02	0.0
16	22	0.0	0.0	0.0	0.0	-58.83	2.8	0.00	0.0
16	23	0.1	0.0	-0.1	0.0	48.46	5.4	0.00	0.0

Epno	Trig	max deformation (10-7) E1	(10-7) sE1	min deformation (10-7) E2	(10-7) sE2	max direction (deg) teta	(deg) steta	rotation (sec) R	(sec) sR
17	1	0.4	0.0	-0.1	0.0	-85.36	1.1	0.00	0.0
17	2	0.2	0.0	-0.1	0.0	61.00	2.0	0.00	0.0
17	3	0.1	0.0	-0.1	0.0	43.04	1.6	0.00	0.0
17	4	0.1	0.0	-0.1	0.0	37.15	0.9	0.00	0.0
17	5	0.0	0.0	-0.2	0.0	10.56	0.6	0.00	0.0
17	6	0.0	0.0	0.0	0.0	-20.00	10.2	0.00	0.0
17	7	0.1	0.0	-0.2	0.0	20.92	0.9	0.00	0.0
17	8	0.1	0.0	-0.2	0.0	52.24	0.8	0.00	0.0
17	9	0.1	0.0	-0.1	0.0	49.92	1.2	0.00	0.0
17	10	0.1	0.0	0.0	0.0	-70.08	2.4	0.00	0.0
17	11	0.0	0.0	0.0	0.0	13.70	9.0	0.00	0.0
17	12	0.3	0.0	-0.2	0.0	40.89	0.5	-0.01	0.0
17	13	0.1	0.0	0.1	0.0	-20.68	4.1	0.00	0.0
17	14	0.1	0.0	0.0	0.0	-82.34	2.1	0.00	0.0
17	15	0.1	0.0	-0.3	0.0	-26.66	1.4	0.00	0.0
17	16	0.5	0.0	-0.1	0.0	-83.29	0.8	0.00	0.0
17	17	0.0	0.0	-0.1	0.0	86.66	3.9	0.00	0.0
17	18	1.0	0.0	-0.8	0.0	48.55	0.4	-0.02	0.0
17	19	0.3	0.0	-2.1	0.0	21.80	0.4	-0.02	0.0

17	20	0.0	0.0	-0.5	0.0	-2.33	0.9	0.00	0.0
17	21	0.7	0.0	-1.3	0.0	36.50	0.5	-0.02	0.0
17	22	0.0	0.0	0.0	0.0	-58.83	2.8	0.00	0.0
17	23	0.1	0.0	-0.1	0.0	48.40	5.4	0.00	0.0

Epno	Trig	max deformation (10-7) E1	(10-7) sE1	min deformation (10-7) E2	(10-7) sE2	max direction (deg) teta	(deg) steta	rotation (sec) R	(sec) sR
18	1	0.4	0.0	-0.1	0.0	-85.36	1.1	0.00	0.0
18	2	0.2	0.0	-0.1	0.0	61.01	2.0	0.00	0.0
18	3	0.1	0.0	-0.1	0.0	43.04	1.6	0.00	0.0
18	4	0.1	0.0	-0.1	0.0	37.16	0.9	0.00	0.0
18	5	0.0	0.0	-0.2	0.0	10.55	0.6	0.00	0.0
18	6	0.0	0.0	0.0	0.0	-21.54	11.3	0.00	0.0
18	7	0.1	0.0	-0.2	0.0	20.79	0.9	0.00	0.0
18	8	0.1	0.0	-0.2	0.0	52.16	0.8	0.00	0.0
18	9	0.1	0.0	-0.1	0.0	49.79	1.2	0.00	0.0
18	10	0.1	0.0	0.0	0.0	-70.21	2.4	0.00	0.0
18	11	0.0	0.0	0.0	0.0	13.32	9.1	0.00	0.0
18	12	0.3	0.0	-0.2	0.0	41.01	0.5	-0.01	0.0
18	13	0.1	0.0	0.1	0.0	-21.66	4.2	0.00	0.0
18	14	0.1	0.0	0.0	0.0	-82.24	2.1	0.00	0.0
18	15	0.1	0.0	-0.3	0.0	-26.55	1.4	0.00	0.0
18	16	0.5	0.0	-0.1	0.0	-83.32	0.8	0.00	0.0
18	17	0.0	0.0	-0.1	0.0	86.32	3.9	0.00	0.0
18	18	1.0	0.0	-0.8	0.0	48.55	0.4	-0.02	0.0
18	19	0.3	0.0	-2.1	0.0	21.80	0.3	-0.02	0.0
18	20	0.0	0.0	-0.5	0.0	-2.33	0.9	0.00	0.0
18	21	0.7	0.0	-1.3	0.0	36.50	0.5	-0.02	0.0
18	22	0.0	0.0	0.0	0.0	-58.83	2.8	0.00	0.0
18	23	0.1	0.0	-0.1	0.0	48.35	5.4	0.00	0.0

Epno	Trig	max deformation (10-7) E1	(10-7) sE1	min deformation (10-7) E2	(10-7) sE2	max direction (deg) teta	(deg) steta	rotation (sec) R	(sec) sR
19	1	0.4	0.0	-0.1	0.0	-85.36	1.1	0.00	0.0
19	2	0.2	0.0	-0.1	0.0	61.01	2.0	0.00	0.0
19	3	0.1	0.0	-0.1	0.0	43.05	1.6	0.00	0.0
19	4	0.1	0.0	-0.1	0.0	37.16	0.9	0.00	0.0
19	5	0.0	0.0	-0.2	0.0	10.53	0.6	0.00	0.0
19	6	0.0	0.0	0.0	0.0	-23.41	12.7	0.00	0.0
19	7	0.1	0.0	-0.2	0.0	20.69	0.9	0.00	0.0
19	8	0.1	0.0	-0.2	0.0	52.11	0.8	0.00	0.0
19	9	0.1	0.0	-0.1	0.0	49.67	1.3	0.00	0.0
19	10	0.1	0.0	0.0	0.0	-70.33	2.4	0.00	0.0
19	11	0.0	0.0	0.0	0.0	13.01	9.3	0.00	0.0
19	12	0.3	0.0	-0.2	0.0	41.13	0.5	-0.01	0.0
19	13	0.1	0.0	0.1	0.0	-22.53	4.3	0.00	0.0
19	14	0.1	0.0	0.0	0.0	-82.14	2.1	0.00	0.0
19	15	0.1	0.0	-0.3	0.0	-26.46	1.4	0.00	0.0
19	16	0.5	0.0	-0.1	0.0	-83.35	0.8	0.00	0.0
19	17	0.0	0.0	-0.1	0.0	86.01	3.9	0.00	0.0
19	18	1.0	0.0	-0.8	0.0	48.55	0.4	-0.02	0.0
19	19	0.3	0.0	-2.1	0.0	21.80	0.3	-0.02	0.0
19	20	0.0	0.0	-0.5	0.0	-2.34	0.9	0.00	0.0
19	21	0.7	0.0	-1.3	0.0	36.50	0.5	-0.02	0.0
19	22	0.0	0.0	0.0	0.0	-58.84	2.8	0.00	0.0
19	23	0.1	0.0	-0.1	0.0	48.31	5.4	0.00	0.0

Epno	Trig	max deformation (10-7) E1	(10-7) sE1	min deformation (10-7) E2	(10-7) sE2	max direction (deg) teta	(deg) steta	rotation (sec) R	(sec) sR
20	1	0.4	0.0	-0.1	0.0	-85.36	1.1	0.00	0.0
20	2	0.2	0.0	-0.1	0.0	61.02	2.0	0.00	0.0
20	3	0.1	0.0	-0.1	0.0	43.06	1.6	0.00	0.0
20	4	0.1	0.0	-0.1	0.0	37.16	0.9	0.00	0.0
20	5	0.0	0.0	-0.2	0.0	10.51	0.6	0.00	0.0
20	6	0.0	0.0	0.0	0.0	-25.55	14.3	0.00	0.0
20	7	0.1	0.0	-0.2	0.0	20.64	0.9	0.00	0.0

20	8	0.1	0.0	-0.2	0.0	52.09	0.8	0.00	0.0
20	9	0.1	0.0	-0.1	0.0	49.56	1.3	0.00	0.0
20	10	0.1	0.0	0.0	0.0	-70.44	2.4	0.00	0.0
20	11	0.0	0.0	0.0	0.0	12.70	9.4	0.00	0.0
20	12	0.3	0.0	-0.2	0.0	41.22	0.5	-0.01	0.0
20	13	0.1	0.0	0.1	0.0	-23.29	4.4	0.00	0.0
20	14	0.1	0.0	0.0	0.0	-82.08	2.2	0.00	0.0
20	15	0.1	0.0	-0.3	0.0	-26.36	1.4	0.00	0.0
20	16	0.5	0.0	-0.1	0.0	-83.37	0.8	0.00	0.0
20	17	0.0	0.0	-0.1	0.0	85.74	3.9	0.00	0.0
20	18	1.0	0.0	-0.8	0.0	48.54	0.4	-0.02	0.0
20	19	0.3	0.0	-2.1	0.0	21.80	0.3	-0.02	0.0
20	20	0.0	0.0	-0.5	0.0	-2.34	0.9	0.00	0.0
20	21	0.7	0.0	-1.3	0.0	36.50	0.5	-0.02	0.0
20	22	0.0	0.0	0.0	0.0	-58.85	2.9	0.00	0.0
20	23	0.1	0.0	-0.1	0.0	48.26	5.5	0.00	0.0

Epno	Trig	max deformation (10-7) E1	(10-7) sE1	min deformation (10-7) E2	(10-7) sE2	max direction (deg) teta	(deg) steta	rotation (sec) R	(sec) sR
21	1	0.4	0.0	-0.1	0.0	-85.35	1.1	0.00	0.0
21	2	0.2	0.0	-0.1	0.0	61.03	2.0	0.00	0.0
21	3	0.1	0.0	-0.1	0.0	43.07	1.6	0.00	0.0
21	4	0.1	0.0	-0.1	0.0	37.16	0.9	0.00	0.0
21	5	0.0	0.0	-0.2	0.0	10.50	0.6	0.00	0.0
21	6	0.0	0.0	0.0	0.0	-27.45	15.7	0.00	0.0
21	7	0.1	0.0	-0.2	0.0	20.56	1.0	0.00	0.0
21	8	0.1	0.0	-0.2	0.0	52.05	0.8	0.00	0.0
21	9	0.1	0.0	-0.1	0.0	49.47	1.3	0.00	0.0
21	10	0.1	0.0	0.0	0.0	-70.53	2.4	0.00	0.0
21	11	0.0	0.0	0.0	0.0	12.46	9.6	0.00	0.0
21	12	0.3	0.0	-0.2	0.0	41.28	0.5	-0.01	0.0
21	13	0.1	0.0	0.1	0.0	-23.94	4.5	0.00	0.0
21	14	0.1	0.0	0.0	0.0	-82.01	2.2	0.00	0.0
21	15	0.1	0.0	-0.3	0.0	-26.28	1.4	0.00	0.0
21	16	0.5	0.0	-0.1	0.0	-83.39	0.8	0.00	0.0
21	17	0.0	0.0	-0.1	0.0	85.52	3.9	0.00	0.0
21	18	1.0	0.0	-0.8	0.0	48.54	0.4	-0.02	0.0
21	19	0.3	0.0	-2.1	0.0	21.79	0.3	-0.02	0.0
21	20	0.0	0.0	-0.5	0.0	-2.35	0.9	0.00	0.0
21	21	0.7	0.0	-1.3	0.0	36.49	0.5	-0.02	0.0
21	22	0.0	0.0	0.0	0.0	-58.87	2.9	0.00	0.0
21	23	0.1	0.0	-0.1	0.0	48.23	5.5	0.00	0.0

Epno	Trig	max deformation (10-7) E1	(10-7) sE1	min deformation (10-7) E2	(10-7) sE2	max direction (deg) teta	(deg) steta	rotation (sec) R	(sec) sR
22	1	0.4	0.0	-0.1	0.0	-85.34	1.1	0.00	0.0
22	2	0.2	0.0	-0.1	0.0	61.05	2.0	0.00	0.0
22	3	0.1	0.0	-0.1	0.0	43.08	1.6	0.00	0.0
22	4	0.1	0.0	-0.1	0.0	37.17	0.9	0.00	0.0
22	5	0.0	0.0	-0.2	0.0	10.49	0.6	0.00	0.0
22	6	0.0	0.0	0.0	0.0	-29.29	17.4	0.00	0.0
22	7	0.1	0.0	-0.2	0.0	20.52	1.0	0.00	0.0
22	8	0.1	0.0	-0.2	0.0	52.03	0.8	0.00	0.0
22	9	0.1	0.0	-0.1	0.0	49.40	1.3	0.00	0.0
22	10	0.1	0.0	0.0	0.0	-70.61	2.5	0.00	0.0
22	11	0.0	0.0	0.0	0.0	12.26	9.8	0.00	0.0
22	12	0.3	0.0	-0.2	0.0	41.31	0.5	-0.01	0.0
22	13	0.1	0.0	0.1	0.0	-24.47	4.6	0.00	0.0
22	14	0.1	0.0	0.0	0.0	-81.97	2.2	0.00	0.0
22	15	0.1	0.0	-0.3	0.0	-26.20	1.4	0.00	0.0
22	16	0.5	0.0	-0.1	0.0	-83.40	0.8	0.00	0.0
22	17	0.0	0.0	-0.1	0.0	85.33	3.9	0.00	0.0
22	18	1.0	0.0	-0.8	0.0	48.54	0.4	-0.02	0.0
22	19	0.3	0.0	-2.1	0.0	21.79	0.3	-0.02	0.0
22	20	0.0	0.0	-0.5	0.0	-2.36	0.9	0.00	0.0
22	21	0.7	0.0	-1.3	0.0	36.49	0.5	-0.02	0.0
22	22	0.0	0.0	0.0	0.0	-58.88	2.9	0.00	0.0
22	23	0.1	0.0	-0.1	0.0	48.19	5.5	0.00	0.0

Epno	Trig	max deformation (10-7) E1	(10-7) sE1	min deformation (10-7) E2	(10-7) sE2	max direction (deg) teta	(deg) steta	rotation (sec) R	(sec) sR
23	1	0.4	0.0	-0.1	0.0	-85.33	1.1	0.00	0.0
23	2	0.2	0.0	-0.1	0.0	61.07	2.0	0.00	0.0
23	3	0.1	0.0	-0.1	0.0	43.10	1.6	0.00	0.0
23	4	0.1	0.0	-0.1	0.0	37.17	0.9	0.00	0.0
23	5	0.0	0.0	-0.2	0.0	10.48	0.6	0.00	0.0
23	6	0.0	0.0	0.0	0.0	-31.10	19.2	0.00	0.0
23	7	0.1	0.0	-0.2	0.0	20.52	1.0	0.00	0.0
23	8	0.1	0.0	-0.2	0.0	52.02	0.9	0.00	0.0
23	9	0.1	0.0	-0.1	0.0	49.34	1.3	0.00	0.0
23	10	0.1	0.0	0.0	0.0	-70.67	2.5	0.00	0.0
23	11	0.0	0.0	0.0	0.0	12.12	9.9	0.00	0.0
23	12	0.3	0.0	-0.2	0.0	41.33	0.5	-0.01	0.0
23	13	0.1	0.0	0.1	0.0	-24.90	4.7	0.00	0.0
23	14	0.1	0.0	0.0	0.0	-81.94	2.2	0.00	0.0
23	15	0.1	0.0	-0.3	0.0	-26.13	1.4	0.00	0.0
23	16	0.5	0.0	-0.1	0.0	-83.40	0.8	0.00	0.0
23	17	0.0	0.0	-0.1	0.0	85.17	4.0	0.00	0.0
23	18	1.0	0.0	-0.8	0.0	48.54	0.4	-0.02	0.0
23	19	0.3	0.0	-2.1	0.0	21.79	0.3	-0.02	0.0
23	20	0.0	0.0	-0.5	0.0	-2.37	0.9	0.00	0.0
23	21	0.7	0.0	-1.3	0.0	36.49	0.5	-0.02	0.0
23	22	0.0	0.0	0.0	0.0	-58.90	2.9	0.00	0.0
23	23	0.1	0.0	-0.1	0.0	48.16	5.6	0.00	0.0

Epno	Trig	max deformation (10-7) E1	(10-7) sE1	min deformation (10-7) E2	(10-7) sE2	max direction (deg) teta	(deg) steta	rotation (sec) R	(sec) sR
24	1	0.4	0.0	-0.1	0.0	-85.32	1.1	0.00	0.0
24	2	0.2	0.0	-0.1	0.0	61.09	2.0	0.00	0.0
24	3	0.1	0.0	-0.1	0.0	43.12	1.6	0.00	0.0
24	4	0.1	0.0	-0.1	0.0	37.17	0.9	0.00	0.0
24	5	0.0	0.0	-0.2	0.0	10.47	0.6	0.00	0.0
24	6	0.0	0.0	0.0	0.0	-32.54	20.8	0.00	0.0
24	7	0.1	0.0	-0.2	0.0	20.51	1.1	0.00	0.0
24	8	0.1	0.0	-0.2	0.0	52.00	0.9	0.00	0.0
24	9	0.1	0.0	-0.1	0.0	49.30	1.3	0.00	0.0
24	10	0.1	0.0	0.0	0.0	-70.72	2.5	0.00	0.0
24	11	0.0	0.0	0.0	0.0	12.05	10.1	0.00	0.0
24	12	0.3	0.0	-0.2	0.0	41.33	0.5	-0.01	0.0
24	13	0.1	0.0	0.1	0.0	-25.22	4.9	0.00	0.0
24	14	0.1	0.0	0.0	0.0	-81.91	2.2	0.00	0.0
24	15	0.1	0.0	-0.3	0.0	-26.06	1.4	0.00	0.0
24	16	0.5	0.0	-0.1	0.0	-83.41	0.8	0.00	0.0
24	17	0.0	0.0	-0.1	0.0	85.05	4.0	0.00	0.0
24	18	1.0	0.0	-0.8	0.0	48.54	0.4	-0.02	0.0
24	19	0.3	0.0	-2.1	0.0	21.79	0.3	-0.02	0.0
24	20	0.0	0.0	-0.5	0.0	-2.38	0.9	0.00	0.0
24	21	0.7	0.0	-1.3	0.0	36.48	0.5	-0.02	0.0
24	22	0.0	0.0	0.0	0.0	-58.91	2.9	0.00	0.0
24	23	0.1	0.0	-0.1	0.0	48.14	5.6	0.00	0.0

Epno	Trig	max deformation (10-7) E1	(10-7) sE1	min deformation (10-7) E2	(10-7) sE2	max direction (deg) teta	(deg) steta	rotation (sec) R	(sec) sR
25	1	0.4	0.0	-0.1	0.0	-85.31	1.1	0.00	0.0
25	2	0.2	0.0	-0.1	0.0	61.11	2.0	0.00	0.0
25	3	0.1	0.0	-0.1	0.0	43.14	1.6	0.00	0.0
25	4	0.1	0.0	-0.1	0.0	37.18	0.9	0.00	0.0
25	5	0.0	0.0	-0.2	0.0	10.47	0.7	0.00	0.0
25	6	0.0	0.0	0.0	0.0	-33.73	22.1	0.00	0.0
25	7	0.1	0.0	-0.2	0.0	20.51	1.1	0.00	0.0
25	8	0.1	0.0	-0.2	0.0	51.99	0.9	0.00	0.0
25	9	0.1	0.0	-0.1	0.0	49.27	1.4	0.00	0.0
25	10	0.1	0.0	0.0	0.0	-70.76	2.6	0.00	0.0
25	11	0.0	0.0	0.0	0.0	11.99	10.2	0.00	0.0

25	12	0.3	0.0	-0.2	0.0	41.33	0.5	-0.01	0.0
25	13	0.1	0.0	0.1	0.0	-25.47	5.0	0.00	0.0
25	14	0.1	0.0	0.0	0.0	-81.91	2.3	0.00	0.0
25	15	0.1	0.0	-0.3	0.0	-26.00	1.4	0.00	0.0
25	16	0.5	0.0	-0.1	0.0	-83.41	0.8	0.00	0.0
25	17	0.0	0.0	-0.1	0.0	84.96	4.0	0.00	0.0
25	18	1.0	0.0	-0.8	0.0	48.54	0.4	-0.02	0.0
25	19	0.3	0.0	-2.1	0.0	21.78	0.3	-0.02	0.0
25	20	0.0	0.0	-0.5	0.0	-2.39	0.9	0.00	0.0
25	21	0.7	0.0	-1.3	0.0	36.48	0.5	-0.02	0.0
25	22	0.0	0.0	0.0	0.0	-58.93	3.0	0.00	0.0
25	23	0.1	0.0	-0.1	0.0	48.11	5.7	0.00	0.0

Epno	Trig	max deformation (10-7) E1	(10-7) sE1	min deformation (10-7) E2	(10-7) sE2	max direction (deg) teta	(deg) steta	rotation (sec) R	(sec) sR
26	1	0.4	0.0	-0.1	0.0	-85.29	1.1	0.00	0.0
26	2	0.2	0.0	-0.1	0.0	61.13	2.0	0.00	0.0
26	3	0.1	0.0	-0.1	0.0	43.16	1.6	0.00	0.0
26	4	0.1	0.0	-0.1	0.0	37.18	0.9	0.00	0.0
26	5	0.0	0.0	-0.2	0.0	10.47	0.7	0.00	0.0
26	6	0.0	0.0	0.0	0.0	-34.53	23.2	0.00	0.0
26	7	0.1	0.0	-0.2	0.0	20.51	1.1	0.00	0.0
26	8	0.1	0.0	-0.2	0.0	51.99	0.9	0.00	0.0
26	9	0.1	0.0	-0.1	0.0	49.26	1.4	0.00	0.0
26	10	0.1	0.0	0.0	0.0	-70.79	2.6	0.00	0.0
26	11	0.0	0.0	0.0	0.0	11.98	10.4	0.00	0.0
26	12	0.3	0.0	-0.2	0.0	41.33	0.5	-0.01	0.0
26	13	0.1	0.0	0.1	0.0	-25.61	5.1	0.00	0.0
26	14	0.1	0.0	0.0	0.0	-81.91	2.3	0.00	0.0
26	15	0.1	0.0	-0.3	0.0	-25.96	1.4	0.00	0.0
26	16	0.5	0.0	-0.1	0.0	-83.40	0.8	0.00	0.0
26	17	0.0	0.0	-0.1	0.0	84.91	4.0	0.00	0.0
26	18	1.0	0.0	-0.8	0.0	48.54	0.4	-0.02	0.0
26	19	0.3	0.0	-2.1	0.0	21.78	0.4	-0.02	0.0
26	20	0.0	0.0	-0.5	0.0	-2.40	0.9	0.00	0.0
26	21	0.7	0.0	-1.3	0.0	36.48	0.5	-0.02	0.0
26	22	0.0	0.0	0.0	0.0	-58.95	3.0	0.00	0.0
26	23	0.1	0.0	-0.1	0.0	48.10	5.7	0.00	0.0

Epno	Trig	max deformation (10-7) E1	(10-7) sE1	min deformation (10-7) E2	(10-7) sE2	max direction (deg) teta	(deg) steta	rotation (sec) R	(sec) sR
27	1	0.4	0.0	-0.1	0.0	-85.28	1.1	0.00	0.0
27	2	0.2	0.0	-0.1	0.0	61.14	2.0	0.00	0.0
27	3	0.1	0.0	-0.1	0.0	43.17	1.6	0.00	0.0
27	4	0.1	0.0	-0.1	0.0	37.18	0.9	0.00	0.0
27	5	0.0	0.0	-0.2	0.0	10.47	0.7	0.00	0.0
27	6	0.0	0.0	0.0	0.0	-34.90	23.7	0.00	0.0
27	7	0.1	0.0	-0.2	0.0	20.49	1.1	0.00	0.0
27	8	0.1	0.0	-0.2	0.0	51.99	0.9	0.00	0.0
27	9	0.1	0.0	-0.1	0.0	49.25	1.4	0.00	0.0
27	10	0.1	0.0	0.0	0.0	-70.81	2.6	0.00	0.0
27	11	0.0	0.0	0.0	0.0	11.99	10.5	0.00	0.0
27	12	0.3	0.0	-0.2	0.0	41.32	0.5	-0.01	0.0
27	13	0.1	0.0	0.1	0.0	-25.71	5.2	0.00	0.0
27	14	0.1	0.0	0.0	0.0	-81.92	2.3	0.00	0.0
27	15	0.1	0.0	-0.3	0.0	-25.92	1.4	0.00	0.0
27	16	0.5	0.0	-0.1	0.0	-83.40	0.8	0.00	0.0
27	17	0.0	0.0	-0.1	0.0	84.88	4.0	0.00	0.0
27	18	1.0	0.0	-0.8	0.0	48.54	0.4	-0.02	0.0
27	19	0.3	0.0	-2.1	0.0	21.78	0.4	-0.02	0.0
27	20	0.0	0.0	-0.5	0.0	-2.42	0.9	0.00	0.0
27	21	0.7	0.0	-1.3	0.0	36.48	0.5	-0.02	0.0
27	22	0.0	0.0	0.0	0.0	-58.97	3.0	0.00	0.0
27	23	0.1	0.0	-0.1	0.0	48.09	5.8	0.00	0.0

Epno	Trig	max deformation (10-7) E1	(10-7) sE1	min deformation (10-7) E2	(10-7) sE2	max direction (deg) teta	(deg) steta	rotation (sec) R	(sec) sR

28	1	0.4	0.0	-0.1	0.0	-85.28	1.1	0.00	0.0
28	2	0.2	0.0	-0.1	0.0	61.15	2.1	0.00	0.0
28	3	0.1	0.0	-0.1	0.0	43.18	1.6	0.00	0.0
28	4	0.1	0.0	-0.1	0.0	37.18	0.9	0.00	0.0
28	5	0.0	0.0	-0.2	0.0	10.47	0.7	0.00	0.0
28	6	0.0	0.0	0.0	0.0	-35.03	24.2	0.00	0.0
28	7	0.1	0.0	-0.2	0.0	20.49	1.2	0.00	0.0
28	8	0.1	0.0	-0.2	0.0	51.99	1.0	0.00	0.0
28	9	0.1	0.0	-0.1	0.0	49.25	1.4	0.00	0.0
28	10	0.1	0.0	0.0	0.0	-70.81	2.7	0.00	0.0
28	11	0.0	0.0	0.0	0.0	11.99	10.6	0.00	0.0
28	12	0.3	0.0	-0.2	0.0	41.32	0.6	-0.01	0.0
28	13	0.1	0.0	0.1	0.0	-25.73	5.4	0.00	0.0
28	14	0.1	0.0	0.0	0.0	-81.92	2.3	0.00	0.0
28	15	0.1	0.0	-0.3	0.0	-25.89	1.4	0.00	0.0
28	16	0.5	0.0	-0.1	0.0	-83.39	0.8	0.00	0.0
28	17	0.0	0.0	-0.1	0.0	84.86	4.0	0.00	0.0
28	18	1.0	0.0	-0.8	0.0	48.54	0.4	-0.02	0.0
28	19	0.3	0.0	-2.1	0.0	21.78	0.4	-0.02	0.0
28	20	0.0	0.0	-0.5	0.0	-2.43	0.9	0.00	0.0
28	21	0.7	0.0	-1.3	0.0	36.47	0.5	-0.02	0.0
28	22	0.0	0.0	0.0	0.0	-58.99	3.1	0.00	0.0
28	23	0.1	0.0	-0.1	0.0	48.08	5.9	0.00	0.0

Strain Rates For Group Three

Epno	Trig	max deformation (10-7) E1	max deformation (10-7) sE1	min deformation (10-7) E2	min deformation (10-7) sE2	max direction (deg) teta	max direction (deg) steta	rotation (sec) R	rotation (sec) sR
4	10	0.1	0.0	0.0	0.0	31.58	2.8	0.00	0.0
5	10	0.1	0.0	0.0	0.0	31.55	2.7	0.00	0.0
6	10	0.1	0.0	0.0	0.0	31.53	2.7	0.00	0.0
7	10	0.1	0.0	0.0	0.0	31.53	2.6	0.00	0.0
8	10	0.1	0.0	0.0	0.0	31.56	2.6	0.00	0.0
9	10	0.1	0.0	0.0	0.0	31.61	2.6	0.00	0.0
10	10	0.1	0.0	0.0	0.0	31.69	2.5	0.00	0.0

11	10	0.1	0.0	0.0	0.0	31.80	2.5	0.00	0.0

Epno	Trig	max deformation (10-7) E1	(10-7) sE1	min deformation (10-7) E2	(10-7) sE2	max direction (deg) teta	(deg) steta	rotation (sec) R	(sec) sR
12	5	0.0	0.0	-0.1	0.0	-8.06	5.9	0.00	0.0
12	6	0.3	0.0	-0.2	0.0	54.67	1.2	0.00	0.0
12	7	0.3	0.0	-0.1	0.0	56.15	1.1	0.00	0.0
12	8	-0.1	0.0	-0.1	0.0	-20.13	13.7	0.00	0.0
12	9	0.0	0.0	-0.1	0.0	49.27	4.8	0.00	0.0
12	10	0.1	0.0	0.0	0.0	31.93	2.5	0.00	0.0

Epno	Trig	max deformation (10-7) E1	(10-7) sE1	min deformation (10-7) E2	(10-7) sE2	max direction (deg) teta	(deg) steta	rotation (sec) R	(sec) sR
13	5	0.0	0.0	-0.1	0.0	-7.93	5.3	0.00	0.0
13	6	0.3	0.0	-0.2	0.0	54.28	1.2	0.00	0.0
13	7	0.3	0.0	-0.2	0.0	56.28	1.1	-0.01	0.0
13	8	-0.1	0.0	-0.1	0.0	-18.52	11.6	0.00	0.0
13	9	0.0	0.0	-0.1	0.0	49.36	4.6	0.00	0.0
13	10	0.1	0.0	0.0	0.0	32.07	2.5	0.00	0.0

Epno	Trig	max deformation (10-7) E1	(10-7) sE1	min deformation (10-7) E2	(10-7) sE2	max direction (deg) teta	(deg) steta	rotation (sec) R	(sec) sR
14	5	0.0	0.0	-0.1	0.0	-7.86	5.1	0.00	0.0
14	6	0.3	0.0	-0.2	0.0	54.09	1.2	0.00	0.0
14	7	0.3	0.0	-0.2	0.0	56.34	1.1	-0.01	0.0
14	8	-0.1	0.0	-0.1	0.0	-17.63	10.8	0.00	0.0
14	9	0.0	0.0	-0.1	0.0	49.46	4.5	0.00	0.0
14	10	0.1	0.0	0.0	0.0	32.21	2.6	0.00	0.0

Epno	Trig	max deformation (10-7) E1	(10-7) sE1	min deformation (10-7) E2	(10-7) sE2	max direction (deg) teta	(deg) steta	rotation (sec) R	(sec) sR
15	5	0.0	0.0	-0.1	0.0	-8.17	5.0	0.00	0.0
15	6	0.3	0.0	-0.2	0.0	53.94	1.2	0.00	0.0
15	7	0.3	0.0	-0.2	0.0	56.28	1.1	-0.01	0.0
15	8	-0.1	0.0	-0.1	0.0	-17.57	10.6	0.00	0.0
15	9	0.0	0.0	-0.1	0.0	49.56	4.4	0.00	0.0
15	10	0.1	0.0	0.0	0.0	32.32	2.6	0.00	0.0
15	11	0.1	0.0	0.0	0.0	64.64	3.4	0.00	0.0
15	12	0.1	0.0	0.1	0.0	-29.32	16.2	0.00	0.0

Epno	Trig	max deformation (10-7) E1	(10-7) sE1	min deformation (10-7) E2	(10-7) sE2	max direction (deg) teta	(deg) steta	rotation (sec) R	(sec) sR
16	5	0.0	0.0	-0.1	0.0	-8.23	4.9	0.00	0.0
16	6	0.3	0.0	-0.2	0.0	53.87	1.2	0.00	0.0
16	7	0.3	0.0	-0.2	0.0	56.27	1.1	-0.01	0.0
16	8	-0.1	0.0	-0.1	0.0	-17.07	10.7	0.00	0.0
16	9	0.0	0.0	-0.1	0.0	49.62	4.3	0.00	0.0
16	10	0.1	0.0	0.0	0.0	32.40	2.6	0.00	0.0
16	11	0.1	0.0	0.0	0.0	64.61	3.5	0.00	0.0
16	12	0.1	0.0	0.1	0.0	-29.03	16.0	0.00	0.0

Epno	Trig	max deformation (10-7) E1	(10-7) sE1	min deformation (10-7) E2	(10-7) sE2	max direction (deg) teta	(deg) steta	rotation (sec) R	(sec) sR
17	5	0.0	0.0	-0.1	0.0	-7.98	4.9	0.00	0.0
17	6	0.3	0.0	-0.2	0.0	53.89	1.2	0.00	0.0
17	7	0.3	0.0	-0.2	0.0	56.34	1.1	-0.01	0.0
17	8	-0.1	0.0	-0.1	0.0	-15.91	10.9	0.00	0.0
17	9	0.0	0.0	-0.1	0.0	49.66	4.2	0.00	0.0
17	10	0.1	0.0	0.0	0.0	32.45	2.7	0.00	0.0

17	11	0.1	0.0	0.0	0.0	64.55	3.6	0.00	0.0
17	12	0.1	0.0	0.1	0.0	-28.77	15.9	0.00	0.0

Epno	Trig	max deformation (10-7) E1	(10-7) sE1	min deformation (10-7) E2	(10-7) sE2	max direction (deg) teta	(deg) steta	rotation (sec) R	(sec) sR
18	5	0.0	0.0	-0.1	0.0	-8.08	4.9	0.00	0.0
18	6	0.3	0.0	-0.2	0.0	53.88	1.2	0.00	0.0
18	7	0.3	0.0	-0.2	0.0	56.30	1.1	-0.01	0.0
18	8	-0.1	0.0	-0.1	0.0	-15.51	11.2	0.00	0.0
18	9	0.0	0.0	-0.1	0.0	49.70	4.1	0.00	0.0
18	10	0.1	0.0	0.0	0.0	32.46	2.8	0.00	0.0
18	11	0.1	0.0	0.0	0.0	64.49	3.6	0.00	0.0
18	12	0.1	0.0	0.1	0.0	-28.53	15.7	0.00	0.0
18	13	0.1	0.0	0.0	0.1	-14.97	15.9	0.00	0.0

Epno	Trig	max deformation (10-7) E1	(10-7) sE1	min deformation (10-7) E2	(10-7) sE2	max direction (deg) teta	(deg) steta	rotation (sec) R	(sec) sR
19	5	0.0	0.0	-0.1	0.0	-8.32	4.9	0.00	0.0
19	6	0.3	0.0	-0.2	0.0	53.86	1.2	0.00	0.0
19	7	0.3	0.0	-0.2	0.0	56.21	1.1	-0.01	0.0
19	8	-0.1	0.0	-0.1	0.0	-15.43	11.7	0.00	0.0
19	9	0.0	0.0	-0.1	0.0	49.70	4.1	0.00	0.0
19	10	0.1	0.0	0.0	0.0	32.46	2.8	0.00	0.0
19	11	0.1	0.0	0.0	0.0	64.41	3.7	0.00	0.0
19	12	0.1	0.0	0.1	0.0	-28.34	15.7	0.00	0.0
19	13	0.1	0.0	0.0	0.1	-14.98	15.8	0.00	0.0

Epno	Trig	max deformation (10-7) E1	(10-7) sE1	min deformation (10-7) E2	(10-7) sE2	max direction (deg) teta	(deg) steta	rotation (sec) R	(sec) sR
20	5	0.0	0.0	-0.1	0.0	-8.68	5.0	0.00	0.0
20	6	0.3	0.0	-0.2	0.0	53.84	1.2	0.00	0.0
20	7	0.3	0.0	-0.2	0.0	56.08	1.1	-0.01	0.0
20	8	-0.1	0.0	-0.1	0.0	-15.67	12.3	0.00	0.0
20	9	0.1	0.0	-0.1	0.0	49.69	4.0	0.00	0.0
20	10	0.1	0.0	0.0	0.0	32.44	2.9	0.00	0.0
20	11	0.1	0.0	0.0	0.0	64.34	3.7	0.00	0.0
20	12	0.1	0.0	0.1	0.0	-28.16	15.6	0.00	0.0
20	13	0.1	0.0	0.0	0.1	-14.96	15.8	0.00	0.0

Epno	Trig	max deformation (10-7) E1	(10-7) sE1	min deformation (10-7) E2	(10-7) sE2	max direction (deg) teta	(deg) steta	rotation (sec) R	(sec) sR
21	5	0.0	0.0	-0.1	0.0	-8.75	5.0	0.00	0.0
21	6	0.3	0.0	-0.2	0.0	53.85	1.2	0.00	0.0
21	7	0.3	0.0	-0.2	0.0	56.05	1.1	-0.01	0.0
21	8	-0.1	0.0	-0.1	0.0	-15.31	12.8	0.00	0.0
21	9	0.1	0.0	-0.1	0.0	49.68	4.0	0.00	0.0
21	10	0.1	0.0	0.0	0.0	32.44	3.0	0.00	0.0
21	11	0.1	0.0	0.0	0.0	64.27	3.8	0.00	0.0
21	12	0.1	0.0	0.1	0.0	-28.02	15.7	0.00	0.0
21	13	0.1	0.0	0.0	0.1	-14.96	15.8	0.00	0.0
21	14	0.1	0.0	0.0	0.0	-85.18	41.1	0.00	0.0
21	15	0.1	0.0	0.0	0.0	85.74	10.1	0.00	0.0

Epno	Trig	max deformation (10-7) E1	(10-7) sE1	min deformation (10-7) E2	(10-7) sE2	max direction (deg) teta	(deg) steta	rotation (sec) R	(sec) sR
22	5	0.0	0.0	-0.1	0.0	-8.52	5.0	0.00	0.0
22	6	0.3	0.0	-0.2	0.0	53.89	1.2	0.00	0.0
22	7	0.3	0.0	-0.2	0.0	56.10	1.1	-0.01	0.0
22	8	-0.1	0.0	-0.1	0.0	-14.17	13.2	0.00	0.0
22	9	0.1	0.0	-0.1	0.0	49.66	4.0	0.00	0.0
22	10	0.1	0.0	0.0	0.0	32.43	3.1	0.00	0.0
22	11	0.1	0.0	0.0	0.0	64.21	3.8	0.00	0.0

22	12	0.1	0.0	0.1	0.0	-27.90	15.7	0.00	0.0
22	13	0.1	0.0	0.0	0.1	-14.95	15.8	0.00	0.0
22	14	0.1	0.0	0.0	0.0	-85.34	41.2	0.00	0.0
22	15	0.1	0.0	0.0	0.0	85.74	10.1	0.00	0.0

Epno	Trig	max deformation (10-7) E1	(10-7) sE1	min deformation (10-7) E2	(10-7) sE2	max direction (deg) teta	(deg) steta	rotation (sec) R	(sec) sR
23	4	0.1	0.0	0.0	0.0	63.74	10.2	0.00	0.0
23	5	0.0	0.0	-0.1	0.0	-8.39	5.1	0.00	0.0
23	6	0.3	0.0	-0.2	0.0	53.92	1.2	0.00	0.0
23	7	0.3	0.0	-0.2	0.0	56.12	1.1	-0.01	0.0
23	8	-0.1	0.0	-0.1	0.0	-13.34	13.5	0.00	0.0
23	9	0.1	0.0	-0.1	0.0	49.64	4.0	0.00	0.0
23	10	0.1	0.0	0.0	0.0	32.42	3.1	0.00	0.0
23	11	0.1	0.0	0.0	0.0	64.14	3.9	0.00	0.0
23	12	0.1	0.0	0.1	0.0	-27.83	15.8	0.00	0.0
23	13	0.1	0.0	0.0	0.1	-14.95	15.8	0.00	0.0
23	14	0.1	0.0	0.0	0.0	-85.51	41.2	0.00	0.0
23	15	0.1	0.0	0.0	0.0	85.74	10.0	0.00	0.0
23	16	0.1	0.1	-0.1	0.1	79.24	13.2	0.00	0.0
23	17	0.0	0.1	-0.1	0.1	21.79	30.2	0.00	0.0
23	18	0.1	0.0	-0.1	0.0	57.71	9.1	0.00	0.0
23	19	0.1	0.0	0.0	0.0	64.18	10.7	0.00	0.0

Epno	Trig	max deformation (10-7) E1	(10-7) sE1	min deformation (10-7) E2	(10-7) sE2	max direction (deg) teta	(deg) steta	rotation (sec) R	(sec) sR
24	1	0.2	0.0	-0.2	0.0	-58.31	3.0	0.00	0.0
24	2	0.3	0.0	-0.4	0.0	47.01	1.2	-0.01	0.0
24	3	0.0	0.0	-0.1	0.0	42.54	6.9	0.00	0.0
24	4	0.1	0.0	0.0	0.0	63.73	10.2	0.00	0.0
24	5	0.0	0.0	-0.1	0.0	-8.27	5.1	0.00	0.0
24	6	0.3	0.0	-0.2	0.0	53.94	1.2	0.00	0.0
24	7	0.3	0.0	-0.2	0.0	56.14	1.1	-0.01	0.0
24	8	-0.1	0.0	-0.1	0.0	-12.65	13.8	0.00	0.0
24	9	0.1	0.0	-0.1	0.0	49.63	4.0	0.00	0.0
24	10	0.1	0.0	0.0	0.0	32.41	3.2	0.00	0.0
24	11	0.1	0.0	0.0	0.0	64.08	4.0	0.00	0.0
24	12	0.1	0.0	0.1	0.0	-27.78	15.9	0.00	0.0
24	13	0.1	0.0	0.0	0.1	-14.95	15.9	0.00	0.0
24	14	0.1	0.0	0.0	0.0	-85.67	41.2	0.00	0.0
24	15	0.1	0.0	0.0	0.0	85.73	10.0	0.00	0.0
24	16	0.1	0.1	-0.1	0.1	79.22	13.2	0.00	0.0
24	17	0.0	0.1	-0.1	0.1	21.80	30.3	0.00	0.0
24	18	0.1	0.0	-0.1	0.0	57.66	9.2	0.00	0.0
24	19	0.1	0.0	0.0	0.0	64.05	10.6	0.00	0.0
24	20	0.4	0.0	-0.5	0.0	-47.32	0.9	0.01	0.0
24	21	0.1	0.1	-0.3	0.1	55.75	10.5	0.00	0.0
24	22	0.0	0.0	0.0	0.0	45.66	9.9	0.00	0.0
24	23	0.5	0.1	-0.5	0.1	-48.05	2.3	0.01	0.0

Epno	Trig	max deformation (10-7) E1	(10-7) sE1	min deformation (10-7) E2	(10-7) sE2	max direction (deg) teta	(deg) steta	rotation (sec) R	(sec) sR
25	1	0.2	0.0	-0.2	0.0	-58.42	3.0	0.00	0.0
25	2	0.3	0.0	-0.4	0.0	47.00	1.2	-0.01	0.0
25	3	0.0	0.0	-0.1	0.0	42.53	6.9	0.00	0.0
25	4	0.1	0.0	0.0	0.0	63.74	10.2	0.00	0.0
25	5	0.0	0.0	-0.1	0.0	-8.27	5.1	0.00	0.0
25	6	0.3	0.0	-0.2	0.0	53.95	1.2	0.00	0.0
25	7	0.3	0.0	-0.2	0.0	56.13	1.1	-0.01	0.0
25	8	-0.1	0.0	-0.1	0.0	-12.31	14.0	0.00	0.0
25	9	0.1	0.0	-0.1	0.0	49.61	4.0	0.00	0.0
25	10	0.1	0.0	0.0	0.0	32.40	3.3	0.00	0.0
25	11	0.1	0.0	0.0	0.0	64.03	4.0	0.00	0.0
25	12	0.1	0.0	0.1	0.0	-27.73	16.0	0.00	0.0
25	13	0.1	0.0	0.0	0.1	-14.93	15.9	0.00	0.0
25	14	0.1	0.0	0.0	0.0	-85.83	41.1	0.00	0.0

25	15	0.1	0.0	0.0	0.0	85.73	10.0	0.00	0.0
25	16	0.1	0.1	-0.1	0.1	79.20	13.2	0.00	0.0
25	17	0.0	0.1	-0.1	0.1	21.83	30.3	0.00	0.0
25	18	0.1	0.0	-0.1	0.0	57.61	9.2	0.00	0.0
25	19	0.1	0.0	0.0	0.0	63.96	10.6	0.00	0.0
25	20	0.4	0.0	-0.5	0.0	-47.37	0.9	0.01	0.0
25	21	0.1	0.1	-0.3	0.1	55.73	10.5	0.00	0.0
25	22	0.0	0.0	0.0	0.0	45.70	9.9	0.00	0.0
25	23	0.5	0.1	-0.5	0.1	-48.06	2.3	0.01	0.0

Epno	Trig	max deformation (10-7) E1	(10-7) sE1	min deformation (10-7) E2	(10-7) sE2	max direction (deg) teta	(deg) steta	rotation (sec) R	(sec) sR
26	1	0.2	0.0	-0.2	0.0	-58.48	3.0	0.00	0.0
26	2	0.3	0.0	-0.4	0.0	47.00	1.2	-0.01	0.0
26	3	0.0	0.0	-0.1	0.0	42.53	6.9	0.00	0.0
26	4	0.1	0.0	0.0	0.0	63.75	10.2	0.00	0.0
26	5	0.0	0.0	-0.1	0.0	-8.14	5.2	0.00	0.0
26	6	0.3	0.0	-0.2	0.0	53.98	1.2	0.00	0.0
26	7	0.3	0.0	-0.2	0.0	56.16	1.1	-0.01	0.0
26	8	-0.1	0.0	-0.1	0.0	-11.69	14.2	0.00	0.0
26	9	0.1	0.0	-0.1	0.0	49.60	4.0	0.00	0.0
26	10	0.1	0.0	0.0	0.0	32.39	3.4	0.00	0.0
26	11	0.1	0.0	0.0	0.0	63.99	4.1	0.00	0.0
26	12	0.1	0.0	0.1	0.0	-27.69	16.1	0.00	0.0
26	13	0.1	0.0	0.0	0.1	-14.92	16.0	0.00	0.0
26	14	0.1	0.0	0.0	0.0	-85.96	41.2	0.00	0.0
26	15	0.1	0.0	0.0	0.0	85.72	10.0	0.00	0.0
26	16	0.1	0.1	-0.1	0.1	79.18	13.2	0.00	0.0
26	17	0.0	0.1	-0.1	0.1	21.88	30.4	0.00	0.0
26	18	0.1	0.0	-0.1	0.0	57.59	9.2	0.00	0.0
26	19	0.1	0.0	0.0	0.0	63.91	10.6	0.00	0.0
26	20	0.4	0.0	-0.5	0.0	-47.40	0.9	0.01	0.0
26	21	0.1	0.1	-0.3	0.1	55.72	10.5	0.00	0.0
26	22	0.0	0.0	0.0	0.0	45.72	9.9	0.00	0.0
26	23	0.5	0.1	-0.5	0.1	-48.06	2.3	0.01	0.0

Epno	Trig	max deformation (10-7) E1	(10-7) sE1	min deformation (10-7) E2	(10-7) sE2	max direction (deg) teta	(deg) steta	rotation (sec) R	(sec) sR
27	1	0.2	0.0	-0.2	0.0	-58.50	3.0	0.00	0.0
27	2	0.3	0.0	-0.4	0.0	47.00	1.2	-0.01	0.0
27	3	0.0	0.0	-0.1	0.0	42.54	6.9	0.00	0.0
27	4	0.1	0.0	0.0	0.0	63.76	10.3	0.00	0.0
27	5	0.0	0.0	-0.1	0.0	-7.89	5.2	0.00	0.0
27	6	0.3	0.0	-0.2	0.0	54.02	1.2	0.00	0.0
27	7	0.3	0.0	-0.2	0.0	56.23	1.1	-0.01	0.0
27	8	-0.1	0.0	-0.1	0.0	-10.85	14.3	0.00	0.0
27	9	0.1	0.0	-0.1	0.0	49.60	4.1	0.00	0.0
27	10	0.1	0.0	0.0	0.0	32.39	3.6	0.00	0.0
27	11	0.1	0.0	0.0	0.0	63.97	4.2	0.00	0.0
27	12	0.1	0.0	0.1	0.0	-27.67	16.2	0.00	0.0
27	13	0.1	0.0	0.0	0.1	-14.93	16.1	0.00	0.0
27	14	0.1	0.0	0.0	0.0	-86.03	41.2	0.00	0.0
27	15	0.1	0.0	0.0	0.0	85.71	10.0	0.00	0.0
27	16	0.1	0.1	-0.1	0.1	79.17	13.2	0.00	0.0
27	17	0.0	0.1	-0.1	0.1	21.91	30.5	0.00	0.0
27	18	0.1	0.0	-0.1	0.0	57.57	9.2	0.00	0.0
27	19	0.1	0.0	0.0	0.0	63.87	10.6	0.00	0.0
27	20	0.4	0.0	-0.5	0.0	-47.42	0.9	0.01	0.0
27	21	0.1	0.1	-0.3	0.1	55.71	10.5	0.00	0.0
27	22	0.0	0.0	0.0	0.0	45.74	9.9	0.00	0.0
27	23	0.5	0.1	-0.5	0.1	-48.07	2.3	0.01	0.0

Epno	Trig	max deformation (10-7) E1	(10-7) sE1	min deformation (10-7) E2	(10-7) sE2	max direction (deg) teta	(deg) steta	rotation (sec) R	(sec) sR
28	1	0.2	0.0	-0.2	0.0	-58.51	3.0	0.00	0.0
28	2	0.3	0.0	-0.4	0.0	47.00	1.2	-0.01	0.0

28	3	0.0	0.0	-0.1	0.0	42.54	6.9	0.00	0.0
28	4	0.1	0.0	0.0	0.0	63.77	10.3	0.00	0.0
28	5	0.0	0.0	-0.1	0.0	-7.72	5.2	0.00	0.0
28	6	0.3	0.0	-0.2	0.0	54.05	1.2	0.00	0.0
28	7	0.3	0.0	-0.2	0.0	56.28	1.1	-0.01	0.0
28	8	-0.1	0.0	-0.1	0.0	-10.30	14.4	0.00	0.0
28	9	0.1	0.0	-0.1	0.0	49.60	4.1	0.00	0.0
28	10	0.1	0.0	0.0	0.0	32.38	3.7	0.00	0.0
28	11	0.1	0.0	0.0	0.0	63.95	4.2	0.00	0.0
28	12	0.1	0.0	0.1	0.0	-27.66	16.3	0.00	0.0
28	13	0.1	0.0	0.0	0.1	-14.92	16.1	0.00	0.0
28	14	0.1	0.0	0.0	0.0	-86.06	41.3	0.00	0.0
28	15	0.1	0.0	0.0	0.0	85.71	10.0	0.00	0.0
28	16	0.1	0.1	-0.1	0.1	79.16	13.2	0.00	0.0
28	17	0.0	0.1	-0.1	0.1	21.92	30.5	0.00	0.0
28	18	0.1	0.0	-0.1	0.0	57.56	9.2	0.00	0.0
28	19	0.1	0.0	0.0	0.0	63.87	10.6	0.00	0.0
28	20	0.4	0.0	-0.5	0.0	-47.42	0.9	0.01	0.0
28	21	0.1	0.1	-0.3	0.1	55.71	10.5	0.00	0.0
28	22	0.0	0.0	0.0	0.0	45.75	10.0	0.00	0.0
28	23	0.5	0.1	-0.5	0.1	-48.07	2.3	0.01	0.0

Strain Rates For Group Four

Epno	Trig	max deformation (10-7) E1	(10-7) sE1	min deformation (10-7) E2	(10-7) sE2	max direction (deg) teta	(deg) steta	rotation (sec) R	(sec) sR
1	6	0.8	0.0	-0.7	0.0	74.67	0.3	0.02	0.0
1	10	0.6	0.0	0.1	0.0	40.58	0.8	0.00	0.0
1	16	0.0	0.0	0.0	0.0	29.71	1.8	0.00	0.0

Epno	Trig	max deformation (10-7) E1	(10-7) sE1	min deformation (10-7) E2	(10-7) sE2	max direction (deg) teta	(deg) steta	rotation (sec) R	(sec) sR
2	6	0.8	0.0	-0.7	0.0	74.68	0.3	0.02	0.0
2	7	0.3	0.0	0.0	0.0	11.02	0.8	0.00	0.0
2	10	0.6	0.0	0.1	0.0	40.64	0.8	0.00	0.0
2	15	0.5	0.0	-0.1	0.0	17.66	1.3	-0.01	0.0
2	16	0.0	0.0	0.0	0.0	30.16	1.7	0.00	0.0

Epno	Trig	max deformation (10-7) E1	(10-7) sE1	min deformation (10-7) E2	(10-7) sE2	max direction (deg) teta	(deg) steta	rotation (sec) R	(sec) sR
3	6	0.8	0.0	-0.7	0.0	74.70	0.3	0.02	0.0
3	7	0.3	0.0	0.0	0.0	11.05	0.8	0.00	0.0
3	8	0.6	0.0	0.1	0.0	51.86	2.3	0.00	0.0
3	9	0.2	0.0	-0.8	0.0	-44.30	1.5	0.00	0.0
3	10	0.6	0.0	0.1	0.0	40.81	0.7	0.00	0.0
3	15	0.5	0.0	-0.1	0.0	17.51	1.4	-0.01	0.0
3	16	0.0	0.0	0.0	0.0	31.40	1.6	0.00	0.0

Epno	Trig	max deformation (10-7) E1	(10-7) sE1	min deformation (10-7) E2	(10-7) sE2	max direction (deg) teta	(deg) steta	rotation (sec) R	(sec) sR
4	6	0.8	0.0	-0.7	0.0	74.73	0.3	0.02	0.0
4	7	0.3	0.0	0.0	0.0	11.09	0.8	0.00	0.0
4	8	0.6	0.0	0.1	0.0	51.00	2.4	0.00	0.0
4	9	0.2	0.0	-0.8	0.0	-45.19	1.5	0.00	0.0
4	10	0.6	0.0	0.1	0.0	41.08	0.7	0.00	0.0
4	15	0.5	0.0	-0.1	0.0	16.78	1.4	0.00	0.0
4	16	0.0	0.0	0.0	0.0	32.99	1.7	0.00	0.0

Epno	Trig	max deformation (10-7) E1	(10-7) sE1	min deformation (10-7) E2	(10-7) sE2	max direction (deg) teta	(deg) steta	rotation (sec) R	(sec) sR
5	6	0.8	0.0	-0.7	0.0	74.77	0.2	0.02	0.0
5	7	0.3	0.0	0.0	0.0	11.16	0.7	0.00	0.0

5	8	0.5	0.0	0.1	0.0	49.75	2.6	0.00	0.0
5	9	0.2	0.0	-0.8	0.0	-46.26	1.6	-0.01	0.0
5	10	0.6	0.0	0.1	0.0	41.44	0.6	0.00	0.0
5	15	0.4	0.0	-0.1	0.0	15.73	1.5	0.00	0.0
5	16	0.0	0.0	0.0	0.0	35.99	1.7	0.00	0.0

Epno	Trig	max deformation (10-7) E1	(10-7) sE1	min deformation (10-7) E2	(10-7) sE2	max direction (deg) teta	(deg) steta	rotation (sec) R	(sec) sR
6	6	0.8	0.0	-0.7	0.0	74.81	0.2	0.02	0.0
6	7	0.3	0.0	0.0	0.0	11.23	0.7	0.00	0.0
6	8	0.5	0.0	0.1	0.0	48.94	3.1	0.00	0.0
6	9	0.2	0.0	-0.7	0.0	-47.19	1.7	0.00	0.0
6	10	0.6	0.0	0.1	0.0	41.88	0.6	0.00	0.0
6	15	0.4	0.0	0.0	0.0	15.10	1.7	0.00	0.0
6	16	0.0	0.0	0.0	0.0	42.47	1.7	0.00	0.0

Epno	Trig	max deformation (10-7) E1	(10-7) sE1	min deformation (10-7) E2	(10-7) sE2	max direction (deg) teta	(deg) steta	rotation (sec) R	(sec) sR
7	6	0.8	0.0	-0.7	0.0	74.85	0.2	0.02	0.0
7	7	0.3	0.0	0.0	0.0	11.32	0.7	0.00	0.0
7	8	0.3	0.0	0.1	0.0	48.75	4.6	0.00	0.0
7	9	0.2	0.0	-0.6	0.0	-47.49	2.0	0.00	0.0
7	10	0.6	0.0	0.1	0.0	42.39	0.6	0.00	0.0
7	15	0.3	0.0	0.0	0.0	15.02	2.3	0.00	0.0
7	16	0.0	0.0	0.0	0.0	51.02	1.5	0.00	0.0

Epno	Trig	max deformation (10-7) E1	(10-7) sE1	min deformation (10-7) E2	(10-7) sE2	max direction (deg) teta	(deg) steta	rotation (sec) R	(sec) sR
8	1	0.0	0.0	0.0	0.0	51.23	2.5	0.00	0.0
8	6	0.8	0.0	-0.7	0.0	74.89	0.2	0.02	0.0
8	7	0.3	0.0	0.0	0.0	11.43	0.7	0.00	0.0
8	8	0.2	0.0	0.1	0.0	52.66	13.5	0.00	0.0
8	9	0.1	0.0	-0.3	0.0	-46.23	3.1	0.00	0.0
8	10	0.6	0.0	0.1	0.0	42.95	0.5	0.00	0.0
8	15	0.2	0.0	0.0	0.0	17.01	4.3	0.00	0.0
8	16	0.0	0.0	0.0	0.0	58.04	1.2	0.00	0.0

Epno	Trig	max deformation (10-7) E1	(10-7) sE1	min deformation (10-7) E2	(10-7) sE2	max direction (deg) teta	(deg) steta	rotation (sec) R	(sec) sR
9	1	0.0	0.0	0.0	0.0	51.35	2.5	0.00	0.0
9	6	0.9	0.0	-0.7	0.0	74.93	0.2	0.02	0.0
9	7	0.3	0.0	0.0	0.0	11.56	0.6	0.00	0.0
9	8	0.1	0.0	0.1	0.0	-50.47	14.3	0.00	0.0
9	9	0.1	0.0	-0.1	0.0	-42.33	6.1	0.00	0.0
9	10	0.6	0.0	0.1	0.0	43.54	0.5	0.00	0.0
9	15	0.1	0.0	0.0	0.0	35.90	18.3	0.00	0.0
9	16	0.1	0.0	-0.1	0.0	62.10	1.0	0.00	0.0

Epno	Trig	max deformation (10-7) E1	(10-7) sE1	min deformation (10-7) E2	(10-7) sE2	max direction (deg) teta	(deg) steta	rotation (sec) R	(sec) sR
10	1	0.0	0.0	0.0	0.0	51.47	2.4	0.00	0.0
10	6	0.9	0.0	-0.6	0.0	74.98	0.2	0.02	0.0
10	7	0.3	0.0	0.0	0.0	11.69	0.6	0.00	0.0
10	8	0.1	0.0	0.0	0.0	-44.43	6.2	0.00	0.0
10	9	0.1	0.0	0.0	0.0	-36.04	15.7	0.00	0.0
10	10	0.6	0.0	0.1	0.0	44.14	0.5	0.00	0.0
10	15	0.1	0.0	0.0	0.0	-83.22	10.6	0.00	0.0
10	16	0.1	0.0	-0.1	0.0	64.39	0.9	0.00	0.0

Epno	Trig	max deformation (10-7) E1	(10-7) sE1	min deformation (10-7) E2	(10-7) sE2	max direction (deg) teta	(deg) steta	rotation (sec) R	(sec) sR

Epno	Trig	max deformation (10-7) E1	(10-7) sE1	min deformation (10-7) E2	(10-7) sE2	max direction (deg) teta	(deg) steta	rotation (sec) R	(sec) sR
11	1	0.0	0.0	0.0	0.0	51.58	2.4	0.00	0.0
11	6	0.9	0.0	-0.6	0.0	75.02	0.2	0.01	0.0
11	7	0.3	0.0	0.0	0.0	11.83	0.6	0.00	0.0
11	8	0.1	0.0	-0.1	0.0	-42.53	4.6	0.00	0.0
11	9	0.1	0.0	0.1	0.0	-37.41	62.5	0.00	0.0
11	10	0.6	0.0	0.1	0.0	44.72	0.5	0.00	0.0
11	15	0.1	0.0	-0.1	0.0	-77.40	5.8	0.00	0.0
11	16	0.1	0.0	-0.1	0.0	65.70	0.8	0.00	0.0

Epno	Trig	max deformation (10-7) E1	(10-7) sE1	min deformation (10-7) E2	(10-7) sE2	max direction (deg) teta	(deg) steta	rotation (sec) R	(sec) sR
12	1	0.0	0.0	0.0	0.0	51.69	2.3	0.00	0.0
12	6	0.9	0.0	-0.6	0.0	75.06	0.2	0.01	0.0
12	7	0.3	0.0	0.0	0.0	11.96	0.6	0.00	0.0
12	8	0.1	0.0	-0.1	0.0	-41.67	3.9	0.00	0.0
12	9	0.1	0.0	0.1	0.0	80.10	79.8	0.00	0.0
12	10	0.6	0.0	0.1	0.0	45.27	0.5	0.00	0.0
12	15	0.1	0.0	-0.1	0.0	-75.50	4.5	0.00	0.0
12	16	0.1	0.0	-0.1	0.0	66.42	0.8	0.00	0.0

Epno	Trig	max deformation (10-7) E1	(10-7) sE1	min deformation (10-7) E2	(10-7) sE2	max direction (deg) teta	(deg) steta	rotation (sec) R	(sec) sR
13	1	0.0	0.0	0.0	0.0	51.79	2.3	0.00	0.0
13	2	0.1	0.0	0.0	0.0	62.46	4.4	0.00	0.0
13	3	0.1	0.0	0.0	0.0	45.27	12.7	0.00	0.0
13	4	0.1	0.0	-0.6	0.0	-46.71	0.7	0.01	0.0
13	6	0.9	0.0	-0.6	0.0	75.10	0.2	0.01	0.0
13	7	0.3	0.0	0.0	0.0	12.08	0.6	0.00	0.0
13	8	0.1	0.0	-0.1	0.0	-40.90	3.7	0.00	0.0
13	9	0.1	0.0	0.1	0.0	72.52	38.5	0.00	0.0
13	10	0.6	0.0	0.1	0.0	45.81	0.5	0.00	0.0
13	11	0.2	0.0	-0.2	0.0	-15.48	0.9	0.00	0.0
13	12	0.5	0.0	-0.6	0.0	29.58	0.4	-0.01	0.0
13	13	0.0	0.0	-0.6	0.0	-12.88	1.6	0.00	0.0
13	14	0.0	0.0	0.0	0.0	81.15	38.6	0.00	0.0
13	15	0.1	0.0	-0.1	0.0	-73.98	4.1	0.00	0.0
13	16	0.1	0.0	-0.1	0.0	66.81	0.8	0.00	0.0

Epno	Trig	max deformation (10-7) E1	(10-7) sE1	min deformation (10-7) E2	(10-7) sE2	max direction (deg) teta	(deg) steta	rotation (sec) R	(sec) sR
14	1	0.0	0.0	0.0	0.0	51.88	2.3	0.00	0.0
14	2	0.1	0.0	0.0	0.0	62.51	4.4	0.00	0.0
14	3	0.1	0.0	0.0	0.0	45.86	12.7	0.00	0.0
14	4	0.1	0.0	-0.6	0.0	-46.79	0.7	0.01	0.0
14	6	0.8	0.0	-0.6	0.0	75.13	0.2	0.01	0.0
14	7	0.3	0.0	0.0	0.0	12.19	0.6	0.00	0.0
14	8	0.1	0.0	-0.1	0.0	-40.27	3.7	0.00	0.0
14	9	0.1	0.0	0.1	0.0	77.58	30.1	0.00	0.0
14	10	0.6	0.0	0.1	0.0	46.30	0.5	0.00	0.0
14	11	0.2	0.0	-0.2	0.0	-15.78	1.0	0.00	0.0
14	12	0.5	0.0	-0.6	0.0	29.51	0.4	-0.01	0.0
14	13	0.0	0.0	-0.6	0.0	-12.88	1.6	0.00	0.0
14	14	0.0	0.0	0.0	0.0	81.03	38.2	0.00	0.0
14	15	0.1	0.0	-0.1	0.0	-72.69	4.0	0.00	0.0
14	16	0.1	0.0	-0.1	0.0	66.96	0.8	0.00	0.0

Epno	Trig	max deformation (10-7) E1	(10-7) sE1	min deformation (10-7) E2	(10-7) sE2	max direction (deg) teta	(deg) steta	rotation (sec) R	(sec) sR
15	1	0.0	0.0	0.0	0.0	51.97	2.2	0.00	0.0
15	2	0.1	0.0	0.0	0.0	62.57	4.4	0.00	0.0
15	3	0.1	0.0	0.0	0.0	46.42	12.7	0.00	0.0
15	4	0.1	0.0	-0.7	0.0	-46.87	0.7	0.01	0.0
15	6	0.8	0.0	-0.6	0.0	75.15	0.2	0.01	0.0

15	7	0.3	0.0	0.0	0.0	12.30	0.6	0.00	0.0
15	8	0.1	0.0	-0.1	0.0	-39.81	3.8	0.00	0.0
15	9	0.2	0.0	0.1	0.0	85.09	25.1	0.00	0.0
15	10	0.6	0.0	0.1	0.0	46.82	0.5	0.00	0.0
15	11	0.2	0.0	-0.2	0.0	-16.14	1.0	0.00	0.0
15	12	0.5	0.0	-0.6	0.0	29.44	0.4	-0.01	0.0
15	13	0.0	0.0	-0.6	0.0	-12.88	1.6	0.00	0.0
15	14	0.0	0.0	0.0	0.0	80.77	37.8	0.00	0.0
15	15	0.1	0.0	-0.1	0.0	-71.57	4.1	0.00	0.0
15	16	0.1	0.0	-0.1	0.0	66.94	0.9	0.00	0.0

Epno	Trig	max deformation (10-7) E1	(10-7) sE1	min deformation (10-7) E2	(10-7) sE2	max direction (deg) teta	(deg) steta	rotation (sec) R	(sec) sR
16	1	0.0	0.0	0.0	0.0	52.06	2.2	0.00	0.0
16	2	0.1	0.0	0.0	0.0	62.63	4.4	0.00	0.0
16	3	0.1	0.0	0.0	0.0	46.89	12.8	0.00	0.0
16	4	0.1	0.0	-0.7	0.0	-46.94	0.7	0.01	0.0
16	6	0.8	0.0	-0.6	0.0	75.18	0.3	0.01	0.0
16	7	0.3	0.0	0.0	0.0	12.41	0.6	0.00	0.0
16	8	0.1	0.0	-0.1	0.0	-39.86	3.8	0.00	0.0
16	9	0.2	0.0	0.1	0.0	89.02	23.0	0.00	0.0
16	10	0.6	0.0	0.1	0.0	47.30	0.6	0.00	0.0
16	11	0.2	0.0	-0.2	0.0	-16.50	1.0	0.00	0.0
16	12	0.5	0.0	-0.6	0.0	29.38	0.4	-0.01	0.0
16	13	0.0	0.0	-0.6	0.0	-12.87	1.5	0.00	0.0
16	14	0.0	0.0	0.0	0.0	80.42	37.4	0.00	0.0
16	15	0.1	0.0	-0.1	0.0	-71.22	4.2	0.00	0.0
16	16	0.1	0.0	-0.1	0.0	66.81	0.9	0.00	0.0

Epno	Trig	max deformation (10-7) E1	(10-7) sE1	min deformation (10-7) E2	(10-7) sE2	max direction (deg) teta	(deg) steta	rotation (sec) R	(sec) sR
17	1	0.0	0.0	0.0	0.0	52.15	2.2	0.00	0.0
17	2	0.1	0.0	0.0	0.0	62.70	4.4	0.00	0.0
17	3	0.1	0.0	0.0	0.0	47.24	12.8	0.00	0.0
17	4	0.1	0.0	-0.7	0.0	-47.00	0.7	0.01	0.0
17	6	0.8	0.0	-0.6	0.0	75.20	0.3	0.01	0.0
17	7	0.3	0.0	0.0	0.0	12.50	0.6	0.00	0.0
17	8	0.1	0.0	-0.1	0.0	-40.31	3.9	0.00	0.0
17	9	0.1	0.0	0.1	0.0	-89.44	23.3	0.00	0.0
17	10	0.6	0.0	0.1	0.0	47.74	0.6	0.00	0.0
17	11	0.2	0.0	-0.1	0.0	-16.86	1.1	0.00	0.0
17	12	0.5	0.0	-0.6	0.0	29.33	0.4	-0.01	0.0
17	13	0.0	0.0	-0.6	0.0	-12.86	1.5	0.00	0.0
17	14	0.0	0.0	0.0	0.0	79.82	37.1	0.00	0.0
17	15	0.1	0.0	-0.1	0.0	-71.60	4.2	0.00	0.0
17	16	0.1	0.0	-0.1	0.0	66.63	0.9	0.00	0.0

Epno	Trig	max deformation (10-7) E1	(10-7) sE1	min deformation (10-7) E2	(10-7) sE2	max direction (deg) teta	(deg) steta	rotation (sec) R	(sec) sR
18	1	0.0	0.0	0.0	0.0	52.25	2.2	0.00	0.0
18	2	0.1	0.0	0.0	0.0	62.77	4.4	0.00	0.0
18	3	0.1	0.0	0.0	0.0	47.50	12.8	0.00	0.0
18	4	0.1	0.0	-0.7	0.0	-47.06	0.7	0.01	0.0
18	6	0.8	0.0	-0.6	0.0	75.21	0.3	0.01	0.0
18	7	0.3	0.0	0.0	0.0	12.59	0.6	0.00	0.0
18	8	0.1	0.0	-0.1	0.0	-40.69	3.9	0.00	0.0
18	9	0.1	0.0	0.1	0.0	-84.80	23.3	0.00	0.0
18	10	0.6	0.0	0.1	0.0	48.13	0.6	0.00	0.0
18	11	0.2	0.0	-0.1	0.0	-17.20	1.1	0.00	0.0
18	12	0.5	0.0	-0.6	0.0	29.29	0.4	-0.01	0.0
18	13	0.0	0.0	-0.6	0.0	-12.85	1.5	0.00	0.0
18	14	0.0	0.0	0.0	0.0	79.09	37.0	0.00	0.0
18	15	0.1	0.0	-0.1	0.0	-71.84	4.2	0.00	0.0
18	16	0.1	0.0	-0.1	0.0	66.46	0.9	0.00	0.0

Epno	Trig	max deformation	min deformation	max direction	rotation

		(10-7) E1	(10-7) sE1	(10-7) E2	(10-7) sE2	(deg) teta	(deg) steta	(sec) R	(sec) sR
19	1	0.0	0.0	0.0	0.0	52.34	2.2	0.00	0.0
19	2	0.1	0.0	0.0	0.0	62.85	4.4	0.00	0.0
19	3	0.1	0.0	0.0	0.0	47.67	12.9	0.00	0.0
19	4	0.1	0.0	-0.7	0.0	-47.10	0.7	0.01	0.0
19	6	0.8	0.0	-0.6	0.0	75.23	0.3	0.01	0.0
19	7	0.3	0.0	0.0	0.0	12.67	0.6	0.00	0.0
19	8	0.1	0.0	-0.1	0.0	-40.61	4.0	0.00	0.0
19	9	0.1	0.0	0.1	0.0	-81.65	25.3	0.00	0.0
19	10	0.6	0.0	0.1	0.0	48.48	0.6	0.00	0.0
19	11	0.2	0.0	-0.1	0.0	-17.52	1.1	0.00	0.0
19	12	0.6	0.0	-0.6	0.0	29.25	0.4	-0.01	0.0
19	13	0.0	0.0	-0.6	0.0	-12.84	1.5	0.00	0.0
19	14	0.0	0.0	0.0	0.0	78.30	37.1	0.00	0.0
19	15	0.1	0.0	-0.1	0.0	-71.40	4.3	0.00	0.0
19	16	0.1	0.0	-0.1	0.0	66.39	1.0	0.00	0.0

Epno	Trig	max deformation (10-7) E1	(10-7) sE1	min deformation (10-7) E2	(10-7) sE2	max direction (deg) teta	(deg) steta	rotation (sec) R	(sec) sR
20	1	0.0	0.0	0.0	0.0	52.44	2.2	0.00	0.0
20	2	0.1	0.0	0.0	0.0	62.91	4.4	0.00	0.0
20	3	0.1	0.0	0.0	0.0	47.79	12.9	0.00	0.0
20	4	0.1	0.0	-0.7	0.0	-47.14	0.7	0.01	0.0
20	6	0.8	0.0	-0.6	0.0	75.24	0.3	0.01	0.0
20	7	0.3	0.0	0.0	0.0	12.74	0.7	0.00	0.0
20	8	0.1	0.0	-0.1	0.0	-40.12	4.1	0.00	0.0
20	9	0.1	0.0	0.1	0.0	-80.73	32.0	0.00	0.0
20	10	0.6	0.0	0.1	0.0	48.77	0.7	0.00	0.0
20	11	0.2	0.0	-0.1	0.0	-17.80	1.2	0.00	0.0
20	12	0.6	0.0	-0.6	0.0	29.22	0.4	-0.01	0.0
20	13	0.0	0.0	-0.6	0.0	-12.82	1.5	0.00	0.0
20	14	0.0	0.0	0.0	0.0	77.44	37.2	0.00	0.0
20	15	0.1	0.0	-0.1	0.0	-70.30	4.5	0.00	0.0
20	16	0.1	0.0	-0.1	0.0	66.41	1.0	0.00	0.0

Epno	Trig	max deformation (10-7) E1	(10-7) sE1	min deformation (10-7) E2	(10-7) sE2	max direction (deg) teta	(deg) steta	rotation (sec) R	(sec) sR
21	1	0.0	0.0	0.0	0.0	52.53	2.2	0.00	0.0
21	2	0.1	0.0	0.0	0.0	62.97	4.4	0.00	0.0
21	3	0.1	0.0	0.0	0.0	47.86	13.0	0.00	0.0
21	4	0.1	0.0	-0.7	0.0	-47.17	0.7	0.01	0.0
21	6	0.8	0.0	-0.6	0.0	75.26	0.3	0.01	0.0
21	7	0.3	0.0	0.0	0.0	12.81	0.7	0.00	0.0
21	8	0.1	0.0	-0.1	0.0	-40.02	4.2	0.00	0.0
21	9	0.1	0.0	0.1	0.0	-75.47	36.4	0.00	0.0
21	10	0.6	0.0	0.1	0.0	49.02	0.7	0.00	0.0
21	11	0.2	0.0	-0.1	0.0	-18.04	1.2	0.00	0.0
21	12	0.6	0.0	-0.6	0.0	29.20	0.4	-0.01	0.0
21	13	0.0	0.0	-0.6	0.0	-12.79	1.5	0.00	0.0
21	14	0.0	0.0	0.0	0.0	76.52	37.5	0.00	0.0
21	15	0.1	0.0	-0.1	0.0	-69.89	4.6	0.00	0.0
21	16	0.1	0.0	-0.1	0.0	66.39	1.1	0.00	0.0

Epno	Trig	max deformation (10-7) E1	(10-7) sE1	min deformation (10-7) E2	(10-7) sE2	max direction (deg) teta	(deg) steta	rotation (sec) R	(sec) sR
22	1	0.0	0.0	0.0	0.0	52.61	2.2	0.00	0.0
22	2	0.1	0.0	0.0	0.0	63.02	4.4	0.00	0.0
22	3	0.1	0.0	0.0	0.0	47.90	13.1	0.00	0.0
22	4	0.1	0.0	-0.7	0.0	-47.19	0.7	0.01	0.0
22	6	0.8	0.0	-0.6	0.0	75.27	0.3	0.01	0.0
22	7	0.3	0.0	0.0	0.0	12.86	0.7	0.00	0.0
22	8	0.1	0.0	-0.1	0.0	-40.37	4.3	0.00	0.0
22	9	0.1	0.0	0.1	0.0	-68.59	32.6	0.00	0.0
22	10	0.6	0.0	0.1	0.0	49.21	0.7	0.00	0.0

22	11	0.2	0.0	-0.1	0.0	-18.22	1.3	0.00	0.0
22	12	0.6	0.0	-0.6	0.0	29.18	0.4	-0.01	0.0
22	13	0.0	0.0	-0.6	0.0	-12.78	1.5	0.00	0.0
22	14	0.0	0.0	0.0	0.0	75.73	37.7	0.00	0.0
22	15	0.1	0.0	-0.1	0.0	-70.30	4.6	0.00	0.0
22	16	0.1	0.0	-0.1	0.0	66.30	1.1	0.00	0.0

Epno	Trig	max deformation (10-7) E1	(10-7) sE1	min deformation (10-7) E2	(10-7) sE2	max direction (deg) teta	(deg) steta	rotation (sec) R	(sec) sR
23	1	0.0	0.0	0.0	0.0	52.69	2.2	0.00	0.0
23	2	0.1	0.0	0.0	0.0	63.06	4.4	0.00	0.0
23	3	0.1	0.0	0.0	0.0	47.93	13.2	0.00	0.0
23	4	0.1	0.0	-0.7	0.0	-47.21	0.7	0.01	0.0
23	6	0.8	0.0	-0.6	0.0	75.28	0.3	0.01	0.0
23	7	0.3	0.0	0.0	0.0	12.91	0.7	0.00	0.0
23	8	0.1	0.0	-0.1	0.0	-40.51	4.3	0.00	0.0
23	9	0.1	0.0	0.1	0.0	-66.18	31.0	0.00	0.0
23	10	0.6	0.0	0.1	0.0	49.36	0.8	0.00	0.0
23	11	0.2	0.0	-0.1	0.0	-18.37	1.3	0.00	0.0
23	12	0.6	0.0	-0.6	0.0	29.17	0.4	-0.01	0.0
23	13	0.0	0.0	-0.6	0.0	-12.75	1.5	0.00	0.0
23	14	0.0	0.0	0.0	0.0	74.97	37.9	0.00	0.0
23	15	0.1	0.0	-0.1	0.0	-70.37	4.7	0.00	0.0
23	16	0.1	0.0	-0.1	0.0	66.26	1.1	0.00	0.0

Epno	Trig	max deformation (10-7) E1	(10-7) sE1	min deformation (10-7) E2	(10-7) sE2	max direction (deg) teta	(deg) steta	rotation (sec) R	(sec) sR
24	1	0.0	0.0	0.0	0.0	52.75	2.3	0.00	0.0
24	2	0.1	0.0	0.0	0.0	63.09	4.4	0.00	0.0
24	3	0.1	0.0	0.0	0.0	47.93	13.3	0.00	0.0
24	4	0.1	0.0	-0.7	0.0	-47.22	0.7	0.01	0.0
24	6	0.8	0.0	-0.6	0.0	75.29	0.4	0.01	0.0
24	7	0.3	0.0	0.0	0.0	12.96	0.7	0.00	0.0
24	8	0.1	0.0	-0.1	0.0	-40.41	4.4	0.00	0.0
24	9	0.1	0.0	0.1	0.0	-66.54	31.9	0.00	0.0
24	10	0.6	0.0	0.1	0.0	49.48	0.8	0.00	0.0
24	11	0.2	0.0	-0.1	0.0	-18.48	1.4	0.00	0.0
24	12	0.6	0.0	-0.6	0.0	29.17	0.4	-0.01	0.0
24	13	0.0	0.0	-0.6	0.0	-12.74	1.5	0.00	0.0
24	14	0.0	0.0	0.0	0.0	74.40	38.2	0.00	0.0
24	15	0.1	0.0	-0.1	0.0	-70.11	4.7	0.00	0.0
24	16	0.1	0.0	-0.1	0.0	66.28	1.1	0.00	0.0

Epno	Trig	max deformation (10-7) E1	(10-7) sE1	min deformation (10-7) E2	(10-7) sE2	max direction (deg) teta	(deg) steta	rotation (sec) R	(sec) sR
25	1	0.0	0.0	0.0	0.0	52.80	2.3	0.00	0.0
25	2	0.1	0.0	0.0	0.0	63.12	4.4	0.00	0.0
25	3	0.1	0.0	0.0	0.0	47.94	13.4	0.00	0.0
25	4	0.1	0.0	-0.7	0.0	-47.23	0.7	0.01	0.0
25	6	0.8	0.0	-0.6	0.0	75.30	0.4	0.01	0.0
25	7	0.3	0.0	0.0	0.0	13.00	0.7	0.00	0.0
25	8	0.1	0.0	-0.1	0.0	-40.36	4.5	0.00	0.0
25	9	0.1	0.0	0.1	0.0	-66.91	30.3	0.00	0.0
25	10	0.6	0.0	0.1	0.0	49.55	0.9	0.00	0.0
25	11	0.2	0.0	-0.1	0.0	-18.56	1.5	0.00	0.0
25	12	0.6	0.0	-0.6	0.0	29.16	0.4	-0.01	0.0
25	13	0.0	0.0	-0.6	0.0	-12.73	1.5	0.00	0.0
25	14	0.0	0.0	0.0	0.0	73.93	38.5	0.00	0.0
25	15	0.1	0.0	-0.1	0.0	-69.97	4.8	0.00	0.0
25	16	0.1	0.0	-0.1	0.0	66.30	1.2	0.00	0.0

Epno	Trig	max deformation (10-7) E1	(10-7) sE1	min deformation (10-7) E2	(10-7) sE2	max direction (deg) teta	(deg) steta	rotation (sec) R	(sec) sR
26	1	0.0	0.0	0.0	0.0	52.84	2.3	0.00	0.0

26	2	0.1	0.0	0.0	0.0	63.13	4.4	0.00	0.0
26	3	0.1	0.0	0.0	0.0	47.93	13.5	0.00	0.0
26	4	0.1	0.0	-0.7	0.0	-47.23	0.7	0.01	0.0
26	6	0.8	0.0	-0.6	0.0	75.30	0.4	0.01	0.0
26	7	0.3	0.0	0.0	0.0	13.02	0.8	0.00	0.0
26	8	0.1	0.0	-0.1	0.0	-40.54	4.6	0.00	0.0
26	9	0.1	0.0	0.1	0.0	-67.14	27.6	0.00	0.0
26	10	0.6	0.0	0.1	0.0	49.60	0.9	0.00	0.0
26	11	0.2	0.0	-0.1	0.0	-18.61	1.5	0.00	0.0
26	12	0.6	0.0	-0.6	0.0	29.16	0.4	-0.01	0.0
26	13	0.0	0.0	-0.6	0.0	-12.72	1.5	0.00	0.0
26	14	0.0	0.0	0.0	0.0	73.64	38.7	0.00	0.0
26	15	0.1	0.0	-0.1	0.0	-70.24	4.9	0.00	0.0
26	16	0.1	0.0	-0.1	0.0	66.28	1.2	0.00	0.0

Epno	Trig	max deformation (10-7) E1	(10-7) sE1	min deformation (10-7) E2	(10-7) sE2	max direction (deg) teta	(deg) steta	rotation (sec) R	(sec) sR
27	1	0.0	0.0	0.0	0.0	52.87	2.4	0.00	0.0
27	2	0.1	0.0	0.0	0.0	63.14	4.4	0.00	0.0
27	3	0.1	0.0	0.0	0.0	47.91	13.6	0.00	0.0
27	4	0.1	0.0	-0.7	0.0	-47.24	0.7	0.01	0.0
27	6	0.8	0.0	-0.6	0.0	75.30	0.4	0.01	0.0
27	7	0.3	0.0	0.0	0.0	13.04	0.8	0.00	0.0
27	8	0.1	0.0	-0.1	0.0	-40.84	4.6	0.00	0.0
27	9	0.1	0.0	0.1	0.0	-67.41	26.7	0.00	0.0
27	10	0.6	0.0	0.1	0.0	49.62	1.0	0.00	0.0
27	11	0.2	0.0	-0.1	0.0	-18.64	1.6	0.00	0.0
27	12	0.6	0.0	-0.6	0.0	29.16	0.4	-0.01	0.0
27	13	0.0	0.0	-0.6	0.0	-12.71	1.6	0.00	0.0
27	14	0.0	0.0	0.0	0.0	73.47	39.0	0.00	0.0
27	15	0.1	0.0	-0.1	0.0	-70.75	4.9	0.00	0.0
27	16	0.1	0.0	-0.1	0.0	66.26	1.3	0.00	0.0

Epno	Trig	max deformation (10-7) E1	(10-7) sE1	min deformation (10-7) E2	(10-7) sE2	max direction (deg) teta	(deg) steta	rotation (sec) R	(sec) sR
28	1	0.0	0.0	0.0	0.0	52.88	2.4	0.00	0.0
28	2	0.1	0.0	0.0	0.0	63.14	4.4	0.00	0.0
28	3	0.1	0.0	0.0	0.0	47.91	13.7	0.00	0.0
28	4	0.1	0.0	-0.7	0.0	-47.24	0.7	0.01	0.0
28	6	0.8	0.0	-0.6	0.0	75.30	0.4	0.01	0.0
28	7	0.3	0.0	0.0	0.0	13.05	0.8	0.00	0.0
28	8	0.1	0.0	-0.1	0.0	-41.00	4.7	0.00	0.0
28	9	0.1	0.0	0.1	0.0	-67.75	27.6	0.00	0.0
28	10	0.6	0.0	0.1	0.0	49.64	1.0	0.00	0.0
28	11	0.2	0.0	-0.1	0.0	-18.66	1.6	0.00	0.0
28	12	0.6	0.0	-0.6	0.0	29.16	0.5	-0.01	0.0
28	13	0.0	0.0	-0.6	0.0	-12.71	1.6	0.00	0.0
28	14	0.0	0.0	0.0	0.0	73.41	39.3	0.00	0.0
28	15	0.1	0.0	-0.1	0.0	-71.04	5.0	0.00	0.0
28	16	0.1	0.0	-0.1	0.0	66.26	1.3	0.00	0.0

KEY FOR TRIANGLE NUMBER

GROUP ONE

1	REYK	NYAL	ONSA
2	NYAL	ONSA	VAAS
3	NYAL	VAAS	VARD
4	VARD	VAAS	MDVO
5	VAAS	MDVO	JOZE
6	JOZE	MDVO	SOFI
7	SOFI	MDVO	ZECK
8	SOFI	ZECK	NICO
9	SOFI	NICO	NOTO
10	SOFI	NOTO	GRAZ
11	GRAZ	NOTO	ZIMM
12	ZIMM	NOTO	VILL
13	VILL	NOTO	MASP
14	REYK	VILL	HERS
15	VILL	REYK	MASP
16	REYK	HERS	ONSA
17	HERS	VILL	ZIMM
18	HERS	ZIMM	ONSA
19	ONSA	ZIMM	WTZR
20	ZIMM	WTZR	GRAZ
21	WTZR	GRAZ	JOZE
22	ONSA	WTZR	JOZE
23	ONSA	JOZE	VAAS
24	GRAZ	SOFI	JOZE
25	MASP	NOTO	NICO

GROUP TWO

1	TROM	MAR6	SODA
2	MAR6	SODA	RIGA
3	SODA	RIGA	ZWEN
4	RIGA	ZWEN	ANKR
5	RIGA	ANKR	MATE
6	RIGA	MATE	GOPE
7	GOPE	MATE	MEDI
8	MEDI	MATE	CAGL
9	MEDI	CAGL	EBRE
10	EBRE	MEDI	DOUR
11	EBRE	DOUR	MADR
12	MADR	EBRE	SFER
13	MEDI	DOUR	GOPE
14	DOUR	GOPE	STAV
15	STAV	GOPE	OSLO
16	OSLO	GOPE	MAR6
17	GOPE	MAR6	RIGA
18	OSLO	MAR6	TRON
19	TRON	OSLO	TROM
20	TRON	TROM	MAR6
21	STAV	TRON	OSLO
22	MADR	DOUR	STAV
22	EBRE	SFER	CAGL

GROUP THREE

1	HOFN	THU1	KELY
2	HOFN	VIL0	KIR0
3	HOFN	VIL0	WSRT
4	WSRT	VIL0	VIS0
5	VIL0	VIS0	METS
6	VIL0	METS	KIR0
7	KIR0	METS	JOEN
8	VIS0	METS	LAMA
9	VIS0	LAMA	BOR1
10	BOR1	LAMA	PENC
11	BOR1	PENC	OBER
12	OBER	PENC	VENE
13	OBER	VENE	PFAN
14	PFAN	VENE	TOUL
15	TOUL	PFAN	DENT
16	DENT	PFAN	WSRT

```
 17  WSRT PFAN OBER
 18  WSRT OBER BOR1
 19  WSRT VIS0 BOR1
 20 THU1 KIR0 HOFN
 21 HOFN WSRT DENT
 22 HOFN DENT TOUL
 23 HOFN KELY TOUL

GROUP FOUR

  1  POTS KIRU BOGO
  2  KIRU BOGO SVTL
  3  POTS BOGO WROC
  4  POTS WROC WETT
  5  POTS WTZR HFLK
  6  POTS HFLK GRAS
  7  GRAS POTS WARE
  8  WARE KOSG DELF
  9  DELF BRUS WARE
 10  GRAS HFLK UPAD
 11  HFLK UPAD MOPI
 12  HFLK MOPI WETT
 13  WETT MOPI WROC
 14  WROC MOPI BOGO
 15  KOSG WARE POTS
 16  KOSG POTS KIRU
```

Appendix G

(Estimated Velocities for the UK Tide Gauge Monitoring Project)

GROUP ONE

fixed-interval smoothing results (vN=Velocity in Northing, vE=Velocity in Easting)
(vH=Velocity in Height, svN,svE and svH are standard errors)

Ep	S.Name	vN	vE	vH	svN	svE	svH

fixed-interval smoothing results

	91.66			1			
1	ABE1	-0.042	20.38	23.25	2.715	3.794	3.025
1	HER1	14.998	22.443	0.266	0.144	0.425	0.273
1	HERS	14.995	22.443	0.265	0.144	0.425	0.273
1	HRM1	16.08	23.841	6.385	2.983	4.242	3.688
1	LER2	0.056	9.943	13.773	2.166	2.731	2.193
1	MADR	14.987	25.493	2.358	0.001	0.001	0
1	NEW1	10.216	18.526	4.636	3.045	3.825	3.536
1	NOT1	-0.695	18.699	-0.518	2.196	3.266	2.761
1	ONSA	13.199	33.861	-1.057	0	0.001	0.001
1	POR1	7.579	24.567	6.345	2.522	3.19	2.915
1	PPA1	9.63	15.166	7.168	2.315	3.282	2.609
1	TROM	7.144	1.316	24.645	0.061	0.055	0.087
1	WETT	12.645	30.237	-4.172	0.001	0.001	0.001
	92.56	0		2			
2	HER1	14.986	22.444	0.269	0.13	0.42	0.267
2	HERS	14.988	22.444	0.271	0.129	0.42	0.267
2	KOSG	13.359	23.458	-0.19	0.377	1.281	0.739
2	LER2	1.503	10.384	14.264	1.206	1.78	1.255
2	MADR	14.984	25.492	2.361	0	0.001	0
2	NEW1	13.064	16.639	1.813	1.753	2.252	2.039
2	ONSA	13.199	33.86	-1.057	0	0.001	0
2	POR1	6.971	24.015	7.266	1.46	1.904	1.694
2	PPA1	9.768	16.016	5.327	1.515	2.498	1.837
2	TROM	7.144	1.313	24.644	0.197	0.586	0.21
2	WETT	12.648	30.238	-4.175	0	0.001	0
	93.57	0.00E+		3			
	5. 0.	00					
3	ABE1	13.915	21.914	8.873	1.673	2.126	1.818
3	HER1	14.947	22.446	0.285	0.127	0.419	0.265
3	HERS	14.962	22.445	0.29	0.127	0.419	0.265
3	HRM1	12.356	24.149	3.646	1.893	2.394	2.202
3	KOSG	13.359	23.458	-0.19	0.377	1.281	0.739
3	LER2	9.388	11.514	9.349	1.443	2.049	1.498
3	MADR	14.979	25.492	2.367	0	0.001	0
3	METS	8.751	41.158	-2.312	0.602	2.373	0.968
3	NEW1	14.002	13.129	1.252	1.797	2.386	2.208
3	NOT1	14.7	22.312	3.3	1.44	1.763	1.631
3	ONSA	13.197	33.858	-1.055	0	0.001	0
3	POR1	13.031	20.909	5.023	1.558	2.105	1.924
3	PPA1	10.799	17.851	1.253	1.661	2.287	1.955
3	TROM	7.144	1.314	24.644	0.187	0.488	0.212
3	WETT	12.654	30.241	-4.182	0	0.001	0
	93.84	0		4			
4	HER1	14.944	22.446	0.287	0.127	0.419	0.265
4	HERS	14.959	22.446	0.292	0.127	0.419	0.265
4	KOSG	13.359	23.458	-0.19	0.377	1.281	0.739
4	LER2	10.259	11.593	8.47	1.459	2.121	1.53
4	MADR	14.979	25.492	2.367	0	0.001	0
4	METS	8.751	41.158	-2.312	0.602	2.373	0.968
4	NEW1	13.562	13.036	1.644	1.695	2.386	2.182
4	NOT1	15.374	22.448	3.465	1.36	1.755	1.599
4	ONSA	13.197	33.858	-1.055	0	0.001	0
4	POR1	14.104	20.577	4.496	1.519	2.142	1.946
4	STO1	39.008	-13.576	4.318	0.329	1.182	0.534
4	TROM	7.144	1.314	24.644	0.187	0.492	0.212
4	WETT	12.654	30.241	-4.182	0	0.001	0
4	ZIMM	13.812	20.646	3.003	0.398	1.382	1.13
	94.16	0.00E+		5			
	8. 0.	00					
5	HER1	14.94	22.446	0.289	0.128	0.419	0.266
5	HERS	14.954	22.446	0.294	0.128	0.419	0.266
5	KOSG	13.359	23.458	-0.19	0.377	1.281	0.739
5	LER2	11.18	11.817	8.095	1.545	2.262	1.632
5	MADR	14.978	25.492	2.368	0.001	0.001	0
5	METS	8.751	41.158	-2.312	0.602	2.373	0.968

5	NEW1	13.54	13.076	1.373	1.68	2.44	2.208
5	NOT1	16.282	22.559	3.461	1.285	1.767	1.578
5	ONSA	13.197	33.858	-1.055	0	0.001	0
5	POR1	15.43	20.305	3.458	1.571	2.236	2.037
5	STO1	39.006	-13.576	4.317	0.328	1.182	0.533
5	TROM	7.144	1.314	24.644	0.187	0.492	0.212
5	WETT	12.655	30.241	-4.182	0	0.001	0
5	ZIMM	13.812	20.646	3.003	0.398	1.382	1.13
	95.22	0.00E+		6			
	. 0.	00					
6	HER1	14.909	22.447	0.315	0.139	0.423	0.272
6	HERS	14.903	22.448	0.314	0.14	0.423	0.272
6	KOSG	13.359	23.458	-0.19	0.377	1.281	0.739
6	MADR	14.976	25.493	2.37	0.001	0.001	0
6	METS	8.751	41.158	-2.312	0.602	2.373	0.968
6	NEW1	22.835	14.443	-0.563	1.729	3.417	2.79
6	NOT1	16.797	24.006	-0.891	1.14	2.03	1.511
6	ONSA	13.195	33.857	-1.051	0.001	0.001	0
6	STO1	38.944	-13.576	4.315	0.321	1.18	0.529
6	TROM	7.144	1.314	24.644	0.187	0.492	0.212
6	WETT	12.656	30.242	-4.184	0.001	0.001	0
6	ZIMM	13.812	20.646	3.003	0.398	1.382	1.13
	95.64	0.00E+		7			
	3. 0.	00					
7	ABE1	10.348	25.792	-12.273	1.658	3.099	2.076
7	HER1	14.904	22.448	0.318	0.142	0.424	0.273
7	HERS	14.896	22.448	0.316	0.143	0.424	0.273
7	HRM1	11.887	23.17	-4.737	1.667	3.266	2.54
7	KOSG	13.359	23.458	-0.19	0.377	1.281	0.739
7	MADR	14.976	25.493	2.371	0.001	0.001	0
7	METS	8.751	41.158	-2.312	0.602	2.373	0.968
7	NEW1	23.644	14.444	0.101	2.214	3.901	3.304
7	NOT1	15.995	24.608	-2.2	1.117	2.155	1.571
7	ONSA	13.195	33.857	-1.051	0.001	0.001	0
7	POR1	13.828	22.772	-9.313	1.402	2.659	2.038
7	PPA1	12.724	22.595	-5.471	1.724	3.324	2.328
7	STO1	38.936	-13.576	4.315	0.322	1.18	0.53
7	TROM	7.144	1.314	24.644	0.187	0.492	0.212
7	WETT	12.656	30.242	-4.184	0.001	0.001	0
7	ZIMM	13.812	20.646	3.003	0.398	1.382	1.13
	95.87	0.00E+		8			
	2. 0.	00					
8	ABE1	9.873	25.844	-12.363	1.648	3.124	2.083
8	HER1	14.903	22.448	0.319	0.143	0.424	0.274
8	HERS	14.894	22.448	0.316	0.144	0.425	0.274
8	HRM1	11.952	23.147	-4.849	1.639	3.289	2.548
8	KOSG	13.359	23.458	-0.19	0.377	1.281	0.739
8	LER2	17.055	16.294	18.804	2.782	4.965	3.263
8	MADR	14.976	25.493	2.371	0.001	0.001	0
8	METS	8.751	41.158	-2.312	0.602	2.373	0.968
8	NEW1	23.592	14.418	0.107	2.456	4.059	3.486
8	NOT1	15.871	24.781	-2.593	1.146	2.208	1.616
8	ONSA	13.195	33.857	-1.051	0.001	0.001	0
8	POR1	13.381	22.884	-9.351	1.42	2.704	2.074
8	PPA1	12.675	22.624	-5.457	1.703	3.351	2.337
8	STO1	38.935	-13.576	4.315	0.322	1.18	0.53
8	TROM	7.144	1.314	24.644	0.187	0.492	0.212
8	WETT	12.656	30.242	-4.184	0.001	0.001	0
8	ZIMM	13.812	20.646	3.003	0.398	1.382	1.13
	96.56			9			
9	ABE1	7.159	26.125	-12.815	2.114	3.564	2.551
9	HER1	14.898	22.448	0.322	0.159	0.43	0.281
9	HERS	14.889	22.448	0.317	0.159	0.431	0.281
9	HRM1	12.13	23.028	-5.428	2.196	3.823	3.105
9	NOT1	15.389	25.714	-4.751	2.036	3.013	2.498
9	POR1	10.879	23.489	-9.517	2.505	3.725	3.186
9	PPA1	12.347	22.767	-5.346	2.268	3.899	2.927
9	STO1	38.935	-13.576	4.316	0.33	1.183	0.535

GROUP TWO

fixed-interval smoothing results

95.87200000000000			8				
8	MATE	18.311	32.016	-2.833	0.473	1.493	1.712
8	DOV1	15.056	24.302	2.566	0.124	0.275	0.164
8	NWH1	20.370	25.898	-3.075	0.214	0.631	0.427
8	LOW1	15.332	11.304	3.687	0.219	0.662	0.424
8	NSH1	25.347	-75.207	40.985	9.514	21.398	15.379
8	IMM1	-0.008	-0.115	-0.132	7.501	20.143	12.610
8	SHE1	18.583	29.582	1.979	0.133	0.325	0.191
8	MIL1	8.724	18.733	4.637	1.839	6.364	2.993
8	HOL1	5.531	27.691	-12.415	1.900	6.563	3.566
8	HEY1	8.092	40.985	6.523	1.813	6.134	3.222
8	AVO1	16.702	36.907	-17.550	1.651	5.646	3.334
8	NEW2	19.921	-15.884	44.198	1.030	2.998	1.786
8	LER3	19.036	-36.018	-67.305	1.106	3.183	1.759
8	DOV2	15.038	24.278	2.570	0.282	0.514	0.244
8	POR3	32.574	-27.607	12.449	0.650	2.074	1.170

fixed-interval smoothing results

95.64300000000000			7				
7	MATE	18.308	32.016	-2.833	0.473	1.493	1.712
7	SHE1	18.591	29.582	1.981	0.132	0.324	0.189
7	MIL1	8.724	18.733	4.637	1.840	6.364	2.993
7	HOL1	5.531	27.691	-12.415	1.900	6.563	3.566
7	HEY1	8.092	40.985	6.523	1.813	6.134	3.222
7	NSH1	25.347	-75.207	40.985	9.514	21.398	15.379
7	AVO1	16.702	36.907	-17.550	1.651	5.646	3.334
7	DOV1	15.056	24.302	2.566	0.122	0.274	0.163
7	NEW2	19.921	-15.884	44.198	1.029	2.998	1.786
7	LER3	19.036	-36.018	-67.305	1.106	3.183	1.759
7	DOV2	15.038	24.278	2.570	0.281	0.513	0.243
7	POR3	32.574	-27.607	12.449	0.649	2.074	1.170
7	NWH1	20.370	25.898	-3.075	0.212	0.630	0.426
7	LOW1	15.332	11.304	3.687	0.218	0.662	0.423

fixed-interval smoothing results

95.20200000000000			6				
6	MATE	18.299	32.016	-2.833	0.473	1.493	1.712
6	DOV1	15.055	24.302	2.566	0.117	0.272	0.159
6	NEW2	19.921	-15.884	44.198	1.029	2.998	1.785
6	LER3	19.036	-36.018	-67.305	1.105	3.183	1.759
6	DOV2	15.038	24.278	2.570	0.278	0.511	0.239
6	POR3	32.575	-27.607	12.449	0.649	2.074	1.169
6	NWH1	20.373	25.898	-3.075	0.208	0.629	0.424
6	SHE1	18.620	29.584	1.988	0.126	0.322	0.185
6	LOW1	15.331	11.304	3.688	0.214	0.661	0.421

fixed-interval smoothing results

94.16800000000001			5				
5	MATE	18.261	32.019	-2.832	0.476	1.493	1.713
5	DOV1	15.038	24.301	2.567	0.093	0.262	0.143
5	NEW2	19.922	-15.884	44.198	1.029	2.998	1.786
5	LER3	19.035	-36.018	-67.304	1.106	3.183	1.759
5	DOV2	15.041	24.279	2.570	0.264	0.502	0.218
5	POR3	32.575	-27.607	12.449	0.651	2.075	1.171
5	NWH1	20.406	25.900	-3.080	0.189	0.623	0.415
5	SHE1	18.791	29.591	2.032	0.106	0.314	0.171
5	LOW1	15.320	11.298	3.697	0.194	0.654	0.411

fixed-interval smoothing results

93.84000000000000			4				
4	MATE	18.260	32.020	-2.832	0.477	1.494	1.713
4	DOV1	15.036	24.300	2.567	0.092	0.261	0.143
4	NEW2	19.922	-15.884	44.198	1.029	2.998	1.786
4	LER3	19.035	-36.018	-67.304	1.106	3.183	1.759
4	DOV2	15.041	24.279	2.570	0.264	0.502	0.218
4	POR3	32.575	-27.607	12.449	0.651	2.075	1.171
4	NWH1	20.410	25.900	-3.081	0.188	0.622	0.414
4	SHE1	18.807	29.592	2.036	0.106	0.314	0.170
4	LOW1	15.318	11.297	3.699	0.193	0.654	0.410

fixed-interval smoothing results

93.57500000000000			3				
3	MATE	18.260	32.020	-2.832	0.478	1.494	1.713
3	DOV1	15.035	24.300	2.567	0.092	0.261	0.143
3	NWH1	20.413	25.900	-3.081	0.187	0.622	0.414

```
  3 SHE1       18.817       29.592        2.039        0.106        0.314        0.170
  3 LOW1       15.317       11.297        3.699        0.192        0.654        0.410
fixed-interval smoothing results
   92.560000000000000                     2
  2 MATE       18.262       32.020       -2.832        0.488        1.497        1.716
  2 DOV1       15.027       24.299        2.567        0.106        0.267        0.154
  2 NWH1       20.440       25.901       -3.086        0.190        0.623        0.416
  2 SHE1       18.915       29.596        2.065        0.120        0.319        0.178
  2 LOW1       15.307       11.292        3.707        0.194        0.654        0.411
fixed-interval smoothing results
   91.660000000000000                     1
  1 DOV1       15.025       24.299        2.567        0.131        0.279        0.173
  1 NWH1       20.448       25.901       -3.087        0.205        0.627        0.422
  1 SHE1       18.939       29.597        2.072        0.143        0.329        0.194
  1 LOW1       15.304       11.291        3.709        0.208        0.658        0.417
```